



Klaas van 't Riet
Johannes Tramper

Start of Citation[PU]M. Dekker[/PU][DP]1991[/DP]End of Citation

title: Basic Bioreactor Design
author: Riet, Klaas van 't.
publisher:
isbn10 | asin: 0824784464
print isbn13: 9780824784461
ebook isbn13: 9780585157214
language:
subject
publication date:
lcc:
ddc:
subject:

[< previous page](#)

page_i

[next page >](#)

Page i

Basic Bioreactor Design

Klaas van 't Riet
Johannes Tramper

Wageningen Agricultural University
Wageningen, The Netherlands



MARCEL DEKKER, INC.

NEW YORK • BASEL

Start of Citation[PU]M. Dekker[/PU][DP]1991[/DP]End of Citation

[< previous page](#)

page_i

[next page >](#)

Library of Congress Cataloging--in--Publication Data

Riet, Klaas van't.

Basic bioreactor design / Klaas van 't Riet and Hans Tramper.

p. cm.

Includes bibliographical references and index.

ISBN 0--8247--8446--4 (acid--free paper)

1. Bioreactors---Design. I. Tramper, Hans II. Title.

TP248.25.B55R54 1991

660'.62---dc20

90--23465

CIP

This book is printed on acid-free paper.

Copyright © 1991 by MARCEL DEKKER, INC. All Rights Reserved

Neither this book nor any part may be reproduced or transmitted in any form or by any means, electronic or mechanical, including photocopying, microfilming, and recording, or by any information storage and retrieval system, without permission in writing from the publisher.

MARCEL DEKKER, INC.

270 Madison Avenue, New York, New York 10016

Current printing (last digit):

10 9 8 7 6

PRINTED IN THE UNITED STATES OF AMERICA

Start of Citation[PU]M. Dekker[/PU][DP]1991[/DP]End of Citation

PREFACE

Basic Bioreactor Design is based on the course material of the graduate course in biochemical engineering at Wageningen Agricultural University.

This course has two objectives:

- 1 To provide the basic principles of reactor design
- 2 To select the relevant principles and data for practical process engineering purposes

These objectives determined the scope of material covered in this book. A limited number of reactor types as well as a limited number of phenomena are discussed. Yet we assume that the ones dealt with are enough to solve 95% of the problems and questions encountered in commercial fermentation. The book is intended for two groups of people: first, graduate students, to use as a textbook for learning the basic principles and methods of bioreactor design, and second, company engineers and biotechnologists, to use it as a handbook of fermenter design and engineering.

Part of this book also originated from the time when Professor K. van 't Riet (then a Gist brocades employee) together with Professor J.J. Heijnen (then a Gist brocades employee, now with Delft Technical University) cotaught a course on biochemical engineering with Dr. N.W.F. Kossen (then at Delft Technical University, now with Gist brocades). A substantial portion of Part Three originates from this lecture series.

The authors wish to acknowledge Dr. N.W.F. Kossen and Prof. J.J. Heijnen for the contribution they made to this book. Prof. A. Prins is acknowledged for Chapter 12.

Further, a number of the examples were contributed by Dr. L.E.S. Brink, Ir. C.D. de Gooyer, Ir. M.H. Zwietering and Dr. P. Verlaan. Dr. R.G.J.M. van der Lans and Mr. B. Brandt made many useful suggestions and corrections.

Also, we thank Mr. C. Rijpma and Mr. M. Schimmel for the artwork. Finally, layout and final preparation has been done by Mr. G. Heida and Ms. H.S. Wessels. Without their dedication this book never would have reached the final completion.

KLAAS VAN 'T RIET
HANS TRAMPER

Start of Citation[PU]M. Dekker[/PU][DP]1991[/DP]End of Citation

CONTENTS

Preface	iii
Part One	
Introduction	
1	3
Introduction	
Part Two	
Basics	
2	27
Balances	
3	51
Yield	
4	68
Kinetics	
5	91
Stability	
6	104
Flow, Flooding, Dispersion	
7	122
Medium	
8	136
Shear	
Part Three	
Reactor Engineering	
9	183
Mixing	
10	220
Hold-Up	
11	236
Mass Transfer	
12	274
Foam	
13	293
Heat Transfer	

14	303
Power Consumption	
Part Four	
Reaction Engineering: Integration	
15	319
Macrokinetics: Particle Level	
16	342
Apparent Stability	
17	370
Macrokinetics: Reactor Level	
18	401
Process Engineering	
Symbols	451
Index	461

Start of Citation[PU]M. Dekker[/PU][DP]1991[/DP]End of Citation

[< previous page](#)

[page_v](#)

[next page >](#)

PART I

Introduction

1

Introduction

1.1 Defining the subject

Bioreactor design is an integral part of biotechnology, an area with rather loose and contested borders. A widely distributed, much advertised, but unfortunately wrong definition of biotechnology is:

Microbiology
Genetics
Biochemistry
Engineering
Chemistry
Pharmacy
Food Technology

BIOTECHNOLOGY

Biotechnology is not simply the sum of microbiology, genetics, biochemistry, engineering, etc.; no, it is the integration of these disciplines, and this involves quite a bit more than just simple addition. Integration and application are the keywords which can be found in most definitions of biotechnology (Fig. 1.1). Especially when designing bioreactors, integration of biological and engineering principles is essential. The bioreactor should be designed such that specific biological and technological demands of a process are met. Naturally, quality and price of the product are decisive for commercial realization. The aim of bioreactor design can thus be defined as "minimization of the costs of the pertinent product while retaining the desired quality, and this within the biological and technological constraints." This does not mean *a priori* that minimizing the costs of the bioreactor also means minimizing the costs of the integral process. This depends largely on the cost-determining part(s) of the process. If running the bioreactor is cost determining, then maximization of the overall volumetric productivity of

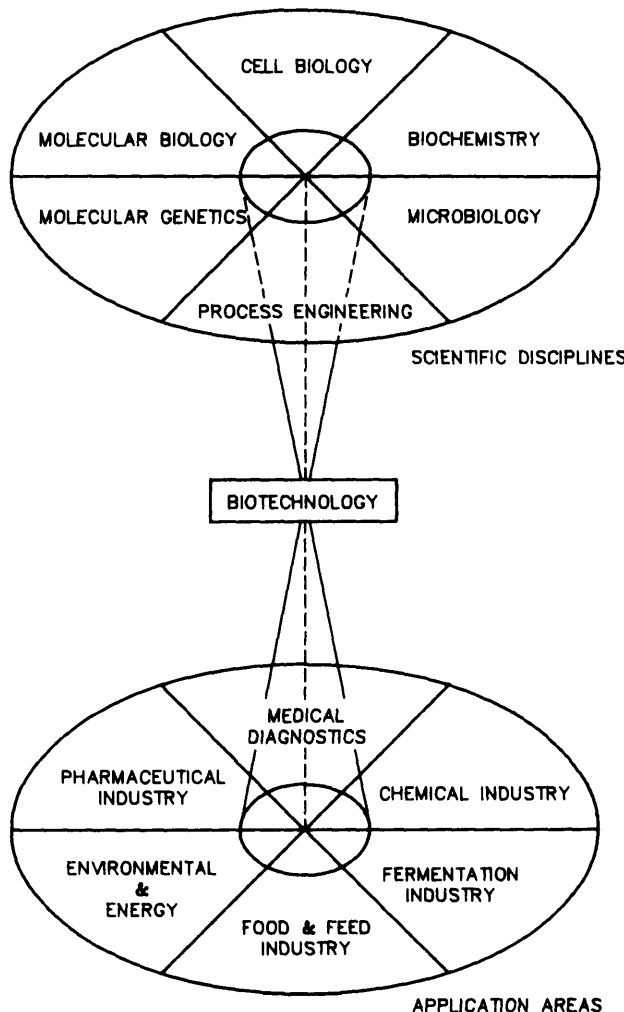


Fig. 1.1 Biotechnology: application-oriented integration of biodisciplines and engineering.

the bioreactor is, in general, the rational approach. If, on the other hand, the downstream processing is cost determining, then maximization of the product concentration in the bioreactor is, in general, the rational thing to do. However, here again integration is the keyword. Bioreactor design should be an integral part of the overall process design.

The words bioreactor, biocatalyst and product have been used in general terms. In the following sections of this chapter the bioreactor will be defined, though still in general terms, with respect to reactor concepts and types and to tools in bioreactor design. The meaning of product is obvious with the annotation that biomass can be the desired product too. In this book biocatalyst means either an enzyme, an enzyme complex, a cell organelle or a whole cell. The latter can be growing or nongrowing, viable or nonviable, etc. Furthermore, a biocatalyst can be free or immobilized, which has far-reaching consequences not only with respect to mass transfer, but sometimes also for the physiology of viable cells. Integration of mass transfer and biokinetics is essential in the description (microkinetics) of immobilized biocatalysts. The source of biocatalysts can be of either microbial, plant or animal origin and examples of all three are used in this book.

1.2 Productivity and product concentration

1.2.1 Overall volumetric productivity

Overall volumetric productivity Q_p ($\text{mol m}^{-3} \text{s}^{-1}$) (it is also common to use a yearly basis) is the average production capacity per unit volume and time of the bioreactor. The overall volumetric productivity is confined on the one hand by physical constraints such as mass and heat transfer, and on the other hand by biocatalyst concentration C_x (mol m^{-3}) and activity of the biocatalyst, expressed as substrate consumption rate $-r_s^*$ ($\text{mol m}^{-3} \text{s}^{-1}$). Maximization of the overall volumetric productivity of the bioreactor in principle means minimization of the costs of investment, because one can suffice with smaller equipment. It usually also means lower operating costs. In general, it means too that it is desired to operate the bioreactor as close as possible to the physical constraints, the horizontal dotted line in Fig. 1.2. This physical limitation is the result of mass and heat transfer limitations, which are stoichiometrically related to product formation. The vertical dotted line in Fig. 1.2 symbolizes the limitation which is a consequence of the fact that the concentration of the biocatalyst is bound to certain defined limits, for instance solubility in case of isolated enzymes and "space" in case of suspended cells. Fig. 1.2 also shows that the biocatalyst should have a minimum specific activity to be able to operate the bioreactor close to its physical ceiling.

1.2.2 Overall biocatalyst productivity

In addition to limitations by mass and heat transfer and concentration of biocatalyst, the overall volumetric productivity of the bioreactor is deter-

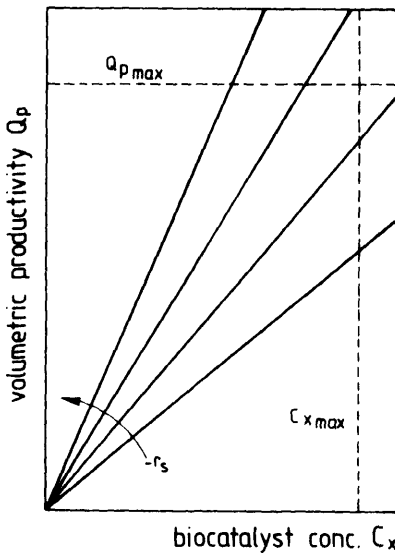


Fig. 1.2 Constraints of overall volumetric productivity. (Adapted from Cooney, 1983.)

mined by the overall productivity of the biocatalyst, Pr_{px} (-), defined as the total moles of product which are produced by 1 mol of biocatalyst during its operational lifetime t_l (s). Pr_{px} is related to the specific product production rate q_p (s^{-1}) (moles of product produced per mol of biocatalyst per second) as

$$Pr_{px} = \int_0^{t_l} q_p dt = - \int_0^{t_l} Y_{ps}^{ov} \frac{r_s^u}{C_x} dt \quad (1.1)$$

The definition of Y_{ps}^{ov} (-), the overall yield of product on substrate (total moles of product produced per total mol of substrate), leads to

$$Q_p = \frac{1}{t_l} \int_0^{t_l} q_p C_x dt \quad (\text{mol m}^{-3} \text{s}^{-1}) \quad 1.2a$$

$$Q_p = \frac{1}{t_l} \int_0^{t_l} -Y_{ps}^{ov} r_s^u dt \quad (\text{mol m}^{-3} \text{s}^{-1}) \quad 1.2b$$

The time needed to empty, clean, refill, restart, etc., the bioreactor between two operations is the so-called down-time, which is symbolized by t_d (s). In case t_d is relevant it can be introduced in Eq. (1.2) by replacing $1/t_1$, preceding the integral, by $1/(t_1 + t_d)$. In addition to the molar productivity used above, the mass productivity (kg product instead of mol) is also quite commonly used in engineering (conversion from one to the other by means of the molecular weights). It is also common practice to use hour, day or year as unit of time.

The search for and the development of a useful biocatalyst with a suitable yield, specific activity and stability is in the beginning the task of microbiologists, biochemists, molecular biologists, protein engineers, etc. However, especially with respect to stability, the process engineer also has means available, among others immobilization, to improve the stability of biocatalysts. This is covered in this book.

1.2.3 Product concentration

The effect of the composition of the product stream leaving the bioreactor on the costs of the downstream processing is large. Therefore, it is essential to take this into account when designing the bioreactor. This often means in practice that the bioreactor is designed such that the concentration of product is as high as possible. The end concentration of product C_p (mol m⁻³) in the bioreactor depends on r_s^u , Y_{ps}^{ov} and the residence time in the bioreactor. For a batch reactor, with t_b (s) as the time that the batch lasts, this leads to

$$C_p = Y_{ps}^{ov} \int_0^{t_b} -r_s^u dt \quad (\text{mol m}^{-3}) \quad 1.3$$

and for a continuous reactor with a liquid throughflow F_1 (m³ s⁻¹) and a volume V (m³):

$$C_p = -Y_{ps}^{ov} r_s^u \frac{V}{F_1} \quad (\text{mol m}^{-3}) \quad 1.4$$

Concentration of product is especially a key-parameter when the downstream processing is the cost-determining part of the integral process. Product recovery is often a laborious and expensive operation, especially when diluted aqueous solutions are involved such as we usually encounter in biotechnology. However, it has become clear that the aqueous reaction medium, which was for a long time supposed to be essential for biocatalysis, can be replaced to a large extent by a suitable organic solvent (Laane et al., 1987).

1.3 Bioreactor types

1.3.1 The stirred vessel

In Fig. 1.3 a schematic view of a stirred vessel is given. The vessel is cylindrical with a height H_v (m) and a diameter T_v (m). Usually H_v is equal to or greater than $2 T_v$. It is equipped with a stirrer in the lower compartment. This stirrer is mounted near the bottom usually at a distance equal to the stirrer diameter. At a lower position the stirrer and bottom interact leading to a decrease in power consumption. At a higher position liquid circulation problems can occur because at increased gas flow rate in case of aeration the bubbles will not be recirculated in the lower compartment. Sometimes the upper compartment(s) are also equipped with a stirrer. The vessel is equipped with baffles to prevent rotation of the contents as a whole. For aeration an air sparger is mounted below the stirrer. For mass transfer its construction is generally not relevant, so it is chosen on the basis of sterility and cleaning criteria.

Fig. 1.4 shows a number of stirrers that are used. It will be shown in Chapter 11 that the stirrer is needed to provide a certain level of power input needed

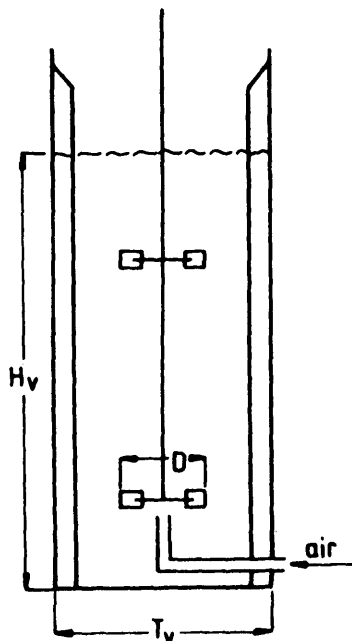


Fig. 1.3 Schematic representation of a stirred fermenter.

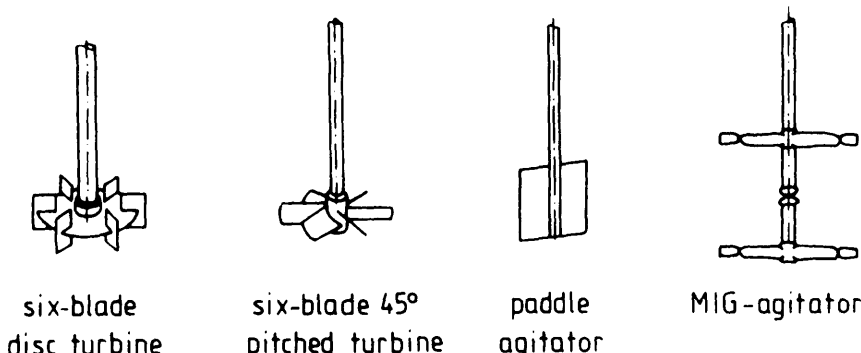


Fig. 1.4 Schematic representation of a number of stirrers. (Adapted from Zlokarnik, 1972.)

for aeration purposes. Therefore, the turbine stirrer, being easy to construct and having a high power number, is the most widely used. The other types are less intensively applied. A detailed description of all types of stirrers can be found in Zlokarnik (1972).

Special design considerations like stirrer drives and sealings are not dealt with here. Also self-aerating stirrers are not discussed. Information about them can be found in Sittig (1983).

1.3.2 The bubble column

A schematic representation of this simple reactor is given in Fig. 1.5. Usually it is $H_r \geq 2 T_v$. At the bottom a sparger is mounted. To prevent too heterogeneous flow patterns in the lower compartment, the sparger nozzles have to be distributed over the cross section of the bottom. Therefore, one ring or a small number of parallel pipes or a starlike construction of pipes is commonly used. In the pipes holes are drilled. In the chapter on mass transfer it is shown that complicated spargers or very small holes merely have disadvantages for most applications.

1.3.3 The air lift

The air lift consists of two pipes, interconnected at top and bottom. In one of the pipes (the riser) air is sparged at the bottom. The air rises and escapes at the top. Therefore, under most circumstances there is no air present in the other pipe (the downcomer). The density difference between riser and

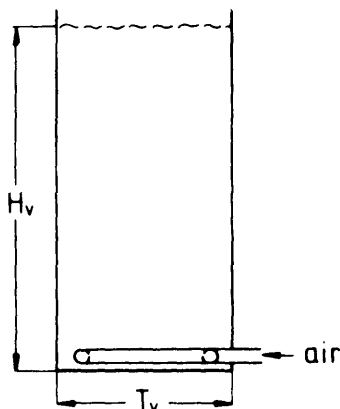


Fig. 1.5 Schematic representation of a bubble column reactor.

downcomer causes an intensive liquid circulation. Two designs can be used, i.e., the internal (Fig. 1.6A) and the external loop reactor (Fig. 1.6B). When an internal loop reactor is built underground, we refer to this as a deep shaft. Volumes can be up to thousands of m^3 . H_v generally is much larger than T_v , usually of the order of 10 T_v , but for the deep shaft up to 100 T_v .

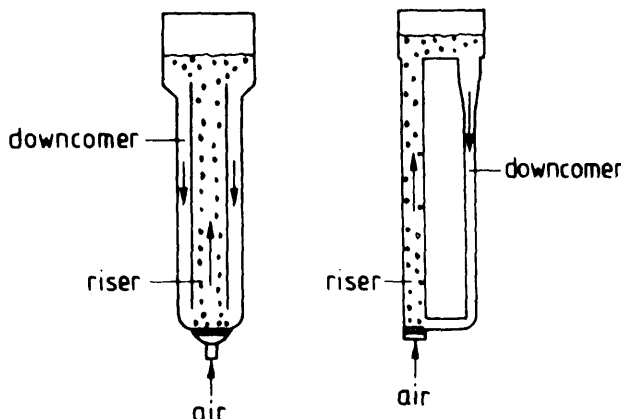


Fig. 1.6 Schematic representation of the air lift. A. Internal loop reactor. B. External loop reactor.

1.3.4 The packed bed

The packed bed is very simple in nature and differs largely from the other three types. It consists of a tubular pipe, packed with the biocatalyst particles. It can be operated in the upflow or downflow mode, i.e., the reaction medium is introduced either at the bottom or the top of the reactor.

1.3.5 Discussion of reactor types

The four basic reactor types discussed in this book are the ones described above. The difference between the packed bed and the other three is so great that the choice usually is straightforward. On the basis of detailed mixing, mass transfer and cost calculations a rational choice can be made between stirred vessel, bubble column and air lift. Many times, however, this is not needed and the following general rules suffice.

- Mixing and mass transfer do not differ very much between the three types. In the air lift the flow is controlled, which enables the introduction of a controlled substrate addition at more than one place.
- For mass transfer the maximum attainable value is higher for stirred vessels, because of the larger power that can be introduced with the stirrer. For air lift and bubble column mass transfer collapses above a viscosity of about 0.1 N s m^{-2} .
- At increasing scale mechanical problems can occur in the stirred vessel because of the large power values of the stirrer motor.

Based on these three reasons the following rules of thumb apply:

- In those cases where viscosities can rise above 0.1 N s m^{-2} (mycelial, biopolymer fermentations) a stirred vessel is chosen because air lift and bubble column will fail.
- In those cases where flexibility in viscosity and mass transfer is needed (pilot plant) a stirred vessel is chosen because air lift and bubble column cannot offer this flexibility.
- In low viscosity fermentations at large scale ($50\text{--}500 \text{ m}^3$) a bubble column is chosen because it is the cheapest fermenter.
- In low viscosity fermentations at very large scale ($200\text{--}10,000 \text{ m}^3$) an air lift is chosen because it permits local and controlled substrate addition. (The stirred fermenter would offer immense mechanical problems at $V > 500 \text{ m}^3$ because the stirrer power P , could easily rise above 1 MW).
- Viscous fermentations cannot be scaled up to scales $> \sim 500 \text{ m}^3$ because the stirred fermenters that are needed for these cases will offer mechanical problems ($P > 1 \text{ MW}$).

These rules of thumb explain why most fermenters < 200 m³ are stirred (viscous, pilot) or bubble type (SCP, Single Cell Protein) while the very large ones are of the more recently developed air lift type.

1.4 Reactor concepts

1.4.1 Introduction

The bioreactor has been introduced in general terms in Section 1.3. In this section the basic bioreactor concepts, i.e., the batch, the fed-batch, the continuous-flow stirred-tank reactor (CSTR), the cascade of CSTRs and the plug-flow reactor, will be described. Integration with the (micro)kinetics, in other words the kinetics of the pertinent free biocatalysts or of the immobilized biocatalysts including mass transfer, yields the overall reactor description or macrokinetics in later chapters. In order to come up with these descriptions, a mass balance over the bioreactor should be drawn up (Fig. 1.7).

In words:

The accumulation of a compound *A* with a concentration in the reactor C_{Ar} is equal to the amount of *A* that comes in, substracted by the amount that goes out, and augmented by the amount that is produced.

In formula:

$$\frac{d(V C_{Ar})}{dt} = F_i C_{Ai} - F_o C_{Ao} + \int r_A^u dV \quad (\text{mol s}^{-1}) \quad 1.5$$

In this equation *V* is the liquid volume in the bioreactor (m³), C_A the concentration of *A* (mol m⁻³) by which the subscripts *i* and *o* refer to

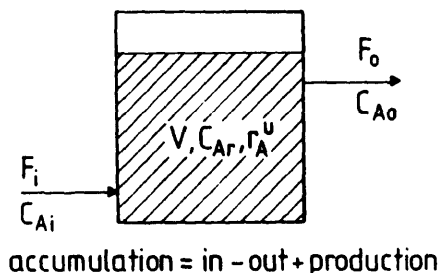


Fig. 1.7 The mass balance over the bioreactor.

the concentration in the influent and effluent, respectively, t is time (s), F_i and F_o the flow ($\text{m}^3 \text{s}^{-1}$) of the in and outgoing stream, respectively, and r_A^u the production rate per unit volume ($\text{mol m}^{-3} \text{s}^{-1}$) of A .

1.4.2 The batch reactor

The most-prominent characteristic of the batch reactor is the fact that there are no in- and outgoing flows (Fig. 1.8). This means that all that is produced is accumulated. The mass balance [Eq. (1.5)] thus simplifies to, assuming ideal mixing:

$$\frac{d(V C_{Ar})}{dt} = r_A^u V \quad (\text{mol s}^{-1}) \quad 1.6$$

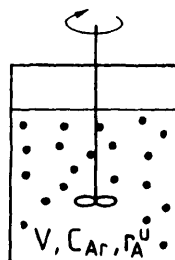
When the volume V remains constant, Eq. (1.6) even further simplifies:

$$\frac{dC_{Ar}}{dt} = r_A^u \quad (\text{mol m}^{-3} \text{s}^{-1}) \quad 1.7$$

With boundary conditions $C_{Ar} = C_{Ar}(0)$ on $t = 0$ and $C_{Ar} = C_{Ar}(t_b)$ at $t = t_b$, the time one batch lasts, separation of variables and integration lead to:

$$t_b = \int_{C_{Ar}(0)}^{C_{Ar}(t_b)} \frac{dC_{Ar}}{r_A^u} \quad (\text{s}) \quad 1.8$$

Substitution of the pertinent rate equation yields the time a run should last to obtain a desired conversion.



accumulation = production

Fig. 1.8 The batch reactor.

1.4.3 The fed-batch reactor

The distinguishing feature of the fed-batch reactor is that there is only an ingoing flow and no outgoing flow (Fig. 1.9). Eq. (1.5) thus becomes, assuming ideal mixing:

$$\frac{d(V C_{Ar})}{dt} = F_i C_{Ai} + r_A^u V \quad (\text{mol s}^{-1}) \quad 1.9$$

or

$$V \frac{d(C_{Ar})}{dt} + C_{Ar} \frac{dV}{dt} = F_i C_{Ai} + r_A^u V \quad (\text{mol s}^{-1}) \quad 1.10$$

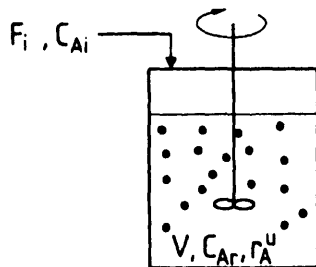
This equation cannot be solved analytically without further simplification and data.

1.4.4 The continuous-flow, stirred-tank reactor (CSTR)

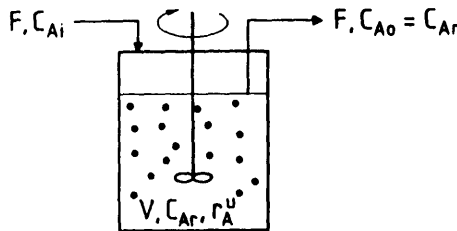
The CSTR defined here (Fig. 1.10) is that the volume V is constant and ideally mixed and that the inflow equals the outflow, i.e. $F_i = F_o = F$. For solving the mass balance [Eq. (1.5)] of a CSTR it is assumed that the reactor essentially is in a steady state:

$$\frac{d(V C_{Ar})}{dt} = 0 \quad (\text{mol s}^{-1}) \quad 1.11$$

Eq. (1.5) thus becomes



accumulation = in + production Fig. 1.9 The fed-batch reactor.



$$0 = \text{in-out} + \text{production}$$

Fig. 1.10 The CSTR.

$$0 = FC_{A_i} - FC_{A_o} + r_A^u V \quad (\text{mol s}^{-1}) \quad 1.12$$

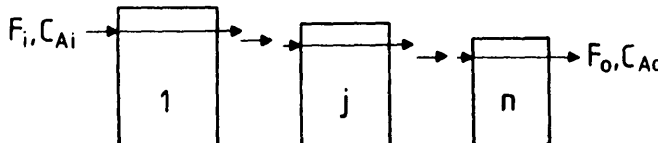
or

$$\tau_{CSTR} = \frac{V}{F} = \frac{C_{A_o} - C_{A_i}}{r_A^u} \quad (\text{s}) \quad 1.13$$

in which τ_{CSTR} is the average residence time (s). As in an ideally mixed vessel the concentration in the reactor is equal to C_{A_r} , this equation can immediately be solved by substituting for r_A^u the appropriate rate equation with $C_{A_r} = C_{A_o}$.

For n CSTRs in series (Fig. 1.11) the same assumptions are made for each vessel as for the single CSTR above. For each vessel in the series Eq. (1.13) thus holds:

$$\tau_{CSTR(j)} = \frac{V_j}{F} = \frac{C_{A_r(j)} - C_{A_r(j-1)}}{r_A^u} \quad (\text{s}) \quad 1.14$$



$$0 = \text{in-out} + \text{production}$$

Fig. 1.11 The cascade of CSTRs.

The subscript j refers to the j -th vessel. In later chapters the optimal design for fermentation using the Monod equation with a linear relation between the microorganism and substrate concentration will be worked out, as well as the optimal design for n CSTRs in series containing (immobilized) biocatalyst of constant activity and following Michaelis-Menten kinetics.

1.4.5 The plug-flow reactor

In the ideal plug-flow reactor (Fig. 1.12) the continuous phase flows as a plug through the reactor; i.e., there is no mixing or, in other words, no axial dispersion. Consequently, if a compound is consumed or produced, a concentration gradient will exist in the direction of flow. The mass balance is therefore first set up over an infinite small slice perpendicular to the direction of the flow with volume dV of the bioreactor. Assuming steady state and $F_i = F_o = F$, Eq. (1.5) then is reduced to:

$$0 = FC_{Ar} - F(C_{Ar} + dC_{Ar}) + r_A^u dV \quad (\text{mol s}^{-1}) \quad 1.15$$

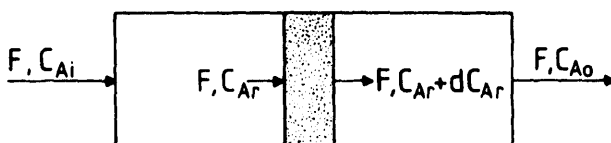
Rewriting gives:

$$\frac{dC_{Ar}}{r_A^u} = \frac{dV}{F} \quad (\text{s}) \quad 1.16$$

Integration over the whole reactor:

$$\int_{C_{Ai}}^{C_{Ao}} \frac{dC_{Ar}}{r_A^u} = \int_0^V \frac{dV}{F} \quad (\text{s}) \quad 1.17$$

or:



$$0 = \text{in-out} + \text{production}$$

Fig. 1.12 The plug-flow reactor.

$$\tau_{pf} = \frac{V}{F} = \int_{C_{A1}}^{C_{A0}} \frac{dC_{Ar}}{r_A^u} \quad (s) \quad 1.18$$

in which τ_{pf} (s) is the residence time of the plug-flow reactor. This equation is in principle the same as that of the batch reactor and integration with the (micro)kinetics is identical.

1.4.6 Discussion of the reactor concepts

A comparison of the various types of reactor concepts, in a general sense, is actually only possible between the batch, the CSTR and the plug-flow reactor. The cascade of CSTRs, depending on the number of vessels n in the series, more or less behaves as an ideal mixer for $n \rightarrow 1$ or an ideal plug flow for $n \rightarrow \infty$. The fed-batch reactor is more difficult to situate. Although the concentration of compounds important for the rate of reaction can be controlled optimally during the whole fed period, the reactor volume is only partially utilized, especially in the beginning. Nevertheless, this reactor concept certainly has decisive advantages in many cases as shown by the fact that it is one of the most widely used.

For the batch, the CSTR and the plug-flow reactor the following equations for the "residence time" have been derived, respectively:

$$t_b = \int_{C_{Ar}(0)}^{C_{Ar}(t_b)} \frac{dC_{Ar}}{r_A^u} \quad (s) \quad 1.8$$

$$\tau_{CSTR} = \frac{C_{A0} - C_{A1}}{r_A^u} \quad (s) \quad 1.13$$

$$\tau_{pf} = \int_{C_{A1}}^{C_{A0}} \frac{dC_{Ar}}{r_A^u} \quad (s) \quad 1.18$$

In general, the rate of reaction decreases if the reactant concentration decreases (reaction-order > 0). For a CSTR this means that the rate of reaction is low for the whole reactor as it is determined by the low concentration in the reactor, equal to that of the outflow. For the other two

reactor types the conversion takes place at concentrations less than the higher incoming concentration. This means that in case of "ordinary" kinetics $\tau_{CSTR} > t_b = \tau_{pf}$, in other words that the CSTR should be larger than the batch and the plug-flow reactor in order to accomplish the same degree of conversion. Naturally, the down-time of the batch reactor is not taken into account here.

In an autocatalytic reaction, i.e., the more product the faster the rate of reaction, or when there is substrate inhibition, the $1/r_A^u$ versus C_{Ar} curves can look quite different. In that case $t_b = \tau_{pf} > \tau_{CSTR}$. For these types of kinetics it is thus advantageous to use a CSTR. Only when zero-order kinetics are involved is there no difference in "residence times" and thus volumina, of the three types of reactors.

1.5 Overall outline

As can be extracted from the preceding sections, the overall volumetric productivity of the bioreactor forms the basis of this book. Built on that are chapters concerning general aspects such as reactor concepts and types, balances, product concentration and medium (viscosity, coalescence, etc.). On the same level are chapters dealing with the limitations of the biocatalyst, i.e., yield, kinetics and stability, as well as chapters discussing the physical constraints resulting from mass and heat transfer, mixing, foaming, flooding, hold-up, shear and power consumption. Integration of kinetics and mass transfer on the particle level in immobilized biocatalysts yields the microkinetics. Similarly, the effect of diffusion limitation of substrate on the apparent stability of the immobilized biocatalyst can be quantified. Integration of (micro)kinetics in the various reactor concepts yields the macrokinetics. These last chapters form the integration block. In this block a division between gas/liquid and liquid/solid mass transfer is carried out for reasons of clarity. Taking into account all pertinent parameters derived in the various preceding blocks, the overall reactor models for the batch, the fed-batch and the continuous stirred-tank reactor (CSTR), the cascade of CSTRs and the plug-flow reactor are derived. Finally, the process engineering aspects and the economic evaluation form the last part. The various chapters are illustrated by means of exercises.

1.6 Examples

Example 1.1 The productivity of an enzyme reaction

Glucose is isomerised into fructose by means of immobilized glucose isomerase in a continuous bioreactor.

Calculate :

- The overall productivity of the biocatalyst
- The overall productivity of the bioreactor on a yearly basis
- The product concentration at time $t = 0$ and $t = t_i$

Data:

- $-\frac{r_s^u(T)}{C_x} = 10^{12} e^{-7.5 \times 10^4 / RT} \text{ s}^{-1}$
- $r_s^u(t) = r_s^u(0) e^{-k_d t} \text{ kg m}^{-3} \text{ s}^{-1}$
- $k_d = 10^{35} e^{-2.5 \times 10^3 / RT} \text{ s}^{-1}$
- $Y_{ps} = 0.9 \text{ kg kg}^{-1}$
- operational life time = half-time $t_{0.5}$ of biocatalyst (s)
- concentration of biocatalyst C_x is 0.1 kg m^{-3}
- $F = 0.01 \text{ m}^3 \text{ s}^{-1}$
- $V = 100 \text{ m}^3$
- $T = 305, 310, 315 \text{ and } 320 \text{ K}$
- down-time is 1 week
- $R = \text{gas constant} = 8.314 \text{ J mol}^{-1} \text{ K}^{-1}$

(Kinetic data adapted from Roels, 1983)

Solution:

$$r_s^u(t_i) = r_s^u(t_{0.5}) = \frac{1}{2} r_s^u(0) = r_s^u(0) e^{-k_d t_i}$$

Rewriting: $t_i = t_{0.5} = \frac{\ln 2}{k_d}$

Substitution in Eq. (1.1) gives

$$Pr_{px}(t) = -Y_{ps} \int_0^{t_i} \frac{r_s^u(0)}{C_x} e^{-k_d t} dt$$

or

$$Pr_{px}(t_{0.5}) = -Y_{ps} \frac{r_s^u(0)}{C_x} \frac{(1 - e^{-k_d t_i})}{k_d} = -\frac{Y_{ps} r_s^u(0)}{2 k_d C_x}$$

Introducing the temperature dependency yields subsequently

$$Pr_{px}(t_{0.5}, T) = \frac{Y_{ps} 10^{12} e^{-7.5 \times 10^4 / RT}}{2 \times 10^{35} e^{-2.5 \times 10^5 / RT}}$$

and for the overall volumetric productivity on a yearly basis

$$Q_p = \frac{365}{t_{0.5} + 7} C_x Pr_{px}(t_{0.5}, T)$$

The product concentration in this case can be described by

$$C_p = \frac{Y_{ps} r_s^u(t, T) V}{F}$$

Substituting the given data in these equations gives Table 1.1

It is clear that as result of the down-time an optimum occurs and obvious that at $t = t_{0.5}$ the concentration of product is half of that at $t = 0$.

Example 1.2 Production of D-(-)-4-hydroxyphenylglycin

D-(-)-4-hydroxyphenylglycin is the optically active intermediate in the synthesis of the broad-spectrum antibiotic amoxicilline. This intermediate is among others produced from a hydantoin derivative by means of the enzyme hydantoinase. The hydantoin derivative is poorly soluble in water,

Table 1.1 The productivity of glucose isomerase

T (K)	305	310	315	320
$r_s^u(0)$	0.14	0.23	0.36	0.56
$Pr_{px}(t_{0.5})$	4.4×10^6	1.4×10^6	0.5×10^6	0.2×10^6
$t_{0.5}$ (days)	552	112	24	5.4
Q_p	2.85×10^5	4.38×10^5	5.72×10^5	5.04×10^5
$C_p(0)$	127	204	324	507
$C_p(t_{0.5})$	63	102	162	254

about 1 kg m^{-3} . The price of the substrate is cost determining and the degree of conversion should therefore be very high, at least 99%.

Calculate the volume needed to produce 1000 kg of product per day by immobilized hydantoinase in a

- batch reactor
- CSTR
- plug-flow reactor

Data:

- Michaelis-Menten reaction kinetics with $v_{max} = 1.5 \times 10^{-4} \text{ kg s}^{-1} \text{ m}^{-3}$ biocatalyst and $K_m = 5 \times 10^{-3} \text{ kg m}^{-3}$
- $Y_{ps} = 1 \text{ kg kg}^{-1}$
- degree of conversion 99%
- down-time for batch reactor 1 day
- The activity of the biocatalyst can be assumed to be constant in time.
- The reactors contain 0.1 m^3 immobilized biocatalyst per m^3 , except the plug-flow reactor, which is packed with 0.5 m^3 immobilized biocatalyst per m^3 reactor.

Solution for the batch reactor:

$$t_b = \int_{C_{Ar}(0)}^{C_{Ar}(t_b)} \frac{dC_{Ar}}{Y_{ps} r_A^u} = - \int_{C_{sr}(0)}^{C_{sr}(t_b)} \left(\frac{0.1 v_{max} C_{sr}}{K_m + C_{sr}} \right)^{-1} dC_{sr}$$

$$t_b = \frac{1}{0.1 v_{max}} \left[K_m \ln \left(\frac{C_{sr}(0)}{C_{sr}(t_b)} \right) + (C_{sr}(0) - C_{sr}(t_b)) \right]$$

Substituting the numerical values gives:

$$t_b = 67535 \text{ s} = 18.76 \text{ h.}$$

Taking into account the down-time of about 1 day, it can be concluded that 1 batch takes about 2 days. The concentration of substrate at time zero is 1 kg m^{-3} and the yield 1 kg kg^{-1} . Therefore, to produce 1000 kg d^{-1} , one batch should have the size of 2000 m^3 , which is thus the working volume of the batch reactor. Note that $0.1 v_{max}$ is substituted due to the biocatalyst loading of $0.1 \text{ m}^3 \text{ m}^{-3}$.

Solution for the CSTR:

$$\tau_{CSTR} = \frac{V}{F} = \frac{C_{A0} - C_{A1}}{r_A^u} = \frac{(C_{sr} - C_{so})(K_m + C_{so})}{0.1 v_{max} C_{so}}$$

Substituting the numerical values yields

$$\tau_{CSTR} = 99 \times 10^3 \text{ s} = 27.5 \text{ h.}$$

In order to produce 1000 kg d^{-1} the flow rate should be:

$$F = \frac{1000 \text{ kg d}^{-1}}{(1 \text{ kg m}^{-3})(24 \text{ h d}^{-1})} = 41.7 \text{ m}^3 \text{ h}^{-1}$$

$$V = \tau_{CSTR} \times F = 1146 \text{ m}^3$$

The minimum working volume of the CSTR is thus 1146 m^3 .

Solution for the plug-flow reactor

$$\tau_{PFR} = \int_{C_{in}}^{C_{eo}} \frac{dC_{Ar}}{r_A^u} = - \int_{C_{in}}^{C_{eo}} \frac{0.5v_{max} C_{sr}}{K_m + C_{sr}} dC_{sr}$$

$$\tau_{PFR} = \frac{1}{0.5v_{max}} \left[K_m \ln \left(\frac{C_{sr}}{C_{eo}} \right) - (C_{eo} - C_{sr}) \right]$$

Substituting the numerical values gives

$$\tau_{PFR} = 13507 \text{ s} = 3.75 \text{ h.}$$

$$V = \tau_{PFR} \times F = 3.75 \times 41.7 = 156 \text{ m}^3.$$

As result of the continuous character of the plug-flow reactor (negligible down-time) and the high volumetric activity, the required volume for the plug-flow reactor is relatively low.

References

- Cooney C.L. "Bioreactors: Design and operation." *Science* **219**, 728 (1983).
- Laane N.C.M., de Bont J.A.M. and Tramper J. "Biocatalysis in nonaqueous media." Elsevier, Amsterdam (1987).

Roels J.A. "Energetics and kinetics in biotechnology." Elsevier Biomedical Press, Amsterdam (1983).

Sittig W. "Fermentation reactors." Chem. Tech. 606 (1983).

Zlokarnik M. "Rührtechnik." Ullmann Encyklopädie der Technischen Chemie. Band II, Verlag Chemie, Weinheim (1972) p. 259.

PART II

Basics

2

Balances

2.1 Introduction

A standard tool in process engineering is the use of elemental balances. According to this method, the balances are written down for each separate chemical element. For bioreactor design, they provide useful information about the flows through and production in the apparatus. For instance, at a given sugar feed rate to a fermenter, growth and maintenance of the microorganisms determine the ammonia consumption rate. Because accumulation should be prevented, the ammonia feed rate to the fermenter should have the same value. Balances can provide the relation between sugar and ammonia feed rate. In the same way the total mass of the fermenter and the concentrations at the end of the fermentation can be calculated. These data can be used to calculate the fermenter volume that is required and can be used as input variables for downstream processing design. In the design of a new production plant balances are the basis for the whole flow sheet. Finally, it should be possible to provide design criteria based on very limited input data such as: "This amount of *BOD* should be removed," or "That amount of product should be produced in a day." This chapter will deal with the principles of balances for bioreactor design.

2.2 Elemental balances

2.2.1 General principles

The principle behind the elemental balances is very simple: The elemental flow into the system equals the flow out of the system, corrected for accumulation in the system. The production term is absent in this balance equation because elements are neither formed nor destroyed.

$$F'_{Ai} - F'_{Ao} = \frac{dVC_A}{dt} \quad (\text{mol s}^{-1}) \quad 2.1a$$

in which

F'_{A1}	= flow rate of element A entering the system	(mol s ⁻¹)
F'_{A0}	= flow rate of element A leaving the system	(mol s ⁻¹)
V	= volume (of the system)	(m ³)
C_A	= concentration of element A (in the system)	(mol m ⁻³)
t	= time	(s)

If accumulation is absent Eq. (2.1a) leads to:

$$F'_{A1} = F'_{A0} \quad (\text{mol s}^{-1}) \quad 2.1\text{b}$$

In Eq. (2.1a) and (2.1b) the kinetics or any other indication about conversion processes of the molecules that contain the elements is absent. It is a black box or unstructured model. The equations can be written down for all elements that are relevant. The elements flow in and out of the system as part of the flows, like the substrate flow, in and out of the system. Fig. 2.1 shows the flow rates that are relevant for a given fermentation with a given N, S, P and C substrate. The system is not defined as the fermenter, but as the biomass only. It is also defined in such a way that accumulation of any of the components is absent. This allows it to replace the flow rates by the production rates r . The following remarks can be made:

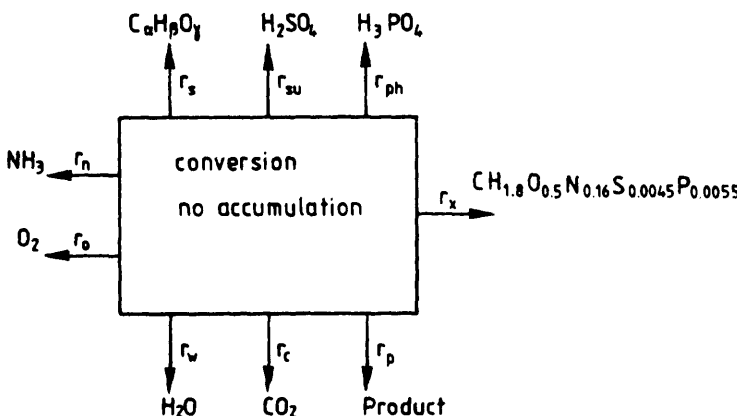


Fig. 2.1 The production rates in the black box model.

- All rates are regarded as production rates. This means that a consumption like that of the C substrate (r_C) appears in the equations as a production with a negative value. Where rates are mentioned as consumption this is given as the production rate preceded by a negative sign. This also explains that all arrows in Fig. 2.1 have to be directed out of the system. It may be noted that there does not exist a consistent sign convention for the rates. Therefore care should be taken in using literature data.
- The black box system consists of only the biomass and the substrates and products processed by the biomass. Because this usually will not be identical to the fermenter contents, the production rates do not always have the same value as the feed rates to the fermenter, because the production rates are only that part that is taken out or added to the fermenter contents by the biomass. For instance, for a batch fermentation the production rates are equal to the amounts produced (or consumed from the available substrates in the batch) by the microorganism.
- Accumulation in the black box model is assumed to be absent. This can be done because the system boundary is defined as the microorganisms only. It is assumed that accumulation of a given compound within the microorganism does not occur. The system boundary definition states that in case accumulation of feed components in the fermenter occurs, this accumulation is kept outside of the model. Product and biomass accumulation is generally included in the model, by a stepwise procedure. For biomass growth the inclusion in the black box is needed because the newly formed biomass will participate in the conversion processes. At a defined t value these accumulations for a time dt are calculated from the production rates. Then these values are added to the mass present in the model at $t = t$, to give the mass at $t = t + dt$.
- Substrates can vary from fermentation to fermentation. In Fig. 2.1 only the C substrate is given with a variable composition. The N, P and S substrates are given with a fixed composition, to prevent the equations to be derived from becoming too complicated. If a substrate different from those given here is used, the equations can easily be set up again, following the lines given in this chapter.
- To determine the elemental balances the elemental composition of all flows, i.e., production rates, has to be known. For biomass this is complicated. However, usually biomass composition is rather constant. It has been determined experimentally (reviewed by Roels, 1983) that for most applications the composition given in Fig. 2.1 can be used. Normalized to C, basis it corresponds to a molar mass of 24.4 g.

By application of Eq. (2.1b) the elemental balances are made by careful addition of the contribution of all production rates for each element. For example, for carbon the production rate of 1 mol of C substrate involves α atoms of carbon, that of biomass involves 1 atom and that of CO_2 also involves 1 atom. In the other production rates no carbon is involved. In this way Eq. (2.2a) is formed. In the same way Eqs. (2.2b-2.2f) are obtained as the balance equations for the other elements. These equations are derived for use when accumulation is absent and $r_p = 0$.

Eq. (2.2) shows the balances for the elements given in the first column, derived from the production rates of the molecules given in the upper row:

	$\text{CH}_{1.8}\text{O}_{0.5}..$	$\text{C}_{\alpha}\text{H}_{\beta}\text{O}_{\gamma}$	NH_3	O_2	CO_2	H_2O	H_2SO_4	H_3PO_4	
Carbon	$1r_x$		$+\alpha r_s$		$+1r_c$				$= 0$
Hydrogen	$1.8r_x$		$+\beta r_s$	$+3r_n$		$+2r_w$	$+2r_{su}$	$+3r_{ph}$	$= 0$
Oxygen	$0.5r_x$		$+\gamma r_s$		$+2r_o$	$+2r_c$	$+1r_w$	$+4r_{su}$	$+4r_{ph} = 0$
Nitrogen	$0.16r_x$			$+1r_n$					$= 0$
Sulfur	$0.0045r_x$						$+1r_{su}$		$= 0$
Phosphorus	$0.0055r_x$							$+1r_{ph}$	$= 0$

It can also be written in matrix notation. With Φ as the matrix containing the production rate row

$$\Phi = (r_x \ r_s \ r_n \ r_o \ r_c \ r_w \ r_{su} \ r_{ph}) \quad (\text{mol s}^{-1}) \quad 2.3$$

and E as the matrix for the elemental flow columns

$$E = \begin{pmatrix} 1 & 1.8 & 0.5 & 0.16 & 0.0045 & 0.0055 \\ \alpha & \beta & \gamma & 0 & 0 & 0 \\ 0 & 3 & 0 & 1 & 0 & 0 \\ 0 & 0 & 2 & 0 & 0 & 0 \\ 1 & 0 & 2 & 0 & 0 & 0 \\ 0 & 2 & 1 & 0 & 0 & 0 \\ 0 & 2 & 4 & 0 & 1 & 0 \\ 0 & 3 & 4 & 0 & 0 & 1 \end{pmatrix} \quad (-) \quad 2.4$$

The balances become

$$\Phi \cdot E = 0 \quad (\text{mol s}^{-1}) \quad 2.5$$

This matrix notation can be very useful for computer calculations, particularly when substrates of different composition have to be included.

2.2.2 The elemental balances

The 6 balance equations given above contain 8 variables; thus all rates can be written as a function of 2 of the other rates. When we are mainly interested in biomass growth and if carbon is the main substrate, r_x and r_s are chosen as the parameters. The equations can then be rewritten as:

$$r_c = -1 r_x - \alpha r_s \quad (\text{mol s}^{-1}) \quad 2.6a$$

$$r_o = +1.094 r_x + (\alpha + \beta/4 - \gamma/2) r_s \quad (\text{mol s}^{-1}) \quad 2.6b$$

$$r_w = -0.647 r_x + (-\beta/2) r_s \quad (\text{mol s}^{-1}) \quad 2.6c$$

$$r_n = -0.16 r_x \quad (\text{mol s}^{-1}) \quad 2.6d$$

$$r_{su} = -0.0045 r_x \quad (\text{mol s}^{-1}) \quad 2.6e$$

$$r_{ph} = -0.0055 r_x \quad (\text{mol s}^{-1}) \quad 2.6f$$

These equations are derived without any knowledge about the reactions that take place in the reactor.

Without further knowledge about these reactions it is not possible to simplify these relations further. Biochemical reactions are extremely complicated and modeling of the complete reaction scheme is impossible. However, only knowledge about the relation between the rates given in Eq. (2.6) is needed. In Chapter 3 it will be shown that generally the substrate consumption rate shows a linear relation with the biomass production rate and the biomass M_x (mol):

$$-r_s = \frac{r_x}{Y_{xs}} + m_s M_x \quad (\text{mol s}^{-1}) \quad 2.7$$

The yield value Y_{xs} , (-) and the maintenance coefficient m_s , (mol substrate per mol biomass per second) both appear to be nearly constant if conditions do not change too drastically. Eq. (2.7) shows that r_x and r_s cannot be chosen independently and after that be introduced in Eq. (2.6). They are related to each other by the biomass present, the yield value and the maintenance coefficient. The first term on the right-hand side of Eq. (2.7) gives the amount of substrate needed for growth and the second term the

amount needed for maintenance. At a given substrate flow rate, the maintenance requirements always have to be fulfilled and the amount of substrate given by the second term is used for this process. Then the growth rate is given by the amount of substrate that remains after subtracting the maintenance requirements. By introducing the linear growth equation, our black box model is transformed into a gray box. The equations then can be given as a function of a single rate value and the biomass. The last one can be regarded as a starting value at time zero. Eq. (2.6) gives, when r_s is chosen as the single variable:

$$r_x = -Y_{xs} r_s - m_s Y_{xs} M_x \text{ (mol s}^{-1}\text{)} \quad 2.8a$$

$$r_c = (-\alpha + Y_{xs}) r_s + m_s Y_{xs} M_x \text{ (mol s}^{-1}\text{)} \quad 2.8b$$

$$r_o = (\alpha + \beta/4 - \gamma/2 - 1.094 Y_{xs}) r_s - 1.094 m_s Y_{xs} M_x \text{ (mol s}^{-1}\text{)} \quad 2.8c$$

$$r_w = (-\beta/2 + 0.647 Y_{xs}) r_s + 0.647 m_s Y_{xs} M_x \text{ (mol s}^{-1}\text{)} \quad 2.8d$$

$$r_n = 0.16 Y_{xs} r_s + 0.16 m_s Y_{xs} M_x \text{ (mol s}^{-1}\text{)} \quad 2.8e$$

$$r_{su} = 0.0045 Y_{xs} r_s + 0.0045 m_s Y_{xs} M_x \text{ (mol s}^{-1}\text{)} \quad 2.8f$$

$$r_{ph} = 0.0055 Y_{xs} r_s + 0.0055 m_s Y_{xs} M_x \text{ (mol s}^{-1}\text{)} \quad 2.8g$$

Some remarks are appropriate here:

- Eq. (2.8) is the generally valid general balance equation [Eq. (2.6)] combined with a model for substrate consumption [Eq. (2.7)] and therefore not anymore generally valid.
- r_s is used here as a parameter because in continuous culture and fed batch this rate can be used as a control variable. Of course, other parameters can be chosen like r_o if oxygen is the limiting substrate or r_x if the growth rate needs to be controlled, with r_x related to the specific growth rate μ (s^{-1}) by

$$r_x = \mu M_x \text{ (mol s}^{-1}\text{)} \quad 2.9$$

- As parameter usually the rate is chosen that can be controlled in the process or the rate that has to follow a predefined pattern during the fermentation.
- Some insight can be gained by qualitative interpretation of the equations. Eq. (2.8a) shows that the growth rate becomes zero when the substrate feed rate equals the maintenance requirements. Eq. (2.8c) gives insight into the oxygen requirements depending on growth. The equation shows that oxygen is required at any r_s value because both terms on

the right-hand side have a negative value (r_s has a negative value). The last part on the right-hand side of the equation is the maintenance-related oxygen consumption. At a given r_H , maintenance always will lead to an extra oxygen consumption because both terms are negative.

- For nitrogen, sulfate and phosphorus both a substrate and maintenance term appear. However, they are of opposite sign when the actual values are introduced. The substrate flow rates define the maximum rates for N, S and P when all substrate would be used for growth. Maintenance diminishes the amount of substrate available for growth and therefore the rate of N, S and P because they are needed only for cell growth. By combining Eqs. (2.8e-f) with Eq. (2.8a) it can be seen that at zero growth the rates for N, S and P indeed become zero.
- To solve the seven Eqs. (2.8) with the nine unknown parameters, two parameter values have to be known. Usually this will include the starting value of the amount of biomass at time zero. The other parameter can be a control variable like one of the substrate rate patterns or the growth rate pattern. The way to use the equations is shown in Examples 2.1 and 2.2.

2.3 The heat-balance equations

A balance can also be set up for the free enthalpies of the flows entering and leaving the system. The difference between these quantities is the heat production r_H (W) of the system. An extensive discussion is presented by Roels (1983). Here we will only discuss the main features.

Enthalpy has to be defined relative to a reference level. Usually enthalpy of combustion to CO₂, (liquid) H₂O and N₂ is chosen because these compounds are not transformed further by the microorganisms. With ΔH (W) defined as the free enthalpy of combustion of component i , the heat balance reads

$$r_s \Delta H_s + r_x \Delta H_x + r_n \Delta H_n + r_p \Delta H_p + r_H = 0 \quad (W) \quad 2.10$$

Phosphorus and sulfate have been left out of the equation. Their contribution is less than 1%. This balance can be solved for each specific case.

For aerobic fermentations it can be shown that there is a simpler way to calculate heat production values. Roels (1983) and other authors have shown that for aerobic production the heat production can be related to the oxygen consumption, because the consumption of oxygen delivers 460×10^3 J mol⁻¹, within very reasonable margins.

$$r_H = -460 \times 10^3 r_o \quad (\text{aerobic}) \quad (W) \quad 2.11$$

This equation is rather accurate for a wide range of conditions, also for most fermentations in which a product is made. Examples 2.3 and 2.4 show how heat production values can be calculated.

For anaerobic conditions such a general rule cannot be derived. Here the enthalpy difference between product and substrate is the main determining factor. For engineering purposes it is preferred in anaerobic fermentations to relate the heat production to the C-substrate consumption rate. This is worked out in Example 2.4.

2.4 The total mass balance

For a commercial fermentation, particularly when executed as a fed batch, the total weight balance of the system is important. This can be set up by adding all feed rates. The water that is usually part of the substrate flows also should be added, as well as the vapor in the outflowing air. The balance differs from the balance given in the preceding chapters because it is a balance for feed rates, not for production rates. Also, the system boundary is now the fermenter instead of the microorganisms. Example 2.5 shows such a balance.

2.5 Conclusions

The balances can be set up for each fermentation. They provide, when combined with the kinetics, the data needed for engineering purposes. They also are a useful tool in that they give the data for the different feed streams. Also, the heat production and the weight development of the fermenter can be calculated.

2.6 Examples

Example 2.1 The effects of carbon and oxygen limitation

Usually the mass of inoculation, $M_x(0)$, in a fermenter has a low value. Thus in the first period of the fermentation the growth is limited by the maximum growth rate of the microorganism. This is called the exponential growth phase. Exponential growth automatically leads to a limitation of one of the substrates after a period of time. Here we will simulate the examples of carbon and oxygen limitation.

- Carbon limitation

Assume that the carbon feed rate is limited by the value $r_{s,max}$. For the exponential growth phase where the carbon is not yet limiting the following calculation can be made.

After rewriting Eq. (2.9) into

$$r_x = \frac{dM_x}{dt} = \mu_{max} M_x \quad (\text{mol s}^{-1}) \quad 2.12$$

this can be solved as

$$M_x = M_x(0) e^{\mu_{max} t} \quad (\text{mol}) \quad 2.13$$

Using Eq. (2.7) leads to the substrate consumption rate:

$$r_s = -\left(\frac{\mu_{max}}{Y_{xs}} + m_s\right) M_x(0) e^{\mu_{max} t} \quad (\text{mol s}^{-1}) \quad 2.14$$

Eqs. (2.13) and (2.14) can be used to calculate the other rates from Eqs. (2.8b-2.8g).

At time $t = t'$, at the value of M'_x , r_s just will reach the value $r_{s,max}$. For $t \geq t'$ we then deal with limitation in carbon substrate feeding rate, i.e.,

$$r_s = r_{s,max} \quad (\text{mol s}^{-1}) \quad 2.15$$

For $t \geq t'$ it can also be derived by introduction of the first part of Eq. (2.12) into Eq. (2.8a) and followed by integration

$$M_x = \left(M'_x + \frac{r_{s,max}}{m_s}\right) e^{Y_{xs} m_s (t' - t)} + \frac{-r_{s,max}}{m_s} \quad (\text{mol}) \quad 2.16$$

Eqs. (2.13) and (2.16) can be used to calculate all the rates at all times, as is illustrated in Fig. 2.2, which was generated using the following data:

Fermenter volume 100 m³

C substrate C₁H₂O₁

$r_{s, \text{max}}$	= -1.85 mol s ⁻¹ (= -2 kg glucose m ⁻³ h ⁻¹)
μ_{max}	= 1.4×10^{-4} s ⁻¹ (= 0.5 h ⁻¹)
Y_{xs}	= 0.67 mol biomass (mol C ₁ H ₂ O ₁) ⁻¹ (= 0.55 kg kg ⁻¹)
m_s	= 4.6×10^{-6} mol C ₁ H ₂ O ₁ (mol biomass) ⁻¹ s ⁻¹ (= 0.02 kg kg ⁻¹ h ⁻¹)
$M_x(0)$	= 4000 mol (= 1 kg m ⁻³ , with the mol mass of biomass = 24.4 g)

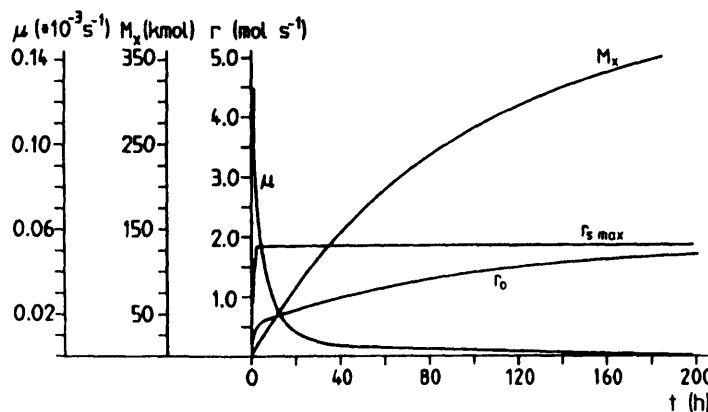
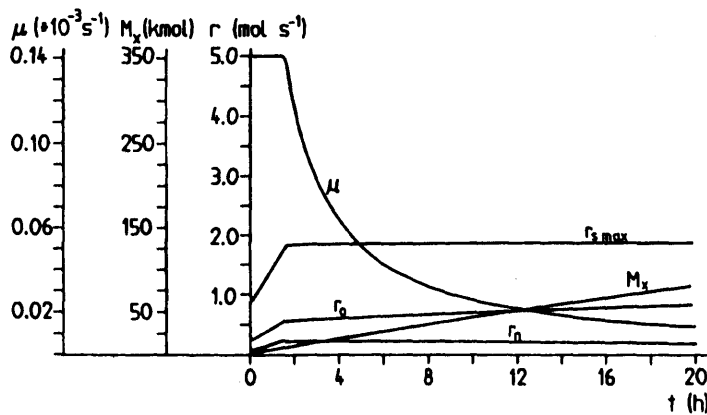


Fig. 2.2 Simulations for CH₂O limitation.

Fig. 2.2 shows an exponential growth phase up to $t = 1.5$ h. For $t > 1.5$ h, r_s limits the growth. The further increasing biomass leads to an increase of the relative part of the substrate that is used for maintenance. Because for a given amount of C substrate, maintenance consumes more oxygen than growth, the value of r_o slowly increases in time. Maintenance does not require any nitrogen, and therefore, r_n slowly decreases in time at $t > t'$. At maximum growth, maintenance requirements can be neglected.

$$\frac{\mu}{Y_{xs}} \gg m_s \quad (\text{s}^{-1}) \quad 2.17$$

as can be seen from combining Eq. (2.7) and Eq. (2.9) into

$$-r_s = \frac{\mu}{Y_{xs}} M_x + m_s M_x = \left(\frac{\mu}{Y_{xs}} + m_s \right) M_x \quad (\text{mol s}^{-1}) \quad 2.18$$

With the data used this means for this example that maintenance can be neglected at $\mu \gg 0.01 \text{ h}^{-1}$.

- Oxygen limitation

The equations can be derived in the same way as was done for the case of carbon limitation. The resulting simulations are given in Fig. 2.3, using as additional data: $r_{o,max} = -1.4 \text{ mol s}^{-1}$ ($OUR = 50 \text{ mol m}^{-3} \text{ h}^{-1}$). In the exponential growth phase the phenomena are the same as for the preceding case. When there is oxygen limitation, however, the increase of biomass with time leads to an increasing part of the oxygen being used for maintenance. For maintenance, less carbon source is needed for a given amount of oxygen used than for growth, and therefore, the carbon consumption rate decreases with time. Finally, a value will be reached at which all carbon and oxygen are needed for maintenance. In that case the growth becomes zero.

Example 2.2 The influence of the degree of oxidation

The degree to which the substrate is oxidized before consumption is important when oxygen limitation occurs. Fig. 2.4 presents simulations for $C_1H_2O_1$, C_1H_4 and $C_1H_4O_1$ using the same data as given in Example 2.1. Fig. 2.4 shows the tremendous effect of the oxidation state of the substrate. The differences in the biomass that can be produced can differ by more than a factor of 2.

Example 2.3 The heat production

The heat production in an aerobic fermentation is calculated for the case of r_s limitation presented in Example 2.1. Both Eqs. (2.10) and (2.11) are

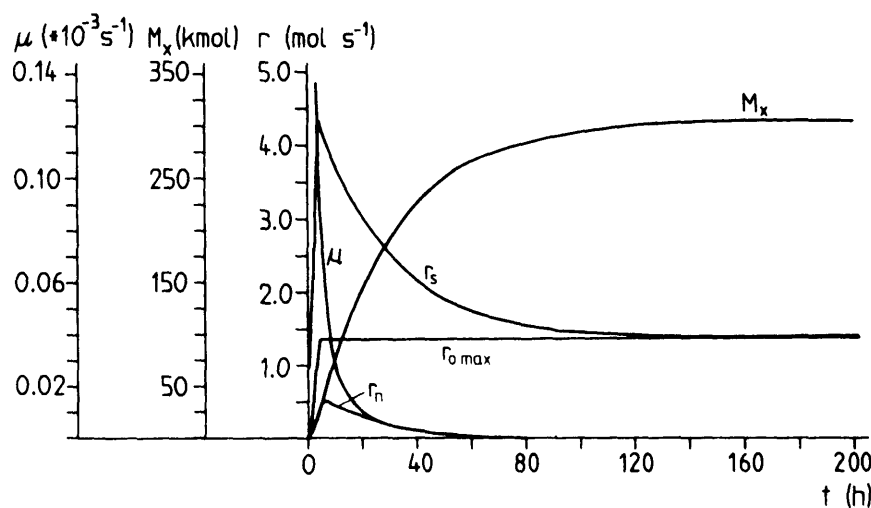
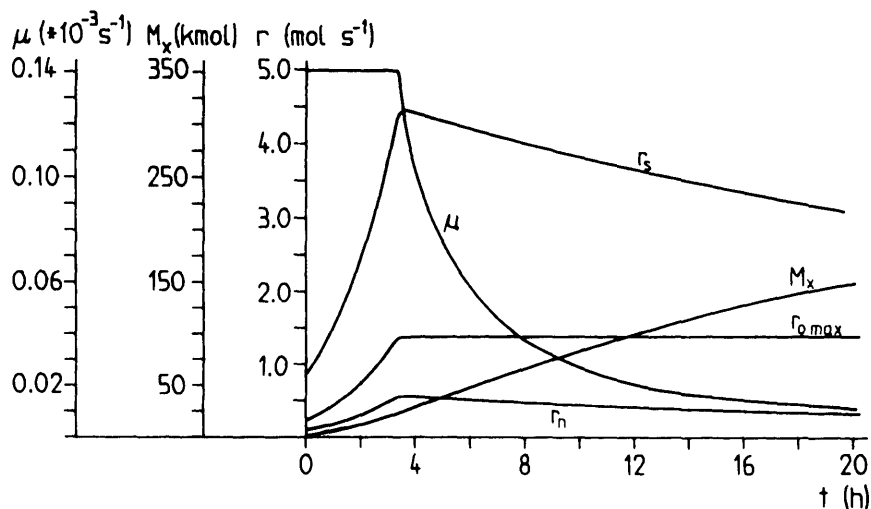


Fig. 2.3 Simulations for oxygen limitation.

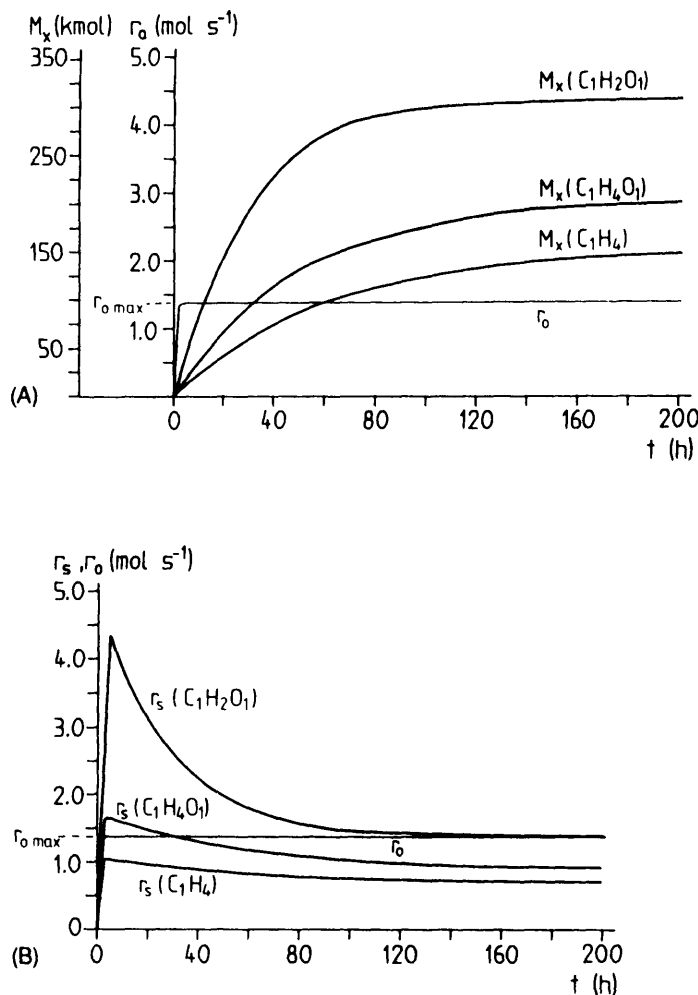


Fig. 2.4 The influence of the substrate degree of oxidation.

used. The enthalpy of combustion data is taken from Roels and is based on gaseous CO₂ and N₂ and liquid H₂O.

Data used: Same as in Example 2.1

$$\Delta H_s = 479 \times 10^3 \text{ J (mol } C_1H_2O_1)^{-1}$$

$$\Delta H_x = 541 \times 10^3 \text{ J (mol } C_1H_{1.8}O_{0.5}N_{0.16})^{-1}$$

$$\Delta H_n = 329 \times 10^3 \text{ J (mol } N_1H_3)^{-1}$$

No product formation

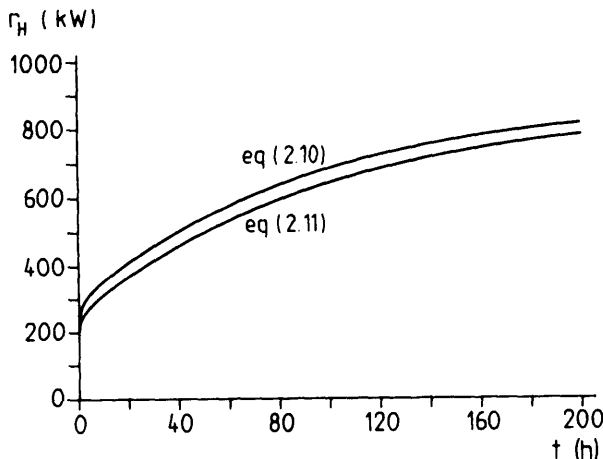


Fig. 2.5 The calculated heat production values.

The results given in Fig. 2.5 show that Eqs. (2.10) and (2.11) both predict rather similar heat production values. Small deviations always occur, because ΔH is dependent on a large number of parameters, such as molarity, pH and temperature. In Fig. 2.2 it can be seen that r_o increases with fermentation time. Eq. (2.11) then predicts and Fig. 2.5 confirms that this results in an increase of the heat production. We have already stated that at constant r , this is caused by the decrease in growth rate during fermentation. When less oxidized substrates like CH_4 are used, the heat production will be considerably higher than for CH_2O because the oxygen consumption is considerably higher.

Example 2.4 The heat production of aerobic and anaerobic fermentations

The heat production related to substrate consumption rate for aerobic and anaerobic fermentations is calculated in this example.

- Aerobic

For an aerobic fermentation without product formation Eq. (2.10) together with the ΔH data of Example 2.3 leads to:

$$479 \times 10^3 r_s + 541 \times 10^3 r_x + 329 \times 10^3 r_n = -r_H \quad (\text{W}) \quad 2.19$$

With Eqs. (2.8a) and (2.8e) this can be rewritten into

$$-r_H = 479 \times 10^3 r_s + 488 \times 10^3 (-Y_{xs} r_s - m_s Y_{xs} M_x) \quad (\text{W}) \quad 2.20$$

This equation will be discussed for two cases:

$\mu \rightarrow 0$, or maintenance is the main source for energy consumption. In that case Eq. (2.20) can be rewritten with Eq. (2.7) into

$$-r_H = 479 \times 10^3 r_s \quad (\text{aerobic, } \mu = 0) \quad (\text{W}) \quad 2.21$$

In case of maintenance all substrate is completely oxidized and, with CH_2O used in this example, 1 mol of substrate consumes 1 mol of oxygen. The value found here should equal that of Eq. (2.11). Small deviations can occur, as shown in Fig. 2.5.

$\mu \gg 0$. Here it is assumed that maintenance can be neglected. Eq. (2.19) now can be rewritten with Eq. (2.7) and $Y_{xs} = 0.67$ into

$$-r_H = 156 \times 10^3 r_s \quad (\text{aerobic, } \mu \gg 0) \quad (\text{W}) \quad 2.22$$

Comparing Eqs. (2.21) and (2.22) shows that heat production related to the substrate consumption rate is much smaller for cell growth than for maintenance. This is because for cell growth less oxygen is required. Eq. (2.22) gives the minimum amount of heat that can be produced in an aerobic fermentation per mol substrate CH_2O .

- Anaerobic

For anaerobic processes like the fermentation of glucose to ethanol the product formation is related to cell growth and maintenance. No separate term for maintenance occurs. The balance reads:

$$-r_H = r_p \Delta H_p + r_s \Delta H_s + r_x \Delta H_x + r_n \Delta H_n \quad (\text{W}) \quad 2.23$$

Here we will work out the example in which biomass growth rate is zero, for ethanol production:

Data used: $C_1H_2O_1 : \Delta H_s = 479 \times 10^3 \text{ J mol}^{-1}$
 $C_1H_3O_{0.5} : \Delta H_p = 660 \times 10^3 \text{ J mol}^{-1}$
 $C_1H_2O_1 \rightarrow 0.67 C_1H_3O_{0.5} + 0.33 CO_2$ thus $r_p = -0.67 r_s$

Eq. (2.23) then gives

$$-r_H = 39 \times 10^3 r_s \quad (\text{anaerobic, } \mu = 0, \text{ ethanol}) \quad (W) \quad 2.24$$

This value is considerably lower than for the aerobic fermentation. This is logical because the substrate has not been oxidized by far as much as for the aerobic fermentation. Roels (1983) gives semi-empirical data for the ethanol fermentation of $11.5 \times 10^3 \text{ J (mol } C_1H_2O_1)^{-1}$. In the balance the value of 39×10^3 is calculated from the difference between two large numbers. It has already been stated that these numbers can vary depending on the conditions. Therefore, this type of difference can occur.

Example 2.5 The total mass balance

The weight balance is the most interesting for a fed-batch system. The feed rates R_f (kg s^{-1}) that leave and enter the system will be considered for the case that none of the substrates is accumulated in the fermenter:

- The substrate feed rate R_f (kg s^{-1}). If the weight fraction of the substrate in the substrate feed is given by f_s (-), then R_f is given by

$$R_f = -10^{-3} r_s M W_s f_s^{-1} \quad (\text{kg s}^{-1}) \quad 2.25$$

in which $M W_s$ is the molecular weight of the substrate in g mol^{-1} . The negative sign appears because R_f is defined as a feed rate, i.e., the rate that enters the vessel, while r_s is defined as a production rate. f_s appears because usually each feed is diluted with water.

- The nitrogen, sulfuric acid and phosphorus acid feed rates, R_n , R_{su} and R_{ph} , respectively. They are given by

$$R_n = -10^{-3} r_n M W_n f_n^{-1} \quad (\text{kg s}^{-1}) \quad 2.26$$

$$R_{su} = -10^{-3} r_{su} M W_{su} f_{su}^{-1} \quad (\text{kg s}^{-1}) \quad 2.27$$

$$R_{ph} = -10^{-3} r_{ph} M W_{ph} f_{ph}^{-1} \quad (\text{kg s}^{-1}) \quad 2.28$$

- The oxygen feed rate R_o is defined by the difference between the weight of oxygen that enters and leaves the fermenter, or

$$R_o = -10^{-3} r_o M W_o \quad (\text{kg s}^{-1}) \quad 2.29$$

- The carbon feed rate R_c is defined as the amount of carbon dioxide that leaves the vessel. It is assumed that the carbon dioxide entering the vessel can be neglected. It is further assumed that carbon dioxide is not accumulated in the fermenter. R_c can then be written as

$$R_c = -10^{-3} r_c M W_c \quad (\text{kg s}^{-1}) \quad 2.30$$

- The water feed rate R_w is defined as the difference between the water vapor weight entering the fermenter in the air flow and the amount of water vapor weight leaving the fermenter with the air flow at a top pressure p_t . The air flow rate F_g ($\text{m}^3 \text{s}^{-1}$) is the value normalized to atmospheric conditions p_n .

$$R_w = -F_g \left(\frac{p_n}{p_t} \rho_{vo} - \rho_{vi} \right) \quad (\text{kg s}^{-1}) \quad 2.31$$

In which

$$\rho_{vi} = \text{vapor concentration of the incoming air at normalized conditions} \quad (\text{kg m}^{-3})$$

$$\rho_{vo} = \text{vapor concentration of the (fully saturated) air above the broth at the temperature and pressure conditions in the top of the fermenter} \quad (\text{kg m}^{-3})$$

- Contributions due to sampling, etc., are neglected. The balance for the weight of the fermenter contents G now becomes

$$\frac{dG}{dt} = R_s + R_n + R_{su} + R_{ph} + R_o + R_c + R_w \quad (\text{kg s}^{-1}) \quad 2.32$$

- The weight of a fed batch at a time t , when $G(0)$ is the weight at $t = 0$, thus becomes

$$G = G(0) + \int_0^t dG \quad (\text{kg}) \quad 2.33$$

All the equations together then yield

$$G = G(0) + 10^{-3} \int_0^t \left[-r_s MW_s f_s^{-1} - r_{su} MW_{su} f_{su}^{-1} - r_n MW_n f_n^{-1} - r_{ph} MW_{ph} f_{ph}^{-1} - r_o MW_o - r_c MW_c - 10^3 F_g \left(\frac{P_n}{P_t} \rho_{vo} - \rho_{vl} \right) \right] dt \quad (\text{kg}) \quad 2.34$$

Here we will show simulations of the value of G for a fed-batch fermentation as a function of time for three values of f_s . The data used are the same as in Example 2.1 for r , limitation with added values of:

$$\begin{aligned} G(0) &= 50000 \text{ kg} \\ f_s &= 1.0 \text{ (case A)}, \quad f_s = 0.5 \text{ (case B)}, \quad f_s = 0.1 \text{ (case C)} \\ f_{ph} &= 0.5 \\ f_{su} &= 0.5 \\ f_n &= 1 \\ F_g &= 0.3 \text{ m}^3 \text{ s}^{-1} \\ \rho_{vl} &= 0.004 \text{ kg m}^{-3} \\ \rho_{vo} &= 0.05 \text{ kg m}^{-3} \\ P_t &= 1 \text{ bar} \end{aligned}$$

Eq. (2.34) can be worked out with the balances as a function of r_s and r_x only:

$$\begin{aligned} G(t) = G(0) + 10^{-3} \int_0^t &\left[r_s (-MW_s f_s^{-1} - MW_o + MW_c) \right. \\ &+ r_x (0.16 MW_n f_n^{-1} + 0.0045 MW_{su} f_{su}^{-1} + 0.0055 MW_{ph} f_{ph}^{-1} \\ &\left. - 1.094 MW_o + 1 MW_c) - 10^3 F_g \left(\frac{P_n}{P_t} \rho_{vo} - \rho_{vl} \right) \right] dt \quad (\text{kg}) \quad 2.35 \end{aligned}$$

This is yet a general equation. Now the values can be introduced, which leads to:

$$G(t) = G(0) + 10^{-3} \int_0^t \left[r_s \left(-\frac{30}{f_s} + 12 \right) + r_x(13.7) - 13.8 \right] dt \quad (\text{kg}) \quad 2.36$$

For the period of 0 up till 1.5 h (5400 s) Eqs. (2.12-2.14) are valid. Introduction of these equations, integration and introduction of the parameter values leads to:

For $t < 1.5$ h (5400 s) the weight equation now reads

$$G(t) = G(0) + 10^{-3} \times \left[\left\{ -6.19 \times 10^3 \left(-\frac{30}{f_s} + 12 \right) + 5.48 \times 10^4 \right\} \times \left(e^{1.4 \times 10^{-4} t} - 1 \right) - 13.8 t \right]$$

Simulations are presented in Fig. 2.6.

For the period of $t > 1.5$ h (5400 s) Eqs. (2.15) and (2.16) can be worked out to

$$G(t) = G(5400) + 10^{-3} \int_{5400}^t \left[-1.85 \left(-\frac{30}{f_s} + 12 \right) + \frac{d \left\{ \left(M'_x + \frac{r_{s, \max}}{m_s} \right) e^{r_{x, m_s} (t' - t)} + \frac{-r_{s, \max}}{m_s} \right\}}{dt} \times 13.7 - 13.8 \right] dt$$

or

$$G(t) = G(5400) + 10^{-3} \times \left[-1.85 \left(-\frac{30}{f_s} + 12 \right) (t - 5400) + \left((M'_x - 4.02 \times 10^5) e^{3.08 \times 10^{-6} (5400 - t)} + 4.02 \times 10^5 \right) \times 13.7 - 13.8 (t - 5400) \right]$$

Simulations are presented in Fig. 2.6.

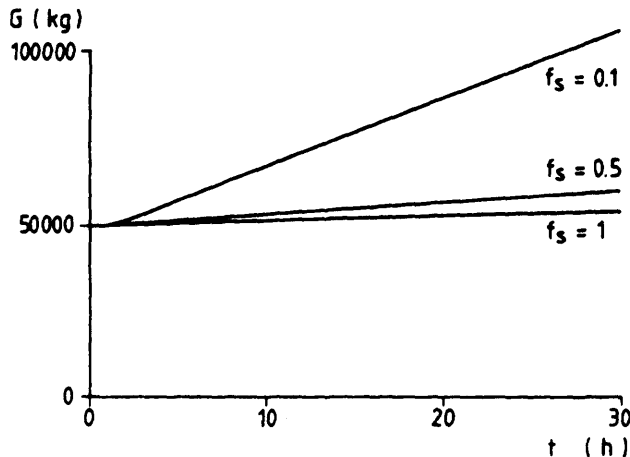


Fig. 2.6 The weight development for $f_s = 1$, 0.5 and 0.1, respectively.

It is seen that the weight of the fermenter increases rather rapidly for $f_s = 0.1$. At $t = 27$ h, a value of 100,000 kg is reached, for $f_s = 0.1$, which is the limit for this reactor. When the different feed flows are analyzed, it appears that the C substrate, carbon dioxide and oxygen are very important. The importance of the substrate feed also indicates that the concentration should be as high as possible. However, even for $f_s = 1$, the weight keeps increasing with time. This is due to the origination of H_2O at the breakdown of the substrate. However, at $f_s = 1$ this effect is limited because of the evaporation of water.

Example 2.6 The balances for the anaerobic ethanol fermentation

The balances can be determined on the basis of the following rates.

Component	C-mol-basis	Rate
Biomass	$CH_{1.8}O_{0.5}$	r_x
Glucose	CH_2O	r_s
Alcohol	$CH_3O_{0.5}$	r_p
Carbon dioxide	CO_2	r_c
Water	H_2O	r_w

The element balances are

$$r_x + r_s + r_p + r_c = 0 \quad 2.37a$$

$$1.8r_x + 2r_s + 3r_p + 2r_w = 0 \quad 2.37b$$

$$0.5r_x + r_s + 0.5r_p + 2r_c + r_w = 0 \quad 2.37c$$

$$\begin{pmatrix} 1 & 1 & 1 & 1 & 0 \\ 1.8 & 2 & 3 & 0 & 2 \\ 0.5 & 1 & 0.5 & 2 & 1 \end{pmatrix} \begin{pmatrix} r_x \\ r_s \\ r_p \\ r_c \\ r_w \end{pmatrix} = 0 \quad 2.38$$

These are 3 equations with 5 unknowns. We will change them in dependencies of r_x and r_s only.

$$\begin{array}{l} 1.8r_x + 2r_s + 3r_p + 2r_w = 0 \\ r_x + 2r_s + r_p + 4r_c + 2r_w = 0 \\ \hline 0.8r_x + 2r_p - 4r_c = 0 \end{array}$$

or:

$$r_c = 0.2r_x + 0.5r_p \quad 2.39$$

Combination with Eq. (2.37a) gives

$$1.2r_x + r_s + 1.5r_p = 0$$

$$r_p = -0.8r_x - 0.67r_s \quad 2.40$$

Eqs. (2.40) and (2.37a) give

$$r_c = -0.2r_x - 0.33r_s \quad 2.41$$

and Eqs. (2.40), (2.41) and (2.37c) give:

$$1.8r_x + 2r_s + 3r_p + 2r_w = 1.8r_x + 2r_s - 2.4r_x - 2r_s + 2r_w = -0.6r_x + 2r_w = 0 \quad 2.42$$

Or summarizing:

$$r_p = -0.8r_x - 0.67r_e \quad 2.40$$

$$r_c = -0.2r_x - 0.33r_e \quad 2.41$$

$$r_w = 0.3r_x \quad 2.42$$

The relation between r_x and r_s is given by Eq. (2.7) for anaerobic fermentation as

$$-r_s = \frac{r_x}{Y_{xs}^a} + m_s^a M_x \quad 2.43$$

with superscript a indicating the anaerobic case.

A combination of the equations describes the biomass dry mass and product production rates in a batch fermentation as:

$$r_x = \frac{dM_x}{dt} = \mu M_x \quad 2.44$$

$$-r_s = -\frac{dM_s}{dt} = \frac{r_x}{Y_{xs}^a} + m_s^a M_x = \left(\frac{\mu}{Y_{xs}^a} + m_s^a \right) M_x \quad 2.45$$

$$r_p = -0.8r_x - 0.67r_e = \left(-0.8\mu + \frac{2\mu}{3Y_{xs}^a} + 0.67m_s^a \right) M_x \quad 2.46$$

$$r_c = -0.2r_x - 0.33r_e = \left(-0.2\mu + \frac{\mu}{3Y_{xs}^a} + 0.33m_s^a \right) M_x \quad 2.47$$

$$r_w = 0.3r_x = 0.3\mu M_x \quad 2.48$$

Similar to that for the substrate consumption [Eq. (2.43)], an equation for the product production can be written as

$$r_p = \frac{r_x}{Y_{xp}^a} + m_p^a M_x \quad 2.49$$

Eq. (2.46) gives for r_p :

$$r_p = \left(-0.8\mu + \frac{2\mu}{3Y_{xs}^a} + 0.67m_s^a \right) M_x = \left(-0.8 + \frac{2}{3Y_{xs}^a} \right) r_x + 0.67m_s^a M_x \quad 2.50$$

Eqs. (2.49) and (2.50) give

$$\left. \begin{aligned} Y_{xp}^a &= \frac{1}{-0.8 + \frac{2}{3Y_{xs}^a}} \\ m_p^a &= 0.67 m_s^a \end{aligned} \right\} \quad \text{For this ethanol fermentation} \quad 2.51$$

Values from Roels (1983) are on the basis of CH_2O and $\text{CH}_3\text{O}_{0.5}$:

$$\begin{aligned} Y_{xs}^a &= 0.14 \text{ mol mol}^{-1} \\ m_s^a &= 0.15 \text{ mol mol}^{-1} \text{ h}^{-1} \\ Y_{xp}^a &= 0.24 \text{ mol mol}^{-1} \\ M_x(0) &= 40 \text{ mol} \\ M_s(0) &= 1000 \text{ mol} \\ \mu_{max} &= 0.5 \text{ h}^{-1} \end{aligned}$$

For this case the growth rate is constant and μ_{max}

$$r_x = \frac{dM_x(t)}{dt} = \mu_{max} M_x(t) \quad 2.52$$

$$\int_0^t \frac{dM_x(t)}{M_x} = \int_0^t \mu_{max} dt \quad 2.53$$

$$\ln\left(\frac{M_x(t)}{M_x(0)}\right) = \mu_{max} t \quad 2.54$$

$$M_x(t) = M_x(0) e^{(\mu_{max} t)} \quad 2.55$$

Eq. (2.45) leads to:

$$-r_s = -\frac{dM_s(t)}{dt} = \left(\frac{\mu_{max}}{Y_{xs}^a} + m_s^a \right) M_x(0) e^{(\mu_{max} t)} \quad 2.56$$

Integration of Eq. (2.56) gives

$$M_s(t) - M_s(0) = -\left(\frac{1}{Y_{xs}^a} + \frac{m_s^a}{\mu_{max}} \right) M_x(0) (e^{(\mu_{max} t)} - 1) \quad 2.57$$

Similarly:

$$M_p(t) - M_p(0) = \left(-0.8 + \frac{2}{3Y_{xs}^a} + \frac{2m_s^a}{3\mu_{max}} \right) M_x(0) (e^{(\mu_{max} t)} - 1) \quad 2.58$$

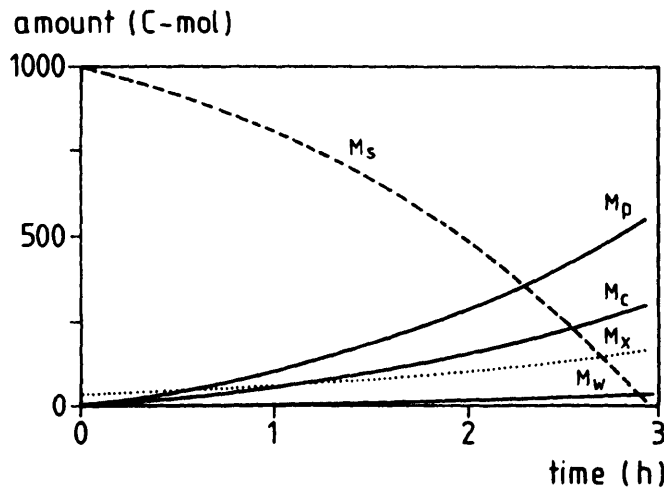


Fig. 2.7 The mass values for the anaerobic alcohol fermentation.

$$M_c(t) - M_c(0) = \left(-0.2 + \frac{1}{3Y_{xc}^a} + \frac{m_i^a}{3\mu_{max}} \right) M_x(0) (e^{(\mu_{max}t)} - 1) \quad 2.59$$

$$M_w(t) - M_w(0) = 0.3 M_x(0) (e^{(\mu_{max}t)} - 1) \quad 2.60$$

Fig. 2.7 shows the mass values for this fermentation.

Reference

Roels J.A. "Energetics and kinetics in biotechnology." Elsevier Biomedical Press, Amsterdam (1983).

3

Yield

3.1 Introduction

The yield Y_{ij} is defined as the ratio between the product (i) production rate r_i and the corresponding substrate (j) consumption rate $-r_j$:

$$Y_{ij} = -\frac{r_i}{r_j} \quad (-) \quad 3.1$$

r is defined as the production rate (mol s^{-1}); thus the consumption rate is $-r$. In consumption the value of r is negative. In this chapter the yield equations for microorganism growth and production and for enzymatic conversion will be dealt with.

3.2 Microorganism growth and production

3.2.1 The linear growth equation

An organism consumes the C substrate for different purposes. In the aerobic case these are product formation and cell growth and maintenance. Schematically this is represented in Fig. 3.1. For each of these flows there exists a relation between the substrate "production" rate and the product production rate that results from this specific flow, as given in Eq. (3.1).

In case of biomass growth the yield is given by Y_{xs} , the moles of biomass, M_x , made from a mol of s , the substrate. In this specific case, the amount of substrate is the substrate that is involved in the biomass formation only. All the other substrate flows are kept outside of this definition. For Fig. 3.1 in this way two yield values can be determined, one for product formation

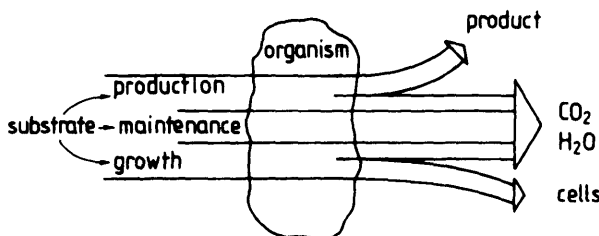


Fig. 3.1 Schematic representation of the substrate flow.

and another one for cell growth. If we include the substrate flow needed for maintenance, the aerobic substrate consumption is then given as

$$-r_s = \frac{r_x}{Y_{xs}} + \frac{r_p}{Y_{ps}} + m_s M_x \quad (\text{mol s}^{-1}) \quad 3.2$$

in which m_s is the maintenance coefficient ($\text{mol substrate mol biomass}^{-1} \text{ s}^{-1}$) and M_x the biomass in the fermenter (mol). This is called the linear substrate consumption equation or the linear growth and production equation. It must be remembered that this equation is the result of a model in which we regard the substrate to be consumed in three separate processes. The strength of the model lies in the fact that it has appeared that under most circumstances Eq. (3.2) is valid. An interesting phenomenon is that the experimentally determined yield and maintenance parameters are nearly independent of growth rate and a number of operating parameters like pH and medium composition, in case these parameters are varied for a limited range. To the model a mechanistic basis can be given. It will be shown that the yield values also can be derived from the biochemical pathways. In a commercial fermentation the total amount of substrate that is needed for product formation is important. This is defined as Y_{ps}^{ov} , the overall yield of product on substrate given as

$$Y_{ps}^{ov} = -\frac{r_p}{r_s} \quad (-) \quad 3.3a$$

and for biomass formation

$$Y_{xs}^{ov} = -\frac{r_x}{r_s} \quad (-) \quad 3.3b$$

3.2.2 The yield values

3.2.2.1 Aerobic systems

The yield value reflects the biochemical reaction mechanism that results in the product or biomass. By analyzing this mechanism it appears that in many cases the yield value can be calculated from the pathway.

An example is the microbial oxidation of ethylene to the epoxide. When the chemical reaction formula is written, we get

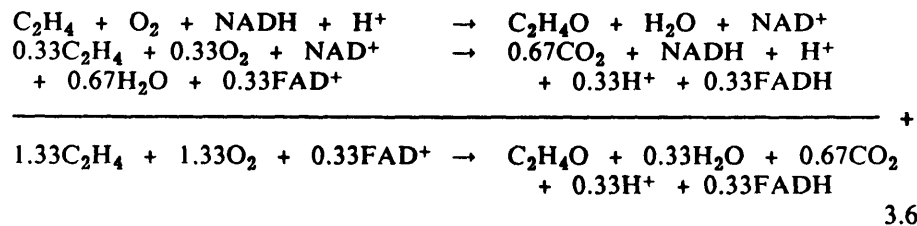


Thus 1 mol of ethylene yields 1 mol of the epoxide, or

$$(Y_{ps}, \text{ chemically}) = 1 \text{ mol mol}^{-1} = 1.57 \text{ kg kg}^{-1} \quad (-) \quad 3.5$$

The yield value on a kg basis is larger than 1 because of the oxygen that is introduced into the molecule.

The biochemical pathway for the epoxide is not as simple as the chemical reaction formula. It is given in Fig. 3.2. This figure shows that a cofactor regeneration is required which is assumed here to originate by partial further oxidation of the formed epoxide. Thus the amount of ethylene consumed to produce 1 mol of the epoxide, is larger than the 1 mol that appears in the chemical reaction formula. By balancing the NADH required for the oxidation of ethylene with the NADH that can be generated by the complete oxidation of the epoxide, the following equations can be written:



This equation, based on the pathway, gives us the reaction mechanism for the epoxide production. The definition of the yield then gives:

$$Y_{ps} = 0.75 \text{ mol mol}^{-1} = 1.18 \text{ kg kg}^{-1} \quad (-) \quad 3.7$$

This example shows that the maximum theoretical yield value can be calculated when the pathway is known.

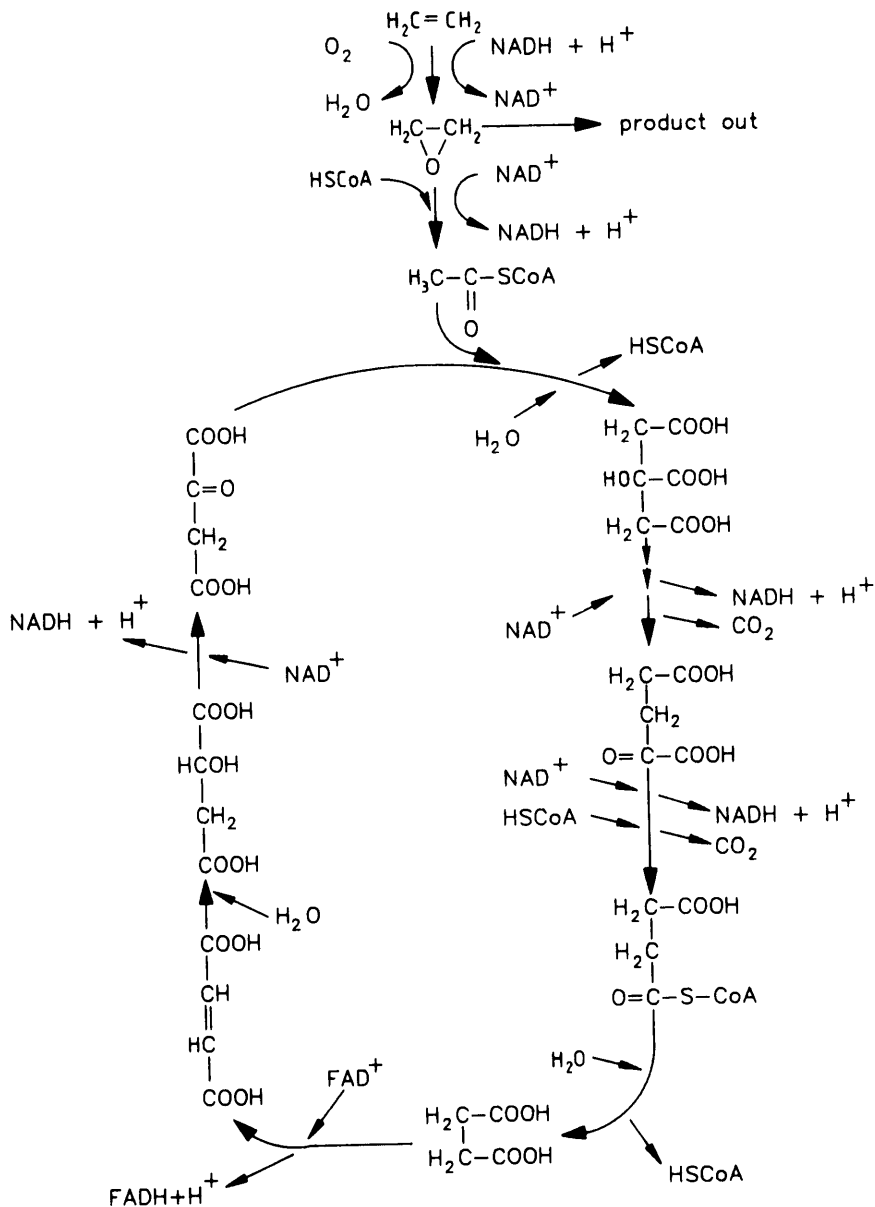


Fig. 3.2 The epoxidation pathway.

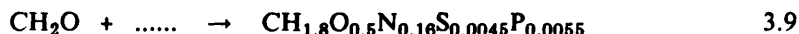
The yield value given in Eq. (3.7) is defined as the yield value on the carbon substrate. Although less usual, other yield values can be defined also. An example is the yield of product on oxygen Y_{po} given as:

$$Y_{po} = - \frac{r_p}{r_o} \quad (-) \quad 3.8$$

For the example of ethylene oxide Eq. (3.6) shows that $Y_{po} = 0.75 \text{ mol mol}^{-1} = 1.03 \text{ kg kg}^{-1}$.

For more complicated product formation routes, the calculation from the pathways becomes more difficult. However, in case of penicillin Cooney and Acevedo (1977) show that even for such a complicated product a yield value can be calculated. They include all the amino acids, etc., needed for penicillin production. For a product like penicillin the calculation is particularly important because the measurement of the yield value is impossible. The reason for this is the relatively small amount of substrate that is used for product formation. Experimental determination by application of Eq. (3.2), with known Y_{xs} , and m , values, then leads to very inaccurate numbers.

A very important yield value is that of biomass production. When the chemical formula is used we get



or

$$(Y_{xs}, \text{ chem}) = 1 \text{ mol mol}^{-1} = 0.81 \text{ kg kg}^{-1} \quad (-) \quad 3.10$$

The pathway is extremely complicated because a cell consists of an immense amount of different products. Therefore, the only thing that can be said is that the value should in any case be < 0.81 . The value can be measured by application of Eq. (3.2) in case of low maintenance requirements ($\mu \gg 0.01 \text{ h}^{-1}$) and absence of, or very low, product requirements. It has been determined experimentally that, in general, for aerobic growth on glucose or similar substrates under normal conditions the yield value is around:

$$Y_{xs} = 0.67 \text{ mol mol}^{-1} = 0.55 \text{ kg kg}^{-1} \quad (-) \quad 3.11$$

This number is indeed somewhat lower than the value based on the chemical formula. A large number of yield values for a range of organisms and a range of substrates is given by Roels (1983).

3.2.2.2 Anaerobic systems

For anaerobic systems calculation of the specific yield values is different. In anaerobic systems the energy involved in the pathways is not provided by the substrate oxidation with O₂ to CO₂ and H₂O but is provided by transformation of the substrate to the product. This means that the substrate is transformed into the product, while feeding the energy metabolism. This results in the absence of a separate product production term in the substrate consumption equation, because this production is already included in the growth and maintenance terms. Thus the substrate consumption equation can be written as

$$-r_s = \frac{1}{Y_{xs}^a} r_x + m_s^a M_x \quad (\text{mol s}^{-1}) \quad 3.12$$

in which the superscript a indicates the anaerobic case. The production rate can be written as

$$r_p = \frac{1}{Y_{xp}^a} r_x + m_p^a M_x \quad (\text{mol s}^{-1}) \quad 3.13$$

It should be noted that a specific yield of biomass on product is introduced here. This is simply a matter of application of the yield definition. The same applies for the product-based maintenance coefficient. Again it must be remembered that this type of equations is based on a model. For Eqs. (3.2) and (3.12) these models can be related to mechanisms in the organism, but for Eq. (3.13) it is more difficult to find the relation with a reaction mechanism. Because all the equations represent only models of the processes that take place, it is not necessary that there will always be a straightforward relation between a model parameter and a reaction mechanism.

3.2.3 The overall yield for microorganisms

3.2.3.1 Aerobic product formation

Generally for a fermentation one is interested in the overall yield value. This is the number that gives the efficiency at which the substrate is converted to the product. For aerobic product formation this reads with application of Eq. (3.2)

$$Y_{ps}^{ov} = -\frac{r_p}{r_s} = \frac{r_p}{\frac{r_x}{Y_{xs}} + \frac{r_p}{Y_{ps}} + m_s M_x} \quad (-) \quad 3.14$$

The growth and production can be expressed with the specific growth rate μ and the specific production rate q_p as

$$r_x = \mu M_x \quad (\text{mol s}^{-1}) \quad 3.15$$

$$r_p = q_p M_x \quad (\text{mol s}^{-1}) \quad 3.16$$

By using Eqs. (3.15) and (3.16), Eq. (3.14) can be rewritten as

$$\frac{Y_{ps}^{ov}}{1 + \frac{\mu Y_{ps}}{q_p Y_{xs}} + \frac{m_s Y_{ps}}{q_p}} \quad (-) \quad 3.17$$

Example 3.1 gives some insight in the relevance of the different parameters of Eq. (3.17).

3.2.3.2 Aerobic biomass production

When there is no product formation, as in the production of a single cell protein, Eq. (3.2) can be simplified to

$$-r_s = \frac{r_x}{Y_{xs}} + m_s M_x \quad (\text{mol s}^{-1}) \quad 3.18$$

Now the overall yield of biomass on substrate is written as

$$Y_{xs}^{ov} = -\frac{r_x}{r_s} = \frac{Y_{xs}}{1 + \frac{m_s Y_{xs}}{\mu}} \quad (-) \quad 3.19$$

Simulations with parameter variations are given in Example 3.2.

3.2.3.3 Anaerobic product formation

The overall yield for anaerobic product formation is defined in the usual way as

$$Y_{ps}^{ova} = -\frac{r_p}{r_s} \quad (-) \quad 3.20$$

With Eqs. (3.12), (3.13) and (3.15) this can be written as

$$Y_{ps}^{ova} = \frac{\frac{\mu}{Y_{xp}^a} + m_p^a}{\frac{\mu}{Y_{xs}^a} + m_s^a} \quad (-) \quad 3.21$$

At zero growth rate all substrate is used for cell energy requirements and therefore it is completely transformed into product. Eq. (3.21) shows that for that case

$$Y_{ps}^{ova} = \frac{m_p^a}{m_s^a} \quad (\mu = 0) \quad (-) \quad 3.22$$

It is convenient to rewrite Eq. (3.21) in such a way that Eq. (3.22) is part of it

$$Y_{ps}^{ova} = \frac{m_p^a}{m_s^a} \frac{\frac{\mu}{Y_{xp}^a m_p^a} + 1}{\frac{\mu}{Y_{xs}^a m_s^a} + 1} \quad (-) \quad 3.23$$

In cases when all substrate goes into product and CO_2 ($\mu = 0$), the stoichiometry of the reaction equation can be used



In that case it can be seen with Eq. (3.23) that

$$Y_{ps}^{ova} = \frac{m_p^a}{m_s^a} = \frac{b}{a} \quad (-) \quad 3.25$$

Thus the maximum yield value for anaerobic product formation equals the value found for the chemical reaction equation. Example 3.3 shows how these equations can be used. This example shows that growth rate has a strong influence on the overall yield. In processes like ethanol formation this yield is the determining factor for the economy of the process. Therefore, processes in which the growth rate is very low or even absent are preferred.

3.2.3.4 Anaerobic biomass production

In the anaerobic case, the production cannot be assumed to be absent as for the aerobic case, because it is needed for biomass production also.

With Eqs. (3.12) and (3.15) it can be derived.

$$Y_{xs}^{ova} = \frac{Y_{xs}^a}{1 + \frac{y_{xs}^a m_s^a}{\mu}} \quad (-) \quad 3.26$$

The relation with the overall yield for production can be seen from Eq. (3.26) combined with Eq. (3.21):

$$Y_{xs}^{ova} = Y_{ps}^{ova} \frac{\mu}{\frac{\mu}{y_{xp}^a} + m_p^a} \quad (-) \quad 3.27$$

In Example 3.4, Fig. 3.10 shows that Y_{xs}^{ova} will generally be much smaller than 1. Comparison with Example 3.2 shows that, in general, the overall yield for growth will be much larger for aerobic systems than for anaerobic systems.

3.3 Enzymatic conversions

The most simple equation for an enzymatic conversion of a substrate S into a product P is given by the equation



Thus the yield of product on substrate becomes

$$Y_{ps} = n \text{ (mol product} \times \text{mol substrate})^{-1}$$

In a large number of cases the value of $n = 1$. In those cases where the reaction stops at zero substrate concentration, the value of Y_{ps} equals the overall yield. However, in case of an equilibrium such as for glucose isomerase the situation becomes more complicated. At equilibrium conditions, indicated by C^* , it is shown in Chapter 4 that an equilibrium constant K can be defined as

$$\frac{C_p^*}{C_s^*} = K \quad (-) \quad 3.29$$

The overall yield (at end of reaction or at equilibrium) is defined as

$$Y_{ps}^{ov} = \frac{\text{total mol of product in the reactor}}{\text{total mol of substrate added to the reactor}} \quad (-) \quad 3.30$$

With $C_s(0)$ = concentration of substrate at time zero and no product present at time zero, it can be derived that

$$Y_{ps}^{ov} = \frac{C_p^*}{C_s(0)} \quad (-) \quad 3.31$$

with

$$Y_{ps} = \frac{C_p^*}{C_s(0) - C_s^*} \quad (-) \quad 3.32$$

This can be rewritten to

$$Y_{ps}^{ov} = \frac{Y_{ps}}{1 + \frac{Y_{ps}}{K}} \quad (-) \quad 3.33$$

Example 3.5 shows applications of this formula.

3.4 Conclusions

The yield concept can be used in models that can be related in many cases to biochemical reaction mechanisms. For aerobic systems it leads to the linear substrate consumption equation. The parameters in this equation can be related to biochemical reaction mechanisms. The overall yield can be calculated from basic microbiological or enzymatic parameters, usually available from literature or small-scale experiments. It gives a clear insight into the efficiency of the transformations. For anaerobic systems the mechanistic background of some of the parameters is less clear. Yet the parameters appear to be constant and the model gives a clear insight into the influence of the operating variables.

3.5 Examples

Example 3.1 The aerobic overall yield of product on substrate

To provide some insight into the relevance of the different parameters of Eq. (3.17) a number of simulations have been made. In each simulation one of the parameters has been varied. The parameter values are chosen in the region where a penicillin fermentation occurs.

Data used (unless taken as parameter to be varied):

$$\begin{aligned}
 Y_p &= 1 \quad \text{kg kg}^{-1} \\
 \mu &= 0.01 \quad \text{h}^{-1} \\
 q_p &= 10^{-2} \quad \text{kg kg}^{-1} \text{ h}^{-1} \\
 Y_x &= 0.55 \quad \text{kg kg}^{-1} \\
 m_s &= 0.025 \quad \text{kg kg}^{-1} \text{ h}^{-1}
 \end{aligned}$$

Remark: The equations are written in the preceding sections on a mol basis. They are dimensionless and can also be used on a kg basis. (Note that in Chapter 2 the balances are derived for the elements. Therefore, these balances cannot be used with parameters on a kg basis, but only on a mol basis).

In Fig. 3.3A-E the overall yield is given. These figures show a number of trends that will be discussed.

- The specific production rate.

For values of $q_p \ll \mu$ as well as $q_p \ll m_s$, the second and third term in the denominator of Eq. (3.17) become $\gg 1$. Therefore, the overall yield becomes proportional to the specific production rate. This is clearly seen in Fig. 3.3A. Only at $q_p > 0.01 \text{ h}^{-1}$ does the influence of q_p start to decrease. The specific production rate therefore is the main important variable that influences the overall yield.

- The specific growth rate.

The substrate that is used for biomass production decreases the overall yield for production. This results in a decrease of the overall yield with an increase of the growth rate. Fig. 3.3B shows this effect. It shows that below $\mu = 0.01 \text{ h}^{-1}$ the effects of substrate loss related to growth can be neglected; 0.01 h^{-1} is also the order of magnitude for which the influence of the q_p value starts to decrease. The second term in the denominator of Eq. (3.17) shows that this can be expected. For larger growth rates, $\mu > 0.1 \text{ h}^{-1}$, the influence of substrate used for growth is rather drastic. Here too much of the substrate is used for growth.

- The maintenance coefficient.

The maintenance coefficient cannot be varied as much as the growth and production rates. Therefore, the simulations are done for only one decade (see Fig. 3.3C). The effect is rather limited with the set of parameters chosen here. This can change in cases where both the growth rate is very low ($\mu < 0.01$) and specific production rate values are low ($q_p \ll m_s$). Then the third term in the denominator of Eq. (3.17) is $\gg 1$ and Y_p'' becomes inversely proportional to the maintenance requirements.

- The yield coefficients.

Both yield coefficients can be varied only over a very limited range of values. Fig. 3.3D and 3.3E show that under those limitations the influ-

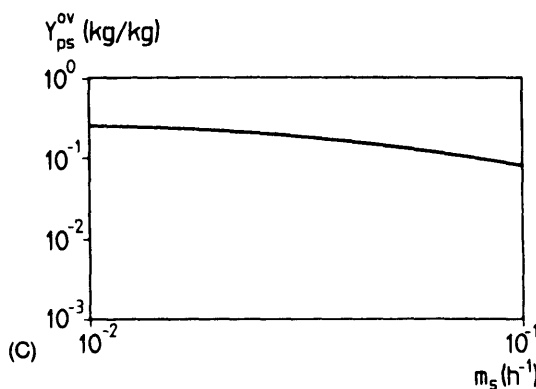
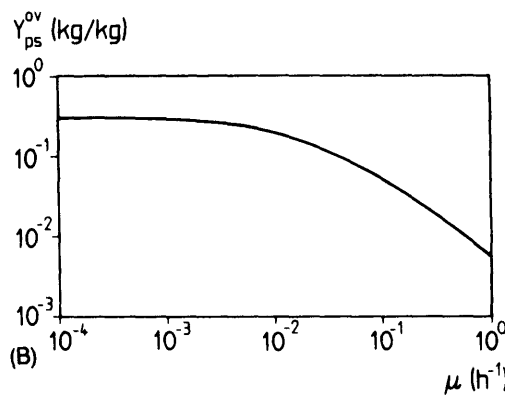
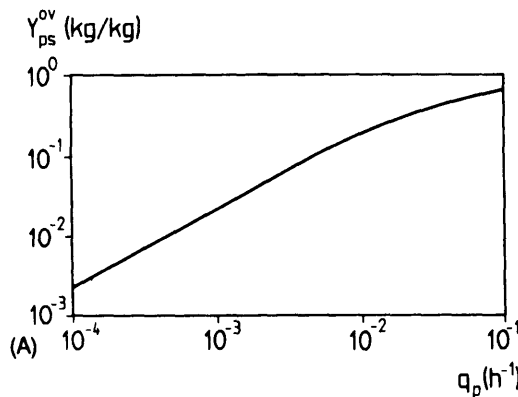


Fig. 3.3A-E Simulations for Y_{ps}^{ov} .

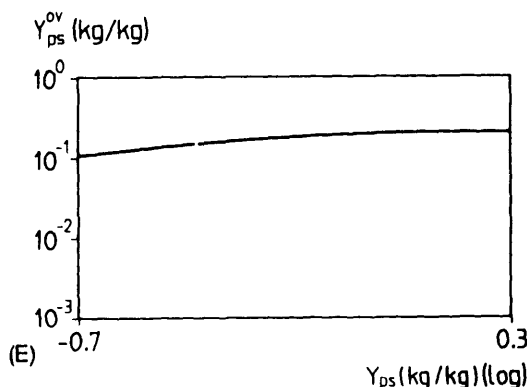
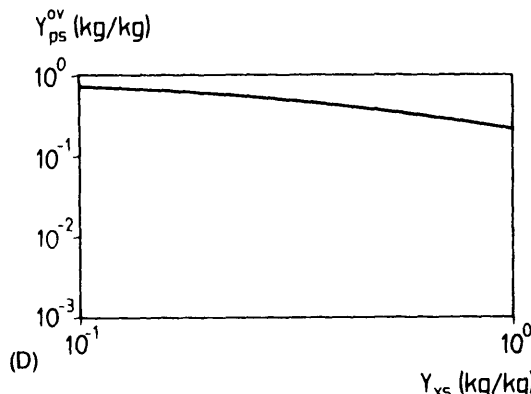


Fig. 3.3A-E (continued)

ence is rather limited. Fig. 3.3E shows also that the difference between the Y_{ps} value and the overall Y_{ps}^{ov} usually is considerable.

Example 3.2 The aerobic overall yield of biomass on substrate

Fig. 3.4 shows simulations of Eq. (3.19) for the overall yield of biomass on substrate. The same set of parameter values as given in Example 3.1 is used. The trends shown in these figures can be understood when realizing what the different substrate flows are meant for. When the growth rate becomes too small ($\mu < m_s$) too much substrate is used for maintenance and the overall yield starts to decrease. If maintenance requirements can be neglected, the overall yield equals the yield Y_{xs} . The maintenance and yield coefficients themselves again can be varied only in a limited range. The influence of these two parameters is therefore limited.

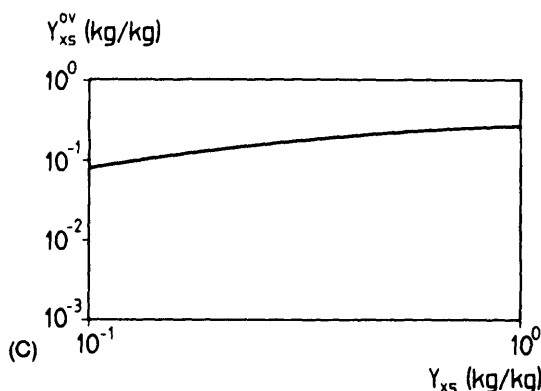
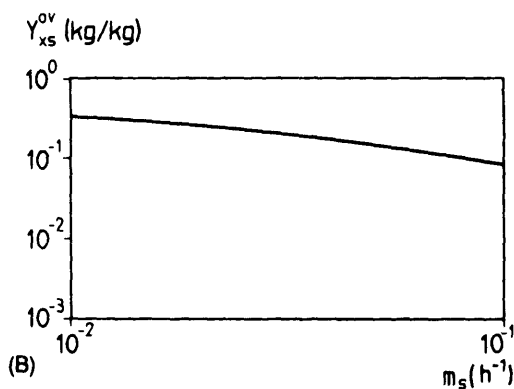
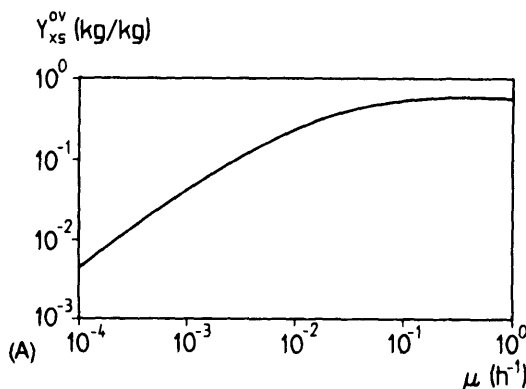
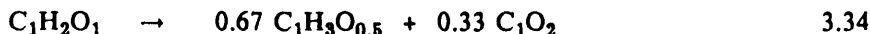


Fig. 3.4A-C Simulations for Y_{xs}^{ov} .

Example 3.3 The anaerobic overall yield of product

The formation of ethanol from glucose with *S. cerevisiae* can be described by the following equations



Roels (1983) gives the following data on a molar basis:

- Low maintenance case

$$-r_s = 7.25 r_x + 0.15 M_x \quad (\text{mol s}^{-1}) \quad 3.35$$

$$r_p = 4.1 r_x + 0.1 M_x \quad (\text{mol s}^{-1}) \quad 3.36$$

- High maintenance case

$$-r_s = 7.25 r_x + 0.9 M_x \quad (\text{mol s}^{-1}) \quad 3.37$$

$$r_p = 4.1 r_x + 0.6 M_x \quad (\text{mol s}^{-1}) \quad 3.38$$

From Eqs. (3.35) to (3.37) it can be calculated, with the dimensions on the molar basis as given in Eq. (3.34):

- Low maintenance

$$\alpha = 1, \quad b = 0.67, \quad Y_{xs}^a = 0.138, \quad m_s^a = 0.15, \quad Y_{xp}^a = 0.24,$$

$$m_p^a = 0.1, \quad b/\alpha = 0.67, \quad m_p^a/m_s^a = 0.67$$

- High maintenance

$$\alpha = 1, \quad b = 0.67, \quad Y_{xs}^a = 0.138, \quad m_s^a = 0.9, \quad Y_{xp}^a = 0.24,$$

$$m_p^a = 0.6, \quad b/\alpha = 0.67, \quad m_p^a/m_s^a = 0.67$$

Simulations for the overall yield are presented in Fig. 3.5, using the data given in this example and substituted in Eq. (3.21).

Example 3.4 The anaerobic overall yield of biomass

Fig. 3.6 shows simulations of Eq. (3.26) with the data used in Example 3.3. The curve of Example 3.2 for the aerobic biomass formation is also given. This figure clearly shows that anaerobic biomass production has a relatively low yield value, as could be expected because product formation is coupled to biomass formation in this case.

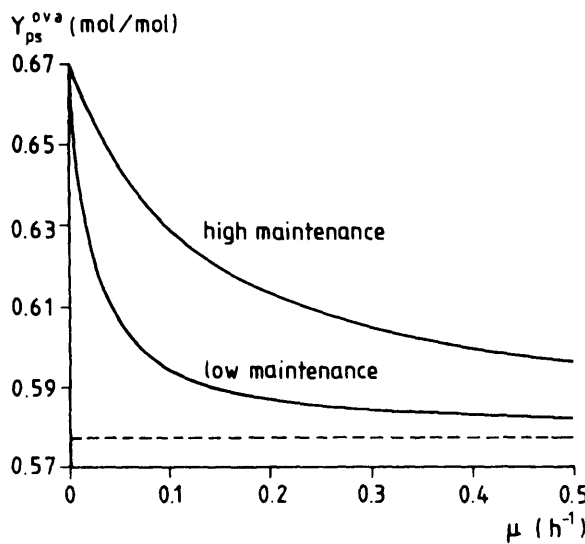


Fig. 3.5 Simulations for Y_{ps}^{ova} .

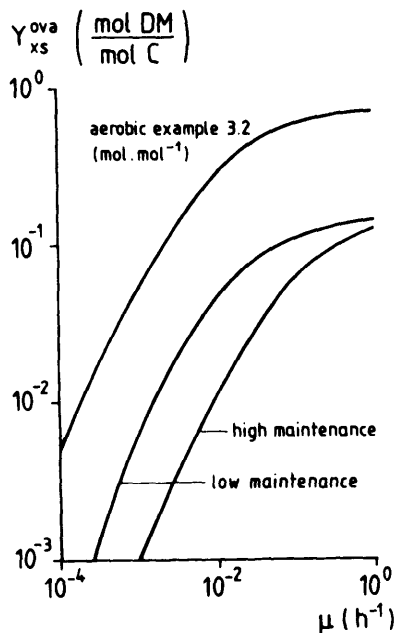


Fig. 3.6 Simulations for Y_{xs}^{ova} .

Example 3.5 The enzymatic overall yield of product

Two examples are given of rather straightforward calculations of the overall yield. An example of a reaction that reaches an equilibrium is the glucose isomerase reaction of glucose to fructose. At equilibrium about 45% of fructose is present. Starting from glucose only, this means that the overall yield is 0.45. This can also be calculated from Eq. (3.33). As 1 mol of glucose is converted into 1 mol of fructose, $Y_{ps} = 1$. At equilibrium conditions, $K = 0.45/0.55 = 0.82$. Eq. (3.33) shows with these parameter values that the overall yield = 0.45. Another example is the production of stereoisomers from a racemic mixture. If, for example, 2 mol of substrate deliver 1 mol of each isomer, then the Y_{ps} , for each of them is 0.5. If the reaction proceeds until the substrate is depleted, $K = \infty$. Then $Y_{ps}^{ov} = 0.5$.

References

Cooney C.L. and Acevedo F. "Theoretical conversion yield for penicillin synthesis." Biotechnol. Bioeng. **19**, 1449 (1977).

Roels J.A. "Energetics and kinetics in biotechnology." Elsevier Biomedical Press, Amsterdam (1983).

4

Kinetics

4.1 Introduction

In this chapter the most-common reaction-rate equations on the level of cell and enzyme will be introduced as well as methods of estimation of the kinetic constants herein. The rate equations are based on the consumption of substrate, and especially in the case of cells, there generally is no stoichiometric relation with product formation. From a mathematic point of view there is no difference between the rate equations for consumption of substrate in conversions by either cells or enzymes. However, because cells can grow and need maintenance energy (see Chapter 3), the eventual models for description of the bioprocess on the level of the bioreactor are quite different. Therefore, cell and enzyme kinetics are treated separately in this chapter.

4.2 Cell kinetics

An extensive description of cell kinetics is given by Pirt (1985) and appropriate parts are presented here. In many respects the bacterial growth process is similar to a chemical reaction in which the components of the medium (the reactants) produce cells in addition to excreted products. This process is catalyzed by the bacterial population (autocatalysis). The chemical reaction rate is determined by the concentration of reactants, but generally the bacterial growth rate remains constant until the medium is almost exhausted of the limiting nutrient. This seeming paradox is explained by the action of enzymes (permeases) which are capable of maintaining constant intracellular concentrations of nutrients over a wide range of external concentrations. Nevertheless, usually at extremely low concentrations of external nutrients the permease enzymes are no longer able to maintain the intracellular concentrations, and the growth rate falls.

The curves relating growth rate to nutrient concentration are typically hyperbolic in form (Fig. 4.1) and can be described by the Monod equation

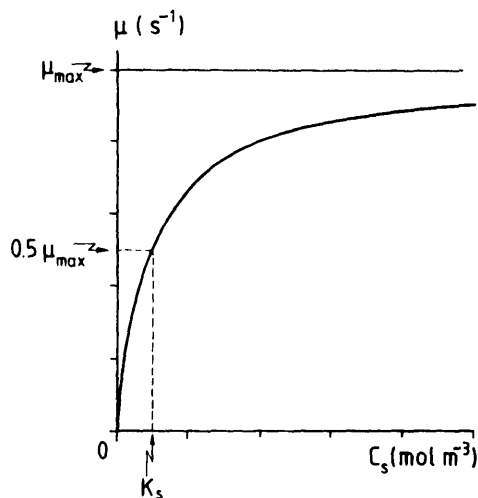


Fig. 4.1 The effect of nutrient concentration on the specific growth rate in case of Monod kinetics.

$$\mu = \mu_{max} \frac{C_s}{K_s + C_s} \quad (\text{s}^{-1}) \quad 4.1$$

where μ is the specific growth rate (s^{-1}) at limiting nutrient concentration C_s (mol m^{-3}), μ_{max} is the growth rate (s^{-1}) at infinite concentration of nutrient and K_s (mol m^{-3}) is a constant analogous to the Michaelis-Menten constant of enzyme kinetics (see Section 4.3), being numerically equal to the substrate concentration supporting a growth rate equal to $0.5 \mu_{max}$. Typical values of K_s and μ_{max} are given in Table 4.1 and 4.2, respectively.

Table 4.1 Typical K_s -values

Organism	Substrate	K_s (mol m^{-3})
<i>E. coli</i>	glucose	3.8×10^{-4}
<i>E. coli</i>	phosphate ions	0.016
<i>Pseudomonas sp.</i>	methanol	0.022
<i>A. niger</i>	glucose	0.028
<i>S. cerevisiae</i>	glucose	0.14

Source: Adapted from Trevan et al. (1987) and references cited therein.

Table 4.2 Typical μ_{max} -values

Organism	μ_{max} (s^{-1})
<i>Beneckeia natriegens</i>	1.178×10^{-3}
<i>Methyloimonas methanolytica</i>	0.147×10^{-3}
<i>Penicillium chrysogenum</i>	0.033×10^{-3}

Source: Adapted from Trevan et al. (1987) and references cited therein.

A cell culture undergoing balanced growth mimics a first-order autocatalytic reaction; i.e., the rate of increase of cells at any particular time is proportional to the number or mass of cells present at that time. The constant of proportionality is the specific growth rate μ . Since we assume the growth rate to be balanced, μ also relates the rate of increase of any given cellular component to the amount of that cellular component, or in mathematical terms

$$\frac{dN_x}{dt} = \mu N_x(t) \quad (s^{-1}) \quad 4.2a$$

$$\frac{dC_x}{dt} = \mu C_x(t) \quad (\text{mol m}^{-3} s^{-1}) \quad 4.2b$$

$$\frac{dC_z}{dt} = \mu C_z(t) \quad (\text{mol m}^{-3} s^{-1}) \quad 4.2c$$

where N_x is the number of cells, C_x the molar concentration of cells (based on the average elemental composition) in the bioreactor (mol m^{-3}), C_z the molar concentration of cellular component Z (mol m^{-3}). All types of other cell kinetics can be used to describe more special cases. We refer to the more specialized literature, e.g., Moser (1985a), for detailed discussions. For engineering purposes Eqs. (4.1) and (4.2) are satisfying for most cases.

4.3 Enzyme kinetics

An extensive discussion is given by Roels (1983) and again appropriate parts are summarized here. The rate of reaction of many enzyme-catalyzed conversions can reasonably well be described by the so-called Michaelis-

Menten equation. This equation was derived theoretically in 1913 by Michaelis and Menten in consequence of the observed kinetics for the conversion of sucrose into glucose and fructose by the enzyme invertase. The equation has the following form

$$r_s^u = -v_{max} \frac{C_s}{K_m + C_s} \quad (\text{mol m}^{-3} \text{s}^{-1}) \quad 4.3$$

where r_s^u is the number of moles of substrate 'produced' per second per unit volume. Because substrate is converted, and r_s^u is always defined as production, the minus sign at the right hand side appears. v_{max} is the number of moles converted per second per unit volume at an infinite substrate concentration ($\text{mol m}^{-3} \text{s}^{-1}$), C_s , the concentration of substrate (mol m^{-3}) and K_m the Michaelis-Menten kinetic constant (mol m^{-3}). As with Monod kinetics this kinetic constant is numerically equal to the substrate concentration at which $r_s^u = 0.5 v_{max}$ (Fig. 4.2).

As enzyme kinetics is actually nothing else than chemical reaction kinetics, treatment along similar lines is obvious. When a conversion of species *A* into species *B* is given an infinite amount of time, thermodynamic equilibrium is reached. The composition of the equilibrium mixture is exclusively determined by the thermodynamic properties of the reactants and the products, in particular the standard free enthalpy. It is independent of the manner in which the reaction is executed. In other words, this means that

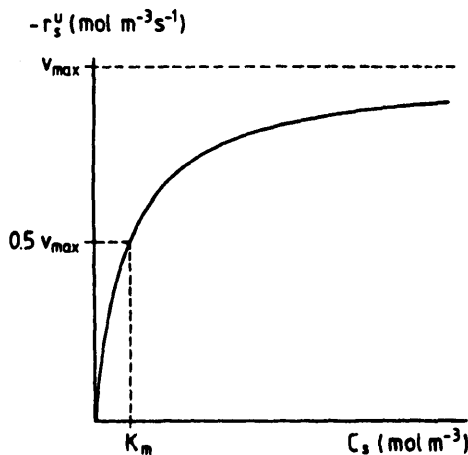
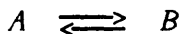


Fig. 4.2 The Michaelis-Menten plot.

the composition of the starting reaction mixture does not influence the equilibrium. It also means that an enzyme in principle catalyzes the reaction in both directions, a principle currently actively studied in the area of biocatalysis in nonaqueous media. The equilibrium constant K of the reaction



is defined as

$$K = \frac{C_B^*}{C_A^*} \quad (-) \quad 4.4$$

in which C_A^* and C_B^* are the equilibrium concentration of A and B , respectively (mol m^{-3}). K is a function of the change in standard free enthalpy ΔG° (J mol^{-1}), which is the difference in standard free enthalpy or thermodynamic potential G° (J mol^{-1}) of A and B shown in Fig. 4.3, and the temperature T :

$$\ln K = -\frac{\Delta G^\circ}{RT} = -\frac{\Delta H^\circ}{RT} + \frac{\Delta S^\circ}{R} \quad (-) \quad 4.5$$

with R the gas constant ($8.31 \text{ J mol}^{-1} \text{ K}^{-1}$), ΔH° the standard enthalpy change or heat of reaction (J mol^{-1}) and ΔS° the standard entropy change ($\text{J mol}^{-1} \text{ K}^{-1}$). The superscript $^\circ$ refers to the situation at unit activity of the pertinent compound(s) at the temperature and pressure under consideration. For enthalpy a definition of the standard enthalpy is not really necessary, as the concentration dependence of the partial molar enthalpies is only of minor importance. In contrast to ΔG° , both ΔH° and ΔS° are not very sensitive to temperature, which implies that generally a linear relationship is found in a plot of $\ln K$ versus $1/T$, though over a limited range of temperatures. Thus at rising temperature K increases in case $\Delta H^\circ > 0$ (endothermic) and decreases if $\Delta H^\circ < 0$ (exothermic). In brief, thermodynamics specify the end situation, not the speed at which this situation is reached.



Fig. 4.3 The free enthalpy of compound A and B .

Description of the rate of reaction, in other words the kinetics, usually occurs by means of the activation energy theory (Fig. 4.4). The activation-energy barrier prevents instantaneous formation of thermodynamic equilibrium.

When the mass action laws are applied to a one-enzyme E , one-substrate S , one-enzyme/substrate-complex ES and one-product P system:



the following equations can be derived, in which $C = C(t)$:

$$\frac{dC_s}{dt} = r_s^u = -k_1 C_e C_s + k_{-1} C_{es} \quad (\text{mol m}^{-3} \text{s}^{-1}) \quad 4.6$$

$$\frac{dC_p}{dt} = r_p^u = -k_2 C_e C_p + k_{-2} C_{es} \quad (\text{mol m}^{-3} \text{s}^{-1}) \quad 4.7$$

$$\begin{aligned} \frac{dC_{es}}{dt} &= k_1 C_e C_s - k_{-1} C_{es} + k_2 C_e C_p - k_{-2} C_{es} \quad (\text{mol m}^{-3} \text{s}^{-1}) \quad 4.8 \\ &= -(r_s^u + r_p^u) \end{aligned}$$

molar free enthalpy

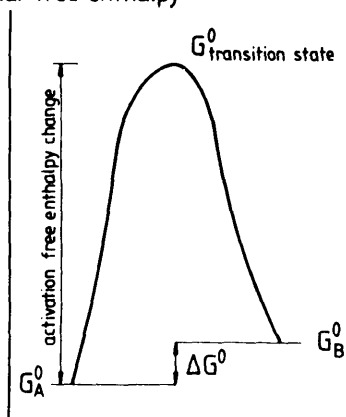


Fig. 4.4 The activation energy barrier.

$$C_e^T = C_e + C_{es} \quad (\text{mol m}^{-3}) \quad 4.9$$

$$C_s(0) = C_s + C_{es} + C_p \quad (\text{mol m}^{-3}) \quad 4.10$$

with the k 's denoting the reaction-rate constants (dimensions depending on the order of the reaction: first order s^{-1} (k_1 and k_{-1}) and second order $\text{m}^3 \text{ mol}^{-1} \text{ s}^{-1}$ (k_2 and k_{-2})) and r_s^u and r_p^u the rate of production ($\text{mol m}^{-3} \text{ s}^{-1}$) of substrate and product, respectively; the C stands for concentration (mol m^{-3}) with the subscript referring to the pertinent species and the superscript T to total concentration and $C_s(0)$ is the situation on time $t = 0$. It is assumed that at the start no product or enzyme substrate complex is present [Eq. (4.10)].

When the thermodynamic equilibrium has been reached

$$r_s^u = r_p^u = 0 \quad (\text{mol m}^{-3} \text{ s}^{-1}) \quad 4.11$$

Substitution in Eqs. (4.6) and (4.7) gives:

$$-k_1 C_e^* C_s^* + k_{-1} C_{es}^* = 0 \quad (\text{mol m}^{-3} \text{ s}^{-1}) \quad 4.12$$

and

$$-k_2 C_e^* C_p^* + k_{-2} C_{es}^* = 0 \quad (\text{mol m}^{-3} \text{ s}^{-1}) \quad 4.13$$

with the asterisk referring to the equilibrium situation.

Multiplication of Eq. (4.12) by k_{-2} , division by k_{-1} and then subtraction by Eq. (4.13) gives

$$\frac{k_{-2} k_1 C_e^* C_s^*}{k_{-1}} - k_2 C_e^* C_p^* = 0 \quad (\text{mol m}^{-3} \text{ s}^{-1}) \quad 4.14$$

or

$$\frac{C_p^*}{C_s^*} = \frac{k_{-2} k_1}{k_2 k_{-1}} = K \quad (-) \quad 4.15$$

Substituting Eq. (4.5) yields

$$\frac{k_{-2}k_1}{k_2k_{-1}} = e^{-\Delta G^0/RT} \quad (-) \quad 4.16$$

From this it appears that as a consequence of a thermodynamic constraint not all four reaction-rate constants are independent of each other. If three are known, the fourth follows immediately from Eq. (4.16). For the general case [Eqs. (4.6-4.10)] there is no easy straightforward analytical solution. Solving is, however, possible when a pseudo-steady-state with respect to C_{es} is assumed:

$$-\frac{dC_{es}}{dt} = r_s^u + r_p^u = 0 \quad (\text{mol m}^{-3} \text{s}^{-1}) \quad 4.17$$

With Eqs. (4.6) and (4.7) this gives

$$C_e(k_1C_s + k_2C_p) = C_{es}(k_{-1} + k_{-2}) \quad (\text{mol m}^{-3}) \quad 4.18$$

Substitution of Eq. (4.9) yields

$$C_{es} = \frac{C_e^T(k_1C_s + k_2C_p)}{k_{-1} + k_{-2} + k_1C_s + k_2C_p} \quad (\text{mol m}^{-3}) \quad 4.19$$

Combination of Eqs. (4.6), (4.14) and (4.19) together with some algebraic work results in

$$-r_s^u = \frac{C_e^T(k_1k_{-2}C_s - k_{-1}k_2C_p)}{k_{-1} + k_{-2} + k_1C_s + k_2C_p} \quad (\text{mol m}^{-3} \text{s}^{-1}) \quad 4.20$$

Substitution of Eq. (4.16) yields

$$-r_s^u = \frac{k_1k_{-2}C_e^T(C_s - C_p e^{\Delta G^0/RT})}{k_{-1} + k_{-2} + k_1\left(C_s + \frac{k_{-2}}{k_{-1}}C_p e^{\Delta G^0/RT}\right)} \quad (\text{mol m}^{-3} \text{s}^{-1}) \quad 4.21$$

When studying this equation more closely one special case can be recognized. If ΔG^0 is negative and large in absolute value, in other words the thermodynamic equilibrium mixture merely consists of product P , then Eq. (4.21) simplifies to:

$$-r_s^u = \frac{k_1 k_{-2} C_e^T C_s}{k_{-1} + k_{-2} + k_1 C_s} \quad (\text{mol m}^{-3} \text{s}^{-1}) \quad 4.22$$

With

$$v_{max} = k_{-2} C_e^T \quad (\text{mol m}^{-3} \text{s}^{-1}) \quad 4.23$$

and

$$K_m = \frac{k_{-1} + k_{-2}}{k_1} \quad (\text{mol m}^{-3}) \quad 4.24$$

the Michaelis-Menten Eq. (4.3) appears. To derive this equation the following assumptions had to be made:

1. $\Delta G^\circ \ll 0$
2. Pseudo-steady-state with respect to C_{ss} ,

The reaction equation for Michaelis-Menten kinetics can thus be written as:



Many other reaction and rate equations are applied to describe more complex enzyme kinetics, but we refer to the more specialized literature, e.g., Cornish-Bowden (1976) and Segel (1975), for extensive discussions. Although several industrial enzymes, e.g., glucose isomerase and glucoamylase, do not obey Michaelis-Menten kinetics, only this type of kinetics will be used in later chapters. The mathematics involved in the other types is too complex to be useful in the context of this book. For engineering calculations the Michaelis-Menten kinetics are satisfying for a large number of applications. Yet even Michaelis-Menten kinetics are sometimes too complex for analytical solutions and in that case simplifications are looked for. Two obvious simplifications of the Michaelis-Menten equation thrust themselves forward:

- i. If $K_m \ll C$, zero-order kinetics are approached and

$$-r_s^u = v_{max} \quad (\text{mol m}^{-3} \text{s}^{-1}) \quad 4.25$$

- ii. If $K_m \gg C$, first-order kinetics are approached and

$$-r_s^u = v_{max} \frac{C_s}{K_m} \quad (\text{mol m}^{-3} \text{s}^{-1}) \quad 4.26$$

In cases where Michaelis-Menten kinetics prohibit analytical solutions, these simplifications or hybrids of these simplifications can be very practical, as we will see later. As stated above, several industrial enzymes do not obey Michaelis-Menten kinetics and the more general case described by Eq. (4.21) should be used. If it is further assumed that the molar concentration of enzyme is low compared to the substrate concentration, which generally is the case, the following equation can be derived from Eq. (4.21):

$$-r_s^u = \frac{v_{max}^* (C_s - C_s^*)}{K_m^* + (C_s - C_s^*)} \quad (\text{mol m}^{-3} \text{s}^{-1}) \quad 4.27$$

with the following parameters (constant at a given temperature)

$$v_{max}^* = k_{-2} C_e^T \frac{1 + e^{\Delta G^0 / RT}}{1 - \frac{k_{-2}}{k_{-1}} e^{\Delta G^0 / RT}} \quad (\text{mol m}^{-3} \text{s}^{-1}) \quad 4.28$$

$$K_m^* = \frac{(k_{-1} + k_{-2}) \left(1 + \frac{k_1}{k_{-1}} C_s^* \right)}{k_1 \left(1 - \frac{k_{-2}}{k_{-1}} \right) e^{\Delta G^0 / RT}} \quad (-) \quad 4.29$$

$$C_s^* = \frac{C_s(0) e^{\Delta G^0 / RT}}{1 + e^{\Delta G^0 / RT}} \quad (\text{mol m}^{-3}) \quad 4.30$$

Eq. (4.27) has a similar form as the ordinary Michaelis-Menten Eq. (4.3). However, K_m^* is dependent on C_s^* and thus $C_s(0)$, in other words, depends on the initial substrate concentration.

4.4 Determination of kinetic constants

4.4.1 The measurement of cell growth

To follow the course of growth of cells, it is necessary to make quantitative measurements. When cells are in the exponential growth phase, the growth is usually balanced, so any property of the biomass can be measured to determine growth rate. As a matter of convenience, the properties usually

measured are cell dry mass or cell number. The only direct way to measure cell mass is to determine the dry weight of cell material in a fixed volume of culture by removing the cells from the medium, drying them and then weighing them. An indirect method for determination of cell mass of unicellular organisms is an optical one: the determination of the amount of light scattered by a suspension of cells. When calibrated against cell suspensions of known density, it is a relatively rapid and accurate way to estimate the dry weight of cells per unit volume of culture. For bacterial cell suspensions that contain 10 million or more cells per cm^3 , the number of cells can be determined microscopically by counting the individual cells in an accurately determined very small volume. Such counting is usually done with special microscope slides known as counting chambers. For larger cells such as animal and especially plant cells, smaller magnifications are needed and thus less dense cell suspensions are required for this technique to be suitable. Another technique of total cell count makes use of the so-called Coulter counter, an electronic device. The number of viable cells can be estimated by means of a plate count. All techniques have specific advantages and disadvantages. Refer to Pirt (1985) and references cited therein for further details. For calculations based on balances and the average molar composition of the cell, the cell dry weight is the only one to be used.

4.4.2 Cell kinetic constants

The kinetic constant K , in Eq. (4.1) is generally very low, which complicates its determination very much. The maximal specific growth rate μ_{\max} , on the contrary, can easily be determined in a batch experiment by measuring the increase in cell mass during the exponential growth phase when all the essential nutrients are still present in excess. A neater, but more laborious, method is by measuring the washout curve in a chemostat. A chemostat can also be used to determine K . When μ_{\max} has been determined, the dilution rate D of the chemostat can be set such that $D = 0.5 \mu_{\max}$. When steady state is reached, determination of the substrate concentration in a sample from the chemostat yields the K , as K is numerically equal to the substrate concentration at $\mu = 0.5 \mu_{\max}$. Other procedures, with reference to the original literature, are mentioned by Pirt (1985).

4.4.3 Enzyme kinetic constants

In order to determine the kinetic constants K_m and v_{\max} in Eq. (4.3), two procedures are generally followed. The procedure usually followed by biochemists is measurement of the rate of substrate consumption (or product formation) by an appropriate analytical procedure at various substrate concentrations. This yields $-r$, C , data pairs, which can be plotted in a regular Michaelis-Menten plot (Fig. 4.2). From this plot v_{\max} and K_m can

roughly be read. More accurate is fitting Eq. (4.3) to these data pairs using a suitable mathematical procedure. Generally, a number of graphic linearization procedures are used to reduce the $-r_s^u$, C_s data pairs to K_m and v_{max} values. Transformation of Eq. (4.3) into

$$-\frac{1}{r_s^u} = \frac{K_m}{v_{max} C_s} + \frac{1}{v_{max}} \quad (\text{mol}^{-1} \text{m}^3 \text{s}) \quad 4.31$$

and plotting $-1/r_s^u$ against $1/C_s$, gives the double reciprocal plot according to Lineweaver-Burk (Fig. 4.5). The kinetic constants can be evaluated from the intercept and the slope as illustrated in Fig. 4.5. In this plot the region with 5% deviation is indicated by the dotted line, representing an area of 95% confidence. As a consequence of the double reciprocal plot, large deviations occur at low substrate concentrations, making this procedure not very accurate (Moser, 1985b).

Another linearization of Eq. (4.3) is achieved by transformation according to Eady and Hofstee:

$$\frac{-r_s^u}{C_s} = \frac{v_{max}}{K_m} + \frac{r_s^u}{K_m} \quad (\text{s}^{-1}) \quad 4.32$$

The corresponding plot is shown in Fig. 4.6, where estimation of the parameters is indicated together with the 95% confidence interval. Again, large deviations occur at low substrate concentrations.

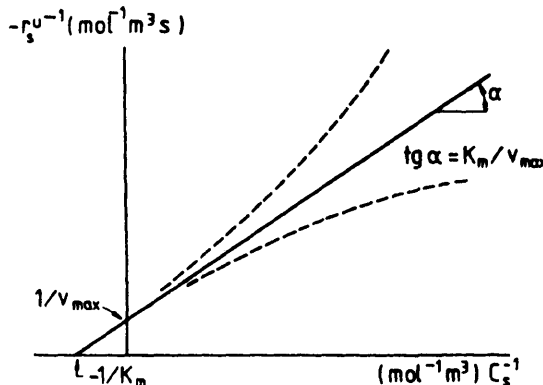


Fig. 4.5 The Lineweaver-Burk plot (broken lines indicate 95% confidence region).

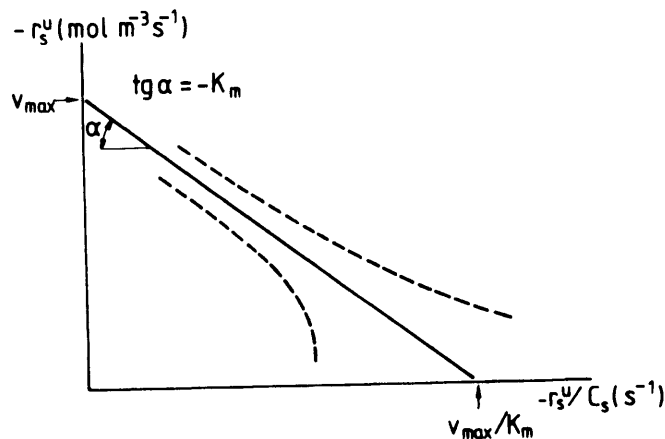


Fig. 4.6 The Eady-Hofstee plot (broken lines indicate 95% confidence region).

Similarly, Eq. (4.33) and Fig. 4.7 represent the linearization according to Langmuir.

$$\frac{-C_s}{r_s^u} = \frac{K_m}{v_{max}} + \frac{C_s}{v_{max}} \quad (s) \quad 4.33$$

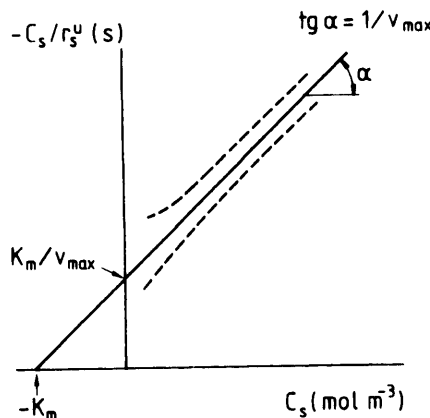


Fig. 4.7 The Langmuir plot (broken lines indicate 95% confidence region).

As can be seen, this plot realizes the smallest deviation and is therefore recommended (Moser, 1985b).

A more recent, completely different method of plotting enzyme kinetic data has been described by Eisenthal and Cornish-Bowden (1974). If the experimental C_s -values are plotted on a negative horizontal axis and the corresponding reaction rates on a vertical axis, then straight lines drawn through the corresponding C_s and $-r_s^u$ -points intersect at $C_s = K_m$ and $-r_s^u = v_{max}$ (Fig. 4.8).

While Fig. 4.8b represents the conventional $-r_s^u = f(C_s)$ plot for better comprehensiveness, Fig. 4.8a demonstrates this simple graphic procedure for estimating the enzyme kinetic constants, which is in agreement with the following rearrangement of Eq. (4.3):

$$v_{max} = -r_s^u + \frac{-r_s^u K_m}{C_s} \quad (\text{mol m}^{-3} \text{s}^{-1}) \quad 4.34$$

Thus, for any value of C_s and $-r_s^u$ it is possible to plot v_{max} against K_m as a straight line with slope $-r_s^u/C_s$, intercept C_s on the negative K_m -axis and intercept $-r_s^u$ on the v_{max} -axis. The second procedure to determine

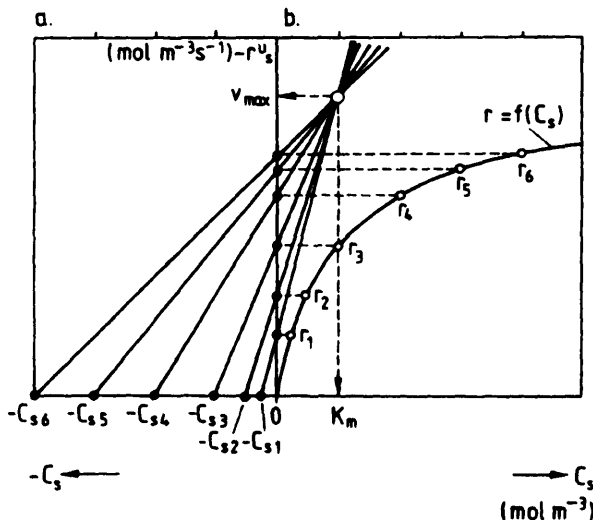


Fig. 4.8 The Eisenthal/Cornish-Bowden plot. (Adapted from Moser, 1985b.)

enzyme kinetic constants in principle only involves one experiment, namely, measurement of the substrate concentration as a function of time in a time course experiment. By fitting the integrated Michaelis-Menten equation

$$t = \frac{K_m}{v_{max}} \ln\left(\frac{C_s(0)}{C_s}\right) + \frac{C_s(0) - C_s}{v_{max}} \quad (s) \quad 4.35$$

to the measured C_s ($= f(t)$) data sets, K_m and v_{max} are obtained. A drawback of this procedure is that deviations of Michaelis-Menten kinetics are not easily detected. This last procedure is also especially suited for determination of the kinetic constants in Eq. (4.27), as only one initial substrate concentration is involved. It is essential that no inactivation of the enzyme occurs during the assay and that Michaelis-Menten kinetics are strictly obeyed.

4.5 Environmental effects

4.5.1 pH effects

The pH of the reaction medium generally has a pronounced effect on both enzyme and cell kinetics. The activity as a function of pH generally displays a bell-shaped profile, both for enzyme catalysis and for cell growth and activity (Fig. 4.9). Although rate equations for the pH-dependency of enzyme kinetics can be derived on the basis of dissociation constants (Moser, 1985b), these correlations have no real practical value. In practice pH-optima are determined experimentally for both enzyme and cell kinetics.

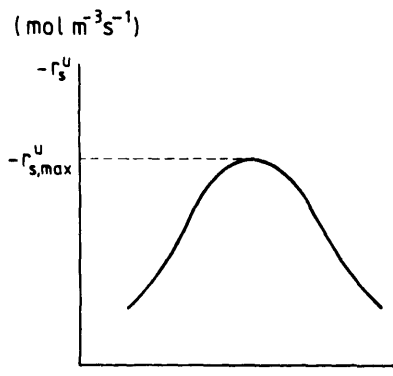


Fig. 4.9 Activity-pH profile.

4.5.2 Temperature effects

The effects of temperature on enzyme and cell kinetics are of considerable interest and importance, but rather complicated. The effects on cell growth and activity have to be explained basically in terms of the temperature dependence of the structure of the cell components, especially proteins and lipids, and of the temperature coefficients of reaction rates, which in turn depend on the activation energies of the reactions (Pirt, 1985). As a consequence, the results normally measured for cell kinetics are similar to those of enzymes. In contrast to the complex mechanisms involved, the experimental results generally exhibit a rather simple behavior: the overall rate passes through a maximum with a sharp decrease with increasing temperature (Fig. 4.10). This behavior is the result of a combined effect. Raising the temperature affects both the enzyme-catalyzed reactions itself and the thermal inactivation of the enzymes (see also Chapter 5). Although the underlying mechanisms are very complex, in the majority of experimental situations the rate of both enzyme catalysis and enzyme denaturation can be described satisfactorily with the Arrhenius equation over a moderate range of temperatures:

$$k = k_\infty e^{-\Delta H^*/RT} \quad (\text{s}^{-1}) \quad 4.36$$

or

$$\ln k = \ln k_\infty - \frac{\Delta H^*}{RT} \quad (-) \quad 4.37$$

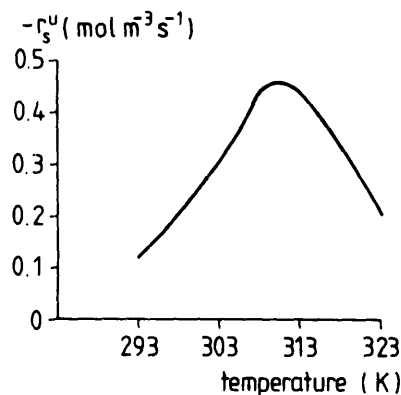


Fig. 4.10 Specific rate as a function of temperature.

where k represents the reaction-rate constant of the pertinent reaction (s^{-1} in case of first-order kinetics), k_* a constant number (s^{-1}) called the frequency factor, dependent on the frequency of formation of activated complexes of the reactants and numerically equal to k at infinite temperature T (K), and $\Delta H'$ the activation enthalpy change ($J mol^{-1}$). It is also common usage to have ΔE as notation instead of $\Delta H'$. Estimation of the parameters $\Delta H'$ and k_* can be carried out with the aid of the Arrhenius plot shown in Fig. 4.11. This plot shows two regimes, which result from the above-mentioned combined effect of biocatalysis and biocatalyst inactivation. One regime (low temperature), where the inactivation effect is insignificant during the duration of the kinetic measurement, can be used for estimation of k_* and $\Delta H'$ of the actual biocatalysis. The other regime (high temperature), when inactivation prevails, can be used for estimation of k_* and $\Delta H'$ of the inactivation reaction. The course of the transition regime will be determined by, among other factors, the duration of the kinetic measurement. For more details refer to Moser (1985b).

4.5.3 Ionic-strength and water-activity effects

While pH and temperature are commonly used experimental variables in enzyme and cell technology research, ionic strength and water activity can be considered neglected variables (Dale and White, 1983; Hahn-Hägerdal, 1986; Pirt, 1985), even though the effects on enzyme activity and stability

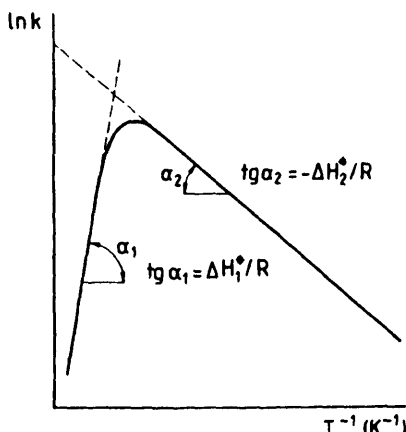


Fig. 4.11 The Arrhenius plot.

and on cell growth and activity can be tremendous; see, for instance, Fig. 4.12 and Fig. 4.13. It is, therefore, not surprising that no correlations exist that more or less are applicable to describe the effects of these neglected variables on enzyme and cell kinetics. Seeing the dramatic effects these variables can have, it is recommended that more experimental attention be given to them in order to

- i) optimize the conditions in the bioreactor not only with respect to temperature and pH, and
- ii) find more generally applicable correlations.

That this type of research can be rewarding was shown by Dale and White (1983). They proposed that the thermodynamic activity of the two histidine residues in the active center of bovine pancreatic ribonuclease, which are absolutely necessary for the enzyme reaction, governs, or at least substantially influences, the enzymic reaction with the negatively charged ribonucleic acid (RNA) substrate. This hypothesis, if accepted, facilitates analysis of the experiments, in which the activity of the immobilized enzyme was measured as a function of ionic strength, according to the Debye-Hückel theory. This simplified theory predicts that the second-order rate constant k ($\text{m}^3 \text{ mol}^{-1} \text{ s}^{-1}$) for a reaction between two charged species, A and B , is

$$\log k = \log k_0 + 0.032 z_A z_B \sqrt{U} \quad (-) \quad 4.38$$

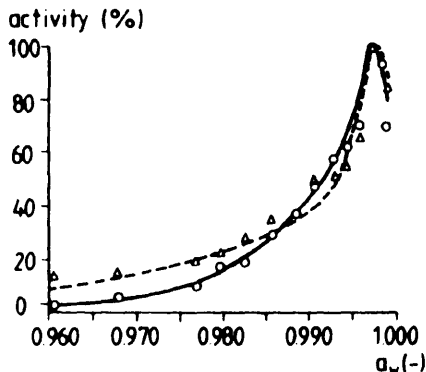


Fig. 4.12 Alkene-oxidizing activity of a free cell suspension of *Mycobacterium PY*, relative to the activity at $\alpha_w = 0.997$ vs. the water activity: (○—○) ethylene and (△—△) propene. (Adapted from Hamstra et al., 1987.)

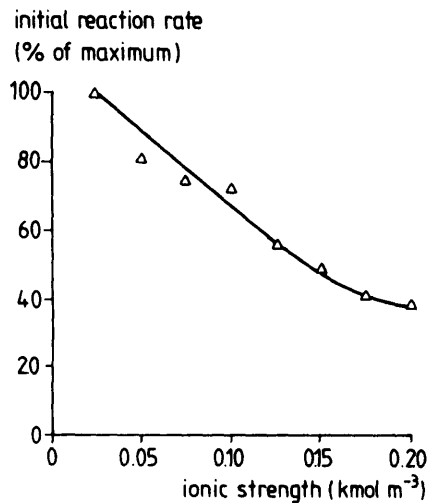


Fig. 4.13 Effect of ionic strength on immobilized ribonuclease.
(Adapted from Dale and White, 1983.)

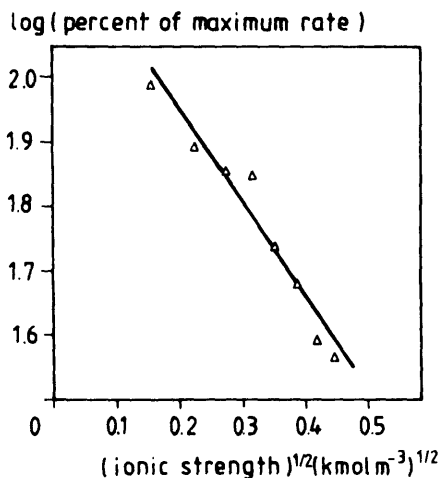


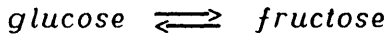
Fig. 4.14 Debye-Hückel plot of data in Fig. 4.13. (Adapted from Dale and White, 1983.)

where k_0 is the rate constant at zero ionic strength, z_A and z_B are the valencies (-) on the reacting species and U is the ionic strength of the reaction medium (mol m^{-3}). Plotting the experimental data in a Debye-Hückel graph (Fig. 4.14) indicates that the Debye-Hückel relationship is a useful model for describing the immobilized ribonuclease activity under the pertinent experimental conditions.

4.6 Examples

Example 4.1 Kinetics of glucose isomerase

The enzyme glucose isomerase catalyzes the following equilibrium reaction:



Calculate at 100 and 52.5°C the equilibrium constant K and $t_{0.5}$ and the kinetic constants at 52.5°C using the following data (adapted from Roels, 1983):

T (°C)	K
50	0.98
60	1.04
70	1.11

$$k_d = 1.46 \times 10^{38} e^{-235/RT} (\text{h}^{-1})$$

$$R = 8.31 \times 10^{-3} \text{ kJ mol}^{-1} \text{ K}^{-1}$$

and

C_s (mol m^{-3})	$-r_A^{\infty}$ ($\text{mmol m}^{-3} \text{ s}^{-1}$)
10.00	8.33
7.50	7.14
6.67	6.25
6.25	5.56
6.00	5.00

The latter data are obtained from one measurement at 52.5°C starting with an initial substrate concentration of 10 mol m^{-3} .

Solution:

$$\ln K = -\frac{\Delta H^0}{RT} + \frac{\Delta S^0}{R}$$

Plotting $\ln K$ versus T^{-1} and linear regression gives $\Delta H^0 = 5.73 \text{ kJ mol}^{-1}$ and $\Delta S^0 = 0.0176 \text{ kJ mol}^{-1} \text{ K}^{-1}$. Substituting T is 373 and 325.5 K yields for the equilibrium constant K 1.3 and 1, respectively. This means that the equilibrium shifts more to the fructose side, which is desirable because it is sweeter.

$$t_{0.5} = \frac{\ln 2}{k_d}$$

Substituting T is 373 and 325.5 K in the equation for k_d gives $t_{0.5}$ of $4.3 \times 10^{-3} \text{ h}$ and 275 h, respectively. Clearly, the very short half-life at 100°C is prohibiting a process at this temperature. Note that it is assumed that the data can be extrapolated to 100°C, which generally is not advisable to do over such a large range.

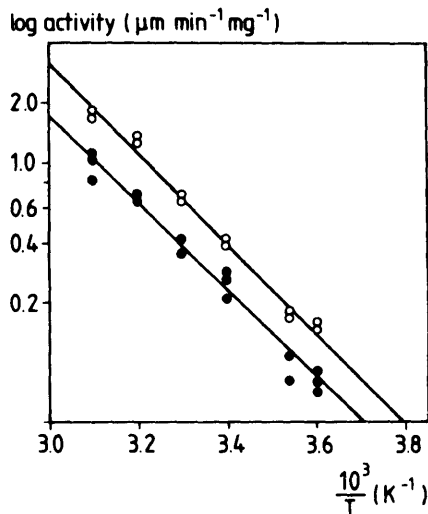


Fig. 4.15 Activity of (o) free and (●) immobilized xanthine dehydrogenase as a function of temperature. (Adapted from Tramper et al., 1979.)

Plotting $1/(C_s - C'_s)$ versus $1/r'$ ('Lineweaver-Burke') or applying a linear regression to this reciprocal data gives $K'_m = 1 \text{ mol m}^{-3}$ and $v'_{max} = 10 \text{ mmol m}^{-3} \text{ s}^{-1}$.

Example 4.2 Calculation of Arrhenius plot

Xanthine oxidase and xanthine dehydrogenase are enzymes which can be used for, among others, analytical purposes. For that immobilization is generally required.

Fig. 4.15 shows the activity of free and immobilized chicken liver xanthine dehydrogenase as a function of temperature in the form of an Arrhenius plot. From the slopes of the lines the activation energies of reaction for the free and immobilized enzyme can be calculated to be 33 and 19 kJ mol⁻¹, respectively. That the activation energy of the immobilized enzyme is about half that of the free enzyme is an indication that the reaction is diffusion controlled in case of the immobilized enzyme. The measured activation energy is, namely, the arithmetic mean of the activation energy for the enzymic reaction and the diffusion process. Since the diffusion activation energy is generally relatively small, the observed activation energy will approach half the true value when diffusion becomes the rate-controlling step.

References

- Cornish-Bowden A. "Principles of enzyme kinetics." Butterworth, London/Boston (1976).
- Dale B.E. and White D.H. "Ionic strength: a neglected variable in enzyme technology." Enz. Micro. Technol. 5, 227 (1983).
- Eisenthal R. and Cornish-Bowden A. "The direct linear plot: a new graphical procedure for estimating enzyme kinetic parameters." Biochem. J. 139, 715 (1974).
- Hahn-Hägerdal B. "Water activity: a possible external regulator in biotechnological processes." Enzyme Microb. Technol. 12, 322 (1986).
- Hamstra R.S., Murris M.R. and Tramper J. "The influence of immobilization and reduced water activity on gaseous-alkene oxidation by *Mycobacterium PY*₁ and *Xanthobacter PY*₂ in a gas-solid bioreactor." Biotechnol. Bioeng. 29, 884 (1987).
- Moser A. "Kinetics of batch fermentations." Chapter 14, pp. 243, in "Biotechnology" edited by Rehm H.-J. and Reed G. Volume 2: "Fundamental aspects".

mentals of biochemical engineering," volume editor Brauer H. VCH, Weinheim (1985a).

Moser A. "Rate equations for enzyme kinetics." Chapter 12, pp. 199, in "Biotechnology" edited by Rehm H.-J. and Reed G. Volume 2: "Fundamentals of biochemical engineering," volume editor Brauer H. VCH, Weinheim (1985b).

Pirt S.J. "Principles of microbe and cell cultivation." Blackwell Scientific Publications, Oxford reprinted 1985.

Roels J.A. "Energetics and kinetics in biotechnology." Elsevier Biomedical Press, Amsterdam (1983).

Segel I.H. "Enzyme kinetics." Wiley Interscience Publications, New York (1975).

Tramper J., Angelino S.A.G.F., Müller F. and Van der Plas H.C. "Kinetics and stability of immobilized chicken-liver xanthine dehydrogenase." Biotechnol. Bioeng. 21, 1767 (1979).

Trevan M.D., Boffey S., Goulding K.H. and Stanbury P. "Biotechnology: The biological principles." Taylor & Francis, New York (1987).

5

Stability

5.1 Introduction

In Chapter 1 it was stated that stability of the biocatalyst is one of the crucial parameters for the overall volumetric productivity of the bioreactor. In this chapter some aspects of enzyme stability are discussed in more detail. As result of their macromolecular structure all enzymes are liable to inactivation at slower or faster rates, depending on the enzyme and the conditions. In principle, the material discussed applies to biocatalysts in general (enzymes, cell organelles and whole cells), provided that the biocatalyst is used for a bioconversion and one enzyme is rate and stability limiting. In biomass production or production of metabolites by growing or at least viable cells, viable-cell stability is crucial. This can be discussed on the basis of the "death" rate of cells, to be added to the specific growth rate. It will not be discussed in this chapter. Mechanical stability or sensitivity to shear and other hydrodynamic forces of fragile cells will be treated separately in Chapter 8.

5.2 Enzymes

5.2.1 Structure

All enzymes are proteins, in other words, long linear chains of amino acids, which are coupled to each other with the so-called peptide bond. There are only 20 naturally occurring amino acids (Table 5.1) and the number of atomic elements involved even less, i.e., 5: carbon, nitrogen, hydrogen, oxygen and sulfur. From the point of view of an engineer the side chain is the most interesting functional group, because the amino and the carboxyl groups, with the exception of the two amino acids at the two ends of the chain, condensate with each other and form the peptide bonds (Fig. 5.1), and are thus excluded from the possibility of modification.

Table 5.1 The naturally occurring amino acids

R GROUPS	R GROUPS	ACIDIC AMINO ACIDS (negatively charged)	
GLYCINE 	ALANINE 	ASPARTIC ACID 	
SERINE 	VALINE 	GLUTAMIC ACID 	
THREONINE 	LEUCINE 		
CYSTEINE 	ISOLEUCINE 		BASIC AMINO ACIDS (positively charged)
TYROSINE 	PROLINE 	LYSINE 	
ASPARAGINE 	PHENYLALANINE 	ARGININE 	
GLUTAMINE 	TRYPTOPHAN 	HISTIDINE (at pH 6.0) 	
	METHIONINE 		

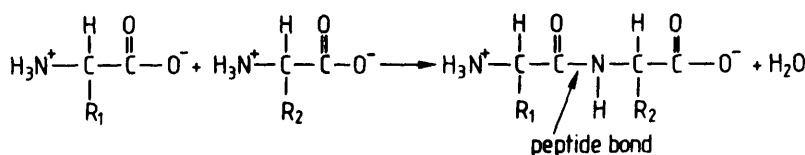


Fig. 5.1 Formation of peptide bonds.

The side chain of the amino acids can be polar, apolar, charged, uncharged, acid, basic, aromatic, etc. (Table 5.1). In connection with enzyme modification and stabilization attention should be paid especially to the side chains of lysine, cysteine, aspartic and glutamic acid, as these can easily undergo a chemical reaction. Through condensation of amino and carboxyl groups the amino acids are coupled (Fig. 5.1), thus forming the polypeptide chain with, for enzymes, molecular weights of 5000 to 7,000,000, in other words, a minimum of 50 amino acids. The enzymes with the larger molecular weights usually consist of more than one polypeptide chain, so-called sub-units, which are more strongly or weakly bound to each other. The strongest bonds are sulfur bridges between cysteines. The protein and thus enzyme synthesis is carried out in the ribosomes of the cell. A piece of DNA is transcribed in messenger RNA, which codes for one or a few related enzymes. In the ribosomes the mRNA is read and translated into amino acids, which subsequently are welded together by means of the peptide bond. Already during the stage of assembling the enzyme starts to fold according to the spatial orientation that eventually leads to the 3-dimensional active conformation (Fig. 5.2).

An enzyme is assigned four structures. The sequence of the constituting amino acids in the polypeptide chain (always unbranched) is called the primary structure. This primary structure, by the nature of the amino acid side chains, determines what is called the secondary and tertiary structure of the enzyme. Smaller or larger pieces of the enzyme chain can be folded according to two regular patterns: the α -helix and the β -pleated sheet.

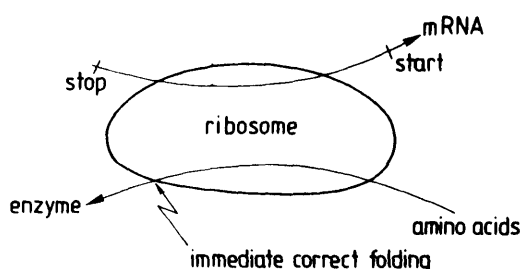


Fig. 5.2 The assembling of an enzyme.

Such microstructures of neighboring amino acids are called the secondary structure of the enzyme. Such regular patterns result from the fact that the peptide bond is fixed in a plane and the "free" rotation of the nearby bonds directed by the neighboring side chains of the amino acids. The α -helix, for instance, is stabilized by leucine, alanine and phenylalanine, destabilized by glutamine, serine and lysine and even broken by glycine. An enzyme thus consists of pieces of α -helix, β -pleated sheet and random parts. The 3-dimensional orientation of the various pieces is what is called the tertiary structure. In general, the orientation is such that a globular macromolecule is formed. The hydrophobic side chains are especially situated in the interior of the sphere and the hydrophilic side chains in the outer layers. When more than one polypeptide chain is involved, the enzyme is called an oligomer enzyme. The spatial orientation of the constituting subunits is the quaternary structure of the oligomer enzyme.

5.2.2 Stability

The 3-dimensional structure of enzymes is stabilized by 5 types of interactions:

1. Hydrogen bonds between polar amino acids
2. Hydrogen bonds between peptide bonds such as in α -helices
3. Hydrophobic interactions between nonpolar amino acids
4. Ionic bonds between oppositely charged side chains
5. Covalent bonds between cysteines (disulfide bridges)

The strength of all these bonds is small, with the disulfide bridge the least weak. Besides, the nature of the bonds is such that the sensitivity for changes in pH, temperature, ionic strength, etc., is very strong. In short, enzymes should be handled with care. The active conformation of enzymes mostly has minimum free enthalpy at the conditions under which they are destined to work. Renaturation is thus possible in principle if a pertinent denaturation has left the primary structure of the enzyme intact. Correct refolding of a reversible denatured enzyme depends strongly on pH, temperature, ionic strength, detergents, etc. Also, the stability and activity of the correct conformation of the enzyme strongly depend on these environmental factors. It is therefore not surprising that the productivity of especially industrial enzymes strongly depends on these factors. However, other factors also play a role, so that for the theoretical productivity the maximum is not always chosen. For instance, in order to prevent microbial contamination, relatively high operational temperatures are chosen, e.g., about 60°C in case of immobilized glucose isomerase, which is considerably above the "theoretical" productivity maximum. Also, in connection with a better solubility of substrate, the operational temperature is sometimes chosen too high, for instance, the use of α -amylase at temperatures of

100°C or higher, so that the point of liquefaction of starch has amply been exceeded.

In addition to temperature, the pH range in which an enzyme can be economically justified is one of the most important factors which determine success from the point of view of application. At an extreme pH the activity is in general nil or very small and a more or less rapid irreversible denaturation occurs. As a result of changes in pH, the degree of ionization of amino acid residue side chains in and outside the active site changes. This can result in larger or smaller changes in conformation, activity and stability. Consequently, enzymes show a pH-activity and a pH-stability optimum.

5.2.3 Inactivation models

As we have seen above, the correct 3-dimensional conformation of enzymes is based on a delicate balance of relatively weak binding forces. Inactivation of enzymes under operational conditions is therefore a fact which should always be taken into account. Inactivation can be the result of covalent modifications, monomolecular incorrect refolding, polymolecular aggregation and loss of cofactors. Covalent modifications occur especially as result of high temperatures and extreme pH and usually are irreversible (Table 5.2).

Irreversible inactivation of enzymes can be thermodynamically or kinetically controlled (Roels, 1983). In thermodynamic control the active enzyme E is in fast equilibrium with a reversibly denatured form D , which eventually is irreversibly inactivated in denatured protein I :

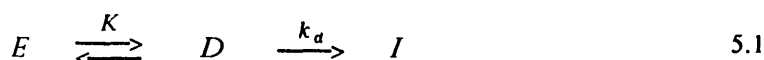


Table 5.2 Covalent modifications that usually result in irreversible enzyme inactivation

-
- * Oxidation/reduction of disulfide bridges
 - * Incorrect formation of disulfide bridges, both intra- and intermolecular
 - * Hydrolysis of disulfide bridges
 - * Isopeptide formation between, for instance, lysine and aspartic acid
 - * Hydrolysis of peptide bonds and Asn, Gln and Arg
 - * Racemization of amino acid residues
 - * β -Elimination of amino acids
 - * Proteolysis of especially unfolded enzymes
 - * Loss of coenzymes, e.g., FAD
-

K is the equilibrium constant and k_d the (first-order) inactivation rate constant (s^{-1}). When the inactivation is kinetically controlled, the active enzyme E is irreversibly transformed into denatured protein I :



5.2.3.1 Thermodynamically controlled inactivation

According to Eq. (5.1) the rate of production of denatured protein I can be written as:

$$\frac{dC_i}{dt} = k_d C_d \quad (\text{mol m}^{-3} \text{s}^{-1}) \quad 5.3$$

with C_i and C_d the concentration (mol m^{-3}) of irreversibly and reversibly, respectively, denatured enzyme. If C_e^T (see Chapter 4) is the active-enzyme concentration and C_e' the total concentration (mol m^{-3}) of active, not irreversibly modified, enzyme protein, then:

$$C_e' = C_e^T + C_d \quad (\text{mol m}^{-3}) \quad 5.4$$

and k_{obs} is assumed to be a hypothetical first-order observed inactivation rate constant, then

$$\frac{dC_i}{dt} = k_{obs} C_e' = k_{obs} (C_e^T + C_d) \quad (\text{mol m}^{-3} \text{s}^{-1}) \quad 5.5$$

and thus

$$k_{obs} = \frac{k_d C_d}{C_e^T + C_d} \quad (\text{s}^{-1}) \quad 5.6$$

With equilibrium conditions:

$$K = \frac{C_d}{C_e^T} \quad (-) \quad 5.7$$

Eqs. (5.4) and (5.6) can be written as, respectively:

$$\frac{C_e^T}{C_e^t} = \frac{1}{1 + K} \quad (-) \quad 5.8$$

and

$$k_{obs} = \frac{k_d}{1/K + 1} \quad (s^{-1}) \quad 5.9$$

The equilibrium constant K is thus an important parameter for the thermodynamically controlled enzyme inactivation. As

$$\ln K = -\frac{\Delta G^0}{RT} = -\frac{\Delta H^0}{RT} + \frac{\Delta S^0}{R} \quad (-) \quad 5.10$$

the rate of inactivation is determined by the difference in standard free enthalpy ΔG^0 ($J \text{ mol}^{-1}$) between D and E (Fig. 5.3). R is the universal gas constant ($8.31 \text{ J mol}^{-1} \text{ K}^{-1}$), T the absolute temperature (K), ΔH^0 and ΔS^0 the difference in standard enthalpy ($J \text{ mol}^{-1}$) and entropy ($J \text{ mol}^{-1} \text{ K}^{-1}$), respectively, between D and E .

When the difference in standard enthalpy between D and E , ΔH^0 , is greater than zero (endothermic reaction), which is usually the case as the native enzyme generally has the minimum energy content, the equilibrium will shift in favor of the denatured form D as the temperature increases. Both ΔH^0 and ΔS^0 are rather insensitive to temperature; thus if T rises K increases as $-\Delta H^0/(RT)$ becomes smaller in absolute value and $\Delta S^0/R$ remains about constant. Both ΔH^0 and ΔS^0 generally have large positive values. The difference in standard free enthalpy ΔG^0 usually is between 200 and 300 kJ mol^{-1} . Consequently, the shift from merely enzyme in the active conformation to merely inactive enzyme occurs over a relatively small range of about 15°C.

The thermodynamically controlled enzyme inactivation can be coupled with the positive temperature effect on the rate of biocatalysis (Chapter 4). The combined models lead to the overall picture of the effect of temperature on enzyme activity, as was schematized in Fig. 4.10. The activity increases until the optimal temperature is reached. At higher temperatures the effect of



Fig. 5.3 Thermodynamically controlled inactivation.

enzyme inactivation in the region of the phase transfer results in a progressive decrease in activity. In Chapter 4 [Eq. (4.23)] it was derived that:

$$v_{max} = k_{-2} C_e^T \quad (\text{mol m}^{-3} \text{s}^{-1}) \quad 5.11$$

with C_e^T the total concentration of active enzyme ($C_e + C_{es}$), and k_{-2} the first-order reaction-rate constant for product formation from the enzyme-substrate complex (s^{-1}). Assuming an Arrhenius type of temperature dependency for k_{-2} , Eq. (5.11) becomes

$$v_{max} = k_\infty C_e^T e^{-\Delta H_r^\bullet / RT} \quad (\text{mol m}^{-3} \text{s}^{-1}) \quad 5.12$$

in which ΔH_r^\bullet is the activation enthalpy of the reaction of enzyme/substrate complex to enzyme and product (J mol^{-1}), and k_∞ the corresponding frequency factor (s^{-1}). Correcting for the fraction of enzyme in the reversible-inactivated form by combination of Eqs. (5.8), (5.10) and (5.12) gives the overall temperature dependence of the maximum apparent forward rate v'_{max} of enzyme reaction:

$$v'_{max} = \frac{k_\infty C_e^T e^{-\Delta H_r^\bullet / RT}}{1 + e^{\Delta S^\bullet / R} e^{-\Delta H^\bullet / RT}} \quad (\text{mol m}^{-3} \text{s}^{-1}) \quad 5.13$$

Eq. (5.13) is graphically worked out in Example 5.1.

5.2.3.2 Kinetically controlled inactivation

In a number of cases the enzyme inactivation can be best described by a model in which the enzyme is directly irreversibly converted to denatured protein I [Eq. (5.2)]. The important parameter in this kinetically controlled inactivation is the enthalpy difference ΔH^\bullet (J mol^{-1}) of the native enzyme E and the transition state (Fig. 5.4).

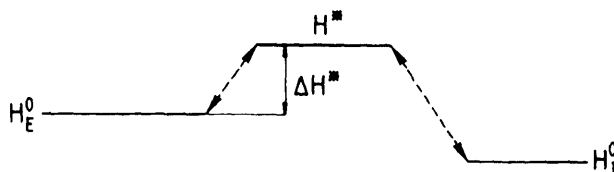


Fig. 5.4 Kinetically controlled inactivation.

The case in which the enzyme is irreversibly inactivated according to a first-order process will be considered here:

$$-\frac{dC_e^T}{dt} = k_d C_e^T \quad (\text{mol m}^{-3} \text{ s}^{-1}) \quad 5.14$$

Integration:

$$C_e^T = C_e^T(0) e^{-k_d t} \quad (\text{mol m}^{-3}) \quad 5.15$$

$C_e^T(0)$ is the initial concentration of active enzyme. A frequently used parameter to describe the stability of an enzyme is the half-life time $t_{0.5}$, i.e., the time in which half of the activity is lost as a result of inactivation. Substitution of $C_e^T = 0.5 C_e^T(0)$ in Eq. (5.15) yields:

$$t_{0.5} = \frac{\ln 2}{k_d} \quad (\text{s}) \quad 5.16$$

In general, k_d is strongly dependent on the temperature. For the range of temperatures of interest from the point of view of application, this dependency can generally be described quite well by an Arrhenius type of relationship:

$$k_d = f(T) = k_\infty e^{-\Delta H' / RT} \quad (\text{s}^{-1}) \quad 5.17$$

k_∞ is the frequency factor (s^{-1}) as introduced in Chapter 4. The activation enthalpy $\Delta H'$ of the enzyme inactivation reaction usually is rather large with values of the order of magnitude of 200–300 kJ mol^{-1} . This means that when the temperature is increased by 10°C , the rate of inactivation increases by a factor of about 10. When it is further considered that the activation enthalpy of the rate of biocatalysis generally is of the order of magnitude of 80 kJ mol^{-1} , in other words, an increase in reaction rate by about a factor of 2.5 when the temperature is raised by 10°C , the crucial role of temperature with respect to overall productivity of the enzyme is obvious.

5.2.4 Stabilization

From the above it is clear that enzyme stability is a crucial factor in the application of enzymes. It is also clear that enzyme inactivation always

occurs more or less rapidly. There are indeed many potential applications for which enzyme instability prohibits practical realization. It is therefore not surprising that much effort is devoted to the stabilization of enzymes. Methods which have been developed and are applied are summarized in Table 5.3.

Immobilization of enzymes can result in fixation of the active conformation. Protection against proteolysis and turbulent environments can also occur. Apparent stabilization as a result of immobilization is discussed at length in Chapter 16. Intramolecular crosslinking with the aid of multifunctional reagents can also result in fixation and, with that, stabilization of the active conformation of the enzyme. Chemical modification without formation of intramolecular bridges occasionally results in stabilization, but the opposite is true as well (a well-known example is microbial rennin). Metal ions such as Ca^{+2} , Zn^{+2} and Mg^{+2} , high concentrations of neutral salts, e.g., ammonium sulfate, presence of ligands such as substrates and inhibitors and polyhydric alcohols (sorbitol, glycerol, polyethylene glycol, etc.) all can result in enzyme stabilization due to especially hydrophilic and hydrophobic interactions. However, until now it has been impossible to predict which method works for which enzyme. Besides, in addition to stabilization, many times loss of activity is observed as well. Two recent developments are the substitution of part or all of the aqueous reaction medium by an organic solvent and protein engineering. Biocatalysis in organic media can have other beneficial effects in addition to stabilization. Protein engineering is also a very potent area for, among others, enzyme stabilization. At present it is possible to change one or more amino acid residues in the polypeptide chain at a desired place by a desired amino acid by so-called site-directed mutagenesis. This can result in a more stable variant of the original enzyme. Naturally, other properties can also be introduced this way. For instance, Genentech and Genencor have elegantly shown this for the enzyme subtilisin.

Table 5.3 Methods of enzyme stabilization

-
- * Immobilization
 - * Intramolecular crosslinking
 - * Chemical modification
 - * Addition of metal ions
 - * Application of high concentrations of neutral salts
 - * Addition of ligands
 - * Addition of polyhydric alcohols
 - * Replacement of aqueous by organic reaction medium
 - * Protein engineering
-

5.3 Examples

Example 5.1 Temperature influence on enzyme activity and stability

In this example Eq. (5.13) is worked out for

$$\Delta H' = 75 \text{ kJ mol}^{-1}$$

$$\Delta S^0 = 0.75 \text{ kJ mol}^{-1} \text{ K}^{-1}$$

$$\Delta H^0 = 225 \text{ kJ mol}^{-1}$$

which are rather typical values for an enzymic reaction. Substitution of these values and $R = 8.31 \times 10^{-3} \text{ kJ mol}^{-1} \text{ K}^{-1}$ in Eq. (5.13), and taking $T = 300 \text{ K}$ as a reference, yields

$$\frac{v'_{\max}(T)}{v'_{\max}(300)} = \frac{e^{-75/(8.31 \times 10^{-3}T)}}{1 + e^{0.75/(8.31 \times 10^{-3})} e^{-225/(8.31 \times 10^{-3}T)}}$$

Fig. 5.5 is the graphic illustration of this equation. As can be seen, the combined mechanisms of reaction and inactivation result in an optimum temperature for enzyme activity.

Example 5.2 Effect of immobilization on stability

In the previous chapter the activity of free and immobilized chicken-liver xanthine dehydrogenase has been analyzed as an example. In the paper of Tramper et al. (1979) stability data are also given (Table 5.4).

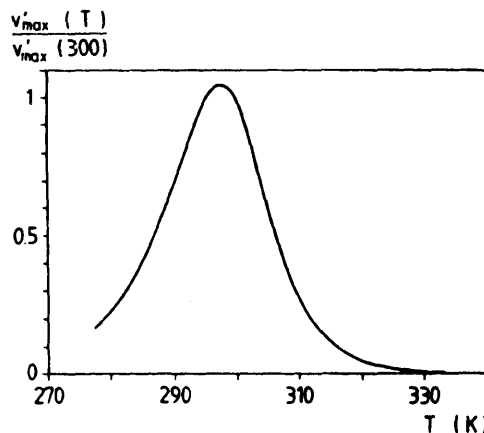


Fig. 5.5 Maximum rate of enzyme reaction as a function of temperature.

Table 5.4 Storage stability of free and immobilized chicken-liver xanthine dehydrogenase as a function of temperature

T °C	Free enzyme $t_{0.5}$ (h)	Immobilized enzyme $t_{0.5}$ (h)
4	423	2114
20	292	1167
30	71	810
40	21	33
50	11	15

Source: Adapted from Tramper et al., 1979.

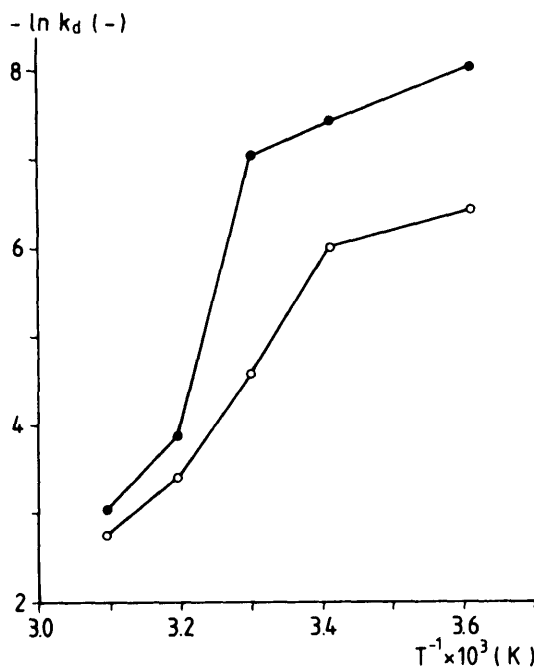


Fig. 5.6 First-order inactivation constant k_d as a function of temperature for free (o) and immobilized (●) chicken-liver xanthine dehydrogenase.

By means of Eq. (5.16), k_d can be calculated from these data as a function of temperature. Eq. (5.17) can be rewritten into

$$\ln k_d = -\frac{\Delta H^*}{RT} + \ln k_\infty$$

Plotting $\ln k_d$ as a function of $1/T$ yields a straight line if the inactivation can be described by a first-order, kinetically controlled mechanism. Fig. 5.6 shows such plots for the reworked data of Table 5.4. Both curves show a linear part over 20°C, but in a different range, and with a different slope. From the slopes a ΔH^* of about 101 and 27 kJ mol⁻¹ is derived for free and immobilized enzyme, respectively.

Immobilization clearly has a pronounced effect. The breakpoint between 30 and 40°C, in the immobilized enzyme, could very well be the result of a change in structure of the pertinent support Sepharose. Gel-like materials like Sepharose are known for such changes (Hulst et al., 1989).

References

- Roels J.A. "Energetics and kinetics in biotechnology." Elsevier Biomedical Press, Amsterdam (1983).
- Tramper J., Angelino S.A.G.F., Müller F. and Van der Plas H.C. "Kinetics and stability of immobilized chicken-liver xanthine dehydrogenase." Biotechnol. Bioeng. 21, 1767 (1979).
- Hulst A.C., Hens H.J.H., Buitelaar R.M. and Tramper J. "Determination of the effective diffusion coefficient of oxygen in gel materials in relation to gel concentration." Biotechnol. Techniques 3, 199 (1989).

6

Flow, Flooding, Dispersion

6.1 Introduction

The basis for most of the transport processes in bioreactors is the flow of liquid and gas bubbles, the dispersion of the gas bubbles and the suspension of particles (i.e., microorganisms or beads). Here we will discuss these phenomena in main lines. A division will be made between stirred vessels, bubble column, air lift type and packed bed reactors.

6.2 The stirred vessel

6.2.1 Flow and flooding

In an aerated bioreactor equipped with one or more stirrers flow phenomena are complicated due to the combined action of stirrer and air bubbles. A simplified description for a disc turbine stirrer is dealt with here. The flow pattern in the absence of gas consists of two circulation loops for each stirrer, as shown in Fig. 6.1A. When gas is sparged, different patterns can exist, as shown by Nienow et al. (1977). At high stirrer speeds and low gas flow rates the circulation pattern largely resembles that of the nonaerated case (Fig. 6.1B). Increasing the gas flow rate changes this pattern gradually until the gas dominates the flow pattern (Figs. 6.1D,E). At even higher gas flow rates the air bubbles will not be distributed at all by the stirrer and the gas escapes in the region of the stirrer axis (Fig. 6.1F). Here again, a circulation loop occurs but the direction of the rotation is just opposite to that of Fig. 6.1A. It will be obvious that for stirred vessels flow patterns like that shown in Figs. 6.1E and 6.1F should be avoided.

The situation in which the gas dominates the flow pattern is called flooding. Nienow et al. (1977) define situation D as flooding, Biesecker (1972) situation F. On small scales a detectable change from D → E → F takes place; however, on large scales the change is gradual (Feijen et al., 1987). All authors give different relations for the flooding point.

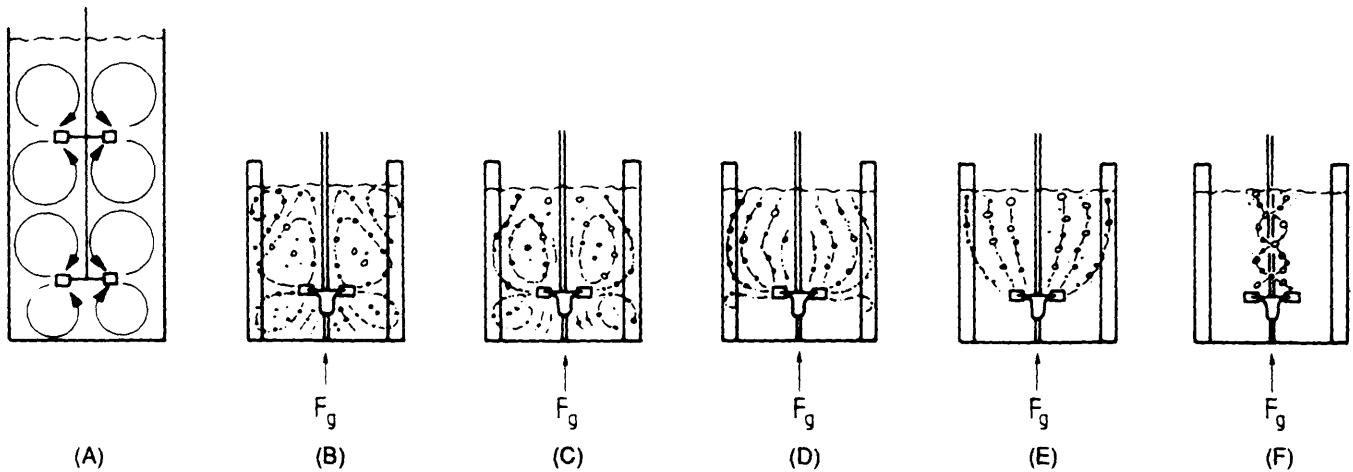


Fig. 6.1 Flow patterns in stirred aerated vessels, according to Nienow et al. (1977).

Biesecker (1972) simply states that flooding occurs when the energy dissipated by the air, $P_g(W)$, exceeds that of the stirrer, $P_s(W)$. For tall vessels, $H_v > T_v$, the energy dissipated by the air above the lower compartment cannot influence the flow field around the stirrer. So, we have to modify his relation: Flooding occurs when the energy dissipated by the gas in the lower compartment, P_{g1} , exceeds P_{s1} , that of the lower stirrer. This is an easy rule of thumb.

Feijen et al. (1987) have measured on large scales with two different methods. They found that flooding is absent for

$$\frac{F_{gs}}{ND^3} < c \frac{N^2 D}{g} \quad (-) \quad 6.1$$

with

- c = 0.34 for the method based on hold-up measurements and
 c = 1.2 for the method based on dissolved oxygen measurements

and further

F_{gs}	= volumetric gas flow rate at the pressure conditions of the lower stirrer	$(m^3 s^{-1})$
N	= stirrer speed	(s^{-1})
D	= stirrer diameter	(m)
g	= gravitational acceleration	$(m s^{-2})$

These formulae indicate that there is no distinct flooding criterium for large vessels. Example 6.1 shows that the criteria of Biesecker and Feijen et al., although very different at first sight, do predict F_g and N values in the same range.

Another important criterion is the minimum stirrer speed for dispersion of air bubbles. At too low stirrer speeds, a situation similar to F occurs due to the incapability of the stirrer to disperse the gas at all, even at extremely low gas flow rates (imagine the situation starting from $N = 0$). This is the case at stirrer tip speed $v_{tip} < 1.5-2.5 m s^{-1}$, as shown by Westerterp et al. (1963).

In conclusion, three design rules can be set:
 Always necessary:

$$v_{tip} > 1.5 - 2.5 \quad (m s^{-1}) \quad 6.2$$

while one of the following equations can be used to calculate the maximum attainable gas flow rate.

$$P_{gI} < P_{sI} \quad (\text{W}) \quad 6.3$$

Or derived from Eq. (6.1)

$$\frac{F_{gs}}{ND^3} < 0.3 \frac{N^2 D}{g} \quad (-) \quad 6.4$$

The experimental conditions underlying reported data in literature about mixing, mass transfer, etc., must be checked for these criteria. If data in the literature do not satisfy these conditions, then the results cannot be regarded as representative for well-designed stirred vessels.

6.2.2 Dispersion and coalescence

In a stirred vessel the main dispersing activity takes place in the immediate vicinity of the stirrer. Knowledge of the flow behavior behind the stirrer blades is essential for a good qualitative understanding of this process. In a one-phase liquid system the flow behind the blades is dominated by a pair of trailing vortices, as shown in Fig. 6.2. Very intensive shear rates, $\dot{\gamma}$ (s^{-1}) up to 100 N, and a distinct downpressure are the result. With a small gas inflow rate, the gas will be entrained in the center of the vortex. In this way a so-called vortex cavity originates (Fig. 6.3A). Intensive dispersion of the gas occurs at the tip of the cavity where dispersed bubbles enter the fluid bulk. With higher gas inflow rates the vortex is completely filled with gas, and it is replaced by a cavity that clings to the back of the blades (Fig. 6.3B). Increasing the gas flow rate further finally leads to the origination of a large cavity (Fig. 6.3C). Systematic arrangements of large and clinging cavities can occur as shown by Warmoeskerken (1986).

The gas dispersion takes place at the back of these cavities. All the gas coming from the sparger situated below the stirrer and also a considerable part of the recirculating gas flow is entrained into these cavities. The suction

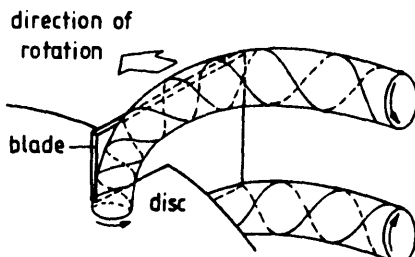


Fig. 6.2 Schematic three-dimensional view of a trailing vortex pair. (Adapted from Van 't Riet, 1975.)

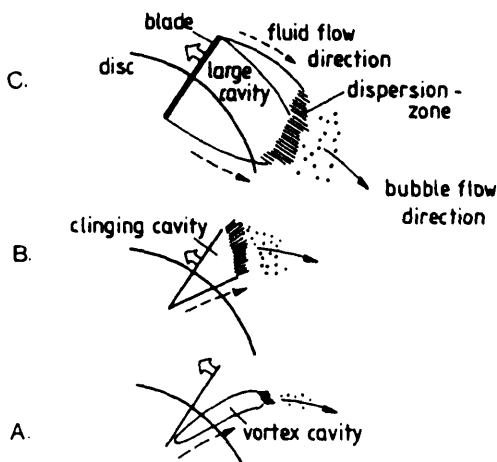


Fig. 6.3 Cavity shapes. (Adapted from Van 't Riet, 1975.)

of recirculating gas into the cavities is important because it results in an intensive mixing of the gas bubbles, even for noncoalescing liquids. The suction of sparger gas and of recirculating gas into the cavities means that practically all bubbles originate from dispersion at the back of these cavities. The nature of these dispersion processes is not well known. Experimentally determined bubble diameters (Koetsier and Thoenes, 1972) indicate that very small bubbles are formed, much smaller than the equilibrium size for coalescing media, which equals about 6 mm. The immediate suction of all sparged air bubbles has an important consequence, namely, that the dispersion in a stirred vessel is independent of the type of sparger. It has indeed been shown that for all those cases where the sparger is situated below the stirrer, no influence of sparger type exists on flooding and mass transfer.

Liquid properties with respect to coalescence can be between two extremes, coalescing and noncoalescing. In a coalescing liquid a substantial part of the collisions between two bubbles leads to coalescence of these two bubbles to a single bubble. In a noncoalescing liquid a collision does not lead to coalescence. In coalescing liquids the small bubbles that were produced at the back of the cavities will coalesce to larger and larger bubbles. This will lead to bubbles that are large enough to be broken up by the average turbulence forces in the vessel. Then a continuous dispersion and coalescence process takes place, leading to an equilibrium bubble size. In stirred vessels this size is about 3-6 mm. The equilibrium bubble size is much larger than the original bubble size at the back of the cavity, because

the average turbulence forces in the vessel are much smaller than the local shear and turbulence forces at the back of the cavities near the stirrer. In noncoalescing liquids the small bubbles originated at the back of the cavity will continue in the bulk volume. Lee and Meyrick (1970) confirmed that bubble size decreases considerably when salts, known coalescence suppressors, are added. In one of their experiments the bubble size at coalescing conditions was 2-3 mm. At constant stirrer speed this decreased to 0.5 mm after salt addition.

The phenomena described above are given schematically in Fig. 6.4. The diagram shows the relations between the mechanisms in a stirred vessel. The complexity of these mechanisms and their relations makes a quantitative assessment very difficult. Much of the results described in the following chapters will therefore have a partly empirical character.

6.2.3 Suspension

Stirring is also required to keep biocatalyst particles from settling out. A rough estimate of the minimal stirrer speed N_{min} (s^{-1}) to just keep the

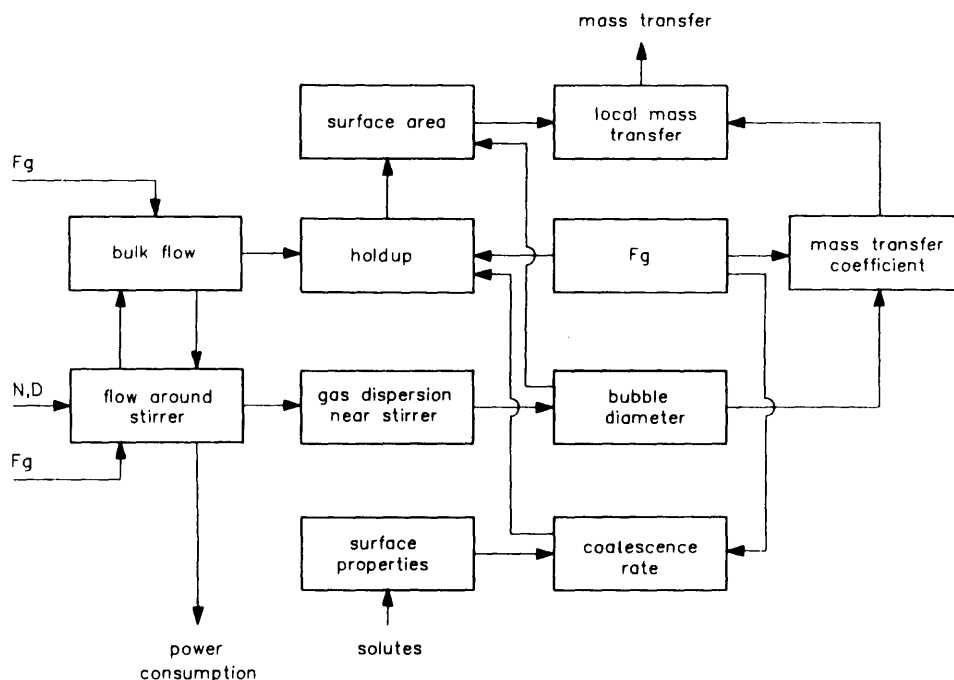


Fig. 6.4 Mechanistic interaction scheme in stirred vessels, according to Kossen (1982).

bottom free of particles can be obtained by the relation given by Zwietering (1958):

$$N_{min} = c_i \nu_t^{0.1} d_p^{0.2} \left(\frac{g (\rho_p - \rho_l)}{\rho_l} \right)^{0.45} X^{0.45} D^{-0.85} \quad (s^{-1}) \quad 6.5$$

in which

c_i = constant

X = weight percentage of particle phase (%)

The constant c_i is dependent on the geometry of the vessel, type of stirrer and particle geometry. The values range from 5 to 10, e.g., for spherical particles and a turbine stirrer 5.5 and for a propellor 6.4.

6.3 The bubble column

6.3.1 Flow and flooding

The flow phenomena in a bubble column are determined by the bubbles that originate at the sparger opening. Two mechanisms are relevant. The first one is the entrainment of liquid in the wake of each bubble. The second are the circulatory flows that arise at most operation conditions.

Homogeneous flow in a bubble column is defined as the regime in which circulatory flows are absent. All bubbles rise upward and mixing is only provided by the liquid in the bubble wake. This flow pattern occurs rather seldom. It can exist only at low gas superficial velocities ($< 1-4 \text{ cm s}^{-1}$) combined with a gas sparger that divides the gas very precisely over the bottom of the bubble column.

Heterogeneous flow in a bubble column is defined as the situation in which circulatory flows are dominant. In a bubble column local density differences can exist due to uneven bubble distribution. This will always be the case with a gas sparger that is unevenly distributed over the vessel bottom. But even at an even distribution, at gas velocities above $0.1-4 \text{ cm s}^{-1}$, in a random way uneven distribution of the bubbles in the vessel starts to occur. At larger scales this happens at lower gas flow rates than at small scales. This causes liquid circulatory flows. It appears that these flows orient themselves in such a way that a time averaged upward flow is present in the center of the vessel, while a downward flow is present at the outward regions. This is a time-averaged situation, because the circulatory loops continuously change and move. The flow pattern is composed of circulatory loops with a diameter value of the same magnitude as the vessel diameter. A more extensive description is given by Joshi (1980) and Heijnen and Van

't Riet (1984). A schematic description is given in Fig. 6.5. When such circulatory flows are present, the bubbles tend to concentrate in the upward flow region.

Flooding in bubble columns is defined as the situation in which the air blows the liquid out of the column. This can happen in small columns, particularly at column diameters < 10 cm. Gas superficial velocities are then on the order of 1 m s^{-1} . For commercial scale columns flooding never happens, because these gas velocities are irrelevant.

6.3.2 Dispersion and coalescence

In a bubble column the bubbles originate at the sparger opening at the bottom of the vessel. At the sparger the bubble size depends mainly upon the gas velocity through the sparger pipe opening and the diameter of the opening. Detailed formulae are given by Heijnen and Van 't Riet (1984). The bubble size can vary from very small (< 1 mm) up to very large (> 1 cm), depending on process conditions.

Once released from the sparger opening, the bubbles are subjected to the dispersion and coalescence processes. In a bubble column an equilibrium

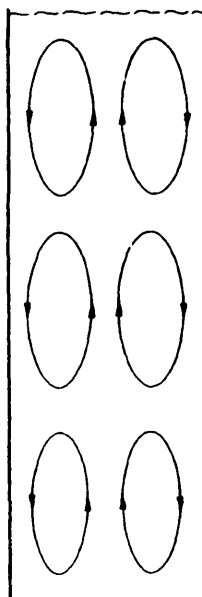


Fig. 6.5 Schematic description of the time-averaged circulatory flows in bubble columns.

bubble size can be defined which has roughly the value of 6 mm. This means that in a coalescing medium bubbles that are smaller than 6 mm will coalesce to larger bubbles. Once they reach a size of about 6 mm, further coalescence will lead to bubbles larger than 6 mm. These bubbles are not stable and will disperse, down to about 6 mm again. Because of this mechanism, the bubble size is always roughly 6 mm for coalescing liquids in a bubble column. The sparger cannot influence this.

In a noncoalescing medium the equilibrium bubble size does not play a role when the bubbles originating from the sparger are smaller than 6 mm. These bubbles will not coalesce due to the liquid properties and they will not disperse because of their small size. That means that in this case the bubble size in the vessel is equal to the bubble size at the sparger. When the bubble size at the sparger is larger than 6 mm, then dispersion will occur down to a bubble size of 6 mm. That means that for a noncoalescing liquid also the bubble size is equal to the equilibrium value under these conditions.

The formulae reviewed by Heijnen and Van 't Riet (1984) predict the bubble size at the sparger. When these formulae are applied for a highly loaded large scale fermenter it appears that for most of the sparger types bubble size at the sparger exceeds 6 mm (see also Example 6.2). This means that the bubble size in the reactor will be the equilibrium size of about 6 mm, independent of liquid composition. Because the sparger does not have a pronounced effect, simple constructions, like rings or pipes with holes, can be used.

The relation between all phenomena is given schematically in Fig. 6.6. As for the stirred vessel, the system is rather complex.

6.3.3 Suspension

Most biocatalyst particles can be easily suspended in bubble column type reactors due to their small size and the relatively small density difference between biocatalyst and the continuous water phase. In those cases where suspension can be critical, as a rule of thumb one can say that the minimum velocity in the bulk phase should be at least twice the terminal settling velocity of the particle. Stokes' law can be used to calculate the single particle settling velocity v_{ps} (m s^{-1}) as:

$$v_{ps} = \frac{d_p^2 (\rho_p - \rho_l) g}{18 \eta_l} \quad (\text{m s}^{-1}) \quad 6.6$$

in which

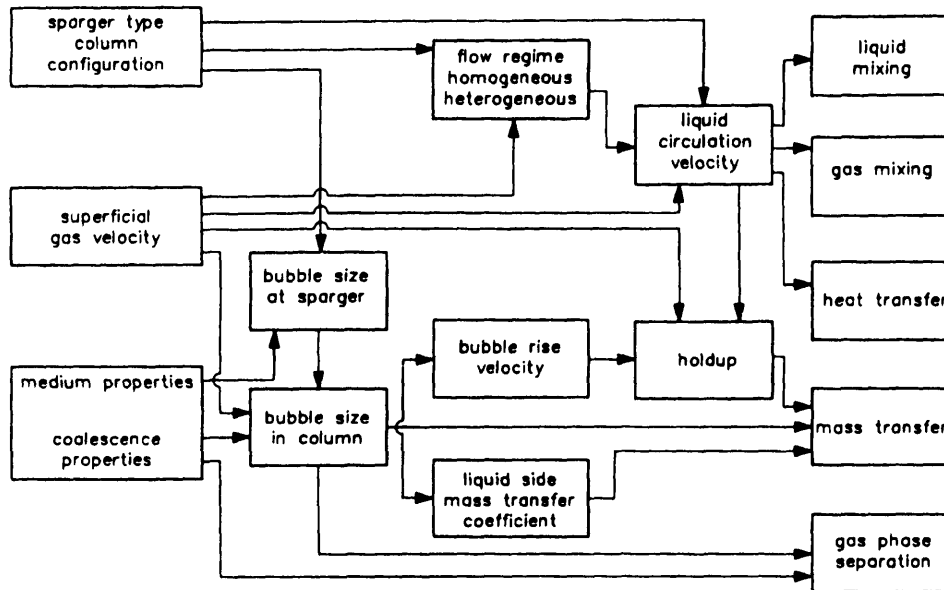


Fig. 6.6 Mechanistic mass transfer model for bubble columns. (Adapted from Heijnen and Van 't Riet, 1984.)

d_p	= diameter of the spherical particle	(m)
ρ_p	= specific density of the particle phase	(kg m ⁻³)
ρ_l	= specific density of the liquid phase	(kg m ⁻³)
η_l	= dynamic viscosity of the liquid phase	(N s m ⁻²)

In order for Stokes' law to be valid, the particle Re number, defined as

$$Re = \frac{\rho_l v_{ps} d_p}{\eta_l} \quad (-) \quad 6.7$$

should be less than 1.

In the intermediate range ($1 < Re < 10^3$) Beek and Mutzall (1975) give a relation for v_{ps} as:

$$c_w Re^2 = \frac{4 d_p^3 \rho_l (\rho_p - \rho_l) g}{3 \eta_l^2} \quad (-) \quad 6.8$$

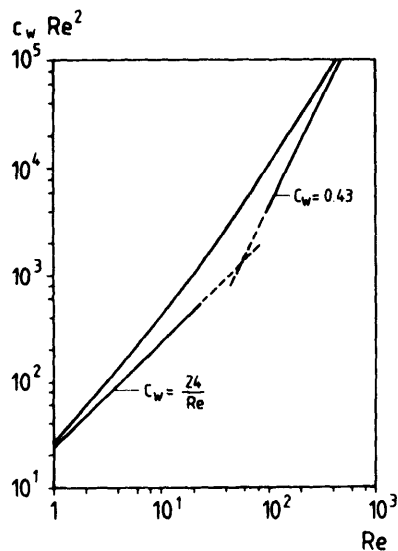


Fig. 6.7 Drag coefficients and related functions for spherical particles.
(Adapted from Beek and Mutzall, 1975.)

in which

$$c_w \quad = \text{drag coefficient} \quad (-)$$

The right hand side of Eq. (6.8) can be calculated for a given situation and by means of Fig. 6.7 the relevant Re can be found, from which v_{ps} can be calculated.

The v_{ps} values can be compared with the liquid velocity data as given in Chapter 9 and an order of magnitude comparison can show to what extent suspension can be a problem. In general, however, the suspension of biocatalyst particles and of small beads is no problem.

6.4 The air lift

6.4.1 Flow and flooding

The principle of the air lift reactor is given in Fig. 6.8. The reactor consists of two vertically mounted tubes, connected to each other at the top and bottom. Air is sparged at the bottom of one of the vertical sections, the so-called riser. The air bubbles rise up and reach the upper connecting section. This part is constructed in such a way that the bubbles can escape. The absence of bubbles in the second vertical section results in a density difference between the two vertical sections. This causes a circulatory flow, upward in the riser and downward in the other section, the downcomer. The

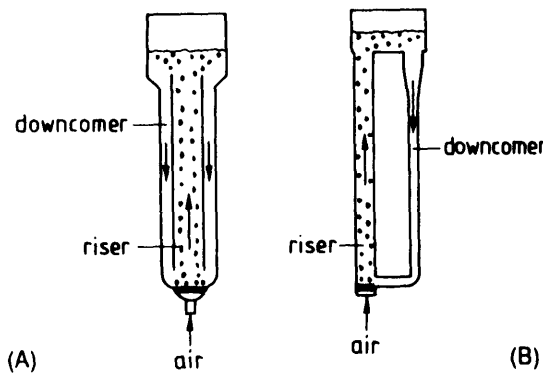


Fig. 6.8 Schematic representation of the air lift. A: Internal loop, B: External loop.

velocity is determined by the driving force and the hydrodynamic resistance resulting in

$$\rho_l \epsilon g H_v = 0.5 K_f \rho_l v_{ls}^2 \quad (\text{kg m}^{-1} \text{s}^{-2}) \quad 6.9$$

with

ρ_l	= liquid density	(kg m^{-3})
ϵ	= gas fraction of the riser	(-)
H_v	= height of the riser	(m)
K_f	= friction coefficient	(-)
v_{ls}	= liquid superficial velocity	(m s^{-1})

In Chapter 9 it will be shown that liquid velocities can be calculated starting from this equation.

The flow in an air lift should be uniform, getting near to a plug flow. However, this is only true when the liquid velocity is relatively large, which means, according to Eq. (6.9), when the hydrodynamic resistance of the flow circuit is limited. At lower liquid velocities, the bubbles in the riser cause a circulatory pattern similar to that of the bubble column circulatory pattern. In the extreme case of a nearly closed downcomer the riser starts functioning as a bubble column. The flow regime between the uniform "air lift" type of flow and the "bubble column" type of flow is called the transition region. Verlaan et al. (1989) derived a criterion that states that uniform flow occurs when the liquid velocity in the riser section is much larger than the circulatory velocity that should occur in a bubble column at the same gas velocity. This will be worked out further in Chapter 9.

Similar to the bubble column, flooding does not occur in properly engineered air lift reactors.

6.4.2 Dispersion and coalescence

The difference between an air lift and a bubble column is the flow field and the construction. The sparger construction is similar. Therefore, the dispersion and coalescence phenomena in an air lift are the same as for the bubble column.

6.4.3 Suspension

For suspension the same formula and reasoning given in Section 6.3.3 are valid.

6.5 The packed bed

6.5.1 Flow and flooding

Immobilized biocatalysts can be used in a packed bed reactor. When the particles are noncompressible and spherical and there is a continuous one-phase system between the packed particles, the pressure drop, over the reactor ΔP_r ($N\ m^{-2}$), is given by the Ergun relation (Beek and Mutzall, 1975):

$$\Delta P_r = \frac{170 \epsilon^2 \eta_l v_{ls} H_v}{(1-\epsilon)^3 d_p^2} + \frac{1.75 \epsilon \rho_l v_{ls}^2 H_v}{(1-\epsilon)^3 d_p} \quad (N\ m^{-2}) \quad 6.10$$

in which

η_l	= dynamic viscosity	$(N\ s\ m^{-2})$
d_p	= particle diameter	(m)
H_v	= reactor height	(m)
ϵ	= particle hold-up	$(-)$

Flooding occurs at upflow conditions when the pressure drop is larger than the total weight of the particles:

$$\Delta P_r > (\rho_p - \rho_c) g H_v \quad (N\ m^{-2}) \quad 6.11$$

with

ρ_p	= density of the particles	$(kg\ m^{-3})$
ρ_c	= density of the continuous phase	$(kg\ m^{-3})$

Before flooding occurs the bed can already expand or fluidize locally. To prevent this problem a packed bed can be used at downflow conditions. The only problem that can occur in that case is compression of the particles. This should be checked for each application by compression experiments. For an expanded or fluidized bed the pressure drop is near the pressure arising from the total weight of the particles.

6.5.2 Dispersion and coalescence

In the packed column these phenomena are absent.

6.6 Examples

Example 6.1 Comparison of the flooding criteria

Two criteria [Eqs. (6.3) and (6.4)] are mentioned for flooding. This example will show that the calculated gas flow rates are in the same range for both criteria. Let us assume a stirred vessel with the geometry as given in Fig. 6.9. Three vessels are used, given by $T_v = 0.25, 1.00$ and 4.00 m , respectively. Further, a stirrer tip speed is given. It has to satisfy Eq. (6.2). In this example two values are stated: 3 and 8 m s^{-1} .

Criterion 6.4 can be worked out for the gas flow rate normalized to atmospheric conditions, F_g , as:

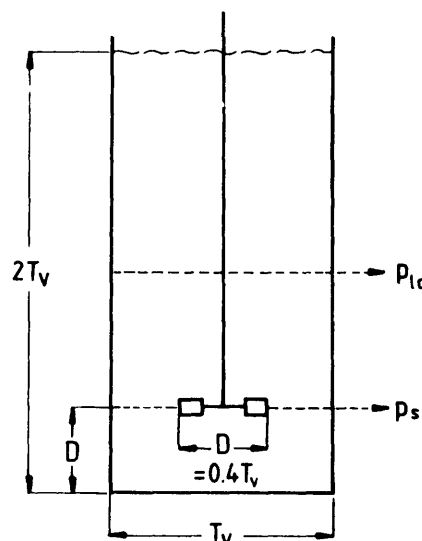


Fig. 6.9 The geometry of the vessel.

$$F_g = c \frac{N^3 D^4}{g} \times \frac{p_s}{p_{atm}} \quad (\text{m}^3 \text{s}^{-1}) \quad 6.12$$

In Table 6.1 the calculated values are given.

Criterion 6.3 can be worked out with Eqs. (14.6) and (14.4) to:

$$F'_g R T \ln \frac{p_s}{p_{lc}} = 2.5 \rho_l N^3 D^5 \quad (\text{mol s}^{-1}) \quad 6.13$$

in which F'_g = the molar gas flow rate and the gassed power number is assumed to have the value of 2.5 (see Chapter 14). p_{lc} is the pressure just at the level between the upper and lower compartment, that is, at a distance T_v above the vessel bottom. When 1 mol of gas is 24.5 dm^3 at $T = 298 \text{ K}$, Eq. (6.13) can be modified to:

$$F_g = 0.0245 \frac{2.5 N^3 D^5}{R T \ln \frac{p_s}{p_{lc}}} \quad (\text{m s}^{-1}) \quad 6.14$$

The results are given in Table 6.1. The gas flow rate is normalized to atmospheric conditions. It can be seen that the power consumption criterion [Eq. (6.3)] predicts a value in the same range as Eq. (6.4) with $c = 1.2$. It can also be seen that at large scales flooding only occurs at impractical large gas flow rates. The two criteria in Eq. (6.4) lead to different gas flow rates, as can be expected from the two different constants. This is a reflection of

Table 6.1 Calculated gas flow rates at which flooding starts

D (m)	v_{tip} (m s ⁻¹)	N (s ⁻¹)			Eq. 6.4 $c = 0.34$	Eq. 6.4 $c = 1.2$	Eq. 6.3
			$p_s \times 10^{-5}$ (N m ⁻²)	$p_{lc} \times 10^{-5}$ (N m ⁻²)			
0.1	3	9.5	1.04	1.025	0.003	0.011	0.014
0.1	8	25.4	1.04	1.025	0.076	0.203	0.274
0.4	3	2.4	1.16	1.10	0.104	0.049	0.065
0.4	8	6.4	1.16	1.10	0.265	0.93	1.24
1.6	3	0.60	1.64	1.40	0.079	0.279	0.350
1.6	8	1.59	1.64	1.40	1.47	5.18	6.52

the fact that particularly at large scales, the change from "fully loaded" to flooding covers a range of gas flow rates. Therefore, there is no single value for the gas flow rate at which flooding starts.

Example 6.2 Small bubble sparging

In this example the consequences of very small bubbles will be determined. Heijnen and Van 't Riet (1984) show that small bubbles can be made by, among others, single orifices and porous discs. For single orifices bubbles will be small only below a maximum value of v_o , the gas velocity in the orifice. With d_o as the orifice diameter, these authors give the criterion:

$$v_o d_o < 5 \times 10^{-4} \quad (\text{m}^2 \text{ s}^{-1}) \quad 6.15$$

Under this condition the bubble diameter at the orifice, d_{vs}^* , is given by:

$$d_{vs}^* = 1.7 \left(\frac{\sigma d_o}{\Delta \rho_{g,l} g} \right)^{0.33} \quad (\text{m}) \quad 6.16$$

with

$$\begin{aligned} \sigma &= \text{surface tension} & (\text{N m}^{-1}) \\ \Delta \rho_{g,l} &= \text{density difference between gas and liquid} & (\text{kg m}^{-3}) \end{aligned}$$

The calculated values for d_o and v_o at given d_{vs}^* values are given in Table 6.2. For bubble diameters below 1 mm the orifice diameter becomes of the order of microns, which is impractically small. At bubble diameters above 1 mm the orifice diameter is still small, but in theory this could be possible. However, the gas velocity in the orifice now becomes on the order of 1-10 m s^{-1} . The distance between the orifices should be large enough to prevent the originating bubbles to influence each other. Let us assume that for the 2-mm bubbles the distance between the holes should be 4 mm. Table 6.2 shows that in that case $d_o = 0.23 \text{ mm}$. With 4-mm distance this means that only 0.26% of the bottom surface area consists of holes. This means that at a v_o value of 2.17 m s^{-1} , as given in Table 6.2, the gas superficial velocity in the vessel is only 6 mm s^{-1} . And for that case the whole bottom has to be covered with the sparger plate. Another problem will show up in that case. Microorganisms tend to grow into such small sparger holes. When such a large amount of holes is present, they tend to block a substantial part of the holes. Therefore, the gas velocity through the open pipes will increase and the bubbles will become larger. The type of calculations given in Table 6.2 can be made for each relevant situation. Only very few cases will prove to be realistic.

Table 6.2 Calculated bubble diameters for an orifice and a porous disc

Orifice			Porous disc	
d_{vs}^* (mm)	d_o (mm)	v_o (max) (m s ⁻¹)	d_o (mm)	v_o (max) (m s ⁻¹)
2	0.23	2.17	0.01	1.4×10^4
1	0.03	17	0.01	1.4×10^1
0.5	0.004	125	0.01	1.4×10^{-2}

Another possibility is the porous disc. In this case the bubble size is given by:

$$d_{vs}^* = 6.1 \times 10^{-3} (v_o d_o)^{0.1} d_o^{0.08} \quad (\text{m}) \quad 6.17$$

Calculations reveal that bubble sizes $\ll 1$ mm are impossible because the low v_o value causes the whole bottom to be covered with the porous disc. For vessel diameters > 1 m this seems to be rather expensive, and besides, it will usually lead to abundant growth of organisms on the porous surface. For bubble sizes larger than 1 mm the v_o data do not imply a limited applicability. Here price and operational problems like cell growth and sterility should be determined for each separate case to make the final decision.

All these calculations are only valid for a fully noncoalescing medium. Usually, for instance because of antifoam addition, some coalescence will take place. In that case these sparger types become even less attractive.

References

- Beek W.J. and Mutzall K.M.K. "Transport phenomena." John Wiley and Sons, London (1975).
- Biesecker B.O. "Begasen von flüssigkeiten mit ruhrern." VDI Forschungssheft 554 (1972).
- Bruyn W., Van 't Riet K. and Smith J.M. "Power consumption with aerated Rushton turbines." Trans. Inst. Chem. Engrs. 52, 88 (1974).

Feijen J., Heijnen J.J. and Van 't Riet K. "Gas hold-up and flooding in large scale fermenters." Proc. Symp. on mixing and dispersion processes. Inst. of Chem Engrs and KIVI/NIRIA Delft Techn Univ., 7 May 1987.

Heijnen J.J. and Van 't Riet K. "Mass transfer, mixing and heat transfer phenomena in low viscosity bubble column reactors." Chem. Engng. J. 28, B21 (1984).

Joshi J.B. "Axial mixing in multiphase contactors. A unified correlation." Trans. Inst. Chem. Engrs. 58, 155 (1980).

Koetsier W.T. and Thoenes D. "Coalescence of bubbles in a stirred tank." Symp. on Chem. React. Engng., Amsterdam, May 1972, B3-15.

Kossen N.W.F. "Models in bioreactor design." Proc. 3rd Int. Conf. on Comp. Appl. in Ferm. Techn., Manchester, Aug. Sept. 1982.

Lee J.C. and Meyrick D.L. "Gas liquid interfacial areas in salt solutions in agitated tanks." Trans. Inst. Chem. Engrs. 48, T37 (1970).

Nienow A.W., Wisdom D.J. and Middleton J.C. "The effect of scale and geometry on flooding, recirculation and power in gassed stirred vessels." 2nd. Eur. Conf. on Mixing, 30th March 1977, Cambridge, England, Paper F1.

Van 't Riet K. "Turbine agitator hydrodynamics and dispersion performance." Thesis, Delft Technical University (May 1975).

Van 't Riet K. and Smith J.M. "The trailing vortex system produced by Rushton turbine agitators." Chem. Engng. Sci. 30, 1093 (1975).

Verlaan P, Vos J.C. and Van 't Riet K. "Hydrodynamics of the flow transition from a bubble column to an airlift loop reactor." J. Chem. Techn. and Biotech. 45, 109 (1989).

Warmoeskerken M.M.C.G. "Gas-liquid dispersing characteristics of turbine agitators." Thesis, Delft Technical University (1986).

Westerterp K.R., Van Dierendonck L.L. and De Kraa J.A. "Interfacial areas in agitated gas liquid contactors." Chem. Engng. Sci. 18, 157 (1963).

Zwietering Th.N. "Suspending of solid particles in liquid by agitators." Chem. Engng. Sci. 8, 244 (1958).

7

Medium

7.1 Viscosity models

In this chapter a short introduction will be given into the rheology of liquids. More detailed information can be found in Charles (1978). In a flowing liquid, neighboring fluid elements with different velocities exert shear onto each other. Fig. 7.1 gives the example of a laminar flow between two parallel plates, one of which is moving. A shear stress τ (N m^{-2}) is exerted onto the plate and onto each of the fluid elements by neighboring fluid elements. The shear stress is dependent upon the velocity gradient. For Newtonian liquids it is given by

$$\tau = -\eta \frac{dv}{dx} = \eta \dot{\gamma} \quad (\text{N m}^{-2}) \quad 7.1$$

in which

$$\begin{aligned} \eta &= \text{dynamic viscosity} & (\text{N s m}^{-2}) \\ \dot{\gamma} &= \text{shear rate} & (\text{s}^{-1}) \end{aligned}$$

τ and $\dot{\gamma}$ can be defined for three dimensions, but in this chapter only one-dimensional cases are considered for the sake of convenience.

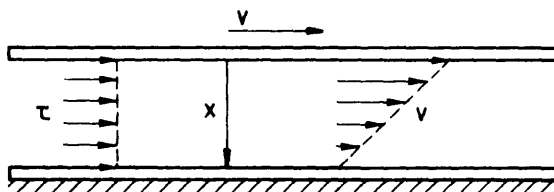


Fig. 7.1 Shear stress and liquid velocity for laminar flow between two parallel plates.

For Newtonian liquids the value of η is independent of the shear rate. Often, however, the viscosity value changes with the shear rate. In a number of cases the power law or Ostwald-de Waele model is valid, given by:

$$\tau = K \dot{\gamma}^n = (K \dot{\gamma}^{n-1}) \dot{\gamma} \quad (\text{N m}^{-2}) \quad 7.2$$

K ($\text{N s}^n \text{m}^{-2}$) is called the consistency index and n (-) is called the power law index.

Combining Eqs. (7.2) and (7.1) delivers the so-called apparent viscosity η_a (N s m^{-2}):

$$\eta_a = K \dot{\gamma}^{n-1} \quad (\text{N s m}^{-2}) \quad 7.3$$

This equation covers the following types of liquid

$n > 1$: dilatant

$n = 1$: Newtonian

$n < 1$: pseudoplastic

For a dilatant liquid the viscosity increases with $\dot{\gamma}$. This can occur with a dispersion of particles in a liquid, when the loading of particles is just below the packed density. Very densely packed yeast or bacterial suspensions sometimes show such dilatant viscosity behavior. For a pseudoplastic liquid the viscosity value decreases with an increasing value of $\dot{\gamma}$. This type of viscosity behavior can occur for (diluted) mycelial suspensions.

A number of suspensions show the existence of a yield stress τ_0 , that has to be exceeded to produce any flow at all. Model equations to describe this behavior are:

$$\tau = \tau_0 + K \dot{\gamma}^n \quad (\text{Bingham}) \quad (\text{N m}^{-2}) \quad 7.4$$

for so-called "Bingham plastic" liquids, and

$$\sqrt{\tau} = \sqrt{\tau_0} + K \sqrt{\dot{\gamma}} \quad (\text{Casson}) \quad (\text{N}^{0.5} \text{ m}^{-1}) \quad 7.5$$

for "Casson" liquids. Both equations can sometimes be applied to concentrated mycelial suspensions. Examples of different kinds of viscosity behavior of liquids are shown in Figs. 7.2 and 7.3.

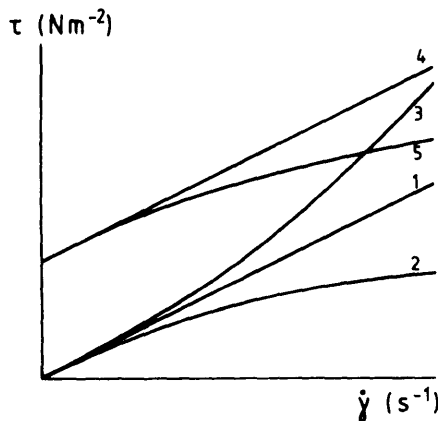


Fig. 7.2 The shear stress-shear rate relation for five model liquids:

1. Newtonian, 2. Pseudoplastic,
3. Dilatant, 4. Bingham plastic,
5. Casson.

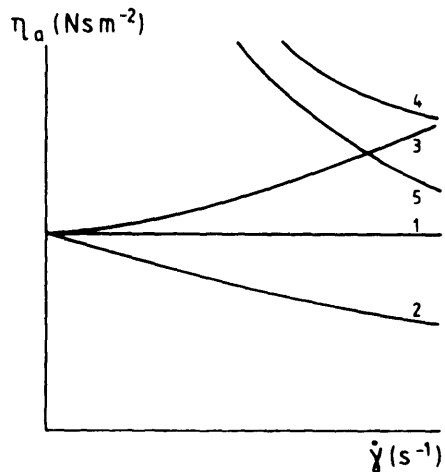


Fig. 7.3 The apparent viscosity values for the curves of Fig. 7.2.

It should be remembered that the equations as given above are only empirical equations to describe the rheological behavior of liquids. As such they have shown to be very useful. Usually, complicated suspensions like mycelial broths also show, to some extent, other effects like a time dependency. This will not be discussed here. The reason is that the rheology of fermentation broths as described in this chapter is already very complicated. The addition of extra effects would make the description only more diffuse and less useful for calculations.

7.2 Rheology data for fermentation liquids

7.2.1 Mycelial broths

The filaments of mycelium can interact with each other. This mechanism can increase the viscosity of the broth and it can even lead to pseudoplastic properties. This influences mass transfer and mixing in a negative way. It is therefore important to know what the viscosity of a given broth can be.

Literature data are available in rather large quantities (e.g. Roels et al., 1974; Charles, 1978; Blakebrough et al., 1978; Manchanda et al., 1982; Henzler and Schäfer, 1987; Van Suydam and Dusseljee, 1987). These data are not consistent. The reason is that an unambiguous relation should not be expected. The viscosity effect originates from the interaction of the hyphae. The hyphae structure, i.e., the morphology of the mould, is dependent upon

many parameters, like culture age, pH, stirring conditions, temperature and aeration conditions. This is even valid for one single strain. Besides this unavoidable cause of viscosity differences of seemingly corresponding broths, the measured values are difficult to relate to the actual values in the fermenter due to a number of reasons involved with the measurement itself:

- the use of different viscosimeter types;
- the broth is not always deaerated;
- the pretreatment is different;
- the times after sampling differ.

It will be clear that only trends can be obtained from the literature. The exact viscosity value and behavior are unique for each broth and can only be measured in that broth.

Two viscosity models are usually applied to mycelial broths: the power law and the Casson model. Fig. 7.4 shows an example of the measured value of the consistency index as a function of the fermentation time. It usually shows a maximum value. Fig. 7.5 shows the trend in the power law index. At the start of the fermentation the biomass dry weight is very low. Therefore, the liquid is near to Newtonian, so $n = 1$. At increasing fermentation times the n value decreases and reaches a rather stable value of 0.2-0.6. A strong relation between K and the biomass dry weight C'_x (kg m^{-3}) does exist. This can be measured with dilution experiments for fermentations at different ages and fermentations with different inoculation quantities. All lead to different relations, usually in the range of

$$K = \text{const.} \times (C'_x)^{1.5-3} \quad (\text{N s m}^{-2}) \quad 7.6$$

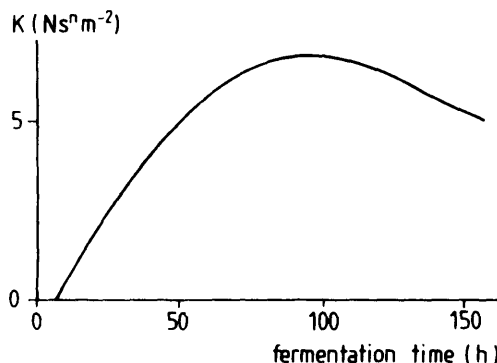


Fig. 7.4 Schematic representation of the value of the consistency index as a function of the fermentation time.

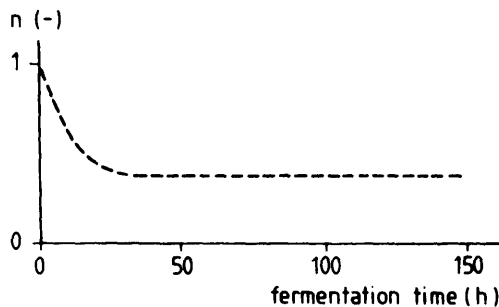


Fig. 7.5 Schematic representation of the value of the power law index as a function of the fermentation time.

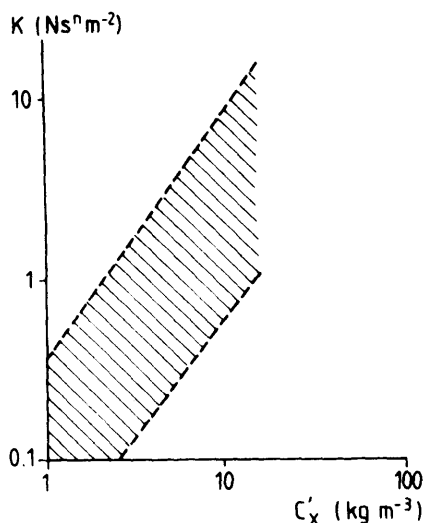


Fig. 7.6 Range of K values for filamentous broth found in literature based on Eq. (7.2).

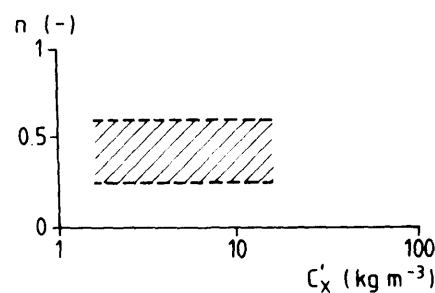


Fig. 7.7 Range of n values for filamentous broth found in literature based on Eq. (7.3).

Figs. 7.6 and 7.7 give the ranges of K and n values compiled from the literature data. From these two figures the η_a ranges can be determined by application of Eq. (7.3). The results are presented in Fig. 7.8. A main important parameter value is the shear rate, $\dot{\gamma}$, and it is just this value that we do not know very much about. An estimation of the value can be made on the basis of the following arguments. Metzner and Otto (1957) state that for laminar flow $\dot{\gamma}$ is of the order of 10 N in the stirrer region. Van 't Riet and Smith (1975) found that $\dot{\gamma}$ can be of the order of 100 N . With N values ranging from 1 up to $10 (\text{s}^{-1})$ this leads to a range for $\dot{\gamma}$ of 10 up to $1000 (\text{s}^{-1})$ near the stirrer. In other parts of the vessel the velocities are lower than the stirrer tip speed. An estimation of the order of magnitude of the liquid velocities then predicts that they can be easily down to about 0.1 times the impeller tip speed. The characteristic distance [dx in Eq. (7.1)] will be on the order of magnitude of 0.1–0.01 times the vessel diameter. With tip speeds of $2\text{--}10 \text{ m s}^{-1}$ and vessel diameters of 0.1 up to 10 m this

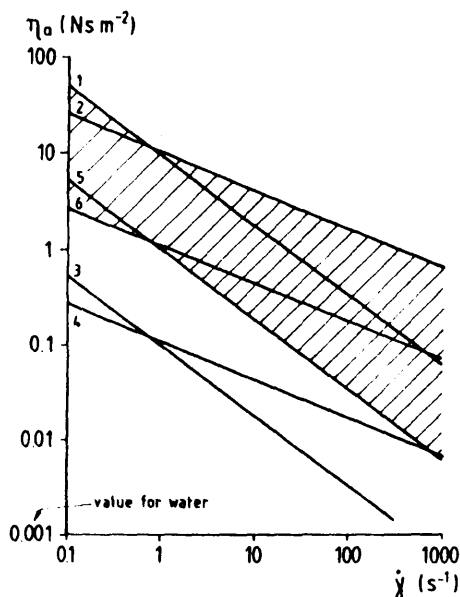


Fig. 7.8 Examples of η_a values based on Figs. 7.6 and 7.7 and Eq. (7.4). The shaded area gives the range for $C'_x = 15 \text{ kg m}^{-3}$.

- | | | | |
|--------------|--------------|--------------|-------------|
| 1. $K = 10$ | $n = 0.25$. | 2. $K = 10$ | $n = 0.6$. |
| 3. $K = 0.1$ | $n = 0.25$. | 4. $K = 0.1$ | $n = 0.6$. |
| 5. $K = 1$ | $n = 0.25$. | 6. $K = 1$ | $n = 0.6$. |

leads to a range of $\dot{\gamma}$ of 0.2 up to 100 (s^{-1}) (The extreme values of 2/10 and 10/0.1, respectively.) Another shear field is that around rising bubbles. Rising bubbles will have a size of 0.001 up to 0.01 m and a rise velocity of 0.001 up to 0.5 $m s^{-1}$, depending on the diameter. This leads to $\dot{\gamma}$ values of 10 up to 500 s^{-1} . Summarizing and excluding the existence of dead zones behind cooling coils, etc., the $\dot{\gamma}$ range can be 0.2 up to 500 s^{-1} , with probably 1-100 s^{-1} being a good estimate. In Fig. 7.8 the range for η_a at $C'_x = 15 \text{ kg m}^{-3}$ is given as the shaded area. It is bordered by the lines representing the extremes for the K and n values at $C'_x = 15 \text{ kg m}^{-3}$ as given in Figs. 7.6 and 7.7. At $\dot{\gamma} = 1-100 \text{ s}^{-1}$ the η_a values range from about 0.05 up to 10 $N s m^{-2}$. This shows that the apparent viscosity can reach extremely high values. The chapters on mixing and mass transfer will show that values like 10 $N s m^{-2}$ are unacceptable. In such cases the first task of the biochemical engineer is not to engineer a suitable reactor, but to decrease the viscosity. The most simple means is to decrease the C'_x value. However, this decreases the productivity of the fermenter. The second means is to influence the morphology by means of culture conditions or strain selection. The third means is to stimulate pellet formation. Pellets usually hardly contribute to the viscosity value.

Although the power law model describes the viscosity reasonably, it does not take into account a yield stress. Several authors have found that concentrated mycelial broths show the existence of a yield stress. For these measurements the Casson equation appeared to give a better correlation. Yet for most of their data the power law model was also satisfying.

7.2.2 Yeast and bacterial broths

Yeasts and bacteria do not influence the viscosity to a great extent. Only in the concentration range where the cells are "loosely" packed can a significant increase of the viscosity value occur. In these cases the viscosity can show a dilatant viscosity behavior. Only a limited further increase in cell density is then enough to cause an infinite viscosity value. The range where this effect can occur is $C_x = 150-300 \text{ kg m}^{-3}$, usually outside the range for commercial fermentations. A more detailed overview is given by Van Suydam and Dusseljee (1987).

7.2.3 Broths with biopolymers

A number of commercial fermentations are directed to the production of biopolymers like Xanthan and Pullulan. In these fermentations the viscosity is mainly determined by the biopolymer itself and the contribution of the cells (bacteria) can be neglected. Therefore, the vast amount of literature about the rheology of polymers can be used by those who want to study this in detail. Here we will limit ourselves to gross relationships.

Usually biopolymer solutions show a yield stress and time dependency. Yet the power law model is usually well suited for the shear rate range of interest. Gross values for Xanthan can be estimated from Charles (1978), Brauer (1985), Henzler and Schäfer (1987), Chang and Ollis (1982) and Bailey and Ollis (1986):

$$\begin{aligned} n &= 0.1 - 0.4 & (-) && 7.7 \\ \eta_a &= 0.1 - 10 & \text{at } \gamma = 1-10 \text{ s}^{-1} \text{ and} & (\text{N s m}^{-2}) & 7.8 \\ && C'_p = 30-50 \text{ kg m}^{-3} & & \\ \eta_a &\sim (C'_p)^{2-3} & & (\text{N s m}^{-2}) & 7.9 \end{aligned}$$

The best way to proceed is to use this type of number for rough estimates and, if more accurate calculations are needed, to measure exactly the data for each product.

7.3 Viscosity measurement methods

7.3.1 Laboratory methods

For viscosity measurements a broad choice of standard equipment is available. We can mention, for instance, the capillary viscosimeter, the plate and cone viscosimeter and the Couette viscosimeter. A summary is given by Charles (1978). All these instruments are very well suited for the measurement of biopolymers. For the measurements of mycelial broths this is not the case for three reasons (see also Bongenaar et al., 1973):

1. Formation of less dense layers (so called "slip" layers) just at the surface of cylinders in rotating-type viscosimeters and just at the capillary boundary in capillary viscosimeters.
2. A tendency of the suspension to become inhomogeneous because of settling.
3. The presence of particles, especially pellets, with a diameter of the same order of magnitude as the capillary diameter or the diameter of the channels in the viscosimeters.

The first reason in particular is problematic because it cannot be detected, except when a comparison is made with other types of instruments. It always takes place and leads to inaccurate, too small viscosity values especially for a dense broth. The measured viscosity value can become more than a factor of 100 too small. For viscous broths a small ($D = 2-5 \text{ cm}$) turbine stirrer can be applied. Chapter 14, on power consumption, shows that the power number [N_p (-)] of such a turbine stirrer is given by:

$$N_p = \frac{c}{Re} = \frac{c \eta}{\rho_l N D^2} \quad Re < 10 \quad (-) \quad 7.10$$

in which

Re	= Reynolds number	(-)
c	= constant	(-)
ρ_l	= liquid density	(kg m ⁻³)
N	= stirrer speed	(s ⁻¹)
D	= stirrer diameter	(m)

The constant c is dependent upon the stirrer geometry only and can be determined with Newtonian test liquids of known viscosity value according to the methods given in Chapter 14. For this measurement a very precise torque measurement is needed. It appears to be just in the range of torque values measured by standard viscosimeters. Thus it is possible to mount the turbine stirrer on a rotary viscosimeter, measuring the torque M (N m). In Chapter 14 it is shown that

$$2\pi NM = N_p \rho_l N^3 D^5 \quad (\text{W}) \quad 7.11$$

In this way N_p can be determined and with Eq. (7.10) the viscosity. Metzner and Otto (1957) have shown that for a turbine stirrer

$$\gamma = c' N \quad (\text{s}^{-1}) \quad 7.12$$

For the standard turbine $c' = 10-15$. If c' has to be known exactly, it can be measured by using a non-Newtonian liquid with a known $\eta_a - \gamma$ relationship. For a number of stirrer speeds N_p is measured. c is known from Newtonian test liquids and with N_p and Eq. (7.10) the η_a value can then be calculated for each N value. From the liquid viscosity data the γ corresponding to the measured η_a can subsequently be determined. Finally, this γ value gives the c' value when introduced in Eq. (7.12).

The turbine stirrer method is now widely used for mycelial broths and can be regarded as the most reliable method. Its disadvantage is that Eq. (7.10) is valid only for $Re < 10$. Under practical circumstances this leads to a lower limit of $10-100 \times N \text{ s m}^{-2}$ for the viscosity that can be measured with this method. Also, because D^2 is present in the Re -number, this method cannot be applied with a stirrer with $D > 2-5 \text{ cm}$, i.e., with the stirrer in the fermenter itself, because Re will become larger than 10. It has to be carried out as an "analytical method," in a very small vessel with a sample taken from the fermenter.

For all methods pretreatment and handling before the measurement is executed are very important. Some aspects are:

- Small bubbles can influence the rheology itself. The turbine method fails with bubbles present because in that case N_p changes (see Chapter 14). Therefore, the sample has to be deaerated.
- The sample contains "living" organisms. In the time period after sampling from the fermenter, the rheology can change, for instance, due to the depletion of oxygen or other substrates. Therefore, the time period after sampling has to be as short as possible and constant.
- During the measurement itself time effects and (de)flocculation can occur. Therefore, the procedure has to be the same for all measurements.

7.3.2 Measurements in the fermenter

Two methods can be distinguished: The use of the fermenter turbine stirrer according to Section 7.3.1 and the use of a specially designed on-line apparatus. The turbine stirrer method, however, is impossible to apply in most cases. Example 7.1 shows that due to the criterion of $Re < 10$, this method fails at pilot scale for low viscosity values and at commercial scale for the whole viscosity range. Besides, there will always be air present in the broth leading to cavity formation and changes in the N_p value. This leads to inaccuracies in measured value. This leaves the turbine method as a useful analytical tool, with sampling from the fermenter and measurement in a separate, small vessel.

A number of companies offer apparatus that can be used in the fermenter or can be used on-line. Because of the limited information given by the fermentation companies about their experiences, not much can be said about the success of these methods. It is, however, known that a number of these methods are used in commercial fermentations. A number of criteria are important for the choice of such methods.

- the reliability and sterility during fermentation
- possibility of steam sterilization
- comparison with laboratory data to find out if the data delivered have any significance.

7.4 Examples

Example 7.1 Viscosity measurement with a turbine stirrer

The turbine method is based on

$$Re = \frac{\rho N D^2}{\eta_l} < 10$$

Table 7.1 gives the value for N at $Re = 10$ for four scales: laboratory 0.01

Table 7.1 N (s^{-1}) values for which $Re = 10$

V (m^3)	D (m)	N (s^{-1}) at:		
		$\eta = 0.001$	$\eta = 0.1$	$\eta = 10$ ($N s m^{-2}$)
0.01	0.074	1.8×10^{-3}	1.8×10^{-1}	18
0.10	0.16	3.9×10^{-4}	3.9×10^{-2}	3.9
1	0.34	8.7×10^{-5}	8.7×10^{-3}	8.7×10^{-1}
200	2.01	2.5×10^{-6}	2.5×10^{-4}	2.5×10^{-2}

— Line above which the turbine in the fermenter can be used for viscosity measurements given by $\pi N D > 0.25 m s^{-1}$ (see Table 7.2) and $N > 0.1 s^{-1}$.

m^3 , pilot $0.1 m^3$ and $1 m^3$ and commercial scale $200 m^3$. For all scales it is assumed that the height of the ungassed volume = 2 times the fermenter diameter and the stirrer diameter = 0.4 times the fermenter diameter. The stirrer speed as calculated in Table 7.1 is the maximum stirrer speed allowed for the viscosity measurement. Table 7.2 gives the stirrer speed needed for dispersion of air bubbles: $\pi N D = 2.5 m s^{-1}$ [Eq. (6.2)]. It appears that the stirrer speed for viscosity measurement has to be lower than the operating speed. The stirrer motor and variable speed drive have to be able to provide this lower speed. Particularly for pilot and commercial scale this leads to unacceptable costs. The torque measurement apparatus has to be blocked at the higher speeds to prevent damage. These reasons lead to the conclusion that there are strong limits to accurate viscosity measurements in a fermenter in general, and unacceptable limits for commercial scale fermenters. If we assume, for instance, that below $\pi N D = 0.25 m s^{-1}$ no accuracy can be obtained and also that the minimum stirrer speed that can be reached is $0.1 s^{-1}$, then the line can be drawn given in Table 7.1. This example gives a clear indication of the limited applicability of this method. Besides the construction problems and costs for the possibility of stirrer

Table 7.2 N (s^{-1}) values for which $\pi N D = 2.5 (m s^{-1})$

V (m^3)	D (m)	N (s^{-1})
0.01	0.074	11
0.10	0.16	5.0
1	0.34	2.3
200	2.01	0.4

speed reduction, the need to stop stirring and aeration for each measurement (10–60 s) also makes this method unattractive even for those limited number of cases where it can be applied.

Example 7.2 Viscosity values of filamentous media

In Example 2.1 M_x (mol) values are calculated as a function of time. When we use these values the C'_x (kg m^{-3}) can be calculated with 24.4 g mol^{-1} of biomass and with a correction (1000) for $\text{g} \rightarrow \text{kg}$ as:

$$C'_x = \frac{M_x}{V} \frac{24.4}{1000} = \frac{M_x}{100} \frac{24.4}{1000} = 24.4 \times 10^{-5} M_x$$

To calculate the viscosity we assume that the fermenter contains a filamentous broth with the following rheology:

From Fig. 7.7:

$$n = 0.5$$

From Fig 7.6:

$$K = 0.07(C'_x)^{1.5}$$

For $\dot{\gamma}$, the values 10 and 100 are chosen.

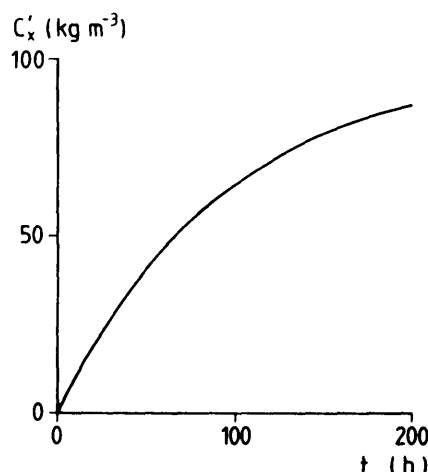


Fig 7.9 Calculated C'_x values for data of Example 2.1.

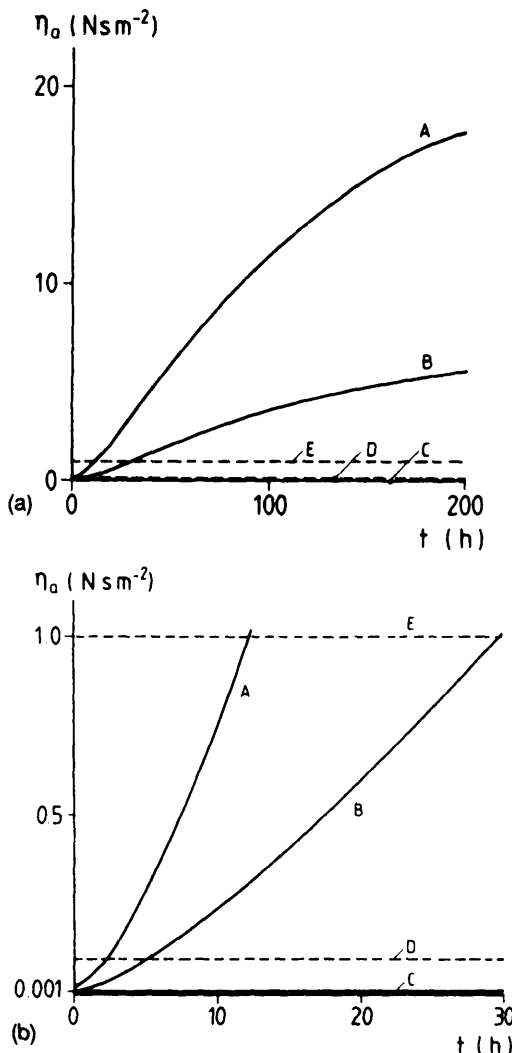


Fig. 7.10A,B The calculated η_a values. A: $\dot{\gamma} = 10 \text{ s}^{-1}$. B: $\dot{\gamma} = 100 \text{ s}^{-1}$. C: Yeast and bacteria. D: Limit for bubble column. E: Limit for stirred tank.

For yeast and bacteria the viscosity is hardly influenced by the microorganisms and thus we assume that $\eta_a = 10^{-3} \text{ N s m}^{-2}$.

The results of the calculations of C'_x are shown in Fig 7.9 and of η_a for the filamentous media in Fig. 7.10. In Chapter 11 it is shown that a bubble column cannot operate at viscosity values above 0.1 N s m^{-2} . The filamentous broth leads to unacceptable viscosity values for the bubble column, almost from $t = 0$ on. Bacteria and yeast do not pose any problem. For a

stirred vessel somewhat higher C_x' values can be reached; however, even for this reactor mass transfer becomes a problem at $C_x' = 10 \text{ to } 30 \text{ kg m}^{-3}$. This example shows very clearly the disastrous effects of high-viscosity mycelia and the need to prevent this type of viscosity behavior.

References

- Bailey J.E. and Ollis D.F. "Biochemical engineering fundamentals." McGraw-Hill Chemical Engineering Series, New York (1986).
- Blakebrough N., McManamey W.J. and Tart K.R. "Rheological measurements on *Aspergillus niger* fermentation systems." *J. Appl. Chem. Biotechnol.* 28, 453 (1978).
- Bongenaar J.J.T.M., Kossen N.W.F., Metz B. and Meyboom F.W. "A method for characterizing the rheological properties of viscous fermentation broths." *Biotechnol. Bioengng.* 15, 201 (1973).
- Brauer H. (ed.) "Biotechnology. Vol. 2. Fundamentals of biochemical engineering." VCH Verlagsgesellschaft Weinheim (1985).
- Chang H.T. and Ollis D.F. "Extracellular microbial polysaccharides: generalized power law for biopolysaccharide solutions." *Biotechnol. Bioengng.* 24, 2309 (1982).
- Charles M. "Technical aspects of the rheological properties of microbial cultures." *Adv. in Biochem. Engng.* 8, 1 (1978).
- Henzler H.J. and Schäfer E.E. "Viskose und elastische Eigenschaften von Fermentationslösungen." *Chem. Ing. Techn.* 59, 940 (1987).
- Manchanda A.C., Jogdand V.V. and Karanth N.G. "Studies on fermentation-broth rheology of a penicillium strain with cellulose as substrate." *J. Chem. Tech. Biotechnol.* 32, 660 (1982).
- Metzner A.B. and Otto R.E. "Agitation of non-Newtonian fluids." *A.I.Ch.E.-J.* 3, 3 (1957).
- Roels J.A., Van den Berg J. and Voncken R.M. "The rheology of mycelial broths." *Biotechnol. Bioengng.* 16, 181 (1974).
- Van Suydam J.C. and Dusseljee P.J.B. "Concept of apparent morphology as a tool in fermentation." In "Physical aspects of bioreactors" Ed. W. Crueger, pp. 107-120 Dechema (1987).
- Van 't Riet K and Smith J.M. "The trailing vortex system produced by Rushton turbine agitators." *Chem. Engng. Sci.* 30, 1093 (1975).

8

Shear

8.1 Introduction

In Chapter 1 it is stated that enzymes, cell organelles and whole cells (viable/nonviable, growing/nongrowing), free or immobilized, of microbial, plant or animal origin, all are considered biocatalysts. In most of the other chapters there is no strong discrimination between these types of biocatalysts, except maybe for growing cells. In this chapter, however, reference to the various types will be made several times, as the fragility and size and thus the sensitivity to hydrodynamic forces of the different species vary widely (Table 8.1). Any of these biocatalyst entities, when placed in a moving fluid with velocity gradients, experiences a shear force whose magnitude depends on the dynamic viscosity of the fluid, the fluid velocity gradient and the size of the pertinent biocatalyst. The effects of this shear force on the biocatalyst largely depend on the properties of the biocatalyst entity itself.

Table 8.1 Size of biocatalysts and sensitivity to shear

Biocatalyst species	Size	Fragility
Enzymes	nanometer range	+/-
Microbial cells	1-10 μm	-
Microbial pellets/flocs	up to 1 cm	+
Animal cells	20 μm	++
Animal cells on microcarriers	150 μm	+++
Plant cells	100 μm	+
Plant cell aggregates	up to at least 1 cm	++
Immobilized biocatalyst	0.015-0.5 cm	+/-

Strictly speaking, shear forces result from spatial differences in the levels of momentum across material stream lines in a moving body of fluid. In a (stirred) bioreactor, however, biocatalysts can encounter a variety of other mechanical forces due to collisions with the vessel walls, the agitator or other objects in the bioreactor. In addition, sparged gas bubbles subject the biocatalyst to surface tension forces and to fluid mechanical forces resulting from the motion, disengagement and bursting of bubbles and from foaming. In this chapter all will be collectively referred to as shear and if possible quantified in terms of shear rate, shear stress, shear force or smallest turbulent eddy length. First, shear will be defined. Further, the equipment and methods most often used for determination of the shear sensitivity of a biocatalyst will be described. Throughout, the consequences for bioreactor design and scale-up will be discussed.

In Chapter 7 the relation between shear stress, viscosity and shear rate is given by Eq. (7.1) as

$$\tau = -\eta_l \frac{dv}{dx} = \eta_l \dot{\gamma} \quad (\text{N m}^{-2}) \quad 8.1$$

in which

τ	= shear stress	(N m^{-2})
η_l	= dynamic viscosity of the liquid	(N s m^{-2})
dv/dx	= fluid velocity gradient	(s^{-1})
$\dot{\gamma}$	= shear rate	(s^{-1})

In Fig. 8.1 the local fluid velocity v (m s^{-1}) is plotted as a function of the local coordinate x (m). According to this figure and to Eq. (8.1) the shear stress τ is assumed to be positive in the direction of decreasing fluid velocity.

Newton's equation for shear stress may also be written as

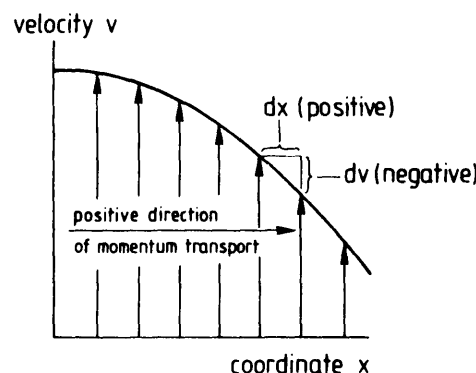


Fig. 8.1 Explanation of shear stress in fluids (corresponds to Fig. 7.1).

$$\tau = -\nu_t \rho \frac{dv}{dx} \quad (\text{N m}^{-2}) \quad 8.2$$

with

$$\nu_t = \frac{\eta_t}{\rho_t} \quad (\text{m}^2 \text{s}^{-1}) \quad 8.3$$

in which

$$\begin{aligned} \nu_t &= \text{kinematic viscosity} & (\text{m}^2 \text{s}^{-1}) \\ \rho_t &= \text{density of the fluid} & (\text{kg m}^{-3}) \end{aligned}$$

Table 8.2 gives the values of η_t , ν_t and ρ_t for water and air, the basic substances of life and thus biotechnology.

The dynamic viscosity of real Newtonian fluids is a constant dependent only of pressure and temperature. All fluids for which η also depends on shear stress, time, elasticity and other parameters are classified as non-Newtonian (see Section 7.1). Mycelial cell suspensions or very thick cell suspensions are typical examples of biotechnological fluids which do not obey Newton's law. For all practical purposes, however, most of the other biotechnological fluids can be considered Newtonian. Furthermore, from an engineering point of view, the existing relations for non-Newtonian behavior are not yet very helpful in describing fluid flow in technical equipment. Therefore, in this chapter only Newtonian fluids will be considered.

The fluid flow can be divided into two types, i.e., laminar and turbulent flow, the difference being that in the first case shear stresses in the fluid are predictable from velocity gradients, but in the latter they are not. This means that the "theory" of turbulent flow relies strongly on empirical

Table 8.2 Dynamic and kinematic viscosity and density of water and air at a pressure of 10^5 N m^{-2} (= 1 bar) and a temperature of 300 K

	ν_t ($\text{m}^2 \text{s}^{-1}$)	η_t (N s m^{-2})	ρ_t (kg m^{-3})
Water	0.857×10^{-6}	0.857×10^{-3}	1000
Air	0.158×10^{-4}	0.186×10^{-4}	1.18

knowledge made generally applicable by scientific reasoning. Hinze (1959) defines turbulent flow as follows: "Turbulent fluid motion is an irregular condition of flow in which the various quantities show a random variation with time and space coordinates, so that statistically distinct average values can be discerned." For instance, average time-averaged shear stress, used later, refers to this situation. Turbulence can be generated by friction forces at solid walls, e.g., impellers, or by the flow of layers of fluids with different velocities past or over one another. As turbulence concerns a situation common in bioreactors, much attention will be given to it.

For the rational design and scale-up of bioreactors the shear sensitivity of biocatalysts should be known quantitatively. This certainly is essential for biocatalysts known to be very fragile, e.g., animal cells. Such information is necessary for each single biocatalyst species which is fragile because the characteristic data can vary considerably from one to the other. Since there is still relatively little information of this kind available in the literature, systematic experiments are usually the only way to collect quantitative data on the influence of shear on a particular biocatalyst. Although these experiments may be rather difficult in many cases, the general strategy is clear (Märkl and Bronnenmeier, 1985). The key parameter measured for quantification of shear effects should be closely related to the aim of the technical process under investigation, for instance, cell viability, cell growth, formation rate or quality of the desired product, yield coefficients, overall biocatalyst productivity and so on. Secondary parameters like release of intracellular material or microscopically obtained morphological data may be very helpful, but they can be misleading when their relation to the direct process aim is not investigated. Furthermore, separation of the influence of damage due to shear and transport effects, like mass and heat transfer limitations, is important as well.

Meijer (1989) gives a schematic representation of a general experimental procedure to determine the shear sensitivity of biocatalysts (Fig. 8.2). As can be seen, various components can contribute to the shear exerted on a biocatalyst in a bioreactor. The overall effect, damage, has many manifestations which can each be quantified by one or more methods. The outcome of the experiment is usually compared with the results of a low-shear experiment. The same author (Meijer, 1989) also expresses the opinion that shear sensitivity data should preferably be collected in a small-scale system that is a down-scaled version of the production system. Therefore, if it is the intention to develop a large-scale process based on an impeller-stirred tank, his recommended method would be to collect data in a small impeller-stirred tank. This author recognizes the disadvantage of the poorly defined and irregular shear levels in such stirred systems, but data collected in a device with well-defined and constant shear levels, on the other hand, usually require an awkward translation to the practical situation. Probably the best

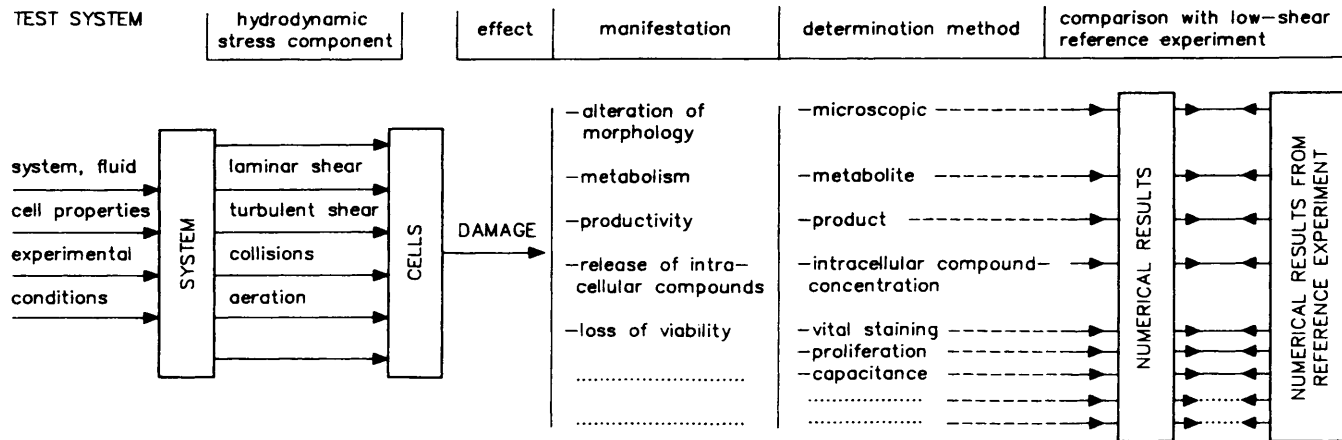


Fig. 8.2 Schematic representation of a general experimental procedure to determine shear sensitivity of biocatalysts. (Adapted from Meijer, 1989.)

approach is to analyze the available shear devices and damage measuring methods for each particular biocatalyst and process aim. An overview of the former two, devices and methods, with examples of the latter two, biocatalyst and aim, is given in the next paragraphs.

8.2 The stirred vessel

8.2.1 Introduction

The standard fermenter (Fig. 8.3) has been and still is the workhorse of the bioreactors used in biotechnology. Consequently, the practical experience with these stirred vessels is great and thus it is desired to use them also for fragile biocatalysts, despite the obvious disadvantage of poorly defined, irregular and often high shear levels. Many studies aiming at the determination of the fragility of biocatalysts have therefore been executed in stirred vessels. In their extensive review, Märkl and Bronnenmeier (1985) give many examples concerning microbial cells. An extensive study on the kinetics and mechanism of shear inactivation of the enzym lipase in a stirred tank has been reported by Lee and Choo (1989). Van Ginkel et al. (1983), among others, studied the effect of stirring on an immobilized biocatalyst. Poncelet and Neufeld (1989) report on the disruption of microcapsules in a stirred vessel as a model and starting point to examine the effects of shear

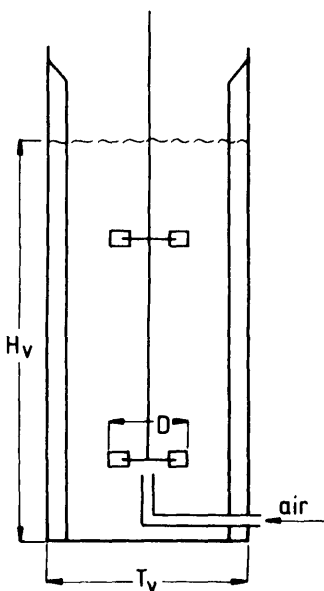


Fig. 8.3 The standard fermenter (same as Fig. 1.3).

on a variety of biological systems. Detailed information and references to many other corresponding studies can be found in these references.

Here attention is focused on animal cells, as shear deterioration is more important for this type of cell. A detailed analysis of the hydrodynamic effects on anchorage-dependent animal cells attached to microcarriers in stirred vessels can be found in Cherry and Papoutsakis (1986) and Croughan et al. (1987 and 1989). Animal cells on microcarriers are especially susceptible to shear due to the lack of a protective cell wall, the relatively large size of animal cells ($\sim 20 \mu\text{m}$, Table 8.1) and the lack of individual cell mobility. Attached cells cannot freely rotate or translate and accordingly cannot reduce the net forces and torques experienced in the shear fields of a stirred vessel.

The purpose of stirring the fluid in a bioreactor is threefold. Stirring first is required to keep solid biocatalysts from settling out and second to assure a homogeneous environment for the biocatalyst, i.e., a continuous, adequate supply of substrates. In biocatalytic reactions in which oxygen is consumed, stirring also is used to improve the oxygen transfer from the gas to the liquid phase. In order to reach these goals, certainly the latter two, the stirrer speed usually should be so high that the fluid flow will be turbulent. Analysis of turbulent flow fields with respect to shear is therefore essential and will be discussed also.

8.2.2 The integrated shear factor

Croughan et al. (1987) correlate the growth of anchorage-dependent animal cells among other with an integrated shear factor ISF (s^{-1}) as given by

$$ISF = \frac{2\pi N D}{T_v - D} \quad (\text{s}^{-1}) \quad 8.4$$

with

N	= stirrer speed	(s^{-1})
D	= stirrer diameter	(m)
T_v	= vessel diameter	(m)

The integrated shear factor is a measure of the strength of the shear field between the impeller and vessel wall. Fig. 8.4 shows that above an ISF of about 19 s^{-1} the growth of animal cells on microcarriers rapidly drops.

The data in Fig. 8.4 concern stirred vessels with volumes of 0.25×10^{-3} and $2 \times 10^{-3} \text{ m}^3$ and the ISF may thus have some usefulness with respect to scale-up, especially as this factor is very easy to calculate. However, the

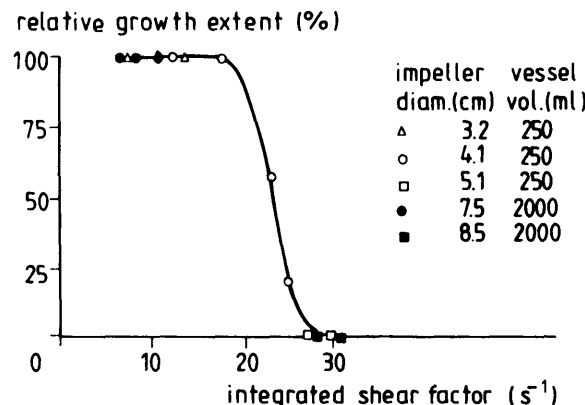


Fig. 8.4 Relative growth extent of FS-4 animal cells on microcarriers as a function of the integrated shear factor. (Adapted from Croughan et al., 1987.)

experimental basis only concerns one set of data on lab scale and no easy incorporation into a mechanistic model is possible. Much more work is therefore needed to establish the real usefulness of this factor for other biocatalysts and for rational design and scale-up.

8.2.3 The time-averaged and maximum shear rate

The same authors (Croughan et al., 1987) also correlate growth with "time-averaged" shear rate $\dot{\gamma}_{ave}$ (s^{-1}) in the region of the reactor with a radius larger than the stirrer radius $0.5 D$ (m). For an unbaffled vessel operated in the turbulent regime they derive $\dot{\gamma}_{ave}$ to be

$$\dot{\gamma}_{ave} = \frac{113.1 N D^{1.8} (T_v^{0.2} - D^{0.2}) \left(\frac{D_f}{D}\right)^{1.8}}{T_v^2 - D^2} \quad (s^{-1}) \quad 8.5$$

with

T_v = vessel diameter (m)

D_f = diameter of the forced vortex zone (m)

The change from laminar to turbulent flow occurs at a Reynolds number Re of about 1000 (Nagata, 1975). The Reynolds number for the bulk flow in a stirred vessel is given by:

$$Re = \frac{N D^2 \rho_l}{\eta_l} \quad (-) \quad 8.6$$

D_f , can be estimated according to Croughan et al. (1987) from:

$$\frac{D_f}{D} = \frac{0.625 Re}{625 + Re} \quad (-) \quad 8.7$$

For geometrically similar systems operated at high Reynolds numbers [$Re \gg 625$, leading to $D_f/D = 0.625$ according to Eq. (8.7)], Eq. (8.5) reduces to the form

$$\dot{\gamma}_{ave} = c N \quad (s^{-1}) \quad 8.8$$

where the constant c takes on a value of 2.4 for a D/T_v ratio of 0.5. This is the same form of equation as found for the shear rate in the impeller region for fluids agitated in the laminar regime (Metzner et al., 1961):

$$\dot{\gamma} = 10 N \quad (s^{-1}) \quad 8.9$$

From the data given by Van 't Riet and Smith (1975) a maximum shear rate in the trailing vortex of the impeller can be determined for both the laminar and turbulent regime. From this case a maximum shear rate $\dot{\gamma}$ of about 100 N and a minimum of about 50 N can be found. This maximum value is much higher than the average value found from Eq. (8.8).

The same data on relative growth extent of FS-4 cells on microcarriers (Fig. 8.4) can be plotted as a function of the average shear rate $\dot{\gamma}_{ave}$ as calculated from Eq. (8.5) (Fig. 8.5). As in Fig. 8.4, a sharp drop in growth occurs at a certain point, in this case at a critical $\dot{\gamma}_{ave}$ of about $2.5 s^{-1}$. Similar results were found for the maximum cell concentration of chicken embryo fibroblasts grown on microcarriers with a critical $\dot{\gamma}_{ave}$ of about $7 s^{-1}$. For geometrically similar systems the $\dot{\gamma}_{ave}$ is proportional to N only. A similar figure therefore will result from a plot for Eq. (8.9) or for $\dot{\gamma} = 100 N$, the maximum shear rate in the trailing vortex.

Croughan et al. (1987) show that if one considers the hydrodynamic forces which arise solely from the spatial gradients in (time-averaged) fluid velocity, then the maximum shear stress τ_{max} ($N m^{-2}$) on a microcarrier surface can be estimated by

$$\tau_{max} = 3 \eta_l \dot{\gamma} \quad (N m^{-2}) \quad 8.10$$

If we substitute for η_l the value of $0.857 \times 10^{-3} N s m^{-2}$ for water and for $\dot{\gamma}$ the average shear rate, $\dot{\gamma}_{ave} = 7 s^{-1}$, a $\tau_{max} = 0.018 N m^{-2}$ is calculated.

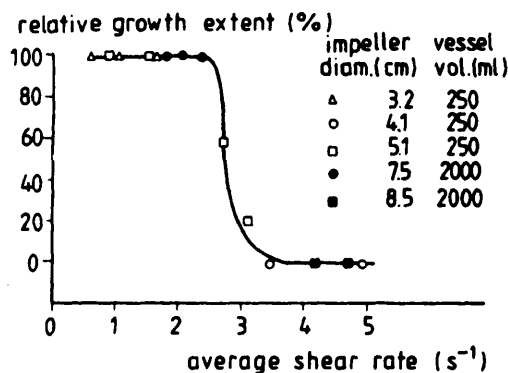


Fig. 8.5 Relative growth extent of FS-4 animal cells on microcarriers as a function of the average "time-averaged" shear rate. (Adapted from Croughan et al., 1987.)

This value is more than an order of magnitude smaller than the value of 0.65 N m^{-2} usually mentioned for animal cells on microcarriers (Croughan et al., 1987, 1989, and refs. cited therein). This indicates that the average shear rate is not the single cause of cell death. The maximum shear stress in the trailing vortex, on the other hand, is on the order of magnitude $0.1\text{-}1 \text{ N m}^{-2}$.

The similarity of the $\dot{\gamma}_{ave}$, ISF and shear rate in the trailing vortex results from the fact that for geometrically similar systems all three are proportional to the rotation rate N of the impeller. Also for the laminar regime [Eq. (8.9)] and for the maximum shear rate in the trailing vortex, this is valid. The data of Croughan et al. therefore cannot discriminate between these models. Like the ISF , the time-averaged shear-rate could be a convenient scale-up parameter, even though there is no direct link with damaging shear stress levels. Croughan et al. (1987) do not deny however, that the good correlations are not coincidental but indicative of dynamic phenomena and therefore recommend a more extensive analysis of the role of time-average shear rates.

8.2.4 Other shear rate models

Croughan et al. (1987) give an equation for the maximum time-averaged shear rate $\dot{\gamma}_{max}$ for the jet off the impeller based on impeller tip speed v_{tip} (m s^{-1}):

$$\dot{\gamma}_{max} = c' v_{tip} \quad (\text{s}^{-1}) \quad 8.11$$

and

$$v_{tip} = \pi N D \quad (\text{m s}^{-1}) \quad 8.12$$

where c' (m^{-1}) is a constant with a value of about 40 m^{-1} for a flat-blade impeller. In their paper, Croughan et al. (1987) plot the relative growth of the FS-4 cells on microcarriers versus impeller tip speed (Fig. 8.6). In contrast to the ISF and time-averaged shear rate, this figure shows that cell growth on different scales does not correlate with impeller tip speed. Maximum cell growth or zero cell growth can be observed at the same tip speed, depending on the size of the vessel. The impeller tip speed, or this maximum time-averaged shear rate, thus does not appear to play a fundamental role in determining in this case whether there are detrimental shear effects.

In some stirred vessels, however, very high maximum time-averaged shear rates may occur in a region of close clearance between the rotating impeller and a stationary vessel component: for instance, if there is a close clearance between the impeller and vessel wall. The tangential flow profile in this region may periodically assume a character similar to the flow between concentric rotating cylinders. The maximum tangential shear rate may then be estimated (Croughan et al., 1989) from the flow profile between concentric rotating cylinders:

$$\dot{\gamma}_{max} = \frac{4\pi N T_v^2}{T_v^2 - D^2} \quad (\text{s}^{-1}) \quad 8.13$$

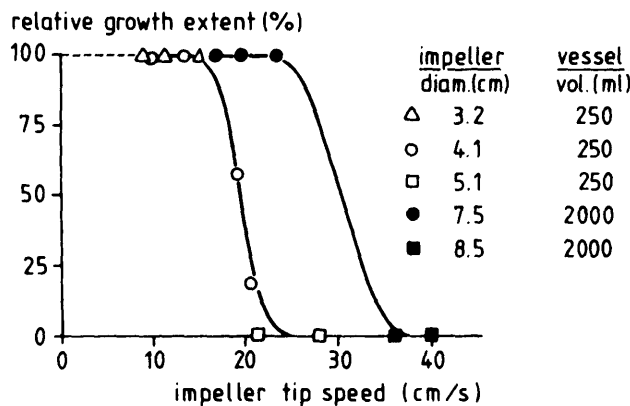


Fig. 8.6 Relative growth extent of FS-4 animal cells on microcarriers versus impeller tip speed. (Adapted from Croughan et al., 1987.)

In this type of vessel, if it contains a medium of high viscosity, maximum time-averaged shear fields at the level of cell-damaging shear stresses are likely. Croughan et al. (1989) investigated this and indeed found that the net growth of FS-4 cells on microcarriers was lower in such a bioreactor with very high maximum time-averaged shear fields when the maximum time-averaged shear stress [calculated by Eqs. (8.13) and (8.10)] was 0.9 N m⁻², i.e., larger than the critical shear of 0.65 N m⁻².

8.2.5 Boundary layer shear forces

Relatively large areas of high shear rate are expected in the boundary layers around the solid objects submerged in the stirred vessel. The moving impeller would be expected to have the highest velocity relative to the liquid and Cherry and Papoutsakis (1986) have analyzed it in detail to characterize the general effect of boundary layer shear forces, again, on animal cells on microcarriers, taking as an example the system specified in Table 8.3.

Table 8.3 Representative microcarriers reactor specification

Liquid		
Volume	V	10^{-3} m ³
Density	ρ_l	10^3 kg m ⁻³
Viscosity	η_l	0.7×10^{-3} N s m ⁻²
Microcarrier beads		
Shape		smooth spheres
Radius	R_p	75 μm
Density	ρ_p	1030 kg m ⁻³
Concentration		
- dry basis		5 kg m ⁻³
- hydrated		7 vol %
Impeller		
Configuration		4 rectangular blades at 45° angle
Diameter	D	0.08 m
Blade width	d_s	0.03 m
Leading edge radius		10^{-3} m
Rotational speed	N	1 s ⁻¹
Tip speed	v_{tip}	0.25 m s ⁻¹

Source: Adapted from Cherry and Papoutsakis, 1986.

As a first approximation marine and angled flat impeller blades can be modelled as stationary flat plates with fluid moving over them. The Reynolds number Re (-) for transition from laminar to turbulent flow over a flat plate is about 3×10^5 (Schlichting, 1979) with

$$Re = \frac{\rho_i v_\infty L}{\eta_i} \quad (-) \quad 8.14$$

in which

v_∞	= free fluid velocity along the plate	$(m s^{-1})$
L	= distance along the plate	(m)
η_i	= liquid viscosity	$(N s m^{-2})$

Taking $v_\infty = v_{tip} = 0.25 \text{ m s}^{-1}$ and substituting this with the appropriate values from Table 8.3 in Eq. (8.14) yields for Re about 11×10^3 ; thus a laminar boundary layer can be expected. However, Schlichting (1979) states that impeller rotation can considerably reduce the Reynolds number for transition. Because of this, Cherry and Papoutsakis (1986), among others, consider both laminar and turbulent boundary layers.

In the laminar case the boundary layer thickness δ_i (m), defined as the distance from the impeller surface at which the fluid velocity reaches 99% of the free fluid velocity v_∞ ($m s^{-1}$), is (Schlichting, 1979)

$$\delta_i \approx 5 \sqrt{\frac{\eta_i}{\rho_i} \frac{L}{v_\infty}} \quad (m) \quad 8.15$$

For the example from Table 8.3 this means:

$$\delta_i \approx 8.3 \times 10^{-3} \sqrt{L} \quad (m) \quad 8.16$$

in which v_∞ was taken as the impeller tip speed $v_{tip} = 0.25 \text{ m s}^{-1}$. The influence of the microcarriers is neglected, as Einav and Lee (1973) have shown that 4 and 6 vol % suspensions of neutrally buoyant spheres do not change the boundary layer shape or development from that predicted for "clean" fluids.

The boundary layer becomes as thick as the diameter of a microcarrier ($150 \mu\text{m}$) at about 0.33 mm from the leading-edge [Fig. 8.7 and Eq. (8.16)]. Cherry and Papoutsakis (1986) arbitrarily say that the boundary layer must be at least three times the microcarrier diameter in order not to be com-

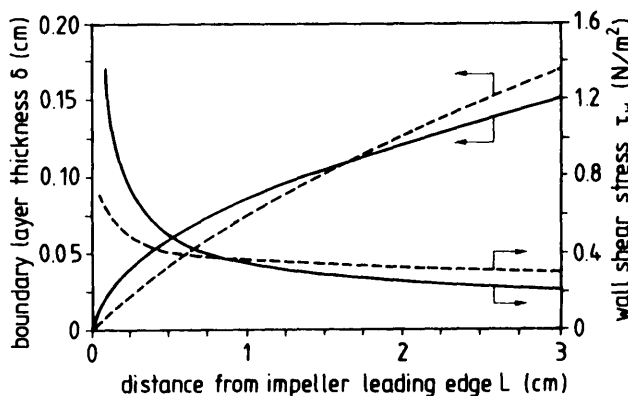


Fig. 8.7 Boundary layer thickness and shear stress on the impeller for the system specified in Table 8.3. —— laminar, ---- turbulent. Arrow indicates microcarrier diameter. (Adapted from Cherry and Papoutsakis, 1986.)

pletely disrupted by the presence of a bead, the corresponding distance being about 3 mm from the leading edge. At the trailing edge of the 3-cm-wide blade the boundary layer thickness is 1.5 mm, or about 10 bead diameters.

Within the boundary layer the highest shear stress occurs at the solid surface. This laminar wall shear stress τ_{wl} ($N\ m^{-2}$) can be calculated by

$$\tau_{wl} = 0.332 \eta_l v_\infty \left(\frac{v_\infty}{\frac{\eta_l}{\rho_l} L} \right)^{0.5} \quad (N\ m^{-2}) \quad 8.17$$

in which 0.332 is the slope of the dimensionless velocity profile at the wall (Schlichting, 1979). Substituting the appropriate values from Table 8.3 with $v_\infty = v_{tip}$ gives

$$\tau_{wl} = 3.5 \times 10^{-2} L^{-0.5} \quad (N\ m^{-2}) \quad 8.18$$

At the position (3 mm) where the boundary layer is three microcarrier diameters thick ($\delta_l = 0.45$ mm), the shear stress calculated is $0.64\ N\ m^{-2}$, which is on the order of shear stresses at which damage to the cells in principle can occur. Over the remainder of the blade the wall shear stress gradually decreases.

For turbulent boundary layers the formulae for boundary layer thickness δ_t (m) and wall shear stress τ_{wl} (N m⁻²) are (Schlichting, 1979):

$$\delta_t = 0.37 L \left(\frac{\rho_t v_\infty L}{\eta_t} \right)^{-0.20} \quad (\text{m}) \quad 8.19$$

and

$$\tau_{wl} = 0.029 \rho_t v_\infty^2 \left(\frac{\rho_t v_\infty L}{\eta_t} \right)^{-0.20} \quad (\text{N m}^{-2}) \quad 8.20$$

Substituting the appropriate values from Table 8.3 with $v_\infty = v_{tip} = 0.25 \text{ m s}^{-1}$ gives

$$\delta_t = 0.029 L^{0.80} \quad (\text{m}) \quad 8.21$$

and

$$\tau_{wl} = 0.14 L^{-0.20} \quad (\text{m}) \quad 8.22$$

In Fig. 8.7 these functions are compared to their laminar equivalents. It is clear that for most of the impeller blade the laminar and turbulent wall shear stress do not differ very much from each other for this particular situation and are below the critical shear stress value where damage can be expected.

In addition to a number of boundary layer forces (Table 8.4), which are qualitatively analyzed by Cherry and Papoutsakis (1986), the shear field in the boundary also causes the bead to rotate. Assuming Couette flow (linear velocity gradient), the magnitude of the average and maximum shear stress on the rotating bead can be estimated (from Cherry and Papoutsakis, 1986):

$$\tau_{ave} = \frac{1}{2} \eta_t \dot{\gamma} \quad (\text{N m}^{-2}) \quad 8.23$$

and

$$\tau_{max} = 3 \eta_t \dot{\gamma} \quad (\text{N m}^{-2}) \quad 8.24$$

respectively, where $\dot{\gamma}$ is the shear rate in the fluid in the absence of the microcarrier. For a linear velocity gradient of 0.25 m s⁻¹ (impeller tip speed)

Table 8.4 Boundary layer forces

Type of Force	Resultant bead motion relative to surface
Fluid drag	Parallel, normal and/or rotational
Gravity and buoyancy	Normal
Effect of pressure gradients ^a	Parallel, and/or normal
Saffman lift force	Normal
Added mass effect	Parallel
Bassett force	Parallel
Magnus force	Normal

^a Important only in turbulent boundary layers
Source: Adapted from Cherry and Papoutsakis, 1986.

over a boundary layer of 10^{-3} m (average thickness for the example, see Fig. 8.7), $\gamma = 0.25/10^{-3} = 250 \text{ s}^{-1}$. The average and maximum shear stress thus calculated for water with Eqs. (8.23) and (8.24) are 0.1 and 0.6 N m^{-2} , the latter being close to the critical shear stress at which cell damage can be expected.

Clearly, the maximum shear stress calculated for both wall shear stress and rotating-shear stress are of the order of magnitude of the critical shear stress at which damage is reported to occur to animal cells. Increase of v_{tip} and η_i can easily bring the value above that reported for damage. Even though no experimental data are reported yet, it certainly is a factor which should be reckoned with in the scale-up and design of bioreactors for growth of cells, in particular animal cells on microcarriers.

8.2.6 Smallest turbulent eddy length

The liquid flow in most stirred vessels is at least locally turbulent, especially at large scale and at relatively high impeller tip speed. If the scale of the smallest turbulent eddies is sufficiently larger than the biocatalyst particles, the particles follow the local flow pattern because most solid biocatalysts, except those immobilized onto dense carriers, are only slightly denser than the reaction medium. The velocity difference between streamlines and biocatalyst will thus be small, except during intermittent brief periods of acceleration when the biocatalyst enters a new eddy. Turbulent eddies of the same size as the biocatalyst or smaller, however, may affect its performance in several possible ways. For sufficiently high bulk flow Reynolds numbers, the smallest eddies exist in a state of isotropic equilibrium. (Croughan et al., 1987). The size of these smallest eddies can then be estimated by the Kolmogorov length scale λ (m) as given by

$$\lambda = \left(\frac{V_l^3}{\epsilon_*} \right)^{0.25} \quad (m) \quad 8.25$$

where ϵ_* is the local power dissipation per unit mass (W kg^{-1}). The size of the smallest eddies decreases with an increase in power input.

Average values of ϵ_* , $\bar{\epsilon}_*$, can be calculated from the stirrer power consumption if the impeller geometry and operating conditions are known. The stirrer power consumption P_s (W) is given by Eq. (14.4) as

$$P_s = N_p \rho_l N^3 D^5 \quad (\text{W}) \quad 14.4$$

in which N_p = impeller power number (-) (see Chapter 14). Then the $\bar{\epsilon}_*$ value can be calculated with V_l as the liquid phase volume as:

$$\bar{\epsilon}_* = \frac{P_s}{\rho_l V_l} = \frac{N_p N^3 D^5}{V_l} \quad (\text{W kg}^{-1}) \quad 8.26$$

In the belief that Kolmogorov's theories can be applied to microcarrier cultures, Croughan et al. (1987) have investigated the role of eddy size on, among others, the relative growth extent of the FS-4 cells (Fig. 8.8).

Detrimental effects appear to come into play when the average Kolmogorov

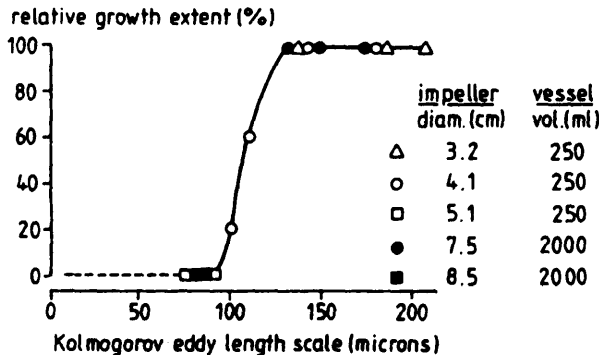


Fig. 8.8 Relative growth of FS-4 cells on microcarriers as a function of the Kolmogorov length scale for the smallest turbulent eddies. (Adapted from Croughan et al., 1987.)

length scale drops below about 100 μm , i.e., about half of the average microcarrier diameter of 185 μm . As expected, excessive agitation apparently leads to the formation of eddies of a small enough size but large enough energy to cause damage to cells.

To determine whether the correlation of cell damage with eddy length has a fundamental basis, Croughan et al. (1987) estimate whether the potentially damaging eddies can produce shear stresses strong enough to indeed damage the cells. With the annotation that only very rough estimates can currently be made, they calculate shear stresses of the order of 0.1 N m^{-2} . These values are only somewhat lower than the critical shear stress at which damage is reported to occur. In order to help to elucidate the mechanisms of damage further, Croughan et al. (1987) set up a model leading to the following equation for the specific death rate q_d (s^{-1}):

$$q_d = k_* \left(\frac{\bar{\epsilon}_*}{v_i^3} \right)^{0.75} \quad (\text{s}^{-1}) \quad 8.27$$

with k_* ($\text{m}^3 \text{s}^{-1}$) the specific death rate constant dependent on cell and microcarrier properties, and reasonably constant for geometrically similar systems.

They apply this model to describe the specific death rate q_d of various cell lines as a function of the average power input per unit mass $\bar{\epsilon}_*$ (Fig. 8.9). As predicted by Eq. (8.27), the slope of 0.75 very nearly matches the slopes for all three sets of data, and the authors conclude: "If the turbulent eddy model is valid, scale-up at constant power input per unit volume should not lead to detrimental hydrodynamic effects."

To further establish the fundamental basis, Croughan et al. (1989) also investigated the effects of viscosity, excluding cell damage from time-averaged flow fields. According to Eq. (8.27), an increase in viscosity should lead to a decrease in specific cell death rate. Similar to Fig. 8.9, the authors plot first the relative growth rate of FS-4 cells as a function of Kolmogorov eddy length for various viscosities (Fig. 8.10). Again, detrimental effects of agitation come into play when the average Kolmogorov length scale falls below about two-thirds (130 μm) of the microcarrier diameter (185 μm). Fig. 8.11 shows the plot for the specific death rate versus the eddy concentration group $(\bar{\epsilon}_*/v_i^3)^{0.75}$ in Eq. (8.27) for two different vessels with the same impeller. The difference in slope, i.e., k_* , for the two geometries is, according to the authors, not statistically significant within a 95% confidence interval. This further supports their hypothesis that the small(est) viscous dissipation eddies are the damaging ones as these depend only on the local power dissipation rate and kinematic viscosity, and not on the

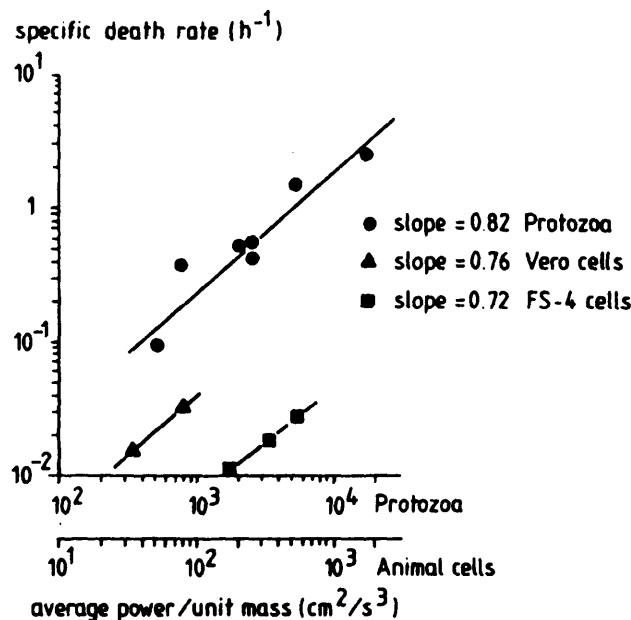


Fig. 8.9 Specific death rate versus average power per unit mass for FS-4 cells on microcarriers, Vero cells on microcarriers and freely suspended protozoa. (Adapted from Croughan et al., 1987.)

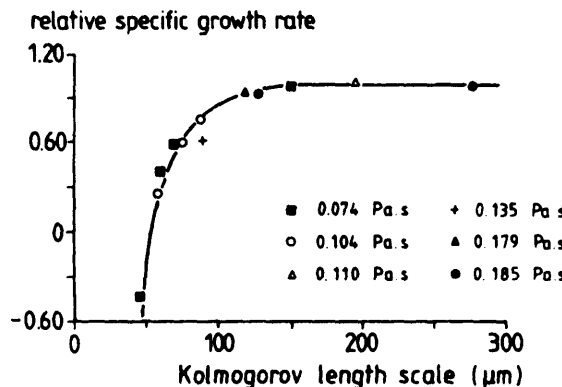


Fig. 8.10 Relative net growth versus Kolmogorov eddy length. (Adapted from Croughan et al., 1989.)

vessel geometry. This in contrast to the larger energy-containing eddies, which are highly dependent on reactor geometry. Nonetheless, experiments have been performed with only a limited number of vessel geometries. For generalization, future experiments should investigate a wider range of geometries and quantitative information on local rates of power dissipation should be incorporated.

As indicated by the data in Fig. 8.11, a 3-fold increase in viscosity can lead to more than a 10-fold reduction in the rate of hydrodynamic cell death. Moderate increases in viscosity can thus lead to very significant reductions in turbulent cell death, according to Eq. (8.27). To see the importance of other reactor variables Eqs. (8.25) and (14.4) can be combined to

$$\lambda = \left(\frac{v_i^3 V}{N_p N^3 D^5} \right)^{0.25} \quad (\text{m}) \quad 8.28$$

in which the reactor volume V can be considered fixed by production requirements. N_p varies in a relatively narrow range for the commonly occurring values of Re , so the 0.25 power of it is ineffectual in significantly changing eddy size. In addition to viscosity (v_i) the important factors to change eddy size are thus impeller speed N and diameter D .

Critical assessment of this application of Komogorov's theory by Croughan et al. (1987 and 1989) yields a weak point (W.A. Berverloo personal com-

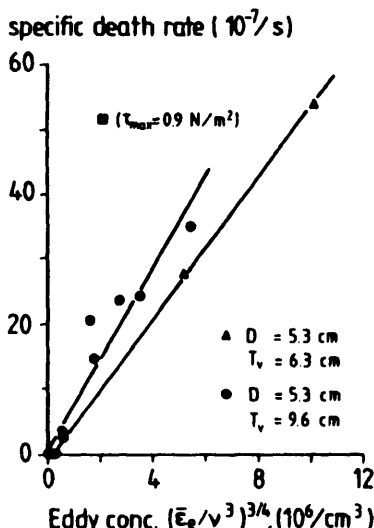


Fig. 8.11 Specific death rate versus concentration of eddies in viscous dissipation regime. (Adapted from Croughan et al., 1989.)

munication). The specific death rate constant k_s in Eq. (8.27) is not dimensionless. This indicates, that k_s depends on one or more unspecified dimensional material properties which is not very satisfactory. Therefore an attempt to make a dimensional analysis of a model of the killing process will be given here.

It is assumed that a cell on a microcarrier is hit by hydrodynamic blows with a frequency proportional to the angular velocity of the "Kolmogorov"-fluctuations $\Omega_k = (\epsilon_s / v)^{0.5}$. This means that:

$$q_d = k_1 \Omega_k = k_1 \left(\frac{\epsilon_s}{v} \right)^{0.5} \quad (s^{-1}) \quad 8.29$$

The dimensionless number k_1 is reversely proportional to the number of hydrodynamic blows needed to kill a cell. If this number would be constant, q_d would be proportional to $\epsilon_s^{0.5}$. Croughan et al. (1987) support the validity of Eq. (8.27) by measurements presented in Fig. 8.9. Apparently q_d is proportional to $\epsilon_s^{0.75}$. This means that k_1 is proportional to $\epsilon_s^{0.25}$ or reversely proportional to $\lambda = (v^3 / \epsilon_s)^{0.25}$ [Eq. (8.25)], the length scale of the Kolmogorov-fluctuations. The microcarrier size d_p , divided by λ is dimensionless, so:

$$q_d \left(\frac{v}{\epsilon_s} \right)^{0.5} = k_1 = k_2 d_p \left(\frac{\epsilon_s}{v^3} \right)^{0.25} \quad (s^{-1}) \quad 8.30$$

or

$$q_d = k_2 d_p \left(\frac{\epsilon_s^3}{v^5} \right)^{0.25} \quad (s^{-1}) \quad 8.31$$

As shown, Croughan et al. (1989) also investigated the validity of the viscosity influence predicted by their model. In Fig. 8.10 measured relative specific growth rates are related to λ and they claim that their results show no other viscosity dependence than by the Kolmogorov length scale λ . However, Eq. (8.31) can be written as:

$$q_d = \frac{k_2 d_p v}{\lambda^3} \quad (s^{-1}) \quad 8.32$$

In accordance with Eq. (8.32) the measurements presented in Fig. 8.10 would even fit better to the drawn line if the length scales were multiplied

with $v^{-0.33}$. Thus Fig. 8.10 supports the model presented here at least as well as the model of Croughan et al.

In Fig. 8.11 Croughan et al. show that the specific death rate is proportional to $\epsilon_v^{0.75}$ for two different vessels with the same impeller. According to these authors the difference in slope is statistically insignificant within a 0.95 confidence interval.

In Chapter 14 will be shown that ϵ_v is proportional to $N^3 D_i^5 / V$, with N (s^{-1}) the revolution rate and D_i (m) the diameter of the impeller. V (m^3) is the volume of the reactor. So:

$$q_d = \frac{k_3 N^{2.25} d_p D^{3.75}}{v^{1.25} V^{0.75}} \quad (s^{-1}) \quad 8.33$$

From Eq. (8.33) the influence of reactor design variables on the death rate q_d can be estimated. The model implies that a 10-fold increase in reactor volume would allow for a 1.6-fold increase in impeller diameter or a 2-fold increase in impeller speed. If reactors of different sizes are built geometrically similar (D_i^3/V is constant):

$$q_d = \frac{k_4 N^{2.25} d_p V^{0.5}}{v^{1.25}} \quad (s^{-1}) \quad 8.34$$

Eq. (8.34) implies that a 10-fold increase in reactor volume has to be compensated by a 1.7-fold decrease in impeller speed. Viscosity has a protecting influence. A 2.5-fold increase in kinematic viscosity allows for a 10-fold increase in reactor volume.

In summary, cells on beads are most affected by turbulence of a scale slightly smaller than the bead diameter, as this causes rotation or high local shear on the bead surface. The turbulent eddies may be made larger, and cell damage presumably reduced, by increasing viscosity, or reducing impeller diameter and speed. These principles will very likely also apply to other biocatalysts, in particular plant cells and animal cells in suspensions, although experimental evidence is even scarcer for these entities.

8.2.7 Collision damage

Turbulent eddies of the same size scale as the microcarrier separation may cause cell damage by promoting bead/bead collisions. Particularly in the case of animal cells on microcarriers this can lead to cell damage. It is easily conceivable that eddies the size of the interbead spacing can accelerate one

bead without disturbing another nearby. The two beads thus have significant relative velocity and a finite chance of a collision with an energy intensity sufficiently to damage the cells. Cherry and Papoutsakis (1986) also have analyzed this aspect and come up with a relation for the severity of collision (SC) ($J s^{-1}$) defined as the energy times the frequency of collision:

$$SC = c \pi \rho_p V_l^3 \frac{\left(\frac{A'}{6}\right)^{0.33}}{6(d_p)^{1.67}} \quad (J s^{-1}) \quad 8.35$$

in which

c	= constant	$(s^3 kg^{-1} m^{-1})$
ρ_p	= specific density of the particle (bead) phase	$(kg m^{-3})$
A'	= specific surface area of beads per volume of suspension	$(m^2 m^{-3})$
d_p	= particle (bead) diameter	(m)

Cherry and Papoutsakis (1986) emphasize that Eq. (8.35) is only valid if the size of the smallest eddies is of the order not only of the interbead spacing, but also of the bead size d_p .

The effect of d_p on the severity of collision may be hard to generalize because smaller beads are expected to result in more collisions of lower energy each. In any case, the cellular responses to frequency and energy are unlikely to be linear - if a certain blow kills the cell, hitting it twice as hard does not make it twice as dead - so the net effect is uncertain. It could be in either direction depending on the relative sensitivity to and the magnitude of frequency and energy terms.

Cells might also be damaged by a collision of the microcarrier with a solid object (impeller, baffles, etc.). Low-velocity collisions may result from a lift force on the bead moving it toward the impeller, gravitational settling or from turbulent velocity fluctuations that propel a bead against a surface. High-velocity collisions with the impeller or other parts of the reactor can occur when the blade advances through the fluid or the fluid flows around a fixed object. Particles flowing on a streamline (Fig. 8.12) that passes within one particle radius of the surface will collide with this surface, a process called interception (Davies, 1973). Inertia and increasing curvature of the streamlines magnify this interception process. Similar to the bead/bead collisions, Cherry and Papoutsakis (1986) derive a relation for the severity of collision with the impeller SC_i , which is of the form:

$$SC_i = \frac{c' \rho_p n_b N^3 D^4 d_p^4}{V} \quad (J s^{-1}) \quad 8.36$$

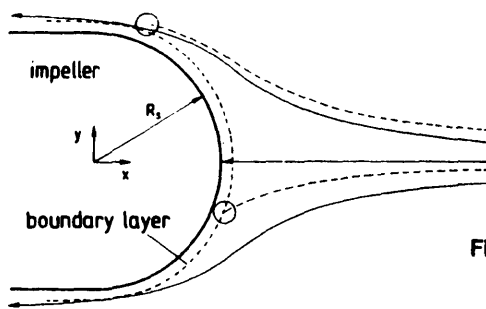


Fig. 8.12 Streamlines around impeller leading edge. (Adapted from Cherry and Papoutsakis, 1986.)

in which

$$\begin{aligned} c' &= \text{constant} & (\text{s}^3 \text{ kg}^{-1} \text{ m}^{-1}) \\ n_b &= \text{the number of impeller blades} & (-) \end{aligned}$$

Even though Cherry and Papoutsakis (1986) did not yet have data to support their reasoning, they speculate on the implication for reactor design. As Eq. (8.36) shows, severity of collision with the impeller is proportional to the cube of agitator speed and the fourth power of impeller diameter and bead diameter. Since tip speed v_{tip} equals $\pi N D$, note that there is also a third power dependence on tip speed:

$$SC_i = \frac{c'' \rho_p n_b v_{tip}^3 D d_p^4}{V} \quad (\text{J s}^{-1}) \quad 8.37$$

in which

$$c'' = \text{constant} \quad (\text{s}^3 \text{ kg}^{-1} \text{ m}^{-1})$$

Because the number of blades appears only as a first-order term, there would seem to be a major advantage to using more impeller blades of lesser diameter in order to reduce collision damage. However, as with bead/bead collisions in turbulence, the effect of collision severity as defined here on such aspects as cell viability or maximum cell density is certainly not linear, and may have even a minimum or maximum within the practical range of severity values. Variables such as impeller diameter, rotational speed and bead diameter affect both frequency and energy in the same direction and should show a simpler behavior. Note that this result may explain the apparently greater resistance to shear of animal cells growing free in suspension. The diameter difference of free cells and microcarriers is roughly a factor of 10, implying a 10,000 times difference in impeller collision severity. Clearly, more experimental studies, including nature of

hitting surface (smoothness, hardness), are necessary to quantify and generalize the collision damage theory, before suitability and applicability for bioreactor design has been proven.

8.2.8 Implications for reactor design

When single particle settling velocities are calculated with Eqs. (6.6-6.8) it appears that these are very low, of the order of 10^{-4} down to 10^{-7} m s^{-1} . (See also Cherry and Papoutsakis, 1986). This means maximum shear stresses smaller than 0.01 N m^{-2} , which is far below any shear stress reported to be damaging to any type of cell or biocatalyst in general. Keeping biocatalysts in suspension should thus not create problems from the point of view of shear sensitivity.

According to Cherry and Papoutsakis (1986), the primary reason for agitating tissue culture reactors is transfer of oxygen and maintaining homogeneity by minimizing variations throughout the reactor of dissolved oxygen and other nutrient concentrations or temperature. Generally speaking, this is the main reason for agitating a bioreactor. The average liquid velocity needed to give effective homogeneity can be estimated by requiring that the biocatalyst moves through the various areas of different conditions in an amount of time that is small compared to their biological response time. Cherry and Papoutsakis (1986) refer to papers concerning microbial cells from which a minimum response time of 2-3 seconds can be derived. Assuming that a 1 dm^3 bioreactor has a characteristic dimension of about 10 cm, the minimum liquid velocity needed to ensure apparent homogeneity is then of the order of 5 cm s^{-1} , which generally means that the bulk liquid flow is turbulent. As the scale increases, even if the minimum liquid velocity is kept the same, turbulence increases due to the increase in diameter. An analysis of shear and turbulence as given in this paragraph is thus generally essential to be able to rationally design and scale-up bioreactors meant for fragile biocatalysts.

As another reason for stirring enhanced oxygen supply was mentioned. Significant improvement can be accomplished by dispersion of the air bubbles in case of sparging, which is unavoidable if the size of the bioreactor increases. A tip speed of the impeller above about 2 m s^{-1} is needed for that [Eq. (6.2)]. The Reynolds number for the bulk flow in a stirred vessel is given by

$$Re = \frac{\rho_l N D^2}{\eta_l} \quad (-) \quad 8.38$$

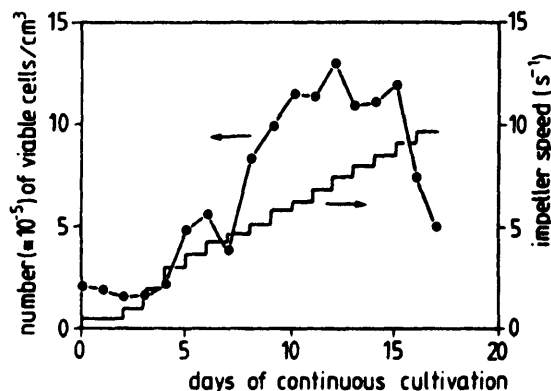


Fig. 8.13 Insect-cell density in a continuous culture at increasing stirrer speeds. (Adapted from Tramper et al., 1986.)

For a small fermenter (volume 1 dm³) with an impeller diameter of $D = 0.05$ m, a minimal tip speed of 2 m s⁻¹ means that the rotation speed N (s⁻¹) should at least be $13\text{ s}^{-1} = 780$ rpm. With a dynamic viscosity η , of 10^{-3} N s m⁻² and a density ρ , of 1000 kg m⁻³, Re can be calculated to be 6.7×10^4 , in other words turbulent flow. Several of the criteria derived in this chapter lead to shear stress values which are of the order of magnitude shown to be critical in various reports for both animal and insect cells (for overview see Tramper and Vlak, 1988, and references cited therein). Fig. 8.13, for instance, shows that insect cells die in a small stirred bioreactor (1.5 dm³) if the impeller stirrer speed is larger than about 9 s⁻¹. We can therefore conclude that stirring from the point of view of substantially improving the oxygen transfer by dispersion of air bubbles in animal and insect cell suspensions generally is impossible (Tramper et al., 1986). The attention should therefore be directed to bubble column and airlift type of bioreactors (Tramper et al., 1988). These will be discussed in the following section.

8.3 Bubble column

8.3.1 Introduction

In contrast to the impeller-stirred vessels, bubble column and airlift type of vessels have been used relatively very little as devices to determine and quantify the fragility of a biocatalyst in particular cells, even though they are of great interest for use as bioreactors for growth of fragile cells (Katinger and Scheirer, 1982). In fact, only three groups have studied and used a bubble column in this respect (Handa et al., 1989; Wudtke and Schugerl, 1987; Tramper et al., 1988; references cited therein). Handa et al.

(1989) particularly studied the effects of sparging on hybridomas and other mammalian cells in suspension culture. They found that damage of cells occurs especially during the bursting of the air bubbles at the suspension surface and that the nonionic surfactant Pluronic has a concentration-dependent protective effect. Wudtke and Schügerl (1987) investigated the fragility of insect cells using various methods, among others a bubble column. In agreement with the findings of Handa et al. (1989), these authors found that covering the suspension with a paraffin layer prevented the appearance of cell debris, indicating that the bubble bursting is indeed the damaging process. Quantitative relationships suitable for bioreactor design and scale-up are not given by these two groups.

8.3.2 Estimation of shear stresses

As stated at the end of the previous section, our incentive to study bubble columns and airlift type of bioreactors for growth of insect and other fragile cells stems from the finding that stirring from the point of view of maximum oxygen transfer is impossible, while supply of oxygen is just the crucial step at larger scales.

In early papers on this topic (Tramper and Vlak, 1988; Tramper et al., 1986) it is stated that insect cells repeatedly failed to grow in an airlift bioreactor, even though the estimated maximum shear stress associated with fluid flow was below the shear stress critical for growth of the cells. It could thus be concluded that the injection, the rising and/or the bursting of the air bubbles are responsible for a faster die-off rate than growth rate. To globally estimate the shear stresses which could be associated with each of these three factors and which an insect cell in principle could experience, Eq. (8.1) can be used:

$$\tau = -\eta_l \frac{dv}{dx} \quad (N m^{-2}) \quad 8.1$$

If it is arbitrary assumed that on one side of the cell the fluid velocity v is equal to that of a nearby air bubble and that on the other side it is zero, dv/dx can be calculated and from that with the dynamic viscosity η_l the shear stress τ . At the injector the velocity v_{bi} ($m s^{-1}$) of the air bubbles can be calculated from the volumetric airflow rate F_g ($m^3 s^{-1}$) and the inner diameter d_i (m) of the injector nozzle:

$$v_{bi} = \frac{F_g}{\frac{1}{4} \pi d_i^2} \quad (m s^{-1}) \quad 8.39$$

With a rather low airflow F_a of $1 \text{ dm}^3 \text{ h}^{-1}$ and a nozzle diameter of 1 mm , the shear stress calculated by means of Eqs. (8.1) and (8.39), substituting for the dynamic viscosity η , $10^{-3} \text{ N s m}^{-2}$ and for dx the insect cell diameter, i.e., $18 \mu\text{m}$, is about 20 N m^{-2} , which is an order of magnitude above the shear stress critical for insect cells to be damaged.

The velocity of a rising air bubble is of the order of 0.25 m s^{-1} (Heijnen and Van 't Riet, 1984). A similar calculation as above yields a shear stress of about 14 N m^{-2} , which again is above the critical value.

The situation of the bursting air bubble at the surface of the cell suspension is more complex. The air bubble forms a "hill" under the liquid surface (Fig. 8.14). As soon as the surface tension of the liquid film, forming the hill with the air bubble, becomes too small, this film will break and the fluid flows back to the bulk. The associated fluid velocity v_{lb} can be estimated by the so-called Culick equation (Havenbergh and Joos, 1983):

$$v_{lb} = 2 \left(\frac{\sigma_l}{\rho_l d_h} \right)^{0.5} \quad (\text{m s}^{-1}) \quad 8.40$$

The surface tension σ_l (N m^{-1}) and the thickness of the liquid film d_h (m) can be assumed to be of the order of $35 \times 10^{-3} \text{ N m}^{-1}$ and $40 \times 10^{-6} \text{ m}$, respectively. With $\rho_l = 1000 \text{ kg m}^{-3}$ it follows from Eq. (8.40) that $v_{lb} = 1.87 \text{ m s}^{-1}$. Substitution in Eq. (8.1) yields $\tau = 104 \text{ N m}^{-2}$, which, again, is far above the value critical for growth of insect and other animal cells to occur.

The above estimate of the shear stresses that an insect cell in theory experiences when sparging the suspension with air and arbitrary assuming that on one side of the cell the fluid velocity is zero and on the other side equal to that of a nearby air bubble, clearly indicates that all associated shear stresses are far above the critical value. The observation that not all cells are instantly broken can be explained by the fact that the critical value

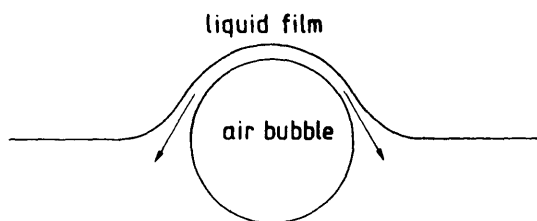


Fig. 8.14 Bursting of an air bubble.

of about 1 N m^{-2} (Tramper et al., 1986) applies to the situation where the cells are constantly exposed to this shear. In the case of sparging, high shear forces, possibly of the order as estimated above, are only momentarily working on the cells. Apparently the flexibility of cells is large enough to withstand most of these short "beatings."

8.3.3 Killing volume hypothesis

In order to be able to find correlations between bubble column design parameters and death rate of the cells, we have derived a model on the basis of the following two assumptions:

1. The loss of viability of the cells is a first-order process:

$$C'_x(t) = C'_x(0) e^{-k_d t} \quad (\text{kg m}^{-3}) \quad 8.41$$

in which

$$\begin{aligned} C'_x(t) &= \text{concentration of viable cells} && (\text{kg m}^{-3}) \\ k_d &= \text{first-order death-rate constant} && (\text{s}^{-1}) \end{aligned}$$

2. Associated with each air bubble, during its lifetime, is a hypothetical volume V_k (m^3) in which all viable cells are killed:

$$-V \frac{dC'_x}{dt} = n_b C'_x V_k = \frac{F_a}{\frac{1}{6} \pi d_b^3} C'_x V_k \quad (\text{kg s}^{-1}) \quad 8.42$$

with

$$\begin{aligned} V &= \text{volume of the bubble column} && (\text{m}^3) \\ n_b &= \text{number of air bubbles generated per second} && (\text{s}^{-1}) \\ F_a &= \text{airflow} && (\text{m}^3 \text{ s}^{-1}) \\ d_b &= \text{diameter of the air bubbles} && (\text{m}) \end{aligned}$$

Separation of variables, and integration assuming V_k to be constant in time, yields:

$$C'_x(t) = C'_x(0) e^{-\left(\frac{6F_a V_k}{\pi d_b^3 V} t\right)} \quad (\text{kg m}^{-3}) \quad 8.43$$

Combining Eqs. (8.35) and (8.36) gives:

$$k_d = \frac{6 F_g V_k}{\pi d_b^3 V} \quad (\text{s}^{-1}) \quad 8.44$$

or

$$k_d = \frac{24 F_g V_k}{\pi^2 d_b^3 T_v^2 H_v} \quad (\text{s}^{-1}) \quad 8.45$$

with T_v the diameter (m) and H_v the height (m) of the bubble column. In order for these equations to become useful, the dependence of V_k on F_g , d_b , T_v and H_v was experimentally determined (Tramper et al., 1986, 1988).

For example, Fig. 8.15 shows the results of the experiments in which only the height of the bubble column was varied and the viability of the insect cells was measured. Conversion of these data points into first-order death-rate constants results in Fig. 8.16, in which k_d is plotted as a function of the reciprocal height. A linear relationship is seen, which can be expected when Eq. (8.45) applies and V_k is independent of H_v . The latter means that the shear stresses associated with the rising of the air bubbles can be assumed to have a negligible damaging effect, a conclusion also reached by the group of Emery for hybridoma, myeloma and baby hamster kidney cells (Emery et al., 1987).

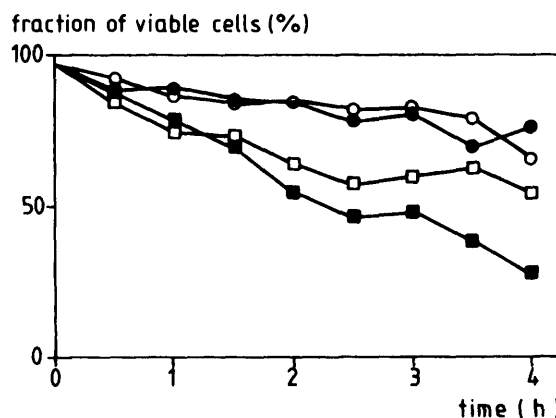


Fig. 8.15 Effect of bubble-column height on the viability of *Spodoptera frugiperda* insect cells in suspension (■, 8 cm; □, 16 cm; ●, 24 cm; ○, 32 cm). (Adapted from Tramper et al., 1986.)

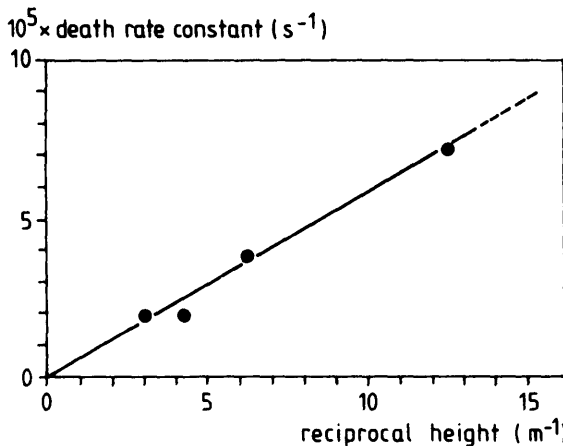


Fig. 8.16 First-order death-rate constant of *Spodoptera frugiperda* insect cells as a function of reciprocal bubble-column height. (Adapted from Tramper et al., 1986.)

The estimations of the various shear stresses already revealed that shear associated with the rising of air bubbles is relatively low in comparison to that associated with the injection of air bubbles into the medium and their bursting at the surface. With $d_b = 6$ mm, $T_v = 3.6$ cm and $F_g = 1.39 \times 10^{-6} m^3 s^{-1}$, V_k can be calculated at the applied heights from the corresponding k_d 's using Eq. (8.45). The average calculated hypothetical volume V_k is $4.6 \times 10^{-10} m^3$, which corresponds to a spherical volume with a diameter of about 1 mm.

Similarly, we have found that k_d is proportional to the airflow F_g and the reciprocal square to bubble-column diameter T_v . In other words, V_k is independent of F_g and T_v . Again, the calculated average V_k was about $4.6 \times 10^{-10} m^3$. Although experimentally much more difficult to establish, it has also been found (Tramper et al., 1988) that k_d is largely independent of the air-bubble diameter d_b (Fig. 8.17). This means that the hypothetical killing volume V_k is roughly proportional to d_b^3 (or the volume of the air bubble). Eq. (8.45) can thus be further reduced by introducing a specific hypothetic killing volume V'_k , that is, the hypothetic killing volume divided by the volume of one air bubble

$$V'_k = \frac{V_k}{\frac{1}{6} \pi d_b^3} \quad (-) \quad 8.46$$

Substitution in Eqs. (8.44) and (8.45) yields the very simple equation:

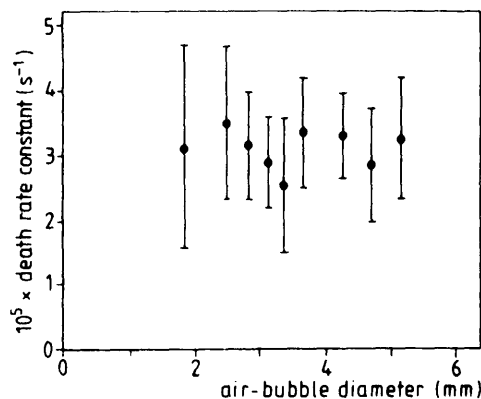


Fig. 8.17 Average death-rate constant of *Spodoptera frugiperda* insect cells in a bubble column as a function of the average air bubble diameter. (Adapted from Tramper et al., 1988.)

$$k_d = \frac{F_g V'_k}{V} = \frac{F_g V'_k}{\frac{1}{4} \pi T_v^2 H_v} \quad (\text{s}^{-1}) \quad 8.47$$

If V'_k is known, which can be measured very simply in a small bubble column (Tramper et al., 1986 and 1988), k_d can thus be easily calculated for each desired bubble column according to Eq. (8.47).

8.3.4 Implications for reactor design

For scale-up of fragile cell cultures, in which oxygen is supplied by sparging air through the suspension, it is important to correlate shear sensitivity with oxygen need of the cells. Based on a m^3 of reactor volume, the oxygen transfer rate OTR' ($\text{mol O}_2 \text{ m}^{-3} \text{ s}^{-1}$) can be written (see Chapter 11) as:

$$OTR' = k_{ot} A' (C_{ot}^* - C_{ot}) = OUR' C_x' \quad (\text{mol m}^{-3} \text{ s}^{-1}) \quad 8.48$$

with

k_{ot}	= oxygen transfer coefficient	(m s^{-1})
C_{ot}^*	= concentration of oxygen in the liquid when in equilibrium with air	(mol m^{-3})
C_{ot}	= actual oxygen concentration in the bulk liquid	(mol m^{-3})
C_x'	= concentration of viable cells	(kg m^{-3})
OUR'	= oxygen uptake rate of a kg of cells	$(\text{mol kg}^{-1} \text{ s}^{-1})$
A'	= specific surface area of the air bubbles	(m^{-1})

A' can also be written as:

$$A' = \frac{n'_b \pi d_b^2}{\frac{1}{4} \pi T_v^2 H_v} \quad (\text{m}^{-1}) \quad 8.49$$

with n'_b being the number of air bubbles present in the reactor

$$n'_b = \frac{F_g H_v}{\frac{1}{6} \pi d_b^3 v_{bw}} \quad (-) \quad 8.50$$

where v_{bw} is the rising velocity of the air bubbles relative to the vessel wall (m s^{-1}). Substitution in Eq. (8.49) gives:

$$A' = \frac{24 F_g}{\pi d_b^2 v_{bw} T_v^2} \quad (\text{m}^{-1}) \quad 8.51$$

From Eq. (8.48) the minimal specific surface area A'_{min} is obtained:

$$OUR' C'_x = k_{ol} A'_{min} (C_{ol}^* - C_{ol,min}) \quad (\text{mol m}^{-3} \text{s}^{-1}) \quad 8.52$$

with $C_{ol,min}$ being the minimum liquid oxygen concentration (mol m^{-3}) at which cells are able to grow.

Growth of cells in a continuous culture can be described by first-order kinetics:

$$C'_x(t) = C'_x(0) e^{k_g t} \quad (\text{kg m}^{-3}) \quad 8.53$$

with k_g the first-order growth rate constant (s^{-1}). In order for growth of insect cells to occur in a bubble column, k_d should be smaller than k_g

$$k_d < k_g \quad (\text{s}^{-1}) \quad 8.54$$

For designing a continuous culture of insect cells in a bubble column Eqs. (8.47–8.54) can be used. It should be stated, however, that the experimental validation was performed in bubble columns all smaller than 1 dm^3 . Experimental validations in larger columns are still to be done.

Inspection of the equations for k_d and A' [Eqs. (8.47) and (8.51)] reveals

that especially the height H_v of the bubble column and the oxygen tension in the gas (C_{ol}^*) are the parameters to adjust in order to meet the demands set by the minimum specific surface area needed to supply sufficient oxygen and by the fact that the growth rate should be faster than the death rate. The rising velocity v_{bw} and the diameter d_b of the air bubbles are not easy adjustable design parameters.

8.4 Shear devices

8.4.1 Laminar shear devices

Midler and Finn proposed in 1966 a constant shear device (Fig. 8.18) resembling a Couette viscometer to produce a well-defined shear stress in the laminar region in order to study effects of shear on biological systems. Since then Couette-type viscometers have been used in several studies aiming at determination of the effects of shear on fragile cells and cell aggregates (Thomas and Janes, 1987; Tramper et al., 1984), in particular animal cells (Tramper et al., 1986; Smith et al., 1987; Wudtke and Schügerl, 1987; Kramer, 1988; Tramper and Vlak, 1988; Chittur et al., 1988; Petersen et al., 1988; Schürch et al., 1988; Hooker et al., 1989). Schürch et al. (1988) show the different flow profiles that can exist, particularly "Taylor" vortices. A schematic representation is given in Fig. 8.19.

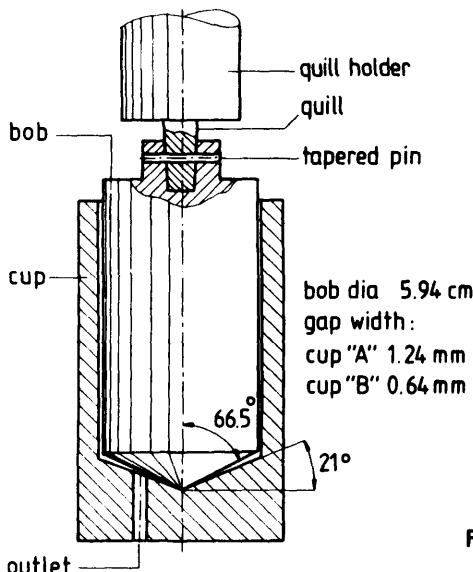


Fig. 8.18 Laminar shear device. (Adapted from Midler and Finn, 1966.)

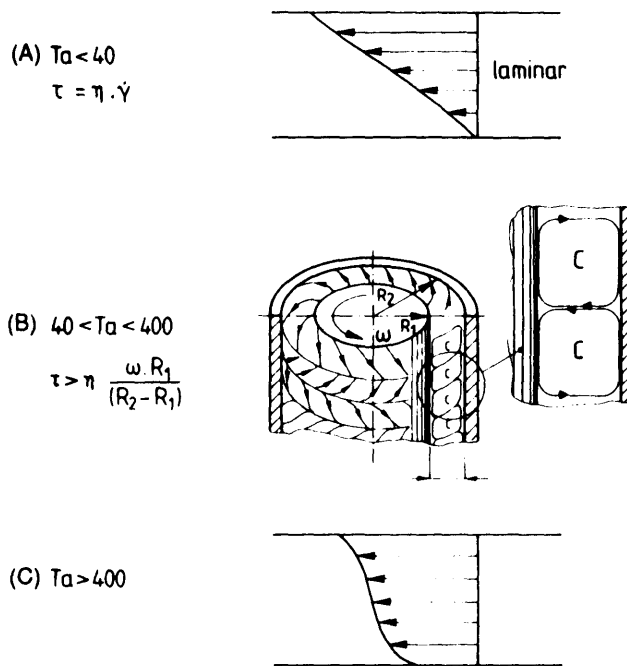


Fig. 8.19 The three different flow profiles in the annular gap of a rotating viscometer:
 (a) laminar flow, (b) "Taylor eddies", (c) turbulent flow. (Adapted from Schürch et al., 1988.)

The advantage of using laminar shear devices is that shear sensitivity can be determined under well-defined laminar conditions, thus avoiding complex flow patterns (Meijer, 1989). The disadvantages, according to this author, are:

1. A laminar shear device allows studying of only one hydrodynamic stress component, i.e., laminar shear.
2. The experiments are restricted to low shear rates and shear stresses. For high shear stresses the viscosity of the cell suspension has to be increased by adding polymers which may have unknown effects on the cells.
3. Large cell aggregates disturb laminar flow. Both cells and aggregates will tend to settle down within the viscometer causing a nonhomogeneous suspension.
4. Experiments are difficult to perform under axenic conditions and therefore can last only for a short period of time.

The latter problem has been solved by a French group (Soule et al., 1987; Mitard and Riba, 1988). In order to study the effect of well-defined shear

stresses on morphology and growth of a fungal strain and on plant cells under axenic conditions, this group designed an annular bioreactor (Fig. 8.20) based on a Couette stable laminar flow. This bioreactor was set up with two coaxial cylinders, so that the cells (plant cells and filamentous fungi) could grow in the gap between the two cylinders. In a similar reactor Hooker et al. (1989) studied the response of *Nicotiana tabacum* to a high shear environment.

Although the experiments in laminar shear devices like Couette viscosimeters come up with numerical values of critical shear stress values, in the case of animal cells mostly slightly below 1 N m^{-2} , at which damaging effects start to occur, the translation to "real-life" bioreactors remains difficult. This was seen, for instance, in the section on stirred vessels, where shear stresses were calculated below those found critical in laminar shear devices, but damage occurred independent of volume (scale).

8.4.2 Other shear-sensitivity measurements

In addition to stirred reactors, bubble columns and Couette vessels, several other approaches have been applied more incidentally to determine the shear

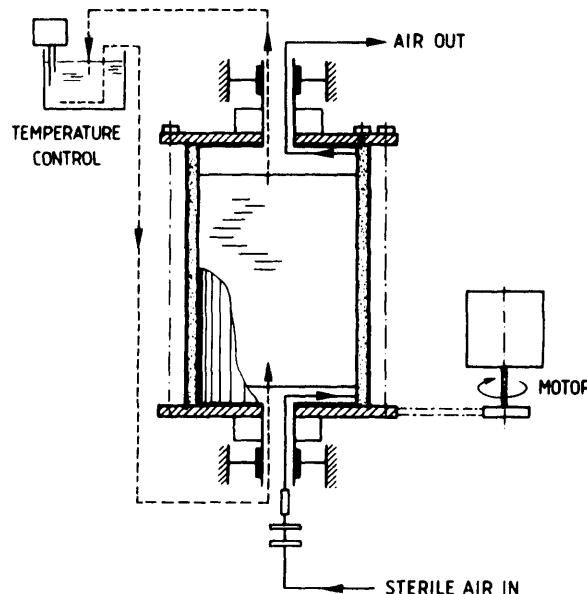


Fig. 8.20 Annular bioreactor for cell cultivation at defined shear stresses. (Adapted from Mitard and Riba, 1988.)

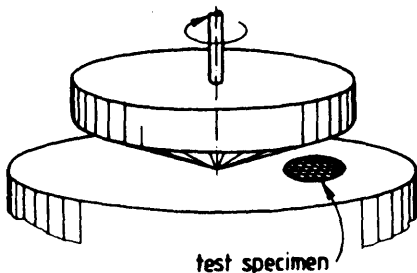


Fig. 8.21 Cone-plate test apparatus.
(Adapted from Dewey et al., 1981.)

sensitivity of cells. Dewey et al. (1981) developed a cone-plate apparatus that produces a uniform fluid shear stress on replicate samples on cultured monolayers of cells (Fig. 8.21). A detailed and profound (mathematical) description can be found in this reference. Stathopoulos and Hellums (1985) used a specifically developed flow channel for studies on the influence of shear stress on cells attached to a flat solid substrate (Fig. 8.22).

Augenstein et al. (1971) and McQueen et al. (1987) used capillary tubes to subject cell suspensions intermittently to flow through a sudden contraction and turbulent flow. The latter authors first observed lysis of mouse myeloma cells at a threshold average wall shear stress of 180 N m^{-2} . Although the flow caused lysis, it had no effect on cell viability. These authors also correlate cell lysis with the Kolmogorov length scale (Fig. 8.23). The figure shows that the threshold value of the Kolmogorov length scale, at which the specific lysis rate became detectably greater than zero, was $3.5 \mu\text{m}$. Therefore, cell lysis began to occur when the smallest turbulent eddy size

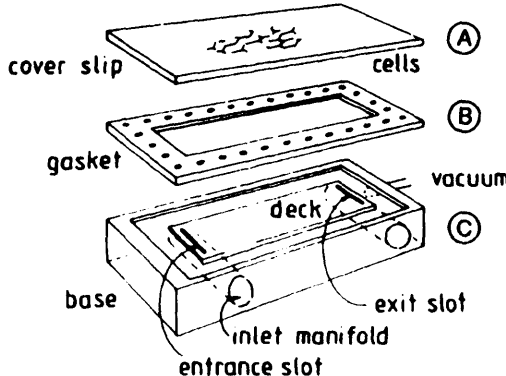


Fig. 8.22 Flow chamber. (Adapted from Stathopoulos and Hellums, 1985.)

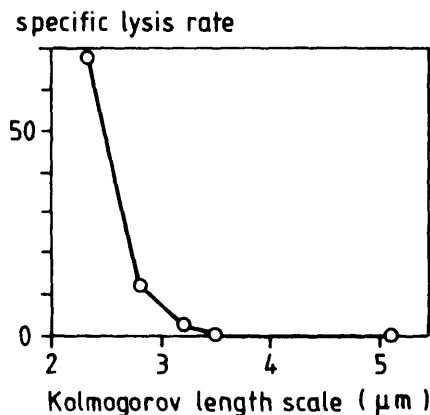


Fig. 8.23 Relationship between the specific lysis rate in units per number of passes through a capillary tube of mouse myeloma cells and the approximate size of the smallest turbulent eddies. (Adapted from McQueen et al., 1987.)

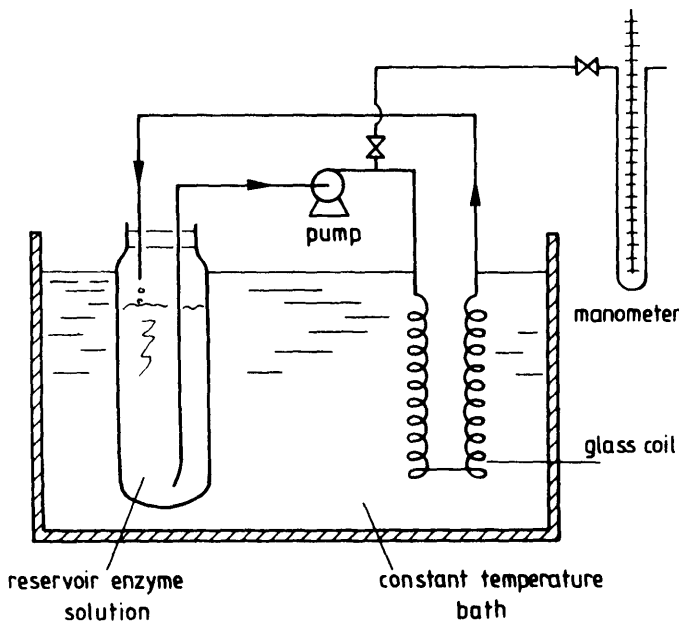


Fig. 8.24 Experimental set-up to measure shear effects in capillary tubing. (Adapted from Reese and Ryu, 1980.)

fell below the cell diameter. This conclusion is remarkably similar to that of Croughan et al. (1987 and 1989) for cells on microcarriers (see Section 8.2.6). This is another indication that the Kolmogorov length scale is a suitable parameter to predict cell damage in turbulent flow regimes. Reese and Ryu (1980) also used a capillary system (Fig. 8.24) to study shear effects, in their case on the enzyme cellulase.

A procedure which in principle can be applied in any bioreactor was developed by Märkl (Märkl and Bronnenmeier, 1985). Märkl developed a test apparatus, in which a free jet generates a defined shear stress in a bioreactor (Fig. 8.25). Part of the culture is forced out of the bioreactor by means of pressure into a second vessel. Other approaches, like shaking cell-culture flasks at various speeds and growing cells in spinner flasks at different agitation speeds (Lee et al., 1988) have been used incidentally too, but these only allow even rougher estimates of the shear stresses involved and translation to large-scale bioreactors is even more awkward. Therefore, no further attention is paid to these.

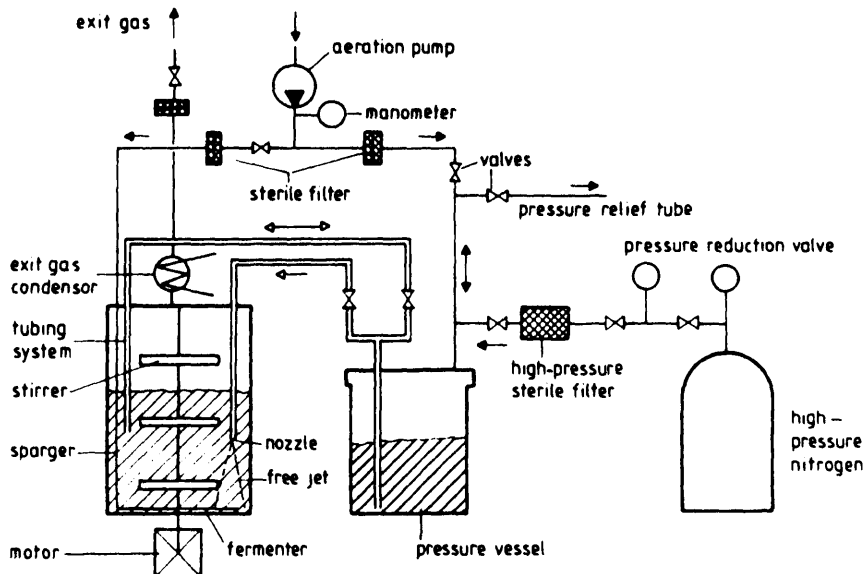


Fig. 8.25 Test apparatus for free-jet shear experiments; ——→ culture flow;
————→ gas flow. (Adapted from Märkl and Bronnenmeier, 1985.)

8.5 Examples

Example 8.1 Insect cells

The minimal doubling time of the insect cells we use in our studies is about 24 h, which means that $k_d = 8 \times 10^{-6} \text{ s}^{-1}$. For growth of these insect cells to occur in a bubble column, k_g should at least be smaller than this value. Tables 8.5 and 8.6 show the results of the calculations for a vessel with $T_v = H_v$ (standard fermenter) and $H_v = 10 T_v$ (typical for bubble column) using the equations given in the preceding section.

Fig. 8.26 illustrates the procedure. The value substituted for k_{ol} is low but extracted from experimental results. The values for OUR' , C_x' , C_{ol} and

Table 8.5 Bubble column data for growth of insect cells, with $H_v = T_v$

V (m ³)	H_v (m)	F_g (m ³ s ⁻¹)	k_d (s ⁻¹)	k_g/k_d (-)
10	2.34	7.96×10^{-3}	3.18×10^{-6}	2.52
1	1.08	1.69×10^{-3}	6.78×10^{-6}	1.18
0.622	0.925	1.24×10^{-3}	8.00×10^{-6}	1.00
0.1	0.503	3.68×10^{-4}	1.47×10^{-6}	0.544
0.01	0.234	7.96×10^{-5}	3.18×10^{-6}	0.252
0.001	0.108	1.96×10^{-5}	6.78×10^{-6}	0.118

Table 8.6 Bubble column data for growth of insect cells, with $H_v = 10 T_v$

V (m ³)	H_v (m)	F_g (m ³ s ⁻¹)	k_d (s ⁻¹)	k_g/k_d (-)
10	10.8	1.69×10^{-3}	6.78×10^{-7}	11.8
1	5.03	3.68×10^{-4}	1.47×10^{-6}	5.44
0.1	2.34	7.96×10^{-5}	3.18×10^{-6}	2.52
0.01	1.08	1.69×10^{-5}	6.77×10^{-6}	1.18
0.00622	0.925	1.24×10^{-5}	8.00×10^{-6}	1.00
0.001	0.503	3.68×10^{-6}	1.47×10^{-5}	0.544

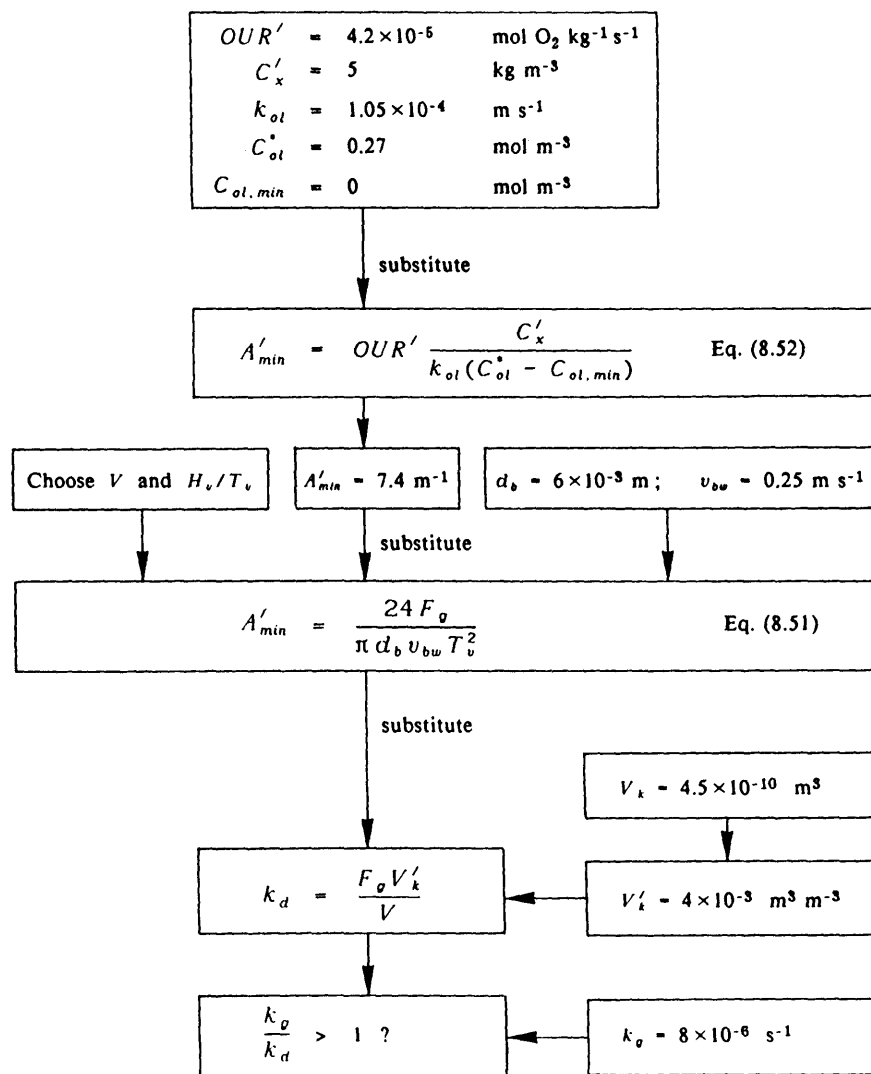


Fig. 8.26 Bubble-column-design calculation scheme for growth of insect cells. (Adapted from Tramper and Vlak, 1988.)

V' are experimental data or derived from experimental data. We have frequently observed, for instance, that the oxygen concentration in a surface-aerated, slowly stirred, continuous culture essentially drops to zero, without significant increase in the number of dead cells. As can be expected from inspection of the formulae, growth of the cells can be expected to improve as the volume or rather the height of the bubble column increases. Naturally, the H_v/T_v ratio cannot be increased unlimitedly, as at a certain point oxygen depletion in the air bubble becomes limiting. Application of this calculation scheme to the small air lift reactor [T_v (riser) = 0.017 m; H_v (riser) = 0.154 m; V (riser) = $35 \times 10^{-6} \text{ m}^3$], in which we initially tried to grow insect cells, yields a k_g/k_d of 0.167 and explains our failures. Boraston et al. (1984), from Celltech, grew hybridoma cells without problems in a 30 dm^3 (H_v/T_v = 12) and a 5 dm^3 (H_v/T_v = 6) air lift, which would give with the data of our insect cells a k_g/k_d = 1.9 and 0.66, respectively. Although hybridoma cells may well be less fragile than insect cells, a k_{oi} value of $4 \times 10^{-4} \text{ m s}^{-1}$ is more likely in an air lift and brings the k_g/k_d ratio well over 1 in both cases. The same company is presently running a 10, 100 and 1000 dm^3 air lift system, and designing a 10 m^3 vessel (Birch et al., 1987). Based on our model, the latter system should operate without problems, since the calculated hydrodynamic effects on cells are not deleterious.

References

- Augenstein D.C., Sinskey A.J. and Wang, D.I.C. "Effect of shear on the death of two strains of mammalian tissue cells." *Biotechnol. Bioeng.* 12, 409 (1971).
- Birch J.R., Lambert K., Thompson P.W., Kennedy A.C. and Wood L.A. "Antibody production with airlift fermenters." in *Large Scale Cell Culture Technology* (B.K. Lydesen, ed.) Hanser Publishers, Munich, pp 1-20, 1987.
- Boraston R., Thompson P.W., Garland S. and Birch J.R. "Growth and oxygen requirements of antibody producing mouse hybridoma cells in suspension culture." *Dev. Biol. Stand.* 55, 103 (1984).
- Cherry R.S. and Papoutsakis E.T. "Hydrodynamic effects on cells in agitated tissue culture reactors." *Bioproc. Engng.* 1, 29 (1986).
- Chittur K.K., Mc Intire L.V. and Rich R.R. "Shear stress effects on human T cell function." *Biotechnol. Progr.* 4, 89 (1988).
- Croughan M.S., Sayre E.S. and Wang D.I.C. "Viscous reduction of turbulent damage in animal cell culture." *Biotechnol. Bioeng.* 33, 862 (1989).

Croughan M.S., Hamel J.F. and Wang D.I.C. "Hydrodynamic effects on animal cells grown in microcarrier cultures." *Biotechnol. Bioeng.* **29**, 130 (1987).

Davies C.N. "Air filtration." Academic Press, New York (1973).

Dewey C.F., Bussolari S.R., Gimbrone M.A. and Davies P.F. "The dynamic response of vascular endothelial cells to fluid shear stress." *J. Biomech. Eng.* **103**, 177 (1981).

Einav S. and Lee S.L. "Particles migration in laminar boundary layer flow." *Int. J. Multiphase Flow* **1**, 73 (1973).

Emery A.N., Lavery M., Williams B. and Handa A. "Large-scale hybridoma culture." *Plant and animal cells: Process possibilities*, C. Webb, F. Mavituna, eds. Ellis Horwood, Chichester (1987), p. 137.

Handa Corrigan A., Emery A.N. and Spier R.E. "Effect of gas-liquid interfaces on the growth of suspended mammalian cells: Mechanisms of cell damage by bubbles." *Enzyme Microb. Technol.* **11**, 230 (1989).

Havenbergh J. and Joos P. "The dynamic surface tension in a free falling film." *J. Coll. Interf. Sci.* **95**, 172 (1983).

Heijnen J.J. and Van 't Riet K. "Mass transfer, mixing and heat transfer phenomena in low viscosity bubble column reactors." *Chem. Engng. J.* **28**, B21 (1984).

Hinze J.O. "Turbulence." McGraw-Hill, New York (1959).

Hooker B.S., Lee J.M. and An G. "Response of plant tissue culture to a high shear environment." *Enzyme Microb. Technol.* **11**, 484 (1989).

Katinger H.W.D. and Scheirer W. "Status and development of animal cell technology using suspension culture techniques." *Acta Biotechnologica* **2**, 3 (1982).

Kramer H.W. "Der Einfluss von Scherkäften in Bioreaktoren auf Proliferation und syntheseleistung tierischer Zeller." Ph.D. Thesis, ETH-Zürich (1988).

Lee G.M., Huard T.K., Kaminski M.S. and Palsson B.O. "Effect of mechanical agitation on hybridoma cell growth." *Biotechnol. Letters* **10**, 625 (1988).

Lee Y.K. and Choo C.L. "The kinetics and mechanisms of shear inactivation of lipase from *Candida cylindracea*." *Biotechnol. Bioeng.* 33, 183 (1989).

Märkl H. and Bronnenmeier R. "Mechanical stress and microbial production" Chapter 18, p. 369, in "Biotechnology" edited by H.-J. Rehm and G. Reed. Vol. 2, "Fundamentals of biochemical engineering." volume-editor H. Brauer. VCH, Weinheim (1985).

McQueen A., Meilhoc E. and Bailey J.E. "Flow effects on the viability and lysis of suspended mammalian cells." *Biotechnol. Letters* 9, 831 (1987).

Meijer J.J. "Effects of hydrodynamic and chemical/osmotic stress on plant cells in a stirred bioreactor." Ph.D. Thesis, Technical University Delft (1989).

Metzner A.B., Feehs R.H., Ramos H.L., Otto R.E. and Tuthill J.D. "Agitation of viscous Newtonian and non-Newtonian fluids." *A.I.Ch.E. J.* 7, 3 (1961).

Midler M. and Finn R.K. "A model system for evaluating shear in the design of stirred fermentors." *Biotechnol. Bioeng.* 8, 71 (1966).

Mitard A. and Riba J.P. "Morphology and growth of *Aspergillus niger* ATCC 26036 cultivated at several shear rates." *Biotechnol. Bioeng.* 32, 835 (1988).

Nagata S. "Mixing: Principles and Applications." Wiley, New York (1975).

Petersen J.F., McIntire L.V. and Papoutsakis E.T. "Shear sensitivity of cultured hybridoma cells (CRL-8018) depends on mode of growth, culture age and metabolite concentration." *J. Biotechnol.* 7, 229 (1988).

Poncelet D. and Neufeld R.J. "Shear breakage of nylon membrane micro-capsules in a turbine reactor." *Biotechnol. Bioeng.* 33, 95 (1989).

Reese E.J. and Ryu D.Y. "Shear inactivation of cellulase of *Trichoderma reesei*." *Enzyme Microb. Technol.* 2, 239 (1980).

Schlichting H. "Boundary layer theory." 7th ed. McGraw-Hill, New York (1979).

Schürch U., Kramer H., Einsele A., Widmer F. and Eppeberger H.M. "Experimental evaluation of laminar shear stress on the behavior of hybridoma mass cell cultures, producing monoclonal antibodies against mitochondrial creatine kinase." *J. Biotechnol.* 7, 179 (1988).

Smith C.G., Greenfield P.F. and Randerson D.H. "A technique for determining the shear sensitivity of mammalian cells in suspension culture." *Biotechnol. Techn.* 1, 39 (1987).

Soule J.C., Wilhelm A.M., Riba J.P. and Ambid C. "Bioréacteur à contraintes mécaniques contrôlées. Application à la culture in vitro de cellules végétales." *Entropie* 22 (136), 24 (1987).

Stathopoulos N.A. and Hellums J.D. "Shear effects on human embryonic kidney cells in vitro." *Biotechnol. Bioeng.* 27, 1021 (1985).

Thomas N.H. and Janes D.A. "Fluid dynamic considerations in airlift and annular vortex bioreactors for plant cell culture." *Ann. NY Acad. Sci.* 506, 171 (1987).

Tramper J. and Vlak J.M. "Bioreactor design for growth of shear-sensitive mammalian and insect cells." A. Mizrahi, ed. *Upstream Process: Equipment and Techniques*, Alan R. Liss, New York (1988), p. 199.

Tramper J., Van Groenestijn J.W., Luyben K.Ch.A.M. and Hulshoff Pol L.W. "Some physical and kinetic properties of granular anaerobic sludge." *Innovations in Biotechnology*, p. 145. (E.H. Houwing, R.R. van der Meer, eds.) Elsevier, Amsterdam (1984).

Tramper J., Williams J.B., Joustra P. and Vlak J.H. "Shear sensitivity of insect cells in suspension." *Enzyme Microb. Technol.* 8, 33 (1986).

Tramper J., Smit D., Straatman J. and Vlak J.M. "Bubble-column design for growth of fragile insect cells." *Bioproc. Engng.* 3, 37 (1988).

Van Ginkel C.G., Tramper J., Luyben K.Ch.A.M. and Klapwijk A. "Characterization of *Nitrosomonas europaea* immobilized in calcium alginate." *Enzyme Microb. Technol.* 5, 297 (1983).

Van 't Riet K. and Smith J.M. "The trailing vortex system produced by Rushton turbine agitators." *Chem. Engng. Sci.* 30, 1093 (1975).

Wudtke M. and Schügerl K. "Investigations of the influence of physical environment on the cultivation of animal cells." *Rheologie und mechanische Beanspruchung biologischer Systeme* GVC. VDI, Düsseldorf (1987), p. 159.

PART III

Reactor Engineering

9

Mixing

9.1 Definitions

Mixing can be defined (Hiby, 1981) as the process that decreases the inhomogeneity of a system, e.g., the contents of a vessel. A system is completely mixed if the chance to find a given component at a certain place is the same for any position in the vessel. Mixing can be characterized by two parameters: the scale of mixing and the intensity of mixing.

The scale of mixing is defined as the smallest dimension in which inhomogeneities are allowed. The scale will always be smaller than the dimension of the system itself and larger than the smallest particles present in the system. Which scale should be chosen is dependent on the process that is studied. For instance, for a solution of salt in water the molecular scale can be chosen. For a mixing process preceding the filling of a container of 1 m diameter with tiny salt crystals and a dry powder, the scale can be 10 or even 100 times the dimension of the largest crystals. If the container is used to fill batches of 10 kg, the scale of 1 or maybe even 10 mm is small enough to obtain batches of equal average composition. When measuring methods involve a sampling or a probe inserted in the vessel, the scale is equal to the size of the sample or the detection part of the probe.

The mixing intensity is defined as the deviation from completely mixed. In theory a system will be completely mixed only after an infinite amount of time. By allowing a deviation from completely mixed we can define a system as mixed after a finite amount of time. An example is given in Fig. 9.1: At $t = 0$ an acid tracer pulse is added to a circulating flow. After this pulse has flown through the lower pipe, the pH electrode detects the passage. This is repeated after each circulation. The pulse will be flattened by the mixing that takes place during the circulation. With the parameters as defined in Fig. 9.1, the mixing intensity can be defined as

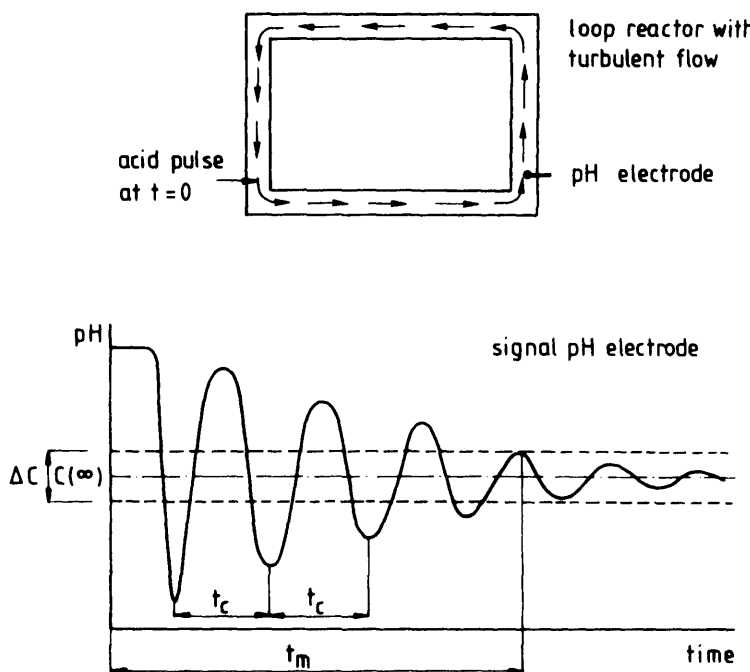


Fig. 9.1 A schematic representation of the relationship of mixing intensity with mixing time.

$$\text{Mixing intensity} = \frac{C(\infty) - 0.5\Delta C}{C(\infty)} \times 100\% \quad (-) \quad 9.1$$

We regard a system as mixed as soon as the deviations from $C(\infty)$ (mol m^{-3}) stay within the given criterion $0.5 \Delta C$, or stated in another way, as soon as the mixing intensity of the system becomes larger than the stated mixing intensity criterion as defined in Eq. (9.1). This confronts us with the fact that the mixing time can have different values for a defined system, because its value increases with the increase of the mixing intensity required.

Usually we are interested only in the mixing at a given scale and intensity. For characterization of this process the mixing time is a useful parameter. The mixing time, t_m (s), is defined as the time needed to reach a given mixing intensity at a given scale, when starting from the completely segregated situation. In the example of Fig. 9.1 an acid pulse is added at $t = 0$. In this case of one single pulse, the system can be regarded as completely segregated at $t = 0$. Fig. 9.1 shows that after a certain time, the mixing time t_m (s), the pH values do not exceed the range of $C(\infty) \pm \Delta C$. In this way the mixing times and intensity are related. The scale in this example is the dimension of the pH probe.

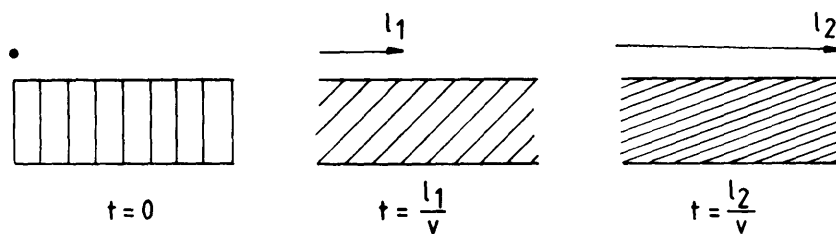


Fig. 9.2 Mixing of a viscous liquid between two parallel plates by shearing action. The upper plate moves with a velocity v . The lower plate is kept in place.

It is evident that a circulation loop exists in Fig. 9.1. This usually is also the case in fermenters, although less strictly defined. In a loop a circulation time, t_c (s), can be defined as the average time needed for the fluid elements to pass one circulation.

9.2 Mechanisms of mixing

Three different mechanisms can be distinguished in mixing: shear, exchange and diffusion.

- Shear: In laminar flow mixing occurs due to fluid layers that shear along each other. This is shown schematically in Fig. 9.2.
- Exchange: In turbulent flow particles are continuously moved with respect to each other. This is a random process. Schematically it is represented in Fig. 9.3.
- Diffusion: This is the mixing process that results from molecular diffusion. It can be regarded as mixing by exchange on a molecular scale.

Assume a bioreactor at a sufficiently high Re number for turbulent conditions. Turbulence is a random fluctuation superimposed on an average velocity (Hinze, 1959). If we want to have a physical idea of this flow it can be described by an infinite number of eddies, all of different size. The largest eddies contain the energy introduced by, for example, the stirrer.

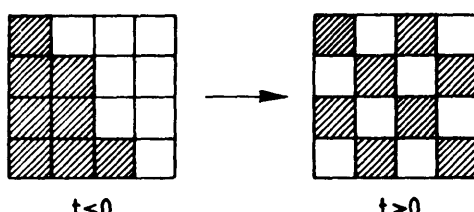


Fig. 9.3 Mixing by exchange.

These eddies are unstable and will break up into smaller ones. This process proceeds to smaller and smaller eddies. In this way the energy is transferred to eddies of decreasing size. The process stops at an eddy size corresponding to $Re = 1$, the so-called Kolmogorov scale. At this size, energy has to be dissipated by viscous dissipation. The diameter, λ (m), of these Kolmogorov eddies can be derived:

$$\lambda = \left(\frac{v^3}{\epsilon_*} \right)^{0.25} \quad (m) \quad 9.2$$

in which

$$\begin{aligned} \epsilon_* &= \text{energy content per unit of mass} && (W \text{ kg}^{-1}) \\ v &= \text{kinematic viscosity} && (\text{m}^2 \text{ s}^{-1}) \end{aligned}$$

In the above-mentioned turbulent bioreactor circulation patterns can be distinguished, usually on the scale of the reactor. Mixing then starts with the transport on the scale of the vessel by these circulations. In this circulation pattern also subpatterns will be present that take care of mixing on a smaller scale. The subpatterns usually are turbulent; i.e., they contain the turbulent eddies of different sizes. These eddies will cause mixing by exchange within the large-scale circulation loops. Finally, mixing will occur by molecular diffusion in the smallest eddies of the turbulence pattern.

9.3 Modeling of mixing

When a liquid flow, F_t ($\text{m}^3 \text{ s}^{-1}$), flows through a tank with a volume V (m^3), the average residence time, τ (s), of the liquid elements will be given by

$$\tau = \frac{V}{F_t} \quad (s) \quad 9.3$$

Fluid elements entering the vessel at a defined moment generally leave the system at different times, due to circulation and mixing phenomena in the tank. This variation is called the residence time distribution.

The residence time distribution can be measured easily for throughflow tanks. Yet it also can be used to understand mixing in batch vessels. Usually circulation loops are present in vessels. Circulation patterns in stirred tanks and air lift fermenters can be modeled by means of a "recirculating flow through pipes" model, comparable to that given in Fig. 9.1. Mixing in these loops leads to a variation of circulation times, which can be described by a residence time model, with an average residence time equal to the circula-

tion time. If the residence time distribution includes fractions with very small and/or very large residence times, then this can cause serious problems in bioreactors. The main problem is oxygen depletion in stagnant zones (infinite residence times) in an aerobic fermenter.

Visualization of the residence time distribution can be done in several ways. Here the example of a turbulent pipe flow is given in Fig. 9.4. At $t = 0$, a tracer is injected at the inlet. After a time t_1 , the tracer with a velocity v will have traveled a distance $L = vt_1$. The tracer particles have different velocities. This leads to so-called dispersion of the tracer particles. This process proceeds along the pipe and the concentration of tracer particles in

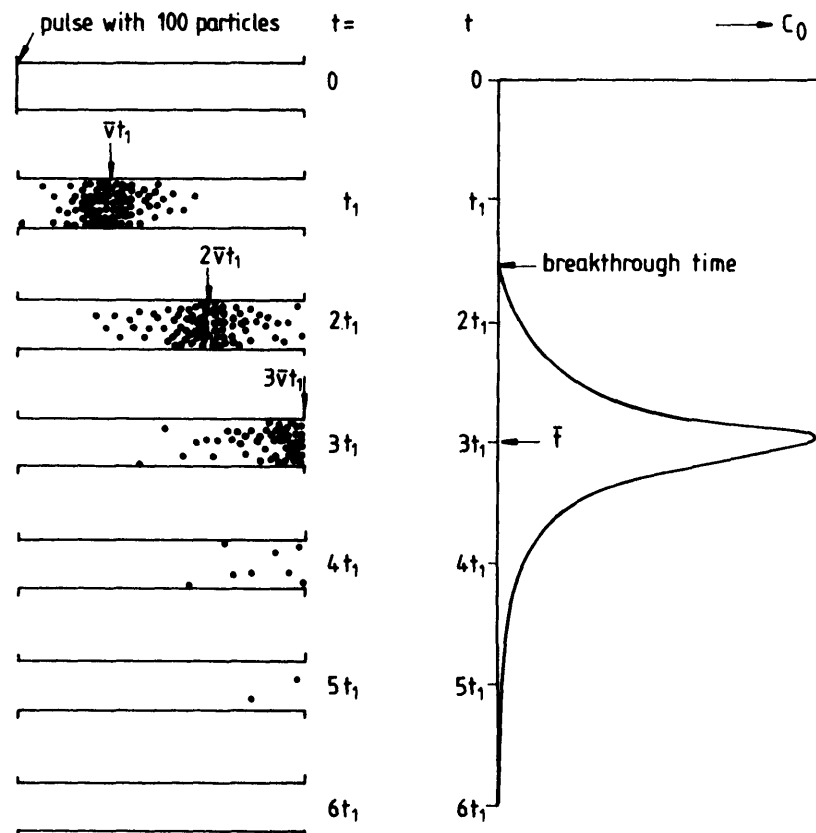


Fig. 9.4 Schematic representation of the residence time distribution and the corresponding curve for the concentration C_0 of the outflowing liquid. In practice the pipe diameter will be \ll than the pipe length.

the outflow will show a distribution as shown in Fig. 9.4. Actually, this is the basis of the pH curve as shown in Fig. 9.1. The tracer particles can be replaced by fluid elements that contain oxygen, leaving the stirrer region in a stirred vessel. The consequences of a residence time distribution for a circulation loop in a stirred vessel are shown in Example 9.1.

The residence time distribution can be described with a number of functions as shown by Levenspiel (1972). Here we will present only two model descriptions. There exist two special types of model reactors that are useful in modeling residence time distribution data, and in relating kinetics to reactor models. These are the ideally mixed reactor and the plug flow reactor. These have already been discussed in Section 1.4. To describe distributions like that given in Fig. 9.4, the tanks-in-series model, also discussed in Section 1.4, is convenient. This model system consists of a series of ideally mixed tanks of equal volume. The inflow of each tank is the outflow of the preceding one. The only parameter is the number of tanks n .

Particularly useful for mixing description of a flow like that given in Fig. 9.4 is the dispersion model. In this model the flow is regarded as a plug flow type with axial dispersion defined by a dispersion coefficient $|D_o|$ ($\text{m}^2 \text{s}^{-1}$). The effects are similar to flow with molecular diffusion with the molecular diffusion coefficient replaced by the dispersion coefficient. The equation is given by

$$\frac{\partial C(z, t)}{\partial t} = |D_o| \frac{\partial^2 C(z, t)}{\partial z^2} - \bar{v} \frac{\partial C(z, t)}{\partial z} \quad (\text{mol m}^{-3} \text{s}^{-1}) \quad 9.4$$

$$\begin{aligned} C(z, t) &= \text{concentration of a component at position } z \text{ and time } t \quad (\text{kg m}^{-3}) \\ z &= \text{axial direction} \quad (\text{m}) \\ \bar{v} &= \text{average velocity in the axial direction} \quad (\text{m s}^{-1}) \end{aligned}$$

Eq. (9.4) can be transformed into

$$\frac{\partial C}{\partial(\theta)} = - \frac{|D_o|}{\bar{v} L} \frac{\partial^2 C}{\partial z'^2} + \frac{\partial C}{\partial z'} \quad (\text{mol m}^{-3} \text{s}^{-1}) \quad 9.5$$

in which L

$$\begin{aligned} L &= \text{length of the pipe reactor} \quad (\text{m}) \\ z' &= \text{dimensionless axial distance } = z/L \quad (-) \\ \theta &= \text{dimensionless time } = t/\tau = t\bar{v}/L \quad (-) \end{aligned}$$

In Eq. (9.5) a dimensionless number, the Bodenstein number can be defined as

$$Bo = \frac{\bar{v}L}{|D_e|} = \frac{\text{mass flow by convection}}{\text{mass flow by dispersion}} \quad (-) \quad 9.6$$

Levenspiel (1972) gives solutions for Eq. (9.5). Comparison of the solutions of the dispersion model and the series of tanks model shows that for large n and Bo values the response curves are similar for the tanks-in-series and the dispersion models. Levenspiel shows that the response curves are the same for

$$Bo = 2n - 1 \quad n \gg 1 \quad (-) \quad 9.7$$

For $n > 5$ the difference between the two models is less than 1%.

From Fig. 9.1 it can be seen that the dispersion causes a flattening of the pulse added at $t = 0$. This is exactly what happens when a tracer is added to a stirred vessel or air lift. Fig. 9.1 shows that the system is regarded as mixed at a mixing time t_m (s), after which the concentration differences do not exceed a predetermined value. The relation of the dispersion and tank-in-series model with mixing time is complex. As discussed, we are mainly interested in mixing as a result of circulating flow in a vessel. The dispersion model fits best the mechanisms that take place in the vessel. Voncken (1966) has shown that the circulation loop in a stirred vessel can be described by a plug flow with dispersion. By coupling the outflow of the circulatory loop with its own inflow, the concentration variation as a function of time can be calculated. Schematically this results in a loop as given in Fig. 9.1. Verlaan et al. (1986) have developed a mathematical procedure to calculate Bo from the concentration profiles. They could relate the Bo value to the mixing time.

The mixing time is dependent on the mixing intensity criterion, the deviation from completely mixed that is allowed; therefore, it is not a fixed value for a given system. Contrary to this, the values for the dispersion coefficient as well as the number of tanks in series are independent variables. This is one of the reasons why the two models are sometimes preferred. The main reason for application of the models is that they are a very useful tool for conversion calculations. Levenspiel shows how the conversion can be calculated when the residence time distribution, either as a tanks-in-series model or as a dispersion model, is known. For the characterization of mixing in fermenters, the mixing time is used most frequently. More complex mixing models are not given, as those given here are adequate for most biotechnological applications. Those interested in additional models can find them in the article of Shah et al. (1978).

9.4 Mixing time data

9.4.1 The stirred vessel

For fermenters we are mainly interested in data for two-phase gas liquid systems. However, this type of information is rather scarce. In contrast to this, the single-phase system is thoroughly researched. As single- and two-phase behavior is related, single-phase models will be dealt with first. With the single-phase knowledge the two-phase data can be understood and organized.

9.4.1.1 Single-phase, liquid mixing times

We can regard the flow through the circulation loops in a stirred vessel as a plug flow (with dispersion) through a pipe. The circulation time t_c (s) is given by

$$t_c = \frac{V_c}{F_c} \quad (\text{s}) \quad 9.8$$

with

$$\begin{aligned} V_c &= \text{volume of the circulation loop} & (\text{m}^3) \\ F_c &= \text{circulation capacity} & (\text{m}^3 \text{ s}^{-1}) \end{aligned}$$

The pumping capacity of the stirrer, F_p ($\text{m}^3 \text{ s}^{-1}$), is defined as the flow that leaves the stirrer region. Due to entrainment of liquid by the impeller flow the circulation capacity is larger than the pumping capacity. It is experimentally found that:

$$\frac{F_c}{F_p} = 2 \quad (-) \quad 9.9$$

Voncken (1966) found that the dispersion in the loop causes a mixing time t_m , given by

$$t_m = 4 t_c \quad (\text{s}) \quad 9.10$$

Eqs. (9.9) and (9.10) contain experimentally determined parameters of the circulation flow model. We can extend this model, to relate mixing time to the operating parameters.

For the fully turbulent case the energy delivered by the stirrer P_{st} , (J s^{-1}) is completely transformed into kinetic energy of the liquid:

$$P_s = F_p \frac{1}{2} \rho_l \bar{v}^2 = N_p \rho_l N^3 D^5 \quad (\text{J s}^{-1}) \quad 9.11$$

with

ρ_l	= liquid density	(kg m ⁻³)
v	= velocity of the liquid just leaving the stirrer	(m s ⁻¹)
D	= stirrer diameter	(m)
N_p	= impeller power number (see Chapter 14)	(-)

For a radially pumping stirrer it is assumed that

$$F_p = \bar{v} \pi D H_s \quad (\text{m}^3 \text{s}^{-1}) \quad 9.12$$

with

H_s	= height of the stirrer blade	(m)
-------	-------------------------------	-----

With the assumption that $V_c = V = \frac{1}{4} \pi T_v^2 H_s$, and $\bar{v}^2 = \bar{v}^2$, Eqs. (9.8-9.12) give the mixing time.

$$t_m = \frac{c}{N} \frac{\left(\frac{T_v}{D}\right)^3 \left(\frac{H_s}{T_v}\right)}{\left[N_p \left(\frac{H_s}{D}\right)^2\right]^{0.33}} \quad \begin{matrix} \text{single-phase} \\ \text{theoretical model} \end{matrix} \quad (\text{s}) \quad 9.13$$

In this equation a constant c is introduced. Eqs. (9.8-9.12) give $c = 0.6$. Experimental verification of this equation is needed, because a number of assumptions have been made.

Eq. (9.13) shows that for $Re > 5000$, for which $N_p = \text{constant}$, $N t_m$ has a constant value. This has been confirmed experimentally by Voncken. Some authors report a slight increase with increasing Re number, but in practice we can assume $N t_m$ to be constant for $Re > 10,000$.

Eq. (9.13) can be simplified. Most fermenters are equipped with a turbine stirrer, with dimensions near to $H_s/D = 0.20$ and $H_s = T_v$ and thus

$$t_m = \frac{c'}{N} \frac{\left(\frac{T_v}{D}\right)^3}{N_p^{0.33}} \quad \begin{matrix} \text{single-phase} \\ \text{theoretical model} \end{matrix} \quad (\text{s}) \quad 9.14$$

in which c' is 1.7 when based on Eqs. (9.8-9.13). The real value of c' can be determined experimentally from mixing time measurements. Table 9.1

Table 9.1 Experimental and calculated values of the mixing time

Reference	Stirrer type	T_v / D	N_p	t_m	
				(-)	(-)
Voncken (1966)	6-blade turbine	2.5	6	20	14
Voncken (1966)	6-blade turbine	3.3	6	35	35
Zlokarnik (1972)	Paddle	2	9.8	10	6
Zlokarnik (1972)	MIG	1.43	0.65	13	6
Zlokarnik (1972)	Propeller	3.33	0.35	150	90
Zlokarnik (1972)	6-blade turbine	3.33	5	50	37
Hoogendoorn and Den Hartog (1967)	6-blade turbine	3	5	32/23*	9

* Different definitions.

presents a number of measured single-phase mixing time values for a large range of N and D values. Although very different stirrer types were used, the experimental values agree in that they all are about a factor 2 larger than calculated from the model Eq. (9.14), with $c' = 1.7$. Introducing this correction we get

$$t_m = \frac{3}{N} \frac{\left(\frac{T_v}{D}\right)^3}{N_p^{0.33}} \quad \text{single-phase experimental} \quad Re > 10,000 \quad (s) \quad 9.15$$

This equation can also be written as [using Eq. (9.11)]:

$$t_m = \left[27 \frac{\rho_f T_v^5}{P_e} \left(\frac{T_v}{D} \right)^4 \right]^{0.33} \quad \text{single-phase experimental} \quad Re > 10,000 \quad (s) \quad 9.16$$

Eqs. (9.15) and (9.16) deliver a reasonable prediction of the single-phase mixing time. Eq. (9.16) can be used if the power number is unknown while the power consumption is known. It has to be realized that mixing time itself is not an objective quantity. Depending on the intensity of the required mixing, mixing time can be smaller or larger than the one calculated with Eqs. (9.15) and (9.16). The equations are valid for a mixing intensity of 90-95%.

All these equations are derived for the turbulent situation ($Re > 10,000$). Hoogendoorn and Den Hartog (1967) and Zlokarnik (1972) show that $N t_m$

increases considerably at decreasing Re number, once $Re < 10,000$. An example for a turbine stirrer is given in Fig. 9.5. Large-scale commercial plants will normally work at large Re numbers. Because of the small diameter value, the Re number in small laboratory-scale fermenters can easily be in the nonturbulent region, at elevated viscosity values. The mixing time values show extremely poor mixing behavior in small fermenters at viscosity values for which large scale fermenters are yet well mixed, as shown in Example 9.2. From this example it can be concluded that for good mixing behavior at laboratory scale, viscosity values $> 0.1 \text{ N s m}^{-2}$ should be avoided. On large scale, values $> 1 \text{ N s m}^{-2}$ should be avoided.

Besides $Nt_m = \text{constant}$ at large Re numbers, there is a gradual increase of mixing time at turbulent conditions with an increase of scale. Example 9.2 shows that this is due to the constant P_f/V scale-up criterion used. This example also shows that scale up with constant mixing time as a criterion is senseless. The gradual increase with increase of scale has to be accepted.

9.4.1.2 Two-phase gas liquid, liquid mixing times

The theory presented so far is derived for single-phase systems. For aerobic fermentations air is a rather essential component. The reason for discussing the single-phase system in such a comprehensive way was that it provides insight for the rather unknown situation of the two-phase system. If we assume that the second phase does not influence the flow phenomena in the

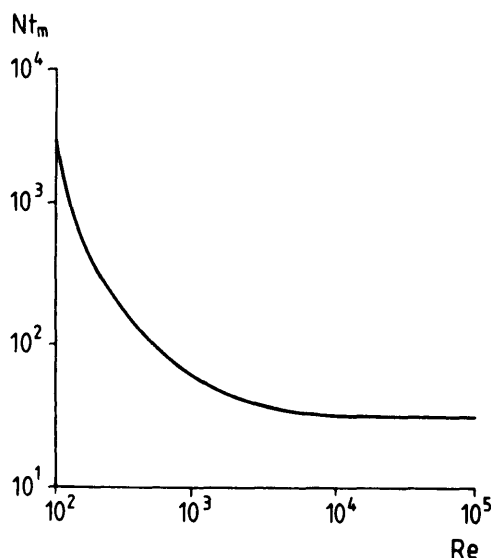


Fig. 9.5 Mixing times for a Rushton type turbine stirrer at low Reynolds numbers. (Adapted from Hoogendoorn and Den Hartog, 1967.)

vessel, then Eq. (9.15) can be applied straightforward. Measured mixing time values are given in Table 9.2, together with single-phase values calculated from Eq. (9.15) or (9.16).

The data in Table 9.2 show that there exists a systematic difference of about a factor 2 between the single-phase calculated and two-phase measured data. Einsele and Finn (1980) and Middleton (1979) also found a factor 1.2-2 due to aeration. Aeration leads to a decrease in the power number (Chapter 14). This is caused by a decrease in pumping capacity due to cavity formation. This is one of the reasons that the mixing time increases, although it cannot explain a factor two increase. The experimental data lead to the conclusion that two-phase and single-phase mixing times are related to each other, with the two-phase mixing times being about two times as large as one-phase mixing times under otherwise identical conditions. Therefore, two-phase large-scale data can be predicted with the following equations:

$$t_m = \frac{6}{N} \frac{\left(\frac{T_v}{D}\right)^3}{N_p^{0.33}} \quad \begin{matrix} \text{two-phase} \\ \text{experimental} \\ Re > 10,000 \end{matrix} \quad (s) \quad 9.17$$

Table 9.2 Experimental values for two-phase liquid mixing times and calculated single-phase values

Reference	V (m ³)	P_s (W)	T_v (m)	t_m	
				exp. (s)	Eq. (9.15), (9.16) (s)
Einsele (1978)	0.14	2100	0.45	15	6
	1	5500	0.86	42	12
	10	25000	1.85	84	26
	20	23000	2.34	51	38
	57	116000	3.31	82	40
Jansen et al. (1978) ^a	1.9	3800	1.08	29	24
	60	120000	3.45	67	52
	120	240000	4.35	119	62

- * Assumptions:
 - $P_s/V = 2 \text{ kW m}^{-3}$ (large scale of Einsele)
 - Single-phase liquid height 75% of H_v
 - $t_m = (H_v/T_v) \times [t_m \text{ calculated from Eq. (9.15) for one compartment with } H_v = T_v]$
 - $H_v/T_v = 2.5$

and

$$t_m = \left[216 \frac{\rho_l T_v^5}{P_s} \left(\frac{T_v}{D} \right)^4 \right]^{0.33} \quad \begin{array}{l} \text{two-phase} \\ \text{experimental} \\ Re > 10,000 \end{array} \quad (s) \quad 9.18$$

It is clear that the accuracy of the t_m prediction is very limited. Again it must be emphasized that t_m is a "subjective" quantity, its value depending upon the criteria used. It is not possible or important to calculate whether it is exactly, say, 100 or 120 s. Yet it is very important to know if the mixing time is 10, 100 or 1000 s. Also, influences of scale and viscosity are important and can be calculated.

For $Re < 10,000$ few data are available for large-scale fermenters. Between $1000 < Re < 10,000$ the influence is limited, as shown in Fig. 9.5. The situation below $Re = 1000$ should be prevented. At $Re < 500$ the mixing time has increased by at least a factor of 10, which is totally unacceptable. If needed, predictions can be made by using Eqs. (9.17) and (9.18) followed by a correction for Re by means of Fig. 9.5. The presence of rising gas bubbles might improve the mixing to some extent; however, for large-scale applications it is unknown to what extent.

The influence of the number of stirrers is unknown. At $Re < 5000$ compartmentalization in regions around each of the stirrers begins to occur. This results in an increase of the mixing time additional to that which occurs at decreasing Re numbers. At $Re < 500$ the mixing time in one-phase systems becomes infinitely long because transport from one compartment to the next one is near to zero. For two-phase systems bubbles moving through the interface provide some mixing, thus increasing mixing between two compartments. For large Re numbers, $Re > 10,000$, Eqs. (9.17) and (9.18) can be applied for each compartment separately. In the case of unhindered transport between the different compartments, the total circulation time will be the sum of the circulation times of each of the separate compartments. Therefore, it seems logical to calculate the total mixing time as the sum of the calculated mixing times from Eqs. (9.17) and (9.18) for each of the separate compartments.

The basis of the two-phase mixing-time equations is the assumption that the gas phase does not influence the flow phenomena to a large extent. In Chapter 6 it was shown that flow phenomena can be influenced to a large extent by gas rates near the flooding region. Therefore, it seems logical that for those gas rates mixing times can differ from those calculated with Eqs. (9.17) and (9.18). It is not known to what extent they will differ.

9.4.1.3 Two-phase gas liquid, gas mixing times

Gas residence times have been measured in vessels up to $T_v = 0.60$ m by Hanhart et al. (1963) and Gal-Or and Resnick (1966). The gas residence time is between that of an ideal mixer and two ideal mixers in series. This is the case only for a complete recirculation flow profile in the vessel. As soon as the flooding region is reached, gas phase mixing can be assumed much less complete. Maybe, just before flooding occurs, the flow region can be accompanied by a less intensive mixing when compared to complete recirculation. No information is available for large-scale vessels and for vessels with $H_v > T_v$ and two or more stirrers. If modeling of the gas phase is needed, compartmentalization will be the best choice.

A distinction has to be made between a well-mixed gas phase leaving the vessel and mixing of the gas bubbles with each other. In the latter case all bubbles have the same composition in the case of a well-mixed situation. For a completely noncoalescing liquid this is not necessarily the case, even when the gas phase leaves the vessel completely well mixed. At recirculating conditions Van 't Riet et al. (1975) have shown that a large part of the recirculating gas stream coalesces with the cavity behind the stirrer blades, thus mixing intensively with the just sparged gas that is sucked nearly instantly into the cavity. This is also the case for a noncoalescing liquid, for which even more coalescence takes place in the cavity than for a coalescing liquid, even though the bubbles do not show any coalescence between each other. Thus there is no difference in composition between different bubbles in a stirred vessel at recirculation conditions. This is in agreement with the results of Reith and Beek (1970), who measured a well-mixed bubble population for noncoalescing liquids, provided that the stirrer speed was large enough.

9.4.1.4 Conclusions for the stirred vessel

The liquid mixing times for one-phase systems can be calculated from an equation that is based on the flow mechanisms in the vessel. For two-phase systems knowledge about the flow mechanisms is rather scarce. Yet it proved to be possible to derive equations from which the mixing times can be calculated, by assuming the mechanisms to be the same as for one-phase systems. For gas rates near the flooding region there might be a large, but unknown influence of the gas flow rate. For gas phase mixing the data are very scarce. At recirculating conditions the gas phase can be regarded as ideally mixed.

9.4.2 The bubble column

9.4.2.1 Liquid mixing

An extensive review of hydrodynamics and mixing in bubble columns is

presented by Heijnen and Van 't Riet (1984). The data in this chapter are taken from that article.

Bubbles that originate at the sparger will rise in the column as a bubble swarm. If there are no circulatory flows, the flow is defined as homogeneous. In that case all the bubbles will rise with the same upward velocity. Mixing originates only from the entrained liquid in the wake of each bubble. This mixing effect is limited. It can be expressed by a dispersion coefficient as

$$D_{el} = 10^{-3} - 10^{-2} \quad \text{homogeneous flow} \quad (\text{m}^2 \text{s}^{-1}) \quad 9.19$$

Homogeneous flow can occur only when the sparger holes are evenly distributed on the bottom of the vessel. Even in that case it occurs only at low gas superficial velocities.

If the sparger holes are not evenly distributed or the gas flow rate is high, local differences in liquid velocities will occur. This leads to differences in coalescence and to differences in hold-up distribution in the fermenter. It appears in bubble columns that a stabilized flow regime occurs, in which there exists an upward current at the center of the column and a downward current at the outer side of the column. The upward and downward currents flow through nearly equal areas. It appears that in tall columns the circulation is divided into loops that have a height of about the column diameter. This so-called heterogeneous flow regime is given schematically in Fig. 9.6 (already shown as Fig. 6.5).

The heterogeneous flow regime occurs at all gas velocities if the sparger holes are unevenly distributed on the vessel bottom. If there is an even distribution, low superficial velocities result in a homogeneous flow regime and high superficial velocities result in a heterogeneous flow regime. The transition can take place at a gas superficial velocity v_{gs} , as high as about 4 cm s⁻¹, however only at extreme conditions like a perfectly even distribution of the sparger holes. Nearly all commercial fermenters show the heterogeneous flow regime.

Mixing for the heterogeneous regime can be described in a number of ways. Due to its character a description with a circulatory velocity is logical. The review of Heijnen and Van 't Riet (1984) gives for v_{lc} (m s⁻¹) the liquid velocity in the center of the column:

$$v_{lc} = 0.9 (g T_v v_{gs}^c)^{0.33} \quad \text{heterogeneous flow} \quad (\text{m s}^{-1}) \quad 9.20$$

The v_{gs}^c is the pressure corrected gas superficial velocity in the column. Due to the large density difference it can be assumed that the actual volume

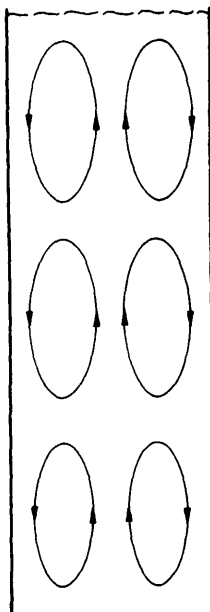


Fig. 9.6 Schematic representation of the time-averaged circulatory flows at the heterogeneous flow regime.

(superficial velocity) of the gas in the column is relevant. It can also be given as a dispersion coefficient:

$$|D_{el}| = 0.33 (g T_v^4 v_{gs}^c)^{0.33} \quad \text{heterogeneous flow} \quad (\text{m}^2 \text{s}^{-1}) \quad 9.21$$

There is no equation available for the mixing time. Yet this can be derived from the circulatory flow. The average liquid upward velocity is about $0.8 \times v_{lc}$. This delivers, with Eq. (9.20) and combined with the knowledge that upward and downward flow go through the same area:

$$F_l = 0.28 (g v_{gs}^c T_v^7)^{0.33} \quad H_v = T_v \quad (\text{m}^3 \text{s}^{-1}) \quad 9.22$$

Introducing the tank volume delivers the circulation time:

$$t_c = 2.8 (g v_{gs}^c T_v^{-2})^{-0.33} \quad H_v = T_v \quad (\text{s}) \quad 9.23$$

Now an assumption has to be made about the relation between mixing time

and circulation time. The same relation as for stirred vessels [Eq. (9.10)] might be the best choice. The equation can be made valid for $H_v > T_v$ by multiplying with the number of compartments = H_v/T_v .

$$t_m = 11 \frac{H_v}{T_v} (g v_{gs}^c T_v^{-2})^{-0.33} \quad \text{heterogeneous flow assumed } t_m = 4 t_c \quad (\text{s}) \quad 9.24$$

9.4.2.2 Gas mixing

For the homogeneous flow regime the gas phase can be regarded as a plug flow. For the heterogeneous regime the liquid circulation will entrain gas bubbles and a certain amount of backmixing will occur. The above mentioned review gives an equation for gas mixing expressed in a dispersion coefficient:

$$D_{eg} = 78 (v_{gs}^c T_v)^{1.5} \quad \text{heterogeneous flow} \quad (\text{m}^2 \text{s}^{-1}) \quad 9.25$$

Eq. (9.25) shows that the dispersion coefficient is strongly dependent on the tank diameter. This is the reason that for small, tall tanks the gas phase can be regarded as a plug flow. In contrast to this, large and not too tall ($H_v/T_v < 3$) tanks have a gas phase that can be regarded as ideally mixed. Example 9.3 elucidates this.

9.4.2.3 Conclusions for the bubble column

Mixing in a bubble column is dependent on the flow regime in the vessel. Two regimes can be distinguished, the homogeneous one, which occurs only at low superficial velocities together with an evenly distributed sparger, and the heterogeneous one, which occurs in all other cases. For each of these situations equations can be given that describe the mixing.

9.4.3 The air lift

9.4.3.1 Liquid mixing

The air lift is shown schematically in Fig. 9.7. The driving force for the liquid circulation is the density difference between riser and downcomer. The gas hold-up in the downcomer is zero or in any case much lower than that of the riser, ϵ_r . The circulating velocity is then given by the balance between the pressure difference originating from ϵ_r and the flow resistance in the loop determined by the liquid velocity v_L , as:

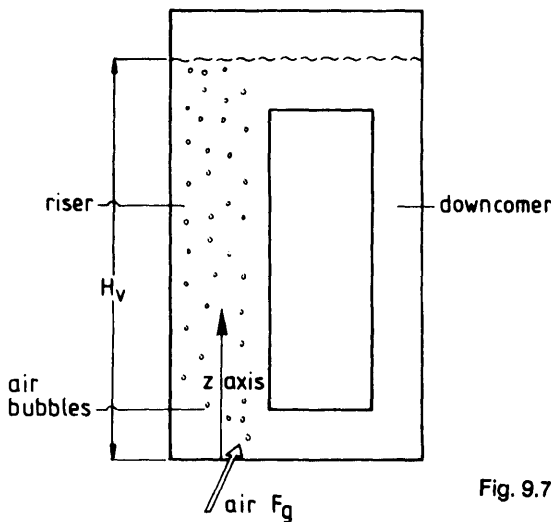


Fig. 9.7 Schematic representation of an air lift reactor.

$$\int_0^{H_v} g \epsilon_r(z) dz = 0.5 K_f (v_{ls})^2 \quad (\text{m}^2 \text{s}^{-2}) \quad 9.26$$

in which

$$\begin{aligned} z &= \text{vertical coordinate} \\ \epsilon(z) &= \text{local gas hold up} \end{aligned} \quad (\text{m}) \quad (-)$$

Eq. (10.3) shows that the local gas hold-up can be calculated from the local liquid velocity, the superficial gas velocity and the velocity difference between bubbles and surrounding liquid. Because the liquid velocity is present in this relation, an iteration procedure has to be developed to solve the equations. This was done by Verlaan et al. (1986). It is given schematically in Fig. 9.8. The resistance to the flow is presented by the friction coefficient K_f . It is the sum of the resistance coefficients of the friction of the riser and downcomer, the friction in the bends that connect the riser and downcomer and the inserts, if present. For engineering of a new fermenter, the K_f values can be estimated from data books and for an existing fermenter, they can be measured accurately by measuring ϵ , and v_{ls} , as Eq. (9.26) shows that a straightforward relation between these two values and K_f does exist (when ϵ in the downcomer is zero). The calculation scheme given in Fig. 9.8 gives us the possibility to calculate the circulation velocity in any air lift fermenter without the need of measurements. Example 9.4 shows calculated values for air lift reactors of

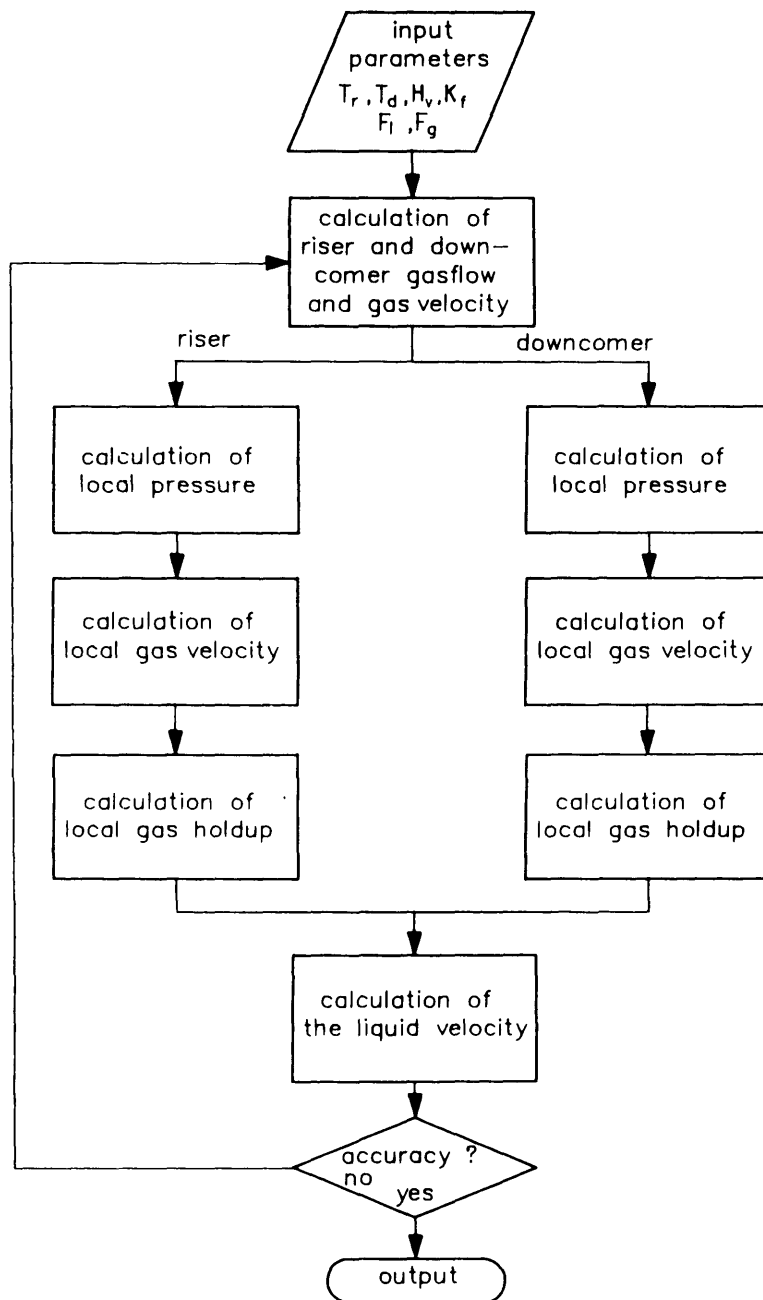


Fig. 9.8 Calculation scheme for calculation of the liquid velocity in an air lift. (Adapted from Verlaan et al., 1986.)

different sizes. Fig. 9.9 shows calculations and measurements for two air lift reactors. The circulating velocities are in the range of 0.5 up to 5 m s⁻¹ for a large range of gas superficial velocities. The calculations also show that large-scale air lift reactors show a larger circulating velocity than small laboratory-scale counterparts. This is due to the fact that the contribution to the friction of the riser and downcomer decreases with increasing diameter.

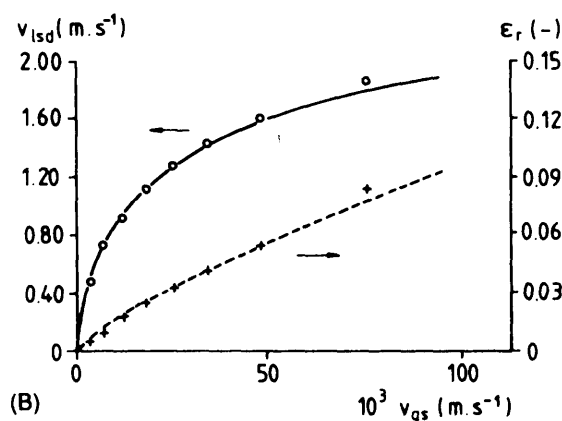
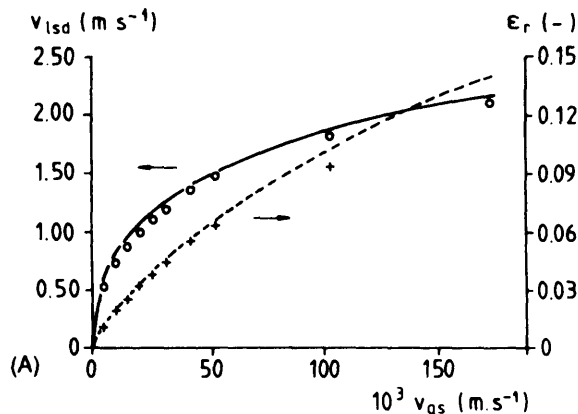


Fig. 9.9 Calculated and measured superficial liquid velocities of the downcomer (v_{lsd}) and gas hold-up in the riser (ϵ_r) as a function of the gas velocity. (Adapted from Verlaan et al., 1986.) A. 0.165 m³ ALR; o, +, experimental; —, —, model predictions. B. 0.6 m³ ALR; o, +, experimental; —, —, model predictions.

The mixing time is related to the circulation time. Verlaan et al. (1986) found that the *Bo* number was in the range of 50–70. With a criterion for the mixing intensity of 95% this results in a mixing time

$$t_m = (4 - 7) t_c \quad \begin{matrix} \text{air lift} \\ 95\% \text{ criterion} \end{matrix} \quad (\text{s}) \quad 9.27$$

This relation offers the possibility of calculating the mixing time by means of the circulation time calculated from v_{ls} . Example 9.5 shows a comparison of the mixing times of stirred tanks, bubble columns and air lifts of the same volume. It appears that at very low superficial gas flow rates the stirred tank shows the best mixing behavior. At high superficial gas flow rates the air lift is preferable, even although its height is 10 times its diameter. In the region in between, the differences are remarkably limited. It is remarkable that at very high superficial velocities the bubble column has lower mixing times than the stirred tank of the same dimensions. The mixing provided by the circulatory flows caused by the bubbles appears to be more efficient than that of the circulating flow of the stirrer.

Until now it has been assumed that a uniform upward-directed flow profile exists in the riser and the same downward-directed flow profile in the downcomer. This is true only for low resistances to flow. Verlaan et al. (1989) show that starting from this situation, an increase of the friction finally leads to a transitional flow regime, between that of the uniform profile of the air lift and the circulatory flows of the bubble column. The existence of such a transition can be expected, because the limit of a totally closed downcomer indeed leaves a riser functioning as a bubble column. The transition occurs at

$$v_{lc} \text{ (bubble column)} \approx v_{ls} \text{ (air lift)} \quad (\text{m s}^{-1}) \quad 9.28$$

or in words: The transition occurs in the region where the liquid superficial velocity in the riser becomes of the same order of magnitude as the liquid circulation velocity [Eq. (9.20)] at the same conditions in a bubble column of that dimensions. In small air lifts or air lifts with inserts these conditions can be met. The mixing time then will be between that of an air lift and that of a bubble column.

9.4.3.2 Gas mixing

In the air lift-type flow regime it can be assumed that the gas mixing is given by the plug flow situation. In the transition region the mixing will be more intensive, until the situation where the bubble column type of flow and corresponding gas mixing [Eq. (9.25)] is reached.

9.4.3.3 Conclusions for the air lift

Mixing times in the air lift can be calculated, although an iteration procedure is needed for that purpose. There are no limitations to these calculations with regard to scale. The flow regime in the air lift has to be checked as there is a possibility that the air lift actually can operate like a bubble column, particularly at small scales.

9.4.4 The packed bed

9.4.4.1 Liquid mixing

Liquid mixing can be characterized by the *Bo* number, corrected for the particle hold up as

$$Bo' = \frac{\bar{v} d_p}{\epsilon_p |D_s|} \quad (-) \quad 9.29$$

Levenspiel and Bischoff (1963) reviewed a number of data and showed

$$2 < Bo' < 5 \quad \text{for } Re = \frac{d_p \bar{v} \rho_l}{\mu_l} < 50$$

$$0.5 < Bo' < 5 \quad \text{for } 50 < Re < 500$$

$$Bo' < 0.5 \quad \text{for } Re > 500$$

This means that for a reactor height $H_v > 100 d_p$, the reactor can be regarded as the plug flow type. It is assumed that short circuiting due to uneven distribution of the particles is absent.

9.5 Measuring methods

9.5.1 Introduction

A wide variety of measuring methods can be found in the literature. Most of them can be applied for measurements in a batch vessel, as well as in throughflow apparatus for input-output measurements. The choice will mainly be made after consideration of the mixing models for which the data are required. Here we will emphasize the practical aspects for each method. In general, a number of requirements can be defined:

- The tracer or tracer fluid must have physical properties similar to the liquid or gas in the vessel. This requires a tracer that is miscible, that, in case of a liquid, has a viscosity and density of the same value as the original liquid, that shows a negligible heat of mixing and that requires a negligible volume to be added.
- The tracer should not interfere with the fermentation broth. It must be nontoxic, sterile, cause no phase changes and have no antifoam properties. No environmental legislations have to be met.
- The tracer must not disappear. Tracers in the gas phase can get transferred to the liquid phase and vice versa. Tracers in the liquid phase can adhere to the microorganisms.
- The detector must not interfere with the process. For small-scale apparatus this means that sampling probes should not interfere with the flow field. For large fermenters this means that sterile sensors and sample points must be present in the vessel.

An extensive review of experimental methods and interpretation of data is given by White (1962).

9.5.2 The conductivity method

With this method an electrolyte tracer is added and the response is measured by a conductivity probe. This method is widely applied on a small scale, as can be concluded from a review by Shah et al. (1978). The advantages are the simplicity of the method and the fast response characteristics of the conductivity probe. For experiments with large-scale fermenters the method is useless. Large volumes of tracer liquid are needed ($100\text{--}500 \text{ dm}^3$ for a 100 m^3 fermenter) and the gas bubbles in the fermenter interfere with the measuring probe. Besides, the addition of an electrolyte and the related increase of osmotic pressure can lead to a change in rheological parameters of the broth and to a change in growth conditions.

9.5.3 The thermal method

With this method a volume of heated liquid is added and the response is measured with thermocouples. This method is seldom used and, if so, only on a small scale with model liquids. Problems are the low density of the tracer liquid and the immense volume to be added for large-scale fermenters.

9.5.4 The pH method

With this method an acid or base is added and the response is measured by one or more pH electrodes. The titration curve presents problems. We can

not simply use this curve because it is not linear. The signal has to be converted to a base or acid concentration curve. To overcome this, a fixed trajectory can be chosen by carefully adjusting the pH to a specific value and by adding a fixed amount of acid. This procedure then has to be repeated for each measurement.

Another limitation in the choice of the trajectory is the equilibrium between carbon dioxide and carbonate. Danckwerts and Sharma (1966) show that the reaction is very fast for carbon dioxide → carbonate but relatively slow for carbonate → carbon dioxide. Indeed, after base addition a drift of the reading seems to take place. This does not occur after acid addition. Thus only acid addition can be used for mixing time measurements.

Although complex, the pH method is often preferred for large-scale mixing time measurements. The probes are fast and sterilizable, often already present in the vessel and acid and base addition circuits usually are present.

9.5.5 The radioactive tracer method

With this method a radioactive tracer is added and mixing is measured by sampling or by measurement in outflow tubes. In the latter case the detector can be placed outside the tube. If safety precautions are satisfied, this method has a number of advantages. Only a small volume of tracer material is needed, it is accurate at low concentrations, sterile addition is easy and small sample volumes or on-line measurement are possible. Disadvantages can be safety aspects and a gas phase tracer might diffuse into the liquid. Applications on a small scale are reviewed by Shah et al. (1978). Large-scale applications are reported by Jansen et al. (1978) and Field and Davidson (1980). This method can be regarded as interesting for mixing measurements on a large scale.

9.5.6 The coloring or decoloring method

With this method a coloring or decoloring agent is added, such as methylene blue or iodine/starch. A review is given by Hiby (1981). The dispersion of the tracer is followed by eye, transparency measurement or spectrophotometry on samples. Decoloring can also be used with a change of pH in combination with an indicator, such as bromine thymol blue or phenolphthalein. Decoloration is particularly useful for the detection of stagnant regions. Examples can be found in the review of Shah et al. (1978).

This method is problematic for large scales and for fermentation broths on all scales. Many of these tracers adsorb to broth particles, some of these experiments are irreversible and some of these methods result in fermenters, filled with colored waste liquids. In addition, most large-scale vessels are

not transparent, and fermentation broths are not. This results in extensive sampling procedures. All these factors lead to the conclusion that, in general, large-scale applications of the (de)coloring method must be discouraged.

9.5.7 The flow follower method

Another technique is the addition of a neutrally buoyant flow follower housing a radio transmitter, the "radio pill." The passage of the pill through the impeller region is registered by a loop aerial surrounding the impeller. Details of this method can be found in Bryant (1976). This method seems to be interesting, but at this time not enough experience is available on large-scale applications and applications under sterile conditions. A principal problem will be the neutral buoyancy in gas liquid dispersions at varying hold-up values.

9.5.8 The chemical reaction method

All the methods described until now are macromixing measurements. The scale of mixing that can be determined is the scale of the probe or the sample and it will vary from about 1 mm up to about 1 cm. For biotechnological applications knowledge about mixing on this scale is adequate. For fast chemical reactions, micromixing on a molecular scale is important. These phenomena can be studied by using a well-defined model reaction system as was done by Bourne et al. (1982). These methods will not be discussed further because they are not important for biotechnological applications.

9.5.9 Conclusions concerning the measuring methods

For small-scale model systems many methods are known of which the conductivity method has been applied most frequently. This method is cheap and reliable for single-phase systems. For fermentation broths, particularly on a large scale, the pH and the radioactive tracer method are recommended. The scale of mixing of the measurement is determined by the size of the probe or the sample and is thus limited to macroscale. With respect to the intensity of mixing, care has to be taken to interpret the pH signal. The advantages and disadvantages of all measuring methods are shown schematically in Table 9.3.

9.6 Conclusions

Mixing can be described in a number of ways. The model descriptions are useful for reactions that take place in the reactor and for a better under-

Table 9.3 Advantages and disadvantages of the mixing time measurements for the model systems liquid and gas-liquid and for the fermentation broth, all separately for small and large scale

	Small scale ($< \sim 1 \text{ m}^3$)			Large scale ($> \sim 10 \text{ m}^3$)		
	Liquid (model)	Gas-liquid (model)	Gas-liquid- organism (fermen- tation)	Liquid (model)	Gas-liquid (model)	Gas-liquid- organism (fermen- tation)
	+	+ -	-	+	-	-
Conductivity	+	+ -	-	+	-	-
Thermal	+ -	+ -	-	-	-	-
pH	+ -	+ -	+	+ -	+ -	+
Radioactive tracer	+	+	+	+	+	+
(De)coloring	+	+ -	+ -	+ -	+ -	+ -
Flow follower	+	+ -	+ -	+	+ -	+ -
Schlieren	+	-	-	-	-	-
Chemical reaction	+	+ -	-	+	+ -	-

standing of the mixing process. Mixing data expressed as mixing times are known for all bioreactors. Measuring methods are readily available.

9.7 Examples

Example 9.1 The influence of a residence time distribution

Problems due to fractions with a very long residence time occur in fermenters. Assume a model for a fermenter as given in Fig. 9.10. Gas liquid

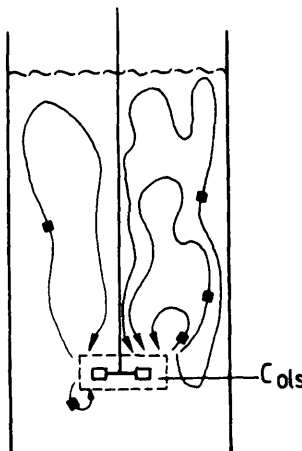


Fig. 9.10 Schematic representation of trajectories of (segregated) fluid elements. ■ Fluid element and its trajectory. — Region where oxygen mass transfer occurs.

mass transfer is assumed to take place only in the stirrer region. Fluid elements leave this region, travel through the vessel and finally will return to the stirrer region. It is assumed now that the fluid elements do not interact with each other; that is, they are completely segregated. All elements have different circulation times, with an average of t_c . For each fluid element the oxygen consumption will decrease the concentration of oxygen in the liquid, starting from C_{ols} , the concentration just after leaving the stirrer region. Assuming the oxygen consumption rate to be independent of the C_{ol} value, this leads to a critical time value t_{cro} , given by (see Fig 9.11).

$$t_{cro} = \frac{C_{ols}}{OUR} \quad (\text{s}) \quad 9.30$$

This means that all fluid fractions with a residence time value that is larger than t_{cro} will be depleted of oxygen before returning to the stirrer region. This is an example where problems do occur due to the large residence time fraction. Problems with oxygen depletion will be discussed more extensively in Chapter 18.

Example 9.2 Mixing times dependent on viscosity and scale

For two scale-up criteria, constant stirrer tip speed and constant power per unit volume, the mixing times given in Table 9.4 have been calculated. The

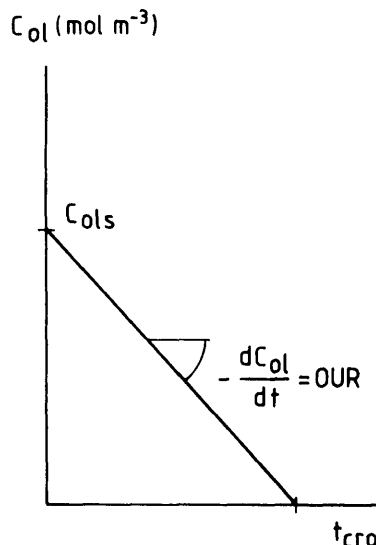


Fig. 9.11 The critical time for oxygen depletion.

Table 9.4 Calculated mixing times

<i>V</i>	<i>T_v</i>	<i>N</i>	η	<i>Re</i>	<i>t_m</i>
(m ³)	(m)	(s ⁻¹)	(10 ⁻³ N s m ⁻²)	(-)	(s)
0.01	0.19	I	25.3	1	99×10^3
				100	994
				1000	99
				10000	10
					$> 10^6$!!
1	0.86	I	5.6	1	86×10^3
				100	857
				1000	86
				10000	9
					$> 10^6$!!
100	3.99	I	1.2	1	451×10^3
				100	4510
				1000	451
				10000	45
					10^5 !!
100	3.99	II	8.2	1	660×10^3
				100	6604
				1000	660
				10000	66
					10^5 !!
100	3.99	II	2.9	1	2.1×10^6
				100	2.1×10^4
				1000	2080
				10000	208
					925 !!
1000	3.99	I	1.2	1	5.0×10^6
				100	5.0×10^4
				1000	5028
				10000	503
					123

Assumptions made to calculate the mixing times:

$$H_v = 2 T_v$$

$$D = 0.33 T_v$$

1 stirrer

$$N_p = 2.5$$

$$\rho_i = 1000 \text{ kg m}^{-3}$$

Scale-up criteria:

$$\text{I: } v_{tip} = 5 \text{ m s}^{-1}$$

$$\text{II: } P_s / V = 2.5 \text{ kW m}^{-3}$$

columns in the table are calculated starting from V as follows:

- T_v is calculated from

$$V = \frac{1}{4} \pi T_v^2 2 T_v$$

- N is calculated for criterion I from

$$\pi N 0.33 T_v = 5$$

and for criterion II from

$$2500 = \frac{2.5 \times 1000 N^3 (0.33 T_v)^5}{V}$$

- η is stated as such
- Re is calculated from

$$Re = \frac{1000 N (0.33 T_v)^2}{\eta}$$

- t_m is calculated with the assumption that $t_m = 2t_m(H_v - T_v)$, with the last one calculated from Eq. (9.17). This is done because for this example $H_v = 2T_v$.
For $Re < 10,000$ the calculated value is corrected with the proportionality derived from Fig. 9.5.

There is a gradual increase of mixing time with scale. This is only valid in the fully turbulent region. The background is that the circulation time increases with scale because the distances increase, while the velocities stay nearly constant. In the low Re number region it can happen that for small scale the mixing time is extremely large, while for large scale, because of the higher Re value, the mixing time is much smaller than on the small scale.

A scale-up criterion of constant mixing time leads to extreme P_s/V values, as shown in Table 9.5. It cannot be applied for that reason.

Example 9.3 Mixing of the gas phase in bubble columns

When the Bo value $\rightarrow 1$, then the gas phase can be regarded as ideally

Table 9.5 The P_s/V required at scale-up with constant t_m value ($T_v/D = 3$)

V (m^3)	T_v (m)	t_m (s)	P_s/V Eq. (9.18) (kW m^{-3})
0.01	0.21	10	0.7
		100	0.0007
1	0.98	10	15.8
		100	0.016
100	4.57	10	349
		100	0.349

mixed. The dispersion coefficient of the gas phase is given by Eq. (9.25). The average convectional velocity of the gas phase can be estimated as follows. Most of the bubbles tend to concentrate in the center of the column. Then they move upward with the liquid with a velocity as given in Eq. (9.20). Additionally they move upward relative to the surrounding liquid, due to their own rise velocity. It is assumed here that this velocity is equal to the terminal rise velocity of 0.25 m s^{-1} . Two cases are worked out, for two bubble upward velocities, v_{bu} (m s^{-1}):

$$\text{Case I: } v_{bu} = v_{lc} + 0.25$$

$$\text{Case II: } v_{bu} = 0.5 v_{lc} + 0.25$$

With $Bo = v_{bu} H_v / D_{sg}$ this gives the Bo values for a number of bubble column fermenters given in Table 9.6.

The calculated values show that for tall columns the gas phase is ideally mixed for the large-scale vessel at a high v_{bu} value. For the columns with $H_v = T_v$, even the small column at high v_{bu} value is ideally mixed, while the gas phase in the large column is ideally mixed also at intermediate v_{bu} values.

Example 9.4 Calculated circulation velocities in air lift reactors

For an air lift reactor calculations for the circulation velocity have been made for reactors of 0.1, 0.5, 1.0, 5.0 and 10.0 m riser diameter, for a range of gas superficial velocities (normalized at atmospheric conditions).

Assumptions are:

- Water air system
- No additional top pressure

Table 9.6 Examples of measured *Bo* values

T_v (m)	H_v (m)	v_{gs} (m s ⁻¹)	$ D_{eg} $ (m ² s ⁻¹)	Case I		Case II	
				Bo (-)	Bo (-)	Bo (-)	Bo (-)
0.10	1.0	0.005	8.7×10^{-4}	463	375		
		0.01	2.5×10^{-3}	180	141		
		0.05	2.8×10^{-2}	21	15		
		0.10	7.8×10^{-2}	8.6	5.9		
0.10	0.1	0.005	8.7×10^{-4}	46	37		
		0.01	2.5×10^{-3}	18	14		
		0.05	2.8×10^{-2}	2.1	1.5		
		0.10	7.8×10^{-2}	0.9	0.6		
0.50	5.0	0.005	9.7×10^{-3}	263	196		
		0.01	2.8×10^{-2}	105	75		
		0.05	3.1×10^{-1}	13	8.6		
		0.10	8.7×10^{-1}	5.5	3.5		
0.50	0.5	0.005	9.7×10^{-3}	26	20		
		0.01	2.8×10^{-2}	11	7.5		
		0.05	3.1×10^{-1}	1.3	0.9		
		0.10	8.7×10^{-1}	0.6	0.3		
5.00	50.0	0.005	3.1×10^{-1}	132	86		
		0.01	8.7×10^{-1}	55	35		
		0.05	9.8×10^0	7.5	4.4		
		0.10	2.8×10^1	3.2	1.8		
5.00	5.0	0.005	3.1×10^{-1}	13	8.6		
		0.01	8.7×10^{-1}	5.5	3.5		
		0.05	9.8×10^0	0.8	0.4		
		0.10	2.8×10^1	0.3	0.2		

The assumed geometry is that given in Fig. 9.12 (for further details, see Verlaan et al., 1986). The total friction coefficient for this reactor is $K_f = 1.5$ for $H_r = 10 T_r$, and $K_f = 1.15$ for $H_r = 2 T_r$, with T_r = riser diameter. The results are given in Table 9.7. They show values of the same order of magnitude as for the stirred tank and the bubble column. Although the liquid velocities increase with scale, the increasing length leads to an increase of mixing time with scale.

Example 9.5 Comparison of mixing times of the stirred tank, the bubble column and the air lift

Results are given in Table 9.8. They were discussed in Section 9.4.3.1.

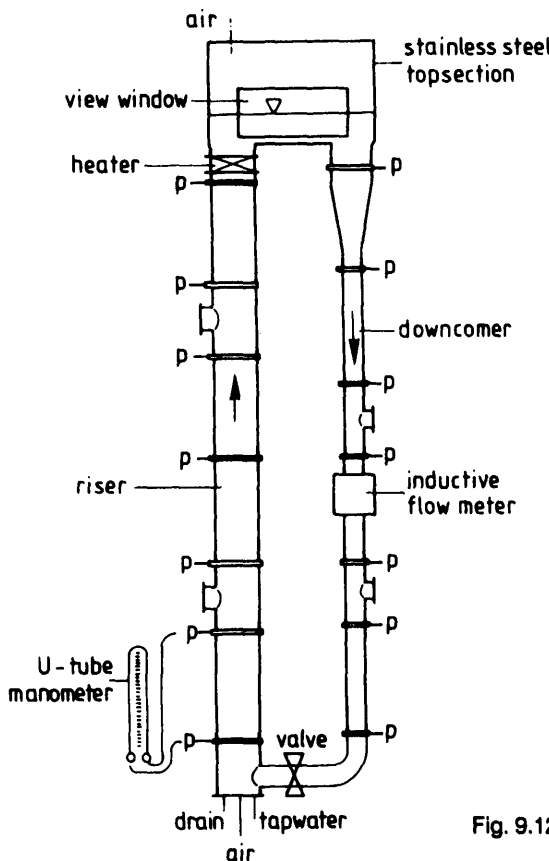


Fig. 9.12 The air lift loop reactor. (Adapted from Verlaan et al., 1986.)

Table 9.7 Circulation times in an air lift reactor

$H_v = 10 T_r$ and $T_d = 0.5 T_r$

V (m ³)	T_r (m)	H_v (m)	v_{sg} (m s ⁻¹)	v_{slr} (m s ⁻¹)	v_{std} (m s ⁻¹)	ϵ_r (-)	t_c (s)
0.01	0.1	1	0.001	0.05	0.200	0.003	33.4
			0.01	0.135	0.542	0.022	12.2
			0.05	0.25	1.009	0.078	6.3
			0.1	0.321	1.285	0.126	4.7
9.8	1.0	10	0.001	0.12	0.479	0.002	139
			0.01	0.30	1.205	0.011	55
			0.05	0.54	2.173	0.036	30
			0.1	0.69	2.758	0.058	24
265	3.0	30	0.001	0.16	0.640	0.001	313
			0.01	0.39	1.572	0.006	127
			0.05	0.703	2.810	0.020	70
			0.1	0.891	3.560	0.032	55
1221	5.0	50	0.001	0.178	0.172	0.001	469
			0.01	0.433	1.733	0.005	192
			0.05	0.772	3.087	0.015	107
			0.1	0.987	3.950	0.023	83

$H_v = 2 T_r$ and $T_d = 0.5 T_r$

V (m ³)	T_r (m)	H_v (m)	v_{sg} (m s ⁻¹)	v_{slr} (m s ⁻¹)	v_{std} (m s ⁻¹)	ϵ_r (-)	t_c (s)
0.01	0.172	0.34	0.001	0.035	0.140	0.003	32.8
			0.01	0.097	0.389	0.026	11.6
			0.05	0.184	0.736	0.093	5.9
			0.1	0.235	0.938	0.152	4.5
9.8	1.71	3.4	0.001	0.093	0.372	0.002	123
			0.01	0.239	0.956	0.016	47.6
			0.05	0.434	1.737	0.052	25.6
			0.1	0.551	2.210	0.084	18.1
265	5.13	10.3	0.001	0.134	0.537	0.002	256
			0.01	0.335	1.340	0.010	102
			0.05	0.602	2.410	0.033	56
			0.1	0.763	3.054	0.053	43
1227	8.55	17.1	0.001	0.156	0.624	0.001	368
			0.01	0.384	1.537	0.008	149
			0.05	0.686	2.747	0.026	82
			0.1	0.880	3.500	0.041	64

Calculations made by P. Verlaan. Information about his program can be obtained from: Wageningen Agricultural University, Section on Food and Bio Process Engineering, Biotechnion De Dreijen, P.O. Box 8129, 6700 EV, Wageningen, The Netherlands.

Table 9.8 Comparison of mixing times

Stirred tank, $H_v = 2 T_v$.
 $v_{up} = 5 \text{ m s}^{-1}$, $D = 0.33 T_v$, $N_p = 2.5$,
 $t_m = t_m, \text{Eq. (9.17)} \times 2$.

V (m ³)	T_v (m)	H_v (m)	D (m)	N (s ⁻¹)	t_m (s)
0.010	0.185	0.37	0.06	13.3	18
9.8	1.84	3.70	0.61	2.61	91
265	5.52	11.1	1.84	0.86	139
1227	9.21	18.4	3.07	0.52	230

Bubble column, $H_v = 2 T_v$.

$t_m = t_m, \text{Eq. (9.24)}$.

V (m ³)	T_v (m)	H_v (m)	v_{gs} (m s ⁻¹)			
			0.001	0.01	0.05	0.10
0.010	0.185	0.37	33	15	9	7
9.8	1.84	3.70	153	71	42	33
265	5.52	11.1	319	148	87	69
1227	9.21	18.4	449	208	122	97

Air lift, $H_v = 2 T_r$.

$t_m = 4 t_c$, t_c data from Example 9.4.

V (m ³)	T_r (m)	H_v (m)	v_{gs} (m s ⁻¹)			
			0.001	0.01	0.05	0.10
0.010	0.172	0.34	131	46	24	18
9.8	1.71	3.4	492	190	102	72
265	5.13	10.3	1024	408	224	172
1227	8.55	17.1	1472	596	328	256

Table 9.8 (continued)**Bubble column, $H_v = 10 T_v$.** $t_m = t_m$, Eq. (9.24).

V (m ³)	T_v (m)	H_v (m)	v_{gs} (m s ⁻¹)			
			0.001	0.01	0.05	0.10
0.010	0.11	1.08	117	54	32	25
9.8	1.08	11	537	249	146	116
265	3.23	32	1116	518	303	240
1227	5.38	54	1568	728	426	338

Air lift, $H_v = 10 T_r$. $t_m = 4 t_c$, t_c data from Example 9.4.

V (m ³)	T_r (m)	H_v (m)	v_{gs} (m s ⁻¹)			
			0.001	0.01	0.05	0.10
0.010	0.1	1.0	134	49	25	19
9.8	1.0	10.0	556	220	120	96
265	3.0	30	1252	508	280	220
1227	5.0	50	1876	768	428	332

References

Bourne J.R., Schwartz G. and Sharma R.N. "A new method for studying diffusive mixing in a tubular reactor." Proceedings 4th BHRA Conference on mixing. Noordwijkerhout (1982), Paper J3.

Bryant J. "The characterization of mixing in fermenters." Adv. Biochem. 5, 101 (1976).

Danckwerts P.V. and Sharma M.M. "The adsorption of carbon dioxide into solutions of alkalis and amines." Chem. Engng. 195 (1966).

Einsele A. "Scaling up bioreactors." Proc. Biochem. (July 1978), p. 13.

Einsele A. and Finn R.K. "Influence of gas flow rates and gas hold up on blending efficiency in stirred tanks." Ind. Engng. Chem. Proc. Des. Dev. 19, 600 (1980).

Field R.W. and Davidson J.F. "Axial dispersion in bubble columns." Trans. Inst. Chem. Engrs. 58, 228 (1980).

Gal-Or B. and Resnick W. "Gas residence time in agitated gas liquid contactor." Ind. Eng. Chem. Proc Des. Dev. 5, 15 (1966).

Hanhart J. Kramers H. and Westerterp K.R. "The residence time distribution of the gas in an agitated gas liquid contactor." Chem. Engng. Sci. 18, 503 (1963).

Heijnen J.J. and Van 't Riet K. "Mass transfer, mixing and heat transfer phenomena in low viscosity bubble column reactors." Chem. Engng. J. 28, B21 (1984).

Hiby J.W. "Definition and measurement of the degree of mixing in liquid mixtures." Internat. Chem. Engng. 21, 197 (1981).

Hinze J.O. "Turbulence." McGraw-Hill, New York (1959).

Hoogendoorn C.J. and Den Hartog A.P. "Model studies on mixers in the viscous flow regime." Chem. Engng. Sci. 22, 1689 (1967).

Jansen H., Slott S. and Gurtler H. "Determination of mixing in large scale fermenters using radioactive isotopes." Preprints 1st Eur. Congr. Biot. Interlaken (1978), Part 2 1/80.

Levenspiel O. "Chemical reaction engineering." John Wiley, New York (1972).

Levenspiel O. and Bischoff K.B. "Patterns of flow in chemical process vessels." Adv. in Chem. Engng. 4, 95 (1963).

Middleton J.C. "Measurements of circulation within large mixing vessels." Reprints Third Eur. Conf. Mixing (April 4-6, 1979).

Reith T. and Beek W.J. "Bubble coalescence rates in a stirred tank contactor." Trans. Inst. Chem. Engrs. 48, T63 (1970).

Shah Y.T., Stiegel G.J. and Sharma M.M. "Backmixing in gas liquid reactors." A.I.Ch.E. J. 24, 369 (1978).

Van 't Riet K., Boom J.H. and Smith J.M. "Power consumption, impeller coalescence and recirculation in aerated vessels." *Trans. Inst. Chem. Engrs.* 54, 124 (1976).

Verlaan P., Tramper J., Van 't Riet K. and Luyben K. Ch. A.M. "A hydrodynamic model for an air lift loop bioreactor with external loop." *Chem. Engng.* 33, B43 (1986).

Verlaan P., Vos J.C. and Van 't Riet K. "Hydrodynamics of the flow transition from a bubble column to an airlift loop reactor." *J. Chem. Techn. Biotechnol.* 45, 109 (1989).

Voncken R.M. "Circulatiestroming en menging in geroerde vaten." Thesis, Delft Technical University (1966).

White E.T. "Sources of error in the measurement of residence time distributions." *J. Imp. Coll. Chem. Engng. Soc.* 14, 72 (1962).

Zlokarnik M. "Rührtechnik." Band II, Verfahrenstechnik. Ullmann Encyclopedie der Technische Chemie, Verlag Chemie, Weinheim (1972).

10

Hold-Up

10.1 Introduction

The hold-up or void fraction, ϵ (-), is the volume of gas, V_g (m^3), present in a fermentation broth, expressed as a fraction of the total volume, $V_g + V_l$ (m^3).

$$\epsilon = \frac{V_g}{V_g + V_l} \quad (-) \quad 10.1$$

If v_{bw} ($m s^{-1}$) is defined as the velocity of the bubbles relative to the vessel wall, the hold-up can be derived as

$$\epsilon = \frac{v_{gs}^c}{v_{bw}} \quad (-) \quad 10.2$$

v_{gs}^c = pressure-corrected gas superficial velocity $(m s^{-1})$

The gas superficial velocity is corrected for the local pressure as this determines the actual gas volume in the reactor. v_{bw} is the sum of v_{bs} ($m s^{-1}$), the bubble rise velocity, or "slip" velocity, relative to the surrounding liquid, and v_{lw} ($m s^{-1}$), the velocity of the liquid relative to the vessel wall. Eq. (10.2) can then be rewritten as

$$\epsilon = \frac{v_{gs}^c}{v_{bs} + v_{lw}} \quad (-) \quad 10.3$$

The liquid velocities are strongly dependent on reactor type and process conditions as shown in Chapter 9. The bubble slip velocity is related to the

single bubble rise velocity v_{br} in an infinite medium. This velocity is given in Fig. 10.1.

The difference between v_{bs} and v_{br} is dependent on e.g. bubble swarm density and turbulence. Yet v_{br} is valuable as a first indication of v_{bs} . Fig. 10.1 shows that two regions can be distinguished. For bubble diameters $d_b < 1 \text{ mm}$, the region where bubbles behave as rigid spheres, v_{br} is strongly dependent on diameter. For $d_b > 1 \text{ mm}$, the region where the bubbles do have a mobile interface, the bubble rise velocity is between 0.2 and 0.5 m s^{-1} . An average value of 0.25 m s^{-1} is generally assumed.

10.2 Hold-up data

10.2.1 The stirred vessel

Flow phenomena in a stirred vessel are very complicated. It is therefore not possible to derive a hold-up formula starting from Eqs. (10.1) and (10.3). Hold-up values in stirred vessels are largely influenced by the coalescence characteristics of the liquid. In Chapters 6 and 11 these phenomena are discussed, as well as the complex composition of fermentation media. Therefore, only hold-up correlations for model systems will be discussed. By using the correlations derived for these model systems and by estimating the influence of fluid properties, an indication of the hold-up value in a fermentation liquid can be obtained.

10.2.1.1 Hold-up in water

Hold-up values in water (tap water, distilled water) have been measured by e.g. Joshi and Sharma (1977), Van 't Riet (1975), Hughmark (1980) and Yung et al. (1979). The first two articles deal with correlations of hold-up

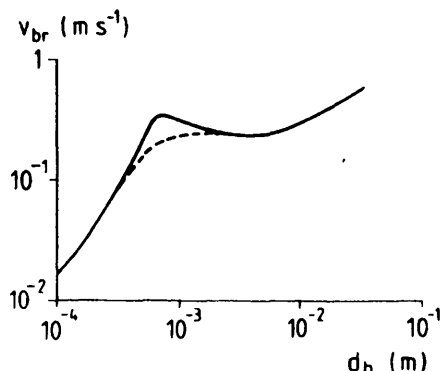


Fig. 10.1 The single-bubble rise velocity in an infinite medium. (Adapted from Heijnen and Van 't Riet, 1984.)

with stirrer power consumption per unit liquid volume, P_s/V_i (W m⁻³), and gas superficial velocity, v_{gs} (m s⁻¹). The last two deal with Froude, Weber and aeration numbers. Van 't Riet measured with different stirrer types, at 5 and 67 dm³ scale. He did not correct for pressure effects, but if a top pressure is applied, the hold-up values do not change when the dependence of the superficial gas velocity is given with the pressure-corrected superficial gas velocity at the stirrer as shown by Feijen et al. (1987). Therefore, the equation becomes:

$$\epsilon = 0.13 \left(\frac{P_s}{V_i} \right)^{0.33} \left(v_{gs} \frac{P_a}{P_s} \right)^{0.67} \quad (-) \quad 10.4$$

with

$$P_s = \text{pressure at the stirrer level} \quad (\text{N m}^{-2})$$

$$P_a = \text{atmospheric pressure} \quad (\text{N m}^{-2})$$

This formula predicts values near those of the other authors, presenting similar P_s/V_i and v_{gs} relationships. Example 10.1 shows also that the results of Feijen et al. (1987), who have measured up to 100 m³, are predicted, with the comment that they found a maximum hold-up value around 0.2 (20%) at larger commercial-scale (100 m³) fermenters. Hughmark (1980) has correlated an extensive number of results and found

$$\epsilon = 0.74 \left(\frac{F_g}{N V_i} \right)^{0.5} \left(\frac{N^2 D^4}{g H_s V_i^{0.67}} \right)^{0.5} \left(\frac{0.0025 \rho_l N^2 D^4}{\sigma V_i^{0.67}} \right)^{0.25} \quad (-) \quad 10.5$$

Remarks: Pure liquids (coalescing)
Turbine stirrer

These two formulae look very different. However, when Eqs. (10.5) and (10.4) are applied to the same data, it appears that both formulae give nearly the same results for small scales as well as for low v_{gs} values, as shown in Example 10.1. Example 10.1 also shows that Eq. (10.5) is rather similar to a P_s/V_i relationship. However, when extrapolating these equations to commercial-scale large vessels (>100 m³) Eq. (10.5) predicts lower values than Eq. (10.4). The conclusion is that Eq. (10.4) should be preferred because it is tested up to 100 m³; however, it can predict excessively high values at $\epsilon > 0.2$.

10.2.1.2 Hold-up in ionic solutions

The addition of salts strongly inhibits the coalescence of bubbles in a dispersion. The resulting smaller bubble size and lower single bubble rise

velocity, (see also Fig. 11.7), increase the hold-up when the bubble diameter becomes smaller than 1 mm.

Lee and Meyrick (1970) found increases up to a factor of 4. No quantitative empirical relation could be given. Qualitatively it can be stated that the ratio between hold-up in ionic solutions and tap water increases with increasing salt concentration, with increasing P_c/V_t values and with decreasing v_g values. Eq. (10.4) can be used to calculate a "bottom" value.

10.2.1.3 Liquids with a complex composition

In Chapter 12 on foaming it is stated that foaming characteristics and coalescence characteristics are usually related. More generally, it can even be said that all types of solutes (proteins, salts, antifoaming agents, alcohols) and culture conditions (pH , T) influence coalescence behavior and thereby the hold-up value. It must be accepted that for complex liquids no relationship can be found. Yet some prediction can be made. Pure water is a coalescing liquid. This means that a fermentation liquid will usually be somewhat or strongly less coalescing than water. Thus hold-up values will be somewhat or considerably higher than the values predicted by Eqs. (10.4) and (10.5). The values from these equations can be regarded as minimum values. Only for extremely coalescing liquids (if at all possible, e.g., by addition of large volumes of antifoam) can the hold-up become somewhat less.

For viscous liquids no data exist. It can be expected that the coalescence leading to extremely large bubbles decreases the hold-up compared to water. However, the presence of very small bubbles (Heijnen et al., 1980) cannot always be ignored and will increase the hold-up.

10.2.1.4 Conclusions for the stirred vessel

There are empirical correlations for hold-up values in pure water. These can be used to calculate minimum values for fermentation liquids. It can be expected that for low viscous fermentation liquids the hold-up will be somewhat larger than for pure water. For highly viscous liquids hold-up can not be predicted at all, as there is the positive effect of small bubbles and the negative effect of extremely large bubbles.

10.2.2 Hold-up values in the bubble column

10.2.2.1 Hold-up values in pure water

Distilled water and also tapwater of a decent quality is a coalescing liquid. This means that the bubbles that originate at the sparger will coalesce up to

the size where they become large enough to become dispersed. This continuous coalescence and dispersion process results in an equilibrium bubble size that is near 6 mm. This phenomenon was discussed more extensively in Chapter 6.

As shown in Chapter 9, two different flow regimes can occur in a bubble column, the homogeneous flow regime and the heterogeneous flow regime. The homogeneous flow regime is reached for special sparger constructions and at low v_{gs} values.

For the homogeneous flow regime Eq. (10.2) can be applied with v_{bw} as the bubble rise velocity v_{bs} . If the influence of the decrease in velocity due to the presence of a swarm is neglected, then $v_{bs} = v_{br}$. From Fig. 10.1 it can be seen that at $d_s = 6$ mm the single-bubble rise velocity is about 0.25 m s⁻¹. Thus the hold-up value becomes

$$\epsilon = \frac{v_{gs}^c}{0.25} \quad \begin{array}{l} \text{Tap water} \\ \text{Homogeneous regime} \\ \text{Swarm neglected} \end{array} \quad (-) \quad 10.6$$

with v_{gs}^c as the superficial gas velocity corrected for the local pressure, because if there are pressures in the fermenter that deviate from the atmospheric pressure, v_{gs} has to be corrected for this pressure. For tall columns this leads to the need for a calculation all over the column height. Usually the flow regime in a large-scale fermenter is heterogeneous. Heijnen and Van 't Riet (1984) show that Eq. (10.3) can then be applied. They also reviewed literature data and correlate these with a simple equation:

$$\epsilon = 0.6 (v_{gs}^c)^{0.7} \quad \begin{array}{l} \text{Tap water} \\ \text{Heterogeneous regime} \end{array} \quad (-) \quad 10.7$$

In commercial-scale fermenters the heterogeneous flow regime nearly always occurs. Therefore, Eq. (10.7) gives the hold-up fermenter for these fermenters. Example 10.2 shows that Eq. (10.7) and a modified Eq. (10.3) predict values in the same range.

10.2.2.2 Hold-up in ionic solutions

An ionic solution is noncoalescing. This means that the bubble size that originates at the sparger will be the bubble size in the column. This is only true when the bubble size is smaller than the equilibrium bubble size in the column. If the bubble size is larger, dispersion will take place down to the equilibrium bubble size, which is about 6 mm. Most of the spargers that are applied on a large scale do produce bubbles with a diameter > 6 mm.

Therefore, also for noncoalescing liquids the bubble size can be equal to that of a coalescing liquid. For the hold-up values this results in the same hold-up for coalescing and noncoalescing liquids in the case of a sparger that produces large (> 6 mm) bubbles. For a sparger that produces smaller bubbles the hold-up can be larger. This will particularly be the case for $d_b < 1$ mm, where the single bubble rise velocity starts to increase considerably. The equations become

$\epsilon = \frac{v_{gs}^c}{0.25}$	Noncoalescing Homogeneous flow Large-bubble sparger	(-)	10.8
$\epsilon > \frac{v_{gs}^c}{0.25}$	Noncoalescing Homogeneous flow Small-bubble sparger	(-)	10.9
$\epsilon = 0.6 (v_{gs}^c)^{0.7}$	Noncoalescing Heterogeneous flow Large-bubble sparger	(-)	10.10
$\epsilon > 0.6 (v_{gs}^c)^{0.7}$	Noncoalescing Heterogeneous flow Small-bubble sparger	(-)	10.11

In commercial-scale fermenters the heterogeneous flow regime nearly always occurs and the sparger nearly always produces large bubbles (see also Example 6.2). Therefore, Eq. (10.10), which is equal to Eq. (10.7), is again the standard hold-up formula that is applicable for these fermenters.

10.2.2.3 Hold-up for liquids with a complex composition

One of the most important phenomena in low-viscous fermentation liquids is the influence of surface-active materials on the coalescence properties of the liquid. Examples are proteins that are produced and surfactants from antifoam liquids that are added to the fermentation and that are sometimes consumed or adsorbed. This means that a fermentation liquid usually will continuously change in the degree to which it is coalescing or noncoalescing, and hold-up can therefore change continuously. Predictions to which extent are not possible. It will be very limited if a large-bubble sparger is applied. For commercial-scale fermenters Eq. (10.7) gives a "lowest" value that will be near the existing value for most situations.

Viscosity also has a large influence. Up to about 10×10^{-3} N s m $^{-2}$ the hold-up can either increase or decrease, most probably due to changes in coalescence characteristics. Usually a liquid also shows a viscosity region

with increased foaming behavior, for instance if a polymer is added. At higher viscosities two effects determine the hold-up. Increased viscosity leads to an increased coalescence. Very large bubbles are formed, whereby diameters of 0.1-1 m are possible. This results in a drastic decrease of the hold-up. On the other hand, highly viscous systems can contain very small bubbles, as shown by Heijnen et al. (1980). These bubbles will have a very low-rise velocity and can increase the hold-up value. In general, the result is a decrease in hold-up at viscosities larger than $10-100 \times 10^{-3} \text{ N s m}^{-2}$. However, for fermentation purposes bubble columns are useless at high viscosity values from the viewpoint of mass transfer, so detailed information is not needed.

10.2.2.4 Conclusions for bubble columns

The hold-up for a coalescing low-viscous liquid with heterogeneous flow can be determined by means of the experimentally found Eq. (10.7). This correlation also can serve as a minimum value for hold-up calculations for not purely coalescing liquids. The extent to which the hold-up in that case deviates from the coalescing value depends on the liquid properties as well as on the sparger characteristics. Many times this will lead to hold-up values that are nearly the same as for coalescing conditions.

An important variable is the liquid viscosity. At viscosities above $10-100 \times 10^{-3} \text{ N s m}^{-2}$ the hold-up will decrease due to the formation of extremely large bubbles.

10.2.3 Hold-up values in the air lift

10.2.3.1 Pure water

The characteristic feature of the air lift is the liquid circulating velocity. This means that bubbles in the riser section are transported upward. In the upper horizontal section they leave the reactor. These phenomena lead to a hold-up value that is lower than for a bubble column at the same conditions. Fig. 10.2 shows results of measurements in a pilot scale air lift reactor, together with values for a bubble column calculated with Eq. (10.7).

In Chapter 9 the existence of a transitional flow regime in an air lift is discussed (Verlaan et al., 1989). This is the region where the flow changes from an air lift type to a bubble column type. The hold-up can be expected to increase with a change from an air lift type to a bubble column type of flow. An example is given in Fig. 10.3.

The existence of the transition region and the dependence of the hold-up value on the circulating velocity make it impossible to give a simple rela-

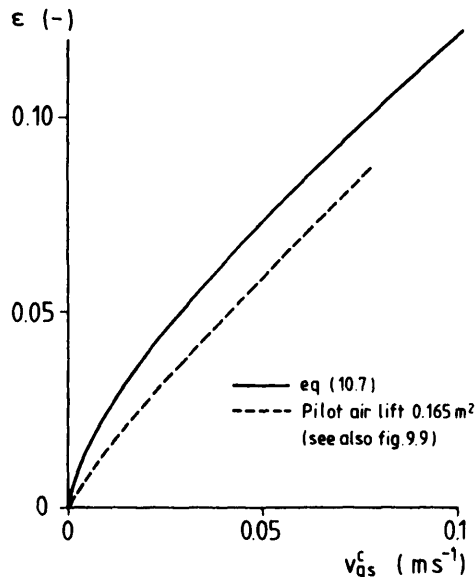


Fig. 10.2 Hold-up values for an air lift fermenter (adapted from Verlaan et al., 1986) and bubble column (Eq. 10.7).

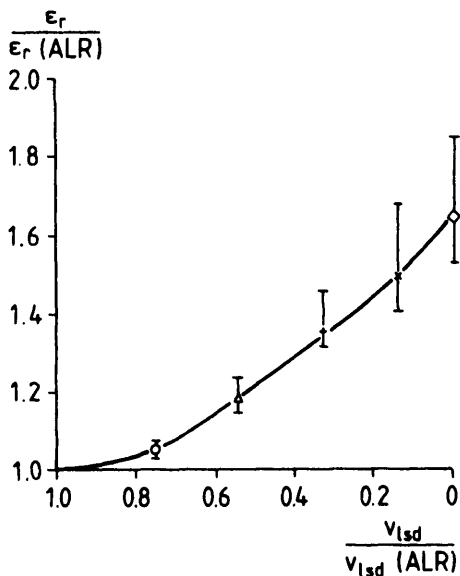


Fig. 10.3 The hold-up value in the riser, ϵ_r (-), relative to $\epsilon_r (ALR)$, the hold-up value for an air lift fully operating as an air lift. Different flow regimes are obtained by changing the position of a valve situated in the lower horizontal tube. $K_f = \infty$, $v_{lsd} = 0$ is a fully closed valve and a riser operating as a bubble column. (Data adapted from Verlaan et al., 1986.)

tionship for hold-up values in an air lift fermenter. Verlaan et al. (1986) were able to calculate hold-up in air lift type of flow by modeling liquid and gas flow in a calculation scheme as given in Fig. 9.8. A simple method to obtain a maximum value is the use of Eq. (10.7). The value in the air lift is always below this value, down to about 50%. For an exact calculation the following procedure should be followed. First, the flow regime has to be established with Eq. (9.28). For an air lift type of flow the calculation given by Verlaan et al. (1986) can be used (see Fig. 9.8). For a bubble column type of flow Eq. (10.7) can be used. For a transition region type of flow the hold-up will be somewhere in between the two values calculated for bubble column and air lift type of flow, respectively.

An air lift-type reactor is well suited for very tall columns. This means that the hold-up can change along the height of the reactor due to the differences in local hydrostatic pressure. Verlaan et al. (1986) give examples of this effect. If these effects become relevant, they should be included in the formula.

10.2.3.2 Ionic solutions and media with a complex composition

The influence of ions, additives and solutes is the same as for the bubble column, as is the influence of the sparger. Therefore, we can refer to Section 10.2.2.

10.2.3.3 Conclusions for the air lift reactor

Hold-up calculations are complicated because the liquid circulating velocity has to be calculated beforehand. Yet they can be calculated when flow modeling is included. The possibility of a transition region makes the calculations complicated.

10.3 Measuring methods

10.3.1 Level measurements

In the simplest case, a transparent fermenter is used and the level of the gas liquid dispersion and of the ungassed level is measured by eye. These level measurements allow the hold-up calculation with Eq. (10.1). In the case of foaming and large fluctuations, the accuracy of this technique is rather poor. This limits the applicability of this method, as does opacity of the stainless steel of most fermenters.

The level can also be measured by a single pressure measurement in the liquid near the surface. This can be done by a tube connected to a manometer, as executed by Rushton and Bimbinet (1968) and Lee and

Meyrick (1970). A general problem is the interference of liquid with the measurement velocities and the related kinetic pressure. To prevent this disturbing effect a perforated tube can be used. Rushton and Bimbinet have for that reason put a loose packing of glass wool between an inner and outer tube to obtain a really quiet surface. These pressure measurements can be applied on a laboratory scale in model liquids. In fermentation liquids the apparatus will be subject to extensive fouling. The advantage of these methods is that they are rather insensitive to the occurrence of a foam layer.

A simple, straightforward method of direct measurement is the use of a float. The accuracy is limited as liquid velocities influence its position and the extensive fluctuations in its position have to be leveled off somehow. At large scales mechanical problems can become severe, particularly in relation to lateral liquid velocities and "signal" transmission to a point outside the vessel, particularly at sterile conditions. A number of methods are known that are based on level measurements by electronic devices. A simple one is measurement of the conductivity between the fermenter wall and two electrodes, one just above and one just below the liquid level. Due to its yes/no discrimination, a number of these electrodes have to be positioned in the vessel. The accuracy is directly dependent on this number. This method does not discriminate between hold-up and foam. In fact, this is applied usually as an alarm device for foaming in fermenters. Other means of measuring the local presence of liquid or air are the thermal conductivity and the capacitance or electrical resistivity sensor. The resistors are cooled when immersed in the liquid. The capacitance between two plates changes with liquid present instead of air. These methods can even discriminate between hold-up and foam. Yet a principal disadvantage is its discontinuous measurement leading to the necessity of a number of sensors above each other, for continuous measurement. Fouling problems can be severe.

10.3.2 Local density measurements

In laboratory model systems a number of methods have been developed for determination of local gas hold-up values. Calderbank (1958) worked with the local sampling of gas, Hills (1974) used an electrical resistivity probe and Calderbank and Rennie (1962) used flashlight photography. Although these methods are applicable for scientific purposes, their use in commercial fermentations is impracticable.

Calderbank et al. (1960) used a measurement with a gamma radiation beam. This enables determination of the mean hold-up along the path between the source and the detector. It appears that this method can be used on production fermenters during normal running. The same principle is applied where microwaves are used as a detection method.

Gas hold-up can be calculated from pressure measurements at various heights. This can be done by a probe in the dispersion (Rushton and Bimbinet, 1968) or by measurement at pressure tap points. The principle is illustrated in Fig. 10.4.

The calculation reads

$$p_2 - p_1 = \rho_d g h \quad (\text{N m}^{-2}) \quad 10.12$$

$$\rho_d = (1 - \epsilon) \rho_l \quad (\text{kg m}^{-3}) \quad 10.13$$

Combining these two delivers

$$\epsilon = 1 - \frac{p_2 - p_1}{\rho_l g h} \quad (-) \quad 10.14$$

ρ_d = density of the dispersion (kg m^{-3})
 ρ_l = density of the liquid (kg m^{-3})

It must be borne in mind that the data will be influenced by the dynamic pressure due to the local liquid velocity. Particularly on a small scale this effect renders this method problematic. However, on large-scale fermenters this method might be favorable, provided that for stirred vessels the pressure taps are situated outside the impeller discharge. One advantage is that the measurement data can also be used as a mass control measurement by a careful positioning of the taps. For large-scale fermenters sterilizable pressure sensors with electrical sensors are commercially available.

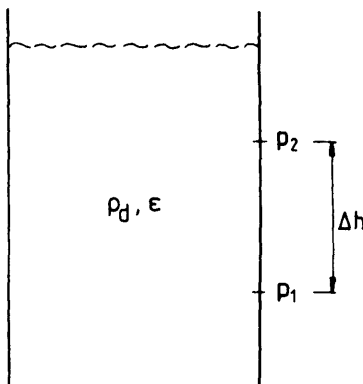


Fig. 10.4 Principle of the hold-up measurement by pressure measurements.

10.3.3 Tracergas method

Matsumara et al. (1978) used a tracergas method. Helium tracer is introduced in the aeration line. The head space of the tank is ventilated with air. Helium concentration in the exhaust gas is analyzed by gas chromatography. After the helium concentration has reached a steady-state value the gas flows entering and leaving the vessel are stopped simultaneously with the rotation of the impeller and hold-up bubbles rise into the head space. From the resulting change in the concentration the hold-up can be calculated.

10.3.4 Conclusions concerning measurement methods

The data given here, together with reasoning about applicability on large scale and commercial availability of sensors, leads to the conclusion that the hold-up (and mass) measurement by means of a number of pressure measurements along the vessel height is favorable for large-scale commercial applications.

10.4 Examples

Example 10.1 Calculated hold-up values for stirred vessels

In this example hold-up values are calculated for vessels of 0.05, 5 and 150 m³ liquid volume, respectively. Assumptions are:

$$T_v / D = 3. \text{ Turbine stirrer}$$

$$H_v / T_v = 1 \text{ (unaerated)}$$

$$P_s / V_t = 1500 \text{ W m}^{-3}$$

$$N_p = 2.5$$

$$\sigma = 0.07 \text{ N m}^{-1}$$

$$\rho_l = 1000 \text{ kg m}^{-3}$$

$$g = 10 \text{ m s}^{-2}$$

v_{gs} is given at normalized atmospheric conditions.

Stirrer is positioned at one stirrer diameter above the bottom.

Calculations used are:

$$N = \left(\frac{P_s}{V_t} \frac{V_t}{N_p \rho_l D^5} \right)^{0.33} \quad \text{as} \quad \frac{P_s}{V_t} = \frac{N_p \rho_l N^3 D^5}{V_t}$$

$$T_v = \left(\frac{4V_t}{\pi} \right)^{0.33} \quad \text{as} \quad V_t = \frac{1}{4} \pi T_v^2 T_v$$

$$\text{Eq. (10.5): } F_g = v_{gs} \frac{1}{4} \pi T_v^2$$

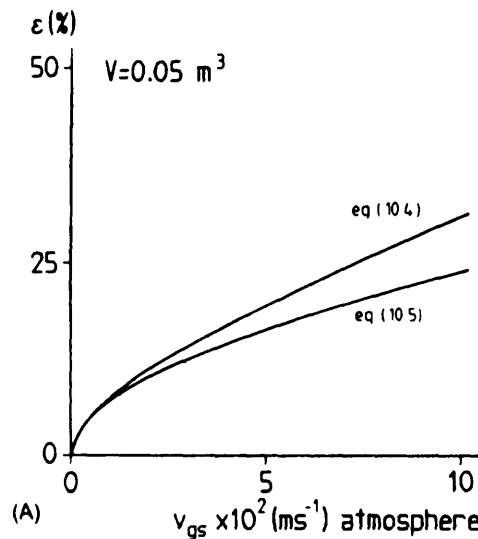


Fig. 10.5A-C Hold-up values for stirred vessels.

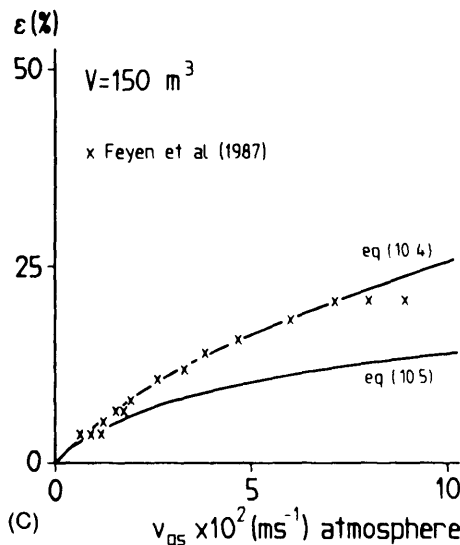
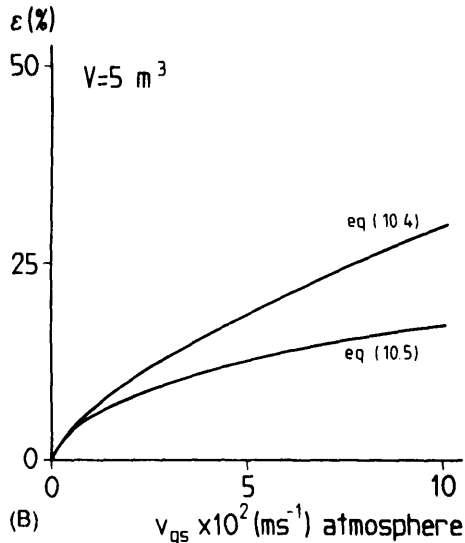
$$\text{Eq. (10.4): } v_{gs} \frac{P_a}{P_s} = v_{gs} \frac{P_a}{P_a + \frac{T_v - D}{10} \times 10^5} = \frac{v_{gs}}{1 + \frac{2T_v}{30}}$$

The following data can be calculated

V_t (m ³)	T_v (m)	D (m)	N (s ⁻¹)	Correction for v_{gs} (-)
150	5.76	1.92	1.51	1.38
5	1.85	0.62	3.20	1.12
0.05	0.40	0.13	9.31	1.03

By applying these data Figs. 10.5A-C are derived. Also, the experimental results of Feijen et al. (1987) for 100 m³ are presented. It is assumed that the pressure correction factor for their v_{gs} data is 1.5. Their results fit perfectly to Eq. (10.4). It must however, be remembered that Feijen et al. do not give accurate P_s/V_t data. These figures show that Eq. (10.4) predicts hold-up values rather well at large scales.

Eqs. (10.4) and (10.5) differ very much at first sight. However, Eq. (10.5) can be rewritten, assuming σ , N_p and ρ_t to be constant, as



$$\epsilon = c \left(\frac{P_s}{V_l} \right)^{0.33} (v_{gs})^{0.5} \frac{D}{T_v} D^{-0.17}$$

This is rather similar to Eq. (10.4), excluding the $D^{-0.17}$ relationship. This might very well be the reason for the low values predicted by Eq. (10.5) at large scales.

Example 10.2 Hold-up formula for a bubble column with a coalescing liquid

Empirical measurements of the hold-up value give the relation

$$\epsilon = 0.6 (v_{gs}^c)^{0.7} \quad (-) \quad 10.7$$

A correction for pressure effects is not applied in this example. Eq. (10.3) can also be used, if we introduce the assumptions (see also Chapter 9)

$$v_{bs} = 0.25$$

$$v_{lw} = 0.5 v_{lc} = 0.45 (g T_v v_{gs}^c)^{0.33}$$

Then Eq. (10.3) leads for a bubble column to

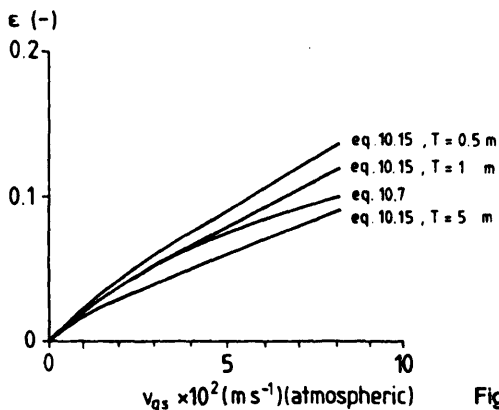


Fig. 10.6 Hold-up values for a bubble column. No pressure corrections were applied.

$$\epsilon = \frac{v_{gs}^c}{0.25 + 0.45(g T_v v_{gs}^c)^{0.33}} \quad (-) \quad 10.15$$

Fig. 10.6 shows the calculated values. They are all in the same range of values at a given gas superficial velocity. As can be seen from Eq. (10.15) the hold-up values calculated with this equation decrease slightly with increasing diameter. It might very well be that this effect will take place in very large fermenters. Then Eq. (10.7) might overestimate the hold-up values for these fermenters.

References

Calderbank P.H. "Physical rate processes in industrial fermentation." Part I: "The interfacial area in gas-liquid contacting with mechanical agitation." Trans. Inst. Chem. Engrs. 36, 443 (1958).

Calderbank P.H., Evans F. and Rennie J. In: Rottenberg P.A. (ed.) Intern. Distillation Symp. 1960 (London: The Inst. of Chem. Engrs.).

Calderbank P.H. and Rennie J. "The physical properties of foams and froths formed on sieve-plates." Trans. Inst. Chem. Engrs. 40, 3 (1962).

Feijen J., Heijnen J.J. and Van 't Riet K. "Gas hold-up and flooding in large scale fermenters." Proceedings Symp. on mixing and dispersion processes. Inst. of Chem. Engrs and KIVI/NIRIA. Delft (7 May 1987).

Heijnen J.J., Van 't Riet K. and Wolthuis A.J. "Influence of very small bubbles on the dynamic kLA measurement in viscous gas liquid systems." Biotechnol. Bioeng. 22, 1945 (1980).

Heijnen J.J. and Van 't Riet K. "Mass transfer, mixing and heat transfer phenomena in low viscosity bubble column reactors." Chem. Engng. J. 28, B21 (1984).

Hills J.H. "Radial nonuniformity of velocity and voidage in a bubble column." Trans. Inst. Chem. Engrs. 52, 1 (1974).

Hughmark G.A. "Power requirements and interfacial area in gas liquid turbine agitated systems." Ind. Eng. Chem. Proc. Des. Dev. 19, 638 (1980).

Joshi J.B. and Sharma M.M. "Mass transfer and hydrodynamic characteristics of gas induced types of agitators." Can. J. of Chem. Engng. 55, 683 (1977).

Lee J.C. and Meyrick D.L. "Gas liquid interfacial area in salt solutions in an agitated tank." Trans. Inst. Chem. Engrs. 48, 537 (1970).

Matsumura M., Masunaga H. Haraya K. and Kobayashi J. "Effect of gas entrainment on the gas hold-up in an aerated stirred tank." J. Ferment. Techn. 56, 128 (1978).

Rushton J.H. and Bimbinet J.J. "Hold-up and flooding in air liquid mixing." The Can. J. Chem. Eng. 46, 16 (1968).

Van 't Riet K. "Turbine agitator hydrodynamics and dispersion performance." Thesis, Delft Technical University (1975).

Verlaan P., Tramper, J., Van 't Riet K. and Luyben K.Ch.A.M. "A hydrodynamic model for an air lift loop bioreactor with external loop." Chem. Engng. J. 33, B43 (1986).

Verlaan P., Vos J.C. and Van 't Riet K. "Hydrodynamics of the flow transition from a bubble column to an airlift loop reactor." J. Chem. Techn. Biotechnol. 1988. 45, 109 (1989).

Yung C.N., Wang C.W. and Chang C.L. "Gas hold up and aerated power consumption in mechanically stirred tanks." Can. J. Chem. Engng. 57, 672 (1979).

11

Mass Transfer

11.1 The mass transfer equations

Mass transfer through a flat sheet boundary can be described with the Fick equation. A rectangular coordinate system (x , y , z) is chosen; x is defined in the direction perpendicular to the flat sheet. If convection is absent and concentration differences in the y and z direction are absent, the Fick equation becomes:

$$F_i''(x, t) = -D_i \frac{\partial C_i(x, t)}{\partial x} \quad (\text{mol m}^{-2} \text{s}^{-1}) \quad 11.1a$$

in which

F_i''	= molar flux of component i	$(\text{mol m}^{-2} \text{s}^{-1})$
D_i	= diffusion coefficient of i	$(\text{m}^2 \text{s}^{-1})$
C_i	= concentration of i	(mol m^{-3})

The mass transfer through a sheet with surface α and thickness dx can be determined from a microbalance. It is assumed that the y and z dependencies can be neglected.

$$\begin{array}{lcl} \text{In} & - & \text{Out} & + \text{ Production} = \text{Concentration change} \\ \alpha F_i''(x, t) & - & \alpha F_i''(x + dx, t) + \alpha dx r_i'(x, t) = \alpha dx \frac{\partial C_i(x, t)}{\partial t} & (\text{mol s}^{-1}) \end{array} \quad 11.1b$$

or

$$-\frac{\partial C_i(x, t)}{\partial x} + D_i \frac{\partial C_i(x + dx, t)}{\partial x} + r_i'(x, t) dx = \frac{\partial C_i(x, t)}{\partial t} dx \quad (\text{mol m}^{-2} \text{s}^{-1}) \quad 11.1c$$

For $C_i(x + dx, t)$ it can be written

$$C_i(x + dx, t) = C_i(x, t) + \frac{\partial C_i(x, t)}{\partial x} dx + \frac{1}{2!} \frac{\partial^2 C_i(x, t)}{\partial x^2} dx^2 + \dots$$

(mol m⁻³) 11.1d

Neglecting the second-order term in dx , because $dx \rightarrow 0$, and introducing Eq. (11.1d) in Eq. (11.1c) finally delivers

$$|D_i \frac{\partial^2 C_i(x, t)}{\partial x^2} + r'_i(x, t) = \frac{\partial C_i(x, t)}{\partial t}$$

(mol m⁻³ s⁻¹) 11.1e

For spherical coordinates the same reasoning leads to:

$$\frac{|D_i}{r_i^2} \frac{\partial}{\partial r} r^2 \frac{\partial C_i(r, t)}{\partial r} + r'_i(r, t) = \frac{\partial C_i(r, t)}{\partial t}$$

(mol m⁻³ s⁻¹) 11.1f

These are the basic equations to calculate mass transfer by diffusion processes.

Many mass transfer processes cannot be easily described with Eq. (11.1e) because convection also plays a role. Because usually the hydrodynamics are not well known, methods are developed to describe mass transfer with bulk concentration values. Particularly for mass transfer from the liquid to a particle and for gas-liquid mass transfer the equation is preferred that relates mass transfer with the bulk concentration values. These concentration values usually can be measured in the bioreactor. Fig. 11.1 gives the concentration profiles around the gas bubble.

With the concentrations as defined in Fig. 11.1, mass transfer from liquid to the gas phase can be described by an overall equation, when a mass transfer coefficient k (m s⁻¹) is introduced. k is a "lumped" parameter in which all mass transfer phenomena are included. Therefore, the value cannot always be determined on the basis of theoretical calculations only. The equation then becomes for the gas phase:

$$F''_i = k_{ig} (C_{ig} - C_{ig,i})$$

(mol m⁻² s⁻¹) 11.2

Based on the liquid phase a similar equation can be written:

$$F''_i = k_{il} (C_{ili} - C_{il})$$

(mol m⁻² s⁻¹) 11.3

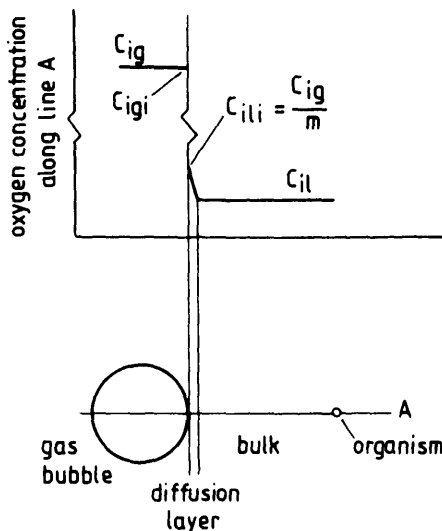


Fig. 11.1 Oxygen mass transfer from a gas bubble to the liquid.

in which

k_{ig}	= gas side mass transfer coefficient	(m s^{-1})
k_{il}	= liquid side mass transfer coefficient	(m s^{-1})
C_{ig}	= concentration of component i in the bulk of the gas phase	(mol m^{-3})
C_{il}	= concentration of component i in the bulk of the liquid phase	(mol m^{-3})
C_{igl}	= concentration of component i in the gas phase just at the gas-liquid interface	(mol m^{-3})
C_{ill}	= concentration of component i in the liquid phase just at the gas-liquid interface	(mol m^{-3})

The ratio of the solubility of component i in gas and liquid is given by the partition coefficient m , defined as

$$m = \frac{C_{igl}}{C_{ill}} = \frac{C_{ig}^*}{C_{il}^*} \quad (-) \quad 11.4$$

in which

C_{ig}^*	= concentration in the gas phase at equilibrium conditions with the liquid phase	(mol m^{-3})
C_{il}^*	= concentration in the liquid phase at equilibrium conditions with the gas phase	(mol m^{-3})

The mass flow can also be written as a function of the concentration in the two bulk phases. Then an overall K_i (m s^{-1}) is used as the "lumped" parameter:

$$F_i'' = K_i \left(\frac{C_{ig}}{m} - C_u \right) \quad (\text{mol m}^{-2} \text{s}^{-1}) \quad 11.5$$

Eqs. (11.2-11.5) show that

$$\frac{1}{K_i} = \frac{1}{m k_{ig}} + \frac{1}{k_{il}} \quad (\text{s m}^{-1}) \quad 11.6$$

These two equations are the general equations for mass transfer.

For gas-liquid mass transfer Eq. (11.5) can be simplified in many cases. This will be shown now for oxygen transfer. For oxygen $m = 32$ in air/water at 25°C. Later in this chapter it will be shown that the k value increases with an increasing diffusion coefficient. The diffusion coefficient of oxygen in the gas phase is larger than that in the liquid phase. These two reasons lead with Eq. (11.6) to the conclusion that for oxygen (index o) the resistance to mass transfer is situated in the liquid, because $1/(mk_{og}) \ll 1/k_{ol}$. Combining Eq. (11.6) with Eq. (11.5) delivers

$$F_o'' = k_{ol} \left(\frac{C_{og}}{m} - C_{ol} \right) \quad (\text{mol m}^{-2} \text{s}^{-1}) \quad 11.7$$

In gas-liquid oxygen transfer literature the notation $F_o'' A = OTR$ ($\text{mol m}^{-3} \text{s}^{-1}$) is usual, wherein A is the specific surface area of the bubbles (m^2 of bubble surface area per m^3 of liquid) and F_o'' is the molar flux of oxygen ($\text{mol m}^{-2} \text{s}^{-1}$) and OTR is the rate of oxygen transfer rate, the rate of the oxygen transfer from the gas to the liquid per m^3 of liquid ($\text{mol m}^{-3} \text{s}^{-1}$). With this notation Eq. (11.7) reads

$$OTR = k_{ol} A (C_{ol}^* - C_{ol}) \quad (\text{mol m}^{-3} \text{s}^{-1}) \quad 11.8$$

This equation will be used in this book for gas-liquid mass transfer.

Mass transfer from the liquid to a (spherical) biocatalyst particle differs from that to or from a gas bubble. In the particle there does not exist a bulk phase concentration, but a concentration profile does exist. Calculations inside the particle therefore are made by application of the Fick diffusion

equations, usually with a term included for consumption of the pertinent component. The boundary values then become

$$C_i = C_{ii} \quad \text{for } r = R_p \quad (\text{mol m}^{-3}) \quad 11.9$$

in which

$$R_p = \text{radius of the spherical particle} \quad (\text{m})$$

Mass transfer from the bulk to the particle surface can be described by an equation similar to Eq. (11.3) as

$$F_i'' = k_{il}(C_{ii} - C_{il}) \quad (\text{mol m}^{-2} \text{s}^{-1}) \quad 11.10$$

The flux F_i'' through the mass transfer boundary layer [Eq. (11.10)] is equal to the flux into the particle at $r = R_p$. For some cases, such as for charged diffusing components together with a charge particle, a partition coefficient has to be introduced in the equations.

11.2 Quantitative relationships for mass transfer

11.2.1 The k_{il} value

11.2.1.1 Gas-liquid k_{il} values

Lewis and Whitman (1924) described mass transfer as a diffusion process limited to a thin liquid film around the bubble, the diffusion layer (see Fig. 11.1). With a film thickness δ (m), and with the assumption of a linear concentration profile, Eqs. (11.1a) and (11.3) lead to

$$k_{il} = \frac{|D_{il}|}{\delta} \quad (\text{m s}^{-1}) \quad 11.11$$

in which

$$|D_{il}| = \text{diffusion coefficient of component } i \text{ in the liquid phase} \quad (\text{m}^2 \text{s}^{-1})$$

δ is not useful as a tool to calculate the k_{il} value, as it cannot be measured easily. But it certainly gives insight in the transport phenomena. For oxygen $|D_{oi}| = 2.3 \times 10^{-9}$ ($\text{m}^2 \text{s}^{-1}$) and $k_{oi} \sim 10^{-4}$ (m s^{-1}), as will be shown later in this chapter. Thus it can be calculated that

$$\delta \approx 10^{-5} \quad (\text{m}) \quad 11.12$$

This is small compared to the size of the bubbles ($1\text{-}6 \times 10^{-3}$ m) and small compared to the distance between the bubbles ($10^{-2}\text{-}10^{-3}$ m). Both results indicate a well-mixed liquid bulk. Then the assumption (Fig. 11.1) of mass transfer, limited to a film around the bubble, is indeed valid.

Another model description for k_{il} is the penetration film theory developed by Higbie (1935). For penetration into an infinite medium the flux after a time t is given by

$$F_i'' = \sqrt{\frac{|D_{il}|}{\pi t}} (C_{il}^* - C_{il}) \quad (\text{mol m}^{-2} \text{s}^{-1}) \quad 11.13$$

This theory is valid for the class of bubbles with a "moving" or "renewing" interface. For that case the bubble rises through the liquid without any liquid entrainment in the film layer. For such a bubble the exposure time of the liquid film can be estimated to be d_b/v_{bs} , [d_b is the bubble diameter (m) and v_{bs} is the bubble rise or slip velocity (m s^{-1})]. By integration over the surface of the bubble with exposure time between zero and d_b/v_{bs} , it can be calculated that

$$k_{il} = \sqrt{\frac{4 |D_{il}| v_{bs}}{\pi d_b}} \quad (\text{m s}^{-1}) \quad 11.14$$

This is a first approximation for k_{il} values for bubbles surrounded by a moving or renewing liquid film.

Just opposite to a moving interface is a completely rigid interface without any convective transport. Eqs. (11.1f) and (11.3) then yield, after extensive calculations not shown here:

$$\frac{k_{il} d_b}{|D_{il}|} = Sh = 2 \quad (-) \quad 11.15$$

in which

$$Sh = \text{Sherwood number} \quad (-)$$

This situation usually will not exist, because bubbles do have a rise velocity and therefore at some distance from the interface convection is also present. For such a rising bubble with a rigid liquid film and with convective

transport at some distance from the interface, an analytical solution is unknown. Calderbank and Moo-Young (1961) found experimentally

$$Sh = \frac{k_{ul} d_b}{D_{ul}} = 2 + 0.31 \left(\frac{d_b^3 \Delta \rho_{gl} g}{\eta_l D_{ul}} \right)^{0.33} \quad (-) \quad 11.16$$

in which

$\Delta \rho_{gl}$ = difference between the specific density of the liquid and the gas phase (kg m^{-3})

g = gravitational acceleration (m s^{-2})

η_l = dynamic viscosity of the liquid phase (N s m^{-2})

Eqs. (11.14-11.16) can be verified with the vast amount of experimentally determined k_{ul} data reported in literature. Data for oxygen taken from a review article by Heijnen and Van 't Riet (1984) are given in Fig. 11.2, together with Eqs. (11.14-11.16). It can be seen that the k_{ul} value depends on the d_b value. Very small bubbles with $d_b \approx 1 \text{ mm}$ tend to have a rigid interface due to the predominance of the surface tension forces. Eq. (11.16) predicts values in the same range. No data are available at $d_b < 0.1 \times 10^{-3} \text{ m}$; thus the theoretical relationship of Eq. (11.15) cannot be verified. Larger bubbles ($d_b > 3 \times 10^{-3} \text{ m}$) tend to have a fully mobile interface. The experimentally determined k_{ul} values show a large scatter, but are in good accordance with Eq. (11.14). For the region between rigid and mobile surfaces a large scatter of data is seen. This is the region where the surface can be either rigid or mobile depending on liquid properties.

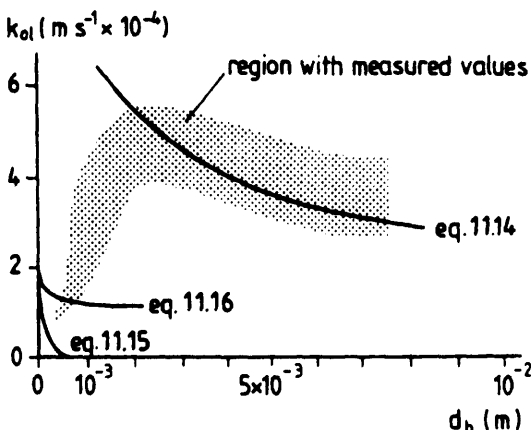


Fig. 11.2 Experimentally determined k_{ul} values for oxygen, compared to calculated values. (Data adapted from Heijnen and Van 't Riet, 1984.)

11.2.1.2 Liquid-solid k_{ii} values

Due to its nature the surface of a solid particle will always be rigid. The k_{ii} equations are therefore of the Sherwood type.

- Freely moving particles

In this category suspended particles are included. The k_{ii} value is dependent on the velocity of the particle relative to the liquid. The velocity usually is unknown. In this section the relations for k_{ii} are given as well as a method to calculate the Reynolds number of the particle Re_p , defined as:

$$Re_p = \frac{\rho_l v_{pl} d_p}{\eta_l} \quad (-) \quad 11.17$$

in which

ρ_l = specific density of the liquid (kg m^{-3})

v_{pl} = velocity of the particle relative to the liquid (m s^{-1})

d_p = diameter of the particle (m)

For $Re_p < 30$, k_{ii} is given by Brian and Hales (1969):

$$\frac{k_{ii} d_p}{|D_{ii}|} = \sqrt{4 + 1.21 \left(\frac{Re_p \eta_l}{\rho_l |D_{ii}|} \right)^{0.67}} \quad (-) \quad 11.18$$

For $Re_p > 30$, k_{ii} is given by Ranz and Marshall (1954):

$$\frac{k_{ii} d_p}{|D_{ii}|} = 2 + 0.57 \sqrt{Re_p} \left(\frac{\eta_l}{\rho_l |D_{ii}|} \right)^{0.33} \quad (-) \quad 11.19$$

The Reynolds number can be calculated from the following set of equations, with the Galilei number defined as

$$Ga = \frac{g d_p^3 \rho_p (\rho_p - \rho_l)}{\eta_l^2} \quad (-) \quad 11.20$$

in which

ρ_p = specific density of the particle (kg m^{-3})

$$\text{For } Ga < 36, \quad \text{then } Re_p = Ga / 18 \quad (-) \quad 11.21$$

$$\text{For } 36 < Ga < 8 \times 10^4, \quad \text{then } Re_p = 0.153 Ga^{0.71} \quad (-) \quad 11.22$$

$$\text{For } 8 \times 10^4 < Ca < 3 \times 10^9, \text{ then } Re_p = 1.74 Ca^{0.5} \quad (-) \quad 11.23$$

- Particles in a packed bed

In a packed bed the liquid velocities around the particle are determined by the superficial liquid velocity and the porosity of the bed. The k_{u} equation is for this case given by

$$\frac{k_u d_p}{D_u} = (1.0 \pm 0.2) \left(\frac{v_{ls} d_p}{v_l \epsilon} \right)^{0.5} Sc^{0.33} \quad (-) \quad 11.24$$

with Sc as the Schmidt number

$$Sc = \frac{v_l}{D_u} \quad (-) \quad 11.25$$

and

- | | | |
|------------|--|-----------------------------------|
| v_{ls} | = superficial liquid velocity, the liquid flow rate
divided by the surface area of the column | (m s ⁻¹) |
| v_l | = kinematic viscosity of the liquid | (m ² s ⁻¹) |
| ϵ | = bed porosity | (-) |

11.2.1.3 The influence of liquid properties on k_{u}

- Gas-liquid

Surface tension has a large influence in the region where the bubble interface can be either rigid or mobile because it can change the mobility of the surface. Outside this region the influence can be neglected.

Calderbank and Moo-Young (1961) have reported some results about the influence of η_l . In general, k_{u} shows a minor increase with increasing η_l . Ionic strength at constant diameter has hardly any influence. Sometimes a minor influence of dissipated power on k_{u} is found.

Although the influence of liquid properties on the k_{u} value for most cases can be neglected at constant bubble diameter, the liquid properties certainly can influence k_{u} by changing the bubble diameter. The bubble diameter can be very sensitive for ionic strength, dissipated power, viscosity and surface tension. The influence on mass transfer is therefore difficult to predict, because the relation between bubble diameter and process variables is usually unknown, as will be discussed later in this section.

- Solid liquid

In this case no change of particle diameter or surface characteristics can occur. The influence of liquid properties is included in the formulae.

11.2.1.4 The influence of temperature

- Gas-liquid

The main influence of temperature is on the diffusion coefficient. Wise and Houghton (1966) show that for oxygen:

$$|D_{ol}| = 4.2 \times 10^{-6} e^{\left(-\frac{10 \times 10^3}{RT} \right)} \quad (\text{m}^2 \text{s}^{-1}) \quad 11.26$$

in which

$$\begin{aligned} R &= \text{gas constant } (= 8.31) & (\text{J mol}^{-1} \text{K}^{-1}) \\ T &= \text{absolute temperature} & (\text{K}) \end{aligned}$$

For the temperature range of 20°C-60°C this can be approached by

$$|D_{ol}| = c T^{0.75} \quad (T \text{ in } ^\circ\text{C}) \quad (\text{m}^2 \text{s}^{-1}) \quad 11.27$$

in which

$$c = \text{constant} \quad (\text{m}^2 \text{s}^{-1} \text{K}^{-0.75})$$

Eqs. (11.14-11.16) show that $|D_{ol}|$ influences k_{ol} in a different way for each of the different hydrodynamic conditions. In general, it can be said that

$$k_{ol} = c' |D|^{0.5 \text{ up to } 1} \quad (\text{m s}^{-1}) \quad 11.28$$

in which

$$c' = \text{constant}$$

Eqs. (11.27) and (11.28) finally lead to the estimation that

$$k_{ol} = c T^{0.4 \text{ up to } 0.7} \quad (T \text{ in } ^\circ\text{C}) \quad (\text{m s}^{-1}) \quad 11.29$$

As a rule of thumb, based also on k_{ol} measurements, the following is used:

$$k_{ol} \text{ increases } 2.5\% \text{ for each } ^\circ\text{C} \quad 11.30$$

11.2.1.5 Conclusions concerning the k_{ol} value

- Gas-liquid

The most important conclusion is that $k_{ol} = 3-4 \times 10^{-4} \text{ m s}^{-1}$ at

$d_b > 2 \times 10^{-3}$ m. At smaller bubble diameters values can decrease down to 1×10^{-4} m s⁻¹, depending on bubble rigidity.

- Solid-liquid

For this system the k_{H_2} value can be directly calculated from the formulae, including important effects like that of temperature and viscosity.

11.2.2 The A value

11.2.2.1 Gas-liquid A values

In the preceding section we have seen that the resistance to mass transfer is localized in the surface layer around the gas bubble. This results in a linear relationship between A and oxygen mass transfer, as shown in Eq. (11.8).

With an (average) bubble diameter d_b , it can be calculated for the specific surface area per m³ meter of reactor volume A' :

$$A' = \frac{6\epsilon}{d_b} \quad (\text{m}^2 \text{ m}^{-3}) \quad 11.31$$

wherein ϵ is the hold-up or void fraction defined as

$$\epsilon = \frac{V_g}{V_l + V_g} \quad (-) \quad 11.32$$

in which

$$\begin{aligned} V_g &= \text{aerated gas volume} & (\text{m}^3) \\ V_l &= \text{unaerated liquid volume} & (\text{m}^3) \end{aligned}$$

In a bioreactor the value of V_g is unknown in most cases. The liquid volume is usually known from the added volume before inoculation and the weight balance and/or weight measurements during the fermentation. Therefore, the specific surface area is preferably taken for each m³ of liquid volume. For the specific surface area per unit of liquid volume A (m² per m³ of liquid) it can be calculated:

$$A = \frac{6}{d_b} \frac{\epsilon}{(1 - \epsilon)} \quad (\text{m}^2 \text{ m}^{-3}) \quad 11.33$$

In Chapter 10 it appeared that hold-up calculations are rather complicated, and that for most cases only experimentally determined relations are

available. With these empirical relationships attempts can be made to solve Eq. (11.33). Yet this appears to be impossible because the bubble diameter needed to solve Eq. (11.33) is unknown. The bubble diameter is a very important parameter for the value of A : directly because of its explicit presence in Eq. (11.33); indirectly it is also present in Eq. (11.33) because of its influence on the ϵ value itself.

Now we will discuss the dispersion and coalescence properties of a liquid and the qualitative influence on A and $k_{\text{u}}A$. Describing the coalescence properties of a liquid, two extreme cases can be distinguished, coalescing and noncoalescing as described in Chapter 6. Fermentation liquids will always be between the two extremes. Due to the complex composition of fermentation liquids, it is impossible to predict where "between." This means that k_{u} , A and $k_{\text{u}}A$ cannot be predicted accurately.

In viscous systems the situation becomes even more complex. Besides the liquid properties, in highly viscous systems the size distribution of the bubble diameter also plays a role. In very viscous liquids, very large ($\gg 1$ cm) bubbles can be present, due to a very fast coalescence process. On the other hand, as Heijnen et al. (1980) show, very small bubbles can also be present, particularly in stirred systems. These tiny bubbles are nearly immobile and have a very large residence time.

In conclusion, it can be said that the processes that determine the bubble diameter are known only qualitatively. This means that a prediction of A from liquid properties and process conditions is impossible. The same applies to the k_{u} value, although that parameter has the advantage that it is not very sensitive to the bubble diameter for $d_b > 3$ mm. These facts explain why mass transfer in bioreactors usually is predicted from experimentally determined $k_{\text{u}}A$ values for model liquids.

11.2.2.2 Solid-liquid A values

The specific surface area per unit of liquid volume A is independent of process conditions and can be calculated by an equation analogous to Eq. (11.33). For this the particle diameter and void fraction should thus be known.

11.2.3 The $k_{\text{u}}A$ value

11.2.3.1 Gas-liquid $k_{\text{u}}A$ values

With Eq. (11.33) it can be derived that

$$k_{ol}A = \frac{6k_{ol}}{d_b} \frac{\epsilon}{(1-\epsilon)} \quad (\text{s}^{-1}) \quad 11.34$$

In the preceding section relations for k_{ol} are given. However, these show a dependency on the generally unknown bubble diameter. The bubble diameter is also explicitly present in Eq. (11.34). Therefore, the $k_{ol}A$ value in gas-liquid dispersion cannot be determined with the formulae presented until now.

A number of researchers have determined $k_{ol}A$ values experimentally. These will be given in this chapter whereby the data will be arranged according to coalescence conditions and process conditions. Only relations for model liquids are presented. Fermentation liquids are always between purely coalescing and purely noncoalescing. Where exactly in between cannot be determined. A fermentation liquid can even vary from moment to moment, for instance as a result of the addition of antifoam to a foaming broth. In Section 11.4 a method will be given to estimate the relationship for a particular fermentation broth.

It is impossible to review all reactor types. Here we will limit ourselves to the most widely used types, the bubble column, the stirred vessel and the air lift column. It appears that in a number of cases, the reactor itself does not make much difference for mass transfer values. Thus these three cases cover most of the applications.

11.2.3.1.1 The bubble column

For a bubble column with a coalescing liquid it has been argued in Section 11.2.2.1 that $d_b = 6 \text{ mm}$. The sparger geometry was irrelevant. Fig. 11.2 shows that this results in a k_{ol} value that is about 4×10^{-4} . The hold-up value is dependent on liquid circulation, bubble diameter and superficial gas velocity. Usually heterogeneous flow will occur. Again, because the bubble diameter is independent of process conditions, the hold-up can be correlated with gas superficial velocity only for heterogeneous flow, as shown in Section 10.2.3.1. Because in this way all variables in Eq. (11.34) are either constant or dependent on superficial gas velocity only, this should lead to a dependence of $k_{ol}A$ on superficial gas velocity only. The review of Heijnen and Van 't Riet (1984) gives, for a coalescing, nonviscous medium:

$$k_{ol}A = 0.32 (v_{gs}^c)^{0.7} \begin{array}{l} \text{coalescing, nonviscous} \\ \text{bubble column} \\ \text{accuracy } \approx 30\% \\ T = 20^\circ\text{C} \end{array} \quad (\text{s}^{-1}) \quad 11.35$$

In this equation and all the following equations v_{gs}^c is the local superficial velocity, i.e., the velocity corrected for the local pressure. In the article it

is also shown that "a rule of thumb" can be used, which predicts that in a bubble column not taller than 45 m at $C_{ol} = 0$, the change in the relative oxygen concentration in the bubbles is 0.55% (absolute) for each meter of unaerated fluid (coalescing) height.

For a noncoalescing liquid the situation is much more complicated because the size of the bubble that forms at the sparger is now important. If the bubble size at the sparger is smaller than 6 mm, the bubbles will keep that diameter throughout the vessel. That means that $k_{ol}A$ can become larger than for a coalescing system. As bubble size and liquid circulation are difficult to predict, it is difficult to predict what the increase will be. Here we will limit ourselves to a noncoalescing, nonviscous medium with a sparger that generates small bubbles. The mass transfer equation becomes:

$$k_{ol}A > 0.32 (v_{gs}^c)^{0.7} \quad \begin{array}{l} \text{noncoalescing, nonviscous} \\ \text{bubble column} \\ \text{small bubble sparger} \\ T = 20^\circ\text{C} \end{array} \quad (s^{-1}) \quad 11.36$$

It seems logical to strive for noncoalescing systems, because of the favorable mass transfer. However, usually for a fermentation liquid noncoalescence also implies severe foaming conditions. This will usually be controlled by addition of an antifoam agent, which, in turn, will also influence coalescence. This complex, and to a large extent yet unknown, relation scheme leads to fermentation liquids that are between coalescing and noncoalescing: not purely coalescing because process conditions are controlled in such a way that this disadvantageous condition is avoided; Not purely noncoalescing because this leads to unacceptable foaming problems.

Another case is that for noncoalescing systems with a bubble size at the sparger larger than 6 mm. This will usually be the case in large-scale systems. The bubbles that are larger than 6 mm will be dispersed down to 6 mm and from that time on they will keep that size. Compared to a coalescing system the size probably may be a fraction smaller because in that case the final bubble size is also the result of a continuous coalescence and dispersion process. A good estimation for mass transfer in noncoalescing, nonviscous media in a bubble column with a large bubble sparger is Eq. (11.35), the formula for a coalescing liquid

$$k_{ol}A = 0.32 (v_{gs}^c)^{0.7} \quad \begin{array}{l} \text{noncoalescing, nonviscous} \\ \text{bubble column} \\ \text{large bubble sparger} \\ \text{accuracy unknown} \\ T = 20^\circ\text{C} \end{array} \quad (s^{-1}) \quad 11.37$$

If the gas superficial velocity is very low, the coalescence sometimes can be limited by the small collision frequency of the bubbles. This means that only

a small number of bubbles should be present. As this means a small hold-up value, it also means that v_{gs}^c should be small. An order of magnitude of $v_{gs}^c = 10^{-3}$ or maybe even 10^{-4} m s^{-1} is necessary for prevention of coalescence by limitation of the collision frequency, the maximum allowable superficial gas velocity. If this condition is met, the mass transfer is large, as for noncoalescing systems [Eq.(11.36)]. This can only be the case in systems with a small gas loading like waste water columns. As soon as v_{gs}^c is increased on such a column, the advantage will disappear. An example can be found in Bacon et al. (1977). They show that $k_{ol}A$ in a coalescing medium decreases with column height. This can be explained by an increase in bubble diameter due to (slowly proceeding) coalescence. The v_{gs}^c value was indeed very low: 10^{-4} m s^{-1} .

The situations given above are valid for heterogeneous flow conditions. At low superficial gas velocities and with a good sparger construction, homogeneous flow can occur. This will lead to a higher $k_{ol}A$ value due to the higher hold-up. Thus

$$k_{ol}A > 0.32 (v_{gs}^c)^{0.7} \begin{array}{l} \text{nonviscous} \\ \text{bubble column} \\ \text{homogeneous flow} \end{array} \quad (\text{s}^{-1}) \quad 11.38$$

It can be concluded that a number of relations exist for $k_{ol}A$ in the bubble column. The right choice must be based on the flow, coalescence conditions and bubble size. None of them usually are known and therefore $k_{ol}A$ predictions seem to be impossible. However, large-scale applications are usually high loaded and not excessively foaming. This means that they usually are coalescing or almost coalescing. Besides, the high loading means that large bubble spargers are involved. Therefore, Eq. (11.35) will usually predict $k_{ol}A$ rather well. For a more accurate prediction the method given in Section 11.4 can be used.

The influence of viscosity on $k_{ol}A$ in a bubble column is very pronounced. Deckwer et al. (1982) report that their own data and reviewed data show the dependency

$$k_{ol}A = c \eta_l^{-0.84} \quad (\text{s}^{-1}) \quad 11.39$$

In practice this means that bubble columns are useless at high viscosity broths. At $100 \times 10^{-3} \text{ N s m}^{-2}$, the $k_{ol}A$ value has already decreased by a factor of 50 compared to water. A viscosity of $100 \times 10^{-3} \text{ N s m}^{-2}$ can therefore be regarded as the upper viscosity limit for bubble column reactors.

The equations for the bubble columns are not based on models for the reactor. Particularly on a large scale, modeling can be needed to correct for

the change in v_g^c , with height due to the hydrostatic pressure differences. In small-scale bioreactors the v_g^c value is nearly constant.

11.2.3.1.2 The stirred vessel

Gas sparged in a stirred vessel is immediately sucked into the gas cavities behind the stirrer blades. It is then dispersed at the end of the cavity into very fine bubbles. These bubbles coalesce to the final bubble size in the vessel. In coalescing systems an equilibrium between coalescence and dispersion of bubbles can be expected, comparable to that in bubble columns. The basic parameters that influence the bubble diameter, the hold-up and $k_{ot}A$, are mainly v_g^c , liquid circulation and turbulence. However, despite the large amount of research done on mass transfer in stirred vessels, the relation with these basic parameters is only touched upon. As a result $k_{ot}A$ relations are merely experimentally determined as a function of v_g^c and P_s/V_t , the latter being the substitute for flow and turbulence. In coalescing liquids a gross correlation is given in a review article by Van 't Riet (1979):

$$k_{ot}A = 2.6 \times 10^{-2} \left(\frac{P_s}{V_t} \right)^{0.4} \left(v_{gs} \frac{P_a}{P_s} \right)^{0.5}$$

coalescing,
nonviscous
stirred vessel (s⁻¹) 11.40
accuracy ≈ 30%
 $T = 20^\circ\text{C}$

For noncoalescing liquids this author gives:

$$k_{ot}A = 2.0 \times 10^{-3} \left(\frac{P_s}{V_t} \right)^{0.7} \left(v_{gs} \frac{P_a}{P_s} \right)^{0.2}$$

noncoalescing,
nonviscous
stirred vessel (s⁻¹) 11.41
accuracy ≈ 30%
 $T = 20^\circ\text{C}$

in which

- | | | |
|----------|--|----------------------|
| P_s | = pressure at the stirrer level | (N m ⁻²) |
| P_a | = atmospheric pressure | (N m ⁻²) |
| v_{gs} | = gas superficial velocity at atmospheric conditions | (m s ⁻¹) |

In these relationships no indication is given for the influence of the sparger. This is absent because as long as the sparger is situated below the stirrer, the bubbles are sucked up and dispersed by the cavity immediately after sparging. Also, the stirrer type does not appear in the relations. The literature shows that only the energy dissipated in the vessel is determining $k_{ot}A$, independent of stirrer type. Because most of the mass transfer occurs in the stirrer region, the v_g^c value is corrected for the pressure conditions at the stirrer position. This is a corrected value for a specific position which is different from v_g^c used in the bubble column. In the bubble column the

mass transfer is evenly distributed over the whole column, and everywhere the local v_{gs}^c should be used.

The influence of viscosity on $k_{ol}A$ in a stirred vessel is not very clear. Most researchers do not find a clear influence up to viscosities of around 50×10^{-3} N s m $^{-2}$. Then $k_{ol}A$ decreases with $\eta^{-0.5}$ up to $\eta^{-0.9}$. Assuming 0.7 to be a good average, this results in the formula:

$$(k_{ol}A)_{viscous} = (k_{ol}A)_{water} \left(\frac{\eta_{broth}}{\eta_{ref}} \right)^{-0.7} \begin{array}{l} \text{stirred vessel} \\ \text{accuracy unknown} \end{array} \quad (s^{-1}) \quad 11.42$$

$\eta_{ref} \sim 50 \times 10^{-3} \text{ Nsm}^{-2}$

Because η_{ref} is much larger than the viscosity of water, the $k_{ol}A$ value for viscous systems in stirred vessels is much larger than that in bubble columns. This is clearly shown in Fig. 11.3. For stirred vessels the $k_{ol}A$ value becomes very small, at viscosity larger than about 1 N s m $^{-2}$. Higher viscosity values should be avoided. Example 9.2 shows that also for mixing reasons these high viscosity values should be avoided.

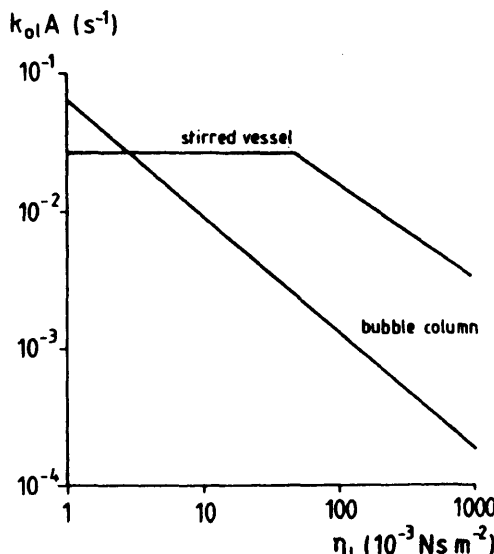


Fig. 11.3 Comparison of a stirred vessel and a bubble column for mass transfer in viscous systems. Values used are Eq. (11.39) with $v_{gs} = 0.1 \text{ m s}^{-1}$ and Eqs. (11.40) and (11.42) with $P_s/V_1 = 1000 \text{ W m}^{-3}$ and $v_{gs} = 0.01 \text{ m s}^{-1}$. No pressure corrections are applied.

The equations for the stirred vessel are completely black box models. At scaling-up this can cause problems when considerable static pressure differences occur (volumes > 100 m³) or when at these large scales more than one stirrer is used. Oosterhuis and Kossen (1983, 1984) have reported a model in which the vessel is divided into a number of compartments. They show that a better prediction of mass transfer on large scales is obtained when the mass transfer formulae are applied to each compartment separately.

Because mass transfer mainly takes place in the stirrer region, C_{ol} differences can exist in the vessel. This will be the case in particular in large-scale vessels. For aerobic organisms that cannot withstand temporary anaerobic conditions, this means that this situation has to be prevented. Usually this results in an allowed minimum value of C_{ol} near the lower stirrer. This phenomenon is worked out in more detail in Chapter 18.

11.2.3.1.3 The air lift

In an air lift reactor a circulation is imposed on the circulation phenomena as is present in a bubble column. For this reason the gas bubbles are transported in a shorter time to the top of the vessel than should be the case in a bubble column under the same conditions. This means that

$$k_{ol}A < 0.32 (v_{gs}^c)^{0.7} \text{ air lift, coalescing liquid} \quad (s^{-1}) \quad 11.43$$

It is possible, with a calculation scheme like shown in Fig. 9.8, to calculate $k_{ol}A$ from local hold-up values, assuming that $k_{ol} = 4 \times 10^{-4}$ m s⁻¹ and $d_b = 6$ mm. Results are given by Verlaan et al. (1989). They show that in a pilot plant air lift reactor the decrease in $k_{ol}A$ value, when compared to a bubble column, can be up to a factor of 3. This value decreases for the transitional region between air lift and bubble column, a phenomenon discussed in Section 9.4.3.1.

One of the reasons to use the air lift, however, is just the circulatory flow. The advantage is that flow profiles are well defined, also on large scales. The result is that modeling of the flow and mass transfer phenomena is possible. Therefore the black box models, like those used for the bubble column, can be replaced by more mechanistic models, as shown in Fig. 9.8.

11.2.3.1.4 Comparisons based on dissipated energy

Mass transfer in reactors is obtained by injecting compressed air and/or by stirring. Both processes consume energy. As this attributes in a significant

way to the cost of a fermentation, much research has been done to improve the energy efficiency of mass transfer. Here we will discuss some general guidelines for energy efficiency.

In Chapter 14 the equation for energy involved with gas sparging is given. This equation is used to calculate the total power consumption involved for mass transfer in a coalescing liquid. In this way Fig. 11.4 is derived, wherein P_t (W) is given by the sum of the energy introduced by the stirrer, P_s (W), and the energy introduced by the gas, P_g (W).

In the section on $k_{o,t} A$ in stirred vessels it was mentioned that the type of stirrer did not influence the mass transfer equations based on P_t/V_t . Fig. 11.4 shows that no difference can even be found between a bubble column and a stirred vessel for coalescing media. Some further remarks can be made.

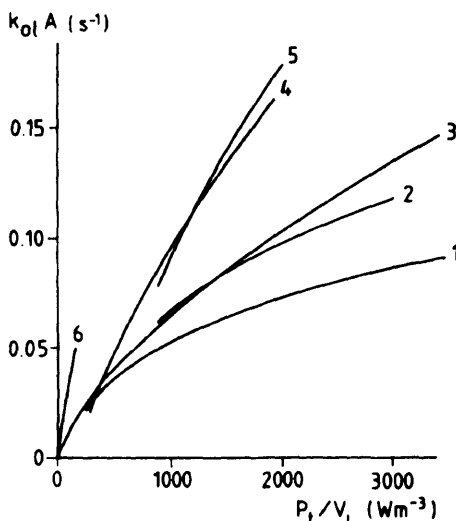


Fig. 11.4 Comparison of $k_{o,t} A$ for stirred tank reactors and bubble columns (air-water system). No pressure corrections applied.

- | | | | |
|----------|----------------|-------------|------------------------------------|
| curve 1, | stirred tank, | water, | $v_{gs} = 0.02 \text{ m s}^{-1}$; |
| curve 2, | stirred tank, | water, | $v_{gs} = 0.04 \text{ m s}^{-1}$; |
| curve 3, | bubble column, | water; | |
| curve 4, | stirred tank, | water-salt, | $v_{gs} = 0.02 \text{ m s}^{-1}$; |
| curve 5, | stirred tank, | water-salt, | $v_{gs} = 0.04 \text{ m s}^{-1}$; |
| curve 6, | bubble column, | water-salt. | |

- In a bubble column the energy needed to compress the air is larger than the energy actually dissipated in the vessel. The last-mentioned value is used in Fig. 11.4. Also, the energy for the stirrer motor exceeds that of the energy dissipated by the stirrer. If very accurate comparisons are needed, these effects should be taken into account.
- A close observation of Fig. 11.4 shows that the curves for the stirred vessel deviate from the bubble column curve at increasing P_t/V_t values. This effect takes place in those cases where the stirrer-dissipated power is much larger than the energy dissipated by the air. In that case the stirrer is used mainly as a liquid mixer instead of a gas-liquid disperser. It can be concluded here that, as a rule of thumb, the stirrer power should not exceed 5 times the gas energy. This is a very important rule from the viewpoint of energy efficiency. Bear in mind that the stirrer power also should not be below the gas energy to prevent flooding.
- The data of Fig. 11.4 could lead to the conclusion that bubble columns should always be preferred. However, there are other reasons that determine the choice, as shown in Chapter 1.
- The air lift is not included in Fig 11.4. The energy introduced by the gas is the same as that for the bubble column. Therefore, the curve for the air lift will be the same as or below the curve for the bubble column.

11.2.3.2 Solid-liquid k_{uA} values

Determination of the solid liquid k_{uA} value is very simple. In Section 11.2.1.2 the equations to calculate k_u values are given. The particle diameter can usually be measured. The hold-up also can be measured. Then application of an equation analogous to Eq. (11.34) gives the k_{uA} value.

11.2.4 The C_{ol} value

The oxygen solubility in fermentation media can deviate from that in pure water due to salts, substrates and other solutes. Quicker et al. (1981) have published a number of experimental values as well as an empirical correlation. They show that the solubility decreases with solute concentration. Ionic solutes have an influence that is different from nonionics. The correlation they give is

$$\log\left(\frac{C_{ol0}}{C_{ol}}\right) = \sum_i 0.25 c_i z_i^2 C_i + \sum_j c_j C_j \quad (-) \quad 11.44$$

in which

c_i, c_j	= constant for component i or j	($\text{m}^3 \text{ mol}^{-1}$)
z_i	= valency for component i	(-)
$C_{i,i}$	= concentration of component i or j	(mol m^{-3})
$C_{o,i}$	= liquid oxygen concentration at zero solute concentration	(mol m^{-3})

Table 11.1 gives $C_{i,i}$ values.

An impression of the order of magnitude of these effects: A 25% decrease in solubility is reached at about 200 kg m^{-3} glucose or 50 kg m^{-3} CaCl_2 or 30 kg m^{-3} NaHPO_4 . These concentrations exceed the usual values for fermentation media. Generally, due to the complexity of the fermentation broth a decrease of 10% or more can be expected as a result of the summation of all the different components. Quicker et al. (1981) measured values of 5-25%.

The change in $C_{o,i}$ considerably complicates the mass transfer calculations. For gas-liquid mass transfer this can be circumvented by using the experimental method that will be discussed in Section 11.4. For liquid-solid

Table 11.1 $c_{i,i}$ values for the solubility of O_2 in solutions at 24°C as given by Quicker et al. (1981)

Cation	$c_i \times 10^{-3}$ (mol m^{-3})	Anion	$c_i \times 10^{-3}$ (mol m^{-3})	Sugar	$c_i \times 10^{-3}$ (mol m^{-3})
H^+	-0.774	F^-	0.982	Glucose	0.119
Li^+	-0.664	Cl^-	0.844	Lactose	0.197
Na^+	-0.550	Br^-	0.820	Sucrose	0.149
K^+	-0.596	J^-	0.821		
Rb^+	-0.662	OH^-	0.941		
Cs^+	-0.666	NO_3^-	0.802		
NH^+	-0.720	ClO_4^-	0.888		
$\text{N} \text{Et}_4^+$	-0.912	SO_4^{2-}	0.453		
Mg^{2+}	-0.314	CO_3^{2-}	0.485		
Ca^{2+}	-0.303	PO_4^{3-}	0.320		
Ba^{2+}	-0.297	H_2PO_4^-	1.037		
Mo^{2+}	-0.311	HPO_4^{2-}	0.485		
		$\text{S}_2\text{O}_3^{2-}$	0.447		
		HCO_3^-	1.058		
		$\text{C}_6\text{H}_5-\text{O}-\text{CH}_2\text{COO}^-$	0.764		

mass transfer the C_{ii} changes should be included in the equations where relevant.

Another important variable influencing C_{oi} is the temperature. Finn (1967) has given data for water. For limited temperature ranges the data can be fitted with a 2.5% decrease in solubility for each degree of temperature difference. When this is compared with the increase of k_{oi} with temperature, it can be concluded that the two effects compensate each other.

11.3 Measuring methods for $k_{\text{oi}}A$

11.3.1 Introduction

For gas-liquid mass transfer it is shown that this can be described by

$$OTR = k_{\text{oi}}A(C_{\text{oi}}^* - C_{\text{oi}}) \quad (\text{mol m}^{-3} \text{ s}^{-1}) \quad 11.8$$

In a bioreactor OTR , C_{oi}^* , and C_{oi} can be measured. The value of the partition coefficient m (Eq. (11.4)) can be calculated from the liquid composition. More problematic is the measurement of k_{oi} and A values. Separate determination of k_{oi} and A is laborious and in many cases even impossible. On the other hand, the product $k_{\text{oi}}A$ is always involved in the equations. Therefore, most of the reported data involve the determination of the product $k_{\text{oi}}A$.

Before applying any measuring method it is important to realize that the $k_{\text{oi}}A$ equation is derived under the assumption of completely mixed gas and liquid phases, with $k_{\text{oi}}A$ assumed to be constant for the whole vessel content. Sometimes modeling of the liquid and gas phase conditions is needed.

11.3.2 The $OTR - C_{\text{oi}}$ method

The basis for this method is the mass transfer equation, Eq. (11.8). All variables, except $k_{\text{oi}}A$, are measured. This implies that this method can be used only in an oxygen-consuming system. The oxygen concentration of the gas phase entering and leaving the bioreactor can be analyzed. With these data OTR can be determined from a balance over the bioreactor:

$$V_t OTR = F_g (C_{\text{og}i} - C_{\text{og}o}) = V_t k_{\text{oi}}A \left(\frac{C_{\text{og}o}}{m} - C_{\text{oi}} \right) \quad (\text{mol s}^{-1}) \quad 11.45$$

in which

F_g	= volumetric gas flow rate	($\text{m}^3 \text{s}^{-1}$)
$C_{o_{\text{gi}}}$	= oxygen concentration of the inflowing air	(mol m^{-3})
$C_{o_{\text{go}}}$	= oxygen concentration of the outflowing air	(mol m^{-3})

When the gas phase is assumed to be ideally mixed then the concentration of the gas phase equals that of the outflowing gas and therewith $C_{o_l} = C_{o_{\text{go}}} / m$. m can be estimated from pure water data eventually corrected for the solutes. The concentration in the liquid phase can be measured directly by means of an oxygen probe. In this way all variables are known and $k_{o_l}A$ can be calculated.

The oxygen concentration will usually be measured by means of a polarographic oxygen sensor. These sensors do not give concentration values, but they record the partial pressure. This means that the oxygen solubility of the liquid should be known, which is not always the case. However, in a fermentation broth a method can be used which overcomes this problem. This will be shown in Section 11.4.

As only in- and outflow conditions are measured, modeling, particularly of the gas phase, is important. For most applications an ideally mixed gas phase is assumed. In that case $C_{o_l} = C_{o_{\text{go}}} / m$, with $C_{o_{\text{go}}}$ the concentration at the (average) pressure in the fermenter. For large oxygen depletion values more detailed modeling is needed. The same applies for the liquid phase for large-scale fermenters. To measure oxygen concentration differences the use of a number of oxygen sensors at different positions can be attractive. If only one sensor is used, it generally is positioned in the stirrer flow region. This is done because the polarographic cell consumes oxygen and therefore a liquid flow is needed to minimize mass transfer resistance in the boundary layer in front of the sensor. When applying cells in other parts of the vessel, the mass transfer resistance by the boundary layer can occur.

The $OTR - C_{o_l}$ method can be applied only to a fermenter for which at least the volumetric air flow rate, the oxygen concentration in the outflowing air and the liquid oxygen concentration can be measured. In many commercial fermentations these measurements are already done for control purposes. If, however, the apparatus has to be bought for $k_{o_l}A$ measurements only, the high cost of the gas concentration measurement in particular has to be considered.

11.3.3 The dynamic method

This method is based on the measurement of the C_{o_l} of a deoxygenated liquid as a function of time, after the air flow is turned on. The deoxygenation can be obtained by passing nitrogen through the liquid or stopping

the air flow in case of an oxygen-consuming fermentation broth. The mass balance gives

$$\frac{dC_{ol}(t)}{dt} = k_{ol}A(C_{ol}^* - C_{ol}(t)) - OUR \quad (\text{mol m}^{-3} \text{s}^{-1}) \quad 11.46$$

with the assumption that $k_{ol}A$ and C_{ol}^* are constant, independent of time. This is also with $C_{ol}(\infty)$ = the equilibrium concentration at stationary conditions,

$$OUR = k_{ol}A(C_{ol}^* - C_{ol}(\infty)) \quad (\text{mol m}^{-3} \text{s}^{-1}) \quad 11.47$$

Eqs. (11.46) and (11.47) can be combined to

$$k_{ol}A = \frac{\ln\left(\frac{C_{ol}(\infty) - C_{ol}(t_1)}{C_{ol}(\infty) - C_{ol}(t_2)}\right)}{t_2 - t_1} \quad (\text{s}^{-1}) \quad 11.48$$

This formula can be applied to model systems without oxygen consumption for which $C_{ol}(\infty) = C_{ol}^*$ ($OUR = 0$) as well as for oxygen-consuming fermentation broths. Although the principles of this method are very simple, a number of limitations will be discussed now which confine its applicability considerably.

The normally used polarographic Clark cell has a characteristic response time τ_p . This is mainly due to the diffusion through the membrane, while additionally in viscous systems and/or systems with a low fluid flow velocity the mass transfer resistance in the boundary layer can also be relevant (Dang et al., 1977; Linek and Vacek, 1976, 1977). Problems occur where τ_p is not much smaller than the characteristic time for mass transfer $1/k_{ol}A$. This results in a response lag and the probe signal is not equal to the instantaneous value of $C_{ol}(t)$. In practice this occurs frequently. Particularly with sterilizable Clark cells, the membrane resistance has a large effect. For these systems many models have been designed, reviewed by Van 't Riet (1979). He shows that the $k_{ol}A$ value can be measured accurately enough up to $k_{ol}A = 0.1 \text{ s}^{-1}$ without correction, by means of commercially available electrodes with $\tau_p = 2-3 \text{ s}$. On the other hand, for sterilizable commercial electrodes, $\tau_p = 10-100 \text{ s}$. In that case it can easily be that $1/k_{ol}A \ll \tau_p$ and thus the $k_{ol}A$ determination becomes very inaccurate, even when a model is applied to correct for this effect.

Quite a different problem is presented by the gas phase average residence time τ_g , in particular when deoxygenation with nitrogen is followed by a

switch to aeration at $t = 0$. If τ_g becomes of the order of magnitude of $1/k_{oi}A$, C_{og} varies with time while the measurement takes place and the assumption of a constant C_{oi}^* needed to derive Eq. (11.48) is not valid any longer. Dunn and Einsele (1975) and Dang et al. (1977) have given models to correct for this effect. It appears from their work that quite large corrections are needed for high ϵ low v_{gs} , (noncoalescing) cases. The problem becomes more serious at larger vessel height H_v (H_v is defined as the height with liquid only). τ_g can be given as

$$\tau_g = \frac{H_v}{v_{gs}^c} \frac{\epsilon}{(1 - \epsilon)} \quad (s) \quad 11.49$$

At scale-up v_{gs}^c values usually do not vary very much with scale. Furthermore, hold-up is a function of v_{gs}^c , and therefore also does not change to a large extent at scale-up. This leads to the conclusion that τ_g becomes about proportional to H_v at scale-up. Consideration of practical ϵ , $k_{oi}A$ and v_{gs}^c values for bubble columns and stirred vessels shows that for this reason it can be safely assumed that $H_v = 1\text{ m}$ is the natural limit for this method because then $1/(k_{oi}A)$ becomes of the same order of magnitude as τ_g . It should be stressed that measurements are indeed useless above this height value. The measurement always leads to a calculated result; however, this result is not representative for the $k_{oi}A$ value. (At very large scales the electrode will measure the change of C_{oi}^* with time and therewith the τ_g value.) The differences are so large that correction models cannot be used to correct for these differences.

In fermentation liquids the method is applied by turning the air flow off and on. This seems to overcome the ϵ_g problem because now the nitrogen is not replaced and the bubbles all originate from the air after turning on the flow. However, after turning on the air flow the hold-up has to build up. Again at about $H_v > 1\text{ m}$ the time to build up the hold-up becomes larger than the characteristic time for mass transfer. Sometimes the liquid is deoxygenated by the addition of a small amount of sulfite. When this is done with continuous air throughflow, the need for correction depends on the extent to which oxygen depletion takes place. Here again, corrections will be needed at larger scales, and again, the limitation of the method will be around $H_v = 1\text{ m}$. The addition of sulfite is completely different from the "sulfite method" discussed in Section 11.3.4. That method is based on reaction controlled mass transfer. In the method given here sulfite is used only as a deoxygenator and conditions should be chosen in such a way that any enhancement or reaction control of mass transfer is absent.

For viscous systems the dynamic method is totally inapplicable, as shown by Heijnen et al. (1980). This is caused by the presence of very small ($\ll 1\text{ mm}$)

bubbles in viscous systems. The very small bubbles are in equilibrium with the oxygen concentration in the liquid phase. In this way they cause an apparent increase of the solubility. Because the oxygen partition coefficient is about 32 (at 25°C) for air/water this effect is already considerable at small-bubble hold-up values of the order of magnitude of 1%. Thus a decrease of $k_{ol}A$ is measured that is only apparent. Correction for this effect by measuring the hold-up of tiny bubbles is very inaccurate because of the gradual change of very small to "normal" bubble sizes.

An advantage of the dynamic method is that the measurement is independent of the oxygen solubility. Eq. (11.48) shows that the partition coefficient is eliminated from this equation. With application of a Clark cell this means that the readings can be used directly, for instance as a percentage of the equilibrium reading. This advantage turns into a disadvantage when OTR values for a specific fermentation broth have to be calculated. Then the solubility, or partition coefficient, for that specific broth has to be known, to be included in Eq. (11.8).

Probably the most pronounced advantage of this method is the low cost of the apparatus involved. This might very well explain the popularity of the method. The total cost might be only 10% of the cost involved with the cost of the apparatus for the $OTR - C_{ol}$ method, because the expensive gas phase analysis is absent. This means that application for small scale, non sterile model systems is obvious. However, as shown in this chapter, it is limited to this application only.

11.3.4 Chemical sorption methods

These methods are based on the reaction of an absorbed gas (O_2 , CO_2) with a chemical added to the liquid phase (Na_2SO_3 , KOH). These reactions are used favorably in a reaction rate region wherein the liquid bulk concentration of the gas component involved equals zero and whereby the absorption is chemically enhanced due to a reaction in the mass transfer boundary layer.

For the sulfite method a review of Van 't Riet (1979) shows that the reaction rate constant can vary in an unknown way. It can safely be said that the application of this method should be strongly discouraged. Without laborious work on reaction conditions this method does not give any information about $k_{ol}A$.

The CO_2 absorption as proposed by Mehta and Sharma (1971) and Robinson and Wilke (1974) is preferable. The reaction kinetics can be determined more accurately. Prasher (1975) is critical of these methods with a view to the prediction of $k_{ol}A$ in fermentation systems.

It will be clear that these types of methods use model liquids. They therefore give relevant data for these liquids only. Usually the addition of chemicals, many times as electrolytes, is involved. The model liquids therefore will be in between coalescing and noncoalescing. Translation of the results to a specific fermentation broth is therefore impossible.

11.3.5 Separate determination of k_{oi} and A

Techniques that can be used include light transmission, photography, suction into a capillary and a microprobe. These methods are laboratory methods, only useful for fundamental research in model liquids. Application on large scale and/or in fermentation liquids does not seem to be useful.

11.3.6 The chemical $OTR - C_{oi}$ method

A method that is in principle similar to the $OTR - C_{oi}$ method is the one in which a small, but accurately known, amount of sulfite is continuously added to the liquid while the reaction conditions are kept in a region such that chemical enhancement is absent and a C_{oi} value is detectable. C_{oi} is measured and OTR can be calculated from the sulfite added. Also, other oxygen-consuming reactions can be used. The results apply for the model liquid only. The liquid changes in time due to the continuously increasing electrolyte concentration. This makes this method less attractive.

11.3.7 Conclusions concerning the measuring methods

The conclusions are summarized in Table 11.2 Whether a method is to be preferred or not depends on the objective that is chosen for the measurement. Here three objectives are selected.

- The first one is the comparison of different apparatus on one scale, for instance to compare the behavior of different stirrer types or the comparison of a bubble column with a stirred vessel. In this case model liquids can be used as well as fermentation liquids.
- The second one is scale-up research. This can be done with fermentation liquids but model liquids are allowed. Now those methods that are problematic or impossible to apply on large scales have to be excluded.
- The third and most important application is the measurement and prediction of OTR for a given fermentation broth. Here most methods which use model liquids are difficult to apply because data about solubility usually are absent. Also, methods limited to small scale only cannot be applied.

Table 11.2 Advantages and disadvantages of the measuring method

Method	Liquid	Objectives										Cost	
		Comparison apparatus		scale-up		OTR							
		one scale		one liquid		prediction							
scale: visc:	small ^b low ^d high ^e	large ^c low high	small low high	large low high									
<i>OTR</i>	Model ^a	- -	- -	- -	- -	- -	- -	- -	- -	- -	no		
C_{ot}	Fermentation ^a	+	+	+	+	+	+	+	+	+	high		
Dynamic gassing out	Model	+	-	-	-	-	±	-	-	-	no		
	Fermentation	+	-	-	-	-	±	-	-	-	low		
CO_2 absorption ^f	Model	+	-	+	-	+	-	+	-	+	kinetics		
	Fermentation	-	-	-	-	-	±	-	±	-	low		
Separate k_{ot} and A	Model	+	+	+	+	+	+	±	±	±	extremely		
	Fermentation	-	-	-	-	-	±	±	±	±	high, low		
Chemical $OTR - C_{ot}$	Model	+	?	+	?	+	?	±	?	±	?	no	
	Fermentation	-	-	-	-	-	±	?	±	?	high, low		

- ^a A model liquid is defined here as a nonfermentation liquid of which the composition can be defined exactly. A fermentation liquid is defined as a specific broth, which can be produced and used by a single laboratory as a model liquid, but by its nature the composition cannot be defined exactly and an exact copy cannot be made by working through the literature data only.
- ^b Small scale ($T_v < 1$ m).
- ^c Large scale ($T_v > 1$ m).
- ^d Low viscous ($1 \text{ to } 2 \times 10^{-3} \text{ N s m}^{-2}$).
- ^e High viscous ($> 100 \text{ to } 1000 \times 10^{-3} \text{ N s m}^{-2}$).
- ^f Sulfite method is not even mentioned because of unreliability.

The $OTR - C_{ot}$ method is the one that should be preferred and that is the most widely applicable. However, it was shown that this method does not give $k_{ot}A$ data when solubility data are not included. Yet this method can be used, as will be shown in the next section.

11.4 The use of the $OTR - C_{ot}$ method for accurate OTR predictions

Although the emphasis in the preceding chapters has been on the

measurement of $k_{ol}A$, the underlying question in fermentation research is the prediction of OTR . Here a method will be presented that can be used for that purpose.

The objectives that have to be reached with this method are:

- Prediction of OTR on all scales
- Prediction of OTR for a fermentation liquid for which the coalescence conditions are not accurately known
- Prediction of OTR for a fermentation liquid for which the partition coefficient is not accurately known

These conditions exclude all methods that involve model liquids as well as those that can be applied at small scales only. The only one that remains is the $OTR - C_{ol}$ method. The question is how this one can be applied to reach the goals.

The concentration in the liquid phase is given by

$$C_{ol} = p_{orec} (C_{ol})_{p=1} \quad (\text{mol m}^{-3}) \quad 11.50$$

with

p_{orec} = partial pressure that is measured by the oxygen sensor (atm)

$(C_{ol})_{p=1}$ = the concentration that belongs to a partial pressure of 1 atm. (mol m⁻³)

$(C_{ol})_{p=1}$ can be written as

$$(C_{ol})_{p=1} = \frac{(C_{og})_{p=1}}{m} \quad (\text{mol m}^{-3}) \quad 11.51$$

with m as the unknown partition coefficient. For a liquid that is used as a reference and for which the partition coefficient, m_{ref} , (-), is known it is valid that

$$(C_{olref})_{p=1} = \frac{(C_{og})_{p=1}}{m_{ref}} \quad (\text{mol m}^{-3}) \quad 11.52$$

Now the general formula can be derived

$$C_{ol} = p_{orec}^* (C_{otref})_{p=1} \frac{m_{ref}}{m} \quad (\text{mol m}^{-3}) \quad 11.53$$

Eq. (11.8) for OTR can then be written as

$$OTR = k_{ol} A \left(p_{orec}^* (C_{otref})_{p=1} \frac{m_{ref}}{m} - p_{orec} (C_{otref})_{p=1} \frac{m_{ref}}{m} \right) \quad (\text{mol m}^{-3} \text{s}^{-1}) \quad 11.54$$

or

$$OTR = k_{ol} A \frac{m_{ref}}{m} \left(p_{orec}^* (C_{otref})_{p=1} - p_{orec} (C_{otref})_{p=1} \right) \quad (\text{mol m}^{-3} \text{s}^{-1}) \quad 11.55$$

in which p_{orec}^* is the measured partial pressure at equilibrium conditions (atm).

OTR , p_{orec}^* and p_{orec} can be measured. $(C_{otref})_{p=1}$ is known, for instance, from databooks. Thus the equation shows that a $k_{ol} A$ value is determined that is a constant times the real $k_{ol} A$ value. The constant is the ratio between the unknown partition coefficient of the fermentation liquid and the partition coefficient for a reference liquid. In this way an apparent $k_{ol} A_a$ value can be calculated from experiments given by

$$k_{ol} A_a = k_{ol} A \frac{m_{ref}}{m} \quad (\text{s}^{-1}) \quad 11.56$$

and Eq. (11.55) and (11.56) can be combined to:

$$OTR = k_{ol} A_a (C_{otref}^* - C_{otref}) \quad (\text{mol m}^{-3} \text{s}^{-1}) \quad 11.57$$

If Eq. (11.55) is used to predict OTR values for the same broth, for instance to predict the maximum OTR value at given stirrer and aeration conditions, thus at $k_{ol} A_a = \text{constant}$, it follows that

$$\frac{OTR_1}{OTR_2} = \frac{p_{orec}^* - (p_{orec})_1}{p_{orec}^* - (p_{orec})_2} \quad (-) \quad 11.58$$

More generally, the equation reads:

$$\frac{OTR_1}{OTR_2} = \frac{(k_{ot}A_a)_1}{(k_{ot}A_a)_2} \frac{P_{orec}^* - (P_{orec})_1}{P_{orec}^* - (P_{orec})_2} \quad (-) \quad 11.59$$

Eqs. (11.57) and (11.59) show that for a given single fermentation broth, the knowledge about the apparent $k_{ot}A_a$ value is satisfactory for the OTR prediction for that broth. Knowledge about the m value is not needed.

For scale-up Eq. (11.59) is very useful. Experiments on pilot scale yield a $k_{ot}A_a$ value for a broth. The process then will be scaled up whereby the liquid composition and therefore m_{ref}/m will be constant and $k_{ot}A_a$ follows the same rules (formulae) at scale-up as $k_{ot}A$. Again, the apparent $k_{ot}A_a$ can be used for scale-up calculations.

The situation becomes more complex when predictions have to be made for extrapolated values of v_{gs} and P_s/V_l . The relationships between $k_{ot}A$, v_{gs} , and P_s/V_l depend on the coalescence character of the liquid. As this is unknown, it seems at first sight that predictions are impossible. However, again an estimation can be made. Fig. 11.5 shows the $k_{ot}A$ relation for a purely coalescing and a purely noncoalescing liquid in a stirred vessel at a

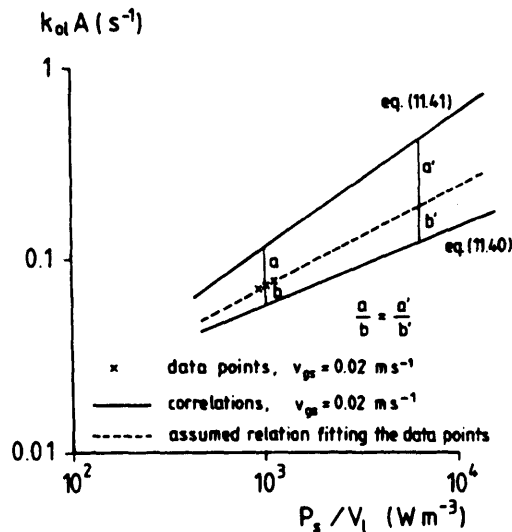


Fig. 11.5 Comparison of experimental values with the values predicted by the equations for coalescing and noncoalescing mass transfer in a stirred tank. The example of $v_{gs} = 0.02 \text{ m s}^{-1}$ is presented. (See also Example 11.2.) No pressure corrections applied.

specified gas superficial velocity. With the $OTR - C_{ot}$ method a limited number of experimental points can be measured at the same gas superficial velocity. These points are apparent values so they cannot be drawn in Fig. 11.5. However, they will be near the real $k_{ot}A$ value if we choose the reference not too far from the fermentation broth, for instance a liquid with the same amount of electrolytes present. When the difference is thus limited we can take this for granted and put the data point(s) in the graph. For the literature data on water the slope of the line of noncoalescing and purely coalescing is different. The slope of the $k_{ot}A$ vs. P_g/V_t graph certainly will change gradually when we change slowly from purely coalescing to purely noncoalescing. If we further assume that this change is proportional to the difference in $k_{ot}A$ value, the line segment given in Fig. 11.5 can be given as a first approximation of P_g/V_t and v_{gs} influence on mass transfer. This type of data can be very useful in research on production scale, where usually only data points from the fermentation itself can be used, while no possibility exists for additional experiments. Example 11.2 shows how this method can be applied.

11.5 Examples

Example 11.1 Hold-up and $k_{ot}A$ for bubble columns

The $k_{ot}A$ value is given by

$$k_{ot}A = \frac{6k_{ot}}{d_b} \frac{\epsilon}{(1-\epsilon)} \quad (\text{s}^{-1}) \quad 11.34$$

For coalescing systems the bubble diameter will be about 6 mm. From Fig. 11.2 it can be seen that for this bubble diameter $k_{ot} \approx 4 \times 10^{-3} \text{ m s}^{-1}$. With this Eq. (11.34) can be transformed into

$$k_{ot}A = \frac{0.4\epsilon}{1-\epsilon} \quad (\text{s}^{-1}) \quad 11.60$$

For a bubble column ϵ is given by Eq. (10.7):

$$\epsilon = 0.6(v_{gs}^c)^{0.7} \quad (-) \quad 10.7$$

Combining this with Eq. (11.1.1):

$$k_{ot}A = \frac{0.24(v_{gs}^c)^{0.7}}{1 - 0.6(v_{gs}^c)^{0.7}} \quad (\text{s}^{-1}) \quad 11.61$$

An even more basic method to calculate ϵ is by means of Eq. (10.3):

$$\epsilon = \frac{v_{gs}^c}{v_{bs} + v_{lw}} \quad (-) \quad 10.3$$

Assuming that for 6-mm bubbles $v_{bs} = 0.25 \text{ m s}^{-1}$ and using the assumption that

$$v_{lw} = 0.5 v_{lc} \quad (\text{m s}^{-1}) \quad 11.62$$

then with Eq. (9.20) for v_{lc} , Eq (10.3) can be written as:

$$\epsilon = \frac{v_{gs}^c}{0.25 + 0.45(g T_v v_{gs}^c)^{0.33}} \quad (-) \quad 11.63$$

Combining Eq. (11.1.4) with Eq. (11.1.1) yields

$$k_{ol} A = \frac{\frac{0.4 v_{gs}^c}{0.25 + 0.45(g T_v v_{gs}^c)^{0.33}}}{1 - \frac{v_{gs}^c}{0.25 + 0.45(g T_v v_{gs}^c)^{0.33}}} \quad (\text{s}^{-1}) \quad 11.64$$

In Fig. (11.6) a comparison is given for $k_{ol} A$ values according to the empirically found $k_{ol} A$ formula [Eq. (11.35)] and the formula based on the basic phenomena, together with the assumptions. These results agree very well. The applicability of Eq. (10.3) gives us the possibility to get more insight in the bubble diameter influence. Fig. 11.7A gives the simplified dependence of bubble rise velocity v_{br} from d_b , Fig. 11.7B gives the simplified dependence of k_{ol} from d_b . $k_{ol} A$ now can be calculated from Eq. (11.34). d_b is the variable. k_{ol} is given in Fig. 11.7B. ϵ can be calculated with Eq. (10.3). In Eq. (10.3) v_{bs} is assumed to be equal to v_{br} and is therefore given in Fig. 11.7A. $v_{lw} = 0.5 v_{lc}$ and then can be calculated with Eq. (9.20). Now $k_{ol} A$ becomes:

$$k_{ol} A = \frac{6 k_{ol}}{d_b} \frac{\frac{v_{gs}^c}{v_{br} + 0.45(g T_v v_{gs}^c)^{0.33}}}{1 - \frac{v_{gs}^c}{v_{br} + 0.45(g T_v v_{gs}^c)^{0.33}}} \quad (\text{s}^{-1}) \quad 11.65$$

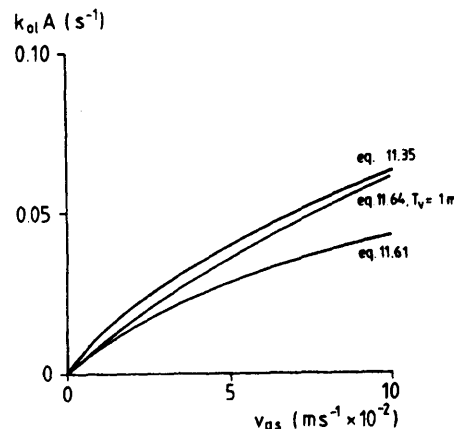


Fig. 11.6 Calculated $k_{oi}A$ values. No pressure corrections applied.

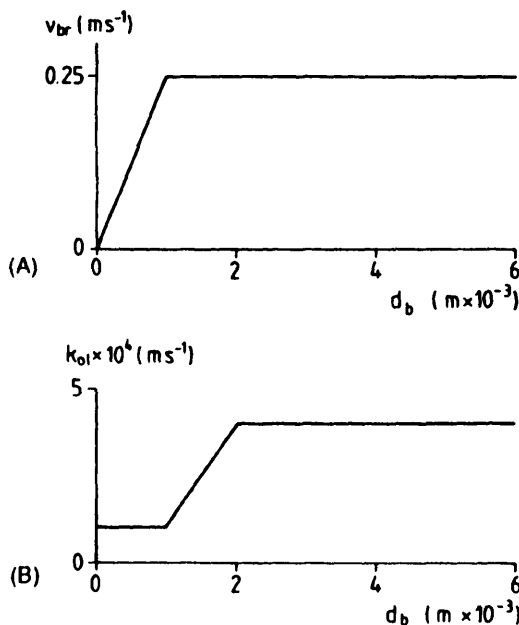


Fig. 11.7 Calculated $k_{oi}A$ values. A: Assumed dependence of v_{br} from d_b . B: Assumed dependence of k_{oi} from d_b . C: Calculated dependence of $k_{oi}A$ from d_b at $v_{gs} = 0.05 m s^{-1}$ and $T_v = 1 m$ with Eq. (11.65). No pressure corrections applied.

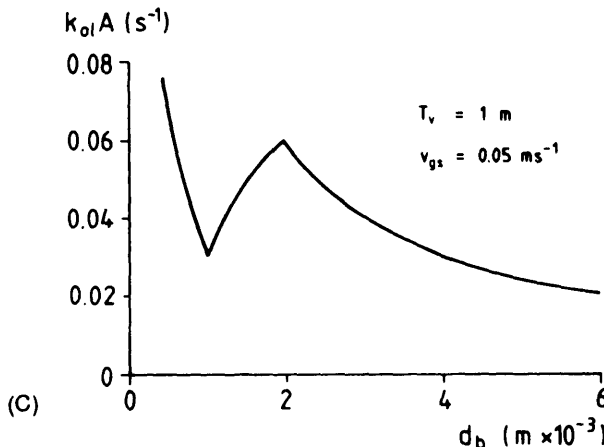


Fig. 11.7 (Continued)

Calculations are presented in Fig. 11.7C. $k_{oi}A$ increases with d_b decreasing from 6 down to 2 mm, due to the decrease of d_b at a constant k_{oi} value. The effect of a decrease of k_{oi} can be seen when d_b decreases from 2 down to 1 mm. When d_b becomes smaller than 1 mm, $k_{oi}A$ strongly increases due to a constant k_{oi} value, a decreasing v_{br} value and a decreasing d_b value. It is clear that for a large effect on $k_{oi}A$, d_b should be less than 0.5 mm. These bubbles are difficult to generate in a bubble column. Besides, very small bubbles can easily lead to foaming problems.

Example 11.2 Large-scale power consumption calculation

Assume a fermentation has been studied on laboratory and pilot scale. The question now is, can this fermentation be scaled up to commercial scale?

The data are:

Fermenter available at pilot scale: $T_v = 0.4\text{ m}$, $H_v = 0.8\text{ m}$ (liquid)
large scale: $T_v = 4\text{ m}$, $H_v = 8\text{ m}$ (liquid)

At pilot scale $P_s/V_t \approx 1000\text{ W m}^{-3}$; v_{gs} can be chosen. At large scale the motor can still be chosen, while the compressor can deliver $v_{gs}(P_a/P_s) = 0.02\text{ m s}^{-1}$, at the total pressure near the stirrer of $3.0 \times 10^6\text{ N m}^{-2}$. Finally the OTR value should be $OTR = 100\text{ mol m}^{-3}\text{ h}^{-1} = 0.028\text{ mol m}^{-3}\text{ s}^{-1}$.

Question: The motor power to be installed.

Solution:

Two problems arise. First, the P_s/V_t value at pilot scale cannot be varied

and will probably not be the value to be used at large scale. Second, the coalescence characteristics at large scale are unknown.

1. What is the $k_{oi}A_a$ value, needed at large scales?
- Let us assume that m is slightly lower for the given fermentation medium than for water. (This can be calculated more accurately if the detailed composition is known; however, it is not strictly needed.) Here we assume that the gross composition leads to:

$$C_{oi}^* = 0.25 \text{ mol m}^{-3} \text{ at air, atmospheric conditions}$$

- At large scale concentration differences do exist. Here we assume that $C_{oi} = 0.10 \text{ mol m}^{-3}$ is needed at the lower stirrer.
- We assume a black box model with ideally mixed gas phase and mass transfer determined by the stirrer conditions. For the gas phase a balance can be made:

$$F_g (C_{ogl} - C_{ogo}) = OTR V_t$$

with the given data:

$$F_g = v_{gs} \frac{1}{4} \pi T_v^2 = 0.02 \times 3 \times \frac{1}{4} \pi \times 4^2$$

$$C_{ogl} = \frac{\text{O}_2 \text{ fraction gas inflow}}{\text{molar volume}} = \frac{0.21}{24.2 \times 10^{-3}}$$

$$V_t = \frac{1}{4} \pi T_v^2 H_v = \frac{1}{4} \pi 4^2 \times 8$$

$$3 \times 0.02 \times \frac{1}{4} \pi \times 4^2 \times \left(\frac{0.21 \times 1000}{24.2} - C_{ogo} \right) = 0.028 \times \frac{1}{4} \pi \times 4^2 \times 8$$

$$\rightarrow C_{ogo} = 4.95 = 0.57 C_{ogl} \quad (\text{mol m}^{-3})$$

$k_{oi}A_a$ now can be calculated with Eq. (11.57):

$$0.028 = k_{oi}A_a (3 \times 0.57 \times 0.25 - 0.10)$$

$$\rightarrow k_{oi}A_a = 0.085 \text{ s}^{-1}$$

2. What are the conditions for the experiment on pilot scales?

$v_{gs} (P_a / P_s)$ should be fixed at 0.02 m s^{-1} because this is the value at large scale. The question to be answered at pilot scale is: where in between coalescing and noncoalescing is the fermentation medium.

3. The experiment

$k_{oi}A_a$ measurements are done at different P_a/V_t values at pilot scale

at $v_{g,i}(P_a/p_i) = 0.02 \text{ m s}^{-1}$ with the $OTR - C_{oi}$ method, assuming again $C_{oi} = 0.25 \text{ mol m}^{-3}$. The data points given in Fig. 11.5 are found. Now the dotted line can be drawn and this line shows

$$k_{oi} A_a = 0.085 \text{ s}^{-1} \text{ at } \frac{P_i}{V_i} = 1300 \text{ W m}^{-3}$$

The motor power $P_i = 1.3 V_i$ (kW) is $1/4 \times \pi \times 4^2 \times 8 \times 1.3 = 131 \text{ kW}$. Including losses, etc., the installed power can be estimated at 150 kW.

References

- Bacon V.W., Balmer R.T. and Griskey R.G. "Water sewage works." (1977), p. 121.
- Brian P.L.T. and Hales H.B. "Effects of transpiration and changing diameter on heat and mass transfer to spheres." A.I.Ch.E. J. 15, 419 (1969).
- Calderbank P.H. and Moo-Young M.B. "The continuous phase heat and mass transfer properties of dispersions." Chem. Engng. Sci. 16, 39 (1961)
- Dang N.D.P., Karrer D.A. and Dunn I.J. "Oxygen transfer coefficients by dynamic moment analyses." Biotechnol. Bioeng. 19, 853 (1977).
- Deckwer W.D., Nguyen-tien K., Schumpe A. and Serpemen Y. "Oxygen mass transfer into aerated CMC solutions in a bubble column." Biotechnol. Bioeng. 24, 461 (1982).
- Dunn I.J. and Einsele A. "Oxygen transfer coefficients by the dynamic method." J. Appl. Chem. Biotechnol. 25, 707 (1975).
- Finn R.K. "Agitation and Aeration." Biochem. and Biol. Eng. Sci., Ed. N. Blakebrough. Academic Press, New York (1967), p. 69.
- Heijnen J.J. and Van 't Riet K. "Mass transfer, mixing and heat transfer phenomena in low viscosity bubble column reactors." Chem. Eng. J. 28, B21 (1984).
- Heijnen J.J., Van 't Riet K. and Wolthuis A.J. "Influence of very small bubbles on the dynamic $k_i A$ measurements in viscous gas-liquid systems." Biotechnol. Bioeng. 22, 1945 (1980).
- Higbie R. "The rate of absorption of a pure gas into a still liquid during short periods of exposure." Trans. A.I.Ch.E. 31, 365 (1935).
- Lewis W.K. and Whitman W.G. "Principles of gas absorption." Ind. Eng. Chem. 16, 1215 (1924).

Linek V. and Vacek V. "Oxygen electrode response lag induced by liquid film resistance against oxygen transfer." *Biotechnol. Bioeng.* 18, 1537 (1976).

Linek V. and Vacek V. "Dynamic measurement of the volumetric mass transfer coefficient in agitated vessels: Effect of the start up period on the response of an oxygen electrode." *Biotechnol. Bioeng.* 19, 983 (1977).

Mehta V.D. and Sharma M.M. "Mass transfer in mechanically agitated gas-liquid contactors." *Chem. Engng. Sci.* 26, 461 (1971).

Oosterhuis N.M.G. and Kossen N.W.F. "Oxygen transfer in a production scale bioreactor." *Chem. Eng. Res. Des.* 61, 308 (1983).

Oosterhuis N.M.G and Kossen N.W.F. "Dissolved oxygen concentration profiles in a production-scale bioreactor." *Biotechnol. Bioeng.* 26, 546 (1984).

Prasher B.D. "Mass transfer coefficients and interfacial areas in agitated dispersions." *A.I.Ch.E. J.* 21, 407 (1975).

Quicker G., Schumpe A., König B., and Deckwer W.D. "Comparison of measured and calculated oxygen solubilities in fermentation media." *Biotechnol. Bioeng.* 23, 635 (1981).

Ranz W.E. and Marshall W.R. "Atomization and spray drying." *Chem. Eng. Progr. Symp. Series* 50 (2), (1954).

Robinson C.W. and Wilke C.R. "Simultaneous measurement of interfacial area and mass transfer coefficients for a well mixed gas dispersion in aqueous electrolyte solutions." *A.I.Ch.E. J.* 20, 285 (1974).

Van 't Riet (1979) K. "Review of measuring methods and results in non-viscous gas-liquid mass transfer in stirred vessels." *Ind. Eng. Chem. Proc. Des. Dev.* 18, 357 (1979).

Verlaan P., Tramper J., Van 't Riet K. and Luyben K.Ch.A.M. "A hydrodynamic model for an air lift loop bioreactor with external loop." *Chem. Eng. J.* 33, B43 (1986).

Verlaan P., Vos J.C. and Van 't Riet K. "Transition from a bubble column to an air lift loop reactor." *J. Chem. Technol. Biotechnol.* 45, 109 (1989).

Wise D.L. and Houghton G. "The diffusion coefficients of ten slightly soluble gases in water at 10-60°C." *Chem. Engng. Sci.* 21, 999 (1966).

12

Foam

12.1 Introduction

The presence of a foam layer is very common, particularly in aerobic fermentations. Foam originates from bubbles and liquid leaving the bulk volume. At the moment that gas and liquid leave the liquid bulk volume, a process of drainage starts. This leads to a decrease in liquid content and a decrease in distance between the bubbles until mainly liquid films are present between the bubbles. Finally a honeycomb structure of air bubbles separated by very thin walls of liquid connected by Plateau borders results from this process. The gas content is very high, usually 60-90%. Foam has to be distinguished from hold-up, which indicates the bubbles in the bulk of the liquid. The gas content for hold-up is usually < 50%, much smaller than for foam. In most cases the difference between hold-up and foam is simply given as hold-up being the bubbles in the broth and foam being the bubbles on top of the broth.

A number of reviews about foaming are known (Bikerman, 1953; Hall et al., 1973; Viesturs et al., 1982). There are a number of definitions and related measuring methods to quantify the foaming behavior of a liquid. The most simple one is given by Bikerman (1953) and Kalischewski et al., (1979). They define the foaminess, Σ (s), of a liquid in a small-bubble column with a porous glass sparger as

$$\Sigma = \frac{V_{f_0}}{F_g} \quad (s) \quad 12.1$$

in which

$$V_{f_0} = \text{equilibrium volume of foam} \quad (\text{m}^3)$$
$$F_g = \text{volumetric gas flow rate} \quad (\text{m}^3 \text{ s}^{-1})$$

A simple method to define the foam stability is given by Bumbullis and Schügerl (1981). A stirrer rotates above the foaming liquid and is moving slowly downward. When it reaches the foam it will destroy the foam. Moving downward further there will be a position at which the foam is not destroyed any more. The corresponding foaminess at this position is Σ_r (s). Foam stability s (-) then is defined as

$$s = \frac{\Sigma_r}{\Sigma} \quad (-) \quad 12.2$$

These two methods give values that are dependent on the measurement method itself, instead of independent absolute values. Viesturs et al. (1982) give more complex definitions. Yet these also do not give absolute values. The existence of different definitions and measuring methods clearly indicates the gap between the complexity of the foam phenomena and the present lack of knowledge.

Foaming has a number of advantages and disadvantages. A negative effect is the decrease of the effective bioreactor volume and even product loss when overflow occurs. Example 12.1 shows that only seconds are needed to get overflow problems when there is a suddenly occurring foam problem. There is also the danger of contamination at overflow conditions. Fragile cells can be damaged when foam collapses. The use of some antifoams can influence the metabolic activity. For pharmaceutical and food applications legislation of antifoams can be a problem. An important positive effect is that usually foaming liquids also tend to be noncoalescing (see, for example, Adler et al., 1980a, b, 1981). Therefore they will have favorable mass transfer characteristics (see also Example 12.2). In practice foam control has to be a subtle balance between the positive effect on mass transfer and the negative effects related to the presence of a foam layer. Generally the process is controlled in such a way that a small foam layer is present on top of the broth.

12.2 Theory of foam stability

The most widely accepted theory is that foam stability is caused by the presence of proteins on the gas-liquid surfaces. A review is given by Prins and Van 't Riet (1987).

12.2.1 Protein properties

Proteins distinguish themselves from low-molecular-weight, surface-active agents in that:

1. They adsorb at an interface at very low concentrations.
2. It is relatively difficult to desorb an adsorbed protein molecule from an interface.
3. Flexible protein molecules change their conformation when they adsorb at an interface.
4. More than one layer of protein molecules can be adsorbed at an interface.
5. Desorption of protein molecules is relatively easy when they are displaced by means of low-molecular-weight surfactants.

Due to these properties the following phenomena can be observed when proteins are adsorbed at a gas-liquid interface.

In equilibrium the conformation of an adsorbed flexible protein molecule is such that those parts of the molecule which prefer to be in the interface form trains and those parts which prefer to be in the liquid form loops and tails, as shown schematically in Fig. 12.1. This conformation of an adsorbed protein molecule is quite different from the conformation of such a molecule in a solution, which is more or less random, as shown in Fig. 12.2. Because a large number of segments are involved in the adsorption process, it takes a relatively long time before the equilibrium conformation of the adsorbed molecules is reached. The value of the interfacial tension is mainly determined by the number of adsorbed segments (trains). Consequently, the attainment of the equilibrium interfacial tension will also take a relatively long time: times of the order of hours are no exception. In short: the value of the interfacial tension when flexible proteins are adsorbed at a gas-liquid interface is determined not only by the amount of proteins that are adsorbed, but also by the way that they are adsorbed. In addition, dynamic effects are important.

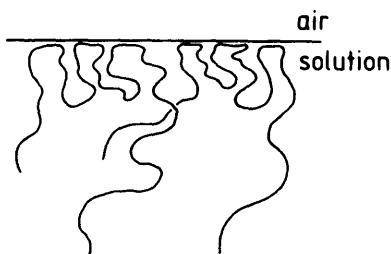


Fig. 12.1 Schematic representation of adsorbed protein molecules.
(From Prins and Van 't Riet, 1987.)

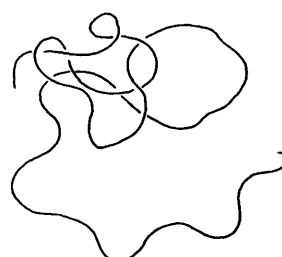


Fig. 12.2 Schematic representation of a protein molecule in a solution.
(From Prins and Van 't Riet, 1987.)

When an interface to which protein is adsorbed is brought out of equilibrium, for instance by means of expansion or compression, the corresponding change in the adsorbed amount of proteins per unit area causes the surface tension to increase or decrease, respectively.

This phenomenon, which gives the surface a certain stiffness, is defined by the parameter E , the surface dilatational modulus (N m^{-1}):

$$E = \frac{d\sigma}{d \ln a} \quad (\text{N m}^{-1}) \quad 12.3$$

in which

$$\begin{aligned} \sigma &= \text{surface tension} & (\text{N m}^{-1}) \\ d \ln a &= \text{relative change in surface area} & (-) \end{aligned}$$

In order to reestablish equilibrium, protein has to be transported to or from the interface, respectively. However, even when this transport is fast, reestablishment of the equilibrium conformation of the adsorbed protein may take a long time.

The important consequence of this behavior is that the surface tension gradients can persist during a relatively long time in a surface to which protein is adsorbed. This phenomenon is important for the behavior of foams and bubbles because a surface tension gradient has the same dimension (N m^{-2}) as a shear stress, indicating that a surface tension gradient is able to compensate for the shear stress exerted by a liquid, because of either flow or gravity forces, along that surface. This phenomenon may cause a considerable slowing down of the liquid velocity close to that surface, which in the limiting case may remain almost motionless with respect to the flowing liquid.

12.2.2 Relevant processes in fermentation

Examples of processes taking place during fermentation in which surface phenomena play a role are:

1. Drainage of liquid from a thin film between two bubbles
2. Drainage of liquid from the Plateau borders in the foam
3. Stability of thin liquid films as affected by the presence of antifoam liquids
4. Oxygen transfer from the rising bubbles to the surrounding liquid

12.2.2.1 Drainage from a thin film between two bubbles

During the fermentation process, thin liquid films are formed between colliding bubbles when they rise through the liquid and in the foam where

bubbles are pressed against each other under more quiet conditions. When the bubbles enter the foam, these films become thinner as a result of drainage and therefore they become more likely to collapse. Drainage of a thin liquid film between gas bubbles is governed mainly by two processes, which can operate independently of each other:

- a. Marginal regeneration
 - b. Viscous flow of film liquid to the surrounding Plateau border. To define thin films and Plateau borders: As stated in the introduction, a honeycomb structure foam consists of thin films (sheets or walls) connected by Plateau borders (threadlike).
- a. In the so-called marginal regeneration process, as a result of the Plateau border suction, thicker parts of the film are drawn to that Plateau border at the expense of thinner film parts that are drawn out of that Plateau border. Because these film parts move along each other in different directions, the stiffness of the film surfaces plays an important role, in the sense that beyond a certain stiffness this process cannot take place. Most protein-stabilized films have surface stiffnesses which are big enough to prevent the performance of the marginal regeneration process. This is an important contribution to the film stability and therefore foaming.
- b. The liquid flows out of a thin liquid film due to the capillary suction exerted by the Plateau border and due to the weight of the film liquid. A thin liquid film has elastic properties, which means that when the film is stretched, the surface tension increases and remains increased as long as the film is stretched. This phenomenon is caused by the limited amount of surfactants present in the thin liquid film, not allowing the film to reach the original equilibrium situation with respect to surfactant adsorption and surface tension, when the film is stretched. As a result of this elastic behavior of the film, the liquid flows out of the film, under the condition that both surfaces of the film remain motionless with respect to the Plateau border. This kind of drainage can therefore be described as the flow of a liquid layer between two parallel solid walls. The amount of liquid F_l^u ($\text{m}^2 \text{s}^{-1}$) leaving the film per unit time and per unit width of the film is given by

$$F_l^u = \frac{2}{3} \frac{\rho_l g}{\mu_l} d_f^3 \quad (\text{m}^2 \text{s}^{-1}) \quad 12.4$$

in which

g	= gravitational acceleration	(m s^{-2})
ρ_l	= liquid density	(kg m^{-3})
μ_l	= liquid dynamic viscosity	(N s m^{-2})
d_f	= film thickness	(m)

The strong dependence of the drainage on the film thickness means that drainage decreases as time proceeds.

In protein-stabilized films, in addition to reestablishment of the amount adsorbed, reestablishment of the equilibrium conformation of the adsorbed protein also contributes to the value of the film elasticity. Consequently, it is to be expected that for protein-stabilized films, the condition of motionless film surfaces is already reached at a thicker film compared to when the film is stabilized with a low-molecular-weight surfactant. The drainage of the film may come to an end when a so-called equilibrium film can be formed. In such a film further drainage is prevented because the two film surfaces repel each other. In the case of flexible proteins this repulsion can be caused by the steric hinderance of the protuding tails and loops of the adsorbed protein molecules. In this way an equilibrium film can be formed which is relatively thick as compared to the equilibrium films stabilised by low-molecular-weight surfactants. It may be that this property of protein-stabilized films is responsible for the well-known relatively high stability of protein foams.

12.2.2.2 Drainage from the Plateau borders in the foam

Apart from trivial parameters such as the geometry of the Plateau border and the viscosity and density of the liquid, the drainage of liquid from the Plateau borders in a foam is determined by the hydrostatic pressure differences over the length of the Plateau border and by the stiffness of the Plateau border surfaces. The hydrostatic pressure in the Plateau border is determined by the height H (m) above the bulk liquid and the Laplace pressure difference ΔP ($N\ m^{-2}$) over the curved Plateau border surface. Assuming a cylindrical shape for the Plateau border surfaces, the following relation exists when both pressures are in equilibrium:

$$\Delta P = \frac{\sigma}{R_c} = \rho_l g H \quad (N\ m^{-2}) \quad 12.5$$

in which

$$R_c = \text{radius of the curvature} \quad (m)$$

A foam at height H reaches equilibrium by allowing the Plateau borders to drain till the radius of curvature of their surfaces is small enough to satisfy Eq. (12.5). Before this equilibrium is reached, it depends on the stiffness of the Plateau border surfaces to what extent these surfaces move with the liquid and consequently to what extent the liquid velocity is slowed down.

In view of the high rigidity of surfaces with adsorbed proteins, it is to be

expected that even for relatively wet foams the drainage proceeds under the condition that the surfaces are motionless. This explains the attempt of several investigators (Kann, 1984; Kann and Feklistov, 1985) to describe the drainage of liquid through a foam quantitatively by means of the liquid flow through a porous bed. This phenomenon is one of the potential factors which contribute to the relatively high stability of protein foams.

12.2.2.3 Stability of thin liquid films

In fermentations antifoam liquids are used to destabilize the foam (Viesturs et al., 1982). These liquids can be composed of, for example, oils, fatty acids, esters, polyglycols and siloxanes (Colbert, 1981). Many of these liquids, particularly the oils, are preferably added as emulsion droplets. Oil droplets can destabilize protein films in the following ways:

- a. They can act as hydrophobic particles which make holes in the films as soon as they contact both film surfaces.
 - b. The droplets may spread over the film surfaces, replacing the adsorbed protein and in this way disturbing the film-stabilizing action of protein.
 - c. The spreading of the oil droplets causes the film liquid to be squeezed away from the spreading droplet.
- a. When a hydrophobic particle contacts both surfaces of a film, a convex surface is formed as a result of the obtuse contact angle. The increased pressure of the liquid under that curved surface causes the liquid to flow away from that particle till ultimately the contact between particle and film is broken and the film collapses, as is shown in Fig. 12.3.
- b. As described above, low-molecular-weight surfactants which are more surface active than the protein will replace the adsorbed protein from the surface. By this process the film can become unstable, for instance, because

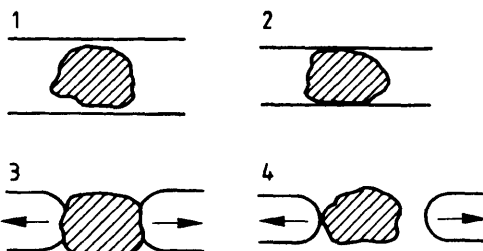


Fig. 12.3 Schematic representation of the draining of the liquid film. (From Prins and van 't Riet, 1987.)

the repulsion between the two film surfaces becomes too small when the low-molecular-weight surfactant is present or because the film becomes thinner, giving one of the other processes the opportunity to break the film.

c. It is well known that foams can be destabilized by adding an oil-in-water emulsion. In a patent of Dupont de Nemours (Walker and Morrow, 1949) it is claimed that the foam-depressing effect reaches a maximum at a certain droplet size of the emulsion. This can be explained by assuming that due to the spreading of the oil droplet (Fig. 12.4) the film liquid is also forced to flow away from the spreading droplet. When the resulting thinning of the film proceeds far enough, the film will break. A maximum in the foam-depressing effect arises, because the formation of a thin spot in the film is promoted when the size of the spreading droplet is increased. However, at a further increase of the droplet size, it has to be taken into account that the number of droplets decreases considerably and this lowers the chance that the film will break.

12.2.2.4 Oxygen transfer to the surrounding liquid

Proteins influence gas bubbles in the broth in two ways: they can change the bubble surface rigidity and they can influence the coalescence phenomena.

As discussed in Chapter 11, a bubble rising in a liquid can have a rigid interface or a freely moving interface. In Chapter 11 (Fig. 11.2) the k_{oi} values show that the transition from rigid to freely moving occurs at a bubble diameter of 1–2 mm. When protein molecules are present, the surface can become more stable. This means that the k_{oi} value can decrease in the range of bubble diameters of 1–2 mm. It is not expected that proteins are

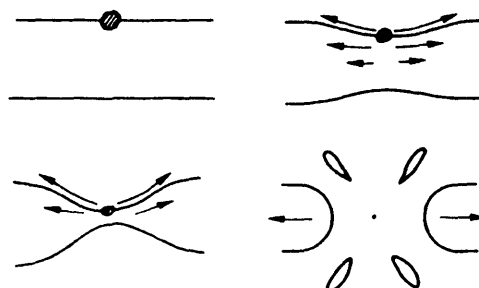


Fig. 12.4 The spreading of an oil droplet. (From Prins and Van 't Riet, 1987.)

able to stabilize the surface at diameters > 3 mm. Usually bubbles in fermentations are larger than 3 mm. Therefore, this negative effect will be limited. It might be that part of the bottom of the bubble will be stabilized, even at diameters > 3 mm. Again this process will have a limited influence, because most of the bubble will keep its freely moving interface.

The final bubble size in a dispersion originates from an equilibrium between dispersion and coalescence, as discussed in Chapter 6. Stabilization of the drainage between two colliding bubbles can change a coalescing liquid into a noncoalescing one. Therefore, the bubble size can decrease. This will improve the mass transfer, as shown in Eq. (11.34). This effect will in general be much more important than the effects on k_{oi} .

In this way the positive effects of foaming on mass transfer can be explained from the stabilizing effects of proteins. When an antifoam is added in abundant quantities, the foam will be destroyed completely, but also the liquid will become a strongly coalescing one, with the coupled negative effects on mass transfer.

12.3 The influence of broth parameters and operating parameters

Some general remarks will be made now about the influence of a number of parameters. These are based on Gaden and Kevorkian (1956), Viesturs et al. (1982), Hall et al. (1973), Bikerman (1953), Bumbullis et al. (1979, 1981), Bumbullis and Schügerl (1979, 1981), Kalischewski et al. (1979), König et al. (1979) and Buchholz et al. (1979).

a. Protein

As discussed in Section 12.2, for fermentation media proteins can be regarded as the main cause of foam stability. Proteins are always present in fermentation media. Many fermentations are directed to the production of extracellular proteins. Those that are not will certainly have proteins available in the medium originating from, for example, extracellular enzymes, cell lysis and substrates. The accumulation of proteins at the interface results in a measurable foaminess already at bulk concentrations of 10^{-3} kg m $^{-3}$ (1 ppm, see also Example 12.3). Foaminess increases with increasing concentration of protein up to $1\text{--}10$ kg m $^{-3}$. At even higher concentrations a decrease can occur due to the coagulation of the proteins. Foaminess due to proteins is very pH dependent. Generally it reaches a maximum value near the isoelectric point.

The proteins mainly originate as extracellular products from the microorganisms. As different organisms can vary considerably in the amount of excretion, the use of mutants is favorable when they produce only minor amounts of proteins, besides the ones needed.

b. Salts

Salts strongly influence the solubility of proteins. They are used therefore to flocculate proteins in a solution. For a given concentration of protein the decrease in solubility also can be regarded as an apparent increase of the protein concentration when seen as a fraction of the saturation concentration. In accordance with this increase is an increase of foaming behavior with the addition of salts, when proteins are present. With the addition of pure salts to pure water no foaming occurs at all.

c. Alcohols

Short-chain alcohols have a definite positive effect on foaminess. A maximum is found at a concentration of 1-2% of alcohol added to a protein water solution.

d. Antifoam agents

Most antifoam agents are strong surface-tension-lowering substances. When they are added to a culture liquid (or protein solution), foaminess is strongly suppressed. Some antifoams show a surprising effect in that they cause foaming when added to a pure water/air dispersion.

e. pH

pH is very important. Protein solutions show a maximum of foaminess at the isoelectric point of the protein. Also, the effect of antifoam agents is pH dependent.

f. Temperature

Increase in temperature leads to a decrease in foaminess. This might be due to an increase of drainage due to a decrease in viscosity. Sometimes increased evaporation of volatile components can occur. At higher temperatures denaturation can influence foaming.

g. Cells

Little is known about the influence of cells. This can be understood from the fact that the presence of cells always will be accompanied by the presence of proteins; other solutes and viscosity increase depending on cell density. In general, very thick suspensions show less foaming activity than very dilute suspensions. This might be a viscosity effect.

h. Gas flow rate

A straightforward relation is the increase of the foam layer with the gas flow rate. This can be expected because more bubbles reach the surface and will convert into foam. Yet in a number of cases a maximum occurs above which the foam layer can even decrease in size with increasing gas flow rate. The reasons are not clear; maybe it is due to a decrease in "monodispersity"

of the bubbles or other changes in bubble diameter. The importance of the effects of gas flow rate is very large for commercial fermentations.

i. Viscosity

The influence of viscosity is not at all clear. Usually foaming increases in a fermentation after inoculation when the viscosity increases from 1 up to 10–100 mPas. It is not clear altogether if this is caused by the viscosity itself or by surface tension effects occurring simultaneously. The same phenomenon can be seen with the addition of a polymer to water. Here it is also questionable whether the foaming is caused by the viscosity or by surface-active trace contaminants. When the viscosity increases further from $10-100 \times 10^{-3} \text{ N s m}^{-2}$ upward, foaming usually decreases. Yet at very high viscosities foaming will start again. The general theory for this phenomenon is that the drainage from the liquid films between the bubbles decreases.

j. Conclusions about the different parameters

It will be clear that some qualitative effects can be predicted, however, in model solutions only. For culture media foam formation is nearly always due to the excretion of proteins from growing cells or from lysis. The quantitative amount of foaminess cannot be predicted from model experiments or from physical data. This should be determined for each type of broth experimentally.

12.4 Foam destruction methods

For commercial fermentations foam control is necessary due to the possibility of overflow. Mass transfer of a foaming liquid is favorable to mass transfer of its nonfoaming counterpart. Thus foam control should not be the complete evasion of foam by an antifoam. An acceptable optimum has to be found for each situation separately. Two groups of foam control methods will be dealt with here.

12.4.1 Antifoam agents

This is the most widely applied method. Reasons are

- the relatively small quantities (< 1% v/v) needed and thus the relatively small contribution to the production costs
- the reliability, also at extreme foaming conditions
- the ease of handling

The negative effects on $k_{o,i} A$ can be minimized to some extent by allowing a certain amount of foam on top of the broth. Usually foam is controlled in such a way that overflow conditions are just prevented within acceptable safety margins.

For the production of foods and pharmaceuticals the agents have to meet the requirements of regulations. Listings of different types of antifoams can be found in Viesturs et al. (1982), Gaden and Kevorkian (1956) and Colbert (1981).

12.4.2 Mechanical and physical methods

Viesturs et al. (1982) and Gaden and Kevorkian (1956) describe a large number of methods, such as high-speed rotating discs, ultrasonics, temperature shocks and other methods. The great advantage of these methods is that the liquid properties are not influenced. In this way the noncoalescing character (high $k_{oi} A$), if present, can be maintained. Also, problems with regulations with the use of antifoam agents are prevented.

The negative effects can best be illustrated on the well-known high-speed centrifugal foam destroyer. The power input of such a destroyer is of the order of 0.5–5 kW per m³ fermenter volume. For commercial large-scale applications this leads to massive constructions and to considerable energy costs. Tip speeds of centrifugal devices are usually > 10 m s⁻¹ (Furchner and Mersmann, 1986). The energy consumption related to these tip speeds makes the use of the centrifugal devices impossible if the liquid is extremely foaming (see Example 12.4). A second disadvantage of great importance is the limited destroying capacity. This leads to an overdimensioned apparatus and always the installment of a back-up control unit equipped with an antifoam dosage unit. The time that is needed for a foam layer to rise from the surface of the vessel to the air outlet is only a matter of seconds for most fermentations (Example 12.1). This means that at suddenly changing foaming conditions (for instance, due to pH control failure) overflow of the broth can easily occur. Once overflow occurs, the vessel content is quickly transported to the exterior of the fermenter (Example 12.1). Fortunately, these extreme conditions will not happen very easily. Yet because of the enormous problems that have to be tackled if a fermentation has a very strong foaming character, the use of antifoams is certainly needed in such cases. Finally, mechanical foam destroyers cannot destroy very small foam bubbles. These return to the broth and can cause serious problems (Furchner and Mersmann, 1986).

The energy and mechanical problems and the need of a back-up system are the main causes that mechanical foam destructors are rarely applied on commercial large-scale fermenters.

12.5 Measuring methods

The methods to quantify the foaminess and the foam stability have already

been dealt with in Section 12.2. The methods used to detect a foam layer in a fermenter are nearly always based on measurement of electrical resistance or conductivity between a number of electrodes and the vessel wall. These electrodes were discussed in Chapter 10.

12.6 Conclusions

The physical background of foaming of the complex fermentation liquids is not well understood. Proteins do play a major role, but all other components can also be important. Foaming is a problem, but its relation to mass transfer leads to the allowance of a certain amount of foam on top of the fermenter. For foam control a number of methods are available. Most widely used are the antifoam liquids and the centrifugal separator. The latter one should be equipped with a safety antifoam dosage device also and is less attractive for large-scale applications.

12.7 Examples

Example 12.1 The consequences of extreme foaming

Usually foam formation is controlled in such a way that the formation of stable foams is prevented. However, sometimes foam stability can suddenly increase, for instance due to foam control failure or a sudden change in pH value. This example shows that operation of a fermenter with stable foam formation can be very problematic and in some cases even impossible.

Assume a commercial large-scale fermenter, with a height $H_s = 10 \text{ m}$ and a diameter $T_s = 5 \text{ m}$. Assume further that the liquid content of the foam is 30% of the gas volume. If the gas superficial velocity, at the conditions of temperature and pressure at the top of the fermenter, is given by v_{gs} , then the stable foam layer originates with a linear velocity v_{rf} , given by

$$v_{rf} = 1.3 v_{gs} \quad (\text{m s}^{-1})$$

The liquid in the foam originates from the fermentation broth; i.e. the liquid level goes downward with a velocity $0.3 v_{gs}$.

If the head space length is given by L , then the time t_f , defined as the time needed for the top of a stable foam layer to rise over a length L , is given by

$$t_f = \frac{L}{1.3 v_{gs} - 0.3 v_{gs}} = \frac{L}{v_{gs}} \quad (\text{s})$$

The broth liquid volume V_b^f , which is transported from the broth to the stable foam, is given by

$$V_b^f = 0.3 v_{gs} \times \frac{1}{4} \pi T_v^2 = 5.9 v_{gs} \quad (\text{m}^3 \text{ s}^{-1})$$

The results for a number of v_{gs} values that are indicative for highly loaded commercial fermentations are given in Table 12.1.

The head space should be as small as possible because this increases the effective volume and thus decreases the costs per unit volume and per unit of product. However, this example shows that there are situations in which overflow can occur within 10 seconds and the vessel can be emptied in minutes. This clearly shows that a stable foam should be prevented. It also makes clear that a subtle foam control is one of the most critical fermenter operational tasks.

Example 12.2 Relation between foam and mass transfer

In Section 11.2 it was shown that the mass transfer coefficient $k_{oi} A$ is strongly dependent on the coalescence and dispersion characteristics of the broth. Differences between a coalescing versus a noncoalescing broth can be up to a factor of 10. As stated in this chapter, the coalescing conditions and

Table 12.1 Times needed to reach overflow conditions

v_{gs} (m s^{-1})	L (m)	t_f (s)	V_b^f ($\text{m}^3 \text{ s}^{-1}$)	V_b^f ($\text{m}^3 \text{ min}^{-1}$)
0.001	0.5	500	0.006	0.35
	1.0	1000		
	2.0	2000		
0.005	0.5	100	0.030	1.77
	1.0	200		
	2.0	400		
0.025	0.5	20	0.148	8.85
	1.0	40		
	2.0	80		
0.050	0.5	10	0.300	17.7
	1.0	20		
	2.0	40		

foaming behavior can be related. This will affect the effectiveness of the reactor. Usually oxygen mass transfer is the limiting variable in fermentation. Increasing the broth liquid volume, V_{eff} , in a given fermenter will increase the total oxygen transfer rate, $OUR \times V_{eff}$ (mol s⁻¹), and also the productivity, linearly, in case of constant $k_{ol} A$. However, the foam suppression has to be increased if the liquid level is increased. This can cause a decrease in $k_{ol} A$ and also a decrease in the total oxygen transfer rate. This example shows this effect.

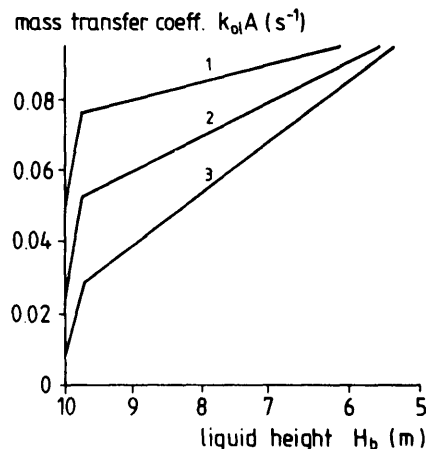
The total oxygen transfer rate is given by (see also Chapter 11)

$$r_o = OUR \times V_{eff} = k_{ol} A (C_{ol}^* - C_{ol}) V_{eff} \quad (\text{mol s}^{-1}) \quad 12.6$$

Let us use $(C_{ol}^* - C_{ol}) = 0.51 \text{ mol m}^{-3}$ and let the reactor be the same as in Example 12.1. Then this equation can be written, introducing the height of the broth in the reactor as H_b (m) and neglecting hold-up effects, as

$$r_o = k_{ol} A \times 0.51 \times \frac{1}{4} \pi T_v^2 H_b = 10.0 k_{ol} A H_b \quad (\text{mol s}^{-1}) \quad 12.7$$

Fig. 12.5 shows three assumed $k_{ol} A$ profiles. These profiles change from a slight to a moderate dependence of $k_{ol} A$ with broth height and therefore antifoam addition. For a broth height below 9.7 m a less drastic decrease is assumed. This decrease is caused by two factors. First, the $k_{ol} A$ value decreases because at constant P_s and increasing V_t , the P_s/V_t value decreases and therewith $k_{ol} A$. Curve 1 is near this situation. Second, with increasing H_b more antifoam is needed to keep the foam level below overflow condition. Curves 2 and 3 show this effect. For extremely high broth heights ($H_b > 9.7 \text{ m}$ in Fig. 12.5) a strong decrease is indicated, because in these cases foam has to be prevented completely, resulting in abundant antifoam addition. These profiles are assumed. No data, let alone formula, can be found about these type of relations. They should be determined for each fermentation separately under the production circumstances. The results for r_o calculated from Eq. (12.7) with the $k_{ol} A$ profiles given in Fig. 12.5 are given in Fig. 12.6. They show that the optimum total oxygen transfer, and therewith the optimal productivity of the fermenter, is strongly dependent on the $k_{ol} A$ characteristics. Only in case of a very limited dependence of $k_{ol} A$ with liquid height should the fermenter be filled up to the top. In other cases the optimum is at lower broth heights. Even more complicated optimizations can be made, like the introduction of a variable power consumption to improve $k_{ol} A$. Besides, in this example the possible effect of coalescence conditions on hold-up is neglected. The conclusion from this example is, however, clear: Foam

Fig. 12.5 Assumed $k_{o1}A$ values.

control is not simply a matter of preventing foam formation, but has far-reaching effects, up to the productivity of a fermenter.

Example 12.3 The concentration of protein that influences foaming

From measurements and calculations reported in the literature, it can be concluded that a monolayer of protein contains $1\text{--}10 \text{ mg (protein) } \text{m}^{-2}$. In a fermenter $k_{o1}A$ can be $10^{-2}\text{--}10^{-1} \text{ s}^{-1}$. With a k_{o1} value of $4 \times 10^{-4} \text{ m s}^{-1}$ this results in an A value of 25 up to $250 \text{ m}^2 \text{ m}^{-3}$. With the reported protein density this results in 25 up to $2500 \text{ mg (protein) } \text{m}^{-3}$ as sufficing for a monolayer around the gas bubbles. Narrowing the outer limits to some extent, this is of the order of 0.1–1 ppm.

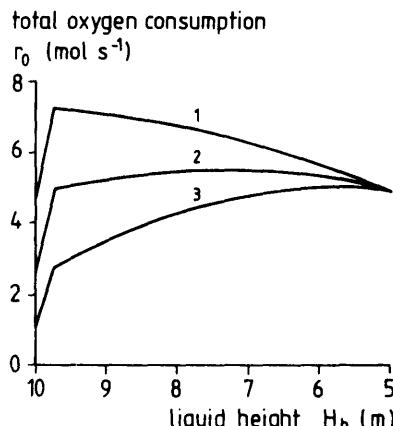
Fig. 12.6 Calculated r_o values.

Table 12.2 The theoretical power consumption P_{th} of a centrifugal foam destroyer

m (kg s ⁻¹)	v_{tip} (m s ⁻¹)				kW
	10	20	40	80	
6	0.3	1.2	4.8	19.2	kW
30	1.5	6	24	96	kW
148	7	30	118	474	kW
300	15	60	236	948	kW

Example 12.4 Power consumption for centrifugal foam destroyers

Centrifugal foam destroyers are based on the principle that the foam is broken up by the high speed and corresponding impact on the vessel wall, liquid surface or other foam bubbles. In case of a fully stable foam the theoretical energy consumption, P_{th} (W), needed to accelerate the liquid in the foam can be calculated from the kinetic energy equation as

$$P_{th} = \frac{1}{2} m v_{tip}^2$$

With the values for the entrained liquid from Example 12.1, Table 12.1 ($m = \rho_s V' = 1000 V' (\text{kg s}^{-1})$) we can calculate the values given in Table 12.2.

The data in this table show that, depending on gas superficial velocity (corrected for the pressure in the top of the vessel) and tip speed of the foam destroyer, a centrifugal separator can be acceptable or totally unacceptable. The last statement is usually true for highly loaded commercial fermenters.

References

Adler I., Buchholz H., Voigt J., Wittler R. and Schügerl K. "Bubble coalescence behavior in biological media. I. Hansenula polymorpha cultivation broths." Eur. J. Appl. Microb. Biotechn. 9, 249 (1980a).

Adler I., Diekmann J., Hartke W., Hecht V., Rohn F. and Schügerl K. "Bubble coalescence behavior in biological media. II. Effect of antifoam additives." Eur. J. Appl. Microb. Biotechn. 10, 171 (1980b).

Adler I., Eberhard U., Habermann W.D. and Schügerl K. "Bubble coalescence behavior in biological media. III. Effect of antifoam concentration." *Eur. J. Appl. Microb. Biotechn.* 12, 212 (1981).

Bikerman J.J. "Foams: theory and industrial applications." Reinhold, New York, 1953.

Buchholz H., Kalischewski K. and Schügerl K. "IV. Hansenula polymorpha cultivation foams." *Eur. J. Appl. Microb.* 7, 21 (1979).

Bumbullis W. and Schügerl K. "V. Alcohol effects." *Eur. J. Appl. Microb.* 8, 17 (1979).

Bumbullis W. and Schügerl K. "VI. Foam stability. Salts effects." *Eur. J. Appl. Microb.* 11, 106 (1981).

Bumbullis W., Kalischewski K. and Schügerl K. "II. Salt effects." *Eur. J. Appl. Microb.* 7, 147 (1979).

Bumbullis W., Kalischewski K. and Schügerl K. "VII. Surface viscosity and viscoelasticity." *Eur. J. Appl. Microb.* 11, 110 (1981).

Colbert J.C. "Foam and emulsion control agents and processes." Noyes Data Corporation, Park Ridge, NJ (1981).

Furchner B. and Mersmann A. "Mechanische schaumzerstörung." *Chem. Ing. Techn.* 58, 332 (1986).

Gaden E.L. and Kevorkian V. "Foams in chemical technology." *Chem. Engng.* 63, 173 (1956).

Hall M.J., Dickinson S.D., Pritchard R. and Evans J.I. "Foams and foam control in fermentation processes." *Progr. Ind. Microb.* 12, 169 (1973).

Kalischewski K., Bumbullis W. and Schügerl K. "I. Protein foams." *Eur. J. Appl. Microb.* 7, 21 (1979).

Kann K.B. "Determination of the flow rate of a liquid through a foam." *Coll. J.* 46, 508 (1984).

Kann K.B. and Feklistov V.N. "Calculation of the flow of liquids in foam channels." *Coll. J.* 46, 1052 (1985).

König B., Kalischewski K. and Schügerl K. "III. Penicillium chrysogenum cultivation foam." *Eur. J. Appl. Microb.* 7, 251 (1979).

Prins A. and Van 't Riet K. "Proteins and surface effects in fermentation: foam, antifoam and mass transfer." *Trends Biotechn.* **5**, 296 (1987).

Viesturs U.E., Kristapsons M.Z. and Levitans E.S. "Foam in microbiological processes." *Adv. Biochem. Engng.* **21**, 169 (1982).

Walker H.W. and Morrow R.W. "Antifoaming agent for elastomeric latexes." DuPont de Nemours E.I., U.S. Patent 2,482,307 (Sept 20, 1949).

13

Heat Transfer

13.1 Heat sources

Before starting the discussion on heat transfer relations, it is useful to summarize the different heat sources and sinks. The general equation is

$$r_{HT} = r_{HS} + r_{HG} + r_{HM} + r_{HV} + r_{HW} + r_{HH} \quad (W) \quad 13.1$$

in which

r_{HT}	= total heat generated (lost)	(W)
r_{HS}	= heat dissipated by the stirrer or mechanical antifoam device	(W)
r_{HG}	= heat generated by the throughflowing gas	(W)
r_{HM}	= heat generated by the metabolic activity of the microorganisms	(W)
r_{HV}	= heat loss resulting from vaporisation	(W)
r_{HW}	= heat loss through the fermenter walls	(W)
r_{HH}	= all other sources	(W)

In the equation all losses are regarded as negative production terms. The different contributions will now be discussed shortly.

r_{HS}

A number of bioreactors, especially those for filamentous fungi are of the stirred fermentor type. Fast rotating mechanical foam destroyers are sometimes used. The resulting r_{HS} value is the dissipated heat due to the mechanical energy exerted by these devices. The calculation for a stirrer is given in Chapter 14 on power consumption. The value in commercial fermentations will generally be 0.5 up to 5 kW m⁻³.

Γ_{HC}

Heat generation can occur due to the expanding rising bubbles. Roels and Heynen (1980) show that this dissipation energy is equal to the heat absorbed by the gas isothermal decompression. Thus the net heat effect is zero. Generally the air is compressed adiabatically, resulting in a temperature that is significantly higher than the broth temperature. This results in a heat production rate given by

$$\Gamma_{HC} = c_{pg} (T_{gi} - T_b) F_g \rho_g \quad (\text{W}) \quad 13.2$$

in which

c_{pg}	= thermal coefficient of the gas	(J kg ⁻¹ °C ⁻¹)
T_{gi}	= temperature inflowing air	(°C)
T_b	= broth temperature	(°C)
F_g	= volumetric gas flow rate	(m ³ s ⁻¹)
ρ_g	= gas density	(kg m ⁻³)

 Γ_{HM}

The organism metabolic activity results in a heat generation for both aerobic and anaerobic fermentations. In Chapter 2 it was shown that for aerobic growth the heat production is a function of oxygen consumption only:

$$\Gamma_{HM} = 460 \times 10^3 OUR \times V_t \quad (\text{W}) \quad 13.3$$

V_t	= broth liquid volume	(m ³)
OUR	= oxygen uptake rate	(mol m ⁻³ s ⁻¹)

For anaerobic systems the heat balance for all production rates has to be set up as shown in Chapter 2.

 Γ_{HV}

Generally the compressed air will be dried for sterilization purposes. On the other hand, the outflowing air will be fully saturated. This results in heat loss due to vaporization.

$$\Gamma_{HV} = -c_v F_g \left(\frac{P_n}{P_t} \rho_{vo} - \rho_{vi} \right) \quad (\text{W}) \quad 13.4$$

c_v	= heat of vaporization	(J kg ⁻¹ °C ⁻¹)
-------	------------------------	--

P_n	= normalized pressure (at which F_g is defined)	(N m ⁻²)
P_t	= fermenter top pressure	(N m ⁻²)
ρ_{vo}	= equilibrium water vapor concentration at broth temperature and top pressure	(kg m ⁻³)
ρ_{vi}	= water vapor concentration of the inflowing air for the conditions at which F_g is defined	(kg m ⁻³)

 r_{HW}

Heat losses also occur through the fermenter wall to the surroundings:

$$r_{HW} = -h_w a_f (T_b - T_s) \quad (\text{W}) \quad 13.5$$

h_w	= total (mainly air side) heat transfer coefficient	(W m ⁻² °C ⁻¹)
a_f	= fermenter surface area	(m ²)
T_s	= temperature of the surrounding air	(°C)

 r_{HH}

Other constituents to the total heat balance are all feed flows (substrate, pH control, antifoam) and specific constituents for each fermentation. The effect is generally small. It can be calculated if necessary.

The effect of all of the processes given above differs widely. Characteristic values are calculated in Example 13.1

13.2 Cooling

13.2.1 General equations

Heat transfer to cooling devices such as coiled tubes is described by

$$H_c = h_t \frac{T_{co} - T_{cl}}{\ln\left(\frac{T_b - T_{cl}}{T_b - T_{co}}\right)} a_c \quad (\text{W}) \quad 13.6$$

and

$$\frac{1}{h_t} = \frac{1}{h_1} + \frac{d_t}{\lambda_t} + \frac{d_w}{\lambda_w} + \frac{1}{h_2} \quad (\text{W}^{-1} \text{ m}^2 \text{ °C}) \quad 13.7$$

in which

H_c	= total heat transfer to the cooling device	(W)
h_t	= total heat transfer coefficient	(W m ⁻² °C ⁻¹)
h_1	= heat transfer coefficient medium 1 (fermentation liquid)	(W m ⁻² °C ⁻¹)
h_2	= heat transfer coefficient cooling medium	(W m ⁻² °C ⁻¹)
d_w	= wall thickness cooling coil	(m ¹)
d_f	= thickness fouling layer	(m ¹)
λ_f	= heat conductivity fouling layer	(W m ⁻¹ °C ⁻¹)
λ_w	= heat conductivity of the wall	(W m ⁻¹ °C ⁻¹)
T_{ci}	= temperature inflow of cooling water	(°C)
T_{co}	= temperature outflow of cooling water	(°C)
a_c	= surface area cooling coils	(m ²)

Usually the wall resistance can be neglected. An exception is stainless steel. The low heat conductivity values of this material makes the wall resistance relevant above a wall thickness of about 5 mm. Sometimes, particularly in the case of wall growth, a fouling layer can become important. In the design of cooling spirals or heat exchangers velocities in the cooling medium are made higher than in the fermentation medium, the last one being 0.1–1 m s⁻¹. Thus heat transfer resistance is mainly located in the fermentation medium. The exception is "riesel cooling," where water flows down the outer wall of the vessel. Here flow can be laminar and the flow velocities can be low. In this case determination of h_1 tends to be more complicated.

In newly designed fermenters cooling is provided in many cases by an external heat exchanger. This prevents the introduction of expensive cooling coils and an optimized unit can be chosen. Conditions of sterility have to be met, the microorganism must be able to withstand the shear in the pump and residence times in the heat exchanger have to be small to prevent deaeration by oxygen consumption of the microorganisms during the unaerated period in the heat exchanger.

13.2.2 Heat transfer coefficients for the fermentation medium

13.2.2.1 The stirred vessel

Heat transfer data are known mainly for unaerated systems. The question is to what extent aeration influences the heat transfer. Kipke (1980) and Steiff et al., (1980) show that aeration can improve as well as deteriorate h_1 . This depends on the stirrer speed and might be related to flooding phenomena. Generally the influence of gassing rate is only minor in relation to the other variables. Thus the data for nonaerated systems can be used as a guideline.

Henzler (1982) has reviewed a number of data. From the figure given in his review it can be derived that

$$\frac{h_1 T_v}{\lambda_b} = 0.6 \left(\frac{N D^2}{v_b} \right)^{0.67} \left(\frac{c_{pb} \eta_b}{\lambda_b} \right)^{0.33} \quad (-) \quad 13.8$$

in which

λ_b	= heat conductivity of the broth	(W m ⁻¹ °C ⁻¹)
v_b	= kinematic viscosity of the broth	(m ² s ⁻¹)
η_b	= dynamic viscosity of the broth	(N s m ⁻²)
c_{pb}	= thermal coefficient of the broth	(J kg ⁻¹ °C ⁻¹)

All types of stirrers are included in this equation. If worked out to a P_s/V , relationship Eq. (13.8) shows a slightly better h_1 value for larger stirrer diameters under otherwise identical conditions. Kipke (1980) reports experiments in which the large-diameter MIG stirrer had about a 45% better h_1 value than a small-diameter turbine stirrer at the same P_s/V , value.

The influence of liquid viscosity is included in Eq. (13.8). For non-Newtonian liquids the apparent viscosity value should be used. However, this value can vary considerably through the vessel. Near the wall the viscosity will be higher than near the stirrer. Sometimes a factor is included to correct for this phenomenon. However, the air bubbles that will interfere with the wall layer make these attempts rather delicate.

13.2.2.2 The bubble column

In a bubble column liquid circulation is determined by the superficial gas velocity. Heat transfer will therefore be related to superficial velocity and liquid properties only. The review of Heijnen and Van 't Riet (1984) delivers

$$h_1 = 9391 (v_{gs}^c)^{0.25} \left(\frac{\eta_w}{\eta_b} \right)^{0.35} \quad (\text{W m}^{-2} \text{ °C}^{-1}) \quad 13.9$$

in which

v_{gs}^c	= pressure corrected gas superficial velocity	(m s ⁻¹)
η_w	= dynamic viscosity of water	(N s m ⁻²)
η_b	= dynamic viscosity of the broth	(N s m ⁻²)

This correlation has proved applicable to $0.1 \text{ m} < T_v < 1 \text{ m}$ and $10^{-3} (\text{N s m}^{-2}) < \eta_b < 5 \times 10^{-2} (\text{N s m}^{-2})$.

Heijnen and Van 't Riet (1984) show that at certain conditions the heat transfer for the stirred vessel given by Eq. (13.8) and the heat transfer coefficient for the bubble column given by Eq. (13.9) are the same when based on the same P_t/V_t value, in which P_t is the total energy introduced in the broth by stirrer and air.

13.2.2.3 The air lift

Heat transfer calculations in the air lift are complicated because the liquid velocity has to be known, and the liquid velocity can be calculated only with a numerical procedure based on a model as given in Chapter 9. Above that the character of the flow field in the riser has to be determined, as it can be from the "real" air lift type of flow, a transitional type of flow or bubble column type of flow (see also Section 9.4.3.1). The flow regime depends on the geometry of the air lift, in particular the total hydrodynamic resistance of the reactor. This means that no single heat transfer value can be given. The following can be done for downcomer and riser, respectively.

a. Downcomer

When the average liquid velocity in the downcomer \bar{v}_d is known from the calculations, the heat transfer coefficient can be calculated from the well-known formula of heat transfer in single-phase turbulent pipe flow, because the bubbles were removed in the upper horizontal section.

$$\frac{h_1 T_d}{\lambda_l} = 0.027 \left(\frac{\rho_l \bar{v}_d T_d}{\eta_l} \right)^{0.8} \left(\frac{\eta_l C_p}{\lambda_l} \right)^{0.33} \quad (-) \quad 13.10$$

in which

T_d = diameter downcomer (m)

b. Riser

In high hydrodynamic resistance the riser acts as a bubble column. In that case Eq. (13.9) can be applied. For the fully air lift type the (average) liquid velocity has to be calculated. For stirred vessels it was found that the bubbles do not contribute to or hinder the heat transfer very much. This might very well be the case for the air lift also. Therefore, when the average velocity is known Eq. (13.10) predicts the heat transfer when the riser diameter is introduced. For transition flow the heat transfer will be between the two values.

13.2.2.4 The packed bed

For a packed bed heat transfer for values cannot be given as it depends on the liquid velocity and the properties of the packing in relation to the contact area between packing and wall. Usually packed beds are used only for enzymatic conversion and no cooling is required.

13.3 Measurement methods

The method to be used is straightforward application of the heat transfer and conservation equations:

$$H_c = \rho_c F_c c_{pc} (T_{co} - T_{ci}) \quad (W) \quad 13.11$$

ρ_c	= density cooling medium	(kg m ⁻³)
F_c	= flow rate cooling medium	(m ³ s ⁻¹)
c_{pc}	= thermal coefficient cooling medium	(J kg ⁻¹ °C ⁻¹)

With Eq. (13.6) this leads to

$$h_t = \frac{\rho_c F_c c_{pc}}{a_c} \ln \left(\frac{T_b - T_{ci}}{T_b - T_{co}} \right) \quad (W m^{-2} °C^{-1}) \quad 13.12$$

Occasionally for more detailed measurements of local heat transfer properties, complicated heat transfer devices have been built, providing the measurement of local heat transfer parameters. These are not discussed here. Examples can be found in Cukierman and Lemcoff (1980).

13.4 Conclusions

Heat transfer in fermenters is determined largely by the resistance in the fermentation medium. Correlations that predict the transfer coefficient are available from the literature. These predictions are not exact because, particularly in non-Newtonian liquids, the flow phenomena are not exactly known.

13.5 Examples

Example 13.1 Heat production and losses: Scale influence

Fermentation conditions		Parameter values	
H_v	$= 2 T_v$	c_{pg}	$= 1300 \text{ J kg}^{-1} \text{ }^{\circ}\text{C}^{-1}$
T_b	$= 40 \text{ }^{\circ}\text{C}$	ρ_g	$= 1.3 \text{ kg m}^{-3}$
T_s	$= 20 \text{ }^{\circ}\text{C}$	c_v	$= 2350 \text{ kJ kg}^{-1}$
T_{oi}	$= 60 \text{ }^{\circ}\text{C}$	ρ_{vo}	$= 0.05 \text{ kg m}^{-3}$
P_t	$= 2 \times 10^6 \text{ N m}^{-2}$	ρ_{vi}	$= 0.004 \text{ kg m}^{-3}$
OUR	$= 10 \text{ mol m}^{-3} \text{ h}^{-1}$	h_w	$= 10 \text{ W m}^{-2} \text{ }^{\circ}\text{C}^{-1}$
Stirrer	$= 1 \text{ kW m}^{-3}$	F_g	$= 0.5 \text{ vvm}$
Dew point air	$= 0 \text{ }^{\circ}\text{C}$	(F_a)	$= \frac{v}{120} \text{ m}^3 \text{ s}^{-1}$

From these values it can be calculated for the following three different volumes

	$V = 100 \text{ m}^3$	$V = 0.1 \text{ m}^3$	$V = 0.001 \text{ m}^3$
r_{HS}	100 kW	100 W	1 W
r_{HC}	28 kW	28 W	0.3 W
r_{HM}	128 kW	128 W	1 W
r_{HV}	-41 kW	-41 W	-0.4 W
r_{HW}	-20 kW	-200 W	-9 W
Total	207 kW	+ 27 W	+ -7 W +

This example clearly shows that heat is mainly produced by the stirrer and by metabolic activity. Heat losses through the wall are relevant in small-scale systems. Dependent on process conditions, metabolic activity and outside temperature, either cooling (large scale) or additional heating (small scale) of the fermenter is required. For large-scale systems cooling will always be required. The change takes place around 100 dm^3 .

Example 13.2 Calculation of the heat transfer area

Let us assume that the 100 m^3 fermenter in Example 13.1 is stirred and that the data are:

$$\begin{aligned} T_v &= 4.24 \text{ m} \\ D &= 1.41 \text{ m} \\ N &= 1.93 \text{ s}^{-1} \end{aligned}$$

The broth has the characteristics of water:

$$\lambda_b = 0.607 \text{ W m}^{-1} \text{ }^{\circ}\text{C}^{-1}$$

$$\nu_b = 10^{-6} \text{ m}^2 \text{ s}^{-1}$$

$$\eta_b = 10^{-3} \text{ N s m}^{-2}$$

$$\rho_b = 10^3 \text{ kg m}^{-3}$$

$$c_{pb} = 4200 \text{ J kg}^{-1} \text{ }^{\circ}\text{C}^{-1}$$

Cooling occurs by steel cooling spirals:

$$d_w = 5 \times 10^{-3} \text{ m}$$

$$\lambda_w = 80 \text{ W m}^{-1} \text{ }^{\circ}\text{C}^{-1}$$

No fouling layer is present and the heat transfer coefficient of the cooling medium can be neglected.

First h_t can be calculated with Eq. (13.8):

$$\frac{h_t \times 4.24}{0.607} = 0.6 \left(\frac{1.93 \times 1.41^2}{10^{-6}} \right)^{0.67} \left(\frac{4200 \times 10^{-3}}{0.607} \right)^{0.33}$$

$$\text{or } h_t = 4192 \text{ W m}^{-2} \text{ }^{\circ}\text{C}^{-1}$$

h_t can be calculated with Eq. (13.7):

$$\frac{1}{h_t} = \frac{1}{2714} + \frac{5 \times 10^{-3}}{80}$$

$$\text{or } h_t = 2320 \text{ W m}^{-2} \text{ }^{\circ}\text{C}^{-1}$$

Note that the steel of the cooling coils makes only a minor contribution to the heat transfer resistance.

Now the surface area can be calculated with Eq. (13.6). Let us assume $T_b = 30^\circ\text{C}$ and $T_{ci} = 10^\circ\text{C}$. The results, dependent on T_{co} , are given in Fig. 13.1. They show that a large surface area fulfills the conditions.

In this example OUR is rather low. It can easily become five times larger. Cooling coils of stainless steel or fouling layers can contribute to the heat transfer resistance. Therefore, the surface area needed for commercial fermenters can be much larger than the area calculated in this example.

To obtain an area of, say, 100 m^2 , a cylindrical cooling coil with an outer diameter of 0.1 m needs a length of 318 m . This is rather a lot. Spiralized

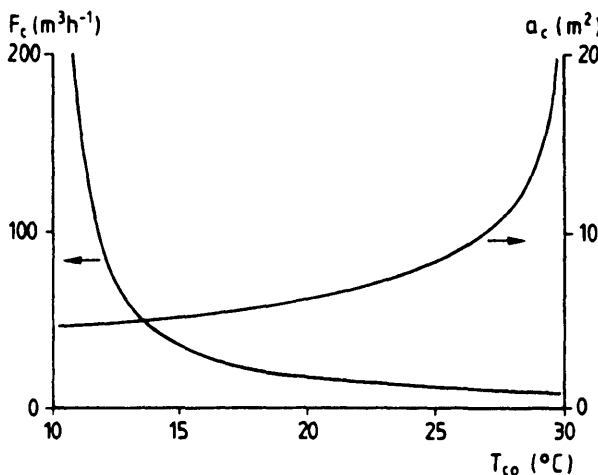


Fig. 13.1 Calculated F_c and a_c as a function of T_{co} .

coils are mainly used. With a spiralized coil and a coil diameter of 4 m, one turn of the spiral has a length of 12.6 m, so 25 spirals are needed. It certainly is a costly part of the fermenter hardware.

References

- Cukierman A.L. and Lemcoff N.O. "Heat and mass transfer in a tank reactor stirred by gaseous jets." *Chem. Eng. J.* **19**, 125 (1980).
- Heijnen J.J. and Van 't Riet K. "Mass transfer, mixing and heat transfer phenomena in low viscosity bubble column reactors." *Chem. Eng. J.* **28**, B21 (1984).
- Henzler H.J. "Verfahrenstechnische Auslegungsunterlagen für Rührbehalter." *Chem. Ing. Techn.* **54**, 461 (1982).
- Kipke K.O. "Wärmeübergang in begasten 'nicht-Newtonischen Flüssigkeiten." *Chem. Ing. Techn.* **52**, 975 (1980).
- Roels J.A. and Heijnen J.J. "Power dissipation and heat production in bubble columns: approach based on nonequilibrium thermodynamics." *Biotechnol. Bioeng.* **22**, 2399 (1980).
- Steiff A., Poggemann R. and Weinsbach P.M. "Wärmeübergang in Rührkesseln mit mehrphasigen Systemen." *Chem. Ing. Techn.* **52**, 492 (1980).

14

Power Consumption

14.1 Introduction

Power is required for mixing and mass transfer. The intensified circulation improves macroscale mixing. The turbulent dynamic forces cause bubble breakup and this improves mass transfer. The turbulent dissipation scale improves the microscale mixing. In contrast to the positive influence of increased power consumption, there are also a number of negative effects. Ultimately all energy introduced in the fermenter will be transformed into heat, thus leading to an increase of cooling requirements. Further, due to the high energy costs, it is rational to economize. Finally, the supply of energy to the system, e.g., by means of a stirrer, can lead to intense shear fields which can damage the microorganisms and other type of cells, in particular animal cells. The balancing of negative and positive effects is an important feature in fermentation operations.

14.2 Quantitative relationships for power consumption

14.2.1 The stirred vessel

14.2.1.1 The single-liquid-phase system

The most widely applied method to introduce power into the vessel is the application of a stirrer. The types range from standard propellers and turbines to exotic types like rods and sieves. General guidelines will be given here to calculate the power consumption. For a stirred tank this energy finally will be equal to the amount of heat due to the stirring action dissipated in the broth.

Let us assume a stirrer in a one-phase system, pumping radially or axially. In the turbulent regime the power is converted mainly into the kinetic energy of the outflowing liquid.

$$P_s = F_p \frac{1}{2} \rho_l \bar{v}^2 \quad (\text{W}) \quad 14.1$$

in which

P_s = stirrer power consumption (W)

F_p = pumping capacity of the stirrer (m³ s⁻¹)

\bar{v} = velocity of the outflowing liquid (m s⁻¹)

ρ_l = specific density of the liquid (kg m⁻³)

For an axially pumping stirrer the following is valid:

$$F_p = \frac{1}{4} \pi D^2 \bar{v} \quad (\text{m³ s⁻¹}) \quad 14.2$$

in which

D = stirrer diameter (m)

and for a radially pumping stirrer

$$F_p = \pi D H_s \bar{v} \quad (\text{m³ s⁻¹}) \quad 14.3$$

in which

H_s = height of the stirrer blade (m)

Eqs. (14.1-14.3) with $H_s = c D$, with c = constant lead to

$$P_s = N_p \rho_l N^3 D^5 \quad (\text{W}) \quad 14.4$$

in which N_p is a dimensionless constant, called the power number. When for a standard turbine we assume:

$$\bar{v} = \pi N D \quad \text{and} \quad \bar{v}^2 = \bar{v}^2 \quad \text{and} \quad H_s = 0.2 D$$

then Eqs. (14.1), (14.3) and (14.4) deliver $N_p \approx 9.7$. This value is very near the experimentally determined value for an 18-blade turbine stirrer. For an axially pumping stirrer like a propeller, the calculation for the average velocity is difficult because it will vary with distance from the axis. F_p for an axially pumping propeller stirrer has to be calculated by integration.

The model given above predicts the power to some extent. More interesting is that the ρ_l , N^3 and D^5 relation holds for all stirrer types and that Eq.

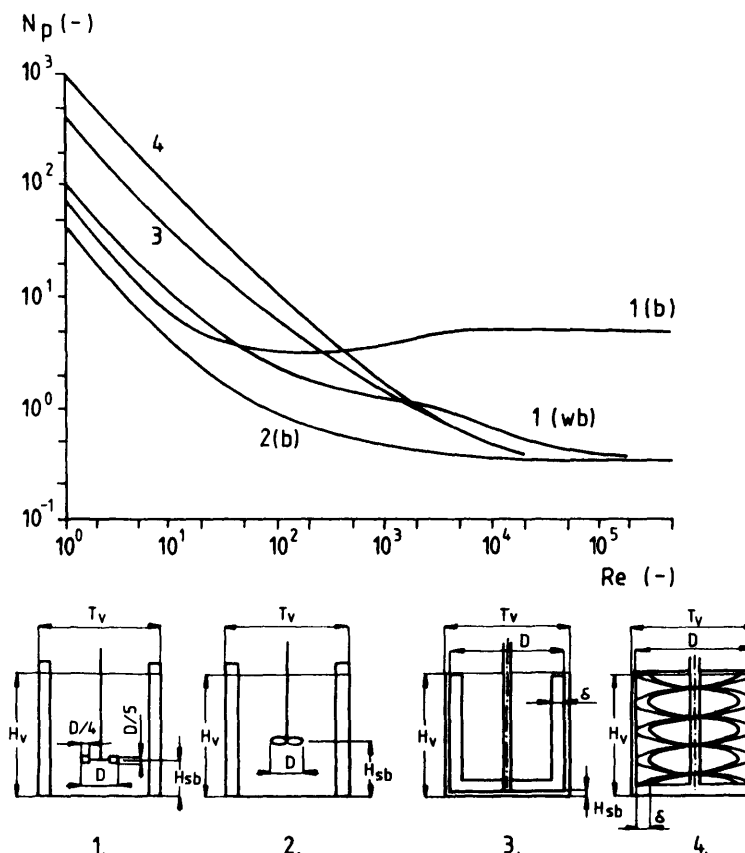


Fig. 14.1 N_p values as a function of the Re -number. b = with baffles; wb = without baffles.

- | | | | |
|----------------------|----------------|-------------------|---------------------|
| 1. Turbine stirrer | $T_v/D = 3.33$ | $H_{sb}/D = 1$ | |
| 2. Propeller stirrer | $T_v/D = 3.33$ | $H_{sb}/D = 1.5$ | $\alpha = 25^\circ$ |
| 3. Anchor stirrer | $T_v/D = 1.02$ | $H_{sb}/D = 0.01$ | $\delta/D = 0.1$ |
| 4. Helix stirrer | $T_v/D = 1.02$ | $H_{sb}/D = 0.01$ | $\delta/D = 0.1$ |

The linear relation at low Re -number also can be calculated from:

- | | | |
|----------------------|----------|--------------|
| 1. Turbine stirrer | $Re = 1$ | $N_p = 70$ |
| 2. Propeller stirrer | $Re = 1$ | $N_p = 40$ |
| 3. Anchor stirrer | $Re = 1$ | $N_p = 420$ |
| 4. Helix stirrer | $Re = 1$ | $N_p = 1000$ |

(Adapted from Zlokarnik, 1972).

(14.4) can be regarded as the general equation for the power consumption. For fully turbulent conditions the measured N_p value for any stirrer type in a baffled vessel is constant. For not fully turbulent conditions, i.e., for lower Re numbers, N_p is a function of Re only. Therefore the calculation of power consumption becomes a determination of the N_p values as a function of Re only. For one-phase systems N_p values are given in Fig. 14.1 and Table 14.1. Example 14.1 shows how to calculate power consumption values by means of Fig. 14.1.

Complications can occur when the vessel is equipped with two or more stirrers. The determination becomes difficult when interaction with other stirrers or the vessel bottom becomes relevant. As a rule of thumb, this interaction can be neglected as long as the distance between two stirrers or between the stirrer and the vessel bottom exceeds the stirrer diameter.

The N_p values in Fig. 14.1 show that the turbine stirrer has a higher N_p value than most of the other stirrer types. This means that it uses relatively more energy. The model showed that the consumed energy is proportional to the pumping capacity of the stirrer. This means that large-scale mixing in the turbine stirred vessel will be better than for the lower N_p stirrers at the same stirrer speed and diameter. In Chapter 11 it appeared that $k_{o,A}$ values were related to P_o/V_o . As the turbine stirrer has a larger power input than stirrers with a lower power number under otherwise identical conditions, it is logical that the turbine stirrer is the most widely used stirrer in fermenters. As long as the objective has to be to introduce power, because mixing and mass transfer are a function of power consumption, the stirrer with the highest power number should be used.

Table 14.1 Fully turbulent power numbers for different stirrer types
in baffled vessels. ($Re > 10,000$; $H_s = 0.2 D$)

Turbine stirrers Rushton	6 blades	5.5	-	6.5
	12 blades	8	-	9
	18 blades	9	-	10
Curved blade turbine		2	-	4
Paddle agitators		1	-	3
Paddle agitators	45° blades	0.5	-	2
Propeller stirrer		0.1	-	1
MIG stirrer		0.2	-	0.4
Ref.	Bates et al., 1963, 1966 Nienow and Miles, 1971 Rushton et al., 1950 Zlokarnik, 1972 Nagata, 1975			

14.2.1.2 Two-phase stirred vessels

For the prediction of the power consumption, the presence of air is a major complication. It has been found that the introduction of an average density of the two-phase system in Eq. (14.4) does not predict P_p in these systems at all. The reason is that the hydrodynamic phenomena around the stirrer blades change with the presence of air. Bruyn et al. (1974) show that large, gas-filled cavities originate behind the stirrer blades (see also Chapter 6). These decrease the hydrodynamic resistance of the blades and therewith the N_p value down to 0.3-0.5 times the ungassed value. An example for a turbine stirrer is shown in Fig. 14.2.

This process is not yet completely understood in its relation to fluid properties, presence of microorganisms, hold-up value, scale, etc. It even has a random character to some extent. Thus even although the ungassed N_p values are known, the calculation of gassed N_p values will be inaccurate. Experiments and experience with larger scales and with the fermentation broth itself are useful tools to improve the calculations.

The widely used relation of Michel and Miller (1962) is no solution to this problem. In this work the correlating variable for the gas flow rate, $F_g^{0.56}$, is varied over about half a decade only. The results scatter sufficiently to allow a slope on the double log plot of anywhere between 1 and 3. On the other hand, the N value is changed over a number of decades. This completely determines the graph, because in this way it is transformed into a N^3 vs. N^7 graph which inevitably gives the slope of 2.3 found from the

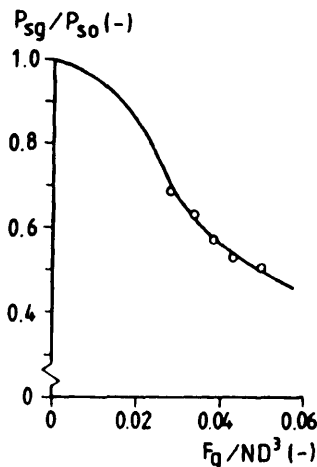


Fig 14.2 The change of the power consumption with gas flow rate for a turbine stirrer. — = measured power consumption; o = predicted power consumption from cavity formation. $T_v = H_v = 0.44$ m, $D = 0.18$ m, $N = 3.3 \text{ s}^{-1}$. (Adapted from Bruyn et al., 1974).

experiments. The scatter due to the gas flow rate variation "disappears" within this N^3 vs. N^7 relation. This method of presentation does not predict much more than that the gassed power consumption is between 0.4 and 1.0 the ungassed value.

Hughmark (1980) has correlated a large number of data for turbine stirrers including those of Michel and Miller. By correlating P_{sg}/P_{so} with the operating parameters, he did overcome the problem stated above. His correlation is

$$\frac{P_{sg}}{P_{so}} = 0.10 \left(\frac{F_g}{N V_t} \right)^{-0.25} \left(\frac{N^2 D^4}{g H_s V_t^{2/3}} \right)^{-0.20} \text{turbine stirrer water } (-) \quad 14.5$$

in which

P_{sg} = gassed power consumption (W)

P_{so} = ungassed power consumption (W)

The average deviation of calculated and experimental values is 11.7%, which, although considerable, is satisfying because of the inherently random character of cavity formation and related power consumption.

The influence of distance between the stirrers and distance from the bottom can be described by the same rule of thumb as for the one-phase systems. A difficult question is the amount of gas that flows to the stirrer(s) above the lower one in case of multiple stirrers. Usually it is assumed that the gas flow rate to these stirrers is the same as that for the lower one. More detailed information can be found in Nienow and Lilly (1979) and Kuboi and Nienow (1982).

The inaccuracy of the prediction does not give rise to serious problems in engineering applications. The N^3 and D^5 relation also holds for aerated systems. Therefore, final adjustment of stirrer power consumption to installed motor power can be done easily by small adjustments of the D value, i.e., by anticipated changes in blade position on the disc. Changes by low or zero aeration (compressor down or sterilization) can be corrected by N control or by a two-speed motor.

In conclusion, it appears that stirrer power consumption values can be predicted, although with limited accuracy.

14.2.2 The bubble column

An extensive evaluation of bubble column power dissipation and heat production, based on thermodynamics, is given by Roels and Heijnen

(1980). The power of the gasflow P_g can be derived from the change of entropy of the gas as

$$P_g = F'_g R T \ln \frac{P_s}{P_t} \quad (\text{W}) \quad 14.6$$

in which

F'_g = molar gas flow rate (mol s^{-1})

P_s = pressure at the sparger (N m^{-2})

P_t = pressure at the top of the fermenter (N m^{-2})

As a rule of thumb, it appears that each 0.01 m s^{-1} of gas superficial velocity corresponds to a dissipated power of 100 W m^{-3} up to $H_v = 1 \text{ m}$. The value gradually decreases for larger H_v values.

When heat production values are calculated, the heat uptake by expansion of the bubbles must be taken into account. It appears, as shown by Roels and Heijnen (1980), that the value of the heat uptake is exactly the value of the heat produced, P_g . Thus the net heat production of the air is zero, when the temperature of the gas flow into the fermenter is equal to the broth temperature. This result is striking but thermodynamically rational.

14.2.3 The air lift

For power consumption predictions the air lift does not differ from the bubble column. All calculations and remarks made for the bubble column are therefore relevant for the air lift also.

14.2.4 The packed bed

Power consumption of the flow through the packed bed can be calculated from the flow rate and the pressure difference along the column [as given by Eq. (6.6)].

14.3 Measuring methods

14.3.1 The torque meter

The torque meter, sometimes called dynamometer, is a compact device that can be placed outside the vessel as part of the stirrer axis. It contains an axis part, usually with a smaller diameter than the axis itself, or a spring. The principle is the measurement of the distortion of that axis part or spring. This can be done, e.g., by strain gauges or by optical or magnetic/electrical

shift measurements. The torque meters are commercially available, usually with the calibration curve included. They can be installed simply and deliver an easily processed signal. They are available for all scales, from pilot plant scale-up to commercial plant scales.

There are some disadvantages such as the high acquisition costs (\$1000 - >\$10000, device only) and the required assembly space. However, the principal drawback is that the torque exerted by the bearings and seals, M_b , is included in the measurements. The required correction can be done by measuring M_b at zero loading (stirrer in air). It appears that M_b is nearly independent of stirrer speed although it is recommended that this be checked for each vessel again. It is assumed that this M_b value is independent of loading conditions.

A second way to determine the M_b value is as follows. The power consumption of the stirrer is given by Eq. (14.4). The power consumption also can be written as

$$P_s = 2\pi N M_s \quad (\text{W}) \quad 14.7$$

in which

$$M_s = \text{torque (moment) on the axis due to the stirrer} \quad (\text{N m})$$

The torque M_t that is measured includes both the torque due to the stirrer and due to the bearings:

$$M_t = M_s + M_b \quad (\text{N m}) \quad 14.8$$

As for $Re > 10000$ the value of N_p is constant, Eq. (14.4) with Eqs. (14.7) and (14.8) delivers

$$M_t = c N^2 + M_b \quad (\text{N m}) \quad 14.9$$

in which

$$c = \text{constant} \quad (\text{N m s}^2)$$

By measuring M_t at different speeds, extrapolation to $N = 0$ of a plot of M_t as a function of N^2 delivers the M_b value. This method is inaccurate if the range of N values is limited and/or the extrapolation is extensive. The value found in this way can be compared with the value found at zero load conditions.

There always exists an uncertainty about the value of M_b . Therefore, the torque meter can be applied only when $M_s > M_b$ and preferably $M_s \gg M_b$.

14.3.2 The strain gauge method

Strain gauges are sometimes applied in the torque meter, but they can also be used as a measuring method as such. They can be adjusted to any given position for the measurement of distortion: for instance, on a number of shaft positions when multiple impellers are used or on each separate stirrer blade for intensive research about hydrodynamics.

For commercial applications, the strain gauge method is less attractive than the torque meter. They are inserted into the vessel and signal transfer from the rotating, and sterile, system to the outside can be problematic. Steam sterilization makes high demands on both the strain gauge and the sticking material. Besides, the calibration has to be done after installment in the vessel, which can be very difficult to do.

The general conclusion is that torque meters are preferably used in commercial plants and for research purposes when overall results are satisfying. The strain gauges are used when the objective is more detailed hydrodynamic research.

14.3.3 Electrical energy measurement

The electrical power, P_{el} , consumed by an AC current motor can be calculated from

$$P_{el} = \sqrt{3} V I \cos\phi \quad (\text{W}) \quad 14.10$$

in which

V = voltage (V)

I = current strength (A)

$\cos\phi$ = phase shift between V and I (-)

Complications lead to a limited applicability of this method. The main problem is the difference between P_{el} and the power delivered to the stirrer axis by the motor. This so-called efficiency factor is given in Fig. 14.3, together with $\cos\phi$. AC motors for small-scale apparatus often show a rather low efficiency and a related strong dependence between efficiency and loading. This is aggravated by the fact that motors for small-scale reactors are generally oversized, lab-scale reactors sometimes more than 10

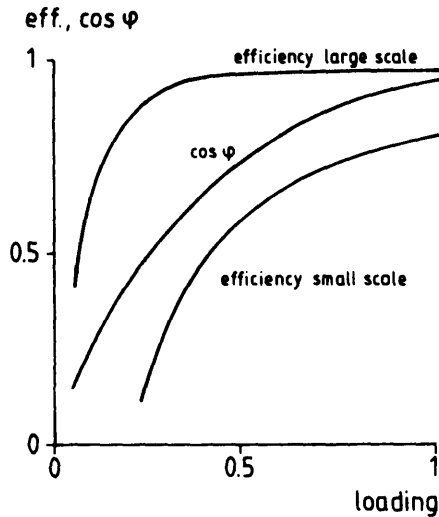


Fig. 14.3 The efficiency factor and $\cos \phi$ for AC motors.

times. Usually motors are equipped with a variable speed control. The losses in this device can be variable with speed and unknown. This leads to the conclusion that although the consumed electrical energy by the motor can be measured by means of Eq. (14.10) or with a so-called Watt meter, this does not necessarily give the stirrer power consumption. This method can be used rather safely on large scales (>10 kW) without speed control and between 0.5 and 1.0 times full load. Validity for other cases is questionable. Example 14.2 makes this very clear for laboratory-scale stirrers.

14.3.4 The heat production measurement

The power dissipated by the stirrer is finally dissipated into heat in the fermenter as

$$P_s = (V_l + V_e) \rho_b c_{pb} \frac{dT_b}{dt} + r_{HL} \quad (W) \quad 14.11$$

in which

- c_{pb} = specific heat of the broth $(J \ kg^{-1} \ ^\circ C^{-1})$
- dT_b = temperature increase of the broth $(^\circ C)$
- V_e = equivalent broth volume due to the heat capacity of the stirrer, shaft, cooling coils, wall, etc. (m^3)
- r_{HL} = other sources of heat losses or sources, e.g., evaporation and heat loss through the wall, see Chapter 13, "Heat Transfer" (W)

V_s can be determined by "calibration" experiments with the addition of a well-defined quantity of heat and with $P_s = 0$. The "long term" temperature change in time after the addition delivers the h_w value for the heat losses through the wall, as defined in Chapter 13. It can be shown that application of this method is reliable at scales > 1 m; at smaller scales the heat losses through the wall are relatively large and make the method inaccurate.

14.4 Conclusions

Power consumption values can be calculated for all fermenter types discussed in this book. For the bubble column and air lift the net heat effect appears to be zero; for the stirred vessel the power consumption of the stirrer will totally be converted into heat dissipated in the broth.

14.5 Examples

Example 14.1 Power consumption calculations

In this example the procedure for the calculation of power consumption and stirrer speed in single-phase systems is given. If N , D , ρ_i and η_i are given, the calculation is simple and as follows:

Step 1: Calculate $Re = \rho_i N D^2 / \eta_i$

Step 2: Determine N_p from Fig. 14.1

Step 3: Calculate P_s

More difficulties can be encountered if the power consumption is given and the stirrer speed has to be determined.

For example: $P_s / V_i = 1500 \text{ W m}^{-3}$,

$$T_v = H_v = 2 \text{ m},$$

$$D = 0.33 T_v,$$

$$\rho_i = 1000 \text{ kg m}^{-3}$$

Liquids: $\eta_i = 1, 10, 100, 1000$ and $10,000 \times 10^{-3} \text{ N s m}^{-2}$, respectively.

Turbine: standard six-blade turbine

The procedure is as follows:

Step 1: Assume a Re number

Step 2: Determine N_p from Fig. 14.1

Step 3: Calculate N

Step 4: Check Re assumption

Step 5: Re OK \rightarrow end calculation

$Re \neq \text{OK} \rightarrow$ Step 1

For our example: Assume $Re > 10\,000$

$$\text{Then: } N_p = 5.5$$

$$V_t = \frac{1}{4}\pi 2^3 = 6.3 \text{ m}^3 \longrightarrow P_t = 9425 \text{ W}$$

$$9425 = 5.5 \times 1000 \times N^3 \times (0.6)^5 \longrightarrow N = 2.8 \text{ s}^{-1}$$

Now Re has to be checked

$\eta_t (\times 10^{-3} \text{ N s m}^{-2})$	1	10	100	1000	10,000	100,000
$Re = \frac{\rho_t N D^2}{\eta_t}$	10^6	10^5	10^4	10^3	10^2	10^1

Concl.: For $\eta_t = 1, 10$ and $100 \times 10^{-3} \text{ N s m}^{-2}$ assumed Re value and check of Re agree and the calculation is finished, with $N = 2.8$. For the higher viscosity values the checked value is much lower than the assumed value of $Re = 10,000$ and a new and lower Re estimation is needed.

For $\eta_t = 1000 \times 10^{-3} \text{ N s m}^{-2}$ the checked Re value is around 10^3 . Fig. 14.1 shows that in this region the N_p value is lower than 5.5. This means that the N value has to increase, because P_t is a given value. The final Re value will therefore be $> 10^3$. Assume 2×10^3 .

$$\begin{aligned} \text{Assumption: } Re &= 2 \times 10^3 \longrightarrow N_p = 4.7 \text{ (Fig. 14.1)} \\ 9425 &= 4.7 \times 1000 \times N^3 \times 0.65 \longrightarrow N = 2.95 \text{ s}^{-1} \\ &\longrightarrow Re = 1062 \end{aligned}$$

The estimation of 2000 has been wrong. Now the procedure can be done again, until a definitive value has been reached. For $\eta_t = 10 \text{ N s m}^{-2}$ the same procedure can be followed.

For very low Re numbers the procedure is simpler:

Assume the N_p curve to be in the linear region.

$$\text{Then } N_p = c'/Re$$

Fig. 14.1 shows that for a turbine stirrer:

$$N_p = \frac{70}{Re} = \frac{70 \eta_t}{\rho_t N D^2}$$

Thus for our example with $\eta_t = 100 \text{ N s m}^{-2}$:

$$9425 = \frac{70 \times 100}{1000 N 0.6^2} 1000 N^3 0.6^5 \longrightarrow N = 2.5$$

Table 14.2 Examples of laboratory stirrer power consumption, water

<i>D</i> (m)	<i>N</i> (rpm)	Stirrer type	<i>N_p</i> (-)	<i>P_s</i> (W)
0.04	300	Turbine	5.5	0.07
0.04	1000	Turbine	5.5	2.6
0.04	300	Propeller	0.35	0.004
0.04	1000	Propeller	0.35	0.17
0.07	300	Turbine	5.5	1.2
0.07	1000	Turbine	5.5	43
0.07	300	Propeller	0.35	0.07
0.07	1000	Propeller	0.35	2.7

Check Re:

$$Re = \frac{1000 \times 2.5 \times 0.6^2}{100} = 9 \quad \longrightarrow \text{Assumption OK}$$

Example 14.2 Laboratory mixer power consumption

Small, laboratory-scale stirrer motors usually have power values of 100 up to 500 W. This power is disappearing mostly in the bearings and the motor and speed control unit itself as this example shows.

Table 14.2 shows calculated values for the stirrer power consumption of laboratory stirrers in water. Even the highest P_s value in this example is $\ll 100$ W. Most of the values are even $\ll 10$ W. This also shows that measurement of motor power consumption by electrical energy measurement on this scale is useless. (From practical experience we also know that most of the power is dissipated in the motor, because we simply can feel that the motor is heated much more than the stirred vessel!)

References

Bates R.L., Fondy P.L. and Corpstein R.R. "An examination of some geometric parameters of impeller power." Ind. Eng. Chem. Proc. Des. and Dev., 2, 311 (1963).

Bates R.L., Fondy P.L. and Fenic J.G. "Impeller characteristics and power."

"Mixing," Vol. 1, Ed. Uhl, V. and Gray, J.B., Academic Press, New York (1966), p. 112.

Bruyn W., Van 't Riet K. and Smith J.M. "Power consumption with aerated Rushton turbines." *Trans. Instn. Chem. Engrs.*, 52, 88 (1974).

Hughmark G.A. "Power requirements and interfacial area in gas-liquid turbine agitated systems." *Ind. Eng. Chem. Proc. Des. Dev.* 19, 638 (1980).

Kuboi R. and Nienow A.W. "The power drawn by dual impeller systems under gassed and ungassed conditions." *Proceedings 4th European BHRA Conference on Mixing*, Noordwijkerhout, Netherlands (April 1982).

Michel B.J. and Miller S.A. "Power requirements of gas liquid agitated systems." *A.I.Ch.E. J.* 8, 262 (1962).

Nagata S. "Mixing, principles and applications." *Kodansha Ltd.*, Tokyo (1975).

Nienow A.W. and Lilly M.D. "The power drawn by multiple impellers in sparged agitated vessels." *Biotechnol. Bioeng.* 21, 2341 (1979).

Nienow A.W. and Miles D. "Impeller power numbers in closed vessels." *Ind. Eng. Chem. Proc. Des. and Dev.* 10, 41 (1971).

Roels J.A. and Heijnen J.J. "Power dissipation and heat production in bubble columns: approach based on non-equilibrium thermodynamics." *Biotechnol. Bioeng.* 22, 2399 (1980).

Rushton J.H., Costich E.W. and Everett H.J. "Power characteristics of mixing impellers." *Chem. Eng. Progr.* 46, 395 Part I, *ibid.* 467 Part II (1950).

Zlokarnik M. "Rührtechnik." Band II *Verfahrenstechnik*, Ullman, *Encyclopedie der Technische Chemie*, Verlag Chemie, Weinheim (1972) p. 259.

PART IV

Reaction Engineering: Integration

15

Macrokinetics: Particle Level

15.1 Qualitative considerations

One of the most important reasons to consider the immobilization of a biocatalyst is the possibility of reuse or continuous utilization. To obtain an immobilized biocatalyst, it is attached to or immobilized in a support. As density, rigidity, size and uniformity of the support increase, the ease by which the heterogeneous biocatalyst can be kept in the bioreactor increases. In a packed-bed bioreactor, for instance, especially rigid, large and uniform biocatalyst beads are desired for the formation of a bed with good and stable flow properties. Small, deformable and irregular-shaped particles usually result in channeling, large pressure drops and quick clogging. Three desired properties for a good retention of the biocatalyst particles in the bioreactor, dense, large and spherical, are in direct conflict with optimal mass transfer. As the density, the size and the approximation of the sphere of the particle in which the biocatalyst is immobilized increase, the chance increases that the rate of biocatalysis is limited by diffusion of substrate.

This can be well explained by means of Fig. 15.1, which shows schematically a porous, spherical particle in which the biocatalyst is immobilized. In this particle mass transfer is, in general, only possible by diffusion. For mass transfer to occur, in other words for a net flow of substrate (or product), a concentration gradient of substrate should exist. When substrate is consumed by the biocatalyst, then the concentration of substrate decreases in the particle and concentration gradients develop, resulting in a net flow of substrate to the particle, and in the particle in the direction from the surface to the center. This molar flux F_s'' ($\text{mol m}^{-2} \text{s}^{-1}$) can be described by Fick's law:

$$F_s'' = - D_{sp} \frac{dC_s(r)}{dr} \quad (\text{mol m}^{-2} \text{s}^{-1}) \quad 15.1$$

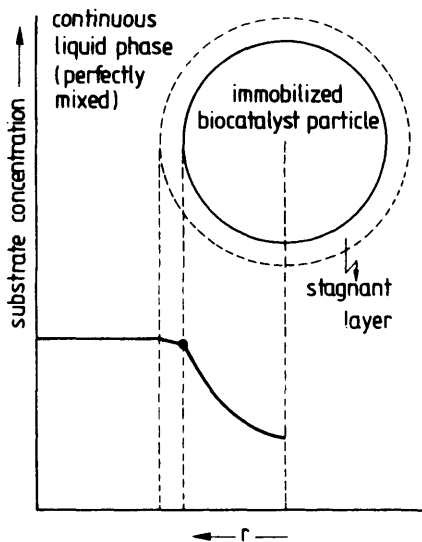


Fig. 15.1 Schematic representation of immobilized biocatalyst bead.

D_{sp} is the effective diffusion coefficient of substrate in the biocatalyst bead ($\text{m}^2 \text{s}^{-1}$), r the spherical coordinate (m) and C_s , the substrate concentration (mol m^{-3}). The net flow F'_s (mol s^{-1}) to one particle with a surface area a (m^2) and a particle radius R_p (m) is thus:

$$F'_s = -a |D_{sp}| \frac{dC_s(r)}{dr} \quad \text{at } r = R_p \quad (\text{mol s}^{-1}) \quad 15.2$$

or to the particles in one cubic meter of reactor volume:

$$F_s^u = -A' |D_{sp}| \frac{dC_s(r)}{dr} \quad \text{at } r = R_p \quad (\text{mol m}^{-3} \text{s}^{-1}) \quad 15.3$$

in which A' = the specific surface area ($\text{m}^2 \text{m}^{-3}$) of the biocatalyst beads per unit of reactor volume. As a result of the biocatalytic activity, accumulation of product occurs, especially in the center of the biocatalyst particle. Consequently a net flow of product will take place, directed from the center of the particle to the surface and from there to the surrounding medium. If the density of the biocatalyst particles increases, in other words if the porosity decreases, $|D_{sp}|$ generally becomes smaller and with that the net flow. The flow also becomes relatively smaller when the biocatalyst particle diameter increases. In case of a sphere it can be calculated (see also Chapter 11) that

$$A' = \frac{3\epsilon}{R_p} = \frac{6\epsilon}{d_p} \quad (\text{m}^2 \text{ m}^{-3}) \quad 15.4$$

with the particle hold-up ϵ defined as

$$\epsilon = \frac{V_p}{V_p + V_l} \quad (-) \quad 15.5$$

Mass transfer by diffusion occurs not only inside the biocatalyst particle, but also in the liquid film immediately surrounding the particle. (See also Section 11.1.) The thickness of the film, δ (m), depends on the turbulence (Reynolds number) of the surrounding liquid. For description of the mass transfer from and to the particle, the film theory (in which it is thus assumed that there is stagnant film through which mass transfer occurs by diffusion exclusively) suffices. The mathematical formulation of the mass transfer to one particle is according to the film theory, for $\delta \ll R_p$:

$$F'_s = k_{sl} A' (C_{sb} - C_{si}) \quad (\text{mol s}^{-1}) \quad 15.6$$

and

$$F_s^u = k_{sl} A' (C_{sb} - C_{si}) \quad (\text{mol m}^{-3} \text{s}^{-1}) \quad 15.7$$

with k_{sl} the mass transfer coefficient (m s^{-1}) and C_{sb} and C_{si} the concentrations of substrate in the ideal-mixed-assumed bulk of the liquid and the interface with the particle, respectively. The mass transfer coefficient is dependent on the turbulence of the liquid. The Reynolds number is the measure for this turbulence. The larger the Reynolds number, the larger the turbulence, the larger k_{sl} and thus the better the mass transfer. It can be seen from Eq. (15.6) that the mass flow is proportional to the concentration gradient over the stagnant liquid film. In addition to these factors which determine mass transfer, it will be obvious that the activity per unit volume of support and the radius of the particle, in other words the maximal length along which substrate has to diffuse to reach all biocatalyst, determines the concentration gradient and thus the net flow.

In Fig. 15.2 the concentration gradients for four situations are given. Case 1 concerns the situation in which the partition coefficient of substrate over bulk liquid and biocatalyst particle is 1, k_{sl} and $|D_{sp}|$ not too small and, further, the radius of the particle and the activity per unit volume not excessive large. All the biocatalyst entities experience a concentration of substrate not much lower than the concentration in the bulk liquid. The

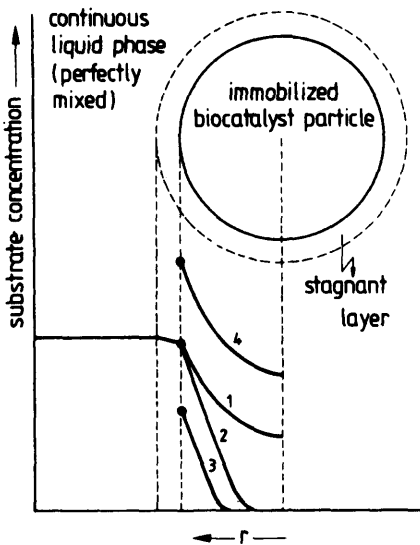


Fig. 15.2 Various substrate concentration profiles in an immobilized biocatalyst particle.

latter is not the case for situation 2. Here a small D_{sp} and/or large radius and/or high biocatalyst activity per unit volume of support is involved. In this case not all biocatalyst entities contribute significantly to the observed immobilized biocatalyst activity.

Cases 3 and 4 concern situations where the partition coefficient of substrate over the bulk liquid and the solid biocatalyst particle differs from 1, being smaller or larger, respectively, than 1. As a result the effect of diffusion limitation of substrate can be magnified or diminished. This kind of partition effects especially occur in cases of charged substrates and supports by which strong attraction or repulsion can occur. The concentration gradients in the biocatalyst particle and in the stagnant liquid layer surrounding it generally have as a result that the immobilized biocatalyst "sees" a lower substrate concentration than the bulk substrate concentration, the lower the more the biocatalyst is in the center of the particle. This means that if the biocatalyst obeys Michaelis-Menten kinetics, the observed rate of reaction will be lower than could be expected on the basis of the bulk concentration. By eye a Michaelis-Menten type of curve is obtained when measured reaction rates are plotted as a function of the concentration of substrate in the bulk liquid. Even a straight line may be seen in the linearized plots when only a limited range of substrate concentrations has been measured. However, description of coupled mass transfer and intrinsic Michaelis-Menten kinetics by means of a Michaelis-Menten type of equa-

tion is principally wrong. Nevertheless, in the literature immobilized biocatalysts are almost without exception described by means of apparent kinetic constants (see also Section 4.3) as follows:

$$-r_s^u = -\frac{dC_{sb}}{dt} = v'_{max} \frac{C_{sb}}{K'_m + C_{sb}} \quad (\text{mol m}^{-3} \text{s}^{-1}) \quad 15.8$$

in which $-r_s^u$ is the number of moles of substrate consumed per second per unit volume, K'_m is the apparent Michaelis-Menten constant (mol m^{-3}) and v'_{max} the apparent maximal rate of conversion ($\text{mol m}^{-3} \text{s}^{-1}$). These apparent constants are, however, dependent on K_m , v_{max} , R_p , D_{sp} , k_{si} , C_{sb} and the activity per unit volume of support. It is better to introduce, as in heterogeneous chemical catalysis, an overall effectiveness factor η_e^{ov} (-) given by:

$$-r_s^u = -\frac{dC_{sb}}{dt} = \eta_e^{ov} v_{max} \frac{C_{sb}}{K_m + C_{sb}} \quad (\text{mol m}^{-3} \text{s}^{-1}) \quad 15.9$$

Although in intrinsic Michaelis-Menten kinetics η_e^{ov} usually lies between 0 and 1, there are situations possible where η_e^{ov} can be greater than 1, for instance situation 4 in Fig. 15.2. Also, in other types of kinetic mechanisms, e.g., substrate inhibition or product activation, it is in principle possible that η_e^{ov} becomes larger than 1.

15.2 External diffusion limitation

In the preceding section we have seen that as a result of the stagnant layer immediately surrounding the biocatalyst particle, the concentration of substrate at the surface of the particle is lower than that in the bulk of the liquid, which is assumed to be ideally mixed. This is in connection with the concentration gradient that is needed for mass transfer to occur through the liquid film. In this section it is assumed that all the biocatalyst is immobilized at the surface of a spherical particle (Fig. 15.3). This surface-immobilized biocatalyst has to suffice with a surface concentration of substrate which is lower than the concentration in the bulk, a concentration we know or can measure. The biocatalyst thus will convert substrate less rapidly than on the basis of "free" Michaelis-Menten kinetics in solution could be expected. In order to correct for this an external effectiveness factor η_e (-) is introduced analogous as in the heterogeneous chemical catalysis. This external effectiveness factor is defined as the ratio of the reaction rate at $C_s = C_{si}$ and the rate at $C_s = C_{sb}$:

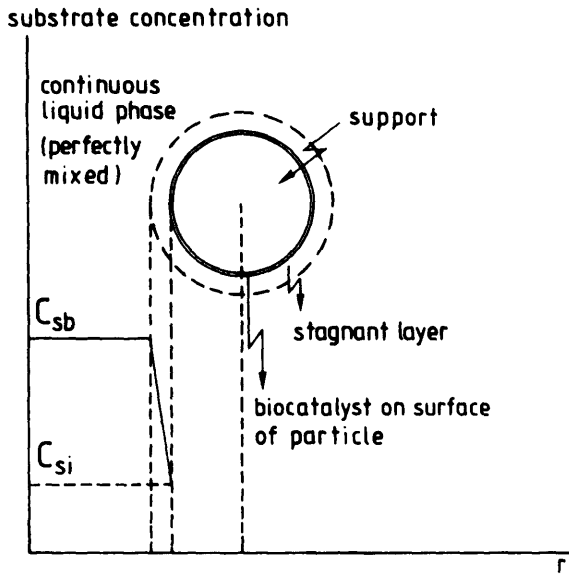


Fig. 15.3 Surface-immobilized biocatalyst.

$$\eta_{ee} = \frac{-r_s^u(C_{si})}{-r_s^u(C_{sb})} \quad (-) \quad 15.10$$

If the intrinsic kinetics of the immobilized biocatalyst are purely Michaelis-Menten, then $0 < \eta_{ee} < 1$, as partition effects are not involved. Substitution of the Michaelis-Menten equation in Eq. (15.10) gives:

$$\eta_{ee} = \frac{v_{max} C_{si} (K_m + C_{sb})}{v_{max} C_{sb} (K_m + C_{si})} \quad (-) \quad 15.11$$

From this it appears that η_{ee} is independent of v_{max} as it cancels in this equation:

$$\eta_{ee} = \frac{C_{si} (K_m + C_{sb})}{C_{sb} (K_m + C_{si})} \quad (-) \quad 15.12$$

For simplicity it is assumed for the present that C_{sb} and K_m are known (C_{sb} can be measured or fixed by a desired conversion in case of a CSTR). This means, in order to calculate η_{ee} , that we have to know C_{si} .

This can be done with Eq. (15.7):

$$F_s^u = -r_s^u = k_{sl} A' (C_{sb} - C_{si}) \quad (\text{mol m}^{-3} \text{s}^{-1}) \quad 15.13$$

The mass transfer coefficient k_{sl} can be estimated by the methods described in Chapter 11. After measurement of r_s^u all the parameters in Eq. (15.13) are known except for C_{si} , and the latter can thus be calculated.

15.3 Internal diffusion limitation

15.3.1 The general case

When the biocatalyst is merely immobilized inside the support, we have to take into account not only external diffusion limitation, but also limitation of the reaction by diffusion of substrate in the support. As a consequence of the consumption of substrate in the particle, there will be a net flow of substrate to and in the particle in the direction of the surface to the center. This means that a radial concentration gradient must exist in the particle in addition to the one in the stagnant liquid film surrounding the particle. The average substrate concentration in the microenvironment of the biocatalyst is thus smaller than the concentration in the ideally mixed bulk liquid, the lower the more the biocatalyst is immobilized in the center of the bead. This in turn results in a lower rate of biocatalysis than could be expected on the basis of the bulk substrate concentration, whereby again the annotation should be made that it is assumed that partition effects do not play a role and that the intrinsic kinetics do obey Michaelis-Menten kinetics. This phenomenon is defined by the internal effectiveness factor η_{ei} (-). In order to correct for both internal and external diffusion limitation of substrate an overall effectiveness factor η_e^{ov} is introduced, which is the product of the external effectiveness factor and the internal effectiveness factor:

$$\eta_e^{ov} = \eta_{ee} \eta_{el} \quad (-) \quad 15.14$$

Quantification of η_{ei} is still possible as described in the preceding section. In order to quantify η_{ei} external diffusion limitation is left without consideration for the present for simplicity. Fig. 15.4 shows some possible substrate concentration profiles inside an immobilized biocatalyst bead. The internal effectiveness factor can be defined as the observed reaction rate $-r_s^u$ divided by the rate which would be observed if all the biocatalyst would "feel" a concentration of substrate equal to that at the surface of the particle:

$$\eta_{ei} = \frac{-r_s^u}{-r_s^u(C_{si})} \quad (-) \quad 15.15$$

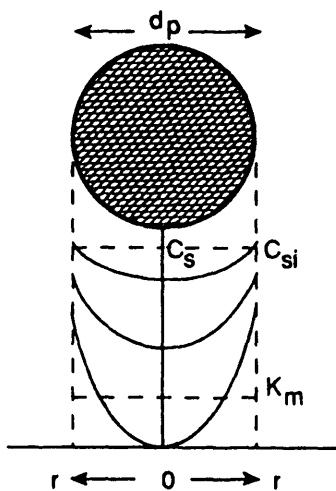


Fig. 15.4 Possible concentration profiles of substrate in an immobilized biocatalyst bead.

In order to be able to quantify η_a , the Thiele modulus Φ (-) is generally used. The Thiele modulus is the ratio of the "kinetic rate" and the "diffusion rate." A generalized Thiele modulus is presented by Aris (1965) and Bischoff (1965):

$$\Phi = \frac{V_{sp}}{\alpha} \frac{-r_s^{ug}(C_{si})}{\sqrt{2}} \left(\int_{C_s^*}^{C_{si}} -D_{sp} r_s^{ug} dC_s \right)^{-0.5} \quad (-) \quad 15.16$$

V_{sp} and α are the volume and the surface area of a single particle, respectively. $-r_s^{ug}$ is the consumption of substrate per unit volume of biocatalyst. C_s^* is the concentration of substrate when the thermodynamic equilibrium is reached. In Michaelis-Menten kinetics C_s^* is zero. When for simplicity it is assumed that the biocatalyst particle is spherical ($V_{sp}/\alpha = d_p/6$), Michaelis-Menten kinetics are obeyed ($C_s^* = 0$) and D_{sp} is independent of the concentration of substrate, Eq. (15.16) reduces to:

$$\Phi = \frac{d_p}{6} \frac{\sqrt{\frac{v_{max}^g C_{si}}{K_m + C_{si}}}}{\sqrt{2 D_{sp} (K_m + C_{si}) \left(1 - \frac{K_m}{C_{si}} \ln \left[1 + \frac{C_{si}}{K_m} \right] \right)}} \quad (-) \quad 15.17$$

with v_{max}^g the maximum rate per unit volume of biocatalyst.

The question now is to find the relation between the Thiele modulus and the internal effectiveness factor. For that a mass balance over an infinite

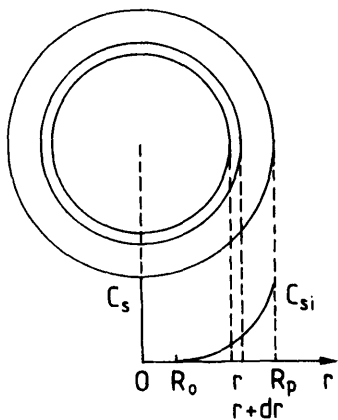


Fig. 15.5 Mass balance over infinite small layer of biocatalyst bead.

thin layer of the biocatalyst bead is set up (Fig. 15.5). In Section 11.1 it is derived that for spherical coordinates and steady state this leads to:

$$\frac{D_{sp}}{r^2} \frac{d}{dr} \left(r^2 \frac{dC_s(r)}{dr} \right) = r_s^{ug}(r) \quad (\text{mol m}^{-3} \text{s}^{-1}) \quad 15.18$$

For Michaelis-Menten kinetics this equation cannot be solved analytically. For the extremes of Michaelis-Menten kinetics, i.e., first-order and zero-order reaction kinetics, analytical solutions do exist (see Section 15.5). As we know that Michaelis-Menten kinetics lie somewhere in between, the effectiveness factors derived from these analytical solutions for zero and first-order kinetics can be used for estimation of the effectiveness factor for Michaelis-Menten kinetics. Therefore, the analytical solutions will be given here and the derivations at the end of this chapter (see Section 15.5).

15.3.2 Zero-order kinetics

For zero-order kinetics the analytical solution of Eq. (15.18) yields the substrate concentration as a function of r in the biocatalyst bead:

$$\frac{C_s(r)}{C_{si}} = 1 + \frac{v_{max}^g R_p^2}{6 D_{sp} C_{si}} \left(\frac{r^2}{R_p^2} - 1 + \frac{2 R_0^3}{r R_p^2} - \frac{2 R_0^3}{R_p^3} \right) \quad (-) \quad 15.19$$

in which R_0 (m) is the radius at which just $C_s(r) = 0$ (see also Fig. 15.5).

When $C_s(r) \gg K_m$ (zero-order kinetics) is substituted in Eq. (15.17) for the Thiele modulus, this equation becomes:

$$\Phi^2 = \frac{v_{max}^g R_p^2}{18 D_{sp} C_{si}} \quad (-) \quad 15.20$$

Substitution of this equation in Eq. (15.19) yields:

$$\frac{C_s(r)}{C_{si}} = 1 + 6\Phi^2 \left(\frac{r^2}{2R_p^2} - \frac{1}{2} + \frac{R_0^3}{rR_p^2} - \frac{R_0^3}{R_p^3} \right) \quad (-) \quad 15.21$$

At $r = R_0$ is $C_s(r) = 0$. Substitution in Eq. (15.21) gives:

$$0 = 1 + 6\Phi^2 \left(\frac{R_0^2}{2R_p^2} - \frac{1}{2} + \frac{R_0^3}{R_0 R_p^2} - \frac{R_0^3}{R_p^3} \right) \quad (-) \quad 15.22$$

Rearrangement gives:

$$\Phi^2 = \left[6 \left(\frac{R_0}{R_p} \right)^3 - 9 \left(\frac{R_0}{R_p} \right)^2 + 3 \right]^{-1} \quad (-) \quad 15.23$$

We further know that for zero-order kinetics, the internal effectiveness factor η_{eio} is equal to the ratio of the volume of the particle where substrate is present and the total volume of the biocatalyst particle:

$$\eta_{eio} = \frac{\frac{4}{3}\pi(R_p^3 - R_0^3)}{\frac{4}{3}\pi R_p^3} = 1 - \left(\frac{R_0}{R_p} \right)^3 \quad (-) \quad 15.24$$

This is because it does not matter how much substrate the biocatalyst "sees" in case of zero-order kinetics. As long as there is substrate present in the microenvironment of the biocatalyst, even if it is only one molecule, it will be converted by the same constant rate. Naturally, this is a theoretical case. Eq. (15.24) can also be written as:

$$\frac{R_0}{R_p} = (1 - \eta_{eio})^{0.33} \quad (-) \quad 15.25$$

Substitution in Eq. (15.23) gives:

$$\Phi^2 = \left[6(1 - \eta_{eio}) - 9(1 - \eta_{eio})^{0.67} + 3 \right]^{-1} \quad (-) \quad 15.26$$

or

$$\eta_{ei0} = -\frac{3}{2}(1 - \eta_{ei0})^{0.67} + \frac{3}{2} - \frac{1}{6\Phi^2} \quad (-) \quad 15.27$$

If R_0 is just 0, then $\eta_{ei0} = 1$ and by means of Eq. (15.26) it can be calculated that for that case $\Phi = 0.33\sqrt{3}$. Therefore, we need two regimes to characterize η_{ei0} :

$$\eta_{ei0} = -\frac{3}{2}(1 - \eta_{ei0})^{0.67} + \frac{3}{2} - \frac{1}{6\Phi^2} \quad \Phi > 0.33\sqrt{3} \quad (-) \quad 15.27$$

$$\eta_{ei0} = 1 \quad \Phi \leq 0.33\sqrt{3} \quad (-) \quad 15.28$$

From Eq. (15.27) the following explicit equation for η_{ei0} can be derived:

$$\eta_{ei0} = 1 - x^3$$

$$\text{with } x = \cos\left(\frac{y + 4\pi}{3}\right) + \frac{1}{2}$$

$$\text{and } y = \cos^{-1}\left(\frac{2}{3\Phi^2} - 1\right) \quad (-) \quad 15.29$$

(Note: cos and cos⁻¹ in radials.)

15.3.3 First-order kinetics

For first-order kinetics Eq. (15.18) can be analytically solved as well (see Section 15.5). The result is

$$\frac{C_s(r)}{C_{si}} = \frac{R_p \sinh\left(r \sqrt{\frac{k}{D_{sp}}}\right)}{r \sinh\left(R_p \sqrt{\frac{k}{D_{sp}}}\right)} \quad (-) \quad 15.30$$

with

$$k = \frac{v_{max}^g}{K_m} \quad (\text{s}^{-1}) \quad 15.31$$

the first-order reaction-rate constant when $C_s \ll K_m$ for Michaelis-Menten kinetics. Sinh has the following mathematical meaning:

$$\sinh z = 0.5(e^z - e^{-z}) \quad (-) \quad 15.32$$

When the generalized Thiele modulus [Eq. (15.16)] is now simplified again with $V_{sp}/a = d_p/6$ (spherical biocatalyst particle), $C_s \approx 0$ (thermodynamic reaction equilibrium at product side) and a substrate-concentration independent D_{sp} , and further by substituting

$$-r_s^{ug} = v_{max}^g \frac{C_s(r)}{K_m} = k C_s(r) \quad (\text{mol m}^{-3} \text{ s}^{-1}) \quad 15.33$$

then the following equation for the Thiele modulus is obtained:

$$\Phi = \frac{\frac{1}{6\sqrt{2}} d_p k C_{si}}{\left(k |D_{sp} | \int_0^{C_{si}} C_s(r) dC_s(r) \right)^{0.5}} \quad (-) \quad 15.34$$

After integration:

$$\Phi = \frac{\frac{1}{6\sqrt{2}} d_p k C_{si}}{\left(\frac{1}{2} k |D_{sp}| C_{si}^2 \right)^{0.5}} \quad (-) \quad 15.35$$

or

$$\Phi = \frac{1}{6} d_p \left(\frac{k}{|D_{sp}|} \right)^{0.5} = \frac{1}{3} R_p \left(\frac{k}{|D_{sp}|} \right)^{0.5} \quad (-) \quad 15.36$$

In this case of first-order reaction kinetics the internal effectiveness factor, η_{si} (-), can be defined as the net flow of substrate to the biocatalyst particle divided by the rate of consumption when all the biocatalyst entities would be confronted by the concentration of substrate at the surface of the biocatalyst particle. In formula:

$$\eta_{ei} = \frac{4\pi R_p^2 D_{sp} \left(\frac{dC_s(r)}{dr} \right)_{r=R_p}}{\frac{4}{3}\pi R_p^3 k C_{si}} \quad (-) \quad 15.37$$

With Eq. (15.30) for the substrate-concentration profile in the biocatalyst particle, $(dC_s(r)/dr)_{r=R_p}$, can be calculated (see Section 15.5). Together with Eq. (15.36) η_{ei} is obtained:

$$\eta_{ei} = \frac{3\Phi \coth(3\Phi) - 1}{3\Phi^2} \quad (-) \quad 15.38$$

Coth has the following mathematical meaning:

$$\coth(z) = \frac{\cosh(z)}{\sinh(z)} = \frac{1}{\tanh(z)} \quad (-) \quad 15.39$$

with

$$\cosh(z) = 0.5(e^z + e^{-z}) \quad (-) \quad 15.40$$

With the radius of the biocatalyst particle R_p , with first-order reaction-rate constant k ($= v_{max}^0 / K_m$) and with the effective diffusion coefficient D_{sp} , which are all assumed to be known, the Thiele modulus and η_{ei} can be calculated by means of Eqs. (15.36) and (15.38).

15.3.4 Michaelis-Menten kinetics

A schematic representation of η_{ei} as a function of the Thiele modulus for both zero- and first-order kinetics is given in Fig. 15.6. As we have seen before, Michaelis-Menten kinetics lies somewhere in between. Since Eq. (15.18) cannot be solved analytically for Michaelis-Menten kinetics, the effectiveness factor can only be calculated by means of numerical solutions in that case. However, a rational analytical estimation of η_{ei} is possible when using the analytical solutions of the zero- and first-order kinetics (Kobayashi and Laidler, 1973):

$$\eta_{ei} = \Theta \eta_{eio} + (1 - \Theta) \eta_{eif} \quad (-) \quad 15.41$$

with

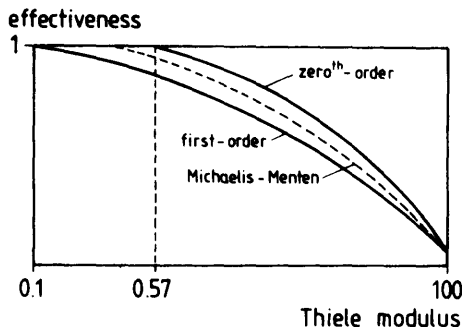


Fig. 15.6 The internal effectiveness factor as a function of the Thiele modulus.

$$\Theta = \frac{C_{si}}{K_m + C_{si}} \quad (-) \quad 15.42$$

If $C_{si} \gg K_m$ (zero-order kinetics) Θ approaches one and from Eq. (15.41) it can be seen that $\eta_{ei} \sim \eta_{e10}$. On the other hand, if $C_{si} \ll K_m$ (first-order kinetics) Θ approaches zero and thus $\eta_{ei} \sim \eta_{e11}$. For cases in between η_{ei} is calculated in between those of zero and first-order kinetics.

15.4 Estimation of intrinsic kinetic constants

In the preceding chapters it is assumed that the intrinsic kinetic constants (v_{max} , K_m) of the immobilized biocatalyst are known. These intrinsic kinetic constants, however, cannot a priori be assumed to be equal to those of the free biocatalyst in solution, as immobilization per se, in other words with exclusion of diffusion and partition effects, can change the intrinsic properties of the biocatalyst. A method to determine the intrinsic kinetic constants is by kinetic measurements using immobilized biocatalyst particles with a very small radius and a low catalytic activity per unit volume of support. Naturally, the biocatalyst should be immobilized by the same procedure and into the same support as the immobilized biocatalyst particles of concern. Furthermore, one has to ascertain that the measurements are not disguised by diffusion limitation and/or partition effects. This can be done, for instance, by executing measurements using immobilized biocatalyst particles of various defined small diameters and/or having various biocatalytic activities per unit volume of support. This should yield constant, equal kinetic constants. Another procedure is to make a series of immobilized biocatalyst particles with a varying diameter but constant activity per unit volume, or constant diameter but varying activity per unit volume. Extrapolation to zero diameter or zero activity, respectively, yields diffusion free kinetic constants (van Ginkel et al., 1983). In our laboratory

we have developed a procedure on the basis of the theory discussed in the preceding chapters. A schematic representation of the principle of this procedure is given in Fig. 15.7. The procedure starts by measurement of the activity of the immobilized biocatalyst by recording the concentration of the substrate. The integrated Michaelis-Menten equation is fitted to the experimental (C_{sb} , t) data pairs. From this the apparent kinetic constants v'_{max} and K'_m of the pertinent immobilized biocatalyst are obtained. As stressed before, these constants only apply for this one particular case and are not suited for modeling, simulation and design purposes. For each data pair a corresponding overall effectiveness factor can be calculated by the methods described in the preceding sections. For that, however, one should know the intrinsic K_m . As a first trial the K_m of the free biocatalyst in solution can be taken, or the apparent K'_m -value calculated as described above. With the aid of the calculated overall effectiveness factors, a "pseudo-experiment" is performed; i.e., the measured reaction rates are corrected for diffusion effects as follows:

$$r_s^u(\text{new}) = (\eta_e^{ov})^{-1} r_s^u(\text{old}) \quad (\text{mol m}^{-3} \text{s}^{-1}) \quad 15.43$$

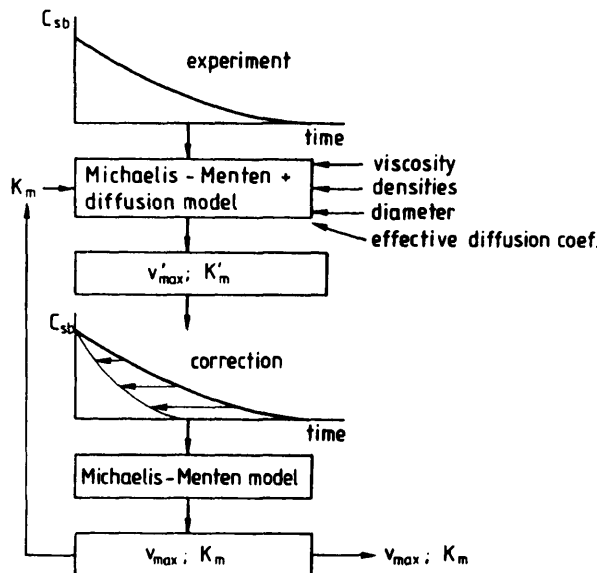


Fig. 15.7 Principle of estimation of intrinsic kinetic constants.

With that a new r^* versus C_{so} -profile can be generated (Fig. 15.7) and with that new kinetic constants and overall effectiveness factors. This iteration procedure can be repeated until the v_{max} and K_m converge to constant values. These are the intrinsic kinetic constants which are the suitable ones for modeling, simulation and design.

15.5 Appendix: Solutions to Eq. (15.18)

15.5.1 Zero-order kinetics

Substitution of $-r_i^{so} = v_{max}^g$ in Eq. (15.18) and integration yields:

$$\frac{v_{max}^g r^3}{3 |D_{sp}|} = r^2 \frac{dC_s(r)}{dr} + IC_1 \quad (\text{mol m}^{-2}) \quad 15.44$$

In order to obtain the integration constant IC_1 , the boundary condition $C_s(r) = 0$ and $dC_s(r)/dr = 0$ at $r = R_0$ (Fig. 15.5) can be used. In that case substrate is present only in part ($r > R_0$) of the immobilized biocatalyst particle. In zero-order kinetics this is also the only situation when the internal effectiveness factor is smaller than one. By means of this boundary condition IC_1 is found to be:

$$IC_1 = \frac{v_{max}^g R_0^3}{3 |D_{sp}|} \quad (\text{mol m}^{-2}) \quad 15.45$$

Substitution in Eq. (15.44) and rearrangement:

$$\frac{dC_s(r)}{dr} = \frac{v_{max}^g r}{3 |D_{sp}|} - \frac{v_{max}^g R_0^3}{3 |D_{sp}| r^2} \quad (\text{mol m}^{-4}) \quad 15.46$$

Separation of variables and integration:

$$C_s(r) = \frac{v_{max}^g r^2}{6 |D_{sp}|} + \frac{v_{max}^g R_0^3}{3 |D_{sp}| r} + IC_2 \quad (\text{mol m}^{-3}) \quad 15.47$$

With the aid of the boundary condition $C_s(r) = C_{si}$ at $r = R_p$ the second integration constant is obtained:

$$IC_2 = C_{si} - \frac{v_{max}^g R_p^2}{6 |D_{sp}|} - \frac{v_{max}^g R_0^3}{3 |D_{sp}| R_p} \quad (\text{mol m}^{-3}) \quad 15.48$$

Substitution in Eq. (15.47) gives:

$$C_s(r) = C_{si} + \frac{v_{max}^g}{6|D_{sp}|} (r^2 - R_p^2) + \frac{v_{max}^g}{3|D_{sp}|} \left(\frac{R_0^3}{r} - \frac{R_0^3}{R_p} \right) \text{ (mol m}^{-3}) \quad 15.49$$

or

$$\frac{C_s(r)}{C_{si}} = 1 + \frac{v_{max}^g R_p^2}{6|D_{sp}| C_{si}} \left(\frac{r^2}{R_p^2} - 1 + \frac{2R_0^3}{rR_p^2} - \frac{2R_0^3}{R_p^3} \right) \quad (-) \quad 15.19$$

15.5.2 First-order kinetics

For first-order kinetics the consumption term in Eq. (15.18) can be written as

$$-r_s^{ug} = \frac{v_{max}^g C_s(r)}{K_m} = k C_s(r) \text{ (mol m}^{-3} \text{ s}^{-1}) \quad 15.50$$

with the result:

$$\frac{k C_s(r)}{|D_{sp}|} r^2 = \frac{d}{dr} r^2 \frac{dC_s(r)}{dr} \text{ (mol m}^{-3}) \quad 15.51$$

or

$$\frac{1}{r^2} \left(2r \frac{dC_s(r)}{dr} + r^2 \frac{d^2C_s(r)}{dr^2} \right) = \frac{k C_s(r)}{|D_{sp}|} \text{ (mol m}^{-5}) \quad 15.52$$

This equation can be solved by means of the following substitutions:

$$C_s(r) = \frac{f(r) C_{si}}{r} \text{ (mol m}^{-3}) \quad 15.53$$

$$\frac{dC_s(r)}{dr} = C_{si} \left(\frac{1}{r} \frac{df(r)}{dr} - \frac{f(r)}{r^2} \right) \text{ (mol m}^{-4}) \quad 15.54$$

$$\frac{d^2C_s(r)}{dr^2} = C_{si} \left(\frac{2f(r)}{r^2} - \frac{2}{r^2} \frac{df(r)}{dr} + \frac{1}{r} \frac{d^2f(r)}{dr^2} \right) \text{ (mol m}^{-5}) \quad 15.55$$

Substitution in Eq. (15.52) yields:

$$\frac{k f(r) C_{si}}{r |D_{sp}|} = \frac{C_{si}}{r^2} \left(\frac{2r}{r} \frac{df(r)}{dr} - \frac{2r f(r)}{r^2} - \frac{df(r)}{dr} + \frac{r^2}{r} \frac{d^2 f(r)}{dr^2} + \frac{2r^2 f(r)}{r^3} - \frac{df(r)}{dr} \right) (\text{mol m}^{-6}) \quad 15.56$$

Reducing further:

$$\frac{d^2 f(r)}{dr^2} = \frac{k}{|D_{sp}|} f(r) \quad (\text{m}^{-1}) \quad 15.57$$

As result of the substitutions the boundary conditions change into:

1. $C_s(r) = C_{si}$ at $r = R_p$ becomes $f(r) = R_p$ at $r = R_p$.
2. $dC_s(r)/dr = 0$ at $r = 0$ changes to $f = 0$ at $r = 0$.

The differential Eq. (15.57) can also be written in the following form:

$$f'' - \frac{k f}{|D_{sp}|} = 0 \quad (\text{m}^{-1}) \quad 15.58$$

This is a homologous differential equation with the characteristic equation:

$$v^2 - \frac{k}{|D_{sp}|} = 0 \quad (\text{m}^{-2}) \quad 15.59$$

The roots of this equation are:

$$1. \quad v_1 = \sqrt{\frac{k}{|D_{sp}|}} \quad 2. \quad v_2 = -\sqrt{\frac{k}{|D_{sp}|}}$$

A solution of the differential Eq. (15.58) can be written in the following form:

$$f(r) = \alpha e^{r \sqrt{\frac{k}{|D_{sp}|}}} + \beta e^{-r \sqrt{\frac{k}{|D_{sp}|}}} \quad (\text{m}) \quad 15.60$$

Substitution of the boundary conditions yields:

$$\alpha = -\beta \quad 15.61$$

and

$$R_p = \alpha e^{R_p \sqrt{\frac{k}{D_{sp}}}} + \beta e^{-R_p \sqrt{\frac{k}{D_{sp}}}} \quad (m) \quad 15.62$$

From this it follows that:

$$\alpha = -\beta = \frac{R_p}{e^{R_p \sqrt{\frac{k}{D_{sp}}}} - e^{-R_p \sqrt{\frac{k}{D_{sp}}}}} \quad (m) \quad 15.63$$

When Eq. (15.52) is substituted back, the solution is found for the concentration profile in the biocatalyst particle for the case of first-order reaction kinetics:

$$r \frac{C_s(r)}{C_{si}} = R_p \frac{e^{r \sqrt{\frac{k}{D_{sp}}}} - e^{-r \sqrt{\frac{k}{D_{sp}}}}}{e^{R_p \sqrt{\frac{k}{D_{sp}}}} - e^{-R_p \sqrt{\frac{k}{D_{sp}}}}} \quad (m) \quad 15.64$$

or

$$C_s(r) = C_{si} \frac{R_p}{r} \frac{\sinh(r \sqrt{\frac{k}{D_{sp}}})}{\sinh(R_p \sqrt{\frac{k}{D_{sp}}})} \quad (m) \quad 15.65$$

Differentiation gives:

$$\begin{aligned} \frac{dC_s(r)}{dr} &= C_{si} R_p \left(-\frac{1}{r^2} \frac{\sinh(r \sqrt{\frac{k}{D_{sp}}})}{\sinh(R_p \sqrt{\frac{k}{D_{sp}}})} + \right. \\ &\quad \left. + \frac{1}{r} \frac{\cosh(r \sqrt{\frac{k}{D_{sp}}})}{\sinh(R_p \sqrt{\frac{k}{D_{sp}}})} \sqrt{\frac{k}{D_{sp}}} \right) (\text{mol m}^{-4}) \quad 15.66 \end{aligned}$$

The substrate concentration gradient at the surface of the immobilized biocatalyst particles thus is:

$$\left(\frac{dC_s(r)}{dr} \right)_{r=R_p} = C_{ss} \left(-\frac{1}{R_p} + \sqrt{\frac{k}{D_{sp}}} \frac{1}{\tanh\left(R_p \sqrt{\frac{k}{D_{sp}}}\right)} \right) \text{ (mol m}^{-4}) \quad 15.67$$

15.6 Examples

Example 15.1 The external effectiveness factor

The enzyme glucose oxidase catalyzes the oxidation of glucose. When glucose is present in excess, oxygen can be considered the limiting substrate, which rate of consumption can be described by Michaelis-Menten type of kinetics. The enzyme is immobilized on the surface of nonporous glass beads.

Calculate:

The overall effectiveness factor for

- i. $v_{max} = 6.5 \text{ mol O}_2 \text{ s}^{-1} (\text{g enzyme})^{-1}$, and
- ii. $v_{max} = 6.5 \times 10^{-7} \text{ mol O}_2 \text{ s}^{-1} (\text{g enzyme})^{-1}$

Data:

$$\begin{aligned} d_p &= 10^{-3} \text{ m} & \eta_i &= 10^{-3} \text{ N s m}^{-2} & D_{oi} &= 2.3 \times 10^{-9} \text{ m}^2 \text{ s}^{-1} \\ K_m &= 0.12 \text{ mol m}^{-3} & \rho_i &= 10^3 \text{ kg m}^{-3} & \rho_p &= 2762 \text{ kg m}^{-3} \\ C_{sb} &= 0.24 \text{ mol m}^{-3} & \text{enzyme load } C_x' &= 10^{-6} \text{ g per bead} \end{aligned}$$

Solution:

The enzyme is immobilized on the surface of nonporous glass beads; thus internal diffusion limitation is absent and in this case $\eta_e'' = \eta_{ee}$.

The mass transfer coefficient k_{oi} can be calculated starting with the Galilei number:

$$Ga = \frac{g d_p^3 \rho_i (\rho_p - \rho_i)}{\eta_i^2} \quad (-) \quad 11.20$$

Substituting the appropriate numerical values gives $Ga = 17,285$ and therefore Eq. (11.22) can be used to calculate Re_p :

$$Re_p = 0.153 Ga^{0.71} = 156 \quad (-) \quad 11.22$$

Substituting this in the Ranz and Marshall relation:

$$\frac{k_{ol} d_p}{|D_{ol}|} = 2 + 0.57 \sqrt{Re} \left(\frac{\eta_l}{\rho_l |D_{ol}|} \right)^{0.33} \quad (-) \quad 11.19$$

with the other numerical values yields a $k_{ol} = 1.3 \times 10^{-4} \text{ m s}^{-1}$. In the steady state we know that the flux of oxygen to one particle is equal to its consumption:

$$k_{ol} a (C_{sb} - C_{si}) = \frac{v_{max} C_{si}}{K_m + C_{si}} C_x'' \quad 15.68$$

Case i: $v_{max} = 6.5 \text{ mol s}^{-1} \text{ g}^{-1}$

Assume first-order kinetics, i.e., $C_{sb} > K_m \gg C_{si}$; then the above equation reduces to

$$k_{ol} a C_{sb} = \frac{v_{max} C_{si}}{K_m} C_x'''$$

Substitution of numerical values yields $C_{si} = 1.8 \times 10^{-6} \text{ mol m}^{-3}$, which indeed is much smaller than K_m , so that the above assumption is justified.

$$\eta_e^{ov} = \eta_{ee} = \frac{r_s^u(C_{si})}{r_s^u(C_{sb})} = \frac{C_{si}(K_m + C_{sb})}{C_{sb}(K_m + C_{si})} = 2.2 \times 10^{-5}$$

Case ii: $v_{max} = 6.5 \times 10^{-7} \text{ mol s}^{-1} \text{ g}^{-1}$

The low activity makes first-order kinetics unlikely and the bulk-liquid concentration is only twice the K_m -value so that application of zero-order kinetics is also inappropriate. This means that Eq. (15.68) has to be used as such. Substitution of numerical values yields a quadratic equation in C_{si} with 2 solutions of which $0 < C_{si} < C_{sb}$ is the valid one. The result is $C_{si} \approx C_{sb}$; in other words, external diffusion limitation is negligible.

Example 15.2 The internal effectiveness factor

Nitrate in groundwater is becoming more and more a problem. In addition to measures aiming at applying lower loads of fertilizers, the need for effective treatment procedures is increasing. One of the alternatives investigated is removal of nitrate by conversion to gaseous N_2 using denitrifying bacteria immobilized in gel beads. Calculate the content of an ideally mixed bioreactor treating $100 \text{ m}^3 \text{ h}^{-1}$ of ground water.

Data:

Influent concentration of nitrate	C_{si} = 50 g m ⁻³
Effluent concentration of nitrate	C_{so} = 1 g m ⁻³
Load of gel beads in reactor	ϵ = 0.2 m ³ gel m ⁻³ reactor
Radius of gel beads	R_p = 1.5 mm
Intrinsic value of	K_m = 10 g m ⁻³ reactor
Intrinsic value of	v_{max}^g = 0.4 g s ⁻¹ m ⁻³ gel
Diffusion coefficient of nitrate in gel	D_{sp} = 10 ⁻¹⁰ m ² s ⁻¹
Mass transfer coefficient of nitrate	k_{sl} = 10 ⁻⁵ m s ⁻¹

Solution:

The bioreactor is ideally mixed; thus the concentration in the reactor is equal to the concentration in the effluent, i.e., 1 g m⁻³. This is much smaller than the K_m , so assuming the reaction to be first order is valid.

Substituting numerical values in Eq. (15.36)

$$\Phi = \frac{1}{3} R_p \left(\frac{k}{D_{sp}} \right)^{0.5} = \frac{1}{3} R_p \left(\frac{v_{max}^g}{K_m D_{sp}} \right)^{0.5} \quad (-) \quad 15.36$$

yields $\Phi = 10$. Substituting this value in Eq. (15.38) for the first-order effectiveness factor

$$\eta_{eff} = \frac{3\Phi \coth(3\Phi) - 1}{3\Phi^2} \quad (-) \quad 15.38$$

gives $\eta_{eff} = 0.0967$. In the steady state we know that the mass transfer to the beads is equal to the consumption by the beads:

$$\eta_{eff} \frac{v_{max}^g}{K_m} C_{si} = k_{sl} A'' (C_{so} - C_{si})$$

Substituting $A'' = 3/R_p$ and the appropriate numerical values, gives a $C_{si} = 0.83$ g m⁻³. The consumption per unit volume of reactor thus becomes

$$\begin{aligned} -r_s^u &= \eta_{eff} \frac{v_{max}^g \epsilon}{K_m} C_{si} \\ &= 0.64 \times 10^{-3} \text{ g m}^{-3} \text{ s}^{-1} \\ &= 2.32 \text{ g m}^{-3} \text{ h}^{-1} \end{aligned}$$

Per cubic meter ground water 49 g of nitrate is removed. The flow is 100 m³ h⁻¹, i.e., a removal of 4900 g h⁻¹.

The working volume of the reactor should thus be $4900/2.32 = 2111$ m³.

References

- Aris A. "A normalization for the Thiele modulus." Ind. Eng. Chem. Fund. 4, 227 (1965).
- Bischoff K.B. "Effectiveness factors for general rate equation forms." A.I.Ch.E. J. 11, 351 (1965).
- Kobayashi T. and Laidler K.J. "Kinetic analysis for solid-supported enzymes." Biochem. Biophys. Acta 302, 1 (1973).
- van Ginkel C.G., Tramper J., Luyben K.Ch.A.M. and Klapwijk A. "Characterization of *Nitrosomonas europaea* immobilized in calcium alginate." Enzyme Microb. Technol. 5, 297 (1983).

16

Apparent Stability

16.1 Introduction

Stability of the biocatalyst is one of the crucial parameters for the overall volumetric productivity of the bioreactor. All biocatalysts, except usually viable cells, lose catalytic activity in time. The stability of a biocatalyst during continuous operation is called operational stability, which usually is numerically expressed by its half-life, i.e., the elapsed time at which the activity is reduced to half. The half-life is one of the crucial parameters in the economic feasibility of a bioprocess. Reliable determination of the half-life, i.e., stability of a biocatalyst, is therefore a prerequisite for the estimation of the feasibility of a particular bioprocess.

Levenspiel (1972) gives two methods to establish the stability of a catalyst during continuous operation. As we will see later, the better method is to keep the conversion constant by decreasing the flow rate as the biocatalyst activity gradually drops. A precise feedback control is, however, essential for this. In the other method the flow rate is kept constant throughout and the decrease in outlet conversion is measured in time. Because of convenience, the latter method is mostly used for conversions by immobilized biocatalysts. Yamane et al. (1987) give a theoretical discussion of the reliability of the information on biocatalyst stability obtained by either method. In particular, the apparent half-life thus obtained for immobilized biocatalysts in both a plug-flow reactor and a CSTR is evaluated. Because of the importance of biocatalyst stability and because of the fact that basic concepts discussed in earlier chapters are integrated in an illustrative manner, the paper of Yamane et al. (1987) is rather extensively discussed here, in addition to a paper of Ooshima and Harano (1983) concerning apparent stabilization as a result of immobilization. A very detailed and extensive review on biocatalyst deactivation in reactors can be found in Sadana (1989).

16.2 Basic equations

Assuming Michaelis-Menten kinetics, the rate of reaction can be written as (see also Chapter 4):

$$-r_s^u = C_e^T(t) \frac{k_{-2} C_s}{K_m + C_s} = C_e^T(t) f(C_s) \quad (\text{mol m}^{-3} \text{s}^{-1}) \quad 16.1$$

in which

$-r_s^u$	= substrate consumption rate per unit volume	(mol m ⁻³ s ⁻¹)
C_e^T	= total active enzyme concentration	(mol m ⁻³)
C_s	= substrate concentration	(mol m ⁻³)
K_m	= Michaelis-Menten constant	(mol m ⁻³)
k_{-2}	= first-order reaction rate constant	(s ⁻¹)

The simplest and most commonly used expression for biocatalyst inactivation is obtained when first-order decay is assumed (Chapter 5):

$$\frac{C_e^T(t)}{C_e^T(0)} = e^{-k_d t} \quad (-) \quad 16.2$$

in which k_d (s⁻¹) is the first-order inactivation rate constant.

If it is further assumed that the half-life is long in comparison to the residence time, then pseudo-steady state can be applied to develop the performance equations for both plug-flow and continuous-flow stirred-tank reactors containing immobilized biocatalyst (Chapters 1 and 15). For the plug-flow reactor this yields:

$$\tau_{pf} = \frac{V(1-\epsilon)}{F_i} = - \int_{C_{si}}^{C_{so}} \frac{dC_s}{\eta_e^{ov} (-r_s^u)} \quad (s) \quad 16.3$$

and for the CSTR

$$\tau_{CSTR} = \frac{V(1-\epsilon)}{F_i} = \frac{C_{si} x}{\eta_e^{ov} (-r_s^u)} \quad (s) \quad 16.4$$

in which

τ	= residence time	(s)
V	= working volume of the reactor	(m ³)

F_i	= liquid through flow rate	($\text{m}^3 \text{s}^{-1}$)
ϵ	= volume fraction of biocatalyst particles	(-)
C_{si}	= inflow substrate concentration	(mol m^{-3})
C_{so}	= outflow substrate concentration	(mol m^{-3})
η_e^{ov}	= overall effectiveness factor	(-)

and x is the conversion defined by

$$x = \frac{C_{si} - C_{so}}{C_{si}} \quad (-) \quad 16.5$$

16.3 Negligible diffusion limitation ($\eta_e^{ov} = 1$)

When the rate of reaction of the immobilized biocatalyst is not significantly influenced by diffusion of substrate, Eqs. (16.1), (16.3) and (16.4) can be reduced and rearranged into

$$\frac{C_e^T(t)}{F_i(t)} = - \frac{1}{(1-\epsilon)V} \int_{C_{si}}^{C_{so}} \frac{dC_s}{f(C_s)} \quad (\text{mol m}^{-6} \text{s}) \quad 16.6$$

for the plug-flow reactor, and

$$\frac{C_e^T(t)}{F_i(t)} = \frac{C_{si} x}{(1-\epsilon)V f(C_{so})} \quad (\text{mol m}^{-6} \text{s}) \quad 16.7$$

for the CSTR. If the conversion x , i.e., C_{so} , is kept constant by adapting the flow rate F_i , the left-hand side of Eqs. (16.6) and (16.7) remains constant as the values on the right-hand side are constant:

$$\frac{C_e^T(t)}{F_i(t)} = \frac{C_e^T(0)}{F_i(0)} = \text{constant} \quad (\text{mol m}^{-6} \text{s}) \quad 16.8$$

or

$$\frac{F_i(t)}{F_i(0)} = \frac{C_e^T(t)}{C_e^T(0)} \quad (-) \quad 16.9$$

It can thus be concluded from Eq. (16.9) that the time course of $F_e(t)/F_e(0)$ yields the true intrinsic stability of the biocatalyst regardless of the expression for $f(C_s)$ and no matter how the biocatalyst decays.

When the flow rate is kept constant, on the other hand, it is difficult to get the real stability of the immobilized biocatalyst from the time course of the conversion $x(t)/x(0)$. Substitution of Eqs. (16.1) and (16.2) in the plug-flow reactor Eq. (16.6), integration and rearrangement gives:

$$\frac{C_e^T(t)}{C_e^T(0)} = \frac{x(t) - K \ln(1-x(t))}{x(0) - K \ln(1-x(0))} = e^{-k_d t} \quad (-) \quad 16.10$$

with $K = K_m/C_{sl}$. If K approaches infinity, i.e., first-order kinetics, Eq. (16.10) reduces to

$$\frac{C_e^T(t)}{C_e^T(0)} = \frac{\ln(1-x(t))}{\ln(1-x(0))} = e^{-k_d t} \quad (-) \quad 16.11$$

and for K approaches zero, i.e., zero-order kinetics, to

$$\frac{C_e^T(t)}{C_e^T(0)} = \frac{x(t)}{x(0)} = e^{-k_d t} \quad (-) \quad 16.12$$

Similary, for the CSTR it can be derived that

$$\frac{C_e^T(t)}{C_e^T(0)} = \frac{x(t) + \left(\frac{K x(t)}{1-x(t)}\right)}{x(0) + \left(\frac{K x(0)}{1-x(0)}\right)} = e^{-k_d t} \quad (-) \quad 16.13$$

which reduces to

$$\frac{C_e^T(t)}{C_e^T(0)} = \frac{\left(\frac{x(t)}{1-x(t)}\right)}{\left(\frac{x(0)}{1-x(0)}\right)} = e^{-k_d t} \quad (-) \quad 16.14$$

for K approaches infinity (first-order kinetics). For K approaches zero (zero-order kinetics) Eq. (16.12) can again be derived. Eq. (16.12) for zero-order kinetics, for both a plug-flow reactor and a CSTR, shows that for this case the $x(t)/x(0)$ profile yields the true operational stability of

the immobilized biocatalyst. Plotting Eqs. (16.10) and (16.13) (Fig. 16.1) with K as parameter shows, on the contrary, that as $K > 0$ the stability apparently increases, an effect which is magnified as the initial conversion $x(0)$ is higher. Caution is thus needed in determining the operational stability of a biocatalyst in this way. Taking representative samples of the immobilized biocatalyst from the continuous reactor at regular intervals and determining the activity of such samples under standard conditions can

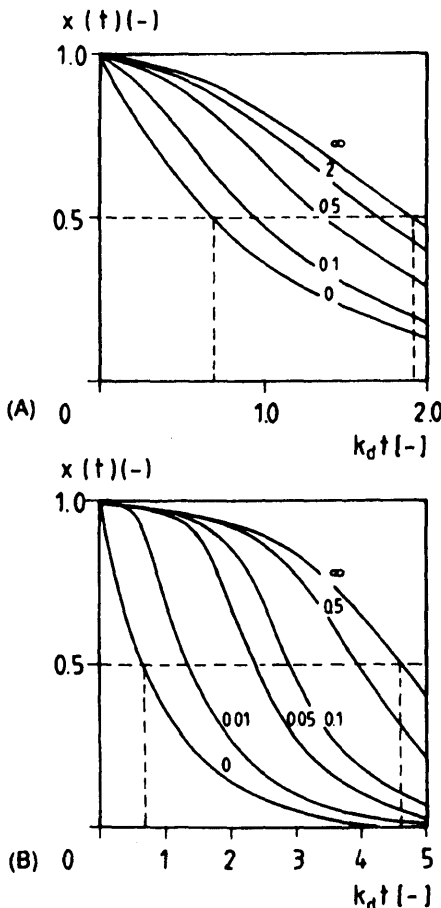


Fig. 16.1 Conversion x as a function of dimensionless time $k_d t$ in (A) a plug-flow reactor and (B) a CSTR (parameter $K = K_m / C_{s,i}$) for Michaelis-Menten kinetics, first-order inactivation, no diffusion limitation, constant flow and an initial conversion of 99%. (Adapted from Yamana et al., 1987.)

largely solve this problem of apparent stability. The standard conditions preferably should exclude mass transfer limitations, as this can also mask true intrinsic stability of an immobilized biocatalyst, as we will see in the next section.

16.4 Diffusion-limited kinetics ($\eta_s^{\text{ov}} < 1$)

16.4.1 Qualitative considerations

In addition to the effects on kinetics (see Chapter 15), limitation of the reaction rate by mass transfer can also influence the stability of the immobilized biocatalyst, or more precisely: apparently can stabilize the immobilized biocatalyst. For that, situation 2 in Fig. 15.2 has to be worked out a little further in detail (Fig. 16.2). Fig. 16.2A corresponds to the situation at $t = 0$. As time passes more and more biocatalyst will be inactivated. As a result the biocatalyst activity per unit volume of support decreases and substrate can penetrate the biocatalyst particle further and further. At time $t = t_1$ (Fig. 16.2B) the situation is reached that all active biocatalyst "feels" substrate and participates in the catalysis. Until that time the observed rate of reaction decreases less in time as could be expected on the basis of the intrinsic inactivation rate constant, because inactivated biocatalyst in the outer layers of the biocatalyst particle is replaced by not-yet-inactivated biocatalyst farther in the interior of the biocatalyst particle and so far not significantly participating in the biocatalysis as a result of substrate exhaustion. At time $t = t_2$ (Fig. 16.2C), when diffusion of substrate is not limiting the rate of reaction any more to a large extent, the decrease in time of the observed rate of reaction approaches that corresponding to the intrinsic inactivation rate constant. Naturally, this transfer from merely rate

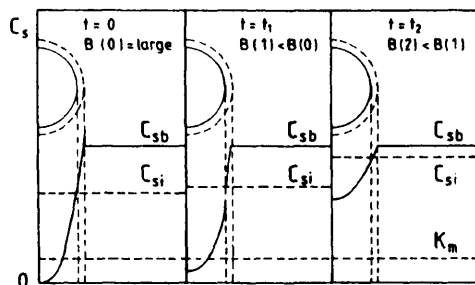


Fig. 16.2 Apparent stabilization, concentration profiles. $B(t)$ = biocatalyst activity as a function of time.

limitation by diffusion of substrate and strong apparent stabilization, to the situation of nil rate limitation by diffusion of substrate and intrinsic stability, is a gradual process (see also Fig. 16.3).

16.4.2 Apparent stabilization for first-order kinetics

16.4.2.1 The general case

In this section the apparent stabilization of an immobilized biocatalyst as a result of rate limitation by diffusion of substrate will be quantified for the case that the biocatalyst follows first-order kinetics. The basis of this quantification comes from Ooshima and Harano (1983). When the kinetics of the pertinent biocatalyst can generally be described by Michaelis-Menten kinetics, this means that the situation is considered where $K_m \gg C_s$, or [see also Eqs. (4.3) and (4.26)]:

$$-r_s^u = v_{max} \frac{C_s}{K_m} = k C_s \quad (\text{mol m}^{-3} \text{s}^{-1}) \quad 16.15$$

The first-order reaction rate constant k (s^{-1}) is thus equal to v_{max}/K_m . Eq. (16.15) describes the rate of reaction when limitation by diffusion of substrate can be neglected. When diffusion limitation is involved, the observed rate of reaction can be described by:

$$-r_s^u = \frac{-dC_{sb}}{dt} = k^{ov} C_{sb} \quad (\text{mol m}^{-3} \text{s}^{-1}) \quad 16.16$$

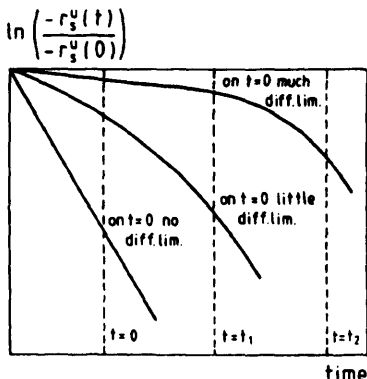


Fig. 16.3 Apparent stabilization, activity profiles.

In this equation C_{sb} (mol m⁻³) is the substrate concentration in the bulk liquid and k^{ov} (s⁻¹) is a kind of overall first-order reaction rate constant, which is equal to:

$$\frac{1}{k^{ov}} = \frac{1}{k_{sl} A'} + \frac{1}{\eta_{el} k} \quad (s) \quad 16.17$$

in which k_{sl} (m s⁻¹) is the liquid-side mass-transfer coefficient, A' (m⁻¹) the specific surface area of the beads in 1 m³ of reactor volume as defined by Eq. (15.4) and η_{el} the internal effectiveness factor for first-order kinetics.

Or, in words, k^{ov} is the reciprocal of the sum of the resistances against external and internal diffusion limitation. Eq. (16.17) can be derived from the fact that the observed rate of reaction is equal to the net flow of mass through the stagnant liquid film surrounding the biocatalyst particle and also equal to the product of the internal effectiveness factor for first-order reaction kinetics and the rate of reaction that would be measured if all the biocatalyst entities experienced the concentration of substrate at the surface of the biocatalyst particle. In equation form:

$$-r_s^u = k^{ov} C_{sb} = k_{sl} A' (C_{sb} - C_{si}) = \eta_{el} k C_{si} \text{ (mol m}^{-3} \text{s}^{-1}\text{)} \quad 16.18$$

in which C_{si} (mol m⁻³) here is the substrate concentration just at the particle/bulk interface. The two right terms can be reworked to:

$$k_{sl} A' C_{sb} = (\eta_{el} k + k_{sl} A') C_{si} \text{ (mol m}^{-3} \text{s}^{-1}\text{)} \quad 16.19$$

or

$$C_{si} = \frac{k_{sl} A' C_{sb}}{\eta_{el} k + k_{sl} A'} \text{ (mol m}^{-3}\text{)} \quad 16.20$$

Substitution in $-r_s^u = \eta_{el} k C_{si}$ yields:

$$-r_s^u = \frac{\eta_{el} k k_{sl} A' C_{sb}}{\eta_{el} k + k_{sl} A'} \text{ (mol m}^{-3} \text{s}^{-1}\text{)} \quad 16.21$$

or

$$-r_s^u = \frac{C_{sb}}{\frac{1}{k_{sl}A'} + \frac{1}{\eta_{sl}k}} \quad (\text{mol m}^{-3} \text{ s}^{-1}) \quad 16.22$$

In this equation Eq. (16.17) for k^{ov} has appeared. An overall dimensionless rate of reaction $\lambda_e^{ov}(t)$ can be defined as

$$\lambda_e^{ov}(t) = \frac{r_s^u(t)}{r_s^u(0)} \quad (-) \quad 16.23$$

or

$$\lambda_e^{ov}(t) = \frac{k^{ov}(t) C_{sb}}{k^{ov}(0) C_{sb}} = \frac{k^{ov}(t)}{k^{ov}(0)} \quad (-) \quad 16.24$$

Substitution of Eq. (16.17) in Eq. (16.24) gives:

$$\lambda_e^{ov}(t) = \frac{(\eta_{sl}(0)k(0) + k_{sl}A')\eta_{sl}(t)k(t)}{(\eta_{sl}(t)k(t) + k_{sl}A')\eta_{sl}(0)k(0)} \quad (-) \quad 16.25$$

η_{sl} , k and λ_e^{ov} are a function of t as indicated in Eq. (16.25). For the sake of convenience the notation (t) will be left out in most of the following equations.

In order to get more insight into this equation, a Damköhler number Da (-) can be introduced, which is a measure between rate of reaction and mass transfer by diffusion:

$$Da(t) = \frac{\eta_{sl}(t)k(t)}{k_{sl}A'} \quad (-) \quad 16.26$$

Substitution in Eq. (16.25) yields:

$$\lambda_e^{ov} = \lambda_{sl} \frac{Da(0) + 1}{Da + 1} \quad (-) \quad 16.27$$

with λ_{sl} (-), the internal dimensionless rate of reaction, defined as

$$\lambda_{ei} = \frac{\eta_{ei}(t) k(t)}{\eta_{ei}(0) k(0)} = \frac{Da}{Da(0)} \quad (-) \quad 16.28$$

If $Da(0)$ and Da are much smaller than 1, that is $k_{st} A' \gg \eta_{ei} k$, in other words limitation of the rate of reaction by external mass transfer is negligably small, it follows from Eq. (16.27) that

$$\lambda_e^{ov} = \lambda_{ei} \quad (-) \quad 16.29$$

Thus λ_{ei} is indeed the dimensionless rate of reaction in the absence of external diffusion limitation. When, in addition, the internal diffusion limitation is neglected, i.e., $\eta_{ei} = \eta_{ei}(0) = 1$, Eq. (16.27) becomes:

$$\lambda_e^{ov} = \lambda_{ei} = \lambda_{er} = \frac{k}{k(0)} = \frac{v_{max}}{v_{max}(0)} \quad (-) \quad 16.30$$

in which λ_{er} = the dimensionless rate of reaction without any diffusion limitation, i.e., of the biocatalyst itself. Because

$$\eta_{ei}(0) \leq \eta_{ei} \leq 1 \quad (-) \quad 16.31$$

(equals sign applies when internal diffusion limitation is absent) and besides

$$Da \leq Da(0) \quad (-) \quad 16.32$$

(equals sign applies when external diffusion limitation is absent) the following applies:

$$\lambda_e^{ov} \geq \lambda_{ei} \geq \lambda_{er} \quad (-) \quad 16.33$$

In words it means that the dimensionless rate of reaction decreases less rapidly in the presence of diffusion limitation, or in still other words: diffusion limitation stabilizes. As a result of diffusion, however, the effective biocatalytic activity per unit immobilized biocatalyst decreases, which results in a decrease of productivity as well. There is therefore an optimal productivity of the bioreactor when an "inactivating" biocatalyst is used (even apart from the time needed to empty the bioreactor, to clean it, to refill it and to start it up again, the so-called down-time between two

operations). The optimal productivity has to be calculated for each process. The main parameters that influence the result are the cost of the biocatalyst, the cost of immobilization, reactor costs and the need for continuous operation at a certain activity level. In order to lay the relation between λ_e^{ov} and the intrinsic stability of the biocatalyst, it is assumed that the inactivation occurs by a first-order process:

$$-\frac{dv_{max}}{dt} = k_d v_{max} \quad (\text{mol m}^{-3} \text{s}^{-2}) \quad 16.34$$

With $k = v_{max}/K_m$ this becomes:

$$-\frac{dk}{dt} = k_d k \quad (\text{s}^{-2}) \quad 16.35$$

or

$$-\frac{dk}{k} = -d \ln\left(\frac{k}{k(0)}\right) = k_d dt \quad (\text{s}^{-1}) \quad 16.36$$

or

$$-\frac{d \ln\left(\frac{k}{k(0)}\right)}{dt} = k_d = -\frac{d \ln \lambda_{er}}{dt} \quad (\text{s}^{-1}) \quad 16.37$$

The absolute value of the slope of line A in the stability plot (Fig. 16.4), in which $\ln(\lambda_e^{ov})$ is plotted as a function of time, is equal to the first-order inactivation constant k_d . This is a straightforward consequence of Eq. (16.30) for first-order inactivation.

The relation now between $d(\ln \lambda_{er})/dt$ and $d(\ln \lambda_e^{ov})/dt$ can be derived as follows. With the aid of Eq. (16.25) it can be obtained that

$$\begin{aligned} \ln \lambda_e^{ov} &= \ln(\eta_{eii}(0)k(0) + k_{st}A') + \ln(\eta_{eii}k) \\ &\quad - \ln(\eta_{eii}k + k_{st}A') - \ln(\eta_{eii}(0)k(0)) \end{aligned} \quad (-) \quad 16.38$$

Differentiation with respect to time gives

$$\frac{d \ln \lambda_e^{ov}}{dt} = \frac{d \ln(\eta_{eii}k)}{dt} - \frac{d \ln(\eta_{eii}k + k_{st}A')}{dt} \quad (-) \quad 16.39$$

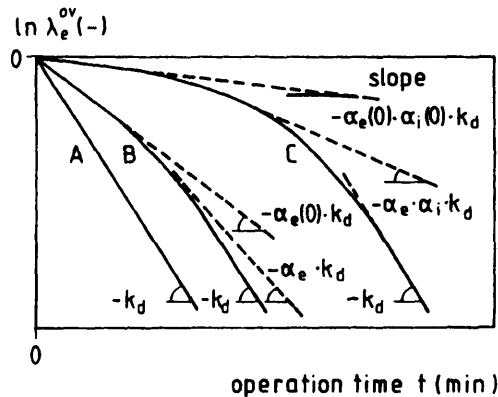


Fig. 16.4 Schematic relations of $\ln(\lambda_e^{\text{ov}})$ as a function of operating time t , for first-order enzyme decay, showing: (A) no diffusion limitation, (B) only internal diffusion limitation, (C) both internal and external diffusion limitation. (Adapted from Ooshima and Harano, 1983.)

because $\eta_{eii}(0)k(0)$ and $k_{s,i}A'$ are independent of time. The middle term can be rewritten into

$$\frac{d \ln(\eta_{eii} k)}{dt} = \frac{d \ln \eta_{eii}}{dt} + \frac{d \ln k}{dt} \quad (-) \quad 16.40$$

or

$$\frac{d \ln(\eta_{eii} k)}{dt} = \frac{d \ln \eta_{eii}}{d \ln \Phi} \frac{d \ln \Phi}{dt} + \frac{d \ln k}{dt} \quad (-) \quad 16.41$$

In the preceding chapter Eq. (15.36) was derived for a first-order reaction with the Thiele modulus equal to:

$$\Phi = \frac{1}{3} R_p \left(\frac{v_{\max}^0}{K_m |D_{sp}|} \right)^{0.5} = \frac{1}{3} R_p \left(\frac{k(1-\epsilon)}{|D_{sp}|} \right)^{0.5} \quad (-) \quad 16.42$$

or

$$\ln \Phi = \ln R_p - \ln 3 + \frac{\ln k}{2} + \frac{\ln(1-\epsilon)}{2} - \frac{\ln |D_{sp}|}{2} \quad (-) \quad 16.43$$

Differentiation with respect to time:

$$\frac{d \ln \Phi}{dt} = \frac{1}{2} \frac{d \ln k}{dt} \quad (-) \quad 16.44$$

Substitution in Eq. (16.41) yields:

$$\begin{aligned} \frac{d \ln(\eta_{\text{eff}} k)}{dt} &= \frac{d \ln \eta_{\text{eff}}}{d \ln \Phi} \frac{1}{2} \frac{d \ln k}{dt} + \frac{d \ln k}{dt} \\ &= \left(1 + \frac{1}{2} \frac{d \ln \eta_{\text{eff}}}{d \ln \Phi} \right) \frac{d \ln k}{dt} \end{aligned} \quad (-) \quad 16.45$$

The right term in Eq. (16.39) also can be worked out further to

$$\begin{aligned} \frac{d \ln(\eta_{\text{eff}} k + k_{\text{st}} A')}{dt} &= \frac{d \ln \left(\frac{\eta_{\text{eff}} k}{k_{\text{st}} A'} + 1 \right)}{dt} = \frac{d \ln(Da + 1)}{dt} \\ &= \frac{1}{Da + 1} \frac{d(Da + 1)}{dt} = \frac{1}{Da + 1} \frac{d Da}{dt} = \frac{Da}{Da + 1} \frac{d \ln Da}{dt} \end{aligned} \quad (-) \quad 16.46$$

In this equation ($k_{\text{st}} A'$ is constant)

$$\frac{d \ln Da}{dt} = \frac{d \ln(\eta_{\text{eff}} k)}{dt} \quad (-) \quad 16.47$$

Eqs. (16.45-16.47) lead to

$$\frac{Da}{Da + 1} \frac{d \ln Da}{dt} = \frac{Da}{Da + 1} \left[\left(1 + \frac{1}{2} \frac{d \ln \eta_{\text{eff}}}{d \ln \Phi} \right) \frac{d \ln k}{dt} \right] \quad (-) \quad 16.48$$

Substitution of Eqs. (16.45), (16.46) and (16.48) into Eq. (16.39) yields

$$\frac{d \ln \lambda_{\text{ov}}^{\text{ov}}}{dt} = \left[\frac{1}{Da + 1} \left(1 + \frac{1}{2} \frac{d \ln \eta_{\text{eff}}}{d \ln \Phi} \right) \right] \frac{d \ln k}{dt} \quad (-) \quad 16.49$$

Substituting

$$-\frac{d \ln k}{dt} = -\frac{d \ln \left(\frac{k}{k(0)} \right)}{dt} = k_d = -\frac{d \ln \lambda_{er}}{dt} \quad (-) \quad 16.50$$

in Eq. (16.49) yields:

$$-\frac{d \ln \lambda_e^{ov}}{dt} = \alpha_e \alpha_i \left(-\frac{d \ln \lambda_{er}}{dt} \right) = \alpha_e \alpha_i k_d \quad (-) \quad 16.51$$

In this equation α_e is the stabilization factor as result of external diffusion limitation, which is equal to:

$$\alpha_e = \frac{1}{Da + 1} \quad (-) \quad 16.52$$

The stabilization factor as a consequence of internal diffusion limitation, α_i , is equal to:

$$\alpha_i = 1 + \frac{1}{2} \frac{d \ln \eta_{oil}}{d \ln \Phi} \quad (-) \quad 16.53$$

Although not visible at first glance, this laborious derivation has yielded a relationship between the apparent and the intrinsic stability of an immobilized biocatalyst, which is particularly useful. This will become obvious when α_e and α_i are studied in more detail.

16.4.2.2 Apparent stabilization by external diffusion limitation

With respect to α_e there are the following two extreme situations:

No external diffusion limitation.

Infinite large rate limitation by diffusion of substrate.

In the first extreme $Da \ll 1$; in other words, α_e approaches 1, or in still other words, there is no stabilization of the immobilized biocatalyst as a result of external diffusion limitation. In the other extreme $Da \gg 1$. This means that α_e approaches 0. In this case the immobilized biocatalyst is infinitely stabilized. This at the same time means that the rate of conversion of substrate approaches the physical ceiling as described in Chapter 1 (i.z.i.; Fig. 1.2) and that biocatalyst approaches zero. The compromise between a sufficient stability and a sufficiently large rate of reaction is thus clearly shown here.

16.4.2.3 Apparent stabilization by internal diffusion limitation

The stabilization factor as result of internal diffusion limitation is less easy to analyze as it is not immediately clear what the numerical value of the term $d(\ln \eta_{eff})/d(\ln \Phi)$ is in case of infinite large internal diffusion limitation. If internal diffusion limitation can be neglected, the internal effectiveness factor for first-order kinetics η_{eff} approaches 1; i.e., $\ln \eta_{eff}$ approaches zero, and Φ approaches zero, thus $d(\ln \Phi)$ approaches $-\infty$. In this case the term $d(\ln \eta_{eff})/d(\ln \Phi)$ approaches zero and a , therefore 1, in other words no apparent stabilization as a result of internal diffusion limitation, as should be the case. In order to find out the numerical value of $d(\ln \eta_{eff})/d(\ln \Phi)$ when the internal diffusion limitation is very large, the relation between η_{eff} and Φ is needed. In Chapter 15 was derived for first-order kinetics (Eq. (15.38)).

$$\eta_{eff} = \frac{3\Phi \coth(3\Phi) - 1}{3\Phi^2} \quad (-) \quad 16.54$$

or

$$\eta_{eff} = \frac{1}{\Phi} \left(\frac{e^{3\Phi} + e^{-3\Phi}}{e^{3\Phi} - e^{-3\Phi}} \right) - \frac{1}{3\Phi^2} \quad (-) \quad 16.55$$

Differentiation with respect to Φ :

$$\frac{d\eta_{eff}}{d\Phi} = -\frac{1}{\Phi^2} \frac{A}{B} + \frac{1}{\Phi} \left(\frac{3B^2 - 3A^2}{B^2} \right) + \frac{2}{3} \frac{1}{\Phi^3} \quad (-) \quad 16.56$$

with $A = (e^{3\Phi} + e^{-3\Phi}) = 2\cosh(3\Phi)$

and $B = (e^{3\Phi} - e^{-3\Phi}) = 2\sinh(3\Phi)$

What should be known is $d(\ln \eta_{eff})/d(\ln \Phi)$:

$$\frac{d \ln \eta_{eff}}{d \ln \Phi} = \frac{\Phi}{\eta_{eff}} \frac{d \eta_{eff}}{d \Phi} \quad (-) \quad 16.57$$

At very large internal diffusion limitation Φ approaches infinity and η_{eff} zero. For Eq. (16.57) this leads to:

$$\begin{aligned} \lim_{\Phi \rightarrow \infty} \frac{\Phi}{\eta_{eff}} \frac{d\eta_{eff}}{d\Phi} &= \lim_{\Phi \rightarrow \infty} \frac{-\frac{1}{\Phi} \frac{A}{B} + \frac{3B^2 - 3A^2}{B^2} + \frac{2}{3\Phi^2}}{\frac{1}{\Phi} \frac{A}{B} - \frac{1}{3\Phi^2}} \\ &= \lim_{\Phi \rightarrow \infty} \frac{-\frac{1}{\Phi} \frac{A}{B}}{\frac{1}{\Phi} \frac{A}{B}} = -1 \end{aligned} \quad (-) \quad 16.58$$

Together with Eq. (16.53) this means that at very large internal diffusion limitation the internal stabilization factor α , approaches 0.5. In words this means that the immobilized biocatalyst obeying intrinsic first-order kinetics can be stabilized, at best with a factor 2, apparently, as a consequence of internal diffusion limitation.

16.4.2.4 Apparent stabilization on the reactor level

In the preceding section it was shown that in particular, external diffusion limitation can give rise to a large apparent stabilization of an immobilized biocatalyst in first-order reaction kinetics. In this section, however, only internal diffusion limitation will be considered, as on the reactor level the case of external diffusion limitation has not yet been worked out to our knowledge. The internal effectiveness η_{eff} for first-order kinetics has been derived in Chapter 15 and is given by Eq. (16.54), with the Thiele modulus Φ for a sphere given by:

$$\Phi = \frac{1}{3} R_p \left(\frac{V_{max}^\theta}{K_m D_{sp}} \right)^{0.5} \quad (-) \quad 16.59$$

Therefore, η_{eff} , is independent of the substrate concentration and Eq. (16.3) for the plug-flow reactor can thus be integrated, yielding

$$\frac{V}{F_i(t)} = - \frac{R_p^2 \ln(1 - x(t))}{(1 - \epsilon) D_{sp} 3(3\Phi(t) \coth 3\Phi(t) - 1)} \quad (\text{s}^{-1}) \quad 16.60$$

When the flow rate is adapted to keep the conversion constant in time, the following equation can be derived from Eq. (16.60):

$$\frac{F(t)}{F(0)} = \frac{\Phi(0) \sqrt{\frac{c_s^T(t)}{c_s^T(0)}} \coth \left(\Phi(0) \sqrt{\frac{c_s^T(t)}{c_s^T(0)}} \right) - 1}{\Phi(0) \coth \Phi(0) - 1} \quad (-) \quad 16.61$$

From Eq. (16.59) it can also be deduced that

$$\frac{\Phi(t)}{\Phi(0)} = \sqrt{\frac{C_e^T(t)}{C_e^T(0)}} \quad (-) \quad 16.62$$

For the fully reaction-controlled regime [$\Phi(0)$ approaches zero and η_{eff} one] Eq. (16.61) reduces to Eq. (16.9), as it should. For the completely diffusion-controlled regime [$\Phi(0)$ approaches infinity and η_{eff} zero] Eq. (16.61) becomes

$$\frac{F(t)}{F(0)} = \sqrt{\frac{C_e^T(t)}{C_e^T(0)}} \quad (-) \quad 16.63$$

which also holds for the Michaelis-Menten equation. Assuming the half-life to be at $F(t) = 0.5 F(0)$ Eq. (16.63) reveals that this is in fact double the true intrinsic half-life. This conclusion was also reached in the previous paragraph on the particle level. This also agrees with the fact that on the reactor level adaptation of the flow rate gives true operational half-lives in the absence of diffusion limitation, as was shown in the beginning of this chapter. When the flow rate is kept constant Eq. (16.60) can be reworked into

$$\frac{\ln(1-x(t))}{\ln(1-x(0))} = \frac{\Phi(0) \sqrt{\frac{C_e^T(t)}{C_e^T(0)}} \coth\left(\Phi(0) \sqrt{\frac{C_e^T(t)}{C_e^T(0)}}\right) - 1}{\Phi(0) \coth \Phi(0) - 1} \quad (-) \quad 16.64$$

Substituting again the two limiting cases of fully reaction controlled [$\Phi(0)$ approaches zero] and completely diffusion controlled [$\Phi(0)$ approaches infinity] yields Eq. (16.11) for the former and Eq. (16.65) for the latter:

$$\frac{\ln(1-x(t))}{\ln(1-x(0))} = \sqrt{\frac{C_e^T(t)}{C_e^T(0)}} \quad (-) \quad 16.65$$

Fig. 16.5 shows the conversion plotted according to this equation for first-order inactivation with $\Phi(0)$ as the parameter. As can be seen, the apparent stability in the plug-flow reactor is maximally 5.5 times larger than the true operational stability (dotted) line, which is the result of both internal diffusion limitation and the constant flow rate policy at initial conversion of 99%. For the CSTR it can similarly be derived that

$$\frac{V}{F_i(t)} = \frac{R_p^2 x(t)}{(1-\epsilon) D_{sp} 3(\Phi(t) \coth \Phi(t) - 1)(1-x(t))} \quad (\text{s}^{-1}) \quad 16.66$$

for first-order reaction kinetics influenced by intraparticle diffusion. If the flow rate is adapted to keep the conversion constant, Eq. (16.61) is obtained for this case with the same extremes and with the same annotations as for the plug flow reactor, i.e., maximal stabilization by a factor 2 as a result of internal diffusion limitation. However, when the flow rate is kept constant, Eq. (16.66) reduces to

$$\frac{\frac{x(t)}{1-x(t)}}{\frac{x(0)}{1-x(0)}} = \frac{\Phi(0) \sqrt{\frac{C_e^T(t)}{C_e^T(0)}} \coth \left(\Phi(0) \sqrt{\frac{C_e^T(t)}{C_e^T(0)}} \right) - 1}{\Phi(0) \coth \Phi(0) - 1} \quad (-) \quad 16.67$$

In reaction-controlled kinetics [$\Phi(0)$ approaches zero] Eq. (16.67) is further reduced to Eq. (16.14). For fully diffusion-controlled kinetics [$\Phi(0)$ approaches infinity] Eq. (16.67) results in

$$\frac{\frac{x(t)}{1-x(t)}}{\frac{x(0)}{1-x(0)}} = \sqrt{\frac{C_e^T(t)}{C_e^T(0)}} \quad (-) \quad 16.68$$

The time courses of $x(t)$ as given by Eq. (16.67) for first-order decay are shown in Fig. 16.5 with $\Phi(0)$ as the parameter. The dotted line represents the intrinsic stability of the biocatalyst. A maximum apparent stabilization of about 13 times is observed, which is the result of both intraparticle diffusion limitation and feed-rate policy.

16.4.2.5 Conclusions for first-order kinetics

In summary, it can be stated that when the aim is the development of an immobilized biocatalyst as stable as practically possible, external diffusion limitation can apparently stabilize the activity to a large extent. In the most extreme case the activity of the biocatalyst at the surface of the particle is so large that every molecule of substrate that reaches the surface, and thus the biocatalyst, is immediately converted. The effective concentration of substrate at the surface is thus zero. This in principle means not only an infinite apparent stabilization, but also a maximal mass transfer to the pertinent immobilized biocatalyst particle at the applied conditions, as the substrate concentration driving force in

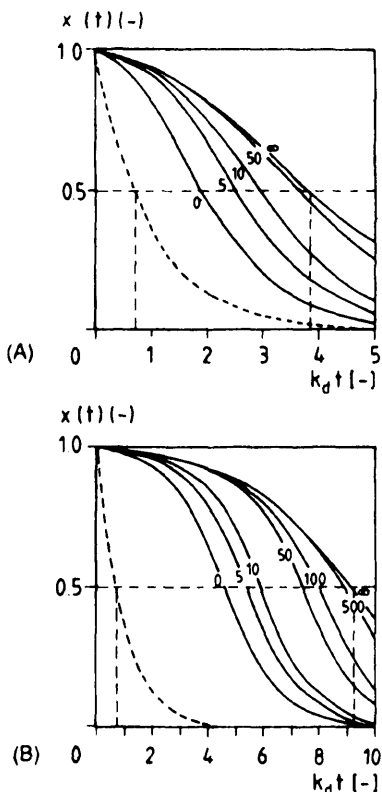


Fig. 16.5 Conversion x as a function of dimensionless time $k_d t$ in (A) a plug-flow reactor and (B) a CSTR for spherical immobilized enzyme particles, first-order enzyme decay, constant flow and an initial conversion of 99%. Figure on each line is the value of $\Phi(0)$. (Adapted from Yamana et al., 1987.)

$$F_s^u = k_{st} A' (C_{sb} - C_{si}) \quad (\text{mol m}^{-3} \text{s}^{-1}) \quad 16.69$$

is maximal ($C_{si} = 0$). This means that the immobilized biocatalyst particles operate against the physical ceiling, as was discussed in Chapter 1. In other words, this means that when the fraction of immobilized biocatalyst particles in the reactor is as high as practically possible, the bioreactor operates at maximal volumetric productivity under the conditions applied. It also means, at the same time, that the efficiency of the biocatalyst is minimal, approaches zero, and this, as we have seen before, is not always desired, especially when a very expensive biocatalyst is involved.

16.4.3 Apparent stabilization for zero-order kinetics

The internal effectiveness factor η_{eo} for zero-order kinetics has been derived in Chapter 15 to be

$$\eta_{eo} = 1 - \left\{ \frac{1}{2} + \cos \left[\frac{1}{3} \cos^{-1} \left(\frac{2}{3\Phi} - 1 \right) + \frac{4\pi}{3} \right] \right\}^3 \quad (16.70)$$

for

$$\Phi = R_p \left(\frac{v_{max}^0}{18 D_{sp} C_{si}} \right)^{0.5} > 0.5774 \quad (16.71)$$

$$\text{and } \eta_{eo} = 1 \quad \text{for } \Phi \leq 0.5774 \quad (16.72)$$

In Eq. (16.71) C_{si} is the substrate concentration at the surface of the biocatalyst particle, which is about the same as the bulk fluid concentration in case of negligible external diffusion limitation as assumed here. At constant-conversion policy the following equations can be derived for the plug-flow reactor by means of Eqs. (16.3), (16.70) and (16.71). First, when $\Phi > 0.5774$ at time zero for the substrate concentration at the inlet of the plug-flow reactor, it can be obtained that

$$\frac{V}{F_i} = \frac{2 R_p^2}{(1 - \epsilon) D_{sp}} \times \int_{\Phi(C_{so})}^{\Phi(C_{si})} \frac{d\Phi}{\Phi^3 \left(1 - \left\{ \frac{1}{2} + \cos \left[\frac{1}{3} \cos^{-1} \left(\frac{2}{3\Phi} - 1 \right) + \frac{4\pi}{3} \right] \right\} \right)} \quad (16.73)$$

When at time $t = t_0$ the activity has dropped so far that $\Phi(C_{si})$ has become 0.5774, the equation after time t reads

$$\frac{V}{F_i} = \frac{2 R_p^2}{(1 - \epsilon) D_{sp}} \left[\int_{\Phi(C_{so})}^{0.5774} \frac{d\Phi}{\Phi^3} + \int_{0.5774}^{\Phi(C_{so})} \frac{d\Phi}{\Phi^3 \left(1 - \left\{ \frac{1}{2} + \cos \left[\frac{1}{3} \cos^{-1} \left(\frac{2}{3\Phi} - 1 \right) + \frac{4\pi}{3} \right] \right\} \right)} \right] \quad (16.74)$$

Using as relationships

$$\Phi(C_{si}, t = t) = \Phi(C_{si}, t = 0) e^{-k_a t / 2} \quad (-) \quad 16.75$$

and

$$\Phi(C_{so}) = 10 \Phi(C_{si}) \quad (-) \quad 16.76$$

Yamane et al. (1987) have numerically worked out Eqs. (16.73) and (16.74) and the results are shown in Fig. 16.6. When $\Phi(t = 0) \ll 0.5774$, i.e., negligible diffusion limitation, $F_i(t)/F_i(0)$ approaches, as it should, Eq. (16.9), whereas when $\Phi(t = 0) \gg 0.5774$ it approaches Eq. (16.63) and the same annotations do apply.

Similarly, equations for the CSTR can be derived:

$$\frac{F_i(t)}{F_i(0)} = \frac{1 - \left\{ \frac{1}{2} + \cos \left[\frac{1}{3} \cos^{-1} \left(\frac{2}{3\Phi^2(t)} \frac{C_s^T(0)}{C_s^T(t)} - 1 \right) + \frac{4\pi}{3} \right] \right\}^3}{1 - \left\{ \frac{1}{2} + \cos \left[\frac{1}{3} \cos^{-1} \left(\frac{2}{3\Phi^2(0)} - 1 \right) + \frac{4\pi}{3} \right] \right\}^3} \frac{C_s^T(t)}{C_s^T(0)} \quad (-) \quad 16.77$$

with

$$\Phi(0) = R_p \left(\frac{V_{max}}{18 D_{sp} C_{so}} \right)^{0.5} \quad (-) \quad 16.78$$

After $\Phi(0) \sqrt{C_s(t)/C_s(0)} < 0.5774$, i.e., no more diffusion limitation, Eq. (16.77) reduces to

$$\frac{F_i(t)}{F_i(0)} = \frac{1}{1 - \left\{ \frac{1}{2} + \cos \left[\frac{1}{3} \cos^{-1} \left(\frac{2}{3\Phi^2(0)} - 1 \right) + \frac{4\pi}{3} \right] \right\}^3} \frac{C_s^T(t)}{C_s^T(0)} \quad (-) \quad 16.79$$

Similar to the plug-flow reactor $F_i(t)/F_i(0)$ for the CSTR approaches for this case Eq. (16.9) when $\Phi(0) \leq 0.5774$ and Eq. (16.63) for $\Phi(0) > 0.5774$. Fig. 16.6 shows that, as can be expected, all lines lie between the fully reaction-controlled extreme ($\eta_{si}(0) = 1$) and the completely diffusion-controlled extreme ($\Phi(0) \rightarrow \infty$) with $F_i(t)/F_i(0) = e^{(-k_a t / 2)}$. This indicates that intraparticle diffusion limitation does not

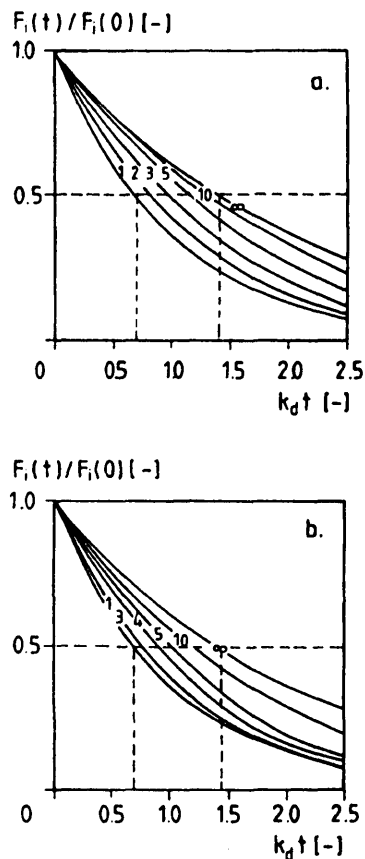


Fig. 16.6 $F_i(t)/F_i(0)$ as a function of dimensionless time $k_d t$ for internal diffusion limited, zero-order reaction kinetics of spherical immobilized enzyme particles (A) packed in plug flow reactor or (B) suspended in CSTR. Operation at constant conversion ($x = 0.99$). First-order enzyme inactivation. Figure on each line is value of $\phi(0)$. Curves of $\phi(0) = 1$ and $\phi(0) = \infty$ correspond to $F_i(t)/F_i(0) = e^{-k_d t}$ and $F_i(t)/F_i(0) = e^{-k_d t/2}$, respectively. (Adapted from Yamane et al., 1987.)

affect to a great extent the apparent stability of an immobilized biocatalyst, obeying zero-order kinetics, when the conversion is kept constant. Yamane et al. (1987) have not worked out the constant-feed rate cases. Also, the Michaelis-Menten kinetics cases, for which no analytical expressions can be derived, have not been worked out.

16.4.4 Effect of initial conversion on apparent stability

In addition to the case of an initial conversion of 99% [$x(0) = 0.99$], Yamane et al. (1987) also have done some calculations for $x(0) = 0.9$. Only the constant-feed rate situations were considered, as "it is no doubt that the apparent half-life does not vary with $x(0)$ at the constant-conversion policy," according to these authors. Table 16.1 shows their results. The apparent half-lives decrease as the initial conversion decreases and the intrinsic stability is better approached as such.

16.5 Conclusions

The apparent stability of an immobilized biocatalyst in a continuous reactor depends on many factors, such as order of reaction, feeding policy, initial

Table 16.1 Comparison of apparent half-life of spherical immobilized enzyme under constant-feed rate policy for cases of $x(0) = 0.99$ and $x(0) = 0.90$; first-order enzyme inactivation.

(i) Michaelis-Menten kinetics at $\eta_*^{\text{ov}} = 1$

K	Plug-flow reactor		CSTR	
	$x(0) = 0.99$	$x(0) = 0.90$	$x(0) = 0.99$	$x(0) = 0.90$
0	0.69	0.69	0.69	0.69
0.1	0.93	0.80	2.91	1.22
0.5	1.37	1.01	3.94	1.84
∞	1.91	1.35	4.62	2.40

(ii) First-order reaction under $\eta_*^{\text{ov}} < 1$

$\Phi(0)$	Plug-flow reactor		CSTR	
	$x(0) = 0.99$	$x(0) = 0.90$	$x(0) = 0.99$	$x(0) = 0.90$
0	1.91	1.35	4.62	2.40
5	2.53	1.87	5.34	3.06
10	2.95	2.20	5.89	3.54
50	3.60	2.59	7.35	4.43
∞	3.82	2.70	9.23	4.80

Source: Adapted from Yamane et al., 1987.

conversion, involvement of diffusion limitation and bioreactor configuration. In this chapter the situations worked out by Yamane et al. (1987) and Ooshima and Harano (1983) have been considered, as they elegantly demonstrate the effects on both particle and reactor level. Although the paper of Sadana (1989) goes even further, the complexity of the material and the scope of this book do not allow an easy and brief incorporation of this interesting work, and it has thus for those reasons been left out. Summarizing with Yamane et al. (1987), the following concluding remarks can be made. If the apparent half-life is regarded as the time at which the flow rate is half of the initial one with the constant-conversion policy, or as the time at which the conversion is half of the initial one with the constant-feed rate policy, it is mostly greater than the intrinsic half-life of the biocatalyst. The cases where the apparent half-lives coincide with the intrinsic one are when the constant-conversion policy applies and diffusion limitation is absent. This is also the case for zero-order kinetics in the constant-flow-rate operation, again in the absence of diffusion limitation. Internal diffusion limitation always increases the apparent half-life, but only to a limited extent; this is in contrast to external diffusion limitation, which in theory can apparently infinitely stabilize the biocatalyst. In comparison to the CSTR, the plug-flow reactor gives closer values to the intrinsic ones, in most cases. So does the constant-conversion policy as compared to the constant-feed rate policy, and the same can be said for zero-order kinetics as compared to higher-order kinetics. Table 16.1, finally, suggests that smaller initial conversions give a smaller, and thus a closer to intrinsic, apparent half-life. In determining the operational stability of an immobilized biocatalyst all these factors should obviously be considered.

16.6 Examples

Example 16.1 Stabilization by external diffusion limitation

The oxygen-consuming enzyme described in Example 15.1 has a half-time of 1 day and inactivates according to a first-order process.

Calculate:

The stabilization factor on day 1 to 30.

Data:

See Example 15.1

Solution:

In Example 15.1 it was shown that for case ii with the low activity there is no significant diffusion limitation. In that case apparent stabilization is also

negligible. For case i, on the other hand, with the high activity, a very small $\eta_e^{ov} = \eta_{ee} = 2.7 \times 10^{-5}$ was calculated. Since there can only be external dif-

fusion limitation - the enzyme is immobilized only on the outer surface - apparent stabilization can only be the result of this external resistance. The stabilization factor as a result of external diffusion limitation α_e can be calculated by means of Eq. (16.52):

$$\alpha_e = \frac{1}{D\alpha + 1} \quad (-) \quad 16.52$$

The Damköhler number $D\alpha$ is

$$D\alpha(t) = \frac{\eta_{ell}(t) k(t)}{k_{sl} A'} \quad (-) \quad 16.26$$

Rewriting this equation for one enzyme particle gives, with $\eta_{ell} = 1$ (no internal diffusion limitation):

$$D\alpha = \frac{k'(t)}{k_{sl} \alpha} = \frac{v_{max}(t) C_x''}{K_m k_{sl} \alpha} \quad (-) \quad 16.80$$

In Example 15.1 $k_{sl} = k_{ol}$ was calculated to be $1.3 \times 10^{-4} \text{ m s}^{-1}$. Substituting this with the other pertinent numerical values in Eq. (16.80) yields $D\alpha$ as a function of $v_{max}(t)$:

$$D\alpha = \frac{v_{max}(t) \times 10^{-6}}{0.12 \times 1.3 \times 10^{-4} \times \pi \times 10^{-6}} = 2.04 \times 10^4 v_{max}(t)$$

Substituting this in Eq. (16.55) and subsequently in Eq. (16.51) gives:

$$\begin{aligned} -\frac{d \ln \lambda_{ov}^{ov}}{dt} &= \alpha_e \alpha_i \left(-\frac{d \ln \lambda_{or}}{dt} \right) = \alpha_e k_d \\ &= \frac{k_d}{D\alpha + 1} = \frac{k_d}{2.04 \times 10^4 v_{max}(t) + 1} \end{aligned}$$

For first-order inactivation $v_{max}(t)$ can be written as

$$v_{max}(t) = v_{max}(0) e^{-k_d t}$$

For an enzyme with a half-life of 1 day $k_d = \ln(2)/1 = 0.69 \text{ d}^{-1}$. This gives with $v_{max}(0) = 6.5 \text{ mol s}^{-1} \text{ g}^{-1}$:

$$-\frac{d \ln \lambda_e^{ov}}{dt} = \frac{0.69}{13.26 \times 10^4 e^{-0.69t} + 1}$$

Integration finally gives

$$\ln \lambda_e^{ov}(t) = -0.69t - \ln\left(1 + \frac{13.26 \times 10^4}{e^{0.69t}}\right) + 11.80$$

Fig. 16.7 is the graphic presentation of this equation, in addition to the intrinsic stability (line with the slope $k_d = 0.69 \text{ d}^{-1}$). Clearly, the external diffusion limitation initially strongly stabilizes the immobilized enzyme.

Example 16.2 Constant conversion vs. constant flow

In a continuous, ideally mixed membrane reactor 1000 kg of a poorly soluble steroid is produced per year using a soluble enzyme (10 kg m^{-3}), which is retained in the reactor. The operational half-time of the enzyme is 10 days (first-order inactivation); the time of one run is 30 days and there are 10

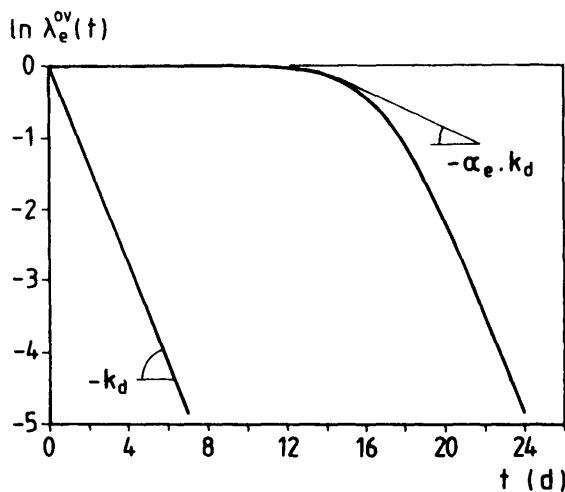


Fig. 16.7 Example of external diffusion limitation.

runs per year. The flow is controlled such that the conversion is always 90%; the product concentration in the outflow is 0.1 kg m^{-3} and the selectivity is $0.85 \text{ kg product per kg substrate}$. The kinetic constants are

$$K_m = 0.01 \text{ kg m}^{-3} \text{ and}$$

$$v_{max} = 10^{-3} \text{ kg s}^{-1} \text{ kg}^{-1} \text{ (Michaelis-Menten kinetics).}$$

Calculate the overall volumetric productivity of the bioreactor on a yearly basis and the initial and end flow of a run. What will be the conversion after 30 days if the flow is kept constant?

Solution:

The product concentration in the effluent is 0.1 kg m^{-3} ; in other words, $0.1/0.85 = 0.118 \text{ kg m}^{-3}$ of substrate has been converted to reach this concentration. The conversion is fixed by control of the flow to 90%; thus $0.118/0.9 = 0.131 \text{ kg m}^{-3}$ is the concentration of substrate in the inflow. Therefore, the concentration of substrate in the reactor is $0.131 - 0.118 = 0.013 \text{ kg m}^{-3}$. Substitution of appropriate values in the Michaelis-Menten equation yields:

$$\begin{aligned} -r_s^u(t=0) &= \frac{10^{-3} \times 10 \times 0.013}{0.01 + 0.013} = 5.67 \times 10^{-3} \text{ kg s}^{-1} \text{ m}^{-3} \\ &= 4.8 \times 10^2 \text{ kg d}^{-1} \text{ m}^{-3} \end{aligned}$$

First-order enzyme inactivation with $t_{0.5} = 10 \text{ days}$ gives $k_d = \ln(2)/10 = 0.069 \text{ d}^{-1}$.

The amount of product Q'_p produced in 1 run in one m^{-3} of reactor can now be calculated from

$$Q'_p = Y_{ps}^{ov} \int_0^{30} -r_s^u(t=0) e^{-0.069t} dt$$

Substitution of appropriate values and integration gives $Q'_p = 5241 \text{ kg m}^{-3}$ in one run. Per run 100 kg should be produced; thus the reactor volume required is 0.019 m^3 . The overall volumetric productivity on a yearly basis is then $1000 (\text{kg y}^{-1})/0.019 \text{ m}^3 = 52\,414 \text{ kg m}^{-3} \text{ y}^{-1}$.

With the aid of Eq. (16.9) the flow rate can be written as a function of time as

$$\frac{F_i(t)}{F_i(0)} = \frac{C_e^T(t)}{C_e^T(0)} = e^{-k_d t}$$

$$F_i(t) = F_i(0) e^{-k_d t}$$

Integration over 30 days gives the total flow per run, which can also be calculated from the product concentration and the total amount of product produced in one run, i.e., $100 \text{ kg}/(0.1 \text{ kg m}^{-3}) = 1000 \text{ m}^3$ per run:

$$\int_{F_i(0)}^{F_i(30)} dF_i(t) = 1000 = -\frac{1}{k_d} \int_0^{30} F_i(0) e^{-k_d t} dt$$

Substitution of the appropriate values and integration gives $F_i(0) = 79 \text{ m}^3 \text{ d}^{-1}$ and from that $F_i(30) = 60.6 e^{-0.069 \times 30} = 10 \text{ m}^3 \text{ d}^{-1}$.

At constant flow rate the conversion after 30 days can be calculated from Eq. (16.13), yielding $x(30) = 0.53$, i.e., 53%, which very likely is unacceptable from the point of view of inefficient substrate use and with regard to downstream processing, unless product separation is easy and substrate recycling is possible.

References

Levenspiel O. "Chemical reaction engineering." 2nd ed. Wiley, New York (1972).

Ooshima H. and Harano Y. "Effects of mass-transfer resistance on apparent stability and performance of fixed-bed immobilized enzyme reactors: theory and experiments with immobilized invertase." Biotechnol. Bioeng. 25, 143 (1983).

Sadana A. "Enzyme deactivation in reactors." Biocatalysis 2, 175 (1989).

Yamane T., Sirirote P. and Shimizu S. "Evaluation of half-life of immobilized enzyme during continuous reaction in bioreactors: a theoretical study." Biotechnol. Bioeng. 30, 963 (1987).

17

Macrokinetics: Reactor Level

17.1 Introduction

In the preceding chapters the most generally used kinetic equations for describing the consumption of substrate as a result of biocatalysis and cell growth have been given and/or derived. In biocatalysis in the absence of limitation of the rate of consumption by diffusion of substrate, the Michaelis-Menten equation usually is a good description:

$$-r_s^u = v_{max} \frac{C_s}{K_m + C_s} \quad (\text{mol m}^{-3} \text{s}^{-1}) \quad 17.1$$

in which

$-r_s^u$	= substrate consumption rate per unit volume	$(\text{mol m}^{-3} \text{s}^{-1})$
v_{max}	= maximum substrate conversion rate	$(\text{mol m}^{-3} \text{s}^{-1})$
C_s	= substrate concentration	(mol m^{-3})
K_m	= Michaelis-Menten constant	(mol m^{-3})

When diffusion limitation cannot be excluded, an overall effectiveness factor η_e^{ov} (-) is introduced:

$$-r_s^u = \eta_e^{ov} v_{max} \frac{C_s}{K_m + C_s} \quad (\text{mol m}^{-3} \text{s}^{-1}) \quad 17.2$$

When substrate is consumed as result of cell growth (or respiration), the Monod equation generally suffices:

$$\mu = \mu_{max} \frac{C_s}{K_s + C_s} \quad (\text{s}^{-1}) \quad 17.3$$

in which

μ	= growth rate	(s ⁻¹)
μ_{max}	= maximum growth rate	(s ⁻¹)
K_s	= Monod constant	(mol m ⁻³)

Similar to the Michaelis-Menten equation, an overall effectiveness factor can be introduced in the Monod equation to account for diffusion limitation of immobilized growing cells. However, no generally proven models exist for this situation yet.

On the basis of a mass balance the following general equations describing the basic reactor concepts, have been derived in Chapter 1. For the batch reactor the time t_b (s) needed for a conversion of a component i from $C_i(0)$ at $t = 0$ to $C_i(\text{end})$ is given by:

$$t_b = \int_{C_i(0)}^{C_i(\text{end})} \frac{dC_i}{r_i^u} \quad (\text{s}) \quad 17.4$$

The mass balance over a continuous stirred-tank reactor (CSTR) in the steady state yields for the average residence τ_{CSTR} (s):

$$\tau_{CSTR} = \frac{V}{F_i} = \frac{C_{ii} - C_{io}}{-r_i^u} \quad (\text{s}) \quad 17.5$$

in which

C_{ii}	= concentration of i in the inflow	(mol m ⁻³)
C_{io}	= concentration of i in the outflow	(mol m ⁻³)

For a CSTR which is assumed to be ideally mixed, the concentration in the reactor, C_{ir} , is equal to the concentration in the outflow, C_{io} .

Similarly, for the j -th reactor in a cascade of n CSTRs:

$$\tau_{CSTR,j} = \frac{V_j}{F_i} = \frac{C_{i,j-1} - C_{i,j}}{-r_{i,j}^u} \quad (\text{s}) \quad 17.6$$

Finally, for the plug-flow reactor it was derived that:

$$\tau_{pf} = \frac{V}{F_i} = \int_{C_{ii}}^{C_{io}} \frac{dC_i}{r_i^u} \quad (\text{s}) \quad 17.7$$

These are the equations which will be integrated below to come up with the basic overall bioreactor models.

17.2 The batch bioreactor

17.2.1 Michaelis-Menten kinetics

Substitution of Eq. (17.1) in Eq. (17.4) gives for the substrate s :

$$t_b = - \int_{C_s(0)}^{C_s(\text{end})} \frac{(K_m + C_s) dC_s}{v_{max} C_s} \quad (\text{s}) \quad 17.8$$

Working this equation out gives:

$$t_b = \frac{K_m}{v_{max}} \ln\left(\frac{C_s(0)}{C_s(\text{end})}\right) + \frac{C_s(0) - C_s(\text{end})}{v_{max}} \quad (\text{s}) \quad 17.9$$

When the kinetic constants, the initial concentration of substrate and the desired conversion are known, the required batch time t_b can thus easily be calculated.

17.2.2 Mass transfer integrated with Michaelis-Menten kinetics

Substitution of Eq. (17.2) in Eq. (17.4) gives:

$$t_b = - \int_{C_s(0)}^{C_s(\text{end})} \frac{(K_m + C_s) dC_s}{\eta_s^{ov} v_{max} C_s} \quad (\text{s}) \quad 17.10$$

This equation cannot be integrated immediately as η_s^{ov} is a function of the substrate concentration C_s . A possible procedure is calculation of the overall effectiveness factor η_s^{ov} at n substrate concentrations in the range of $C_s(0)$ to $C_s(\text{end})$. Through this n (η_s^{ov} , C_s) data pairs an n -th order polynomial is fitted. This polynomial is substituted in Eq. (17.10) such that integration is possible.

17.2.3 Monod growth kinetics

Pirt (1985) shows that in addition to Eq. (17.3) for consumption of substrate as a result of growth of cells, two additional equations are needed to

describe the system. First, the equation describing the biomass production is:

$$r_x^u = \frac{dC_x(t)}{dt} = \mu C_x(t) \quad (\text{mol m}^{-3} \text{s}^{-1}) \quad 17.11$$

Second, the equation defining the yield factor of biomass on substrate Y_{xs} , (-) at zero maintenance requirements is:

$$Y_{xs} = \frac{C_x(t) - C_x(0)}{C_s(0) - C_s(t)} \quad (-) \quad 17.12$$

Rearranging:

$$C_s(t) = C_s(0) - \frac{C_x(t) - C_x(0)}{Y_{xs}} \quad (\text{mol m}^{-3}) \quad 17.13$$

Substitution of Eq. (17.13) in Eq. (17.3) gives:

$$\mu = \mu_{max} \frac{\frac{C_s(0) - \frac{C_x(t) - C_x(0)}{Y_{xs}}}{Y_{xs}}}{K_s + C_s(0) - \frac{C_x(t) - C_x(0)}{Y_{xs}}} \quad (\text{s}^{-1}) \quad 17.14$$

or

$$\mu = \mu_{max} \frac{Y_{xs} C_s(0) - C_x(t) + C_x(0)}{Y_{xs} K_s + Y_{xs} C_s(0) - C_x(t) + C_x(0)} \quad (\text{s}^{-1}) \quad 17.15$$

Substitution of this equation in Eq. (17.11) and integration yields:

$$\int_{C_x(0)}^{C_x(t)} \frac{Y_{xs} K_s + Y_{xs} C_s(0) - C_x(t) + C_x(0)}{Y_{xs} C_s(0) - C_x(t) + C_x(0)} \frac{dC_x(t)}{C_x(t)} = \mu_{max} \int_0^t dt \quad (-) \quad 17.16$$

By conversion to partial fractions, the left-hand side of Eq. (17.16) becomes:

$$A \int_{C_x(0)}^{C_x(t)} \frac{dC_x(t)}{C_x(t)} + B \int_{C_x(0)}^{C_x(t)} \frac{dC_x(t)}{Y_{xs} C_s(0) - C_x(t) + C_x(0)} \quad (-) \quad 17.17$$

with

$$A = \frac{Y_{xs} K_s + Y_{xs} C_s(0) + C_x(0)}{Y_{xs} C_s(0) + C_x(0)} \quad (-) \quad 17.18$$

and

$$B = \frac{Y_{xs} K_s}{Y_{xs} C_s(0) + C_x(0)} \quad (-) \quad 17.19$$

Integration yields:

$$A \ln\left(\frac{C_x(t)}{C_x(0)}\right) - B \ln\left(\frac{Y_{xs} C_s(0) + C_x(0) - C_x(t)}{Y_{xs} C_s(0)}\right) = \mu_{max} t \quad (-) \quad 17.20$$

Eq. (17.20) gives the well-known S-shaped curve of batch growth in which the value of $C_x(t)$ tends asymptotically to the value $[Y_{xs} C_s(0) + C_x(0)]$. By means of Eq. (17.13) for each value of C_x the corresponding C_s can be calculated, such that C_s is also known as a function of time as well.

17.3 The fed-batch reactor

17.3.1 Michaelis-Menten kinetics

For Michaelis-Menten kinetics the fed-batch equations are difficult to solve. As the practical value is also low it will not be discussed in this chapter.

17.3.2 Monod growth kinetics

Pirt (1985) shows the results for this case. In contrast to fed-batch biocatalysis, the practical importance of fed-batch fermentations is very large, either for production of biomass (e.g., baker's yeast) or for production of cell metabolites (e.g., penicillin). Therefore, the appropriate theory of the fed-batch culture will be derived here to show the unique properties.

Assume a homogeneous batch culture in which growth is limited, or will be limited after a batch growth phase, by the concentration of one substrate while all the other essential nutrients are present in excess. If $C_s(0)$ is the initial concentration of this growth-limiting substrate and $C_{sr}(t)$ the biomass concentration at time t , then for the case that the maintenance requirements can be neglected:

$$C_{xr}(t) = C_{xr}(0) + Y_{xs} (C_{sr}(0) - C_{sr}(t)) \quad (\text{mol m}^{-3}) \quad 17.21$$

with $C_{xr}(0)$ the concentration of biomass immediately after inoculation (time $t = 0$). It is further assumed that when the biomass concentration reaches its maximum value, C_{xrmax} (mol m^{-3}), the growth-limiting substrate is practically exhausted so that $C_{sr}(t) \ll C_{sr}(0)$. If the concentration of biomass at time $t = 0$ is small compared to the final concentration, Eq. (17.21) reduces to:

$$C_{xrmax} = Y_{xs} C_{sr}(0) \quad (\text{mol m}^{-3}) \quad 17.22$$

When the situation of Eq. (17.22) is reached, a medium feed is started at flow rate F_i , and with the growth-limiting substrate at concentration $C_{sr}(0)$ in the feed medium. The total amount of biomass in the fed-batch culture is given by:

$$M_{xr}(t) = C_{xr}(t) V(t) \quad (\text{mol}) \quad 17.23$$

or

$$C_{xr}(t) = \frac{M_{xr}(t)}{V(t)} \quad (\text{mol m}^{-3}) \quad 17.24$$

Differentiation gives

$$\frac{dC_{xr}(t)}{dt} = \frac{V(t) \frac{dM_{xr}(t)}{dt} - M_{xr}(t) \frac{dV(t)}{dt}}{(V(t))^2} \quad (\text{mol m}^{-3} \text{s}^{-1}) \quad 17.25$$

In this equation

$$\frac{dM_{xr}(t)}{dt} = \mu M_{xr}(t) \quad (\text{mol s}^{-1}) \quad 17.26$$

and

$$\frac{dV(t)}{dt} = F_i \quad (\text{m}^3 \text{s}^{-1}) \quad 17.27$$

while

$$\frac{F_i}{V(t)} = D \quad (\text{s}^{-1}) \quad 17.28$$

with D as the dilution rate. Substitution in Eq. (17.25) yields

$$\frac{dC_{xr}(t)}{dt} = (\mu - D) C_{xr}(t) \quad (\text{mol m}^{-3}) \quad 17.29$$

The first case that we will discuss is that at the end of the batch period the biomass concentration is equal to $C_{xr\max}$ and is not allowed to increase further. If the relationship between the specific growth rate and the concentration of growth-limiting substrate is of the Monod type [Eq. (17.3)] and when $C_{sr}(0) \gg K_s$, over most of the range of μ from zero upward, the growth-limiting substrate will be almost completely utilized so that when $C_{xr}(t)$ is $C_{xr\max}$ is about $Y_{xs} C_{sr}(0)$. From that moment on $dC_{xr}(t)/dt$ is about zero. Under these conditions it follows from Eq. (17.29) that μ is about D . A substrate mass balance over the reactor gives:

$$\frac{dM_{sr}(t)}{dt} = F_i C_{sr}(0) - \frac{\mu M_{xr}(t)}{Y_{xs}} \quad (\text{mol s}^{-1}) \quad 17.30$$

When $M_{xr}(t) = V(t)C_{xr\max}$ virtually all of the substrate is consumed as fast as it enters the culture so that $F_i C_{sr}(0)$ is about equal to $\mu M_{xr}(t)/Y_{xs}$. Hence $dM_{sr}(t)/dt$ and $dC_{sr}(t)/dt$ are about zero. In this so-called quasi-steady state $dC_{xr}(t)/dt$ and $dC_{sr}(t)/dt$ are thus about zero and μ is about equal to D .

To obtain the concentration of the growth-limiting substrate as a function of the dilution or feed rate D in this quasi-steady state, $\mu = D$ is substituted in the Monod equation:

$$C_{sr}(t) = \frac{D K_s}{\mu_{max} - D} \quad (\text{mol m}^{-3}) \quad 17.31$$

The rate of increase in the total amount of biomass during this quasi-steady state is given by:

$$\frac{dM_{xr}(t)}{dt} = F_i Y_{xs} C_{sr} \quad (\text{mol s}^{-1}) \quad 17.32$$

Integration:

$$M_{xr}(t) = M_{xr}(0) + F_i Y_{xs} C_{sr}(0) t \quad (\text{mol}) \quad 17.33$$

Comparing a fed-batch culture in the quasi-steady state with a CSTR in a steady state (see also next section), in both cases in effect we have $\mu = D$ but, whereas D is constant in the CSTR, the so-called chemostat, in a fed-batch culture D is decreasing and μ is assumed to decrease at the same rate. The unique feature of fed-batch fermentations is that, in the quasi-steady state, the biomass is in a transient state with the growth rate under control.

The second case to be discussed is where C_{xr} is allowed to increase further during the "fed" period. Example 2.1 shows this for oxygen or carbon substrate limitation where the growth rate decreases with time to fit the requirements of the limitation. For each fed-batch situation the relevant equation can be derived and the relevant data can be calculated, either analytically or numerically. Example 2.1 also shows that with a fed-batch very high concentrations of biomass (and product) can be obtained. This is one of the reasons that this is a reactor concept of large practical importance.

17.4 The continuous-flow stirred-tank reactor (CSTR)

17.4.1 Michaelis-Menten kinetics

Substitution of Eq. (17.1) in the general equation for the CSTR [Eq. (17.5)] yields:

$$\tau_{CSTR} = \frac{V}{F_i} = \frac{(C_{si} - C_{sr})(K_m + C_{sr})}{v_{max} C_{sr}} \quad (\text{s}) \quad 17.34$$

with $C_{sr} = C_{so}$ for an ideally mixed solution. For any desired conversion the required residence time can thus be calculated directly.

17.4.2 Mass transfer integrated with Michaelis-Menten kinetics

Analogous to the above ordinary Michaelis-Menten kinetics, substitution of Eq. (17.2) in Eq. (17.5) yields a formula which allows straightforward calculation of the residence time required for a specific conversion:

$$\tau_{CSTR} = \frac{V}{F_i} = \frac{(C_{si} - C_{sr})(K_m + C_{sr})}{\eta_e^{ov} v_{max} C_{sr}} \quad (\text{s}) \quad 17.35$$

again with $C_{sr} = C_{so}$

17.4.3 Monod growth kinetics

Concerning substrate consumption substitution of Eq. (17.3) in the general equation for the CSTR [Eq. (17.5)] is not immediately possible. Pirt (1985) has dealt with this problem. In order to get the units right, for $-r_s^u$ the following should be substituted (when maintenance can be neglected):

$$-r_s^u = \mu \frac{C_{xr}}{Y_{xs}} \quad (\text{mol m}^{-3} \text{s}^{-1}) \quad 17.36$$

or

$$r_s^u = \mu_{max} \frac{C_{sr} C_{xr}}{(K_s + C_{sr}) Y_{xs}} \quad (\text{mol m}^{-3} \text{s}^{-1}) \quad 17.37$$

Substitution of this equation in Eq. (17.5) gives:

$$\tau_{CSTR} = \frac{V}{F_i} = \frac{1}{D} = \frac{(C_{si} - C_{sr})(K_s + C_{sr}) Y_{xs}}{\mu_{max} C_{sr} C_{xr}} \quad (\text{s}) \quad 17.38$$

Substitution of

$$r_x^u = \mu C_{xr} \quad (\text{mol m}^{-3} \text{s}^{-1}) \quad 17.39$$

in Eq. (17.5) yields the equation for biomass:

$$\tau_{CSTR} = \frac{V}{F_i} = \frac{1}{D} = \frac{C_{xi} - C_{xr}}{-\mu C_{xr}} \quad (\text{s}) \quad 17.40$$

With $C_{xi} = 0$ it follows from this equation that:

$$\mu = D \quad (\text{s}^{-1}) \quad 17.41$$

Substitution in Eq. (17.3) gives the steady-state substrate concentration C_{sr}^{ss} in the CSTR:

$$C_{sr}^{ss} = \frac{K_s D}{\mu_{max} - D} \quad (\text{mol m}^{-3}) \quad 17.42$$

Substitution of this equation in Eq. (17.38) gives the steady-state biomass concentration:

$$C_{xr}^{ss} = Y_{xs} \left(C_{si} - \frac{K_s D}{\mu_{max} - D} \right) \quad (\text{mol m}^{-3}) \quad 17.43$$

The maximum possible growth rate for this case is obtained when $C_{sr}'' = C_{si}$. Inserting this value in Eq. (17.3) gives

$$\mu = D_{crit} = \mu_{max} \frac{C_{si}}{K_m + C_{si}} \quad (\text{s}) \quad 17.44$$

with D_{crit} the critical dilution rate at which the steady-state biomass concentration just becomes zero. If $C_{si} \gg K_s$, it follows from Eq. (17.47) that D_{crit} is about μ_{max} . Plots of C_{xr}^{ss} and C_{sr}^{ss} against the dilution rate D with typical parameter values are shown in Fig. 17.1.

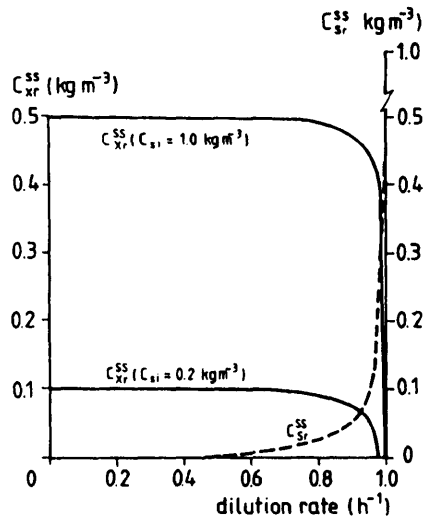


Fig. 17.1 Steady-state values of biomass and growth-limiting substrate concentrations in a chemostat: $\mu_{max} = 1 \text{ h}^{-1}$; $K_s = 5 \text{ g m}^{-3}$; $Y = 0.5$.

(Adapted from Pirt, 1985.)

For a chemostat culture, the rate of output of biomass per unit volume of bioreactor, Q_{px} (mol m⁻³ s⁻¹), is given by:

$$Q_{px} = D C_{xr} \quad (\text{mol m}^{-3} \text{ s}^{-1}) \quad 17.45$$

Substitution of Eq. (17.43) gives the steady-state output:

$$Q_{px} = D Y_{xs} \left(C_{si} - \frac{K_s D}{\mu_{max} - D} \right) \quad (\text{mol m}^{-3} \text{ s}^{-1}) \quad 17.46$$

The steady-state output as a function of the dilution rate with typical values is shown in Fig. 17.2. The biomass output rate reaches a maximum at the dilution rate D_{max} , which is obtained by differentiating Q_{px} with respect to D and equating the derivative to zero. Hence we find:

$$D_{max} = \mu_{max} \left(1 - \sqrt{\frac{K_s}{K_s + C_{si}}} \right) \quad (\text{s}^{-1}) \quad 17.47$$

Substitution of this equation in Eq. (17.43) gives the steady-state biomass concentration at D_{max} :

$$C_{xrmax}^{ss} = Y_{xs} \left(K_s + C_{si} - \sqrt{K_s (K_s + C_{si})} \right) \quad (\text{s}^{-1}) \quad 17.48$$

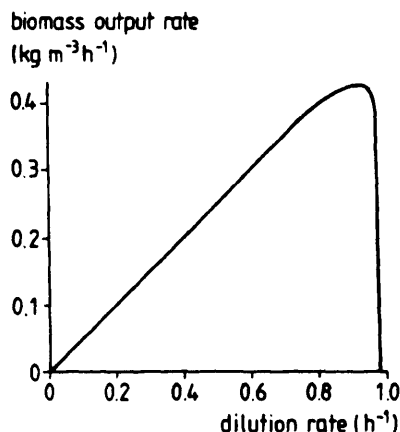


Fig. 17.2 Steady-state rates of biomass output in a chemostat: $\mu_{max} = 1 \text{ h}^{-1}$; $K_s = 5 \text{ g m}^{-3}$; $Y = 0.5$; $C_{si} = 1 \text{ kg m}^{-3}$. (Adapted from Pirt, 1985.)

If $C_{si} \gg K_s$, the maximum output rate Q_{pxmax} is

$$Q_{pxmax} = D_{max} C_{x_{rmax}}^{ss} \approx D_{max} Y_{xs} C_{si} \quad (\text{mol s}^{-1}) \quad 17.49$$

17.4.4 Mass transfer integrated with Monod kinetics

This has been dealt with by Venkatasubramanian et al. (1983). Consider the system as pictured in Fig. 17.3. Immobilized cells are suspended in an ideally mixed culture and can grow to a certain concentration in the support material. When this concentration is reached, cell division proceeds at the same rate, but all extra cells are released into the medium and in turn further divide at the same rate or are washed out from the cultures. A substrate balance over the vessel yields

$$\frac{d(C_{sr} V)}{dt} = F_i C_{si} - \frac{V \mu C_{xr}}{Y_{xs}} - \frac{V \mu C_{xr}^{im}}{Y_{xs}} - F_i C_{sr} \quad (\text{mol s}^{-1}) \quad 17.50$$

Assuming steady state and constant reactor volume V gives after division by V and rearrangement

$$D(C_{si} - C_{sr}) = \mu \frac{C_{xr} + C_{xr}^{im}}{Y_{xs}} \quad (\text{mol m}^{-3} \text{s}^{-1}) \quad 17.51$$

The biomass balance over the vessel

$$\frac{d(C_{xr} V)}{dt} = \mu C_{xr} V + \mu C_{xr}^{im} V - F_i C_{xr} \quad (\text{mol s}^{-1}) \quad 17.52$$

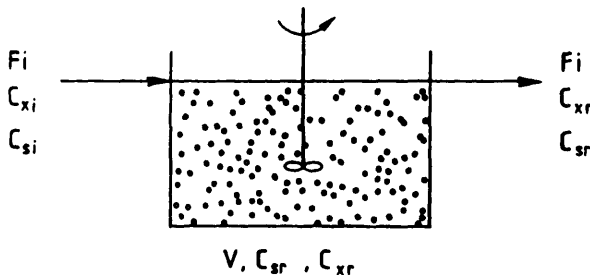


Fig. 17.3 Immobilized growing cells in CSTR.

similarly yields

$$D C_{xr} = \mu (C_{sr} + C_{xr}^{im}) \quad (\text{mol m}^{-3} \text{s}^{-1}) \quad 17.53$$

For all cases that $C_{xr}^{im} > 0$ it follows from this equation that $D > \mu$. Substituting Monod kinetics Eq. (17.3) and Eq. (17.53) in Eq. (17.51) gives

$$\frac{\mu_{max} C_{sr}}{K_s + C_{sr}} = \frac{D Y_{xs} (C_{si} - C_{sr})}{Y_{xs} (C_{si} - C_{sr}) + C_{xr}^{im}} \quad (\text{s}^{-1}) \quad 17.54$$

This is a quadratic equation in C_{sr} with a meaningful solution for $0 < C_{sr} < C_{si}$. Substituting $C_{xr}^{im} = 0$ yields the equations for the "ordinary" chemostat. For $C_{xr}^{im} > 0$ it can be shown that the conversion of substrate is always larger than in the case of $C_{xr}^{im} = 0$. Introduction of the overall effectiveness factor η_e^{ov} can account for diffusion limitation. The equations thus become

$$D(C_{si} - C_{sr}) = \mu \frac{C_{xr} + \eta_e^{ov} C_{xr}^{im}}{Y_{xs}} \quad (\text{mol m}^{-3} \text{s}^{-1}) \quad 17.55$$

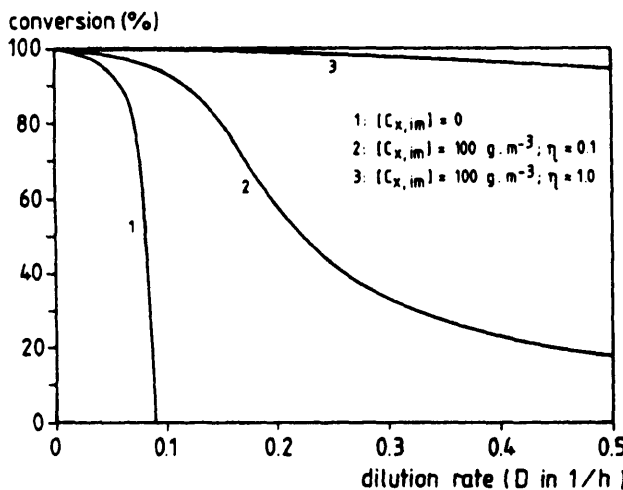


Fig. 17.4 Simulation of conversion by immobilized growing cells as a function of dilution rate.

for the substrate balance,

$$D C_{xr} = \mu (C_{xr} + \eta_e^{ov} C_{xr}^{im}) \quad (\text{mol m}^{-3} \text{s}^{-1}) \quad 17.56$$

for the biomass balance, and

$$\frac{\mu_{max} C_{sr}}{K_s + C_{sr}} = \frac{D Y_{xs} (C_{si} - C_{sr})}{Y_{xs} (C_{si} - C_{sr}) + \eta_e^{ov} C_{xr}^{im}} \quad (\text{s}^{-1}) \quad 17.57$$

when Monod kinetics is substituted. Fig. 17.4 shows a simulation using data taken from our work with nitrifying bacteria (*Nitrosomonas europaea* and *Nitrobacter agilis*). It clearly shows that as more cells are immobilized, the conversion is higher and that this effect is partly nullified by diffusion limitation. It also shows that even in the case that $D > \mu_{max}$ (wash-out conditions for free cells) high and stable conversions can be accomplished.

17.5 The cascade of n CSTRs

17.5.1 Introduction

Much attention has been given in the past to reactor systems consisting of a series of well-stirred tanks, because of the relative simplicity and the great importance of these systems. In standard textbooks on chemical reaction engineering, like Aris (1961) and Levenspiel (1972), general concepts of reactor design are treated and mostly illustrated with n -th order reaction kinetics. The optimization of a series of CSTRs is usually executed by defining the optimum as the smallest total reactor size (holding time) to perform a specific conversion. This definition is also applicable in the derivation of the following sections. Finding the optimal design thus amounts to finding the minimum of the total holding time, which is a function of all intermediate substrate concentrations, i.e., the concentration of substrate in the first, the second, etc., until the last-but-one reactor in the series. Mathematically formulated, this involves finding the intermediate substrate concentration values subject to the following equation [derived from Eq. (17.7)]:

$$C_{so,j} = C_{sr,j} = C_{so,j-1} + r_{e,j} \tau_{CSTR,j} \quad j = 1, 2, \dots, (n) \quad (\text{mol m}^{-3}) \quad 17.58$$

This set of (n) equations has to be solved simultaneously for the (n) intermediate concentrations C_{sr} . The choice of the total number of reactors n is naturally dictated by the economics of the process. Usually, as discussed

by Herbert (1961) and Reusser (1961), only about two to four reactors are justified. Below it will be shown that the introduction of a second reactor considerably reduces the total reactor volume. Because of the complexity in the case of Monod kinetics, only the case of Michaelis-Menten kinetics will be worked out in detail.

17.5.2 Michaelis-Menten kinetics

A simple analytical expression has been derived by Luyben and Tramper (1982) for the optimal design of CSTRs in series, assuming a constant activity of the biocatalyst in the reactor. The optimum is defined as the smallest total reactor size (holding time) to perform a specific conversion. The resulting total holding time can also be used as a good approximation for the total holding time of equal-sized CSTRs. The mathematically more complex case of n equal-sized CSTRs will be illustrated by an example. Consider n CSTRs in series with an inlet concentration of substrate of $C_{si,1}$ (mol m⁻³) for the first reactor (Fig. 17.5).

Introducing Michaelis-Menten kinetics Eq. (17.1) in Eq. (17.6) gives:

$$\tau_{CSTR,i} = \frac{V_i}{F_i} = \frac{(C_{so,i-1} - C_{so,i})(K_m + C_{so,i})}{v_{max} C_{so,i}} \quad (s) \quad 17.59$$

This equation can be written in dimensionless form by introducing the following variables:

$$\alpha_i = \frac{C_{so,i}}{C_{si,1}} \quad (-) \quad 17.60$$

$$\kappa = \frac{K_m}{C_{si,1}} \quad (-) \quad 17.61$$

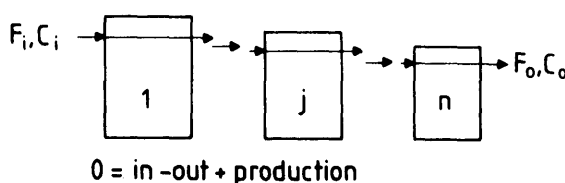


Fig. 17.5 The cascade of CSTRs.

and

$$\Theta_j = \frac{\tau_{CSTR,i} v_{max}}{C_{st,1}} \quad (-) \quad 17.62$$

Substitution of Eqs. (17.60-17.62) in Eq. (17.59) leads to:

$$\Theta_j = \frac{(\alpha_{j-1} - \alpha_j)(\kappa + \alpha_j)}{\alpha_j} \quad (-) \quad 17.63$$

Eq. (17.63) is a general relation that gives the dimensionless holding time required in the j -th reactor to obtain a dimensionless concentration α , starting from α_{j-1} , assuming Michaelis-Menten kinetics. From Θ_j immediately follows the volume of the j -th reactor for a given maximum reaction rate v_{max} , volumetric flow rate F_i , and initial substrate concentration $C_{st,1}$ (Eqs. (17.62) and (17.6)).

Finding the optimal design according to the above definition amounts to finding the minimum of the total holding time, which is a function of all α_j 's. Mathematically formulated, this involves finding the intermediate α_j -values subject to the following equation:

$$\frac{\delta}{\delta \alpha_j} \left[\sum_{j=1}^n \Theta_j \right] = 0 \quad j = 1, 2, \dots, (n-1) \quad (-) \quad 17.64$$

Only two terms of this summation contain α_j , leading to:

$$\frac{\delta}{\delta \alpha_j} \left[\frac{(\alpha_{j-1} - \alpha_j)(\kappa + \alpha_j)}{\alpha_j} + \frac{(\alpha_j - \alpha_{j+1})(\kappa + \alpha_{j+1})}{\alpha_{j+1}} \right] = 0 \quad (-) \quad 17.65$$

Differentiation and rearranging gives:

$$\alpha_j^2 = \alpha_{j-1} \alpha_{j+1} \quad j = 1, 2, \dots, (n-1) \quad (-) \quad 17.66$$

This simple result relates the conversion $(1 - \alpha_j)$ in the j -th reactor to the conversion in the $(j-1)$ th and the $(j+1)$ th reactor for a series of CSTRs, in which a reaction takes place following Michaelis-Menten kinetics. Important to note is that κ dropped out of the relation. This means that the

intermediate substrate concentrations for a series of perfectly mixed tank reactors are independent of the Michaelis-Menten constant K_m . Eq. (17.66) consists of a set of $(n - 1)$ relations which can be solved directly for a given total conversion $(1 - \alpha_n)$ as follows. Writing the set of equations from Eq. (17.66):

$$\alpha_{n-1}^2 = \alpha_{n-2} \alpha_n \quad (-) \quad 17.67$$

$$\alpha_j^2 = \alpha_{j-1} \alpha_{j+1} \quad (-) \quad 17.68$$

$$\alpha_1^2 = \alpha_0 \alpha_2 \quad (-) \quad 17.69$$

Substituting from the bottom up gives:

$$\alpha_j = \alpha_0 \left(\frac{\alpha_1^2}{\alpha_2} \right) \left(\frac{\alpha_3^2}{\alpha_4} \right) \dots \left(\frac{\alpha_{j-1}^2}{\alpha_j} \right) \quad j = 1, 2, \dots, (n-1) \quad (-) \quad 17.70$$

Since the conversion $(1 - \alpha_1)$ is related to the inlet concentration of the first tank, α_0 is equal to 1 by definition of Eq. (17.60) and Eq. (17.70) thus simplifies to:

$$\alpha_j = \alpha_{j+1} \left(\frac{\alpha_1^2}{\alpha_2} \right) \dots \left(\frac{\alpha_{j-1}^2}{\alpha_j} \right) \quad j = 1, 2, \dots, (n-1) \quad (-) \quad 17.71$$

Some results of Eq. (17.71) and subsequent use of Eq. (17.63) are presented in Table 17.1. This table gives the dimensionless concentrations and holding

Table 17.1 Dimensionless concentrations and holding times in the mixed reactors for $\alpha_n = 0.01$ and $x = 0.1$

n	α_j (independent of x)					Θ_j (dependent of x)				
	1	2	3	4	5	1	2	3	4	5
1	0.01					10.89				
2	0.1	0.01				1.80	0.99			
3	0.215	0.046	0.01			1.149	0.533	0.401		
4	0.316	0.100	0.0316	0.010		0.900	0.432	0.285	0.238	
5	0.398	0.158	0.0631	0.025	0.01	0.753	0.391	0.247	0.189	0.166

Source: Adapted from Luyben and Tramper, 1982.

times in the mixed reactors for an initial concentration of ten times the Michaelis-Menten constant and a conversion of 99%. The data show that the difference in holding time between two subsequent reactors is largest for low values of n , especially between the first two reactors, and becomes smaller as n increases.

Table 17.2 gives the total holding times for two values of κ , both for a series of CSTRs with minimal total volume and for a series of equal-sized mixed reactors. Total holding times for equal-sized mixed reactors have been calculated using a zero finding routine. The last value in Table 17.2 is the dimensionless holding time for a plug-flow reactor with Michaelis-Menten kinetics, calculated by means of the following equation (see also Section 17.6):

$$\Theta_{pf} = (\alpha_0 - \alpha_n) - \kappa \ln \alpha_n \quad (-) \quad 17.72$$

An important observation from Table 17.2 is the considerable difference going from one to two or more CSTRs. For the conditions studied, there is only a minor difference (less than 10%) between the total holding time for optimal and equal-sized mixed reactors. Even in extreme cases, i.e., for very

Table 17.2 Dimensionless total holding times for optimal and equal-sized mixed reactors, for $\alpha = 0.01$ and two values of κ

n	$\kappa = 0.1$		$\kappa = 1$	
	$\Theta_{t,opt}$	$\Theta_{t,eq}$	$\Theta_{t,opt}$	$\Theta_{t,eq}$
1	10.890	10.890	99.990	99.990
2	2.790	2.917	18.990	19.006
3	2.082	2.234	11.915	11.947
4	1.855	1.983	9.639	9.677
5	1.746	1.854	8.549	8.588
6	1.683	1.776	7.917	7.954
7	1.641	1.723	7.505	7.540
8	1.613	1.684	7.216	7.249
9	1.591	1.656	7.003	7.033
10	1.575	1.633	6.839	6.867
	Θ_{pf}	1.451		5.595

Source: Adapted from Luyben and Tramper, 1982.

low values of κ and α , this difference remains relatively small (37% for $n = 3$, $\kappa = 10^{-3}$ and $\alpha = 10^{-4}$).

Furthermore, it can be shown that in the limiting cases of first-order kinetics [Eq. (17.66) also holds for this case] and zero-order kinetics the equal and optimal sizes are exactly the same. As shown, the optimal holding times can be calculated very simply by means of Eq. (17.71), and the sum of these can thus be used as a good approximation for the total holding time of equal-sized CSTRs. This makes Eq. (17.62) an even more valuable tool for design equations. The restrictions are imposed by the assumption that the biocatalytic activity is constant in the reactors. Especially in the case of soluble enzymes, for which ordinary Michaelis-Menten kinetics in particular apply, special measures have to be taken. Continuous supply of relatively stable enzyme to the first tank in the series is a possibility, though in general expensive. A more attractive alternative is the application of a series of membrane reactors.

A paper describing the optimization of a series of CSTRs on the basis of the cost minimization or profit maximization criterion has been published by Ong (1986). Michaelis-Menten and Monod kinetics were used as the examples in this paper.

17.5.3 Mass transfer integrated with Michaelis-Menten kinetics

The problem of keeping a constant biocatalyst activity in the ideally mixed reactors is less severe in the case of solid immobilized biocatalyst. Immobilized biocatalysts can easily be retained in the reactors and when the stability is sufficiently high, the activity per unit reactor volume can be considered constant for some time. The introduction of the overall effectiveness factor in the Michaelis-Menten equation [Eq. (17.2)] does not lead to more complex equations in the case of the optimal design described in the preceding section (de Gooijer et al., 1989). Instead of introducing a dimensionless holding time as defined by Eq. (17.62), the following one is used:

$$\Theta_j = \frac{\eta_a^{ov} \tau_{CSTR,j} v_{max}}{C_{si,1}} \quad (-) \quad 17.73$$

As a result, all the other equations derived in the preceding section for the optimal design are the same. Consequently, α , is independent not only of the dimensionless Michaelis-Menten constant, but also of the overall effectiveness factor. Compensation for the lower activity as a result of diffusion limitation of substrate solely occurs by increase of the holding

times (size) of the various reactors in the series. The compensation factor, i.e., the overall effectiveness factor, must be calculated for each tank by the procedures described in Chapter 15. An example will be worked out in the examples.

17.5.4 Monod growth kinetics

Bischoff (1966) worked out an optimal design for several continuous fermentation systems, including a series of stirred tanks. On the basis of the criterion of a minimal total holding time of a series of n reactors, he derives the following equations for biomass:

$$\frac{\partial \left[\sum_{j=1}^n \tau_{CSTR,j} \right]}{\partial C_{xo,j}} = 0 \quad j = 1, 2, \dots, (n-1) \quad (-) \quad 17.74$$

$$= \frac{1}{r_j(C_{xo,j})} - \frac{C_{xo,j} - C_{xo,j-1}}{r_j^2(C_{xo,j})} \frac{dr_j(C_{xo,j})}{dC_{xo,j}} - \frac{1}{r_j(C_{xo,j+1})}$$

or

$$1 = \frac{C_{xo,j} - C_{xo,j-1}}{r_j(C_{xo,j})} \frac{dr_j(C_{xo,j})}{dC_{xo,j}} + \frac{r_j(C_{xo,j})}{r_j(C_{xo,j+1})} \quad (-) \quad 17.75$$

This set of $n-1$ equations should be solved simultaneously for the $(n-1)$ $C_{xo,j}$'s. Aris (1961) has indicated a graphic procedure for aiding in this solution for a related problem.

For a series of two fermenters Eq. (17.75) reduces to

$$1 = \frac{C_{xo,1} - C_{xt,1}}{r_1(C_{xo,1})} \frac{dr_1(C_{xo,1})}{dC_{xo,1}} + \frac{r_1(C_{xo,1})}{r_2(C_{xo,2})} \quad (-) \quad 17.76$$

Bischoff further worked out this equation for Monod kinetics with a single substrate and microorganism. Furthermore, Bischoff compared this with a system consisting of a CSTR followed by a plug-flow reactor. Although a plug-flow reactor generally yields smallest holding times, Herbert (1961) has discussed the fact that a plug-flow reactor cannot operate by itself in the steady state without a source of microorganisms to feed into the reactor, because of the autocatalytic nature of the reaction. The specific example Bischoff uses is the lactic acid fermentation by *Lactobacillus delbrueckii*

Table 17.3 Comparison of fermenter total holding time for various systems

Fermenter system	Intermediate dimensionless concentration $\frac{C_{x0,1}}{C_{xi,1}}$	Total holding time (dimensionless) $\Theta_t = \mu_{max} \tau_i$
One CSTR	-	11
Two equal CSTRs	0.713	$2.72 + 2.74 = 5.48$
Two optimum CSTRs	0.792	$3.41 + 1.82 = 5.23$
CSTR + plug-flow	0.635	$2.37 + 1.60 = 3.97$

Source: Adapted from Bischoff, 1966.

with $C_{xi,1} = 0$ and assuming that 95% of the input substrate is converted to microorganisms. Table 17.3 gives the results of his calculations.

As seen in the previous section a cascade of two CSTRs is significantly better than one single CSTR. Also in agreement with the findings of the previous section is the result that the relative sizes of the two CSTRs in the cascade does not seem to be very critical since almost the same total holding time is obtained for both configurations. The CSTR/plug-flow reactor combination gives the optimum-sized reactor system, as can be expected. A description of two chemostats in series can also be found in more detail in Pirt (1985).

17.6 The plug-flow reactor

17.6.1 Michaelis-Menten kinetics

Substitution of Eq. (17.1) in Eq. (17.7) for the plug-flow reactor gives an equation similar to the one found for the batch reactor:

$$\tau_{pf} = \frac{V}{F_i} = - \int_{C_{si}}^{C_{so}} \frac{K_m + C_{sr}}{v_{max} C_{sr}} dC_{sr} \quad (s) \quad 17.77$$

or

$$\tau_{pf} = \frac{K_m}{v_{max}} \ln\left(\frac{C_{si}}{C_{so}}\right) + \frac{(C_{si} - C_{so})}{v_{max}} \quad (s) \quad 17.78$$

Analogous to the batch reactor with Michaelis-Menten kinetics, this equation for the residence time of the plug-flow reactor can be solved directly when the kinetic constants, the inlet concentration of substrate and the desired conversion are known.

17.6.2 Mass transfer integrated with Michaelis-Menten kinetics

Also in case of diffusion-limited reactions where the overall effectiveness factor is used to describe the effect of diffusion on the rate of biocatalysis, the mathematics are the same as in the case of the batch reactor. Substitution of Eq. (17.2) in Eq. (17.7) thus yields:

$$\tau_{pf} = \frac{V}{F_i} = - \int_{C_{sr}}^{C_{so}} \frac{K_m + C_{sr}}{\eta_e^{ov} v_{max} C_{sr}} dC_{sr} \quad (s) \quad 17.79$$

This equation, again, cannot be integrated immediately as η_e^{ov} is a function of the substrate concentration C_{sr} , which changes when going from the entrance to the exit of the plug-flow reactor. The procedure we use to solve this equation is calculation of the overall effectiveness factor at n substrate concentrations in the interval C_{sr} to C_{so} . Through this n (η_e^{ov} , C_{sr}) data pairs an n -th order polynomial is fitted. This polynomial is substituted in Eq. (17.79) followed by a numerical solution.

17.6.3 Monod growth kinetics

A plug-flow reactor is of no practical value for cultivation of cells if no cell recycle or continuous inoculation is applied. Wash-out of cells, namely, is bound to occur. Plug-flow culture with cell recycle is used on a large scale in the activated sludge process for water purification. As the applicability, however, is limited, and as the theory does not further contribute to a better understanding, no further attention is paid to these systems here. The interested reader is referred to Pirt (1985).

17.7 Examples

Example 17.1 Batch reactor/CSTR. Inactivation; first-order kinetics

A factory is faced with the problem of executing an enzymic conversion batchwise or continuously in a fully depreciated stirred tank reactor. The price of the enzyme is cost determining.

Calculate:

- A For the batch reactor when the batch time is 4 days and the down-time 2 days:
1. The end concentration of substrate.
 2. The capacity of the reactor on a yearly basis.
 3. The price to convert 1 mol of substrate.
- B For the continuous reactor with a flow of $0.052 \text{ m}^3 \text{ h}^{-1}$ the same items.

Data:

Half-time of the enzyme	$t_{0.5} = 4 \text{ d}$
Enzyme concentration	$C_e = 0.002 \text{ kg m}^{-3}$
Michaelis-Menten constant	$K_m = 100 \text{ mol m}^{-3}$
Maximum rate	$v_{max} = 0.6 \text{ mol kg}^{-1} \text{ s}^{-1}$
Inlet/starting substrate concentration	$C_s = 10 \text{ mol m}^{-3}$
Price of enzyme	\$ = 250 \text{ kg}^{-1}
Reactor volume	$V = 5 \text{ m}^3$

Solution:

A1

The Michaelis-Menten constant K_m is much larger than C_s , at all times, thus assuming first-order kinetics is justified.

The mass balance for the batch reactor in this case reads:

$$\frac{dC_s}{dt} = r_s^u = - \frac{v_{max} C_e}{K_m} C_s$$

or

$$C_s(4) \int_{C_s(0)}^{C_s(4)} \frac{dC_s}{C_s} = \int_0^4 - \frac{v_{max}(0) C_e}{K_m} e^{-k_d t} dt$$

For first-order inactivation (Chapter 5) $k_d = \ln 2 / t_{0.5} = 0.17 \text{ d}^{-1}$. Integration and substitution of numerical values yields a $C_s(\text{end})$ of 0.5 mol m^{-3} .

A2

In $4 + 2$ days, 9.5 mol m^{-3} is converted, i.e., in 5 m^3 , 47.5 mol total . Per year this becomes $365 \times 47.5 / 6 = 2890 \text{ mol}$.

A3

In every m^3 0.002 kg enzyme converts $10 - 0.5 = 9.5 \text{ mol}$ of substrate or 4750 mol kg^{-1} enzyme, i.e., $0.053 \text{ $ mol}^{-1}$.

B1

With a flow of $0.052 \text{ m}^3 \text{ h}^{-1}$ the average residence time (of the enzyme) is $5/0.0052 = 96 \text{ h}$, which is just the half-life of the enzyme. Therefore, assume that the activity of the enzyme in the reactor is half that of the initial activity. The mass balance for the CSTR yields in this case:

$$\frac{V}{F} = \tau_{CSTR} = \frac{C_{so} - C_{si}}{-r_s^u} = \frac{\frac{C_{si} - C_{so}}{\frac{v_{max} C_s}{K_m}}}{C_{so}}$$

Substitution of numerical values gives a C_{so} of 3.25 mol m^{-3} .

B2

In every m^3 , 6.75 mol is converted, i.e., with a flow of $0.052 \text{ m}^3 \text{ h}^{-1}$, 0.35 mol h^{-1} or 3075 mol y^{-1} .

B3

In every m^3 0.002 kg enzyme converts $10 - 3.25 = 6.75 \text{ mol}$ of substrate, or 3375 mol kg^{-1} enzyme, i.e., $0.074 \text{ $ mol}^{-1}$.

From the point of view of enzyme costs and conversion it is thus cheaper to work batchwise. Also, the capacity is only slightly less under the pertinent conditions.

Example 17.2 CSTR. Inactivation and zero-order kinetics

An enzyme in intact cells of *Arthrobacter globiformis* catalyzes the conversion of hydrocortisone (molecular weight 333) to prednisolone. The cells are immobilized in alginate gel beads and used in a continuous process for the synthesis of prednisolone. In the range of interest this conversion can be rather well described by apparent Michaelis-Menten kinetics with apparent $K'_m = 30 \text{ mmol m}^{-3}$ and apparent $v'_{max} = 3 \text{ mmol (kg cells)}^{-1} \text{ s}^{-1}$. The biocatalyst decays according to a first-order mechanism with $k_d = 0.046 \text{ d}^{-1}$. The biocatalysis is executed in a CSTR run for 30 days continuously before replacing the biocatalyst. Due to down-time, a maximal of 8 runs per year are possible. The inlet substrate concentration is 10 kg m^{-3} and the initial conversion 99%. The selectivity is $1 (\text{mol mol}^{-1})$. The beads contain 1 kg of cells per m^3 of beads and the bioreactor load is 0.2 m^3 bead per m^3 .

Calculate:

1. The overall productivity of the biocatalyst.
2. The overall volumetric productivity of the CSTR on a yearly basis.
3. The end conversion.

Solution:

1.

The concentration of substrate in the influent is 10 kg m^{-3} , i.e., 30 mol m^{-3} (M.W. 333). With a conversion of 99% initially, the minimum substrate concentration is 0.3 mol m^{-3} in the CSTR, which means zero-order kinetics ($K_m' = 0.03 \text{ mol m}^{-3}$) is a good assumption for the whole run as the substrate concentration only increases.

Eq. (1.1) can thus be written as:

$$Pr_{px} = Y_{ps} \int_0^t v'_{max}(0) e^{-k_d t} dt$$

Substituting numerical values:

$$Pr_{px} = 1 \int_0^{30} 3 \times 10^{-3} \times 24 \times 3600 e^{-0.046t} dt$$

$$= 4217 \text{ mol } (\text{kg cells})^{-1}$$

$$= 1400 \text{ kg } (\text{kg cells})^{-1}$$

2.

The concentration of cells is 0.2 kg per m^3 bioreactor. Therefore, per run 280 kg of substrate are converted per m^3 reactor. Per year this means, with 8 runs, 2240 kg m^{-3} .

3.

The product concentration can be calculated by means of Eq. (1.4):

$$C_p(t) = Y_{ps} v'_{max}(0) e^{-k_d t} \tau_{CSTR}$$

The residence time τ_{CSTR} can be calculated from the data at time zero. The amount of substrate converted per m^3 at $t = 0$ is $30 - 0.3 = 29.7 \text{ mol m}^{-3}$. The activity per m^3 reactor is $0.2 \times 3 = 0.6 \text{ mmol } (\text{m}^3 \text{ bioreactor} \cdot \text{s})^{-1}$. The residence time thus is $29.7 / (0.6 \times 10^{-3}) = 49500 \text{ s} = 825 \text{ min} = 13.75 \text{ h}$. Substituting this in the equation for $t = 30 \text{ d}$ yields $C_p = 7.42 \text{ mol m}^{-3}$, i.e., a conversion of $7.42 / 30 \times 100\% = 24.7\%$, which is not a very economical operation.

Example 17.3 The cascade of CSTRs. External and internal mass transfer resistance at zero-order kinetics

Glucose oxidase catalyzes the oxidation of glucose to glucono- δ -lactone, which spontaneously hydrolyzes to gluconic acid, a commercially interesting product. The enzyme is immobilized in beads with a radius of 1 mm. Since a high conversion is essential and in order to minimize abrasion of the particles and to prevent limitation of the reaction rate by the transport of oxygen, the use of a cascade of two air lift reactors is considered for the production of gluconic acid by the immobilized enzyme in a continuous mode. On the basis of the following specifications a biochemical engineer calculates, in contradiction to what she expected after reading this book, that the cost of investments is higher for two than for one air lift in this case.

Data:

- The air lift can be considered as ideally mixed.
- The desired conversion is 99%.
- 10 m³ of a glucose solution (180 kg m⁻³) must be processed per day.
- The effective diffusion coefficient D_{sp} of glucose in the support is 10⁻⁹ m² s⁻¹.
- The mass transfer coefficient k_t is 10⁻⁴ m s⁻¹.
- The intrinsic Michaelis-Menten constant K_m for glucose is 1 mol m⁻³.
- The intrinsic maximal glucose consumption rate v_{max} is 2 × 10⁻² mol (m³ particles s)⁻¹.
- Load of immobilized enzyme is 0.2 m³ particles per m³ bioreactor.
- Costs Y (k\$) of a reactor with volume V (m³) can be described by:

$$Y = 80 + 220 \times V^{0.6}$$

Solution:

The influent concentration of glucose C_{si} is 180 kg m⁻³, i.e., 1000 mol m⁻³. When the desired conversion of 99% is realized, the effluent concentration $C_{so} = 10$ mol m⁻³, in other words $K_m = 1$ mol m⁻³ ≪ C_{so} , i.e., zero-order kinetics is a justified first assumption. For zero-order kinetics Eq. (15.20) can be applied for calculation of the internal effectiveness factor η_{ei} :

$$\Phi^2 = \frac{v_{max}^g R_p^2}{18 |D_{sp}| C_{si}} \quad 15.20$$

Assuming as a second approximation that the concentration of substrate at the particle surface $C_{si} = C_{so}$, i.e., no external diffusion limitation, the

Thiele modulus ϕ can be calculated to be much smaller than 0.57, which means that $\eta_{ei} = 1$, or negligible internal diffusion limitation.

The net transport of substrate to the particle is equal to the amount converted:

$$k_i A (C_{sb} - C_{si}) = \eta_{ei} v_{max} = v_{max}$$

Substitution of the appropriate numerical values yields that C_{si} is only slightly less than 10 mol m^{-3} , in other words about equal to C_{sb} , so external diffusion limitation is also negligible, as assumed in the calculation of η_{ei} , which makes both calculations valid. Using Eqs. (17.71), (17.63), (17.62) and (17.59) for calculation of the dimensionless concentrations, residence times and volumes, respectively in a "cascade" of 1 and 2 ideally mixed air lifts gives the results shown in Table 17.4.

With the cost equation the reactor investment becomes 1824 k\$ for 1 air lift and $1645 + 494 = 2139$ k\$ for 2. The fact that in this particular case there is only a slight reduction in total volume in going from 1 to 2 reactors is due to the almost zero-order kinetics. It is clearly not enough for investment in 2 reactors.

Example 17.4 The plug-flow reactor. Internal mass transfer resistance and zero-order kinetics

Invertase catalyzes the hydrolysis of sucrose in glucose and fructose (invert sugar) according to Michaelis-Menten kinetics. In a plug-flow reactor with immobilized invertase 31.1 tons of invert sugar should be produced per day.

Calculate:

The volume of the plug-flow reactor.

Table 17.4 Calculated values

	$N = 1$	$N = 2$
Eq. (17.71)	$\alpha_0 = 1; \alpha_1 = 0.01; \alpha_0 = 1; \alpha_1 = 0.1; \alpha_2 = 0.01$	
Eq. (17.63)	$\Theta_1 = 1.089$	$\Theta_1 = 0.909$
Eq. (17.62)	$\tau_{CSTR1} = 3.15 \text{ d}$	$\tau_1 = 2.63 \text{ d}$
Eq. (17.59)	$V_1 = 31.5 \text{ m}^3$	$V_1 = 26.3 \text{ m}^3$
		$V_2 = 2.86 \text{ m}^3$

Data:

- Inlet concentration of sucrose: $C_{in} = 342 \text{ kg m}^{-3}$.
- Conversion 99%.
- Biocatalyst-particle diameter: $d = 3.5 \text{ mm}$.
- Effective diffusion coefficient: $D = 0.5 \times 10^{-9} \text{ m}^2 \text{ s}^{-1}$.
- External mass transfer resistance can be neglected.
- Volume fraction of biocatalyst particles in the reactor is 50%.
- The kinetic data in Table 17.5 have been obtained by very small biocatalyst particles having a very low activity per unit volume.

Solution:

The inlet concentration is 342 kg m^{-3} , i.e., 1 kmol m^{-3} or a 1 molar solution. As the conversion is 99% the outlet concentration $C_{out} = 0.01 \text{ kmol m}^{-3}$. The kinetic data have been obtained using very small biocatalyst particles with a very low activity per unit volume. This means that the assumption that intrinsic kinetics have been measured is justified. From the data it can easily be obtained by the procedures described in Chapter 4 that $K_m = 1 \text{ mol m}^{-3}$ and $v_{max} = 10^{-5} \text{ mol m}^{-3} \text{ s}^{-1}$. Therefore, assuming zero-order kinetics over the whole reactor is appropriate.

With Eq. (15.20) and the particle surface concentration equal to the bulk concentration C_{sb} (no external diffusion limitation)

$$\Phi^2 = \frac{v_{max}^0 R_p^2}{18 D_{sp} C_{sb}} \quad 15.20$$

it can be calculated that $\Phi \leq 0.57$ in the whole reactor, thus $\eta_s^{ov} = 1$ in the whole reactor. Further we know that

Table 17.5 Kinetic data

Substrate concentration (mol m ⁻³)	Reaction rate × 10 ⁶ (mol m ⁻³ (particles) s ⁻¹)
5.00	8.33
2.50	7.14
1.67	6.25
1.25	5.56
1.00	5.00

$$\tau_{pf} = \int_{C_{si}}^{C_{so}} \frac{dC_s}{r_s^u} = \int_{C_{si}}^{C_{so}} \frac{dC_s}{-\epsilon v_{max}} = \frac{C_{so} - C_{si}}{-\epsilon v_{max}} \quad (s) \quad 17.7$$

which yields $\tau_{pf} = 19.8 \times 10^7 \text{ s}$.

Per day 31.1 ton invert sugar is produced, i.e., $0.36 \text{ kg s}^{-1} = 1 \text{ mol s}^{-1}$, which corresponds to a flow F_t of $10^{-3} \text{ m}^3 \text{s}^{-1}$. This means a reactor volume of $\tau_{pf} F_t = 19.8 \times 10^7 \times 10^{-3} = 2 \times 10^5 \text{ m}^3$. Clearly, this is not a realistic volume, which is the result of the very low biocatalyst activity.

Example 17.5 Plug-flow reactor. First-order kinetics with external and internal mass transfer resistance

To prevent accumulation of ammonium ions in consumption fish production ponds the water must be refreshed continuously at a rather high rate. This not only means a significant energy bill because of the large quantities of water which must be heated to about 30°C , but also high environmental taxes due to the high *BOD*. An alternative studied is recirculation of most of the water after removal of the ammonium ions using immobilized bacteria.

Calculate the size of the plug-flow reactor by which 1 m^3 of pond water can be treated per minute.

Data:

Inlet concentration	$C_{si} = 54 \text{ g NH}_4^+ \text{ m}^{-3}$
Outlet concentration	$C_{so} = 18 \text{ g NH}_4^+ \text{ m}^{-3}$
Bed porosity	$\epsilon = 0.5 \text{ m}^3 \text{ m}^{-3}$
Particle diameter	$d_p = 2 \text{ mm}$
Intrinsic Michaelis-Menten constant	$K_m = 100 \text{ mol m}^{-3}$
Intrinsic maximum rate	$v_{max} = 0.1 \text{ mol s}^{-1} \text{ m}^{-3} \text{ particles}$
Effective diffusion coefficient	$ D_{sp} = 10^{-9} \text{ m}^2 \text{ s}^{-1}$
Mass transfer coefficient	$k_t = 2 \times 10^{-4} \text{ m s}^{-1}$

Solution:

The outlet concentration is 18 g m^{-3} , i.e., 1 mol m^{-3} . This means, with $K_m = 100 \text{ mol m}^{-3}$, first-order reaction kinetics is an appropriate assumption. The Thiele modulus thus is

$$\Phi = \frac{1}{3} R_p \left(\frac{v_{max}}{K_m |D_{sp}|} \right)^{0.5}$$

or with numerical values

$$\Phi = \frac{1}{3} 10^{-3} \left(\frac{0.1}{100 \times 10^{-9}} \right)^{0.5} = 0.33$$

The internal effectiveness factor for a first-order reaction is:

$$\begin{aligned}\eta_{oi} &= \frac{1}{3\Phi^2} (3\Phi \coth(3\Phi) - 1) \\ &= \frac{1}{3\Phi^2} \left(3\Phi \frac{e^{3\Phi} + e^{-3\Phi}}{e^{3\Phi} - e^{-3\Phi}} - 1 \right) \\ &= 0.94\end{aligned}$$

The Thiele modulus and thus the internal effectiveness factor for a first-order reaction is independent of the substrate concentration. Therefore, the above calculated η_{oi} holds for the whole reactor.

In the steady state the flux of substrate to the particle is equal to the amount consumed by the particles (C_{si} is here the substrate concentration at the liquid/solid interface):

$$k_l A' (C_s - C_{si}) = \eta_{oi} \frac{\nu_{max} \epsilon}{K_m} C_{si}$$

Substituting numerical values and $C_s = C_{so}$ and $A' = 6\epsilon/d_p$:

$$2 \times 10^{-4} \frac{6 \times 0.5}{2 \times 10^{-3}} (1 - C_{si}) = 0.94 \frac{0.1 \times 0.5}{100} C_{si}$$

$$C_{si} = 0.998 \text{ mol m}^{-3} \approx C_{so}$$

In other words, at the outlet of the reactor the external diffusion limitation is negligible, which means $\eta_{oi} \approx 1$ in the whole reactor (C_{si} is here the inlet substrate concentration):

$$\tau_{pf} = \int_{C_{si}}^{C_{so}} \frac{dC_s}{r_s^u} = - \int_{C_{si}}^{C_{so}} \frac{dC_s}{\eta_{oi} \frac{\epsilon \nu_{max}}{K_m} C_s} = \eta_{oi} \frac{K_m}{\epsilon \nu_{max}} \ln \frac{C_{si}}{C_{so}}$$

Substituting numerical values gives $\tau_{pf} = 2338 \text{ s} = 39 \text{ min}$. The required volume thus is

$$V = \tau_{pf} F = 39 \text{ m}^3$$

References

- Aris R. "The optimal design of chemical reactors." Academic Press, New York (1961).
- Bischoff K. "Optimal continuous fermentation reactor design." Can. J. Chem., October, 281 (1966).
- de Gooijer C.D., Hens H.J.H. and Tramper J. "Optimum design for a series of continuous stirred tank reactors containing immobilized biocatalyst beads obeying intrinsic Michaelis-Menten kinetics." Bioprocess Engineering 4, 153 (1989).
- Herbert D. "Continuous culture of microorganisms." Soc. Chem. Ind. Monograph, London 12, 21 (1961).
- Levenspiel O. "Chemical reaction engineering." John Wiley, New York (1972).
- Luyben K.Ch.A.M. and Tramper J. "Optimal design for continuous stirred tank reactors in series using Michaelis-Menten kinetics." Biotechnol. Bioeng. 24, 1217 (1982).
- Ong S.L. "Optimization of CSTRs in series by dynamic programming." Biotechnol. Bioeng. 28, 818 (1986).
- Pirt S.J. "Principles of microbe and cell cultivation." Blackwell Scientific Publications, Oxford (1985).
- Reusser F. "Theoretical design of continuous antibiotic fermentation units." Appl. Microbiol. 9, 361 (1961).
- Venkatasubramanian K., Karkare S.B. and Vieth W.R. "Chemical engineering analysis of immobilized-cell systems." Appl. Biochemistry and Bioengineering, Vol 4, 311 (1983).

18

Process Engineering

18.1 Relations between parameters: The critical times concept

18.1.1 Introduction

Most of the engineering parameters discussed separately in Chapters 9 to 14 show mutual relationships. Mass transfer is related to foam control. Mass transfer is related to stirrer power and gas flow rate, as well as to hold-up. Increasing mass transfer leads to an increase in hold-up and therewith a decrease in effective reactor volume. Also, mixing is related to these parameters. All stirrer power finally will dissipate into heat and will influence the cooling requirements in this way. The main important relationship, however, is that of mixing with oxygen mass transfer, substrate addition and heat transfer. This will be worked out in a critical time regimes concept.

In an air lift loop reactor the liquid recirculates through riser and down-comer. It is not difficult to understand that this flow can be modeled (Section 9.4.3) by a recirculating flow through pipes representing plug flow with an added dispersion. Also, the flow through a stirred vessel can be modeled with such a loop (Section 9.4.1). In fermenters the carbon substrate is usually added to the vessel at a single point. Thus the substrate addition can be included in the model by a continuous inflow of the substrate at one defined position in the loop. The same applies for oxygen as for stirred fermenters: the oxygen transfer takes place mainly in the stirrer region. A liquid element, including microorganisms, that passes this feed point is "loaded" with substrate and from that point on only consumption will take place. This will go on until the substrate is depleted, unless before that time the liquid element passes the feed point again. A critical time t_{cr} can be defined, at which the substrate will just be depleted, given by

$$t_{cr} = \frac{C_{sf}}{-r_s^u} \quad (s) \quad 18.1$$

with

$$\begin{aligned} C_{sf} &= \text{substrate concentration at the feeding position} & (\text{mol m}^{-3}) \\ -r_s^u &= \text{substrate consumption rate per unit volume} & (\text{mol m}^{-3} \text{s}^{-1}) \end{aligned}$$

The critical time can be related to the circulation time. This can be seen from the following idealized case of plug flow. When the flow through the loop can be described by plug flow then the circulation time should be smaller than the critical time. If this is not the case, then the fluid will be depleted and $C_s = 0$. For a nonideal plug flow the reasoning is that fluid elements that have a circulation time larger than t_{cr} will be depleted. As a criterion, it can be said the t_{cr} should be larger or much larger than the (average) circulation time. In this section critical time values will be calculated for the C substrate, for O_2 and for heat production. These will be compared with the circulation times in fermenters. The t_{cr} values can impose limitations on fermenter design. Other limitations are given by values that are reasonable for parameters like power consumption, viscosity and gas flow rate. The consequences from these limitations will be discussed in Section 18.2.

18.1.2 The critical time for oxygen

18.1.2.1 The definition

If mass transfer takes place at one single position in the circulating loop, then the oxygen available for the microorganisms is given by C_{of} (mol m^{-3}) at that position. After passing this feed position the consumption rate is given by OUR ($\text{mol m}^{-3} \text{s}^{-1}$). If OUR is assumed to be constant in time, then Eq. (18.1) becomes for t_{cro} (s), the critical time for oxygen:

$$t_{cro} = \frac{C_{of}}{OUR} \quad (\text{s}) \quad 18.2$$

18.1.2.2 The stirred vessel

For stirred vessels mass transfer mainly takes place in the stirrer region, particularly for viscous broths. Thus for a stirred fermenter with one stirrer, the concentration in the stirrer region, C_{ols} (mol m^{-3}), is higher than anywhere else in the vessel. If mass transfer outside the stirrer region is totally absent, then the stirrer region can be regarded as the feed position for oxygen and C_{ols} is the C_{of} , as defined above. If t_{cro} is defined on the basis of C_{ols} , Eq. (18.2) becomes:

$$t_{cro} = \frac{C_{ols}}{OUR} \quad (\text{s}) \quad 18.3$$

With C_{ols} and OUR of the order of magnitude of 0.1 mol m^{-3} and $0.01 \text{ mol m}^{-3} \text{ s}^{-1}$, respectively, the critical time is of the order of 10 s. This is the same order of magnitude as circulation time and mixing time for large fermenters. If oxygen mass transfer occurs in the stirrer only, and mass transfer outside this region is absent, then a fluid element that left the stirrer region is depleted in a time equal to t_{cro} . Although in stirred fermenters the mass transfer outside the stirrer region is not zero, it certainly is much lower than that in the stirrer region. This means that depletion will occur at a time value that is indeed of the order of magnitude of t_{cro} . Therefore, the critical time for oxygen should be included in the design and optimization procedure. For this purpose it has to be related to design parameters. This can be done by determination of the relationship with the circulation time, and with the mixing time.

For a vessel with one stirrer and for which oxygen transfer outside the stirrer region is absent, it is valid, for the idealized case that the circulation loop can be modeled by plug flow, that:

$$t_{cro} = t_c \quad \begin{matrix} \text{one stirrer} \\ \text{transfer only at stirrer} \\ \text{plug flow in loop} \end{matrix} \quad (\text{s}) \quad 18.4$$

Eq. (18.4) is thus only valid when the model assumptions are justified. However, in a stirred fermenter there will be some transfer of oxygen outside the stirrer region, of the order of magnitude of the mass transfer in a bubble column with the superficial gas velocity of the stirred vessel. This leads to an increase of the time before oxygen depletion really takes place. The depletion time is thus in reality somewhat larger than t_{cro} calculated with Eq. (18.4). If more than one stirrer is used, the fluid element is loaded each time that a stirrer region is passed. In that case the vessel can be regarded as being divided into a number of compartments each with one stirrer. In that case the t_c value of a compartment with one stirrer should be used instead of the circulation time of the whole vessel. Besides all these effects, the main problem is that the circulation loop is not at all of the plug flow type. A limited amount of mixing (dispersion) can be regarded as an improvement; however, dead zones or regions with a relatively long residence time also occur. This means that the distribution of the circulation times leads to values that are larger as well as smaller than the average value used in Eq. (18.4). No quantitative information is available about the distribution of circulation times. Therefore, Eq. (18.4), although useful, should be regarded as a first indication only.

The driving force for oxygen mass transfer is given by $(C_{ol}^* - C_{ols})$ according to Eq. (11.8).

$$OTR = k_l A (C_{ol}^* - C_{ols}) \quad (\text{mol m}^{-3} \text{ s}^{-1}) \quad 11.8$$

At 1 bar $C_{oi}^* = 0.27 \text{ mol m}^{-3}$. This means that a value of $C_{oi} > 0$ (for instance, 0.10 mol m^{-3}) decreases the driving force for mass transfer considerably. Because the circulation time increases with scale, as shown in Example 9.2, this effect becomes more significant at larger scales. To prevent local oxygen depletion in the vessel, the C_{oi} value should be high; however, to obtain optimum mass transfer the C_{oi} value should be as low as possible, preferably zero. These two requirements contradict each other and an optimum value should be found. For this purpose the C_{oi} value should be known accurately. The theory only predicts order of magnitude values. Section 18.1.2.5 shows experimental methods to obtain more precise values of the critical oxygen concentration C_{oi}^* by means of measurements of OTR under critical and noncritical conditions.

18.1.2.3 The air lift

Eq. (18.2) can be used for localized oxygen transfer at a single position and plug flow. The air lift can be regarded as a loop reactor with nearly plug flow. However, the first assumption of a single point addition of oxygen does not hold at all. Mass transfer takes place in the whole riser part of the air lift. In this part local oxygen depletion due to the mechanism discussed in the previous section will not occur. The down-comer does not contain air bubbles and is a region where mass transfer is absent. Therefore, the liquid in the upper horizontal part entering the down-comer should contain enough oxygen to cover the time that the liquid flows through the down-comer. Eq. (18.2) can be applied in this part of the air lift by introducing the circulation (passing) time through the down-comer. With order of magnitude velocities in the down-comer of 1 up to 10 m s^{-1} and critical times of the order of 10 s this effect only starts to become relevant in air lift reactors exceeding a height of about 10 m, if in the upper part the oxygen concentration in the liquid, C_{oi} , is about 0.1 mol m^{-3} .

Depletion of the liquid phase can also occur by a totally different mechanism: mass transfer limitation in the upper part of very tall air lift reactors. This will be discussed in Section 18.2.2.

18.1.2.4 The bubble column

The t_{cr} concept as defined by Eq. (18.2) does not apply to the bubble column because mass transfer takes place in the whole column. As for the air lift, mass transfer limitation can occur in the upper part of tall columns. This will be discussed in Section 18.2.2.

18.1.2.5 Experimental determination of the critical C_{oi} value

The preceding sections show that at scale-up local oxygen depletion can easily occur. Calculations can be made for the order of magnitude of C_{oi}

at which the effect can become important. The mixing and dispersion in the reactor is, however, too complicated to calculate this value exactly. Therefore, an experimental method will be discussed here that gives additional information.

The objective of most aerobic fermentations is product or microorganism production. For this to be optimal the oxygen consumption and the product production by the microorganism must be optimal. Therefore, the final check for an optimal fermentation can be done by measurement of these two quantities. OUR and production, averaged for the whole vessel, will decrease when the conditions are not favorable, i.e., when oxygen depletion anywhere in the vessel occurs. From the sparsely available literature it appears that for small-scale, ideally mixed reactors, the critical oxygen concentration at which the production of, for instance, penicillin starts to decrease is very small, $< 0.01 \text{ mol m}^{-3}$. For OUR the same applies. This is given schematically in Fig. 18.1, line A. In a small scale, ideally mixed vessel concentration differences of oxygen are absent. Thus no local depletion occurs, and the low C_{ol} values at which OUR and q_p start to decrease can be regarded as the values at which the metabolism of the organism is influenced. If the relationship between C_{ol} and OUR or production for a large scale vessel is recorded, a result as given in Fig. 18.1, line B, will be obtained. Both OUR and q_p show a decrease at much higher values of C_{ol} than in the small ideally stirred tank. This will be due to local depletion somewhere in the large vessel. As local OUR and q_p can start to decrease at different local C_{ol} values (see also the difference in line A) the decrease can start at two different C_{ols} values. The C_{ol} value obtained experimentally in this way can be compared with the one calculated from Eq.

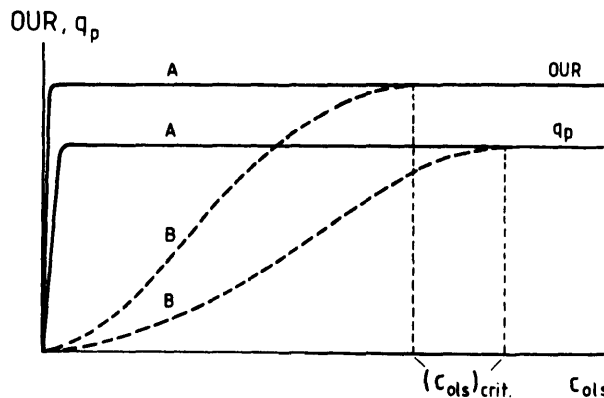


Fig. 18.1 Example of the influence of C_{ol} on OUR and q_p . Line A: A very small-scale, ideally mixed fermenter. Line B: A large-scale, stirred fermenter.

(18.3). This method is particularly useful for optimization of existing equipment. For scale-up its use is limited, although it gives an indication whether the use of the circulation time in Eq. (18.4) is indicative for the critical time. This gives the possibility to estimate large-scale critical C_{ols} values based on the circulation time ratio of the two scales and the critical C_{ols} value at small scale.

Assuming that the mass transfer takes place in the stirrer region, while depletion occurs in the circulation loop, means that concentration differences of the same magnitude as the critical oxygen concentration exist in large-scale fermenters. Cells experience these differences during each circulation loop. Not much is known about the extent to which this influences the cells. It is usually assumed that the effects are limited. This can be examined by estimating concentration differences and time regimes in the large-scale vessel first. Then in a small-scale vessel the regimes are simulated. This can be done by an aeration deaeration process or by two connected vessels. With the aeration deaeration procedure the highest concentration in the large-scale vessel is simulated by the concentration after aeration. The lowest concentration in the large-scale vessel is simulated by the concentration after deaeration. The time between aeration and deaeration is the same as the estimated circulation time for the organism in the large-scale vessel between the two regions. The same aim is reached by using two connected ideally mixed vessels with different oxygen concentration values and with the broth being pumped from one vessel to the other. Both methods are only indicative for the large scale because the complex mixing and dispersion in large vessels is only partly simulated in this way.

The engineering solutions for the critical oxygen concentration are directed to the prevention of local oxygen depletion anywhere in the vessel by keeping the oxygen concentration at the stirrer level (or in the top section of the air lift) above the critical value of C_{ols} . The driving force for mass transfer, $C_{ol}^* - C_{ols}$, decreases with increasing C_{ols} . To obtain an acceptable mass transfer value, $k_{ol}A$ can be increased using appropriate stirrer power consumption or gas flow rate, or the driving force can be increased by increasing C_{ol}^* with increased pressure in the fermenter head space. However, as will be shown in Section 18.3, stirrer power and gas flow rate have their limitations. Also, the fermenter head space pressure cannot be increased unlimitedly because of construction problems.

All discussions in this section apply to aerobic systems, as anaerobic systems do not consume oxygen and this type of limitation thus does not occur.

18.1.3 The critical time for the C substrate

With the loop model and C_{ss} (mol m^{-3}) defined as the concentration just after the feed position, Eq. (18.1) becomes

$$t_{crs} = \frac{C_{sf}}{-r_s^u} \quad (s) \quad 18.5$$

When maintenance is neglected, the Monod equation gives the r_s^u value as

$$-r_s^u = \mu_{max} \frac{C_s}{K_s + C_s} \frac{C_x}{Y_{xs}} \quad (\text{mol m}^{-3} \text{s}^{-1}) \quad 18.6$$

For maximum growth, ($\mu = \mu_{max}$), to occur throughout, care has to be taken that $C_s \gg K_s$, in the whole circulation loop. In that case the height of C_s does not influence the growth rate and the decrease in the circulation loop of only a fraction in C_s then becomes irrelevant for the growth rate. As μ_{max} is usually obtained in batch reactors with excess substrate present, this does not introduce any problem. The situation becomes much more complicated in case of substrate-limited growth. For growth rate $\mu \ll \mu_{max}$ Eq. (18.6) can be modified with $C_s \ll K_s$.

$$-r_s^u = \frac{\mu_{max}}{K_s} C_s \frac{C_x}{Y_{xs}} \quad (\text{mol m}^{-3} \text{s}^{-1}) \quad 18.7$$

Because of the first-order reaction in C_s , the time for total depletion of substrate becomes infinite because the rate (μ) decreases with time and becomes infinitely small. A first approximation of the time for total depletion can be obtained when the substrate consumption rate is assumed to be constant in time and equal to that of the average rate corresponding to C_s . The ratio of Eqs. (18.5) and (18.7) yields:

$$t_{crs} = \frac{Y_{xs} K_s}{\mu_{max} C_x} \frac{C_{sf}}{C_s} \quad (s) \quad 18.8$$

To get the situation that microorganism experiences a nearly constant C_s value in the circulation loop, this automatically means that C_{sf} is about C_s , i.e., the ratio in Eq. (18.8) = 1.

Using for this case values like those presented in Table 4.1 and 4.2 gives values of $t_{cr} \ll 1$ s up to several seconds. Thus it is impossible to obtain conditions in a large fermenter that come even near to a constant value of C_s for the whole loop. In a single feed addition all substrate for the loop is added at that position. This leads to large concentration differences along the circulation loop. With the average growth rate in the reactor being μ , r_s^u is given by the linear growth equation. The concentration at the feed

position should be at least, with t_c assumed to be the circulation time for each fluid element:

$$C_{sf} = -t_c r_s^u \quad (\text{mol m}^{-3}) \quad 18.9$$

For a large-scale fermentation with an r_s^u value of, for instance, $-0.02 \text{ mol m}^{-3} \text{ s}^{-1}$ and a t_c of 50 s this leads to $C_{sf} = 1 \text{ mol m}^{-3}$. This value is much larger than typical K_s values as shown in Table 4.1. For the case $t_c > t_{crs}$, this means that the cells experience at the substrate feed position substrate concentrations in the liquid that are a multitude of the one they should experience according to the Monod equation and that the growth rate should vary very much along the circulation loop, when Monod kinetics are instantly valid. It is questionable if this really occurs, as it is known that in medium-scale fermenters, with circulation times of 1-10 s, no problems with regard to production and growth are encountered. This leads to the assumption that the cells are able to level out the concentration differences to some extent. In very large-scale fermenters, however, it has been observed several times that the overall yield of growth and production can decrease, due to this effect. The solution in this case is the introduction of multiple substrate addition points. For the cell, circulating in the vessel, it is not the mixing in the vessel as a whole that is important, but the time between the presence of two substrate addition positions. For a single addition point the time between two addition positions is equal to the circulation time, but with two addition positions, the time needed to reach the next addition position is the only relevant one for the cell. In the loop model it decreases the time proportionally for equally spaced addition points. Comparable to the dependence on C_{ols} as shown in Fig. 18.1, a relationship with a number of feed positions like that given in Fig. 18.2 can

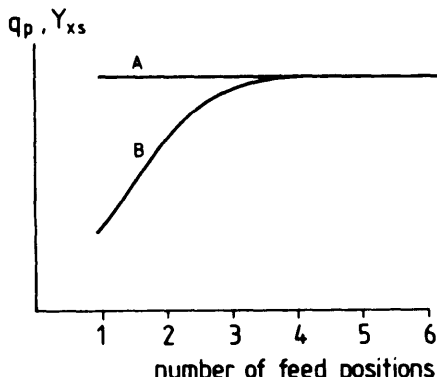


Fig. 18.2 Example of the influence of the number of evenly distributed substrate feed positions. Line A: A very small-scale, ideally mixed fermenter. Line B: A large-scale, stirred fermenter.

be expected. This also gives an experimental means to figure out the existence of this problem for the given fermenter. The measurement is executed by adding the total amount of substrate by a single feed addition position and measuring the relevant parameter such as overall yield. The same measurement is repeated, now with the substrate feed equally divided over two feed addition positions. Similar experiments with an increasing number of feed addition positions are executed until no influence is found any more.

The loop model shows that the feed positions should be evenly distributed along the loop. This can easily be done in an air lift type of fermenter. Because the flow profiles in the stirred fermenter and the bubble column are much less well defined, it cannot be defined exactly where the substrate addition points should be positioned. Trial and error based on assumed flow profiles seems to be the best procedure. It clearly shows one of the advantages of the air lift fermenter for very large ($\gg 100 \text{ m}^3$) scales.

The calculations given above are for an aerobic system. Eq. (18.1) also applies for anaerobic systems. Therefore, the same procedure can be followed. In anaerobic systems mixing is usually very poor and therefore in a feed-type fermentation the cells will nearly always experience a changing environment. However, if this leads to a switch from, for instance, growth to maintenance, this can even be profitable, because many times the product is formed as part of the maintenance process and in this way the yield of product on substrate will increase. This will be one of the reasons for the relatively small attention that is usually paid to mixing in anaerobic systems.

18.1.4 The critical time for heat production

With ΔT ($^{\circ}\text{C}$) the temperature variance that is allowed, ρ_b the broth density (kg m^{-3}), HPR (W m^{-3}) the heat production rate and c_{pb} ($\text{J kg}^{-1} \text{ }^{\circ}\text{C}^{-1}$) the thermal coefficient of the broth, the critical time for heat production, t_{crH} (s), is given by

$$t_{crH} = \frac{\Delta T c_{pb} \rho_b}{HPR} \quad (\text{s}) \quad 18.10$$

With $\Delta T = 0.1 \text{ }^{\circ}\text{C}$ and order of magnitude values for the other parameters, t_{crH} is of the order of 100 s. Cooling coils or cooled vessel wall parts usually will be present at several positions in the loop and therefore temperature differences generally can be neglected. For anaerobic systems the heat production is small compared to the aerobic ones. But mixing is usually poorer also, so this can level out the advantage of the low heat production. Usually no problems will occur. However, for extremely sensitive fermenters

tations like that for pilsener beer, small temperature differences can lead to detectable quality defects. Therefore, scale-up for this type of products should be done with t_{crH} in mind.

18.1.5 Conclusions concerning the critical times

For large-scale aerobic fermenters the critical times for oxygen and C substrate become of the same order of magnitude as the circulation time. Therefore design and operation of these fermenters has to take these effects into account. For oxygen this means that the oxygen concentration at the stirrer position in stirred vessels and in the top of the fermenter for air lift fermenters has to be above a required minimum level. This can become problematic in large vessels. For the C substrate very large fermenters will require multiple substrate addition points. Air lift fermenters have certain advantages in this respect. The biological background of substrate concentration variations is complex and not well understood. Trial-and-error methods are still the only way to find out the influence in a given fermenter. Temperature variations usually will not create any problems.

18.2 Engineering restrictions for design

18.2.1 Introduction

From the critical time concept it appeared that minimum values for mass transfer and mixing are needed to overcome negative effects. However, in Chapter 9 it was mentioned that the mixing time will increase with scale-up and that it is simply impossible to overcome this increase except with absurd stirrer power or gas flow rate. Because mass transfer is related to stirrer power and gas flow rate, its value will be limited too. With the limitation of mass transfer the biomass and product concentration are also limited. A further complication of biomass is the viscosity with filamentous microorganisms. Thus it appears that rational engineering leads to upper limits for productivity. Before discussing the design and optimization procedure in Section 18.3, the engineering restrictions will be discussed in this section. The mixing time restriction is not discussed because that has already been done in Chapter 9 and Section 18.1.

18.2.2 The mass transfer restriction

As shown in Chapter 11, the oxygen mass transfer coefficient $k_{oi}A$ (s^{-1}) is mainly related to gas flow rate and stirrer power consumption. The stirrer power is usually in the range of 1 up to 5 $kW m^{-3}$. The lower limit is determined by the need to prevent flooding. The upper limit is given by the chance of shear damage at increasing stirrer speeds and simply by mech-

anical reasons: a 5-kW m⁻³ power consumption results in a 1-MW motor on top of a 200-m³ fermenter. Gas superficial velocities are usually limited to the range of 0.01 up to 0.10 m s⁻¹, after correction for local pressure. The mass transfer coefficient in a stirred vessel is given by Eqs. (11.40) and (11.41) and in a bubble column by Eq. (11.35). With the limits for stirrer power and gas flow rate these equations give the upper limits that $k_{oi}A$ can reach. These are in the range of 0.2 s⁻¹ for the stirred vessel and 0.06 s⁻¹ for the bubble column, both for coalescing systems.

The second factor that determines the oxygen mass transfer rate (OTR) is the driving force. Here the fermenter top pressure is an important factor. Mechanical reasons limit the top pressure. Costs of compression can also become relevant. The use of pure oxygen or oxygen-enriched air is also a means to increase the driving force, but the costs again can be too high. A side effect is that a high driving force, together with a considerable part of the oxygen consumed, inherently leads to a CO₂ concentration of the same order of magnitude as the O₂ consumed. Many cells show a limit in tolerance to the partial CO₂ pressure in the liquid. When a design has to be made all these considerations have to be worked through, to find the optimal combination. Usually an increased top pressure is economical but only for the range of 2×10^5 up to 5×10^5 N m⁻². With a C_{oi} value that has to be > 0 this leads to driving forces that do not exceed the value of 1 mol m⁻³.

The driving force also decreases due to the transfer process itself. When the gas phase is ideally mixed, the concentration in the reactor is equal to that in the gas outflow. It is economical to use as much of the compressed oxygen (air) as possible. This means that the driving force of 1 mol, stated above, will never be reached. Mass transfer calculations will become much more complex when the H_o/T_o ratio for a vessel becomes large, i.e., for tall columns. Now the assumption of a well mixed gas phase is not valid any more. This is complicated by the change in hydrostatic pressure for large-scale reactors.

In air lift reactors with a height larger than about 10 m the high driving force at the bottom of the reactor gradually decreases with height because of decreasing static pressure. Above that the driving force decreases with distance from the bottom because of oxygen depletion due to the transfer. We can assume that backmixing of the gas phase is absent. For very low or zero OUR values the effect of decreasing static pressure and depletion of the bubbles even leads to transfer from the liquid phase back to the gas bubbles in the upper part of the column. Calculation methods discussed in Section 11.2.3.1.3 include the effects of static pressure and gas phase concentration, thus making possible quantitative calculations. Depending on OUR , top pressure and further design and operating variables a height larger than 50 up to 100 m usually leads to problems with oxygen depletion in the

upper parts of the air lift. A similar problem for the bubble column is shown in Example 18.1.

For tall bubble columns the same two effects as discussed for the riser section of the air lift apply: Decrease of static pressure with height and depletion of the gas phase due to mass transfer in lower areas. Modeling and calculation is not as straightforward as for the air lift fermenter. Example 18.1 shows one of the ways to model a high, tall bubble column as well as the consequences of the effect of gas phase depletion and decreasing static pressure. Because the liquid velocity is smaller than in the air lift, problems can occur at much smaller height values than 50 m.

Combining all the limitations given above, OTR can maximally be up to $0.2 \text{ mol m}^{-3} \text{ s}^{-1}$ for the stirred vessel and 0.06 for the bubble column. As these values are the combination of extremes, values below, say, $0.05 \text{ mol m}^{-3} \text{ s}^{-1}$ ($180 \text{ mol m}^{-3} \text{ h}^{-1}$) are more reasonable maxima. Anyway these calculations show that mass transfer in a fermenter is limited. This imposes limitations on the fermentation. Eq. (2.6b) can be rewritten for CH_2O as substrate as

$$\begin{aligned} -r_o^u &= OTR = -1.094 r_x^u - r_s^u \\ &= -1.094 \mu C_x + \frac{\mu C_x}{Y_{xs}} + m_s C_x \quad (\text{mol m}^{-3} \text{ s}^{-1}) \end{aligned} \quad 18.11$$

or

$$OUR = \left[\left(\frac{1}{Y_{xs}} - 1.094 \right) \mu + m_s \right] C_x \quad (\text{mol m}^{-3} \text{ s}^{-1}) \quad 18.12$$

Fig. 18.3 shows OUR values dependent on growth rate and cell density. The cell density is in a range where limitation due to its physical size does not occur. But depending on the OTR that can be obtained, limitation due to mass transfer occurs, for both cell densities shown in Fig. 18.3, above a certain growth rate for the higher cell density value already at very low growth rates. This example clearly illustrates that OTR is a limiting parameter. It can be said in general that oxygen mass transfer is the determining limitation for most (aerobic) fermentations.

18.2.3 The viscosity restriction

In the preceding section it was shown that low viscous fermentations are limited by the OTR at increasing cell density and growth rate. Fig. 18.3 showed the OUR values as calculated from the balance and kinetic equa-

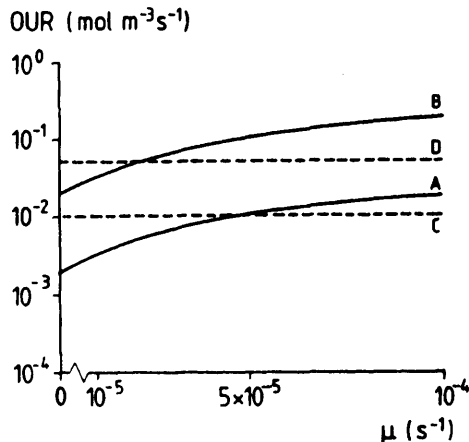


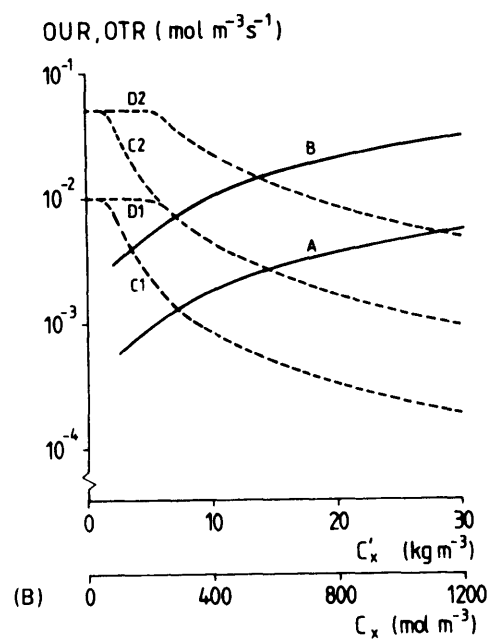
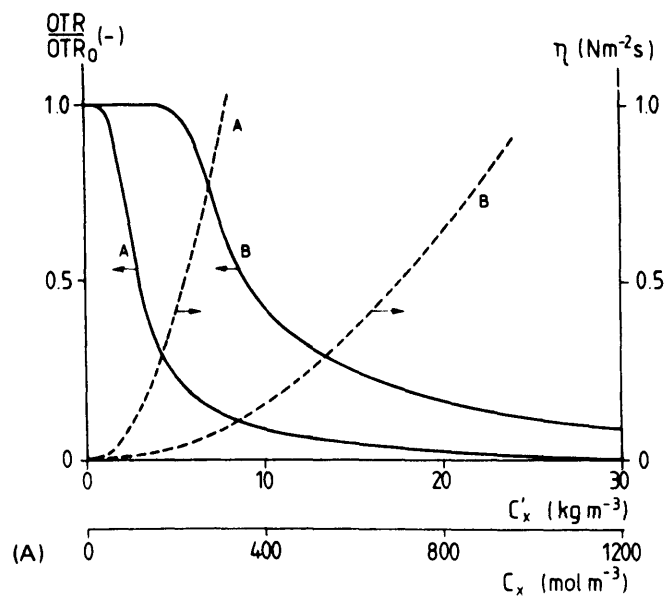
Fig. 18.3 Calculated OUR values from Eq. (18.12) for $Y_{xs} = 0.66$ (-) and $m_1 = 4.6 \times 10^{-6} \text{ s}^{-1}$.
 Line A: $C_x = 400 \text{ mol m}^{-3}$ (10 kg m⁻³). Line B: $C_x = 4000 \text{ mol m}^{-3}$ (100 kg m⁻³). Line C: $OUR = 0.01 \text{ mol m}^{-3} \text{ s}^{-1}$ (36 mol m⁻³ h⁻¹). Line D: $OUR = 0.05 \text{ mol m}^{-3} \text{ s}^{-1}$ (180 mol m⁻³ h⁻¹).

tions with C_x and μ as variables. However, the $k_{o,A}$ and therefore the OUR data in this figure only hold for low viscous fermentations, e.g., for yeast and bacteria. Filamentous microorganisms show an increase in viscosity with cell density as given in Chapter 7. Eq. (11.42) shows that $k_{o,A}$ will decrease at viscosities above $50 \times 10^{-3} \text{ N s m}^{-2}$. This means that the maximum attainable OTR for a given fermenter decreases with increasing cell density. Fig. 18.4A shows two examples of calculated η and OTR values for a filamentous broth. Fig. 18.4B shows a figure similar to Fig. 18.3 with C_x on the horizontal axis. It clearly shows that viscosity limits the attainable C_x value to very low levels, even below values of 10 kg m⁻³. For large-scale fermenters this occurs in a regime where the Re number is large enough to prevent bad mixing. The only solution for this problem is to decrease the viscosity either by changing the physiology of the microorganism or by pellet formation. Increasing the mass transfer capabilities by further increasing stirrer power and gas flow rate is rather useless. This is a clear example where the microbiology and technology should work together. The problems created by the microorganisms cannot be solved economically by process engineering. They should simply be prevented.

18.2.4 Heat, hold-up and foam restrictions

As shown in Chapter 13, the main heat production sources are oxygen consumption and stirrer power consumption. Reasonable values as estimated in Section 18.2.2 are $OUR = 0.05 \text{ mol m}^{-3} \text{ s}^{-1}$ and $P/V = 2000 \text{ W m}^{-3}$. Application of Eq. (13.3) yields for the heat production r_H^u (W m⁻³):

$$r_H^u = 460 \times 10^3 \times 0.05 + 2000 = 25000 \quad (\text{W m}^{-3}) \quad 18.13$$



With the high stirrer power consumption and gas flow rates involved with these maximum *OUR* values, the heat transfer coefficient h_1 ($\text{W m}^{-2} \text{C}^{-1}$) can be calculated with Eqs. (13.8) and (13.9) to be around 4000 ($\text{W m}^{-2} \text{C}^{-1}$). With an assumed average temperature difference of 10°C between broth and cooling water it can be calculated that the requirement for the surface area required for cooling is about 1 m^2 of cooling surface per m^3 reactor volume. This can easily be provided with cooling coils or parallel connected outside heat exchangers. The conclusion is that generally heat production is not a restriction.

Hold-up is no restriction either. The only disadvantageous aspect is that fermenter volume is occupied by the gas hold-up and as such not available for microorganisms. The hold-up values for the conditions as given in Section 18.2.2 are in the range of 15% up to 30% and therefore the effective fermenter volume is only 70% up to 85%.

Foam again is not a restriction. As shown extensively in Chapter 12, foam can be adequately prevented with antifoam agents. It must be remembered that foam and mass transfer are related by means of the coalescence characteristics of the bubbles. Thus it is connected with the mass transfer restriction. Part of the head space is needed as a safety margin for foam control. When this is added to the hold-up volume, it appears that the effective fermenter volume even decreases to less than the 70% up to 85% calculated from the hold-up correction.

18.2.5 The biomass concentration

As shown in Eq. (18.12), the maximum attainable biomass concentration is related to the mass transfer restriction. The values are far below the value where the biomass as such can be a restriction, i.e., where the physical limits

Fig. 18.4A Viscosity and OTR , calculated with Eqs. (7.3), (7.6) and (11.42).

Case A: $K = 0.05 (C'_x)^2$, $n = 0.5$, $\gamma = 10$.

Case B: $K = 0.005 (C'_x)^2$, $n = 0.5$, $\gamma = 10$.

Fig 18.4B Calculated OTR values, based on Fig. 18.4A, and comparison with OUR values, based on Fig. 18.3.

A: OUR at $\mu = 0$. Data the same as for Fig. 18.3.

B: OUR at $\mu = 5 \times 10^{-5} \text{s}^{-1}$. Data the same as for Fig. 18.3.

C: OTR C₁: Case A in Fig. 18.4A with $(OTR)_{\text{water}} = 0.01 \text{ mol m}^{-3} \text{s}^{-1}$.

C₂: Case A in Fig. 18.4A with $(OTR)_{\text{water}} = 0.05 \text{ mol m}^{-3} \text{s}^{-1}$.

D: OTR D₁: Case B in Fig. 18.4A with $(OTR)_{\text{water}} = 0.01 \text{ mol m}^{-3} \text{s}^{-1}$.

D₂: Case B in Fig. 18.4A with $(OTR)_{\text{water}} = 0.05 \text{ mol m}^{-3} \text{s}^{-1}$.

of its size are reached. This is in the range of 150-250 kg m⁻³. Long before this is reached, mass transfer or other limitations will occur.

The biomass concentration value can be calculated from the total biomass M_x and the volume of the broth V_b in the reactor. For the batch and fed-batch reactor the $M_x(t)$ is calculated with the balances and yield equations as shown in Chapter 2 (see also Example 2.1). V_b can be determined from the broth weight $G(t)$ (kg) with the weight balance as shown in Chapter 2 (Example 2.5). Then $C_x(t)$ is given by

$$C_x(t) = \frac{M_x(t)}{V_b(t)} = \frac{M_x(t)}{G(t)} \rho_b \quad (\text{mol m}^{-3}) \quad 18.14$$

with ρ_b (kg m⁻³) the broth density. For a fed-batch the weight will nearly always increase with time, mainly due to the substrate feed component, which means that C_x will increase to a lesser extent than M_x . For a batch the substrate feed component is absent, leaving only O₂, CO₂ and evaporation. Here the weight will usually decrease with time, leading to a faster increase of C_x .

When a fermenter is mass transfer limited, it means that it is only used at its full potential when this limitation is actually reached. Just after inoculation this will not be the case (see also Examples 2.1 and 2.2). This period then should be as short as possible to reach the most economical situation. The inoculum therefore should not be too small. Quantities of .1 up to .5 times the final quantity to be reached are usual. A calculation scheme can be set up, including the balances and the costs of a line of inoculation vessels of increasing size, to calculate the optimal set-up of inoculation vessels and production vessels. The reasoning that the limits of the fermenter should be reached as fast as possible makes the batch fermenter completely unattractive for those applications where the growth rate cannot be controlled. In that case the constant growth rate causes an exponential increase of the OUR (see the start of the fermentation in Example 2.2). At a certain moment the OUR value becomes equal to the mass transfer capacity. This automatically means that the end of the exponential increase is reached. Only at this very last moment is the mass transfer capacity fully used; during the whole period of the fermentation only (a small) part of the capacity is used. For the fed-batch fermentation the mass transfer can be controlled and therefore this reactor concept is favorable.

For a continuous culture cell concentration can be calculated from the growth equations and the balances over the fermenter. The equations are given in previous chapters and can be used for straightforward calculation of C_x and the corresponding OUR. In this case the required OUR and

fermenter capacity can be fitted to each other very precisely. At first sight the maximum attainable C_x is the same for continuous culture and fed-batch. However, in a fed-batch the growth rate can be controlled in such a way that a decrease of μ is used to keep OTR constant at increasing C_x (see also Example 2.2). By doing this a larger C_x can be obtained than in a continuous culture. For the product concentration the difference is even more striking. The cell separation step after the fermentation is usually expensive, and becomes less expensive per kg biomass when the C_x increases. This makes the continuous culture much less favorable than the fed-batch. This is one of the reasons that large-scale commercial fermentations are usually of the fed-batch type.

18.2.6 The product concentration

The product concentration is a very important factor for the economics of the recovery process. A number of unit operations, in particular in the separation and concentration, are "volume dependent," which means that the capacity is independent of the product concentration. This makes the costs inversely proportional with that concentration.

The concentration for a batch and fed-batch is given by the following equation:

$$C_p = \int_0^{t_e} q_p C_x(t) dt \quad (\text{mol m}^{-3}) \quad 18.15$$

This equation shows that the batch fermenter is only attractive for production for those applications at which the C_x value is large for the whole fermentation. For most batch fermentations exponential growth occurs and for a large part the productivity will be low due to the low C_x value. Sometimes the growth rate can be controlled, for instance with N limitation. The fed-batch is usually preferred because it can be controlled with C limitation.

The concentration in the continuous culture is given by

$$C_p = q_p C_x \tau = \frac{q_p C_x}{\mu} \quad (\text{mol m}^{-3}) \quad 18.16$$

This means that the product concentration is dependent on the growth rate. Comparing a continuous culture and a fed-batch with the same cell concentration (both determined by the mass transfer attainable), the product

concentrations have the ratio of t_e/μ^{-1} . t_e can easily be 200 h or more; the μ^{-1} value usually will be much smaller. Dilution effects because of volume increase in the fed-batch are left out from this calculation, but even so we can conclude that for a large number of cases the fed-batch yields much higher product concentrations than the continuous culture. This is again a reason for application of the fed-batch.

The above equations are simple. When more knowledge is available about the production characteristics of the cells, extensive models can be made, including an optimization of product concentration and productivity. This will not be worked out further here because it is dependent on the details of each case. It requires the application of both basics and engineering as given in the preceding chapters, combined in a computer model, and with an optimization routine added. An illustrative example of such a procedure is given by Heijnen et al., (1979).

18.3 General design and optimization schemes for fermenters

18.3.1 The design scheme

For design of fermenters all knowledge about balances, yield and engineering has to be integrated. This is a very complex task. In this chapter the general procedure will be discussed. The general schemes are given in Figs. 18.5 and 18.6. Three steps can be distinguished.

Step 1

Statement and translation of the objective. Simple objectives like "produce 100 tons of biomass per day" or "produce 1 g of interferon per day" are adequate. This objective is translated in r and M values that can be used as input for the second step. This is the procedure shown in the upper half of Fig. 18.5

Step 2

Process engineering calculations with the restriction as the pivot. For aerobic fermentations this will usually be the OTR . This is the part that is given in Fig. 18.6.

Step 3

Final calculation of fermenter layout with the data from step 2. This is the procedure shown in the lower half of Fig. 18.5.

With step 1

For these calculations no knowledge is used yet of the engineering of the large-scale reactor. Only indicative knowledge about the importance of the

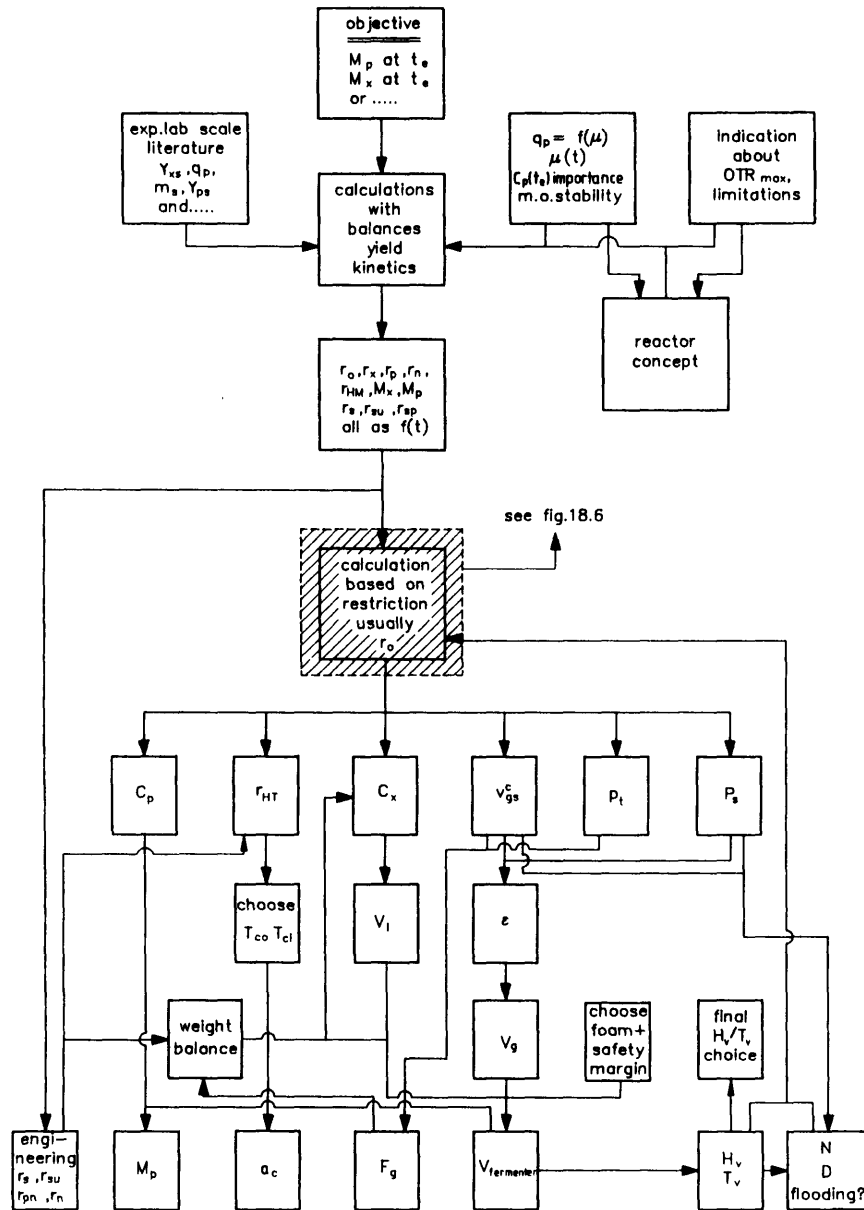


Fig. 18.5 The general design scheme for a fermentation.

OTR restriction is used, to be included in the reactor concept choice. Then the microbiological parameters are determined. All those that are less relevant or to which the end result will be rather independent are taken from the literature. The important ones are determined in lab-scale experiments. Then these data are used to calculate the r and M values. The "simple" objective is translated in this way in useful data.

With step 2

Here a distinction between aerobic and anaerobic processes has to be made. For anaerobic fermentations the limitations are usually absent, so the design can be made straightforward. For aerobic fermentations only the substrate flows can be engineered straightforward. For the other parameters and the likely case of *OTR* limitation the extended scheme is given in Fig. 18.6. Now a reactor type has to be chosen, then an *OTR* limitation. This determines the stirrer power consumption P , and the local pressure-corrected superficial gas velocity v_g^c . These are chosen here to start the iteration procedure that determines the final values. They are chosen on the basis of common sense for what is acceptable for the type of reactor that is chosen. The *OTR* limitation also determines the C_x value, as shown also in Section 18.2. Because M_x is given, with C_x the reactor dimensions can be calculated, of course with an assumption for hold-up and foam. The viscosity also can be calculated from C_x , and if needed a new *OTR* can be calculated for this viscosity value. This will result in the first iteration scheme in which the *OTR*, C_x and η will be adapted to each other. From the data now known the $k_{o,A}$ and the circulation time can be calculated. With the appropriate formula $k_{o,A}$ and *OTR* together determine the required driving force. The required driving force is then obtained by adjusting the top pressure p_t . The gas balance iteration loop corrects this for the gas phase depletion. Now the first iteration loop is ended and the calculations can start again with the new data. Contrary to a normal iteration loop, the following loops are not done straightforward to come to the final p_t value, but each of the parameters P , v_g^c , H , T , and p_t can be changed by subjective choice. This is all paperwork with the formulae given in this book and it can be left to this, except for the viscosity relations. It is useful to determine these for the given strain in pilot experiments. However, when very large fermenters have to be designed, it is recommended to introduce a design for a 1- or 5-m³ fermenter. In pilot plant experiments this gives the opportunity to test the procedure, in particular the formulae used for mass transfer (according to the method given in Section 11.4) and viscosity.

With step 3

These are all simple calculations and the result is the final layout of the fermenter. However, a check has to be made with the 2 calculations to find

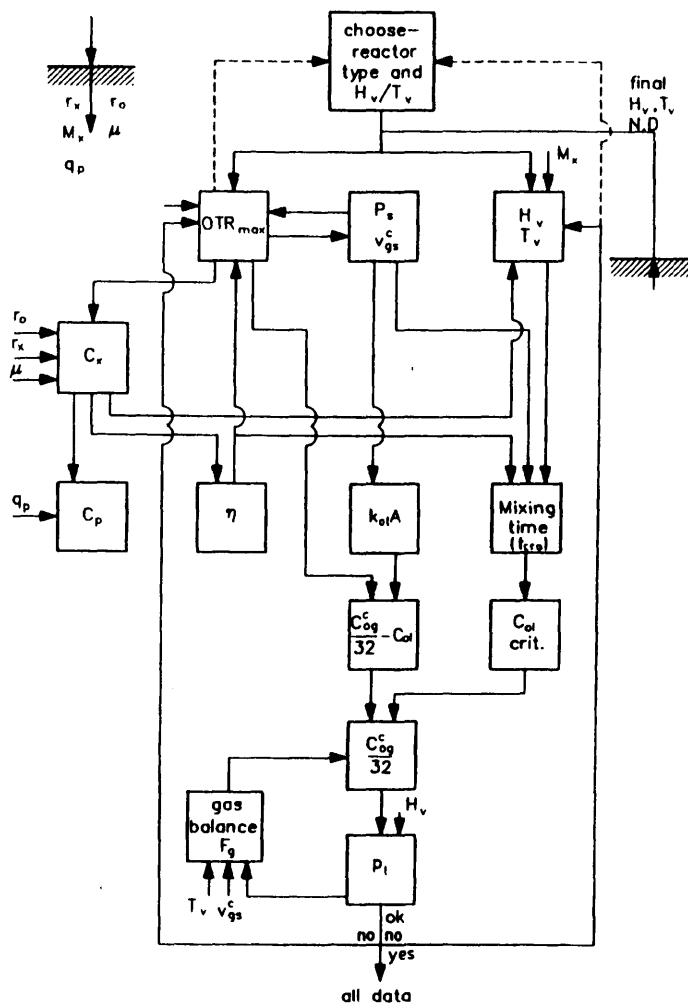


Fig. 18.6 The design scheme for an aerobic fermenter.

out if all assumptions are really valid. Particularly, hold-up and the weight balance (C_x) can be important. After a number of iterations the final design will be ready.

The whole scheme shows that a number of choices have to be made and that the final result will vary with these choices. Further, the final result is just as reliable as the formulae used. It has been mentioned several times that a

fermentation broth cannot be characterized to such an extent that the margins in the formulae become smaller than 10% up to 20%. This has to be accepted. After installment the optimization procedure as given in the next section can be applied.

A complete procedure is too large to be covered by an example. Example 18.2 gives a small part of a total design, based on the data of Example 2.1.

18.3.2 The optimization scheme

The first objective of an optimization is to obtain minimum operation costs. But usually after some time the question is asked, "Can we make more product in this fermenter because there is a market for it". This question can be answered with the method described here. The optimization has to be based on the knowledge of the exact mass transfer, viscosity, mixing and hold-up, and on the relationship between mass transfer and foam destruction. This means that all relevant parameters in the pertinent formulae have to be determined in the production fermenter itself with the production strain. This is unavoidable because it is unknown whether there is a difference between the parameter values on pilot scale and production scale because, as said, the broths will differ to some unknown extent. Reasons can be, for instance, different shear stress regimes (N is always different), differences in substrate concentration variations (t_m is always different), while above that, we do not know how a specific strain responds to these differences, neither do we know how the parameters in the formulae change with the resulting changes in the broth. Sometimes microbiological parameters will also have to be rechecked. The $k_{o,t}A$ relation can be determined with the method described in Fig. 11.5, the critical oxygen concentration with the method given in Fig. 18.1 and the relation between foam layer, effective volume and $k_{o,t}A$ can be determined from $k_{o,t}A$ measurements also. This part of the procedure is shown in the upper part of the total optimization scheme as given in Fig. 18.7. With the known equations a calculation scheme can be set up about the influences of, for instance, changes in $v_{o,t}$, P_t and P_c . This procedure, following the scheme of Fig. 18.7, yields the increase in M_p and also the increase in product gains. Also the costs for introduction of the assumed changes in the operating variables can be calculated. It might very well be that a change in two of the variables, for instance an increase of P_t with decrease in P_c , leads to a more economical fermentation at the same product output. By introducing all data in an optimization routine, the optimum design of the fermenter can be calculated. Besides the optimization itself, a parameter sensitivity analysis can be interesting. For instance, in viscous mycelia it can be determined to what extent the M_p value can increase when a decrease in viscosity (K value) is attained. This can motivate microbiologists considerably to find a better strain with respect to viscosity. (A principle should be that viscous

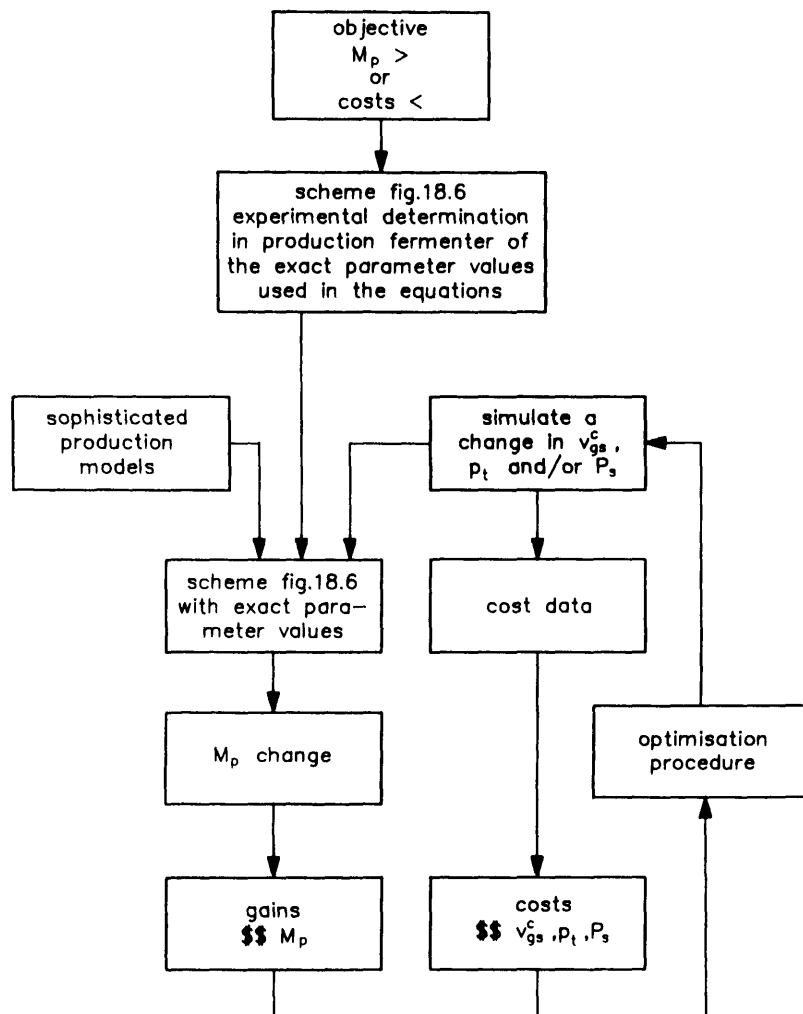


Fig. 18.7 The general optimization scheme for a fermenter.

strains are prevented anyhow because the *OTR* restriction means that production costs for viscous strains always are much larger than for non-viscous strains.) Most of the optimization routine is done by computer optimization procedures. This makes it attractive to use production models like that given by Heijnen et al. (1979).

18.4 Cost aspects of engineering design and optimization

18.4.1 The general case

In the previous section the OTR could be chosen without cost considerations. Increasing OTR results in a decrease in V_t , leading to a cheaper fermenter. But in Section 11.2.3.1.1 it was shown that $k_{ol}A$ increases with the total power with an exponent < 1 . This means that at increasing OTR the (power) costs per mol oxygen increase. Thus it is important to find out the relevance of these cost factors to include in the design scheme.

The quantity used to indicate the oxygen transfer efficiency is the weight of oxygen transferred at a kWh:

$$\frac{\text{kg O}_2}{\text{kWh}} = \frac{OTR \cdot 3600 \times 32 \times 10^{-3}}{\left(\frac{P_s}{V_t} + \frac{P_a}{V_t} \right) 10^{-3}} \quad (\text{kg kWh}^{-1}) \quad 18.17$$

For OTR the equation reads:

$$OTR = k_{ol}A \left(\frac{C_{og}^c}{m} - C_{ol} \right) \quad (\text{mol m}^{-3} \text{s}^{-1}) \quad 11.8$$

Assume a coalescing liquid and two simplified cases. The first case is a stirred fermenter with one stirrer at $0.4 T_v$ above the bottom. The second case is a bubble column with the driving force assumed to be equal to the driving force halfway between bottom and top of the column. For both cases the gas phase is assumed to be ideally mixed. Then the equations read, using Eq. (11.45) to derive Eq. (18.18), Eq. (11.37) for Eq. (18.21), Eq. (11.45) for Eq. (18.24) and local pressure corrections for Eqs. (18.19), (18.20), (18.22) and (18.23):

Stirred tank

$$OTR = 2.6 \times 10^{-2} \left(\frac{P_s}{V_t} \right)^{0.4} \left(v_{gs} \frac{P_a}{P_s} \right)^{0.5} \left(\frac{C_{og}^c}{m} - C_{ol} \right) \quad (\text{mol m}^{-3} \text{s}^{-1}) \quad 18.18$$

$$C_{og}^c = \left(\frac{P_t + (H_v - 0.4T_v)\rho_t g}{P_a} \right) C_{ogo} \quad (\text{mol m}^{-3}) \quad 18.19$$

$$v_{gs} \frac{P_a}{P_s} = F_g \left(\frac{P_a}{P_t + (H_v - 0.4T_v)\rho_t g} \right) \frac{1}{\frac{1}{4}\pi T_v^2} \quad (\text{m s}^{-1}) \quad 18.20$$

Bubble column

$$OTR = 0.32 (v_{gs}^c)^{0.7} \left(\frac{C_{og}}{m} - C_{oi} \right) \quad (\text{mol m}^{-3} \text{s}^{-1}) \quad 18.21$$

$$C_{og}^c = \left(\frac{p_t + 0.5H_v \rho_t g}{p_a} \right) C_{ogi} \quad (\text{mol m}^{-3}) \quad 18.22$$

$$v_{gs}^c = F_g \left(\frac{p_a}{p_t + 0.5H_v \rho_t g} \right) \frac{1}{\frac{1}{4}\pi T_v^2} \quad (\text{m s}^{-1}) \quad 18.23$$

Both:

$$OTR V_t = F_g (C_{ogi} - C_{ogo}) \quad (\text{mol s}^{-1}) \quad 18.24$$

or

$$C_{ogo} = C_{ogi} - \frac{OTR V_t}{F_g} \quad (\text{mol m}^{-3}) \quad 18.25$$

These equations show that OTR and therefore the oxygen transfer efficiency is influenced by p_t , v_{gs} , P_g , F_g and V_t , in a complicated way.

18.4.2 The influence of the operating variables

Example 18.3 shows a number of calculations for the operating variables p_t , P_g and v_{gs}^c . A number of conclusions can be drawn which are not limited to that example only.

- It appears that, as expected, the transfer efficiency decreases with increasing power per unit volume for all simulations. The efficiencies are in the range of 0.5 up to 2 kg O₂/kWh for normal conditions. The decrease could already be expected from the relationship between $k_{oi}A$ and total power per unit volume: Section 11.2.3.1.4 shows that $k_{oi}A$ increases with power with an exponent < 1.
- The kg O₂/kWh is used sometimes as a sales argument. Here we can see that such a number is relevant only when the absolute value of OTR is also given.
- Large differences can exist for the same OTR . In Section 11.2.3.1.4 it appeared that power input due to the gas flow rate should not be « than that due to the stirrer. Indeed when this is included the bubble

column and the stirred vessel are in the same maximum range (curves 3, 5 and 2 in Fig. 18.12).

- With increasing p_i , the oxygen transfer efficiency can become better as well as worse. In general, moderate values of p_i are the optimal ones. At constant F_g , the efficiency can decrease considerably with increasing p_i . This is due to an increasing depletion of the gas phase. Above that the $k_{L,A}$ decreases because $v_{g,i}^c$ decreases. This levels out the advantages of the increased pressure to a large extent, particularly for the bubble column. At constant $v_{g,i}^c$, the stirred tank is optimal. This is because the depletion stays limited and because the gas energy is not the main energy component over a wide range. In this example the bubble column with constant $v_{g,i}^c$ is below the optimal line. This is because the depletion is not large enough, leading to a large F_g and also large compression energy while the gas is not used.

In conclusion, it is clear that the balance between the three components is very subtle. In the case of a new design or an existing fermenter it is useful to make this type of exercise to find the optimum ratio. Large gains are possible.

18.4.3 The choice between V_i and OTR

Increasing V_i at a defined r_o leads to a decrease in OTR and therefore to an increase in the $\text{kg O}_2/\text{kWh}$. Thus a choice is possible between volume costs and energy-related costs. This is relevant only when the two costs are of the same order of magnitude. If we define $\$_o$ as the costs per m^3 per hour due to the energy needed for oxygen transfer and $\$_e$ as the energy costs per kWh ($\$ \text{ kWh}^{-1}$), then it can be derived that

$$\$_o = 32 \times 10^{-3} \times 3600 \ OTR \frac{\$_e}{\text{kg O}_2 / \text{kWh}} \quad (\$ \text{ m}^{-3} \text{ h}^{-1}) \quad 18.26$$

Example 18.4 gives a number of calculations from which it appears that $\$_o$ can be of the order of 0.01 up to $2 \$ \text{ m}^{-3} \text{ h}^{-1}$. In the following section it will be shown that the total costs of each m^3 of a large scale fermenter are of the order of $1 \$ \text{ m}^{-3} \text{ h}^{-1}$. When a design is started, the costs for design of a larger fermenter is much less than linearly related to the volume because only the fermenter itself has to be larger, not all equipment surrounding it. When the $\$_o$ are of the order of .1 and larger, a design with a larger fermenter will decrease this number and that can easily result in a fermentation that is cheaper per hour. For each design this has to be tried out with the given values of fermenter cost and energy cost. Again this will lead to moderate OTR values. An example can be found in Van 't Riet (1983).

An interesting contradiction is the optimization once the fermenter is installed. If more product can be sold it can be profitable to increase the energy input in order to improve the *OTR* following the scheme of Fig. 18.7. This leads to values that are suboptimal when seen from the design reasoning given above. The reason is that the increase in *OTR* is not optimized with respect to minimum total costs (V , is not a variable for an existing vessel) but with respect to additional costs versus additional product gains. Thus such an optimization can be very attractive from the viewpoint of sales, but the total production costs are higher than in the case of an optimized design starting with the input of the increased production value.

18.5 General cost estimates

This book is not directed to cost calculations for bioprocesses. Yet some of the consequences for design on costs are given, as done for oxygen efficiency in the previous section. In this section methods will be discussed how to obtain first estimates of product production costs on the basis of parameter values determined from literature and lab-scale data only. The results can also be used to guide research management decisions as shown by Van 't Riet (1986).

18.5.1 Substrate costs

The overall yield of product on substrate, Y_{ps}^{ov} (-), is given in Chapter 3 as

$$Y_{ps}^{ov} = \frac{Y_{ps}}{1 + \frac{\mu Y_{ps}}{q_p Y_{xs}} + \frac{m_s Y_{ps}}{q_p}} \quad (-) \quad 3.17$$

When $\$, (\$/\text{mol}^{-1})$ are the substrate costs and $\$_{ps}, (\$/\text{mol}^{-1})$ the costs of product related to the substrate, it can be derived that

$$\$_{ps} = \frac{\$}{Y_{ps}^{ov}} = \frac{\$}{Y_{ps}} \left(1 + \frac{\mu Y_{ps}}{q_p Y_{xs}} + \frac{m_s Y_{ps}}{q_p} \right) \quad (\$/\text{mol}^{-1}) \quad 18.27$$

Because all equations in this book are given in molar units, these equations are also given in these units. They can also be used without any change in the formulae on a kg basis. Nearly always $Y_{ps}^{ov} < Y_{ps}$ and in many cases $Y_{ps}^{ov} \ll Y_{ps}$. Therefore, the substrate-related costs can be a multitude of the costs when calculated on the basis of Y_{ps} . This is because the substrate is used for growth and maintenance also, as can easily be seen from the last two terms of Eq. (18.27). This equation also shows that only parameters that

can be determined on a small scale are included. Example 3.1 showed the influence of different parameters on Y_{ps}^{ov} . These results can be used for the calculation of $\$_{ps}$, as shown in Example 18.5. The $\$_{ps}$ value can vary strongly, particularly with q_p , but the other parameters can also be important for certain ranges of values.

Similar equations can be derived for biomass production:

$$Y_{xs}^{ov} = \frac{Y_{xs}}{1 + \frac{m_s Y_{xs}}{\mu}} \quad (-) \quad 3.19$$

and:

$$\$_{xs} = \frac{\$_s}{Y_{xs}} \left(1 + \frac{m_s Y_{xs}}{\mu} \right) \quad (\text{\$/mol}^{-1}) \quad 18.28$$

with $\$_{xs}$ ($\text{\$/mol}^{-1}$) as the substrate related costs for biomass production. When $\mu < m_s$, then the Y_{xs}^{ov} value will be considerably lower than Y_{xs} , due to the significant amount of substrate used for maintenance. Example 3.2 showed simulations of Y_{xs}^{ov} , Example 18.6 shows the related $\$_{xs}$. At low μ values these become $\gg \$_s$. This is also connected with the OTR limitation. For recovery purposes the C_x value should be high. This favors a fed-batch. Example 2.1 gives data for a fed-batch with oxygen limitation. It is seen that μ gradually decreases in time. Example 18.7 shows the increasing biomass costs with time. This means that the fermentation will be stopped before the theoretically maximum attainable biomass concentration is reached. A calculation including the costs as given in this example and the recovery costs dependent on C_x can give the optimum length of the fed-batch.

For anaerobic product formation the substrate related production costs, $\$_{ps}^a$, are calculated with Eq. (3.21) as

$$\$_{ps}^a = \frac{\$_s}{Y_{ps}^{ova}} = \$_s \frac{\frac{\mu}{Y_{xp}^a} + m_p^a}{\frac{\mu}{Y_{xs}^a} + m_s^a} \quad (\text{\$/mol}^{-1}) \quad 18.29$$

Example 3.3 shows that the range of Y_{ps}^{ova} is limited, yet the influence of μ is present. Example 18.8 shows the $\$_{ps}^a$ values.

Anaerobic biomass formation is found from Eq. (3.26) as

$$\frac{\$_{xs}^a}{Y_{xs}^{ova}} = \frac{\$_{xs}}{Y_{xs}^a} \left(1 + \frac{Y_{xs}^a m_s^a}{\mu} \right) \quad (\text{\$/mol}^{-1}) \quad 18.30$$

Example 3.4 showed that $Y_{xs}^{ova} \ll Y_{xs}^{ov}$ at the same μ value. Therefore Example 18.9 shows that $\$_{xs}^a \gg \$_{xs}$, and $\$_{xs}^a \gg \$_s$. When biomass production is the objective, anaerobic fermentation is not very attractive.

The substrate-related cost data can also be used to optimize a fermentation. The procedure starts with a sensitivity analysis of the Y^{ov} formula, to find out the sensitive parameters. Graphs like that given in Examples 3.1-3.4 can also be used for this purpose. Then this result is compared to the chances of success and the costs of research to improve this parameter or to the costs of process improvements like an increase in OTR when μ has to increase. Examples for penicillin and plant secondary metabolites are given by Van 't Riet (1984, 1986).

18.5.2 The fermenter costs

The cost of running a fermenter is constituted of a multitude of factors like depreciation, overhead, labor, energy, cooling, etc. As mentioned before, it is not the objective of this book to give exact cost calculations. Yet to be able to make estimates a gross number is used. For a 200-m³ fermenter the costs of all factors together is about 1 \$ m⁻³ h⁻¹ (Van 't Riet, 1986; Swartz, 1979). This number is not very exact and a more accurate number can be calculated for a given situation if needed. Yet it is useful for estimations. The total hourly fermenter costs are given by $\$_{hf}$ (\$ m⁻³ h⁻¹). The fermenter-related hourly production costs $\$_{ph}$ (\$ mol⁻¹) for aerobic product formation can be calculated as

$$\$_{ph} = \frac{\text{fermenter costs}}{\text{product produced}} = \frac{\$_{hf}}{q_p C_x 3600} \quad (\text{\$/mol}^{-1}) \quad 18.31$$

For aerobic biomass production

$$\$_{xh} = \frac{\$_{hf}}{\mu C_x 3600} \quad (\text{\$/mol}^{-1}) \quad 18.32$$

For anaerobic product production

$$\$_{ph}^a = \frac{\$_{hf}}{\left(\frac{\mu}{Y_{xp}^a} + m_p^a \right) C_x 3600} \quad (\text{\$/mol}^{-1}) \quad 18.33$$

For anaerobic biomass production

$$\$_{xh}^a = \frac{\$_{hf}}{\mu C_x 3600} \quad (\text{\$ mol}^{-1}) \quad 18.34$$

Example 18.10 shows for aerobic product formation the influence of C_x and the other parameters on the $\$_{ph}$ as well as on the costs of the product after fermentation $\$_{pf}$, defined by

$$\$_{pf} = \$_{ps} + \$_{ph} \quad (\text{\$ mol}^{-1}) \quad 18.35$$

C_x and thus the maximum attainable *OTR* in the fermenter and the q_p value are very important. From Example 18.10 the economy of scale can be seen. For small scale fermentations ($1-10 \text{ m}^3$) $\$_{ph}$ is, in that example, the main important factor. Also it is interesting that at volumes $> 200 \text{ m}^3$ the scale does not influence the final result to that degree anymore, because the $\$_{ps}$ becomes relatively important.

The recovery process can be included in a similar way. As this book deals about bioreactor design only, this cost aspect will not be discussed here. Information can be found in Van 't Riet (1986, 1984).

18.6 Conclusions

Fermenter design and optimization are complicated because the optimal design is dependent on many factors. Yet it is possible to use an iteration procedure to get the desired design. Cost aspects have also been discussed. These can be included in the design procedure to find the optimal design for a given objective.

18.7 Examples

Example 18.1 Oxygen depletion in the top section of a large bubble column

In this example the gas and liquid oxygen concentration will be calculated for two tall bubble columns.

Case I: $H_v = 10 \text{ m}$, $T_v = 1 \text{ m}$
 Case II: $H_v = 50 \text{ m}$, $T_v = 1 \text{ m}$

The bubble columns are modeled with a rather simple model, a series of N ideal mixers for gas as well as liquid phase, with each: $H_v = T_v$. This is

shown schematically in Fig. 18.8. A balance can be set up for compartment n (Fig. 18.9) that reads for the liquid phase:

$$OTR V_t - OUR V_t - (F_t)_n (C_{ol})_n + (F_t)_n (C_{ol})_{n-1} \\ - (F_t)_{n+1} (C_{ol})_n + (F_t)_{n+1} (C_{ol})_{n+1} = V_t \frac{d(C_{ol})_n}{dt}$$

and for the gas phase

$$F_g [(C_{og})_n - (C_{og})_{n+1}] = OTR V_t$$

with

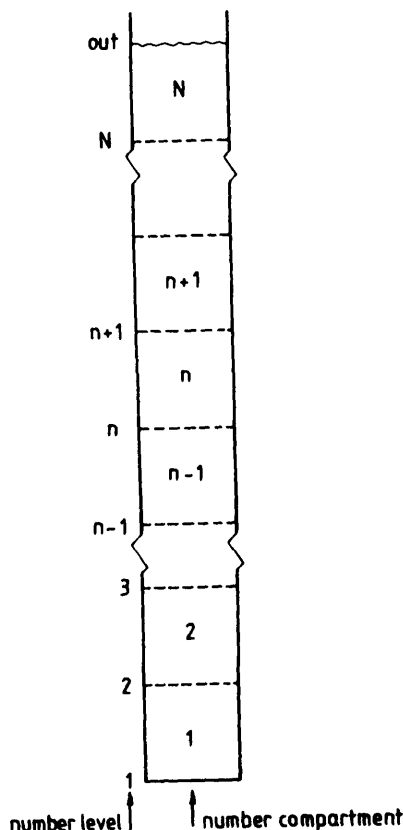
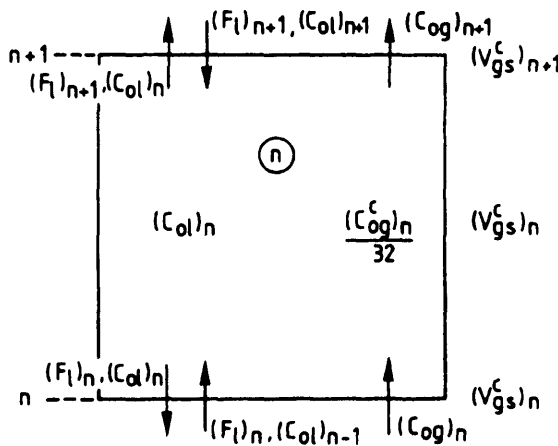


Fig. 18.8 The bubble column model. A series of ideal mixers.

Fig. 18.9 The flow scheme of compartment n .

$$OTR = k_{ol} A \left(\frac{C_{og}^c}{m} - C_{ol} \right)$$

$$k_{ol} A = 0.32 (v_{gs}^c)^{0.7} \quad 11.36$$

$$F_l = 0.28 (g)^{0.33} (v_{gs}^c)^{0.33} (T_v)^{2.33} \quad 9.21$$

$$(C_{og}^c)_n = (C_{og})_n \frac{P_t + \frac{10^4 H_v}{N} (N - n + 1)}{10^5}$$

$$(v_{gs}^c)_n = v_{gs} \frac{10^5}{P_t + \frac{10^4 H_v}{N} (N - n + 1)}$$

$$m = 32$$

$$c_1 = \frac{0.28 (g)^{0.33} (T_v)^{2.33}}{\frac{1}{4} \pi T_v^3} = \frac{0.77}{T_v^{0.67}}$$

$$c_2 = \frac{\frac{1}{4} \pi T_v^2}{\frac{1}{4} \pi T_v^3} = \frac{1}{T_v}$$

The balances read for stationary conditions, when the pressure in compartment n is assumed to be that of level n :

for $n = 1$:

$$(C_{ol})_1 = \frac{0.32(v_{gs}^c)_1^{0.7} \frac{(C_{og})_1}{32} - OUR + c_1(v_{gs}^c)_2^{0.33} (C_{ol})_2}{0.32(v_{gs}^c)_1^{0.7} + c_1(v_{gs}^c)_2^{0.33}}$$

$$(C_{og})_2 = \frac{c_2 v_{gs} (C_{og})_1 - 0.32(v_{gs}^c)_1^{0.7} \left(\frac{(C_{og})_1}{32} - (C_{ol})_1 \right)}{c_2 v_{gs}}$$

for $n = n$:

$$(C_{ol})_n = \frac{0.32(v_{gs}^c)_n^{0.7} \frac{(C_{og})_n}{32} - OUR + c_1(v_{gs}^c)_n^{0.33} (C_{ol})_{n-1} + c_1(v_{gs}^c)_{n+1}^{0.33} (C_{ol})_{n+1}}{0.32(v_{gs}^c)_n^{0.7} + c_1(v_{gs}^c)_n^{0.33} + c_1(v_{gs}^c)_{n+1}^{0.33}}$$

$$(C_{og})_{n+1} = \frac{c_2 v_{gs} (C_{og})_n - 0.32(v_{gs}^c)_n^{0.7} \left(\frac{(C_{og})_n}{32} - (C_{ol})_n \right)}{c_2 v_{gs}}$$

and for $n = N$:

$$(C_{ol})_N = \frac{0.32(v_{gs}^c)_N^{0.7} \frac{(C_{og})_N}{32} - OUR + c_1(v_{gs}^c)_N^{0.33} (C_{ol})_{N-1}}{0.32(v_{gs}^c)_N^{0.7} + c_1(v_{gs}^c)_N^{0.33}}$$

$$(C_{og})_{out} = \frac{c_2 v_{gs} (C_{og})_N - 0.32(v_{gs}^c)_N^{0.7} \left(\frac{(C_{og})_N}{32} - (C_{ol})_N \right)}{c_2 v_{gs}}$$

Two simulations have been made, with an iteration procedure:

- Case I: $H_v = 10 \text{ m}$, $T_v = 1 \text{ m}$, $N = 10$,
 $p_t = 10^5 \text{ N m}^{-2}$ $v_{gs} = 0.06 \text{ m s}^{-1}$ $OUR = 0.01 \text{ mol m}^{-3} \text{ s}^{-1}$
- Case II: $H_v = 50 \text{ m}$, $T_v = 1 \text{ m}$, $N = 50$.
Same parameter values as Case I.

The results for $C_{og}^c / 32$ and C_{ol} are given in Fig. 18.10. C_{og} is given in Fig. 18.11.

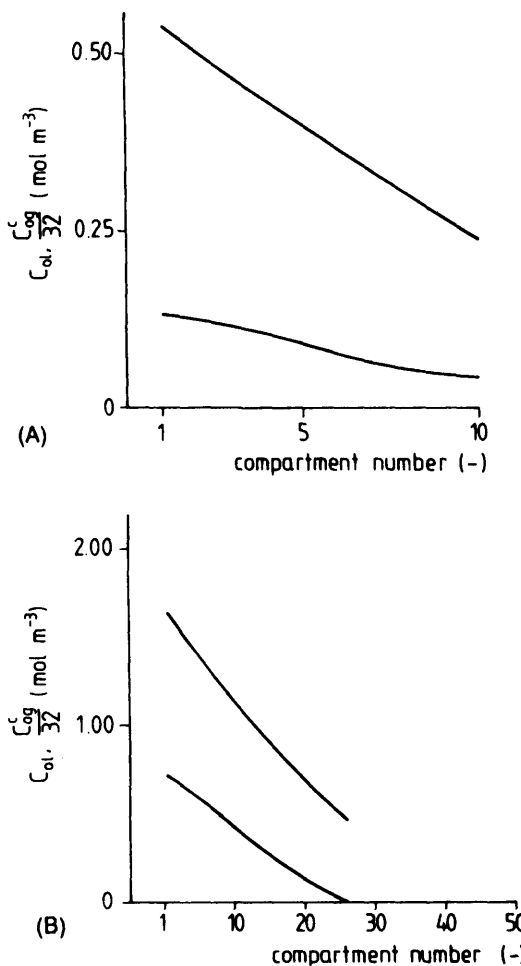


Fig. 18.10 The liquid oxygen concentration values. The upper line is C_{og}^c , the lower line is C_{ol} . A: Case 1. B: Case 2.

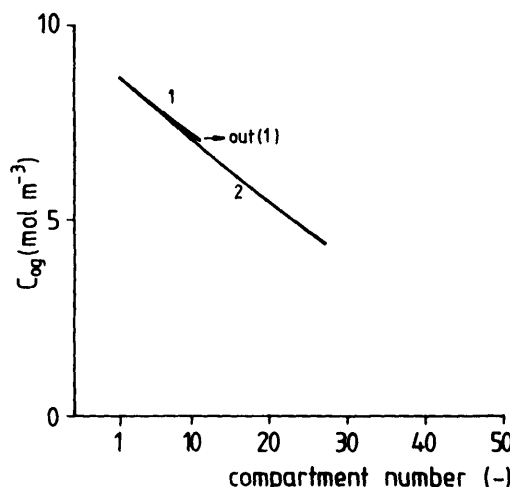


Fig. 18.11 The gas phase concentration at atmospheric conditions.
Line 1: Case 1. Line 2: Case 2.

For $N = 10$ the results show that the whole column is adequately aerated. The gas oxygen concentration decreases, however not to such a degree that a lack of oxygen occurs in the upper part of the column. The gas-liquid mass transfer in the lower compartment is larger than in the upper compartment. A calculation learns that for

$$n = 1: OTR = 0.0113 \text{ mol m}^{-3} \text{ s}^{-1} \text{ and for}$$

$$n = 10: OTR = 0.0094 \text{ mol m}^{-3} \text{ s}^{-1}.$$

The difference between OTR and OUR is equilibrated by mixing in the liquid phase (F_L). Two remarks can be made about this phenomenon.

1. The liquid phase mixing is very intensive. For instance, for $n = 5$ it can be calculated that:

$$OTR V_L = 0.008 \text{ mol s}^{-1}$$

$$(F_L)_5 (C_{ol})_5 = 0.024 \text{ mol s}^{-1}$$

$$(F_L)_5 (C_{ol})_4 = 0.027 \text{ mol s}^{-1}$$

$$(F_L)_5 [(C_{ol})_4 - (C_{ol})_5] = 0.003 \text{ mol s}^{-1}$$

indicating that oxygen transfer to a compartment by gas-liquid transfer (mass transfer) is of the same order of magnitude as that by liquid transport (mixing).

2. The differences in OTR between $n = 1$ and $n = 10$ are much less than would be expected at first sight from the driving force as seen in

Fig. 18.10. The reason is that $v_{g,i}^c$ decreases linearly with pressure. Due to the exponent 0.7 in the $k_{oi}A$ formula, the $k_{oi}A$ decreases for this reason with an exponent 0.7. The increase of C_{oi}^c is linear with pressure. This results, at $C_{oi} = 0$, in an exponent of $-0.7 + 1 = 0.3$ for the OTR increase with pressure. Here the stirred fermenter is advantageous because of the lower exponent ($= 0.4$) for $v_{g,i}^c$ and an increase with an exponent of $-0.4 + 1 = 0.6$.

For $N = 50$ the results show that this reactor does not work well with the given parameter values. At $n > 27$, $C_{oi} = 0$, indicating that the OTR transport by mixing $< OUR$. The depletion of the gas phase is about 50% of the original value and $v_{g,i}^c = 0.03 \text{ m s}^{-1}$ at this level ($n = 25$). These two facts lead to an OTR value that is too small to obtain a satisfactory aeration (at $n = 27$ $OTR = 0.0087$) even with the intensive liquid oxygen transport. Nearly the same would be the case for a 27-m bubble column with a top pressure of $3.3 \times 10^5 \text{ N m}^{-2}$. This example shows that a bubble column has a limitation in the height allowed, mainly dependent on the OUR value, and caused by gas phase depletion and OTR. An air lift shows a more efficient liquid oxygen transport from the lower compartments up to the upper compartments. Yet, although at a larger height, for this fermenter also, the height is limited for the same reasons.

Example 18.2 Example of the design scheme use

In this example the design scheme will be elucidated. The first part of the scheme as shown in Fig. 18.5 calculates the r and M values. This was shown in Example 2.1. For oxygen limitation Fig. 2.3 gives the result. The values are given there as $f(t)$. In Fig 2.3 an r_o value is postulated. The reactor concept is also chosen in Example 2.1: A fed-batch. The results of Example 2.1 are chosen as the basis for this example. Starting from $t = 0$ the calculation scheme can be worked through for a given time interval. That will not be done in this example. It can be expected that at the end of the fermentation, $t = t_f$, the volume will be at its maximum and the concentration will be at its maximum and therefore the design for t_f will cover the whole fermentation. Let us assume we want a fermentation with $t_f = 20 \text{ h}$. At the end $M_x = 205\,600 \text{ mol}$, $r_o = -1.4 \text{ mol s}^{-1}$ and $\mu = 1.0 \times 10^{-5} \text{ s}^{-1}$. That is the start for Fig. 18.6. The scheme is followed now:

- A stirred tank is chosen.
- 1 stirrer, $D = 0.4 T_v$, at D above the bottom, $H_v/T_v = 2$.
- $OTR_{max} = 0.01 \text{ mol m}^{-3} \text{ s}^{-1}$ (chosen).
- Now V_i can be calculated $V_i = r_o/OTR = 140 \text{ m}^3$.
Assuming hold-up + foam = 30%, then $V_i = 182 \text{ m}^3$
 $\rightarrow 0.5 H_v = T_v = 4.87 \text{ m}$.
- From V_i and M_x , C_x can be calculated: $C_x = 1124 \text{ mol m}^{-3}$. This is a rather low value. Maybe later a larger OTR_{max} can be introduced.

- This is a yeast fermentation $\rightarrow \eta$ and C_p not relevant.
- Choose $P_s/V_i = 2000 \text{ W m}^{-3}$ and $v_{gs}^c = 0.03 \text{ m s}^{-1}$; $k_{ol}A$ can then be calculated from

$$k_{ol}A = 2.6 \times 10^{-2} \left(\frac{P_s}{V_i} \right)^{0.4} (v_{gs}^c)^{0.5} = 0.094 \text{ s}^{-1}$$

- $\frac{C_{o_2}^c}{32} - C_{ol} = \frac{OTR}{k_{ol}A} = \frac{0.01}{0.094} = 0.11 \text{ mol m}^{-3}$

- The C_{ols} at critical conditions is needed. The mixing time can be calculated with Eq. (9.18). It is found $t_m = 43 \text{ s}$. This is for $H_v = T_v$. Therefore, it is multiplied by a factor 2. The circulation time is $0.25 t_m$. We assume that $t_{cro} = t_c$.

Then $C_{ols} = \frac{43 \times 2}{4} 0.01 = 0.22 \text{ mol m}^{-3}$

- $C_{o_2}^c/32 = 0.11 + 0.22 = 0.33 \text{ mol m}^{-3}$. This is a minimum value, to obtain the required OTR.
- Now the gas balance has to be set up.

$$F_g (8.68 - C_{o_2}) = OTR V_i = 1.4 \text{ mol s}^{-1}$$

$$v_{gs} \frac{P_s}{P_a} \frac{1}{4} \pi T_v^2 (8.68 - C_{o_2}) = 1.4 \text{ mol s}^{-1}$$

Assume $P_s = 2 \times 10^5 \text{ N m}^{-2}$. Then $P_a = 2.6 \times 10^5 \text{ N m}^{-2}$

$$\rightarrow C_{o_2} = 7.71 \text{ mol m}^{-3}$$

$$C_{o_2}^c/m = 7.71 \times 2.6 / 32 = 0.62 \text{ mol m}^{-3}$$

- All data are known now. It appears that $C_{o_2}^c/m$ is larger than required for effective aeration. Therefore, chosen parameter values can be changed. Possibilities are OTR increase, v_{gs}^c decrease, P_s decrease or r_o increase and OTR increase, leading to M_x increase. Or the last combination and the same M_x , but with a decrease of t_c . If M_x and t_c are kept the same, an OTR increase (and V_i decrease) seems to be most logical. All these schemes can be worked through, completed with the influence of P_s change and finally the best choice is used for the last part of Fig. 18.5.

This part is rather simple, except the weight balance. Here an integration for the whole period is required, following the lines as given in Example 2.5. This will lead to the volume at $t = 0$, that is required to obtain the volume calculated at $t = t_c$. It also can be calculated if OTR is not exceeded at $t < t_c$. Usually this is not the case because the C_x increase due to M_x increase is usually larger than the C_x decrease due to dilution effects. The final results have to be compared with all the assumed values and the whole procedure will be repeated if needed or wished with adapted values.

Example 18.3 The oxygen transfer energy efficiency

Assume, unless stated $V_t = 100 \text{ m}^3$

otherwise:

$$H_v = 2 T_v = 8 \text{ m}$$

$$p_t = p_a = 10^5 \text{ N m}^{-2}$$

$$F_g = 0.63 \text{ m}^3 \text{ s}^{-1}$$

$$C_{ots} = 0 \text{ mol m}^{-3}$$

$$C_{ot} = 0 \text{ mol m}^{-3}$$

For a stirred tank the transfer equation can be written as:

$$OTR = 2.6 \times 10^{-2} \left(\frac{P_s}{V_t} \right)^{0.4} \left(\frac{F_g}{\frac{1}{4} \pi T_v^2} \frac{p_a}{p_t + (H_v - 0.4 T_v) 10^4} \right)^{0.5} \times \\ \left(\frac{p_t + (H_v - 0.4 T_v) 10^4 \left(8.68 - \frac{OTR V_t}{F_g} \right)}{32 p_a} - 0 \right)$$

For a bubble column the transfer equation can be written as:

$$OTR = 0.32 \left(\frac{F_g}{\frac{1}{4} \pi T_v^2} \frac{p_a}{p_t + T_v 10^4} \right)^{0.7} \times \\ \left(\frac{p_t + T_v 10^4}{32 p_a} \left(8.68 - \frac{OTR V_t}{F_g} \right) - 0 \right)$$

For the gas energy the adiabatic compression energy is chosen (Smith and Van Ness, 1987):

$$P_g = \frac{p_a F_g}{\gamma} \left(\left(\frac{p_t + H_v 10^4}{p_a} \right)^{\frac{\gamma-1}{\gamma}} - 1 \right)$$

with

$$\gamma = \frac{C_p}{C_v} = 1.4$$

The results are given in the Tables 18.1-18.7.

Table 18.1 Change in P_s / V_l for a stirred tank

$\frac{P_s}{V_l}$ (W)	OTR (mol m ⁻³ s ⁻¹)	$\frac{\text{kg O}_2}{\text{kWh}}$
600	1.85×10^{-2}	2.33
1,000	2.12×10^{-2}	1.86
2,000	2.51×10^{-2}	1.25
5,000	3.04×10^{-2}	0.66
10,000	3.45×10^{-2}	0.35
20,000	3.83×10^{-2}	0.22

All data are given in Fig. 18.12.

Table 18.2 Change in P_s / V_l for a stirred tank.
Different gas flow rate: $F_g = 5 \times 0.63$
m³ s⁻¹. Lower P_s values are not
included because of flooding

$\frac{P_s}{V_l}$ (W)	OTR (mol m ⁻³ s ⁻¹)	$\frac{\text{kg O}_2}{\text{kWh}}$
2,000	7.35×10^{-2}	2.37
5,000	9.55×10^{-2}	1.67
10,000	1.14×10^{-1}	1.13
20,000	1.34×10^{-1}	0.71

All data are given in Fig. 18.12.

Table 18.3 Change in F_g for a bubble column

F_g ($\text{m}^3 \text{s}^{-1}$)	OTR ($\text{mol m}^{-3} \text{s}^{-1}$)	$\frac{\text{kg O}_2}{\text{kWh}}$
0.1	2.4×10^{-3}	5.96
0.2	4.1×10^{-3}	5.10
0.4	6.9×10^{-3}	4.34
0.6	9.3×10^{-3}	3.93
1.0	1.4×10^{-2}	3.46
2.0	2.3×10^{-2}	2.90
5.0	4.5×10^{-2}	2.27
10.0	7.5×10^{-2}	1.88
20.0	1.2×10^{-1}	1.55

All data are given in Fig. 18.12.

Table 18.4 Change in P_t for the stirred vessel.

Case I: $F_g = 0.63 \text{ m}^3 \text{s}^{-1}$.

P_t (N m^{-2})	OTR ($\text{mol m}^{-3} \text{s}^{-1}$)	$\frac{\text{kg O}_2}{\text{kWh}}$
1×10^5	2.45×10^{-2}	1.19
2×10^5	2.70×10^{-2}	1.22
4×10^5	3.08×10^{-2}	1.22
8×10^5	3.48×10^{-2}	1.18
20×10^5	3.99×10^{-2}	1.09

All data are given in Fig. 18.12.

Table 18.5 Change in P_t for the stirred vessel.
Case II: $v_{gs}^c = 0.04 \text{ m s}^{-1}$

P_t (N m ⁻²)	OTR (mol m ⁻³ s ⁻¹)	$\frac{\text{kg O}_2}{\text{kWh}}$
1×10^5	2.87×10^{-2}	1.39
2×10^5	4.62×10^{-2}	1.69
4×10^5	8.12×10^{-2}	1.74
8×10^5	1.51×10^{-1}	1.51
20×10^5	3.61×10^{-1}	1.08

All data are given in Fig. 18.12.

Table 18.6 Change in P_t for the bubble column.
Case I: $F_g = 0.63 \text{ m}^3 \text{s}^{-1}$

P_t (N m ⁻²)	OTR (mol m ⁻³ s ⁻¹)	$\frac{\text{kg O}_2}{\text{kWh}}$
1×10^5	9.73×10^{-3}	3.82
2×10^5	1.11×10^{-2}	2.32
4×10^5	1.28×10^{-2}	1.62
8×10^5	1.48×10^{-2}	1.23
20×10^5	1.79×10^{-2}	0.92

All data are given in Fig. 18.12.

Table 18.7 Change in P_t for the bubble column.
Case II: $v_{gs}^c = 0.04 \text{ m s}^{-1}$

P_t (N m ⁻²)	OTR (mol m ⁻³ s ⁻¹)	$\frac{\text{kg O}_2}{\text{kWh}}$
1×10^5	1.06×10^{-2}	3.71
2×10^5	1.81×10^{-2}	1.98
4×10^5	3.32×10^{-2}	1.20
8×10^5	6.34×10^{-2}	0.80
20×10^5	1.54×10^{-1}	0.49

All data are given in Fig. 18.12.

Example 18.4 Energy costs

In this example the energy costs are calculated for a fermentation with $r_o = 4 \text{ mol s}^{-1}$. V_f is chosen as 25, 50, 100, 200 and 400 m³. The kg O₂/kWh is taken from Fig. 18.12 from curve 3. The \$_s are chosen as 0.05, 0.10 and 0.15 \$(kWh)⁻¹. Using Eq. (18.26) Table 18.8 has been made.

This example shows that at a given total r_o , the energy costs increase with decrease in scale. This is not surprising, although the extent is larger than might be expected. At very large scale, the value is very low and a further increase in scale is not very interesting anymore.

Example 18.5 The costs of product on substrate

The influence of the parameters that constitute the \$_{ps} equation is shown in Fig. 18.13 A-E. Unless varied, the parameter values are the same as that in Example 3.1. The discussion of the influence of the parameters is also the same as given in Example 3.1.

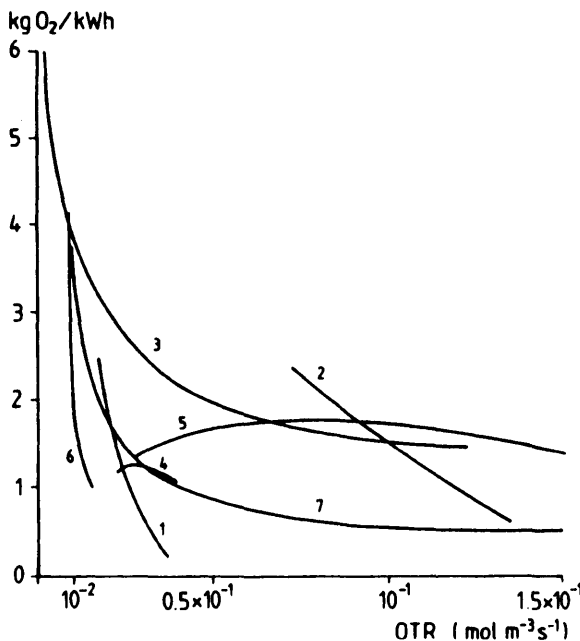


Fig. 18.12 The kg O₂/kWh as a function of OTR. The numbers refer to the numbers of Tables 18.1-18.7.

Table 18.8 Calculated energy costs

V_l (m ³)	OTR (mol m ⁻³ s ⁻¹)	$\frac{\text{kg O}_2}{\text{kWh}}$	\$ _o (\\$ m ⁻³ h ⁻¹)			
			\$ _o = 0.05	0.10	0.15	{\\$}(kWh) ⁻¹
25	0.16	1.4	0.66	1.32	1.97	
50	0.08	1.7	0.27	0.54	0.81	
100	0.04	2.2	0.10	0.21	0.31	
200	0.02	3.1	0.04	0.07	0.11	
400	0.01	3.9	0.01	0.03	0.04	

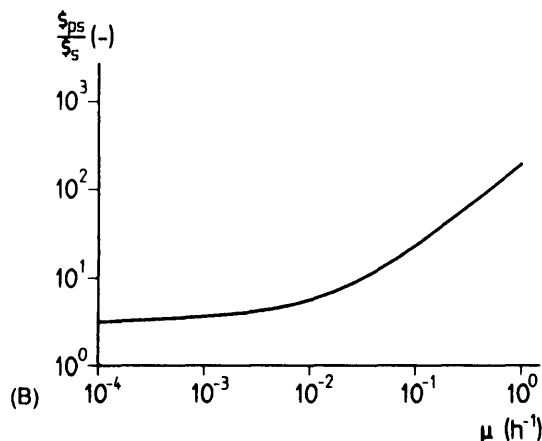
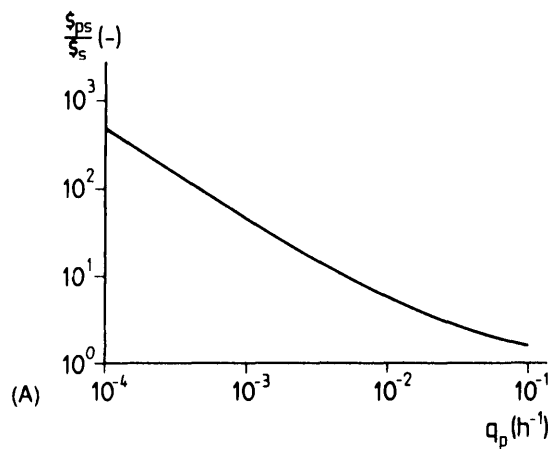


Fig. 18.13 A-E The value of $\frac{s_{ps}}{s_s}$, as a function of a number of parameters (all on a kg basis).

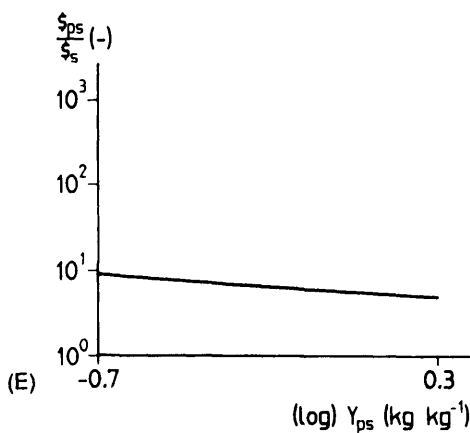
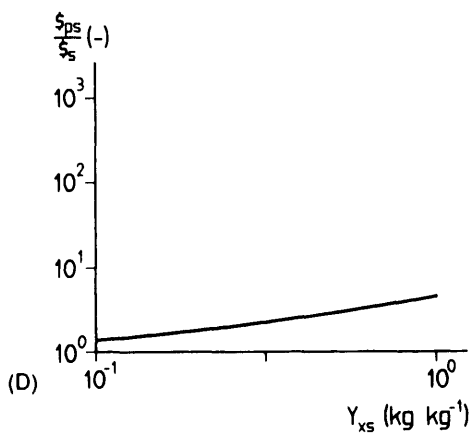
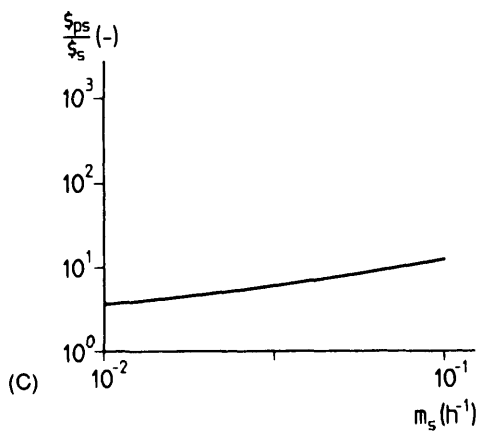


Fig. 18.13 A-E (continued)

Example 18.6 The costs of biomass on substrate

The influence of the parameters that constitute the $\$_{xs}$ equation is shown in Fig. 18.14 A-C. Unless varied, the parameter values are the same as that in Example 3.2. The discussion of the influence of the parameters is also the same as given in Example 3.2.

Example 18.7 The costs of biomass on substrate for a fed-batch

Based on the data given in Example 2.1, the $\$_{xs}/\$$, can be calculated for the additional biomass produced at a time t . According to Fig. 18.15, the influence is rather limited as long as $\mu > 5 \times 10^{-2} (\text{h}^{-1})$, that is, below $t = 20 \text{ h}$. For higher time values the costs increase in an increasingly faster rate with fermentation time.

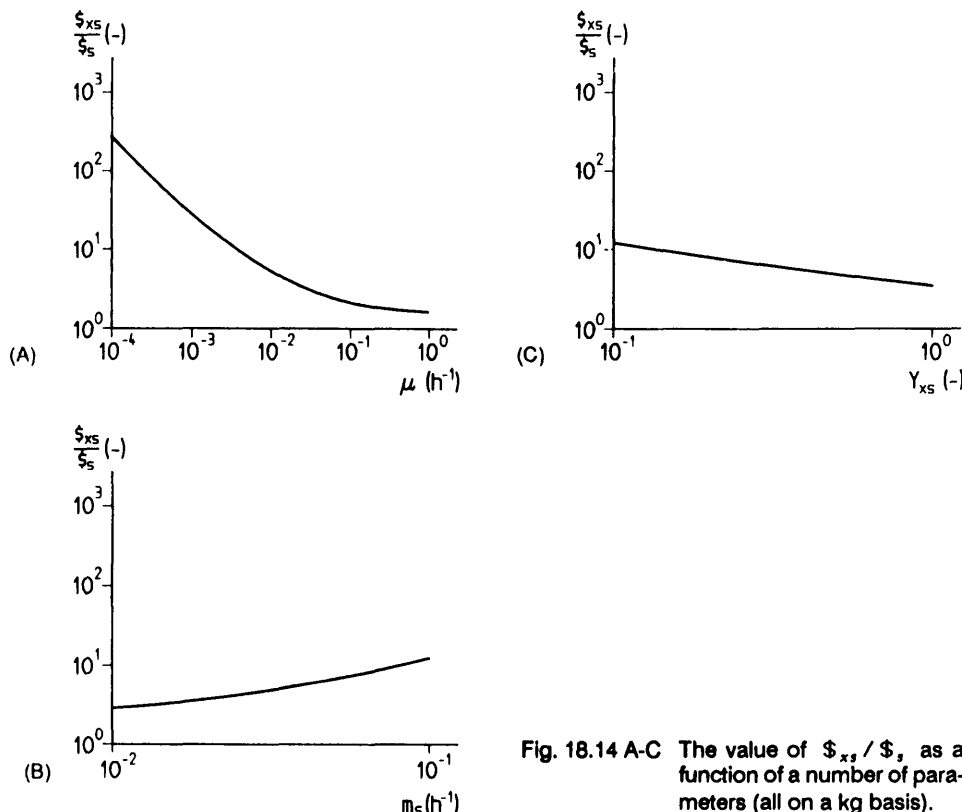


Fig. 18.14 A-C The value of $\$_{xs}/\$$, as a function of a number of parameters (all on a kg basis).

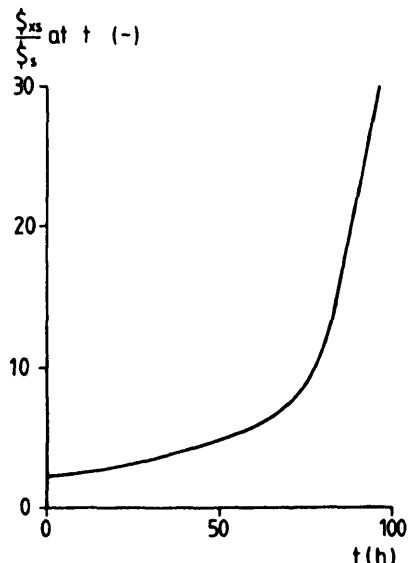


Fig. 18.15 The $\frac{\$_{xs}}{\$_s}$ for the fermentation given in Example 2.1 (Fig. 2.3). All values are on a mol basis.

Example 18.8 The product costs for an anaerobic fermentation

For the anaerobic case a simulation of $\frac{\$_{ps}^a}{\$_s}$ is given in Fig. 18.16 based on Example 3.3. The difference with $\frac{\$_{ps}}{\$_s}$ as found in Fig. 18.13B is large. The overall yield for product formation is usually much better in anaerobic fermentations than in aerobic fermentations. See also the remarks made in Example 3.3.

Example 18.9 The biomass costs for an anaerobic fermentation

Fig. 18.17 shows simulations for $\frac{\$_{xs}^a}{\$_s}$ and $\frac{\$_{xs}}{\$_s}$ (these are on a molar basis in the example). It is clear that aerobic fermentations can lead to much cheaper biomass than anaerobic fermentation. The data used are the same as in Examples 3.2 and 3.3. See also the discussion in Example 3.3.

Example 18.10 The total product costs of the fermenter, aerobic

In this example a number of simulations are made for $\frac{\$_{pf}}{\$_s}$. The parameter values, unless varied, are:

$$\begin{aligned} Y_{ps} &= 1 \quad \text{kg kg}^{-1} \\ \mu &= 0.01 \quad \text{h}^{-1} \\ q_p &= 10^{-2} \quad \text{kg kg}^{-1} \text{ h}^{-1} \end{aligned}$$

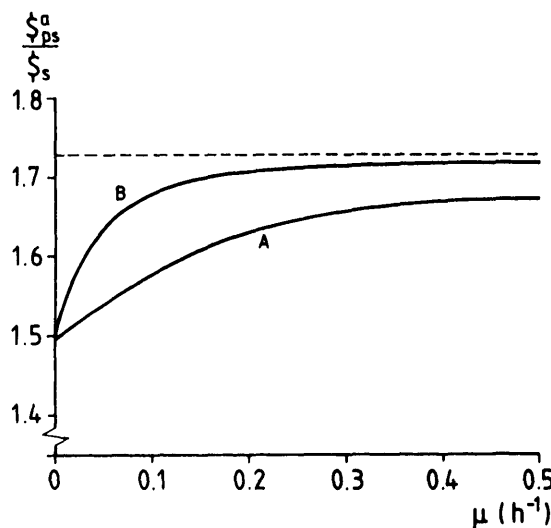


Fig. 18.16 The $\frac{\$_{ps}^a}{\$_s}$ for the fermentation given in Example 3.3 (Fig. 3.5). All data on a kg basis. Line A: High-maintenance case. Line B: Low-maintenance case.

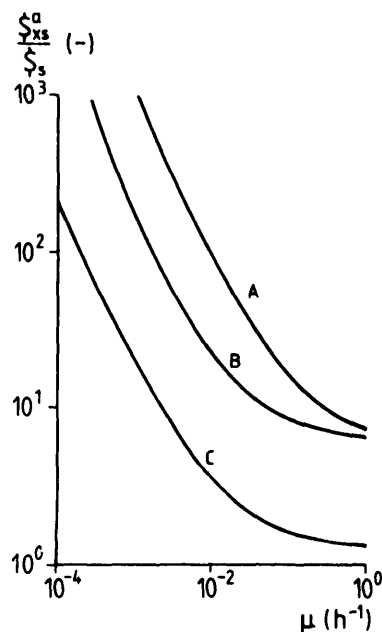


Fig. 18.17 The $\frac{\$_{xs}^a}{\$_s}$ and $\frac{\$_{xs}^a}{\$_{ps}^a}$ as a function of μ .

Line A: Anaerobic, high-maintenance case (data in Example 3.4)
 Line B: Anaerobic, low-maintenance case (data in Example 3.4)
 Line C: Aerobic case (data in Example 3.4). All values are on a mol basis.

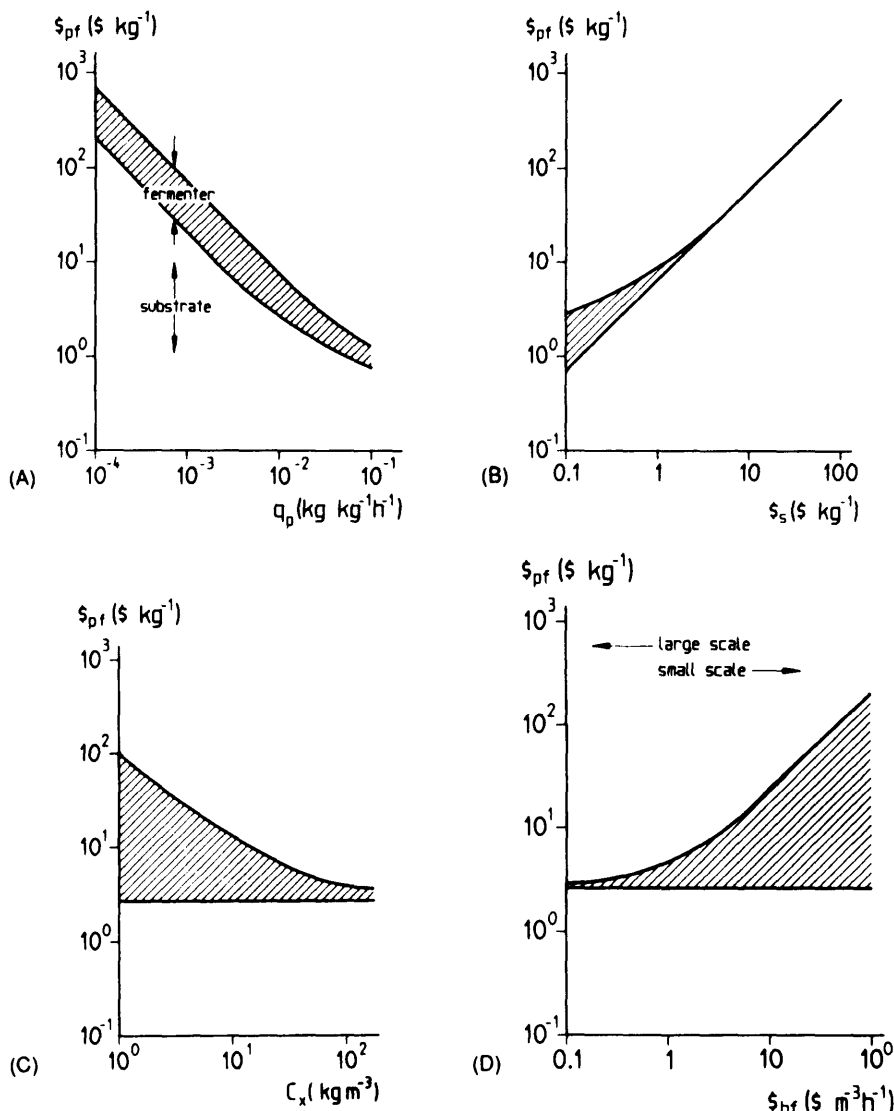


Fig. 18.18 A-D Simulations for $\$_{pf}$. The shaded areas are the fermenter related costs; the area below the lower line, the substrate related costs.

$$\begin{aligned}
 Y_{xs} &= 0.55 \text{ kg kg h}^{-1} \\
 m_s &= 0.025 \text{ kg kg}^{-1} \text{ h}^{-1} \\
 C_x &= 50 \text{ kg m}^{-3} \\
 \$_s &= 0.5 \text{ \$ kg}^{-1} \\
 \$_{h_f} &= 1 \text{ \$ m}^{-3} \text{ h}^{-1}
 \end{aligned}$$

The μ and C_x values are chosen in a region for a moderate OTR value as shown in Fig. 18.3. The μ value is chosen in a region where it hardly influences $\$,_{h_f}$. Simulations are shown in Fig. 18.18 A-D. Because of the logarithmic scale the fermenter costs seem to be limited for a number of cases. However, this is the case only for large $\$,$ values, low $\$,_{h_f}$ values and high C_x values.

References

- Heijnen J.J., Roels J.A. and Stouthamer A.H. "Application of balancing methods in modeling the penicillin fermentation." *Biotechnol. Bioengn.* **21**, 2175 (1979).
- Swartz R.W. "The use of economic analysis of penicillin G manufacturing costs in establishing priorities for fermentation process improvement." *Annual reports on fermentation technology*, Vol. 3. Academic Press, New York (1979).
- Smith J.M. and Van Ness H.C. "Introduction to chemical engineering thermodynamics." *Mc Graw-Hill*, New York (1987).
- Van 't Riet K. "Mass transfer in fermentation." *Trends in Biotechnology* **1**, 113 (1983).
- Van 't Riet K. "Genetic engineering or biochemical engineering. The profitability argument." *The world biotechnology report*, Vol. 1, Europe p. 265 (1984).
- Van 't Riet K. "The selection of research targets based on forecasted production costs." *Trends Biotechnol.* **4**, 236 (1986).

List of Symbols

A	specific A per unit liquid volume	(m^{-1})
A'	specific A per unit reactor volume	(m^{-1})
A''	specific A per unit particle volume	(m^{-1})
A	reacting species A	
a	surface area	(m^2)
a_c	surface area cooling coils	(m^2)
a_f	surface area fermenter	(m^2)
a_w	water activity	(-)
α	constant	(-)
B	reacting species B	(-)
Bo	Bodenstein number	(-)
Bo'	Bo corrected for particle hold-up	(-)
BOD	Biological Oxygen Demand	(-)
b	constant	(-)
C	concentration	(mol m^{-3})
C_A	concentration of A	(mol m^{-3})
C_A^*	concentration of A at equilibrium	(mol m^{-3})
C_B^*	concentration of B at equilibrium	(mol m^{-3})
C_{A1}	inflowing concentration of A	(mol m^{-3})
C_{A0}	outflowing concentration of A	(mol m^{-3})
C_{Ar}	reactor concentration of A	(mol m^{-3})
C_d	concentration denatured enzyme	(mol m^{-3})
C_e	enzyme concentration	(mol m^{-3})
C_e^T	total active enzyme concentration	(mol m^{-3})
C_e'	total not irreversibly modified C_e	(mol m^{-3})
C_{es}	enzyme/substrate complex concentration	(mol m^{-3})
C_i	concentration of component i	(mol m^{-3})
C_i	concentration irreversible inactivated enzyme	(mol m^{-3})
C_{ig}	concentration i in gas bulk phase	(mol m^{-3})
C_{igI}	concentration i at gas interface	(mol m^{-3})

C_{ii}	concentration i in bulk liquid phase	(mol m ⁻³)
C_{il}	concentration i at liquid interface	(mol m ⁻³)
C_{l1}	concentration i in bulk phase 1	(mol m ⁻³)
C_{l2}	concentration i in bulk phase 2	(mol m ⁻³)
C_o	concentration outflowing liquid	(mol m ⁻³)
C_{og}	oxygen concentration in gas bulk	(mol m ⁻³)
C_{og}^e	C_{og} at the local pressure	(mol m ⁻³)
C_{ogl}	oxygen concentration in inflowing air	(mol m ⁻³)
C_{oga}	oxygen concentration in outflowing air	(mol m ⁻³)
C_{ol}	oxygen concentration in liquid bulk	(mol m ⁻³)
C_{ol}^*	interface oxygen concentration	(mol m ⁻³)
C_{ol0}	oxygen conc. liquid without solutes	(mol m ⁻³)
$C_{ol,ref}$	reference oxygen concentration	(mol m ⁻³)
C_{ols}	C_{ol} at stirrer level	(mol m ⁻³)
C_p	product concentration	(mol m ⁻³)
C'_p	product concentration	(kg m ⁻³)
C_p^*	equilibrium product concentration	(mol m ⁻³)
C_s	substrate concentration	(mol m ⁻³)
$C_s(0)$	initial substrate concentration	(mol m ⁻³)
C_s^*	equilibrium substrate concentration	(mol m ⁻³)
C_{sb}	C_s in bulk liquid	(mol m ⁻³)
C_{sf}	C_s at the feed position	(mol m ⁻³)
C_{si}	C_s at particle medium interface	(mol m ⁻³)
$C_{s\mu}$	C_s at growth rate μ	(mol m ⁻³)
C_x	dry cell concentration	(mol m ⁻³)
C'_x	dry cell concentration	(kg m ⁻³)
C_z	concentration of Z	(mol m ⁻³)
$C(\infty)$	tracer concentration at $t = \infty$	(mol m ⁻³)
ΔC	allowed deviation from ideally mixed	(mol m ⁻³)
c	constant	(-)
c'	constant	(-)
c_i, c_j	constant related to i or j	(m ³ mol ⁻¹)
c_{pb}	thermal coefficient of the broth	(J kg ⁻¹ C ⁻¹)
c_{pc}	thermal coefficient cooling medium	(J kg ⁻¹ C ⁻¹)
c_{pg}	thermal coefficient of the gas	(J kg ⁻¹ C ⁻¹)
c_v	heat of vaporization	(J kg ⁻¹)
c_w	drag coefficient	(-)
D	stirrer diameter	(m)
D	dilution rate	(s ⁻¹)
$D\alpha$	Dämkohler number	(-)
D_f	forced vortex zone diameter	(m)
$ D_e $	axial dispersion coefficient	(m ² s ⁻¹)

D_{eg}	axial dispersion coefficient gas phase	(m ² s ⁻¹)
D_{el}	axial dispersion coefficient liquid phase	(m ² s ⁻¹)
D_i	diffusion coefficient of <i>i</i>	(m ² s ⁻¹)
D_{ll}	D_l in the liquid phase	(m ² s ⁻¹)
D_{ol}	diffusion coefficient of oxygen in liquid	(m ² s ⁻¹)
D_{sp}	effective $ D$ of substrate in particle	(m ² s ⁻¹)
d_f	foam film thickness	(m)
d_b	bubble diameter	(m)
d_i	injector inner diameter	(m)
d_h	hill liquid film thickness	(m)
d_t	fouling layer thickness	(m)
d_p	particle diameter	(m)
d_s	stirrer blade width	(m)
d_w	thickness wall cooling coil	(m)
E	refers to enzyme	
E	surface dilatational modulus	(N m ⁻¹)
ES	refers to enzyme substrate complex	(mol m ⁻³)
ΔE	activation energy	(J mol ⁻¹)
F_c	volumetric circulation flow rate	(m ³ s ⁻¹)
F_g	volumetric gas flow rate	(m ³ s ⁻¹)
F'_g	molar gas flow rate	(mol s ⁻¹)
F_{gl}	inflowing volumetric gas flow rate	(m ³ s ⁻¹)
F_{go}	outflowing volumetric gas flow rate	(m ³ s ⁻¹)
F_{gs}	F_g at pressure of the lower stirrer	(m ³ s ⁻¹)
F_l	volumetric inflow rate	(m ³ s ⁻¹)
F_i'	molar flux of <i>i</i>	(mol m ⁻² s ⁻¹)
F'_{A1}	inflowing molar flow rate of <i>A</i>	(mol s ⁻¹)
F'_{A0}	outflowing molar flow rate of <i>A</i>	(mol s ⁻¹)
F_o	volumetric outflow rate	(m ³ s ⁻¹)
F''_o	molar flux of oxygen	(mol m ⁻² s ⁻¹)
F_p	volumetric pumping capacity	(m ³ s ⁻¹)
F_l	volumetric liquid flow rate	(m ³ s ⁻¹)
F_l^u	liquid flow per unit width	(m ² s ⁻¹)
F_m	flow rate cooling medium	(m ³ s ⁻¹)
F'_s	molar flow rate of substrate	(mol s ⁻¹)
F''_s	molar flux of substrate	(mol m ⁻² s ⁻¹)
F_s^u	F'_s per unit reactor volume	(mol s ⁻¹ m ⁻³)
$f(r)$	function	(m)
$G\alpha$	Galilei number	(-)
G_A^0	standard free enthalpy of <i>A</i>	(J mol ⁻¹)
G_B^0	standard free enthalpy of <i>B</i>	(J mol ⁻¹)
ΔG^0	standard free enthalpy change	(J mol ⁻¹)

g	gravitational acceleration	(m s ⁻²)
h_t	total heat transfer coefficient	(W m ⁻² °C ⁻¹)
h_1	heat transfer coefficient in medium 1	(W m ⁻² °C ⁻¹)
h_2	heat transfer coefficient in medium 2	(W m ⁻² °C ⁻¹)
H_v	vessel height	(m)
H	height	(m)
H_c	total heat transfer to cooling device	(W)
H_s	stirrer blade height	(m)
H_{sb}	height stirrer above vessel bottom	(m)
HPR	heat production rate	(W m ⁻³)
ΔH_i	free enthalpy change of combustion of i	(J mol ⁻¹)
ΔH^0	standard enthalpy change	(J mol ⁻¹)
ΔH^\bullet	activation enthalpy change	(J mol ⁻¹)
ΔH_r^\bullet	activation enthalpy change of a reaction	(J mol ⁻¹)
ΔH_p	product free enthalpy change of combustion	(J mol ⁻¹)
ΔH_n	ammonia free enthalpy change of combustion	(J mol ⁻¹)
ΔH_s	C substrate free enthalpy change of combustion	(J mol ⁻¹)
ΔH_x	biomass free enthalpy change of combustion	(J mol ⁻¹)
I	electric current strength	(A)
ISF	integrated shear factor	(s ⁻¹)
j	number (of j -th vessel in a series of n)	(-)
K	equilibrium constant	(-)
K	consistency index	(N s ⁿ m ⁻²)
K_f	friction coefficient	(-)
K_i	total mass transfer coefficient for i	(m s ⁻¹)
K_m	Michaelis-Menten constant	(mol m ⁻³)
K'_m	apparent K_m	(mol m ⁻³)
K_s	Monod constant	(mol m ⁻³)
K_m'	pseudo Monod constant	(mol m ⁻³)
k	reaction rate constant	
k_d	denaturation reaction rate constant	(s ⁻¹)
k_d	first-order death rate constant	(s ⁻¹)
k_e	first-order specific death rate constant	(m ³ s ⁻¹)
k_g	first-order growth rate constant	(s ⁻¹)
k_u	frequency number	
k_{ig}	gas side mass transfer coefficient for i	(m s ⁻¹)
k_{il}	liquid side mass transfer coefficient for i	(m s ⁻¹)
k_j	k of j -th reaction ($j = -2$ to 2)	
k_{obs}	hypothetical observed denaturation k	(s ⁻¹)
k_{og}	gas side k for oxygen	(m s ⁻¹)
k_{ol}	liquid side k for oxygen	(m s ⁻¹)
$k_{ol} A_a$	apparent measured $k_{ol} A$ value	(s ⁻¹)
k_{sl}	liquid side k for substrate	(m s ⁻¹)

k^{ov}	overall first order k	(s ⁻¹)
L	length	(m)
M_b	torque exerted by bearings and seals	(N m)
M_s	torque exerted by stirrer	(N m)
M_t	total torque	(N m)
M_x	biomass	(mol)
m	partition coefficient	(-)
m_s	aerobic maintenance coefficient on substrate	(s ⁻¹)
m_a^s	anaerobic maintenance coefficient on substrate	(s ⁻¹)
m_p^a	anaerobic maintenance coefficient on product	(s ⁻¹)
N	stirrer speed	(s ⁻¹)
N_x	number of cells	(-)
N_p	stirrer power number	(-)
n	number (ideally mixed tanks)	(-)
n	power law index	(-)
n_b	number of impeller blades	(-)
n'_b	number of bubbles per m ³ reactor volume	(m ⁻³)
OTR	oxygen transfer rate	(mol m ⁻³ s ⁻¹)
OTR'	specific oxygen transfer rate	(mol kg ⁻¹ s ⁻¹)
OUR	oxygen uptake rate	(mol m ⁻³ s ⁻¹)
OUR'	specific oxygen uptake rate	(mol kg ⁻¹ s ⁻¹)
P	power consumption	(W)
P	refers to product	
P_{el}	electrical power	(W)
P_g	energy dissipated by the gas	(W)
P_{gl}	energy dissipated by gas in lower compartment	(W)
P_s	stirrer power consumption	(W)
P_{sg}	P_s , at gassed conditions	(W)
P_{su}	P_s , at ungassed conditions	(W)
P_{sl}	energy dissipated by stirrer in lower compartment	(W)
P_t	energy from stirrer and gas	(W)
Pr_{px}	overall productivity of the biocatalyst	(-)
ΔP	Laplace pressure difference	(N m ⁻²)
ΔP_r	pressure drop over the reactor height	(N m ⁻²)
P_a	atmospheric pressure	(N m ⁻²)
P_n	normalized pressure	(N m ⁻²)
P_s	pressure at stirrer level	(W)
P_t	fermenter top pressure	(N m ⁻²)
P_{orec}	sensor measured O ₂ partial pressure	
P_{orec}'	P_{orec} at atmospheric pressure	
q_d	specific death rate	(s ⁻¹)
q_p	specific product production rate	(s ⁻¹)
Q_p	overall volumetric productivity	(mol m ⁻³ s ⁻¹)

R	gas constant	(J mol ⁻¹ K ⁻¹)
Re	Reynolds number	(-)
R_c	radius of the curvature	(m)
R_p	particle radius	(m)
R_s	stirrer radius	(m)
R_v	vessel radius	(m)
R_0	radius at which C_s is just zero	(m)
r	radius	(m)
r_A	production rate component A	(mol s ⁻¹)
r_A^u	production rate A per unit volume	(mol m ⁻³ s ⁻¹)
r_c	carbon dioxide production rate	(mol s ⁻¹)
r_H	heat production rate	(W s ⁻¹)
r_{HG}	heat produced by the throughflowing gas	(W)
r_{HT}	total heat generated or lost	(W)
r_{HS}	r_H dissipated by stirrer	(W)
r_{HM}	r_H generated by microorganisms	(W)
r_{HV}	r_H resulting from vaporization	(W)
r_{HW}	r_H through fermenter walls	(W)
r_{HH}	r_H from all other sources	(W)
$r_{i,j}$	i or j production rate	(mol s ⁻¹)
r_i^u	r_i per unit volume	(mol m ⁻³ s ⁻¹)
r_o	oxygen production rate	(mol s ⁻¹)
r_n	ammonia production rate	(mol s ⁻¹)
r_p	product production rate	(mol s ⁻¹)
r_p^u	product production rate per unit volume	(mol m ⁻³ s ⁻¹)
r_{ph}	phosphoric acid production rate	(mol s ⁻¹)
r_s	substrate production rate	(mol s ⁻¹)
r_s^u	substrate production rate per unit volume	(mol m ⁻³ s ⁻¹)
r_s^{up}	substrate production rate per unit volume of biocatalyst	(mol m ⁻³ s ⁻¹)
r_{su}	sulfuric acid production rate	(mol s ⁻³)
r_x	biomass production rate	(mol s ⁻³)
r_w	water production rate	(mol s ⁻³)
S	refers to substrate	
SC	severity of collision	(J s ⁻¹)
SC_i	severity of collision with impeller	(J s ⁻¹)
Sc	Schmidt number	(-)
Sh	Sherwood number	(-)
ΔS°	standard entropy change of reaction	(J mol ⁻¹ K ⁻¹)
s	foam stability	(-)
t	time	(s)
t_c	circulation time	(s)
t_{cr}	critical time	(s)

t_{cro}	critical time for oxygen depletion	(s)
t_{crs}	critical time for substrate	(s)
t_{crH}	critical time for heat	(s)
t_d	down-time	(s)
t_m	mixing time	(s)
t_i	operational lifetime of the biocatalyst	(s)
$t_{0.5}$	half-life time	(s)
T	temperature	(K)
T_b	broth temperature	(°C)
T_{cl}	temperature of inflowing cooling water	(°C)
T_{co}	temperature of outflowing cooling water	(°C)
T_{gi}	temperature of inflowing gas	(°C)
T_s	temperature of surroundings	(°C)
T_v	vessel diameter	(m)
ΔT	temperature difference	(°C)
U	ionic strength	(mol m ⁻³)
V	volume	(m ³)
V	voltage	(V)
V_c	volume of the circulation loop	(m ³)
V_{fe}	equilibrium volume of foam	(m ³)
V_g	volume of the gas phase	(m ³)
V_k	killing volume	(m ³)
V_l	volume of the liquid phase	(m ³)
V_p	volume of particles	(m ³)
v_{max}	maximum substrate conversion rate	(mol m ⁻³ s ⁻¹)
v_{max}^g	maximum substrate conversion rate per unit volume of biocatalyst	(mol m ⁻³ s ⁻¹)
v'_{max}	apparent v_{max}	(mol m ⁻³ s ⁻¹)
v''_{max}	maximum substrate conversion rate	(mol m ⁻³ s ⁻¹)
v	velocity	(m s ⁻¹)
v_{bi}	bubble velocity at injector	(m s ⁻¹)
v_{br}	single bubble rise velocity	(m s ⁻¹)
v_{bs}	bubble rise or slip velocity	(m s ⁻¹)
v_{bw}	bubble velocity relative to the wall	(m s ⁻¹)
v_{gs}	gas superficial velocity	(m s ⁻¹)
v_{gs}^c	v_{gs} corrected for local pressure	(m s ⁻¹)
v_{lb}	liquid film velocity	(m s ⁻¹)
v_{lc}	liquid velocity in the center	(m s ⁻¹)
v_{ls}	liquid superficial velocity	(m s ⁻¹)
v_{ps}	single particle settling velocity	(m s ⁻¹)
v_{tip}	stirrer tip speed	(m s ⁻¹)
v_{tw}	liquid velocity relative to the wall	(m s ⁻¹)
v_{pl}	particle velocity relative to liquid	(m s ⁻¹)

v_∞	velocity at infinite distance	(m s ⁻¹)
\bar{v}	average velocity	(m s ⁻¹)
W_A	weight of A added	(kg)
X	weight percentage of particle phase	(%)
x	conversion	(-)
Y_{ij}	aerobic yield of component i on j	(-)
Y_{po}	aerobic yield of product on oxygen	(-)
Y_{ps}	aerobic yield of product on substrate	(-)
Y_{ps}^{ov}	aerobic overall yield of product on substrate	(-)
Y_{ps}^{ova}	anaerobic overall yield of product on substrate	(-)
Y_{xp}^a	anaerobic yield of biomass on product	(-)
Y_{xs}^a	aerobic yield of biomass on substrate	(-)
Y_{xs}^{a*}	anaerobic yield of biomass on substrate	(-)
Y_{xs}^{ova}	anaerobic overall yield of biomass on substrate	(-)
z	coordinate	(m)
z_i	valency of component i	(-)
μ	specific growth rate of cells	(s ⁻¹)
μ_{max}	maximum specific growth rate	(s ⁻¹)
ρ_d	density of the gas-liquid dispersion	(kg m ⁻³)
ρ_p	particle specific density	(kg m ⁻³)
ρ_c	continuous phase specific density	(kg m ⁻³)
ρ_m	specific density of cooling medium	(kg m ⁻³)
ρ_l	liquid phase specific density	(kg m ⁻³)
ρ_{vl}	water vapor weight gas in, normalized	(kg m ⁻³)
ρ_{vo}	water vapor weight fermenter top	(kg m ⁻³)
$\Delta \rho_{gl}$	specific density difference gas and liquid	(kg m ⁻³)
δ	film thickness	(m)
δ_l	laminar boundary layer thickness	(m)
δ_t	turbulent boundary layer thickness	(m)
η	dynamic viscosity	(N s m ⁻²)
η_a	apparent dynamic viscosity	(N s m ⁻²)
η_l	liquid dynamic viscosity	(N s m ⁻²)
η_b	broth dynamic viscosity	(N s m ⁻²)
η_{ei}	internal effectiveness factor	(-)
η_e^{ov}	overall effectiveness factor	(-)
η_{eo}	external effectiveness factor	(-)
η_{eio}	zero-order internal effectiveness factor	(-)
η_{eal}	first-order internal effectiveness factor	(-)
ϵ	gas hold-up or porosity	(-)
ϵ_d	gas hold-up downcomer	(-)
ϵ_r	gas hold-up in the riser	(-)
ϵ_e	energy content per unit mass	(W kg ⁻¹)

$\dot{\gamma}$	shear rate	(s^{-1})
$\dot{\gamma}_{ave}$	time-averaged shear rate	(s^{-1})
ν	kinematic viscosity	($m^2 s^{-1}$)
ν_l	liquid kinematic viscosity	($m^2 s^{-1}$)
ν_b	broth kinematic viscosity	($m^2 s^{-1}$)
Θ	dimensionless concentration	(-)
τ	average residence time	(-)
τ	shear stress	($N m^{-2}$)
τ_0	yield stress	($N m^{-2}$)
τ_{CSTR}	average residence time of the CSTR	(s)
τ_g	average gas residence time	(s)
τ_p	characteristic response time of electr.	(s)
τ_{pf}	residence time of a plug flow reactor	(s)
τ_{wl}	laminar wall shear stress	($N m^{-2}$)
τ_{wt}	turbulent wall shear stress	($N m^{-2}$)
τ_{max}	maximum shear stress	($N m^{-2}$)
τ_{ave}	time-averaged shear stress	($N m^{-2}$)
λ_i	heat conductivity of fouling layer	($W m^{-1} ^\circ C^{-1}$)
λ_w	heat conductivity of the wall	($W m^{-1} ^\circ C^{-1}$)
λ_b	heat conductivity of the broth	($W m^{-1} ^\circ C^{-2}$)
λ_e^{ov}	overall dimensionless reaction rate	(-)
λ_{ei}	internal dimensionless reaction rate	(-)
λ_{er}	biocatalyst dimensionless reaction rate	(-)
λ	Kolmogoroff eddy size	(m)
σ	surface tension	($N m^{-1}$)
Σ	foaminess	(s)
Σ_r	foaminess with moving stirrer	(s)
α	propeller blade angle	(deg)
$\cos \phi$	phase shift between V and I	(rad)
Φ	Thiele modulus	(-)
$\$_o$	fermenter energy costs	($\$ m^{-3} h^{-1}$)
$\$_{hf}$	fermenter costs per hour	($\$ m^{-3} h^{-1}$)
$\$_e$	costs of energy	($\$ kW h^{-1}$)
$\$_s$	costs of substrate	($\$ mol^{-1}$)
$\$_{ps}$	substrate-related product costs, aerobic	($\$ mol^{-1}$)
$\$_{xs}$	substrate-related biomass costs, aerobic	($\$ mol^{-1}$)
$\$_{ps}^a$	substrate-related product costs, anaerobic	($\$ mol^{-1}$)
$\$_{xs}^a$	substrate-related biomass costs, anaerobic	($\$ mol^{-1}$)
$\$_{ph}$	fermenter-related product costs, aerobic	($\$ mol^{-1}$)
$\$_{xh}$	fermenter-related product costs, aerobic	($\$ mol^{-1}$)
$\$_{ph}^a$	fermenter-related product costs, anaerobic	($\$ mol^{-1}$)
$\$_{ph}^a$	fermenter-related biomass costs, anaerobic	($\$ mol^{-1}$)
$\$_{pf}$	total costs of product after fermentation	($\$ mol^{-1}$)

INDEX

A

Active conformation, 94

Air bubble:

bursting, 162, 166

injection, 162, 166

rising, 162, 165

rising velocity, 168

specific surface area, 167

Air lift, 9, 114

a-Helix sheet, 93

Amino acids, 91

Animal cells, 139, 142, 145, 147, 157, 161, 169

Antifoam, 223

agent, 284

liquid, 280

Apparent stabilization:

external diffusion limitation, 355

first-order kinetics, 348

internal diffusion limitation, 356

reactor level, 357

zero-order kinetics, 361

Arrhenius, 98, 99

equation, 83

B

Batch:

bioreactor, 372
fermentation, 48
productivity, 417
S-shaped growth curve, 374

Batch reactor, 13, 371
mass transfer, 372
Michaelis-Menten kinetics, 372
Monod kinetics, 372

β -Pleated sheet, 93

Bingham liquids, 123

Biocatalyst:

immobilized, 319, 388
microenvironment, 325

Biomass, 31

concentration, 415
consumption, 29
growth, 31
output rate, 380
production rate, 31

Biopolymers, 128

Bioreactor annular, 171

Black box model, 28, 32

Bodenstein number, 188, 203, 204, 211

Boundary layer, 148

forces, 150
laminar, 148
shear forces, 147
thickness, 148, 150
turbulent, 148, 150

Bubble:

- diameter, 267
- rise velocity, 221, 268

Bubble column, 9, 110, 161, 164, 165

- insect cells, 168

C

Casson equation, 128

Casson liquids, 123

Cell:

- growth measurement, 77
- kinetics, 68
- kinetics constant, 78

Chemical reaction method, 207, 261

Chemostat, 377, 380, 382

Circulation:

- capacity, 190
- loop, 185
- pattern, 186
- time, 190, 195, 198, 203, 403

Coalescence, 108, 111, 116, 117, 120, 196, 197, 222, 223, 225, 282

Coalescing, 247, 249, 254

- non-, 247, 249

Collision:

- bead/bead, 157
- damage, 157
- severity, 158

Compartment, 195

Conductivity method, 205

Continuous culture, 32, 416

Cooling, 295, 415

Cooling coils, 415

Cooling device, 296

Costs:

biomass, 428, 445

energy, 426, 442

fermenter, 429

product, 427, 442

substrate, 427

Couette flow, 150

Start of Citation[PU]M. Dekker[/PU][DP]1991[/DP]End of Citation

[< previous page](#)

[page_461](#)

[next page >](#)

Couette viscosimeter, 169, 171

Critical dilution rate, 379

Critical time, 401

heat production, 409

oxygen, 403

regime, 401

substrate, 406

value, 209

CSTR, 14, 343, 371, 377

biomass concentration, 379

equal-sized, 388

mass transfer, 377, 381

Michaelis-Menten kinetics, 377

Monod kinetics, 378, 381, 389

steady state, 378, 379

substrate concentration, 378

CSTR-cascade, 371, 383, 390

mass transfer, 388

Michaelis-Menten kinetics, 384, 388

Monod kinetics, 389

CSTR-series, 384, 385

Michaelis-Menten kinetics, 385

D

Damköhler number, 350, 366

Death rate, 91

cells, 164

first-order constant, 164, 165

specific, 153
specific constant, 153

Decoloring method, 206

Definition:

bioreactor design, 3
biotechnology, 3

Degree of oxidation, 37

Denaturation, 94, 95

Diffusion, 185, 237, 319

effective coefficient, 320
external limitation, 323, 355
internal limitation, 325, 356
limitation, 351

Dilatant, 123

Dilatational modulus stability, 277

Dispersion, 104, 106, 107, 111, 116, 117, 282

coefficient, 188, 197

Disulfide bridges, 94

Down-time, 7

Dynamic method, 258

Dynamometer, 309

E

Eady and Hofstee, 79

Eddy:

concentration group, 153
damaging, 153
length, 151, 153
size, 152, 155

smallest, 158

Effectiveness:

first-order kinetics, 357

Effectiveness factor:

internal, 325, 328, 357

overall, 323, 370, 372, 382, 391

Eisenthal and Cornish-Bowden, 81

Electrical energy measurement, 311

Elemental balances, 27

Elemental flow, 30

Energy:

efficiency, 255

gas, 254

stirrer, 254

Engineering restriction, 410

Enthalpy combustion, 33

Environmental effects, 82

Enzyme:

kinetics, 70

kinetics constant, 78

structure, 93

Equilibrium constant, 72

Ethanol, 46

Ethanol fermentation, 49

Exchange, 185

Exponential growth, 37

F

Fed-batch, 32, 34, 44, 163, 417

biocatalyst, 374

fermentation, 374, 377

productivity, 417

Fed-batch culture:

growth-limiting substrate, 375

quasi-steady state, 377

Fed-batch reactor, 14, 374

Michaelis-Menten kinetics, 374

Monod kinetics, 374

Fermenter pressure head space, 406

Fick's law, 236, 319

Film theory, 321

First-order decay, 343

Flooding, 104, 110, 114, 116, 117, 195, 410

Flow, 104, 110, 114, 116

Flow follower method, 207

Flow regime:

heterogeneous, 197, 224, 248

homogeneous, 197, 224, 250

transitional, 203, 226

Start of Citation[PU]M. Dekker[/PU][DP]1991[/DP]End of Citation

[< previous page](#)

page_462

[next page >](#)

Foam, 223, 274, 413

centrifugal destroyer, 285, 290

control, 287

stability, 275

stable layer, 286

Foaminess, 274

Fouling layer, 296

Fragile cells, 161, 167, 169

G

Galilei number, 243

Gas cavities, 251

Gas phase depletion, 420

Gray box model, 32

Growth, 51

exponential, 34

specific rate, 32, 57, 61, 69

Growth-limiting substrate, 376

H

Half-life, 342

apparent, 342

time, 99

Heat:

balance, 33

production, 33, 37, 40, 56

production, critical time, 409

transfer coefficient, 296

vaporization, 294

Hold-up, 197, 220, 223, 246, 413

gas, 199

Holding time, 383

total, 383, 384

Hydrodynamic effects, 142

Hydrodynamic forces, 136, 144

I

Ideally mixed:

reactor, 188

serie, tank, 188

Immobilization, 319

Immobilized cells, 381

Impeller:

angled flat blades, 148

marine blades, 148

power number, 152

tip speed, 145, 151

Inactivation, 95

constant rate, 96

first-order, 99

kinetically controlled, 95, 98

thermodynamically controlled, 95, 96

Inhomogeniety, 183

Insect cells, 161, 163, 175

continuous culture, 168

growth, 168

Interbead spacing, 158

Interception, 158

Interface:

freely moving, 281

rigid, 281

Invertase, 71

Ionic solution, 222

Ionic strength, 244

effects, 84

Isoelectrical point, 283

K

Killing volume, 166

hypothesis, 164

specific hypothetic, 166

Kinematic viscosity, 138

Kinetic constant:

apparent, 323

intrinsic, estimation, 332

Kinetics, 28

diffusion-controlled, 359

first-order, 76, 327, 329, 335, 348, 357, 359

reaction-controlled, 359

zero-order, 76, 327, 328, 334, 361

Kolmogorov, 186

length scale, 151, 172

theory, 152

L

Laminar flow, 138, 144, 148

Couette stable, 171

Langmuir, 80

Level measurement, 228

Limitation:

carbon, 34, 37

oxygen, 34, 37

Linear growth equation, 32, 51

Lineweaver-Burk, 79

Liquid velocity, 197

Local density measurement, 229

M

Maintenance, 37, 51, 52, 56, 373

coefficient, 31, 61

Mass balance, 12

Mass transfer, 108, 236, 249, 254

coefficient, 238

Michaelis-Menten:

equation, 70, 76, 370

integrated-equation, 82

kinetics, 327, 331, 384

plot, 78

Mixing, 183, 435

intensity, 183, 192

scale, 183

time, 184, 189, 190, 193, 196, 198, 203, 403

Start of Citation[PU]M. Dekker[/PU][DP]1991[/DP]End of Citation

Monod:

equation, 68, 370, 376

kinetics, 382-384

Morphology, 128

Multiple substrate addition points, 408

N

Newtonian, 123

liquids, 123, 138

O

Oligomer enzyme, 94

Operational lifetime, 6

OTR - Colmethod, 257

Overall productivity:

biocatalyst, 5

volumetric, 5

Overall reaction rate:

dimensionless, 350

first-order constant, 349

Overall yield:

biomass on substrate, 52, 57, 59, 63, 65

product on substrate, 52, 56, 57, 59, 60, 65

Oxygen:

concentration, critical, 404-406

consumption, 33

depletion, 187, 209, 430

enriched air, 411

solubility, 255

transfer, energy efficiency, 438

transfer rate, 239

P

Packed bed, 11, 116

Partition coefficient, 322

Pellet formation, 413

Pellets, 128

Penetration, 241

Peptide bond, 91

pH:

effects, 82

method, 205

Plant cells, 157

Plateau border, 274, 279

Plug-flow reactor, 16, 188, 343, 357, 371, 389, 390, 402

mass transfer, 391

Michaelis-Menten kinetics, 390, 391

Monod kinetics, 391

Polarographic:

Clarck cell, 259

oxygen sensor, 258

Porous disc, 120

Power:

consumption, 118, 222, 254, 47

consumption, gassed, 106, 308

consumption, stirrer, 106, 152, 308

law, viscosity, 123, 128

local dissipation, 152

Product:

concentration, 417

formation, 51, 56

Production:

specific rate, 57, 61

Pseudoplastic, 123

Pump capacity, 190

R

Radioactive tracer method, 206

Reaction rate:

dimensionless, 351

Reactor concepts, 12, 17

Regime:

diffusion-controlled, 358

reaction-controlled, 358

Renaturation, 94

Renewing interface, 241

Residence time:

average, 186

average, gas, 259

distribution, 186, 208

Response time:

characteristic, 259

Reynolds number, 143, 148, 160, 65

S

Scale-up, 209

Schmidt number, 244

Shear, 136, 185

critical, 147
damage, 410
inactivation, 141
integrated factor, 142
sensitivity, 139

Shear device, 169
laminar, 169, 170

Shear rate, 107, 122, 127, 137
maximum, 143
models, 145
time-averaged, 143

Shear stress, 122, 163, 165
average, 151
capillary tubes, 172
cone plate apparatus, 172
critical, 151, 153, 162, 171
critical value, 163

Start of Citation[PU]M. Dekker[/PU][DP]1991[/DP]End of Citation

[< previous page](#)

page_464

[next page >](#)

[Shear stress]:

- estimate, 162, 163, 166, 174
 - flow channel, 172
 - free jet, 174
 - laminar, wall, 149
 - maximum, 151, 162
 - measurement, 171, 172, 174
 - shaking cell-culture flasks, 174
 - spinner flasks, 174
 - wall, 150, 172
- Sherwood number, 241
- Slip velocity, 220
- Solubility, 238
 - oxygen, 255
- Sparger, 112, 119, 197
- Sparging, 162
- Stability, 91
 - apparent, 342
 - operational, 346
- Stabilization, 99
- Stagnant zones, 187
- Stirred vessel, 8, 104, 141, 143, 147, 151, 160
- Stirrer type, 251
- Strain gauge, 311
- Subunits, 93
- Sulfite method, 261
- Support, 319

Surface:

- mobile, 242
- rigid, 242
- tension, 163, 244

Surface area:

- specific, 246, 320

Surfactants, 225

Suspension, 109, 112, 116

T

Temperature effects, 83

Thermal method, 205

Thiele modulus, 326, 357

- generalized, 326

Tiny bubbles, 247, 261

Top pressure, 420

Torque, 130

- meter, 309

Tracer, 205

- gas method, 231

Transitional region, 253

Turbulence, 185

- cell death, 155

- eddies, 151, 157

- smallest eddy length, 151

- smallest eddy size, 172

Turbulent flow, 138, 142, 143, 148, 160, 174, 193

V

Viscosimeter, 129

Viscosity, 122, 137, 153, 225, 244, 250, 284, 412

Viscous broth, 402

Volumetric productivity, 360

W

Water-activity effects, 84

Weight balance, 34, 42

Y

Yield, 51

 biomass on product, 56

 biomass on substrate, 31, 51, 55, 56, 61

 factor, 373

 product on oxygen, 55

 product on substrate, 51, 59, 61

Start of Citation[PU]M. Dekker[/PU][DP]1991[/DP]End of Citation

[< previous page](#)

[page_465](#)